Oregon International Port of Coos Bay

Proposed Section 204(f)/408 Channel Modification Project

Sub-Appendix 4

Offshore and Ocean Entrance Dynamics

February 2024 Draft

EXECUTIVE SUMMARY

The Oregon International Port of Coos Bay (OIPCB or Port) seeks to modify the Coos Bay, Oregon Federal Navigation Channel (FNC); the channel modifications assessed in this evaluation are referred to as the Proposed Alteration (PA). The PA consists of widening the channel to a nominal 450 feet (ft) and deepening it to 57 ft Mean Lower Low Water (MLLW) at the entrance to the Coos Bay FNC and to a depth of 45 ft MLLW from inside the entrance through approximately River Mile (RM) 8.2.

This Sub-appendix supports the *Engineering Appendix* to the *Section 204(f)/408 Report*. Specifically, this Sub-appendix presents the analyses that were used to influence the design of the project and to assess any physical effects associated with the project in the FNC downstream of RM 2.5, where the dynamics are dominated by waves and currents. Project elements located downstream of RM 2.5 include the jetties, Charleston Breakwater, the Entrance Channel, the Entrance Turn, Charleston Marina, and Log-spiral Bay (LSB). Tsunami propagation throughout the entire estuary is considered herein because tsunamis originate offshore. The dynamics upstream of RM 2.5 and in the Charleston Channel/South Slough, dominated by tidal and river currents, are presented in *Estuarine Dynamics* (Sub-appendix 3). Side slope equilibration in the Entrance Channel is discussed in the *Channel Side Slope Analysis* report (Sub-appendix 6). These sub-appendices similarly support the *Engineering Appendix* to the *Section 204(f)/408 Report*. Two project configurations were considered: Existing Condition and PA.

The analyses presented herein include:

- Detail the existing metocean conditions in the offshore area and Entrance Channel;
- Simulate wave propagation and estimate extreme waves at the North and South Jetties, the Charleston Breakwater, in the shorelines adjacent to the inlet, and in the channel under the Existing Condition and PA;
- Determine the wave induced motions in the Entrance Channel;
- Explain sedimentation patterns in the offshore area and Entrance Channel of Coos Bay and estimate how proposed modifications may impact these sedimentation patterns;
- Assess changes to erosion along the shorelines adjacent to the inlet, at the base of the jetties, and within the LSB.
- Estimate Entrance Channel shoaling under the Existing Condition and PA;
- Assess how changes to the extreme wave climate may impact jetty armor stone; and
- Investigate potential changes to tsunami propagation throughout the Coos Bay estuary.

The analyses and results are summarized below and described in detail in the body of this report.

WAVE PROPAGATION AND EXTREME WAVE HEIGHTS

The offshore wave climate and wave propagation within the Coos Bay Entrance Channel were thoroughly analyzed. The objective of these analyses was to understand the wave conditions at Coos Bay entrance and determine any changes in wave heights due to channel modifications and their impacts to the stability of existing infrastructure, such as the North Jetty, the South Jetty, and the Charleston Breakwater.

The offshore wave climate was based on data from Coastal Data Information Program (CDIP) Buoys 139p1 (Umpqua Offshore) and 126p1 (Coos Bay). These buoys together provide an 11-year record of wave data. Buoy data shows that the majority of offshore waves originate from a westerly and northwesterly direction. The winter storms have two directional peaks: the majority of waves approach from the west to west-northwest (WNW), and there is a secondary peak from the southwest. The west to WNW waves are long-period swell waves with periods on the order of 16 to 20 seconds, while the southwest waves have periods generally less than 15 seconds.

Seventy-nine storms were identified from an 11-year record from offshore CDIP buoys, in collaboration with U.S. Army Corps of Engineers (USACE) technical reviewers. The CDIP buoys are suitable for characterizing waves at Coos Bay based on water depth and proximity. These waves were propagated to the shoreline using the MIKE-21 Spectral Wave (SW) Model and the Boussinesq Wave (BW) Model, BOUSS-2D[1]. Propagation was simulated for four tidal conditions: Mean Higher High Water (MHHW), MLLW, ebb current at Mean Sea Level (MSL), and flood current at MSL. The total water level of each simulation included the measured non-tidal residual at the time of the storm plus the tidal level. Wave heights were extracted at multiple locations near the North Jetty, the South Jetty, the Charleston Breakwater, in the Entrance Channel, and in the Entrance Turn.

At each wave extraction point, wave heights were plotted for each project condition as cumulative distribution plots and as plots analyzed by offshore direction. The cumulative distribution plots are useful in analysis of jetty stone stability, as wave height is a key input in the Hudson equation. This is summarized in the section on "Armor Stone Stability" below. The wave direction plots can be used to estimate how waves from different offshore directions are expected to respond to the Project. Design armor size was calculated based on the wave height corresponding to the 95^{th} percentile ranking determined from the cumulative distribution plots. Using the 95^{th} percentile wave height follows the current USACE design practice.

The numerical modeling shows that widening and deepening the navigation channel causes enhanced wave refraction at the offshore portion of the Entrance Channel. Since the Project extends the Entrance Channel further offshore, waves begin to refract further offshore. As a result of the Project, wave energy from the WNW sector (parallel with the channel alignment) is expected to shift from the channel to outside of the jetties. Waves from the south-southwest (SSW) through the west tend to focus more energy on the South Jetty head and less energy on the North Jetty, and waves from the northwest (NW) and north-northwest (NNW) are expected to focus more energy on the North Jetty head and less on the South Jetty. Wave heights are expected to decrease along both the North Jetty trunk and the South Jetty trunk. Essentially, the modeling results show that

[1] *MIKE-21 SW was approved per the May 26, 2016 Memorandum for Record entitled One-Time Authorization for Using MIKE-21 Modeling Suite. BOUSS-2D is a USACE-approved model.*

wave propagation into the channel will be reduced at nearly all locations as a result of implementing the 2023 PA improvements.

It has been noted that extreme wave heights from the NW and NNW sectors can be particularly damaging to the North Jetty (Moritz 2018). These NW and NNW sectors represent only 25 percent of all the incoming waves and only 7 percent of the investigated 79 storm events. Investigating the largest storms from these sectors showed an overall decrease in extreme wave heights at the North Jetty under the 2023 PA.

It is recognized that changes in sea levels predicted in the future is likely to impact design conditions at Coos Bay. The evaluations on future sea level change (SLC) consisted of repeating the wave modeling for the Existing Conditions and the 2023 PA performed for current no SLC condition and including +3.2 feet of SLC (USACE "high" projection for 2080). The modeled SLC cases predict increases in wave heights (up to 2.1 ft) occurred over the entire entrance including the jetties, the navigation channel, Charleston Marina and the LSB with SLC. During the propagation of waves into the entrance, the wave height increases due to SLC are between 1 to 2 ft at South Jetty, higher than those at North Jetty. The comparisons between the Existing Conditions and the 2023 PA, both with future SLC, show increase of extreme waves at the South Jetty head (about 5 percent) and decrease at the North Jetty head, the North Jetty trunk/root, the in LSB, and within the channel.

VESSEL MOTIONS DUE TO WAVES

Wave-induced vessel motions were calculated to provide input for the depth required for the Entrance Channel (see Main Engineering Appendix Report). Vertical motions due to waves were estimated using ANSYS AQWA. The design vessel selected for analysis was the Post-Panamax Containership *Kalina*, representative of the largest vessel likely to visit Coos Bay under the PA.

Vessel motions are influenced by both wave heights and wave periods. In total, over 2,000 dynamic simulations were simulated to evaluate the vertical motion of the vessel due to the range of wave conditions experienced by vessels entering and leaving Coos Bay.

COASTAL SEDIMENT TRANSPORT PROCESSES

Coastal sedimentation and inlet shoaling were evaluated using the following:

- Analysis of historic shorelines;
- Development of conceptual sediment budget; and
- Numerical sediment transport modeling.

A review of historical shoreline development indicates that the construction of the North Jetty in the late 1800s resulted in the formation of the North Spit and, starting in the late 1950s, the formation of LSB. Shoreline movements over the past 10 years indicate that erosion of the North Spit and of LSB has stabilized.

Shoaling results from offshore sediment moving into the Entrance Channel and from longshore transport circumventing the jetty tips. Two distinct shoals develop, one between the jetty tips and one about 1,000-2,000 ft offshore of the jetty tips. Net longshore transport near the inlet is toward the north, with values ranging from 300,000 cubic yards per year (cy/yr) south of the inlet (where longshore transport is limited by sediment availability) to 800,000 cy/yr north of the inlet (where sediment is plentiful due to material placement).

The USACE Coastal Modeling System (CMS) was used to simulate sediment transport in the Entrance Channel and offshore area and its impact on future Operations and Maintenance (O&M) dredging within the Entrance Channel, including the portion of the deeper, wider channel offshore of the jetty tips. The model was used to predict the increase in shoaling under the 2023 PA relative to the Existing Conditions. Both scenarios were modeled directly, rather than one being interpolated from the results of the other. Future O&M dredging volumes were estimated by adding these modeled increases to the present-day average annual dredging volumes. Since the most recent channel deepening in 1998, annual O&M in the Entrance Channel (downstream of RM 2.5) has been approximately 667,000 cy/yr. Sediment transport modeling predicts shoaling in the entrance channel between RM -1 and RM 1 under the 2023 PA to increase by 308,000 cy/year, and between RM 1 and RM 2.5 conservatively by about 51,000 cy/year relative to the Existing Conditions. The total projected increase in shoaling up to RM 2.5 due to the 2023 PA channel dredging, and its impact on expected O&M rates is summarized in Table ES-1.

To account for the natural variability in annual sedimentation in the O&M projections, a similar distribution around the mean expected value of sedimentation as observed in the historical record was assumed. The standard deviation observed from the data record was scaled to the projected mean sedimentation with the 2023 PA. Accordingly, assuming a normal distribution the future annual O&M dredging could be expected to fall between 760,000 cy and 1,290,000 cy about 68% of the time.

Table ES-1
Projected O&M Dredging in the Coos Bay Entrance Channel up to RM 2.5

Estimate	Projected Entrance Channel Dredging in cy/year	
	Existing Conditions	**2023 PA**
Projected Increase in Shoaling[2]	N/A	+359,000
Projected O&M	667,000[3]	1,026,000

Sediment transport results were also used to identify areas that are under the Existing Conditions and where erosion may be expected to increase. Under the Existing Conditions, the Pacific Ocean shorelines, the base of the South Jetty root, and the North Jetty root are erosional. Under the 2023 PA, the erosion is projected to increase along a portion of the North Jetty root. Therefore, a rock apron has been proposed from North Jetty Station 56+50 to 71+90 to protect against the potential increase in erosion. Sedimentation model results also indicate the potential for a minor increase in erosion potential at LSB and Charleston Breakwater. While not sufficient to warrant mitigation measures, these areas have been identified to be monitored as part of the Risk Management Plan.

[2] *Based on model results*
[3] *Based on historical data record*

ARMOR STONE STABILITY

Armor stone on the South Jetty head is sheltered by a concrete monolith that extends 300 ft offshore of the structure at MLLW, which appears to dissipate a portion of the incoming wave energy. The armor stone at the South Jetty head is presently in fair condition (USACE 2012b). The USACE (2017b) report notes the ongoing deterioration of the North Jetty head. The head has been receding since the last repair in 1989. The current North Jetty head is located at Station 82+86; the rate of retreat has been slowing in recent years, and only 5 ft of recession was noted from 2016-2017 (compared to 17 ft/year from 1994-2011 as noted in USACE 2012b). Presently, the USACE has initiated a three-year North Jetty Repair Major Maintenance project on April 1, 2023 and is expected to last until December 2025.

Analysis of armor stone stability was based on the 95th percentile of the cumulative wave height distribution and compared to the wave threshold for armor stone stability at all extraction points along the North and South Jetties.

Design guidance indicates that, under the Hudson equation, an increase in damage is expected for an 8% increase in wave height; this corresponds to roughly a 26% increase in armor stone size. Majority of the extraction points show a decrease in wave height resulting from the 2023 PA. The largest percent increase in wave height occurs at extraction point S2, where the wave height increases by 2.4% (i.e., significantly lower than 8%). Therefore, an increase in damage is not expected per the design guidance. At the North Jetty, the 95th percentile wave heights are all below the wave thresholds. In addition, the 95th percentile wave heights decrease under the 2023 PA, which results in decreases of required armor sizes for all North Jetty locations except at N1. Therefore, the 2023 PA is not expected to result in any increased damage to the jetties.

TSUNAMI PROPAGATION

Tsunamis originating from seismic activity in the Cascadia Subduction Zone (CSZ) represent the most prominent nearfield threat to Coos Bay. The Oregon Department of Geology and Mineral Industries (DOGAMI) has developed and modeled a number of hypothetical events involving the full rupture of this subduction zone to create tsunami inundation maps for the coast of Oregon since 1994. DOGAMI has marked inundation lines corresponding to the XXL scenario in the vicinity of Coos Bay. This same scenario was modeled to examine the impact that the project improvements would have on tsunami propagation in Coos Bay.

The results of the simulations indicate that there are nearly no changes between the Existing Condition and the 2023 PA. Therefore, the project improvements do not affect tsunami runup along the shorelines within Coos Bay.

RISK MANAGEMENT PLAN

Results of the investigations described in this Section 204(f)/408 Report, in the opinion of the OIPCB, show that all project effects on infrastructure and the natural environment have been managed or are minor and manageable. The Corps of Engineers, through their Section 408 and 404 reviews, will make the Federal determination whether the Proposed Alteration is environmentally acceptable and consistent with Federal policy. As is the case with the implementation of any navigation improvement project in such a dynamic physical environment and within an important and ecologically valuable estuary, there will be inherent residual risk and uncertainty associated with project implementation. As such, Risk Management will be a critical element of the project.

This sub-appendix describes analyses that were used to influence the design of the project and to assess any physical effects associated with the project in the Entrance Channel downstream of RM 2.5, where the dynamics are dominated by waves and currents. Project elements located downstream of RM 2.5 include the jetties, Charleston Breakwater, the Entrance Channel, the Entrance Turn, Charleston Marina, and Log-spiral Bay (LSB). Note that potential impacts to physical infrastructure related to the FWP conditions addressed in this sub-appendix relate to wave and current-driven hydrodynamic and littoral sediment transport processes. Potential impacts to physical infrastructure related to side slope equilibration of the deeper and wider FWP navigation channel are addressed in *Sub-Appendix 6 – Channel Side Slope Analysis*.

Throughout the development of the Section 204(f)/408 Report, potential areas of residual risk regarding the potential for impacts within the Coos Bay Entrance Channel area have been identified. While these potential impacts will be further evaluated in the EIS process, preliminary elements of risk identified as warranting quantitative risk management plan are summarized in Table ES-2.

Table ES-2
Risk Management Elements Related to Offshore and Ocean Entrance Dynamics Analyses

Issue or Concern	Primary Monitoring	Monitoring Tools	Frequency and Duration of Monitoring	Trigger(S) for Action	Possible Response Actions
North and South Jetty Stability	Bathymetric surveys	Bathymetric surveys to establish baseline Existing Conditions variability	Annually – 5-year period post construction. Periodic following major storm events.	Erosion beyond predicted limits and / or in close proximity to jetty structure	Temporarily suspend dredging operations; Add or enhance rock apron
Other Infrastructure Stability including LSB and Charleston Breakwater	Bathymetric surveys	Bathymetric surveys to establish baseline Existing Conditions variability	Annually – 5-year period post construction. Periodic following major storm events.	Erosion beyond predicted limits and / or in close proximity to jetty structure	Temporarily suspend dredging operations; Add or enhance rock apron or other protective measures

The Risk Management Plan will be developed based on USACE Risk Management guidance.

Table of Contents

Attachments

List of Tables

List of Figures

ACRONYMS AND ABBREVIATIONS

2D	Two-dimensional
3D	Three-dimensional
3d HD	3D Hydrodynamic
ac	Acres
ADCP	Acoustic Doppler Current Profilers
AIS	Automatic identification system
AMD	Advanced Maintenance Dredging
ASA(CW)	Assistant Secretary of the Army for Civil Works
ATON	Aids to Navigation
BMPs	Best Management Practices
BOE	Basis of Estimate
BW	Boussinesq Wave
CBNS	Coos Bay North Spit
CDF	Confined Disposal Facility
CDIP	Coastal Data Information Program
CFR	Code of Federal Regulations
cfs	Cubic feet per second
CMOP	Coastal Margin Observation and Protection
CMS	Coastal Modeling System
CRA	Cost Risk Analysis
CSZ	Cascadia Subduction Zone
CWA	Clean Water Act
cy	Cubic yards
cy/yr	Cubic yards per year
CZMA	Coastal Zone Management Act
DBB	Design-Bid-Build
DDR	Design Documentation Report
DEA	David Evans and Associates, Inc.
DHI	Danish Hydraulic Institute
DMMP	Dredged Material Management Plan
DOGAMI	Oregon Department of Geology and Mineral Industries
DTM	Digital Terrain Model
EC	Engineering Circular
EIS	Environmental Impact Statement
ENSO	El Niño/Southern Oscillation
ER	Engineer Regulations
ERDC	Engineer Research and Development Center
ESA	Endangered Species Act
ETL	Engineer Technical Letter
FAA	Federal Aviation Administration
FERC	Federal Energy Regulatory Commission
FM	Flexible Mesh
FM HD	Flexible Mesh Hydrodynamic
FNC	Federal Navigation Channel
FR	Federal Register
ft	Foot or feet
FY	Fiscal Year
gpm	Gallons per minute
GRI	Geotechnical Resources, Inc.
HCSS	Heavy Construction Systems Specialists
HOWL	Highest Observed Water Level
HRA	Habitat Restoration Area

ACRONYMS AND ABBREVIATIONS

HSE	Health, safety and environment
IG	Infragravity
ILS	Instrument Landing System
in.	Inches
IWP	Industrial Waste Pond
lf	Linear feet
LiDAR	Light Detection And Ranging
LNG	Liquefied natural gas
LNGC	Liquefied natrual gas carrier
LOA	Length Overall
LSB	Log-spiral Bay
LST	Longshore Transport
M&N	Moffatt & Nichol
MCR	Mouth of the Columbia River
MCX	Mandatory Center of Expertise
mcy	Million cubic yards
MHHW	Mean Higher High Water
MHW	Mean High Water
mi	Miles
MLLW	Mean Lower Low Water
MLW	Mean Low Water
mm	Millimeters
MMR	Major Maintenance Report
MOF	Material Offloading Facility
MorFac	Morphological acceleration factors
MPRSA	Marine Protection, Research, and Sanctuaries Act
MSL	Mean Sea Level
MTL	Mean Tide Level
MTO	Material takeoffs
NAIP	National Agricultural Imagery Program
NAVD88	North American Vertical Datum of 1988
NDBC	National Data Buoy Center
NED	National Economic Development
NEPA	National Environmental Policy Act
NGDC	National Geodetic Data Center
NM	Nautical Mile
NMFS	National Marine Fisheries Service
NNW	North-northwest
NOAA	National Oceanic and Atmospheric Administration
NOS	National Ocean Service
NRC	National Research Council
NTPro	Navi Trainer Pro 5000
NW	Northwest
NWN	North West-north
O&M	Operations and Maintenance
OCMP	Oregon Coastal Management Program
ODEQ	Oregon Department of Environmental Quality

ACRONYMS AND ABBREVIATIONS

ODLCD	Oregon Department of Land Conservation and Development
ODMDS	Ocean Dredged Material Disposal Site
ODSL	Oregon Department of State Lands
OESA	Oregon Endangered Species Act
OGMT	Oregon Gateway Marine Terminal
OIPCB or Port	Oregon International Port of Coos Bay
OPC	Opinion of probable costs
OPRD	Oregon Parks and Recreation Department
OSU	Oregon State University
PA	Proposed Alteration
POT	Peak-Over-Threshold
PRG	Project Review Group
PRG	Project Review Group
psi	pounds per square inch
PSU	Practical salinity unit
QC	Quality control
RAO	Response Amplitude Operators
RFP	Roseburg Forest Products
RM	River mile
RMS	Root-mean-squared
ROD	Record of Decision
SDPP	South Dunes Power Plant
SEF	Sediment Evaluation Framework
SELFE	Semi-implicit Eulerian-Lagrangian Finite Element
SHPO	Oregon State Historic Preservation Office
SL	Screening levels
SLC	Sea level change
SLR	Sea-level Rise
SMMP	Site Management/Monitoring Plan
SOORC	Southern Oregon Ocean Resource Commission
SSE	Safe Shutdown Earthquake
SSW	South-southwest
SW	Spectral Wave
SWORA	Southwest Oregon Regional Airport
TCX	Technical expertise
the “Project”	Coos Bay Section 204(f) Channel Modification Project
TIN	Triangular irregular networks
Transas	Transas Navi Trainer Pro 5000
TSP	Tentatively Selected Plan
U.S.	United States
USACE	U.S. Army Corps of Engineers
USBLM	U.S. Bureau of Land Management
USC	United States Code
USCG	U.S. Coast Guard
USDA	U.S. Department of Agriculture
USEPA	U.S. Environmental Protection Agency
USFWS	U.S. Fish and Wildlife Service

ACRONYMS AND ABBREVIATIONS

USGS	U.S. Geological Survey
USGS	U.S. Geological Survey
VFR	Visual flight rules
WIIN	Water Infrastructure Improvements for the Nation
WNW	West-northwest
WOP	Without Project
WRDA	Water Resources Development Act
WRRDA	Water Resources Reform and Development Act
WSP	Western Snowy Plover
WSW	West-southwest

1. INTRODUCTION

The Oregon International Port of Coos Bay (OIPCB or Port) is home to the second largest deep-draft coastal harbor between San Francisco and the Puget Sound, based on the tonnage of cargo transported through the Port. Access to the Port's facilities is provided by the Coos Bay Federal Navigation Channel (FNC), a federal channel that was first dredged in the early 1900s. The channel was last improved in 1998, when the channel was deepened by 2 feet (ft) from 35 ft to 37 ft. Since 1998, vessels calling at the Port have substantially increased in size.

1.1 Overview

The OIPCB proposes a Pacific Coast Intermodal Port (PCIP) project at Coos Bay, Oregon. The PCIP consists of integrated elements that would link freight arriving by container ship to the Port to Class 1 rail networks in Oregon. The in-water component of the project includes the deepening and widening of the existing FNC for deep-draft container vessels. In support of that work, the Port is conducting economic, engineering, and environmental studies preparatory to improving the Federal navigation project. These investigations are being conducted under the authority granted by Section 204 of the Water Resources Development Act (WRDA), 1986, as modified by Section 1014 of the Water Resources Reform and Development Act (WRRDA), 2014. This action will require approval by the U.S. Army Corps of Engineers under Section 14 of the Rivers and Harbors Appropriation Act of 1899, 33 United States Code 408, to modify the Federal navigation project. The Section 204/408 Report and Environmental Impact Statement (EIS) will propose modifications to the Coos Bay Navigation Channel in Coos County, Oregon, to accommodate larger deep draft vessels and provide local, state, and federal economic benefits. The USACE, Portland District is presumed to be the lead federal agency for the EIS in cooperation with the U.S. Department of Transportation's Federal Rail Administration.

1.2 Study Area Description

Coos Bay is located in Coos County, Oregon, on the southern Oregon coast, about 200 miles (mi) south of the mouth of the Columbia River (MCR) and 445 mi north of San Francisco Bay. It is the navigational approach to Charleston, Empire, North Bend, Glasgow, Coos Bay, and Eastside (Figure 1-1 and Figure 1-2). The bay is formed by the junction of Isthmus Slough, Catching Slough, Coos River, Kentuck & Willanch Sloughs, Haynes Inlet, South Slough, and Winchester Creek, and is located at the foot of the Coast Range. Deep-draft navigation is limited to the lower 15 mi of the estuary.

The surface area of the Coos Bay estuary is about 12,000 acres (ac) (about 19 square mi). Tidelands, located from River Mile (RM) 0 through 15 comprise 20 percent to 30 percent of the estuary area. The inlet to the estuary, referred to as the Entrance Channel, is fully exposed to waves.

The Coos Bay estuary drains directly into the Pacific Ocean. The nearshore zone adjacent to the Entrance Channel is composed of fine- to medium-grained sediments and intermittent rock outcroppings. The coastal shelf within 8 mi of the inlet has a roughly 100:1 (Horizontal:Vertical) slope. Cape Arago, a headland that limits sediment transport and marks the southern boundary of the littoral cell, is located 2.5 mi south of the inlet.

The topography of the lower Coos River area is a combination of rugged mountain terrain, extensive sand dunes adjacent to the ocean, and relatively flat pasture land along the river. The

terrain of the area is quite rugged, because the mountains are relatively young, denoted by the typical narrow, sinuous valleys and steep side slopes. Relief varies from sea level to just under 3,000 ft; however, most of the land lies between 500 ft and 1,500 ft in elevation.

Geotechnical investigations indicate the subsurface conditions in the channel typically vary from relatively clean sand to siltstone and sandstone sedimentary rock. The sedimentary rock is present near the mudline from about RM 2 to RM 6 and at Guano Rock from about RM 0.7 to RM 0.9.

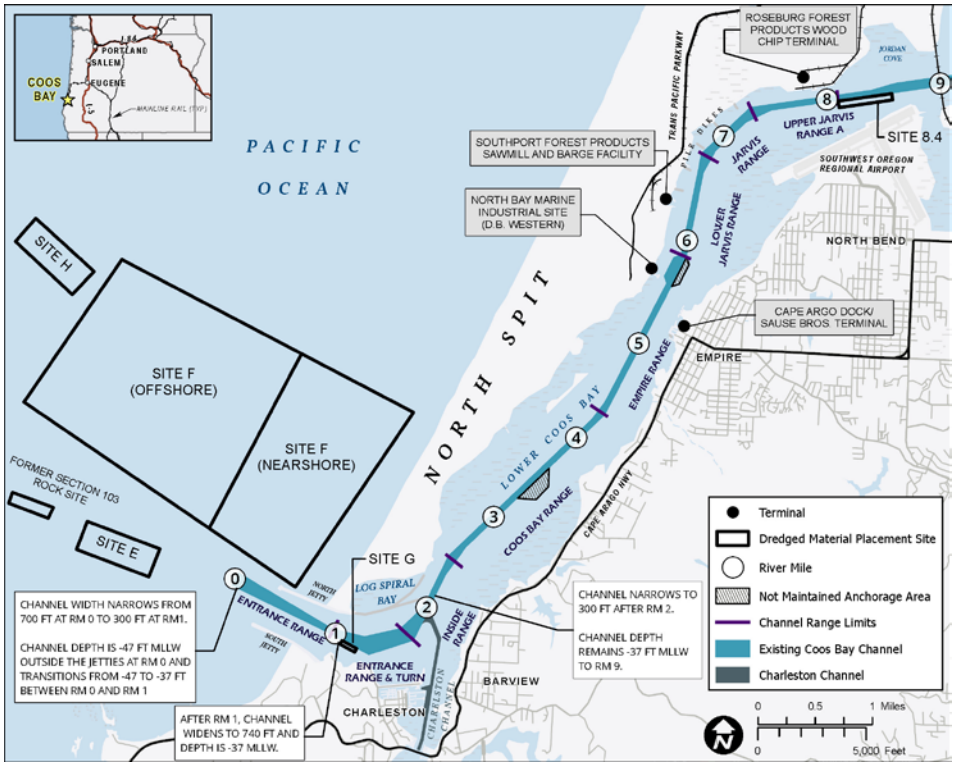

Figure 1-1
Coos Bay Project Vicinity Map, Lower Bay

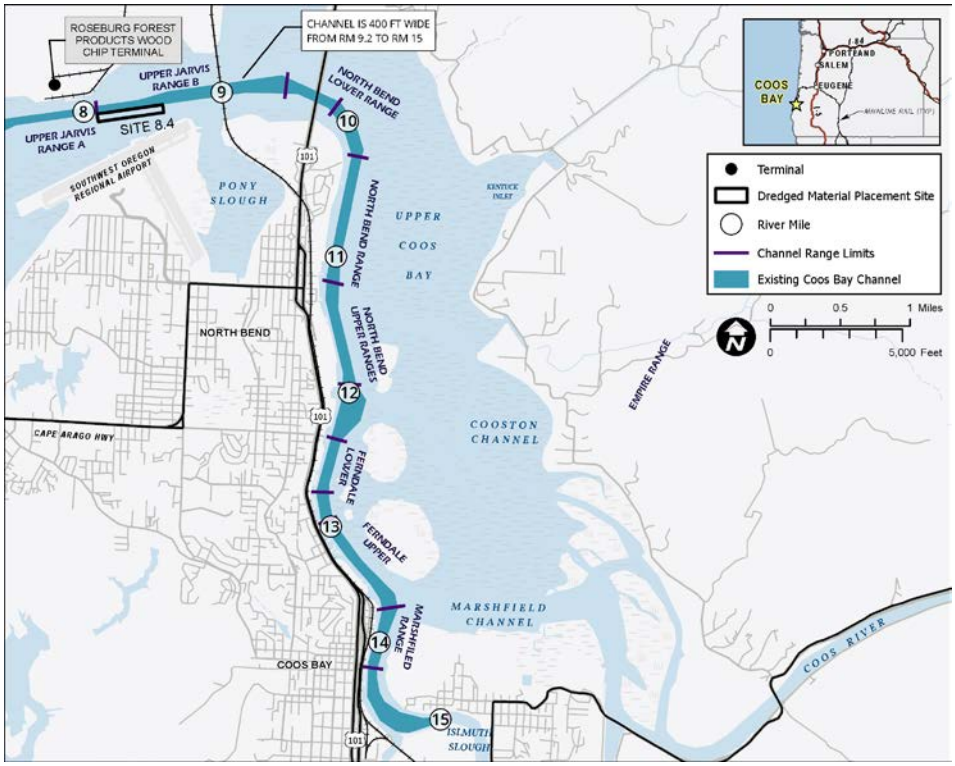

Figure 1-2
Coos Bay Project Vicinity Map, Upper Bay

1.3 Existing Navigation Channel

The Coos Bay Federal Navigation Project was first authorized by the Rivers and Harbors Appropriation Act of March 3, 1899, and has been subsequently modified in 1919, 1937, 1951, 1952, 1979, and 1998. The 1979 project represents the completion of the 1970 authorized which allowed the USACE to deepen and maintain the Entrance Channel at -45 ft Mean Lower Low Water (MLLW) and the inner channel to -35 ft MLLW. The most recent project modification was authorized in the fiscal year (FY) 1996 Energy and Water Development Appropriations Act, Public Law 104-46, which provided for deepening the channel by 2 ft to -47 ft MLLW from the ocean entrance to Guano Rock at RM 1, and to -37 ft MLLW from RM 1 to RM 15. Public Law 104-46 also provided for deepening the turning basin at RM 12 by 2 ft and expanding it by 100 ft, from 800 ft by 1,000 ft to 900 ft by 1,000 ft.

The U.S. Army Corps of Engineers (USACE) Federal Navigation Project consists of the following federally authorized elements:

- North Jetty (9,600 ft long) and South Jetty (3,900 ft long), located on either side of the Entrance Channel, including the two relic structures that extend from the root of the North Jetty, one of which extends into Log-spiral Bay (LSB) and the other of which extends into the estuary.
- An Entrance Channel with an authorized depth of -47 ft MLLW, which decreases from a width of 700 ft at RM 0 to a width of 300 ft at RM 1.
- An inner channel (from RM 1 to RM 15) that has an authorized depth of -37 ft MLLW, a width of 300 ft from RM 1 to RM 9, and a width of 400 ft from RM 9 to RM 15.
- Two (2) turning basins, both of which are 1,000 ft long. The first is located at RM 12, and has a width of 900 ft. The other, located at RM 14, has a width of 730 ft. Both have a depth of -37 ft MLLW, consistent with the channel depth.
- Five (5) pile dikes between RM 6.4 and RM 7.3 in the main channel.
- Continuation of the main channel beyond RM 15 (in the Isthmus Slough) with a width of 150 ft and a depth of -22 ft MLLW.
- A 150-ft-wide Charleston Access Channel that has a depth that varies from –17 to -14 ft MLLW.
- A breakwater and bulkhead at Charleston.
- Charleston Small Boat Basin (10 feet deep) constructed by USACE in 1956 and maintained by the OIPCB.
- Advanced maintenance dredging (AMD) of the channel extends offshore to RM -0.55, where the width of maintenance is 1,060 ft. Authorized AMD is 5 ft of depth in the Entrance Channel (RM 0.55 to RM 1) and 1 ft of depth upstream of RM 1.

The USACE maintains the above elements to provide navigational access to Coos Bay. USACE maintenance of the main navigation channel and jetty features provides ongoing deep-draft navigation access to Coos Bay.

1.4 Description of the 2023 Proposed Alteration (2023 PA)

To accommodate larger deep draft vessels and provide local, state, and federal economic benefits, the Port proposes navigation channel improvements to the Coos Bay Navigation Channel. These proposed channel improvements are hereinafter referred to as the 2023 Proposed Alteration (2023 PA) and they are summarized as follows:

- *Coos Bay Inside Range*: the channel from RM 1.3 to RM 2.8 on the red side of the channel was widened. The range heading of the Coos Bay Inside Range was changed by 1° from 28.0° - 208.0° to 27.0° - 207.0°.

- *Bend Widener at RM 4.0*: a bend widener was included in the 2023 PA to add an additional 50 ft on the green side in the turn from Coos Bay Range to Empire Range.

- *Post Panamax Generation 3 (PPX3) Containership Turning Basin at RM 5.0*: a larger turning basin at the container facility is needed to accommodate the PPX3 containership. Based on the vessel's dimension, the proposed turning basin is 2,000 feet long (parallel to the channel) and 1,600 feet wide. The turning basin's design bottom elevation is -45 ft MLLW, the same as the 2023 PA channel.

- *Capesize Turning Basin at RM 8.0*: a Capesize turning basin was added at RM 8.0 to replace the turning basin that was removed at RM 7.5. Operationally, this turning basin will be used by inbound empty vessels. Therefore, the turning basin's design bottom elevation is -37 ft MLLW. The deeper navigation channel (450-ft wide at -45 ft MLLW) continues through the length of the turning basin.

The above improvements are shown in Table 1-1 and Table 1-2; no dredging is proposed beyond the boundaries in these tables. The project vicinity is represented graphically in Figure 1-3. In this figure, the channel is labeled by RM. Figure 1-3 also shows the location of the adjacent federal infrastructure: the two jetties that run parallel to the channel from RM 0 to RM 1 and the pile dikes located along the north bank of the channel from RM 6.4 to RM 7.5.

Table 1-1
Channel Footprint for Existing Authorized Project and 2023 PA

Range(s) and RM	Existing Conditions	2023 PA
	Offshore Extent	
Offshore Limit including Advanced Maintenance Dredging	RM -0.55[1]	RM -1
Offshore Limit of Navigation Channel	RM 0[1]	RM -0.9
	Channel Width (ft)	
Offshore Inlet Offshore Limit of Navigation Channel to RM 0.3	700 narrowing to 550	1,280 narrowing to 600
Entrance Range RM 0.3 to 1.0	550 narrowing to 300	600
Entrance Range RM 1.0 to 2.0 and Turn	Varies up to 740	Varies up to 1,140
Inside Range RM 2.0 to 2.5	300	500
Coos Bay Range RM 2.5 to 4.3	300	450
Empire Range RM 4.3 to 5.9	300	450
Post Panamax Generation 3 Turning Basin RM 4.7 to 5.6	None	2,000 x 1,600
Lower Jarvis Range RM 5.9 to 6.8	300	450
Jarvis Turn RM 6.8 to 7.3	400	500
Upper Jarvis Range RM 7.3 to 8.2	300	450

Range(s) and RM	Existing Conditions	2023 PA
Capesize Turning Basin RM 7.6 to 8.0	None	2,000 × 1,100

Notes:

1. The authorized FNC starts at RM 0. However, advanced maintenance dredging (AMD) occurs further offshore, typically from the channel entrance to RM -0.55. The channel width at RM -0.55 is approximately 960 ft.

Table 1-2
Channel Depth for Existing Authorized Project and 2023 PA

	Navigation Bottom Elevation (ft, MLLW)		Advance Maintenance Dredging[1] (ft)	
Range(s) and RM	Existing Conditions	2023 PA	Existing Conditions	2023 PA
Offshore Inlet Offshore Limit of Navigation Channel to RM 0.3	-47	-57	5	6
Entrance Range RM 0.3 to 1.0	-47 decreasing to -37[2]	-57 decreasing to -45[3]	Varies 5 to 1[4]	Varies 1 or 6[5]
Entrance Range and Turn RM 1.0 to 2.0	-37	-45	1	1
Inside Range RM 2.0 to 2.5	-37	-45	1	1
Coos Bay Range RM 2.5 to 4.3	-37	-45	1	1
Empire Range RM 4.3 to 5.9	-37	-45	1	1
Post Panamax Generation 3 Turning Basin RM 4.7 to 5.6	None	-45	None	1
Lower Jarvis Range RM 5.9 to 6.8	-37	-45	1	1
Jarvis Turn RM 6.8 to 7.3	-37	-45	1	1

Upper Jarvis Range RM 7.3 to 8.2	-37	-45	1	1
Capesize Turning Basin RM 7.6 to 8.0	None[6]	-37[6]	None	1

Notes:

1. Capital dredging consists of the navigation depth plus AMD plus a rock buffer plus a portion of overdepth.
2. For the existing channel, the navigation depth decreases from a depth of -47 to -37 ft MLLW between RM 0.4 and RM 0.7. The channel is dredged farther offshore to obtain for AMD depth.
3. For the 2023 PA, the navigation depth decreases by 12 ft between RM 0.3 (depth of -57 ft MLLW) and RM 1.0 (depth of -45 ft MLLW).
4. AMD of 5 ft starts at the offshore daylight line, approximately RM -0.6, and continues to RM 0.7.
5. AMD of 6 ft starts at the offshore daylight line. The AMD will be 1 ft in areas where Guano Rock is present (RM 0.7 to RM 1).
6. Under the Existing Conditions, there is no formal turning basin; vessels that visit Roseburg Forest Products turn in existing deeper water at this location. Under the 2023 PA, incoming vessels will enter the channel and turn under ballast load, so it is not necessary to dredge beyond a depth of -37 ft MLLW.

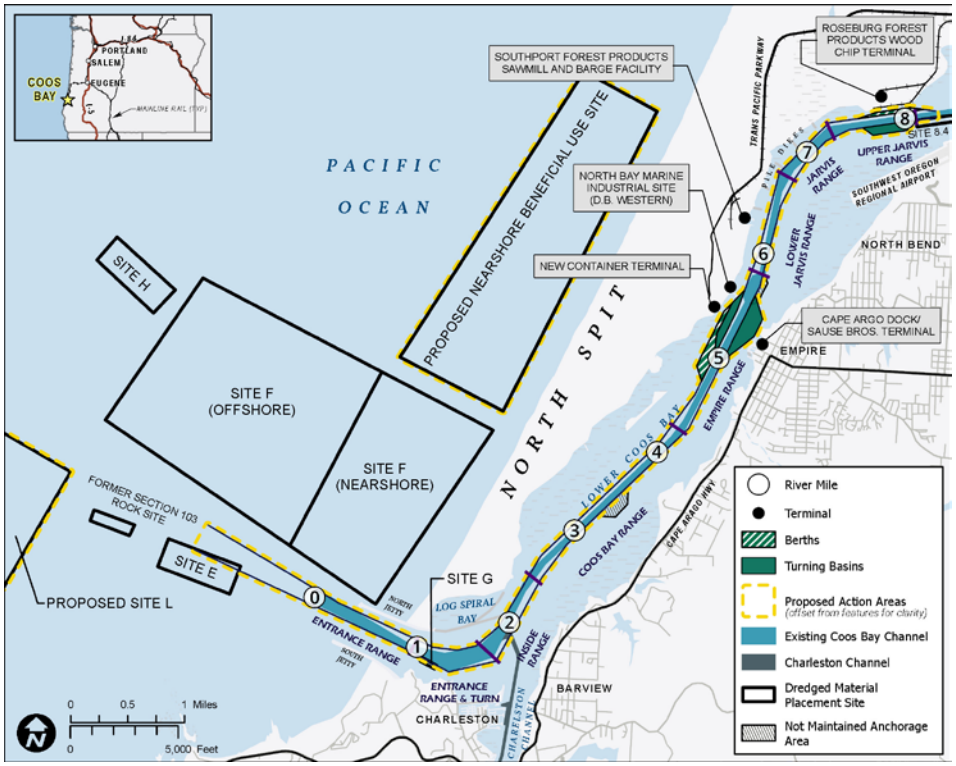

Figure 1-3
Summary of the 2023 Proposed Alteration

1.5 Previous Coos Bay Channel Modification Studies

From 2016 to 2019, the Port evaluated alternatives for modifications to the Coos Bay Federal Navigation Project in support of a previous proposal. In support of that effort, M&N prepared 19 substantial works of engineering and design, economics, modeling, and construction planning. The USACE, Portland District comprehensively reviewed and evaluated the entirety of the Port's proposals as reflected in their Main Report and all appendices (OIPCB 2019).

1.6 Objective

The purposes of this Offshore and Ocean Entrance Dynamics report are to:

- Detail the existing metocean conditions in the offshore area and the Entrance Channel;
- Simulate wave propagation and estimate extreme waves at the North and South Jetties, the Charleston Breakwater, LSB, and in the channel under the Existing Conditions and the 2023 PA;
- Determine the required wave allowance depth in the Entrance Channel to account for wave-induced vessel motions;
- Explain sedimentation patterns in the offshore area and the Entrance Channel of Coos Bay and estimate how proposed improvements may impact these sedimentation patterns;
- Assess changes to erosion along the shorelines adjacent to the inlet, at the base of the jetties, and within the LSB;
- Estimate the Entrance Channel shoaling under the Existing Conditions and the 2023 PA;
- Assess how changes to the extreme wave climate may impact jetty armor stone; and
- Investigate potential changes to tsunami propagation throughout the Coos Bay estuary.

This effort includes the development of conceptual and numerical models of the Coos Bay offshore area and the Entrance Channel to determine the potential effects on hydrodynamics, navigation, shoreline conditions, sediment transport, and tsunami propagation. These models are used to determine physical effects to civil infrastructure and to quantify the effects to annual O&M at Coos Bay. A summary list of applied numerical models with descriptions is presented in Table 1-3.

Analysis of existing or proposed material placement sites is not included in these reports; instead such analysis is contained in Sub-Appendix 10, *Dredged Material Disposal Sites*, and the Dredged Material Management Plan.

Table 1-3
Summary of Numerical Models

Model Name	Model Description and Application
MIKE-21 model suites by the Danish Hydraulic Institute (DHI)	MIKE-21 is a computer program that simulates free surface flows, waves, cohesive and non-cohesive sediment transport, water quality, and ecology in rivers, lakes, estuaries, bays, coastal areas and seas in two dimensions.Wave propagation is computed by MIKE-21 Spectral Wave (SW) module. The Spectral Wave module is used to simulate wave propagation from offshore to the coast. Estuarine hydrodynamics is simulated using MIKE-21 Flexible Mesh Hydrodynamic model (MIKE-21 FM HD), a two-dimensional depth averaged hydrodynamic model. The hydrodynamic model is coupled with sediment transport (ST) model to evaluate sedimentation processes within the estuary. MIKE-21 Classical hydrodynamic model is a two-dimensional hydrodynamic model, which uses finite difference numerical solution over structured grid. The model is capable to accurately resolve flows over land under rapid flooding conditions. The model is used in the evaluation of propagation of a potential tsunami.
BOUSS-2D Boussinesq Wave (BW) modelules by USACE	BOUSS-2D is a comprehensive numerical for simulating the propagation and transformation of waves in coastal regions and harbors. The model is developed by USACE Coastal Inlets Research Program. The model BW module is used to simulate waves in the inlet and wave loading on jetties, and includes a fully integrated wave-current integration module.
Coastal Modeling System (CMS) by USACE	CMS was developed by USACE Coastal Inlets Research Program, was is used to for evaluation of sediment transport in the inlet and offshore areas. The model is the USACE-preferred model for inlet sedimentation. Coastal sedimentation was simulated using CMS, which is the USACE-preferred model for inlet sedimentation. The model consists of two coupled models: CMS-Flow and CMS-Wave. The sediment transport module within CMS-Flow includes formulas for bedload and suspended sediment for sandy material.
Ansys AQWA suite time-domain	Validation of vertical ship motion response in the entrance channel was independently checked using the Ansys AQWA suite time-domain model for hydrodynamic response analysis of floating bodies. ANSYS AQWA software is an engineering analysis suite of tools for the investigation of the effects of wave, wind and current on floating ships and can be executed for six degree-of-freedom analysis in both frequency and time domain.

1.7 Report Organization

This report was prepared to document the data and methodology used, and results of the numerical modeling work for the Coos Bay offshore area and the Entrance Channel. The report is generally organized to first describe the physical characteristics of the site, followed by the numerical modeling used to simulate coastal processes, and finally to apply these studies to specific project elements to develop design recommendations or estimate impacts. Specific sections are as follows:

- Section 2 describes the historical and existing site conditions. The first portion of this section delineates the existing metocean conditions, as well as projected future conditions resulting from sea level rise (SLR). The second portion of this section highlights the history of coastal development of Coos Bay, specifically noting the developments that have influenced waves, currents, or sedimentation.
- Section 3 shows how water level, current, and wave data were used in the design and analysis of the Channel Modification Project. This section also describes the hydrodynamic and wave modeling studies used to perform this assessment.
- Section 4 presents an analysis of vertical motions due to waves in the Entrance Channel.
- Section 5 includes a description of sedimentation patterns at the site. This includes the long-term observed changes (how the site has responded to previous coastal development), a conceptual sediment budget, and numerical sediment transport modeling. The results of this section include estimates of erosion at LSB and estimates of future shoaling rates in the Entrance Channel, and the ability of the USACE to maintain the entrance channel under the 2023 PA.
- Section 6 investigates how the extreme wave heights determined in Section 3 may affect the jetties. This section uses armor stone design guidelines to develop recommendations based on these waves.
- Section 7 presents an analysis of tsunami propagation in Coos Bay under the Existing Conditions and the 2023 PA.

2. HISTORICAL AND EXISTING CONDITIONS

2.1 Project Area

Wave propagation, currents, and sedimentation near the mouth of Coos Bay are subject to existing geology and to ocean forces such as wind, varying water levels, and offshore waves. Local winds generate sea waves. Far-off storms generate swell waves that propagate into the area. The waves mobilize the sandy bottom and currents carry the sediment as sediment transport. These elements are described in detail in the following sections.

2.1.1 Geological Setting

The continental shelf off Coos Bay is approximately 14 mi wide. Regional offshore bathymetric contours generally run northeast to southwest, parallel to the coastline (USACE and USEPA 1986). A previous study of the continental shelf sediments found that the movement of beach sand during lower sea levels was to the north, with a substantial fraction of the material on the beaches in the vicinity of Coos Bay sourced from the Klamath Mountains to the south rather than from the Oregon Coast Range (Komar 1992).

Within the Entrance Channel, the median grain size ranges from 0.27 to 0.36 mm (based on surveys from USACE 2005 and SHN 2007). Beach sand along this portion of the Pacific coastline generally has a median grain size of 0.25 mm (M&N 2008). In the offshore area, sediment grain size data is limited. The most recent and complete data was collected in 1979-1980, which indicates the median grain size to range from 0.15-0.25 mm, increasing up to 0.4 mm near the offshore disposal sites (Hancock et al. 1981). Grain size in this area is shown in Figure 2-1. The concentration of larger grain in the vicinity of the Ocean Dredged Material Disposal Sites (ODMDSs) (E, F, and H – dashed lines) is likely due to placement practices. Sand from the channel is placed in these areas, with the larger grain size staying relatively stationary, thereby increasing the median grain size. Elsewhere, the median grain size is generally less than 0.2 mm, becoming finer further offshore.

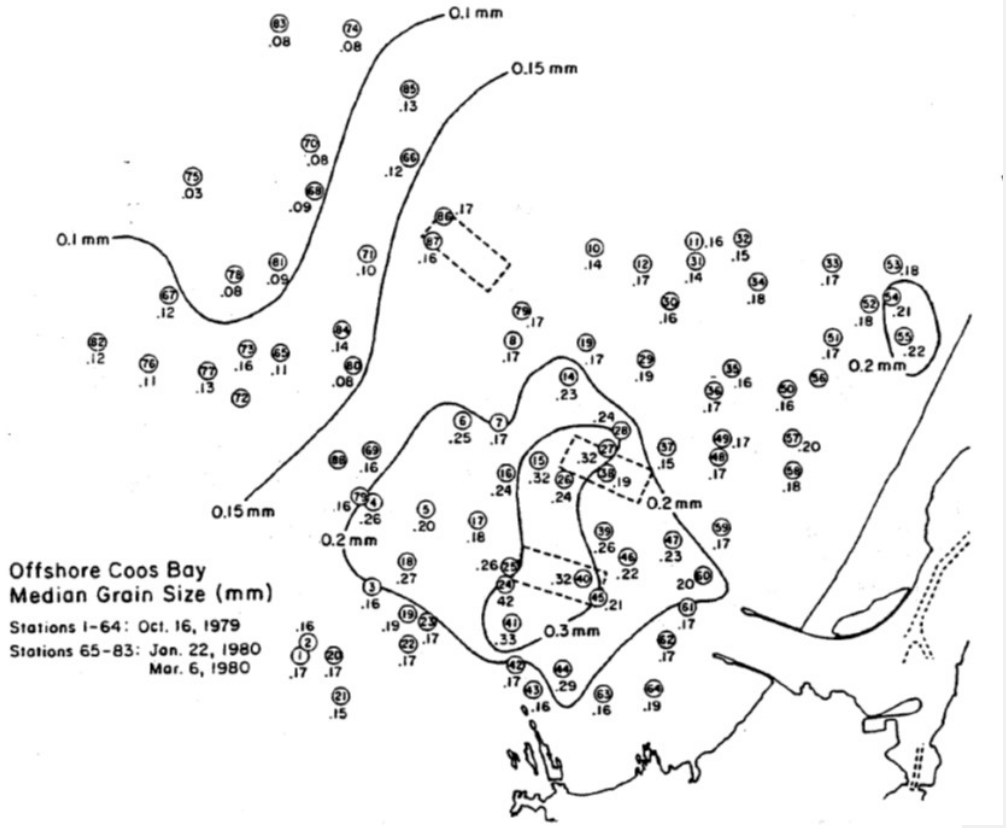

Figure 2-1
Offshore Area Median Grain Size Distribution (Hancock et al. 1981)

2.1.2 Winds

The National Data Buoy Center (NDBC) maintained a C-MAN weather station (Cape Arago) on the Pacific coast approximately two miles southwest of the Coos Bay jetties until December 2012 (NDBC 2015). An anemometer is also maintained at the Southwest Oregon Regional Airport (SWORA) in North Bend. Figure 2-2 shows the location of these stations.

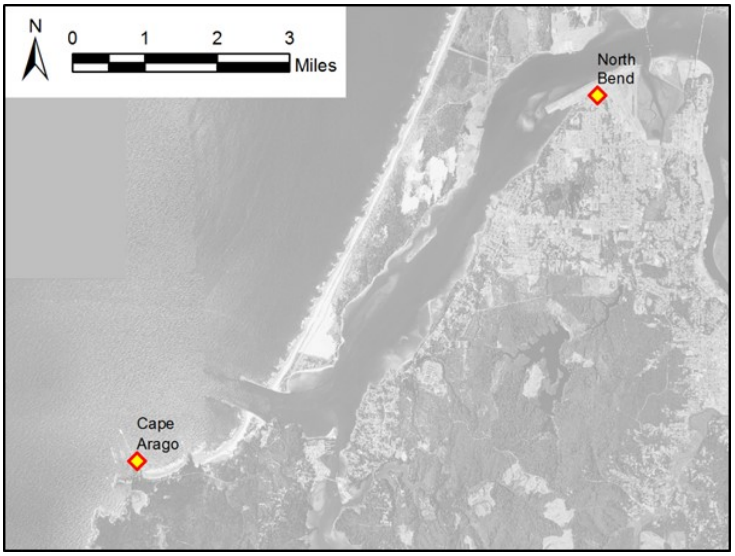

Figure 2-2
Location of Cape Arago C-MAN Station and North Bend Anemometer

Winds throughout the Coos Bay area have strong north-south directionality, as indicated by the wind roses in Figure 2-3. At Cape Arago, the strongest winds are from the south, while at North Bend they are from the north. Onshore-offshore sea breezes are a relatively minor contributor to the winds.

Typically, winds are from the north in the summer and from the south in the winter, as indicated by the seasonal wind roses in Figure 2-4 and Figure 2-5. Winds along the southern Oregon coast are generally dominated by large-scale pressure patterns over the North Pacific and onshore. During winter, the Gulf of Alaska Low produces frequent cyclonic storms that reach the coastline from the west and move towards the north. Winds exceeding 60 knots can occur along the southern Oregon coast several times each winter. Summer storms are rarer and less intense. The strong southerly winds have been instrumental in creating the Coos Bay dune sheet to the north of Coos Bay.

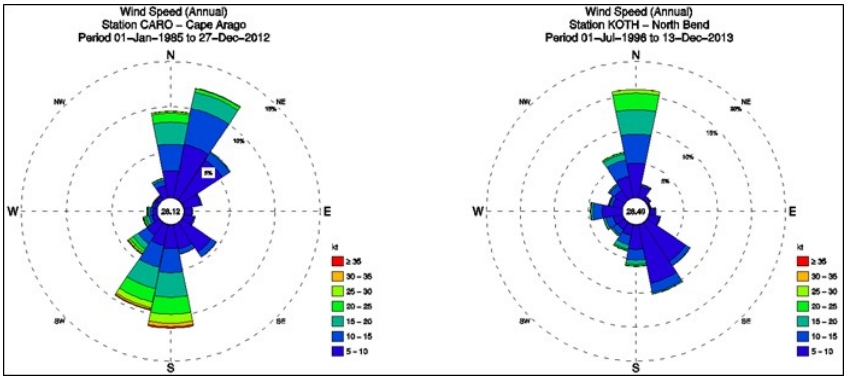

Figure 2-3
Wind Roses at Cape Arago (Left Panel) and North Bend (Right Panel), Full Year

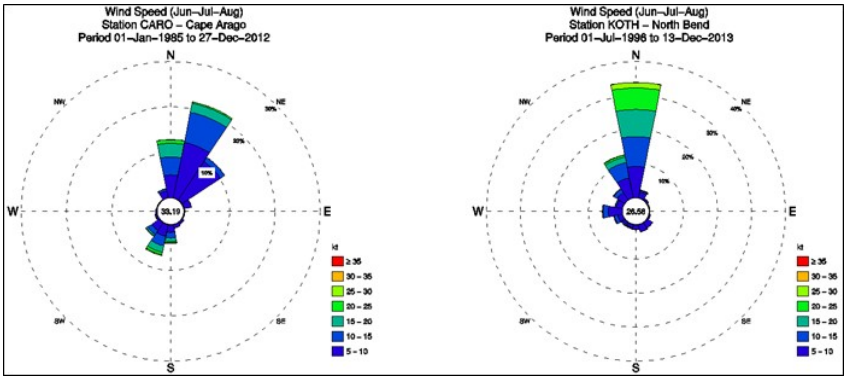

Figure 2-4
Seasonal Wind Roses at Cape Arago (Left Panel) and North Bend (Right Panel),Summer (June through August)

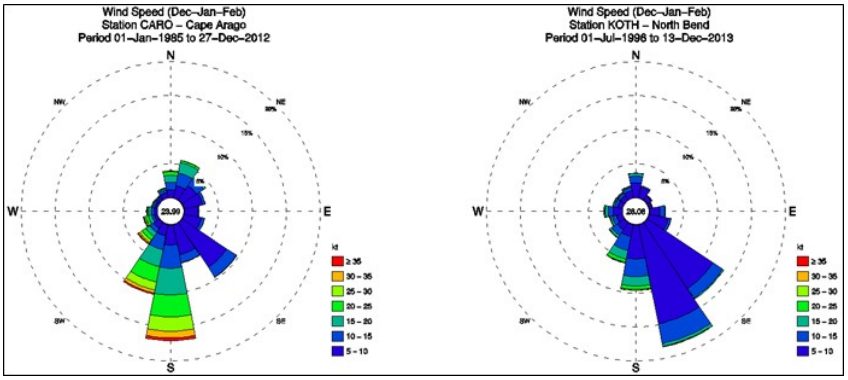

Figure 2-5
Seasonal Wind Roses at Cape Arago (Left Panel) and North Bend (Right Panel), Winter (December through January)

Sustained wind speeds are slightly greater at Cape Arago than at North Bend, as shown in Figure 2-6. However, winds in the jettied entrance may be lower than those measured at Cape Arago. According to the Coos Bay Pilots' Association, the bluffs south of the entrance both shelter the entrance against south winds and slow incident winds from the north.

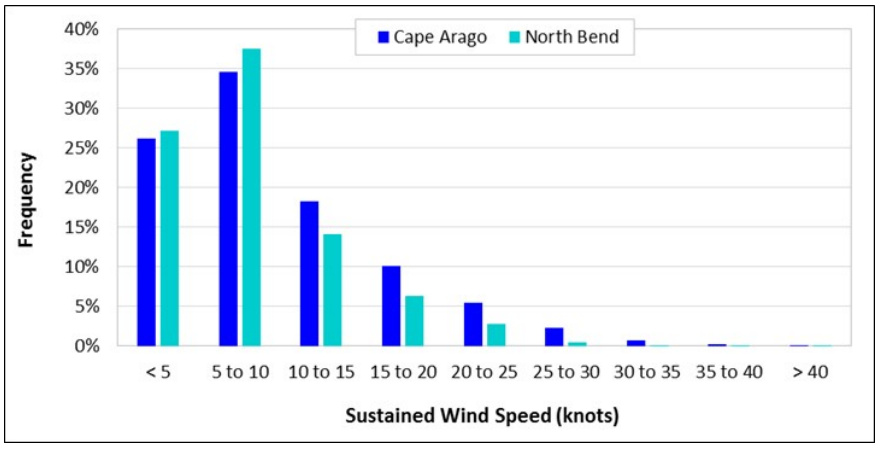

Figure 2-6
Histograms of Wind Speeds at Cape Arago and North Bend

2.1.3 Recorded Water Levels

Total water level consists of astronomical and meteorological tide components. Astronomical tides along the Oregon coast are semi-diurnal mixed; this means that there are, on average, two high and two low water stages of differing elevations each day. Meteorological tides refer to changes in expected astronomical tides caused by local meteorological conditions. It is commonly called

storm surge, as the water surface is elevated due to the passage of a storm. Storm surge is more likely to occur during the winter months; therefore, its effect also causes an apparent seasonal variation in water levels.

The National Oceanic and Oceanographic Administration (NOAA)/National Ocean Service (NOS) maintains a tide gauge, number 9432780, in Charleston near the mouth of Coos Bay. This gauge was selected for use in the present analysis because it is located within the Entrance Channel at Coos Bay, and because it has a long period of record (46 years). Measured tides are available from April 1, 1970 to December 31, 2016 (NOAA 2017). The location of the gauge is shown in Figure 2-7.

Figure 2-7
Location of Tide Gauge at Charleston, Oregon

2.1.3.1 Tides

Water levels near the mouth of Coos Bay are primarily tide-dependent: river flooding has relatively little effect. Tidal datums are listed in Table 2-1; as this table shows, the tidal range can be large in Coos Bay, as Mean Higher High Water (MHHW) is 7.62 ft above MLLW. All elevations in this report are relative to MLLW.

Table 2-1
Tidal Datums for Station 9432780, Charleston, Oregon: 1983–2001 Epoch

Datum	Elevation (ft, MLLW)
Highest Observed Water Level (1/26/1983)	11.18
Mean Higher High Water (MHHW)	7.62
Mean High Water (MHW)	6.96
Mean Tide Level (MTL)	4.11
Mean Sea Level (MSL)	4.08
Mean Low Water (MLW)	1.27
North American Vertical Datum of 1988 (NAVD88)*	0.50*
Mean Lower Low Water (MLLW)	0.00
Lowest Observed Water Level (6/1/1973)	-3.08

Note:

**NAVD88 is a geodetic datum rather than a tidal datum.*

2.1.3.2 Storm Surge

Extreme analysis on storm surge at Charleston (NOAA/NOS tide gauge number 9432780) was calculated using the Peak-Over-Threshold (POT) Method (Goda 2010), based on the difference between the measured and the predicted water levels for the entire period of record. The highest two storm surges were both observed in strong El Niño years: 3.13 ft on 1/26/1983 and 3.06 feet on 12/16/2002. Table 2-2 and Figure 2-8 shows the extreme storm surge based on the Weibull distribution. The two high El Niño storm surges correspond to approximately a 50-year return period; the 100-year return period storm surge is approximately 3.3 feet.

Table 2-2
Storm Surge Values in Coos Bay

Return Period (years)	Storm Surge (ft)
1	1.9
2	2.1
5	2.4
10	2.6
25	2.9
50	3.1
100	3.3

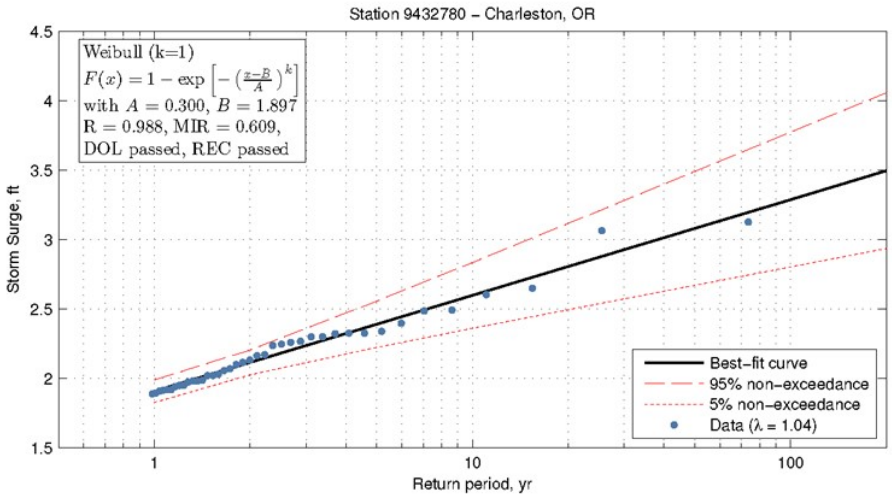

Figure 2-8
Best Fit Curve for Storm Surge Return Periods

2.1.3.3 Seasonal Variation

Data from NOAA tide gauge number 9432780 was also used to estimate how water levels typically change over the course of the year. The entire data record was segmented by month, and the average water level in each month calculated. The results can be seen in Figure 2-9. As this figure shows, the most significant water level variation occurs in December and January, potentially due

to storm surge during these times. Still, the average water level is less than 0.03 ft above MSL (for comparison, the tidal range is 7.62 ft, or 250x this variation); therefore, seasonal variation is insignificant compared to normal tidal fluctuation.

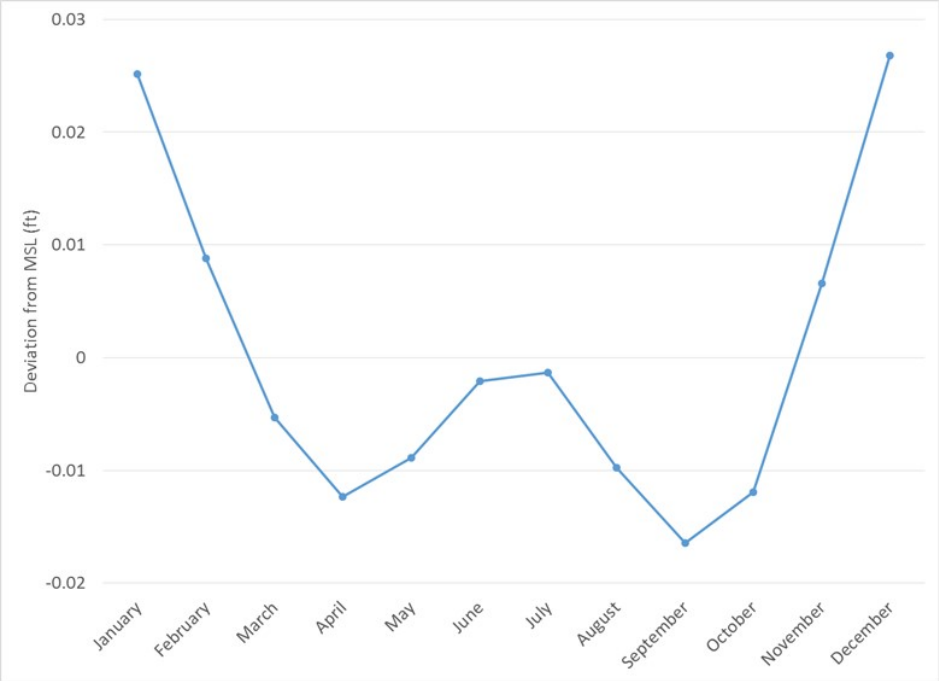

Figure 2-9
Seasonal Water Level Variations at Charleston Tidal Station

2.1.3.4 Extreme Analysis

The Highest Observed Water Level (HOWL) of 11.18 ft occurred on January 26, 1983, during a high tide, approximately 3 hours before the storm surge of record (3.13 ft). The extreme water levels observed generally correspond to a combination of high storm surge superimposed onto a high tide.

Extreme analysis on total water levels at Charleston (NOAA tide gauge number 9432780) was calculated using the POT Method (Goda 2010) for the entire period of record (April 1, 1978 to December 31, 2016). Table 2-3 and Figure 2-10 shows the extreme water levels based on the Weibull distribution.

Table 2-3
Extreme Water Levels in Coos Bay

Return Period (years)	High Water Levels (ft, MLLW)
1	10.10
2	10.42
5	10.71
10	10.90
25	11.12
50	11.28
100	11.43

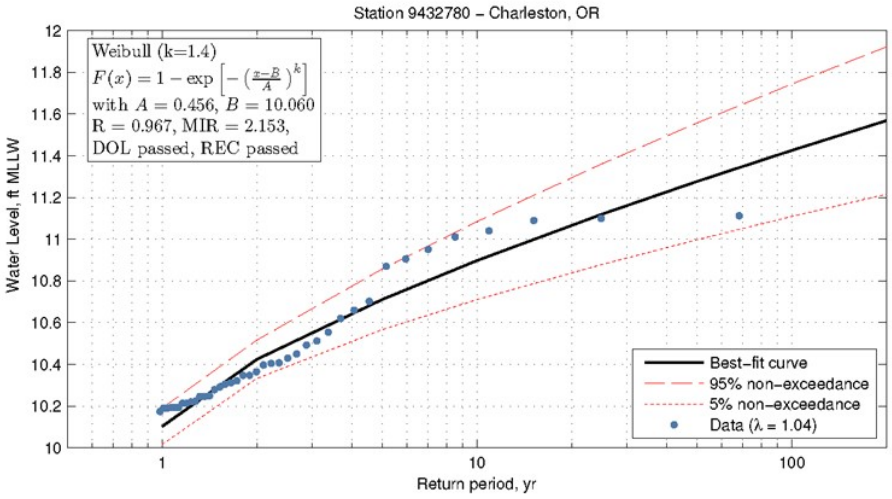

Figure 2-10
Best Fit Curve for Extreme Water Levels Return Periods

The following observations can be made for the three most extreme water levels:

- 100-year return period: 11.43 ft MLLW. This is 0.15 ft higher than the 50-year water level, consistent with the 100-year storm surge being approximately 0.2 ft higher than the 50-year storm surge.

- 50-year return period: 11.28 ft MLLW: This is slightly higher than the HOWL, which occurred over 39 years of data.
- 25-year return period: 11.12 ft MLLW: This is slightly lower than the HOWL.

2.1.3.5 Sea Level Change

Numerous peer-reviewed publications about climate change and sea level change (SLC) have been published in recent years, and SLC projections vary from study to study. Significant uncertainties in future emissions of greenhouse gases, the effects upon global temperatures, and the effects upon ice sheets and other drivers of the sea level compound to give a wide variation in projections of global and regional SLC.

This study uses the guidelines established by the USACE as provided in ER 1100-2-8162. Table 2-4 provides projections of relative SLC at Charleston, OR. The base year of 1992 is selected for the USACE guidance because it is the midpoint of the 1983–2001 tidal epoch, which is used to define MLLW and other tidal datums in this report. According to the USACE guidance, the "low" projection uses an MSL trend of 1.29 ±1.15 mm/year (0.42 ft/century) based on monthly extremes data from 1970 to 2006 (NOAA 2015). The "intermediate" and "high" rates of local SLC are estimated using the modified National Research Council (NRC) curves that account for changes to the rate of SLC, as described by NOAA (2015). The USACE SLC tool (http://www.corpsclimate.us/ccaceslcurves.cfm) calculates the projected SLC and their high, intermediate, and low projection curves are shown in Figure 2-11.

Table 2-4
Projections of Relative Sea Level Rise (ft) for Charleston, OR

Year	Low (Historic Rate)	Medium (per USACE 2013)	High (per USACE 2013)
1992 (base year)	0.0	0.0	0.0
2010	0.1	0.1	0.2
2040	0.2	0.4	1.1
2080	0.4	1.1	3.2
2100	0.5	1.5	4.8

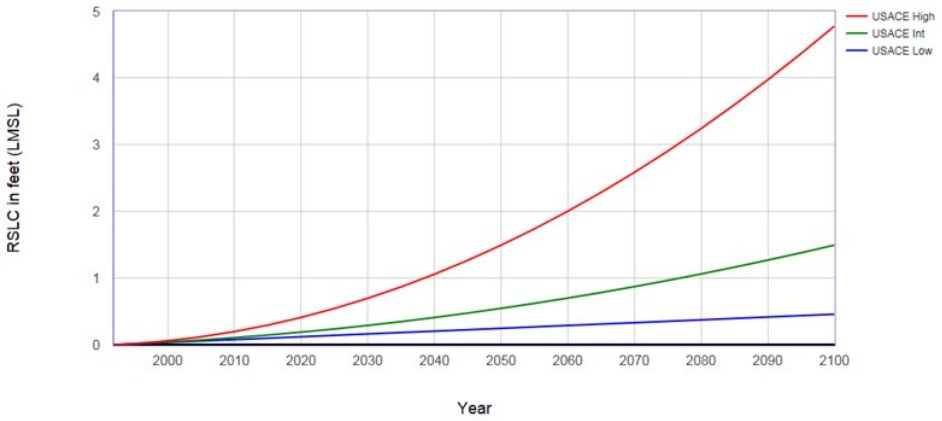

Figure 2-11
Relative Sea Level Change (RSLC) Scenarios for Charleston, Coos Bay (USACE SLC Curve Calculator, 2017.55)

2.1.4 Recorded Currents

Mid-water currents (those measured at one-third the depth) and near-bottom currents are generally between 0.2 to 0.4 knots in the vicinity of ODMDS F and H. Mid-depth summer median currents near ODMDS F are slightly stronger (0.4 to 0.6 knots), while median winter and spring currents near ODMDS F and H may be between 0.6 to 1.2 knots.

Closer to the inlet, currents are propelled by tidal action, freshwater flows, waves, and winds. Current modeling was performed by USACE (2012b) to simulate these effects. It was found that tidal action is the primary influence on currents at the entrance. Tidal currents range from 2 to 3 knots, with up to 4 knots possible; ebb currents tend to be stronger than flood currents.

2.1.5 Recorded Waves

This section presents an analysis of deep water metocean data offshore of Coos Bay, Oregon. Wave data through 2016 was gathered and reanalyzed to derive deep water wave statistics.

2.1.5.1 Offshore NDBC Buoy Data

The NDBC buoys are 10-ft discus buoys (Figure 2-12) that measure several metocean parameters, including wind and waves. The anemometer is located at a 16-ft elevation. The measurements are reported hourly and include standard observations and spectral density parameters. The directional spectra may not be available for all buoys and installation periods.

Figure 2-12
3-meter Discus NDBC Buoy

The standard observations include sustained wind speed and direction (8-minute average), gust speed (5-second average), significant wave height, peak wave period, mean wave period, peak wave direction (if directional data is available), pressure, and air and water temperatures. For the analysis, wind speeds were converted to a standard 32.8-ft elevation using ISO 19901-1:2005(E) formulation. The data were processed to develop wind roses, histograms, and exceedance curves.

The spectral density observations include energy density for each frequency bin (usually between 0.03 to 0.4 Hz).

The directional spectral information is provided in the form of the Fourier coefficients and the mean and principal wave directions. They can be used to reconstruct the full directional energy spectra.

Table 2-5 presents a list of NDBC buoys in the vicinity of Coos Bay. Figure 2-13 shows their location. Buoy 46002 is the farthest from Coos Bay, located approximately 275 nautical miles (NM) offshore. The buoy is exposed to open water winds and waves from all directions. Other buoys are located along the Oregon coast approximately 20 NM offshore, where they are exposed to open water waves from the western sectors. Winds measured at these three buoys are affected by the proximity to the coast.

Availability of the standard data ranges from 14 years (Buoy 46015) to 41 years (Buoy 46002). The spectral density data is usually available since 1996 (over 20 years). However, most of available measurements are not directional. The directional spectral data becomes available later, between 1997 (Buoy 46029) to 2015 (Buoy 46002). While all buoys are currently in service, the temporal coverage of the data herein discussed corresponds to the time when the data was downloaded and processed.

Table 2-5
Buoys Operated by NOAA NDBC

ID	Buoy	Location	Depth (m)	Standard	Spectral Density	Spectral Direction
46002	West Oregon – 275 NM West of Coos Bay, OR	42°36'49" N 130°29'24" W	3368.1	7/1975–8/2016	1/1996–7/2016	9/2015–7/2016
46015	Port Orford – 15 NM West of Port Orford, OR	42°45'52" N 124°49'57" W	420.3	7/2002–8/2016	7/2002–7/2016	5/2007–7/2016
46029	Columbia River Bar – 20 NM West of Columbia River Mouth	46°9'32" N 124°30'52" W	144.8	3/1984–8/2016	1/1996–7/2016	11/1997–7/2016
46050	Stonewall Bank – 20 NM West of Newport, OR	44°39'22" N 124°31'33" W	137.2	11/1991–8/2016	1/1996–7/2016	3/2008–7/2016

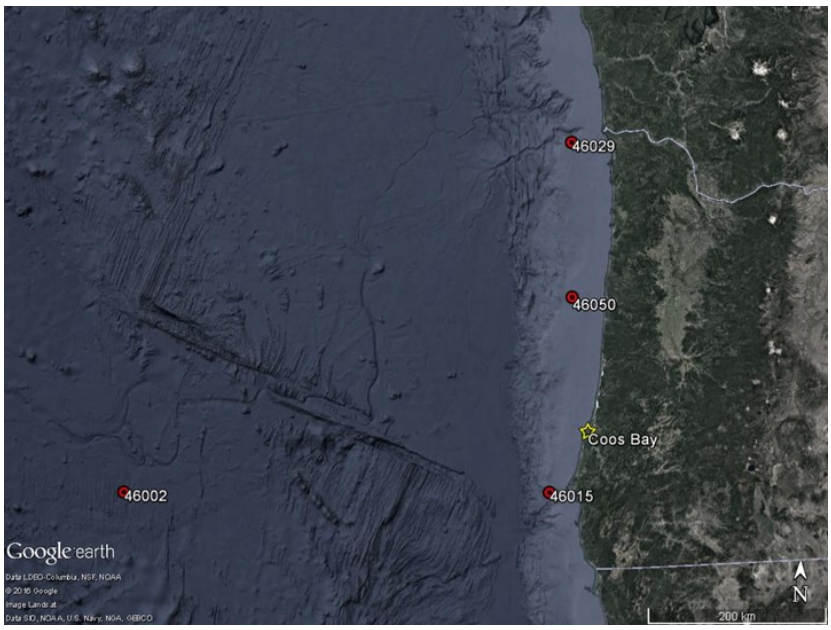

Figure 2-13
Buoys Operated by NOAA NDBC

A comparison of the wave field measured at the aforementioned NDBC buoys was carried out with the attempt to generalize the wave field characteristics in the offshore area.

Table 2-6 presents a comparison of statistics of the significant wave height and peak wave period. The statistics show that the wave fields measured at Buoys 46015, 46029, and 46050 (15-20 NM from the coast) are, in general, very similar. The wave field measured at Buoy 46002 (275 NM from the coast) is slightly more energetic, as shown by the wave height statistics, but does not deviate significantly from the pattern observed at the other three buoys.

Figure 2-14 through Figure 2-17 illustrate the graphical representation of the comparison of wave statistics for Buoys 46002 vs. 46015 and Buoys 46050 vs. 46015. The figures show that differences in the wave fields are evident only in the highest 1 percent of the waves.

Table 2-6
Offshore Wave Height and Period Statistics

NDBC Buoy	25%	50%	75%	90%	95%	99%	Max†	Mean	Mode
Significant Wave Height (m)									
46002	1.7	2.4	3.3	4.4	5.2	6.9	15.1	2.7	1.4
46015	1.6	2.2	3.0	4.0	4.7	6.3	11.9	2.4	1.7
46029	1.4	2.0	2.9	4.0	4.8	6.4	13.8	2.3	1.4
46050	1.5	2.1	2.9	4.0	4.8	6.3	14.1	2.4	1.4
Peak Wave Period (s)									
46002	8.3	11.1	12.9	14.8	16.7	20.0	25.0	11.0	11.1
46015	8.3	10.8	12.9	16.0	16.7	19.1	25.0	11.1	10.0
46029	8.3	10.8	12.5	14.3	16.7	19.1	25.0	10.8	11.0
46050	8.3	10.8	12.5	14.8	16.7	19.1	25.0	10.8	11.0

† Maximum period is limited by spectral resolution

The selected NDBC buoys have 60 to 70 percent of all waves approaching from the west to NW quadrants with the prevailing directions from WNW. Waves from the southwest to west and NW to north sectors account for the rest of the waves. Due to its open exposure, Buoy 46002 captures a small percentage of waves from eastern sectors. Figure 2-18 presents the annual directional distribution of waves for Buoy 46015 as an example of the directional distribution of waves in the area closer to the shore.

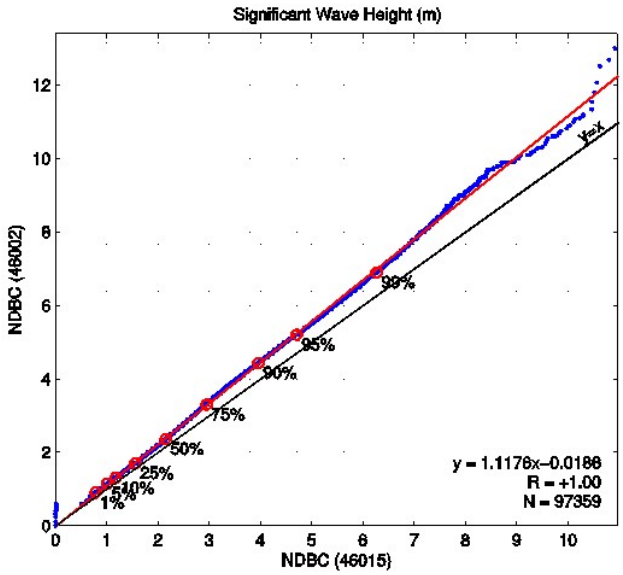

Figure 2-14
Comparison of Significant Wave Height Statistics for Buoys 46002 and 46015

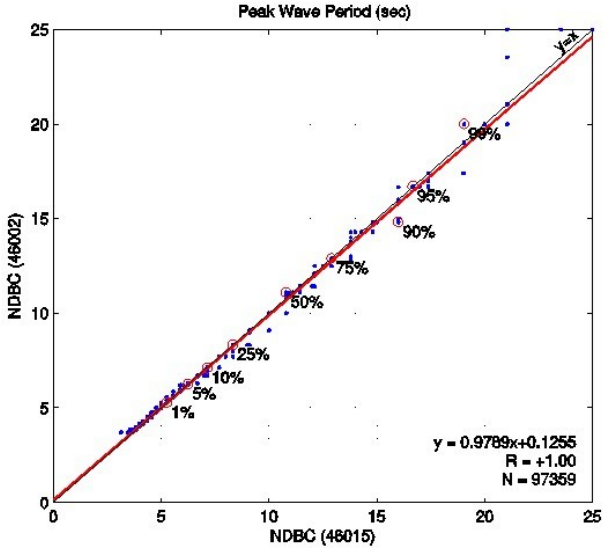

Figure 2-15
Comparison of Peak Wave Period Statistics for Buoys 46002 and 46015

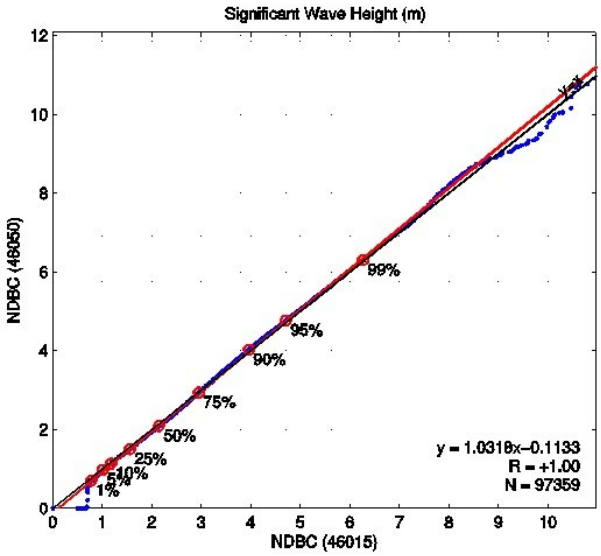

Figure 2-16
Comparison of Significant Wave Height Statistics for Buoys 46050 and 46015

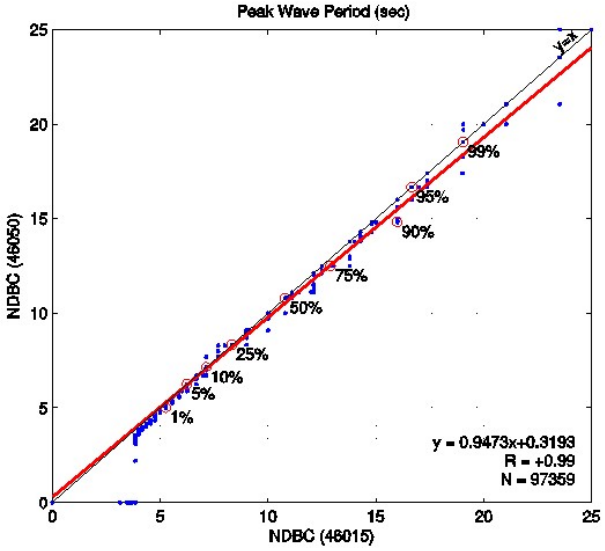

Figure 2-17
Comparison of Peak Wave Period Statistics for Buoys 46050 and 46015

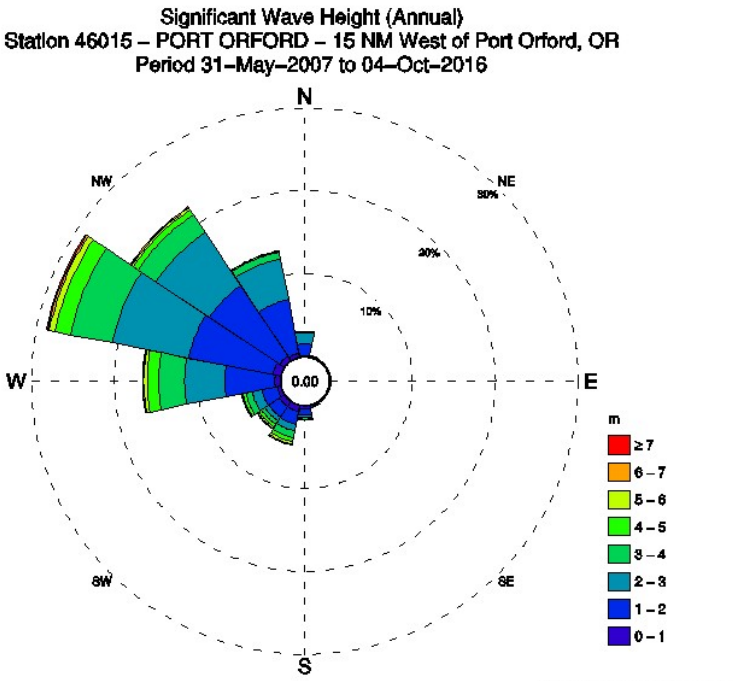

Percentage of Occurrence

Significant Wave Height, m	N	NNE	NE	ENE	E	ESE	SE	SSE	S	SSW	SW	WSW	W	WNW	NW	NNW	Total
Total	3.04	0.16			0.10	0.10		0.27	1.70	4.68	3.99	4.80	16.56	28.62	22.34	13.07	100.00
7														0.16			0.42
6													0.10	0.22	0.12		0.69
5										0.32	0.20	0.11	0.44	0.74	0.28		2.18
4										0.49	0.40	0.36	1.37	1.69	0.69	0.11	5.47
3	0.18								0.18	0.62	0.49	0.79	3.13	5.11	2.60	0.83	14.16
2	1.35								0.31	0.62	0.57	1.16	4.64	9.41	7.75	5.01	31.31
1	1.41							0.16	0.73	1.58	1.54	1.88	8.04	10.34	10.21	8.60	40.64
0									0.37	0.73	0.68	0.41	0.64	0.96	0.66	0.45	5.13
	N	NNE	NE	ENE	E	ESE	SE	SSE	S	SSW	SW	WSW	W	WNW	NW	NNW	Total

Figure 2-18
Annual Directional Distribution of Significant Wave Height at Buoy 46015

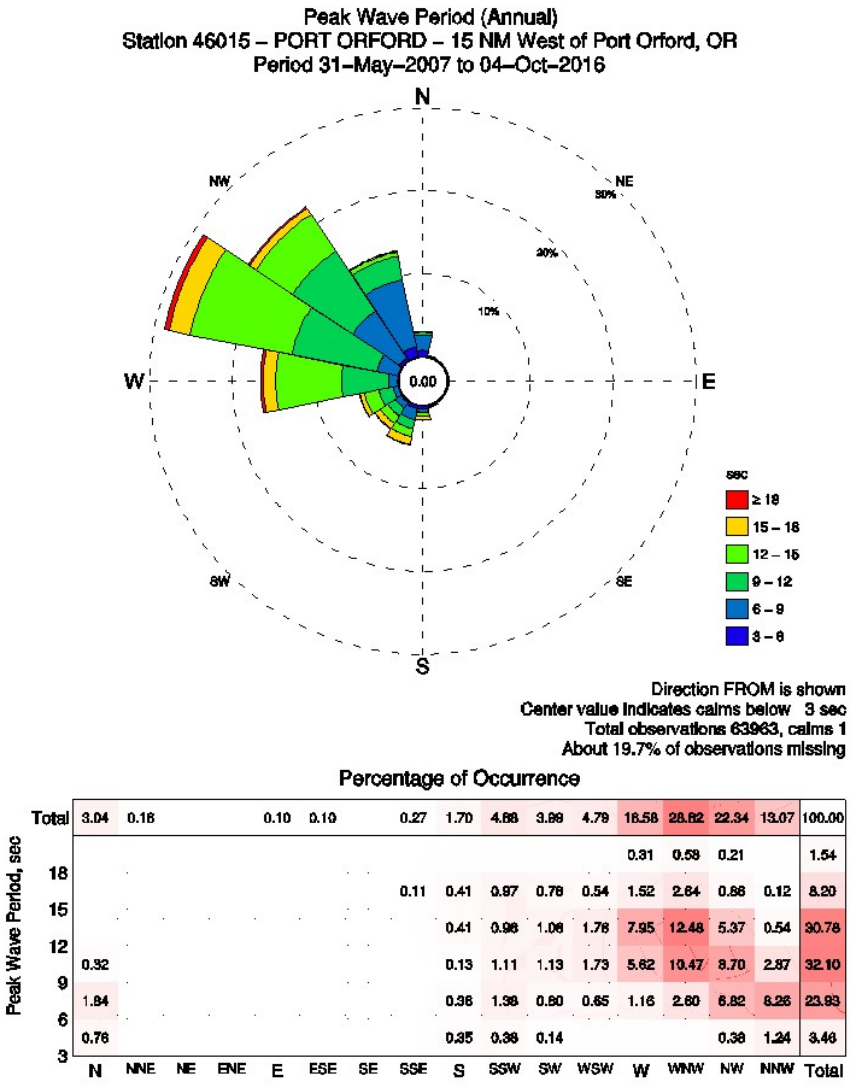

Percentage of Occurrence

Peak Wave Period, sec	N	NNE	NE	ENE	E	ESE	SE	SSE	S	SSW	SW	WSW	W	WNW	NW	NNW	Total
Total	3.04	0.16			0.10	0.10		0.27	1.70	4.66	3.99	4.79	16.58	28.62	22.34	13.07	100.00
18													0.31	0.58	0.21		1.54
15								0.11	0.41	0.97	0.76	0.54	1.52	2.64	0.86	0.12	8.20
12									0.41	0.96	1.06	1.76	7.95	12.48	5.37	0.54	30.78
9	0.32								0.13	1.11	1.13	1.73	5.62	10.47	8.70	2.87	32.10
6	1.84								0.36	1.38	0.80	0.65	1.16	2.60	6.82	8.26	23.93
3	0.76								0.35	0.38	0.14				0.38	1.24	3.46
	N	NNE	NE	ENE	E	ESE	SE	SSE	S	SSW	SW	WSW	W	WNW	NW	NNW	Total

Figure 2-19
Annual Directional Distribution of Peak Period at Buoy 46015

Swells are long-period waves that are not generated or supported by the local winds. Peak wave periods associated with swell are typically greater than 8 seconds. The range of wave periods observed in Table 2-6 indicates that long-period waves or swell occur with a high frequency. The

statistics show that peak wave periods greater than 10 seconds occur about 50 percent of the time. The active presence of swell is characteristic of the open Pacific Ocean coasts.

The selected buoys show that swell approaches from the west to NW quadrant, with accentuation on the WNW sector (Figure 2-19).

Figure 2-20 shows a joint histogram of significant wave height and peak wave period for Buoy 46015 as representative of all other buoys. The histogram shows that swell in this region can be very energetic, reaching wave heights of up to 6 m (20 ft).

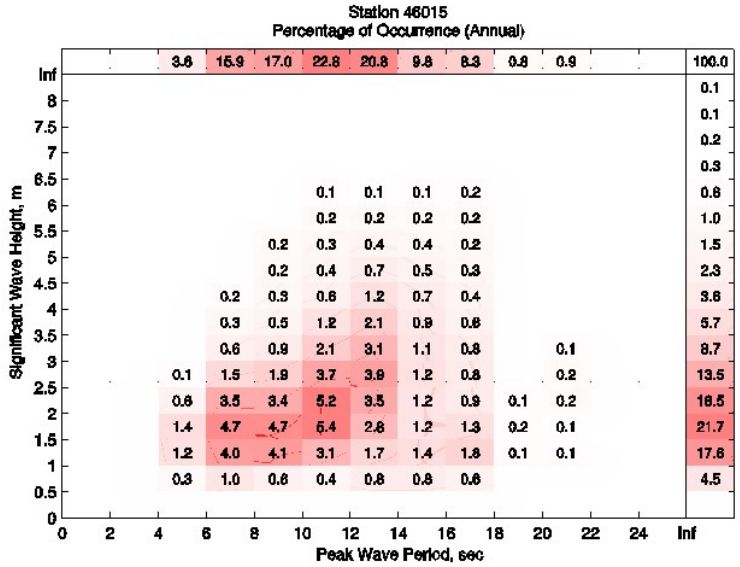

Figure 2-20
Joint Histogram of Significant Wave Height and Peak Wave Period at Buoy 46015

Based on analysis of wave measurements from the four NDBC buoys, it can be concluded that the offshore wave field in the offshore area from Coos Bay is fairly similar in terms of wave heights, peak periods, directionality, and occurrence of swell.

2.1.5.2 Offshore CDIP Buoy Data

The Coastal Data Information Program (CDIP) of the Scripps Institution of Oceanography is dedicated to measuring coastal environment data, including measurements of waves along the coast of the U.S. Measurements from several buoys (Figure 2-21) located in the vicinity of Coos Bay are available from the CDIP. A list of active and historical buoys is presented in Table 2-7 and their locations are shown in Figure 2-22.

Spectral data are available at 30-minute resolution and 3-degree directional resolution. The full directional two-dimensional (2-D) spectra were constructed from the measured data using the Extended Maximum Likelihood Method (Earle et al. 1999).

Wind measurements are not available from the CDIP buoys.

Figure 2-21
Datawell Waverider MKIII CDIP Buoy

Table 2-7
Buoys Operated by Scripps Institution of Oceanography

Buoy ID	Buoy	Location	Depth (m)	Spectral
139p1 (NDBC 46229)	Umpqua Offshore, OR	43°45'58" N 124°33'3" W	182.9	7/2006–8/2016
126p1	Coos Bay, OR (discontinued)	43°23'49" N 124°39'0" W	204.8	3/2005–2/2006
135p1	Coos Bay North, OR (discontinued)	43°37'6" N 124°33'30" W	200	4/2006–5/2006

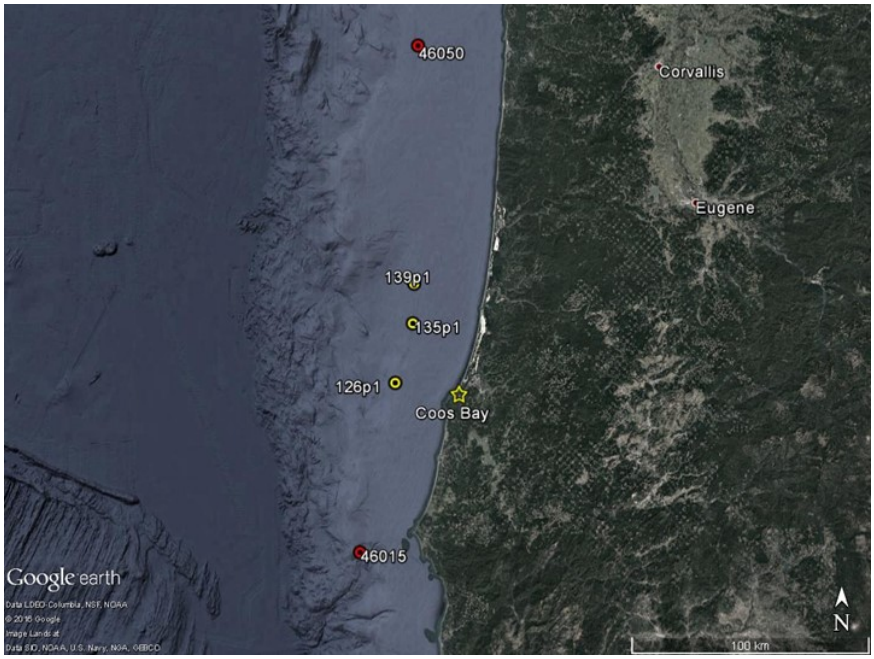

Figure 2-22
CDIP Buoys Operated by the Scripps Institution of Oceanography

Present analysis will be mainly focused on Buoy 139p1 due to short duration of available data at other buoys.

2.1.5.3 Buoy 139p1 Umpqua Offshore

Data from Buoy 139p1 is available from July 2006 until August 2016, with about 1.8 percent of observations missing. Wave roses for the significant wave height are shown in Figure 2-23 (annual) and Figure 2-24 (seasonal). Wave height statistics (percentiles, mode, and maximum values) are gathered in Table 2-8. Figure 2-25 shows monthly variability in significant wave height.

Figure 2-23 shows that the wave directions are prevailing from WNW (modal direction is 286°) followed by west and NW. Wave heights from the dominant directional sectors occur most frequently within the 1-4 m (3-13 ft) range. Figure 2-24 shows that summer waves are predominantly from WNW to north-west-north (NWN) with some waves from the southwest. Wave heights are significantly lower during the summer compared to other seasons. The west to WNW waves are long period swell waves with periods on the order of 16 to 20 seconds generated by distant storms, while the southwest waves tend to be shorter period waves (often with periods under 12 seconds) generated by local storms. The most energetic waves occur during winter months with the prevailing direction from west and WNW. The maximum recorded wave height is 11.3 m (37.1 ft) from 270° (directly west) on December 10, 2015.

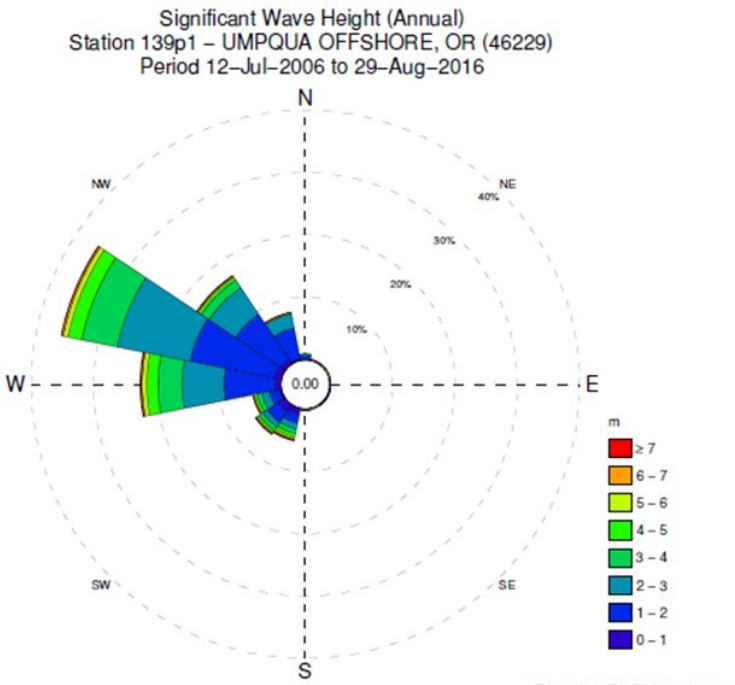

Percentage of Occurrence

Significant Wave Height, m	N	NNE	NE	ENE	E	ESE	SE	SSE	S	SSW	SW	WSW	W	WNW	NW	NNW	Total
Total	0.90								0.22	5.24	5.66	4.61	22.53	35.98	17.01	7.79	100.00
7										0.11			0.12				0.40
6										0.15			0.22	0.27			0.88
5										0.34	0.20	0.17	0.70	0.78	0.21		2.42
4										0.60	0.43	0.44	1.82	2.25	0.56		6.16
3										0.73	0.69	0.78	3.84	5.81	1.50	0.19	13.60
2	0.30									0.94	0.84	1.23	6.74	11.90	5.12	2.33	29.44
1	0.56									1.43	2.16	1.60	8.16	13.79	8.83	4.94	41.55
0										0.95	1.21	0.32	0.92	1.11	0.70	0.30	5.56
	N	NNE	NE	ENE	E	ESE	SE	SSE	S	SSW	SW	WSW	W	WNW	NW	NNW	Total

Figure 2-23
Annual Directional Distribution of Significant Wave Height for Buoy 139p1

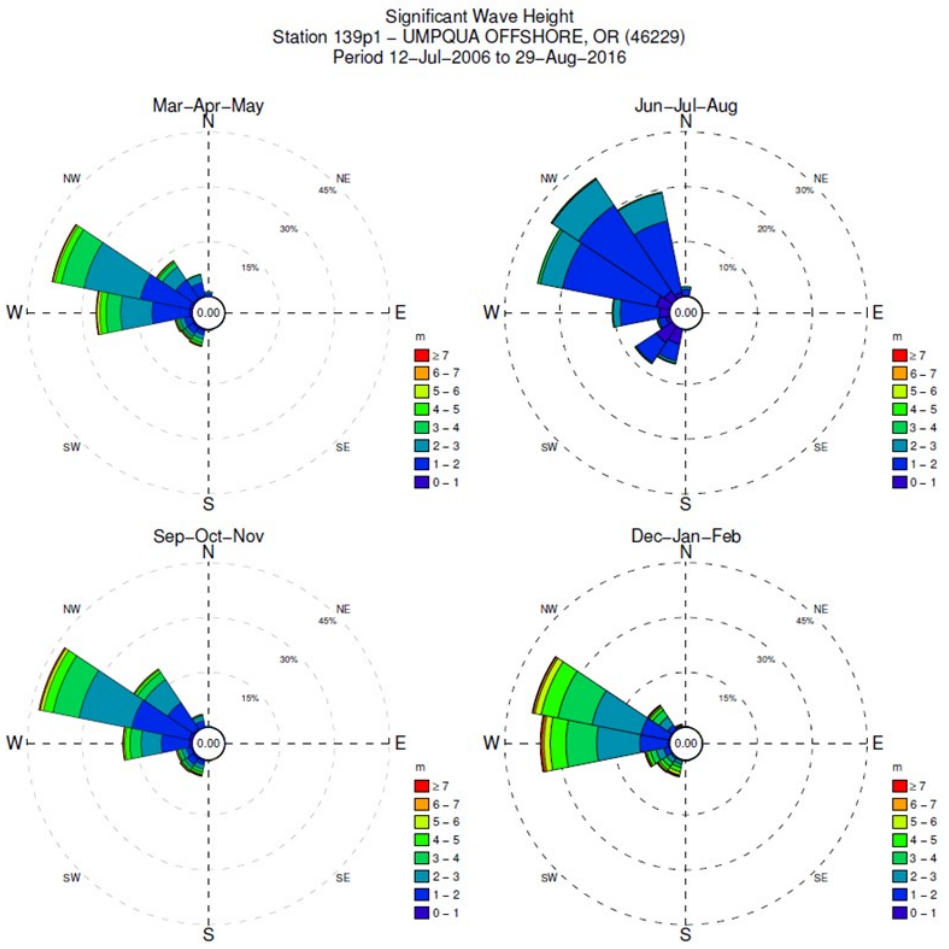

Figure 2-24
Seasonal Directional Distribution of Significant Wave Height for Buoy 139p1

Table 2-8
Significant Wave Height Statistics for Buoy 139p1

	Significant Wave Height (m)								
Period	**25%**	**50%**	**75%**	**90%**	**95%**	**99%**	**Max**	**Mean**	**Mode**
January	2.0	2.8	3.7	4.7	5.4	6.7	9.6	3.0	2.3
February	2.1	2.8	3.6	4.5	5.1	6.3	8.4	3.0	2.5
March	2.0	2.7	3.6	4.6	5.3	6.5	9.8	2.9	2.7
April	1.8	2.3	2.9	3.6	4.1	5.4	7.6	2.4	1.7
May	1.3	1.7	2.2	2.7	3.0	4.0	5.9	1.8	1.4
June	1.1	1.5	1.9	2.5	2.8	3.5	4.7	1.6	1.4
July	1.2	1.6	1.9	2.2	2.4	2.9	3.3	1.6	1.6
August	1.1	1.4	1.7	2.1	2.3	2.8	4.1	1.5	1.6
September	1.3	1.7	2.3	2.9	3.4	4.7	6.7	1.9	1.4
October	1.7	2.2	2.9	3.7	4.3	5.7	8.7	2.4	2.0
November	2.1	2.9	3.8	4.7	5.3	6.7	10.0	3.0	2.6
December	2.2	3.1	4.2	5.4	6.2	7.8	11.3	3.3	2.3
Annual	1.5	2.1	2.9	4.0	4.7	6.2	11.3	2.4	1.4

Table 2-9 shows primary and secondary modal wave directions for significant wave heights. Modal directions were computed from observations in each directional sector. These directions provide a more accurate estimate of most frequent wave direction from a given sector. The primary direction is the most frequent direction, while the secondary direction is the second most frequent direction. Percentage of occurrence is computed relative to all observations, such as most frequently wave heights are in the 1-2 m range in WNW sector with a total of 14 percent of occurrence (see Figure 2-23). In this range and sector, the most frequently observed direction is 286°. Waves above 7 m (23 ft) can arrive from directions of 275° or 201° north most frequently.

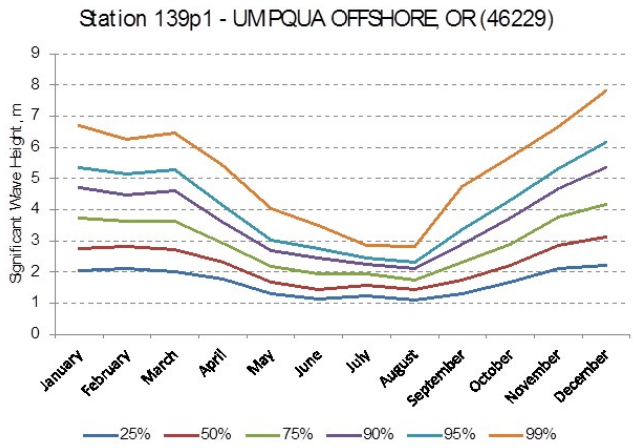

Figure 2-25
Monthly Variability of Annual Significant Wave Height at Buoy 139p1

Table 2-9
Annual Primary and Secondary Modal Wave Directions

Significant Wave Height, m	Primary Direction, degN	% Occurrence	Secondary Direction, degN	% Occurrence
0.00–1.00	218.7	1.21%	286.3	1.11%
1.00–2.00	286.3	13.79%	218.8	2.16%
2.00–3.00	286.3	11.90%	201.8	0.94%
3.00–4.00	286.3	5.81%	201.8	0.73%
4.00–5.00	286.3	2.25%	196.3	0.60%
5.00–6.00	281.6	0.78%	201.8	0.34%
6.00–7.00	286.3	0.27%	201.9	0.15%
>7.00	275.2	0.12%	200.6	0.11%
Total	286.3	35.98%	218.8	5.66%

The extreme significant wave heights for various return periods were derived from the observations at Buoy 139p1. The analysis was performed following the methodology by Goda (2010). A set of peak values were identified using the POT method. The method identifies events using a threshold (a 99.5-percentile value was used). A maximum for each event was identified as the peak value. The extreme values were used to find the best-fit extreme value probability distribution from several distributions.

The Weibull (k=1.0) extreme value probability distribution provided the best-fit to the omnidirectional wave data (Figure 2-26[4]). The extreme wave heights and 5 percent and 95 percent non-exceedance values for selected return periods are given in Table 2-10. Most of the extreme wave heights were from the western quadrant and immediate adjacent quadrants (WSW and WNW).

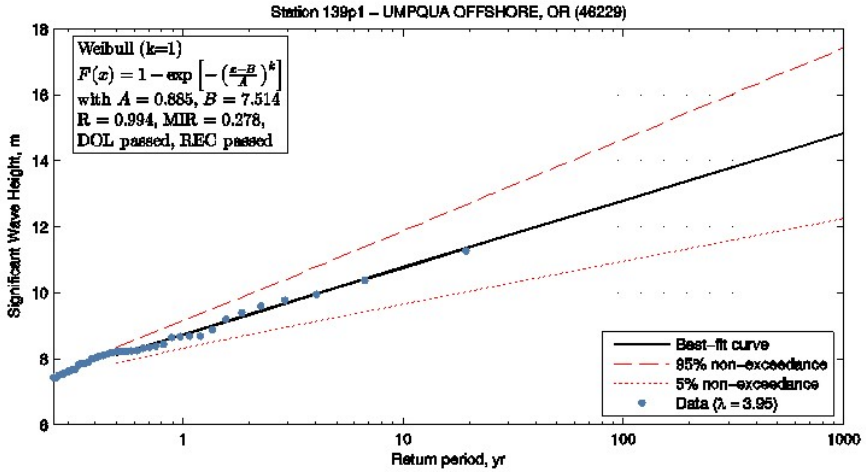

Figure 2-26
Extreme Significant Wave Heights for Buoy 139p1

[4] *The following parameters are shown in the figure: λ is the mean rate of extreme events, R is the correlation coefficient, MIR is the "goodness of fit" test (Minimum Ratio of residual correlation coefficient), DOL is the Deviation of Outlier test, and REC is the Residue of Correlation coefficient test (Goda 2000)*

Table 2-10
Extreme Significant Wave Heights for Buoy 139p1

Return Period (years)	Significant Wave Height, m		
	Best-fit	95% non-exc.	5% non-exc.
5	10.2	11.1	9.3
10	10.8	11.9	9.7
25	11.6	13.0	10.2
50	12.2	13.8	10.6
100	12.8	14.7	11.0

Figure 2-27 shows the annual directional distribution of the peak wave period. Peak wave periods from the dominant directional sectors (west and west-northwest) occur most frequently within the range of 6 to 16 seconds. Peak wave periods exceed 16 seconds about 6.5 percent of the time. Additional peak wave period statistics (percentiles, mode and maximum values) are gathered in Table 2-11.

Figure 2-28 shows the seasonal directional distribution of the peak wave period. Peak wave periods during summer are lower compared to other seasons. Frequency of occurrence of peak periods greater than 15 seconds are observed to considerably increase during winter.

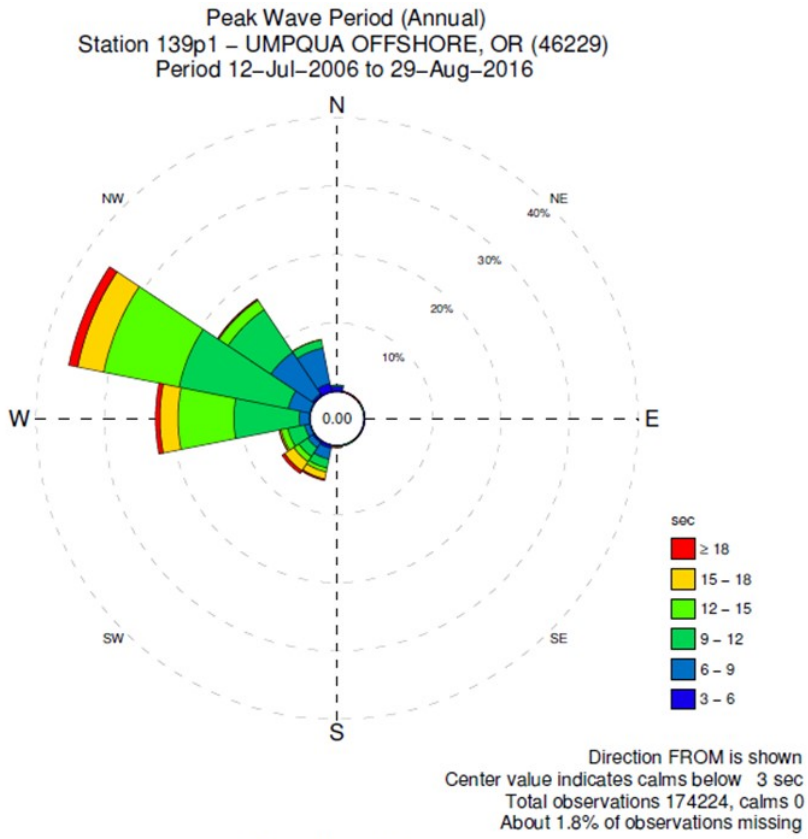

Percentage of Occurrence

Peak Wave Period, sec	N	NNE	NE	ENE	E	ESE	SE	SSE	S	SSW	SW	WSW	W	WNW	NW	NNW	Total
Total	0.90								0.22	5.24	5.66	4.61	22.53	35.98	17.01	7.79	100.00
18										0.21	0.44		0.62	1.30			2.62
15										1.06	1.62	0.26	2.65	3.91	0.19		9.70
12										0.60	0.90	1.00	8.17	11.24	1.64		23.58
9										1.31	1.54	2.50	9.57	16.27	7.52	1.23	40.01
6	0.30									1.63	0.90	0.77	1.48	3.20	7.31	5.32	20.99
3	0.59									0.43	0.26				0.34	1.22	3.11

Figure 2-27
Annual Directional Distribution of Peak Wave Period for Buoy 139p1

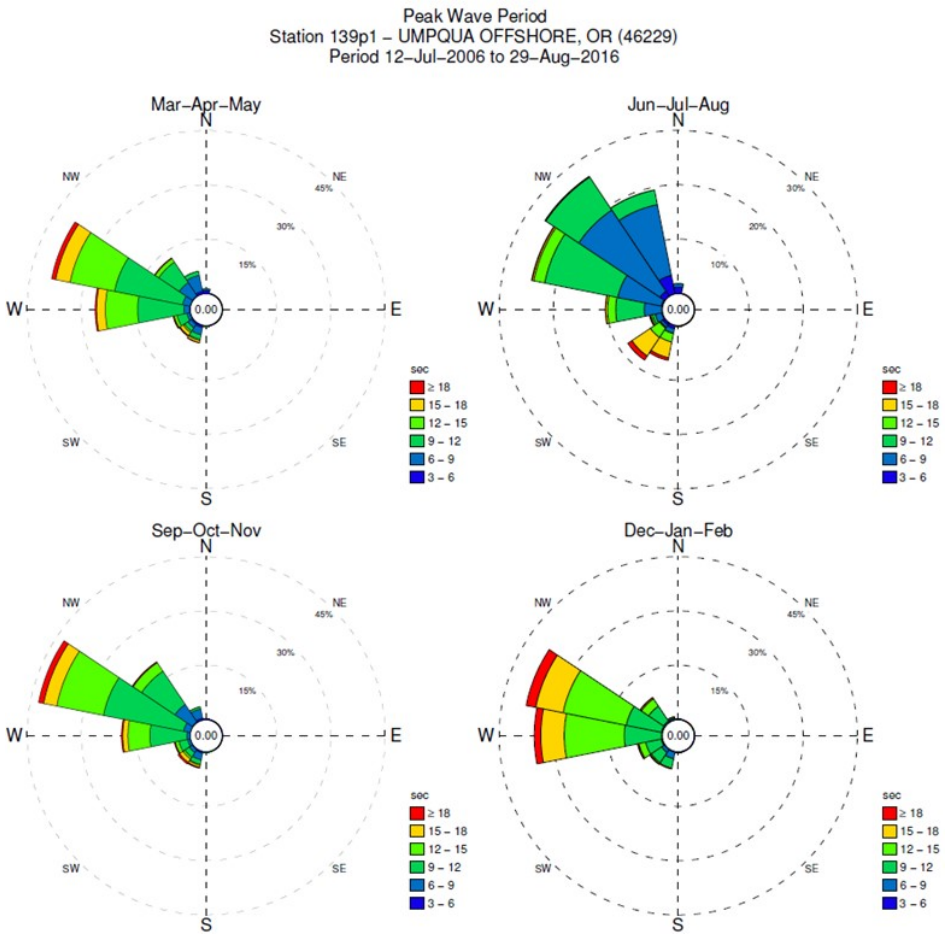

Figure 2-28
Seasonal Directional Distribution of Peak Wave Period for Buoy 139p1

Table 2-11
Peak Wave Period Statistics for Buoy 139p1

	Peak Wave Period (s)								
Period	**25%**	**50%**	**75%**	**90%**	**95%**	**99%**	**Max†**	**Mean**	**Mode**
January	11.8	13.3	14.3	16.7	18.2	20.0	25.0	13.1	13.3
February	11.1	12.5	14.3	15.4	16.7	20.0	25.0	12.7	12.5
March	10.5	11.8	13.3	15.4	16.7	18.2	22.2	12.0	11.8
April	9.9	11.8	13.3	15.4	16.7	18.2	22.2	11.6	11.8
May	8.3	9.9	11.1	13.3	15.4	16.7	20.0	9.9	9.1
June	7.7	9.1	12.5	15.4	16.7	18.2	25.0	10.1	8.3
July	7.1	8.3	9.9	14.3	15.4	18.2	20.0	9.1	8.3
August	7.1	8.3	9.9	13.3	15.4	16.7	20.0	9.0	8.3
September	8.3	10.5	12.5	14.3	16.7	18.2	22.2	10.7	9.9
October	9.9	11.1	12.5	14.3	15.4	18.2	25.0	11.4	11.8
November	10.5	11.8	13.3	15.4	16.7	20.0	22.2	11.9	12.5
December	10.5	12.5	14.3	15.4	16.7	20.0	25.0	12.5	13.3
Annual	9.1	11.1	13.3	15.4	16.7	18.2	25.0	11.1	12.5

† Maximum period is limited by spectral resolution

The joint histogram of significant wave height and peak wave period is shown in Figure 2-29. The histogram shows a correlation between increasing peak wave period ranging from 6–16 seconds and increasing significant wave height. Peak wave periods greater than 16 seconds are generally limited to 3 m (10 ft) significant wave height. The histogram also supports the previous observations based on the annual wave roses that, most of the time, the wave field is characterized by significant wave heights of 1-4 m (3-13 ft) with peak wave periods ranging from 6-16 seconds.

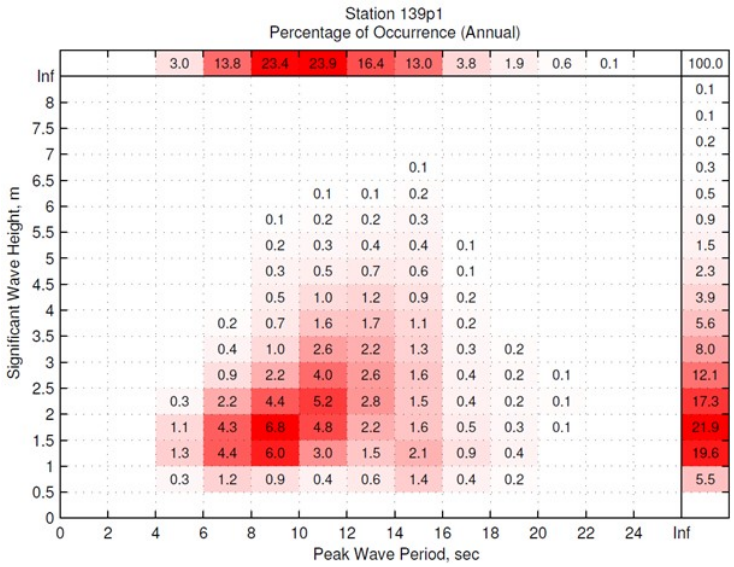

Figure 2-29
Annual Joint Histogram between Peak Wave Period and Significant Wave Height for Buoy 139p1

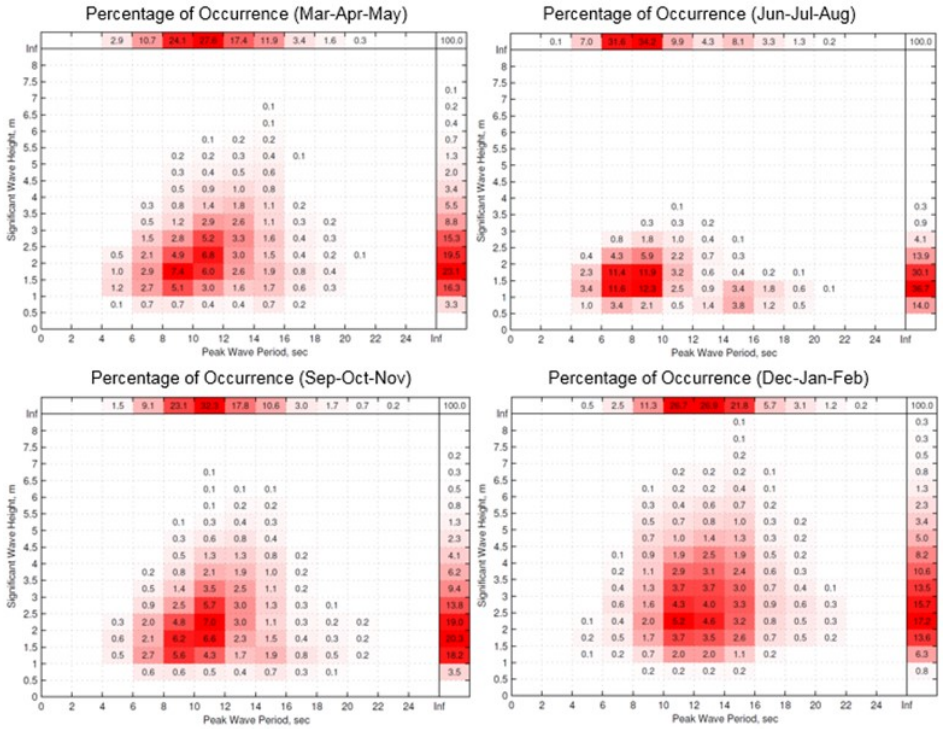

Figure 2-30
Seasonal Joint Histogram between Peak Wave Period and Significant Wave Height for Buoy 139p1

2.1.5.4 Buoy 126p1 Coos Bay

Data from Buoy 126p1 is available from March 2005 until February 2006, with about 18 percent of observations missing. The maximum recorded wave height is 8.7 m (28.5 ft) from 273° on January 4, 2006.

Other results of data analysis are not presented due to the short duration of the data record. However, it was found that the wave conditions were similar to the conditions at Buoy 139p1.

2.1.5.5 Buoy 135p1 Coos Bay North

Data from Buoy 135p1 is available from April 2006 until May 2006, with no observations missing. Maximum significant wave height was 5.2 m (17.1 ft) from 196° on May 23, 2006.

Other results of data analysis are not presented due to short duration of the data record. However, it was found that the wave conditions were similar to the conditions at Buoy 139p1.

2.1.5.6 Summary

The three CDIP buoy deployments presented provide insight on the wave characteristics offshore Coos Bay. From the analysis of the data, the following characterization can be made:

- The dominant directional sector of wave approach is WNW, followed by west and NW.
- Waves approaching from the southwest are usually long-period waves and dominate the wave field about 10 percent of the time. These waves may be present during other periods as well, but they are not as energetic.
- During the summer months of June, July, and August there is some variability in wave directionality, with a higher frequency of occurrence of waves from the NW and north-northwest (NNW).
- Significant wave heights occur most frequently in the 1-4 m (3-13 ft) range with the maximum significant wave heights of above 11 m (36 ft).
- More energetic wave conditions occur during the winter months of December, January, and February with significant wave heights exceeding 4 m (13 ft) about 20 to 25 percent of the time.
- Peak wave periods occur most frequently in the 6-16 second range.
- Joint histograms of significant wave height and peak wave period show that peak wave periods correlate with significant wave heights in the 6-16 second range.

2.1.6 Storms

Storm events were identified from the time series of significant wave height measured at CDIP Buoys 139p1 and 126p1 using the POT method. The threshold was equal to 99.5 percentile value of the recorded wave heights.

A total of 79 storms were identified: 8 from Buoy 126p1 and 71 from Buoy 139p1. The storms cover a period extending from March 2005 to August 2016. The winter storms have two directional peaks: the majority of waves approach from west to WNW, and there is a secondary peak from the southwest. The west to WNW waves are long-period swell waves with periods on the order of 16 to 20 seconds generated by distant storms, while the southwest waves originate from nearby storms with periods generally less than 15 seconds. This southwest peak accounts for the highest storm waves. The selected storms are described in Section 3.3.4.1.

Maximum storm surge extracted from water levels measured at NOAA Station 9432780 Charleston, OR, is within a window of 12 hours before and 6 hours after the peak wave height. Figure 2-31 presents time series of one of the selected storms and illustrates the meaning of the storm parameters shown in Figure 2-31.

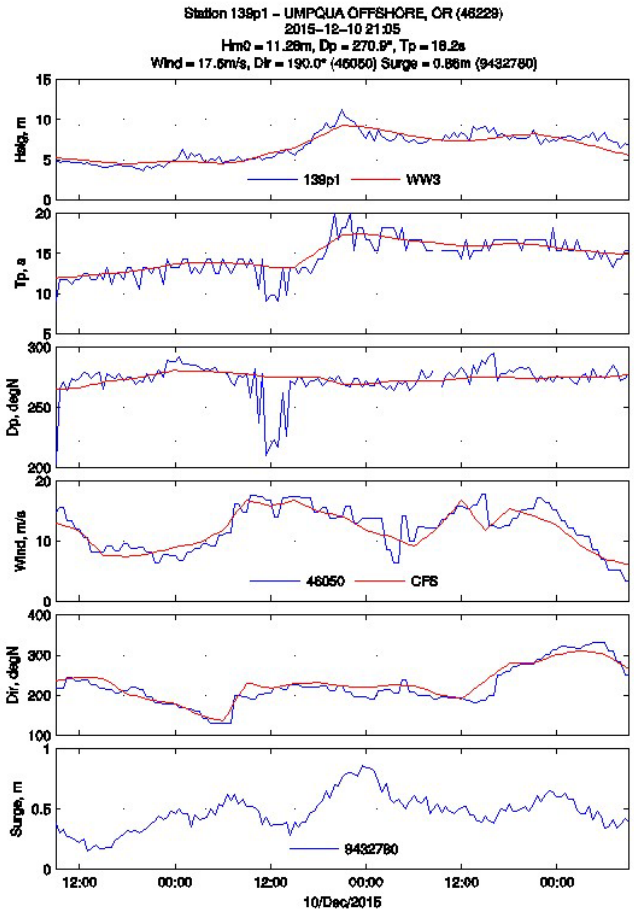

Figure 2-31
Example of Storm Data

2.2 Federal Project History

The USACE began construction on the first jetty in Coos Bay prior to 1890 and followed with dredging shortly after in 1910. This section outlines the history of USACE construction in the Entrance Channel and in the adjacent shoreline or offshore areas.

2.2.1 Navigation Channel

Before the first federal navigation project was constructed in Coos Bay, the original outlet channel from Coos Bay into the Pacific Ocean crossed a bar at the bay mouth and was about 10 ft deep by 200 ft wide. Inside the bar, the natural channel was about 22 ft deep.

Dredging the ocean bar channel was first authorized in 1910, with a 22-ft channel authorized in 1919. Dredging quantities were significant, typically 1 mcy annually was dredged from the entrance bar (Chief of Engineers 1924, 1926, 1927). Since this time, the Entrance Channel has been repeatedly made wider and deeper, and has shifted towards the north:

- A channel 24 ft deep and 300 ft wide was authorized in 1930 and completed in 1932; this depth was authorized to be extended to the turning basin above Marshfield in 1934;
- The outer bar channel was authorized to a depth of 40 ft and the inner channel to 30 ft, with two turning basins and two anchorages in 1946;
- An outer channel 45 ft deep and inner channel 35 ft deep were authorized in 1969 and completed by 1974; 4 ft of AMD at the entrance and in the upper reach was authorized in 1994; and
- An outer channel 47 ft deep at the entrance and 37 ft deep internally was authorized in 1996 and completed in 1997.

2.2.2 Coos Bay Jetties

2.2.2.1 Construction and Repair History

Prior to construction of the existing jetties, the USACE began constructing a jetty from Fossil Point towards the west. In 1890, after several years of construction, the Board of Engineers halted work on the original jetty and recommended the construction of two parallel jetties that would provide a navigable waterway to Coos Bay. Figure 2-32 shows the location of the remnant of this original, partially-built jetty, together with the maximum constructed extent of the North and South Jetties.

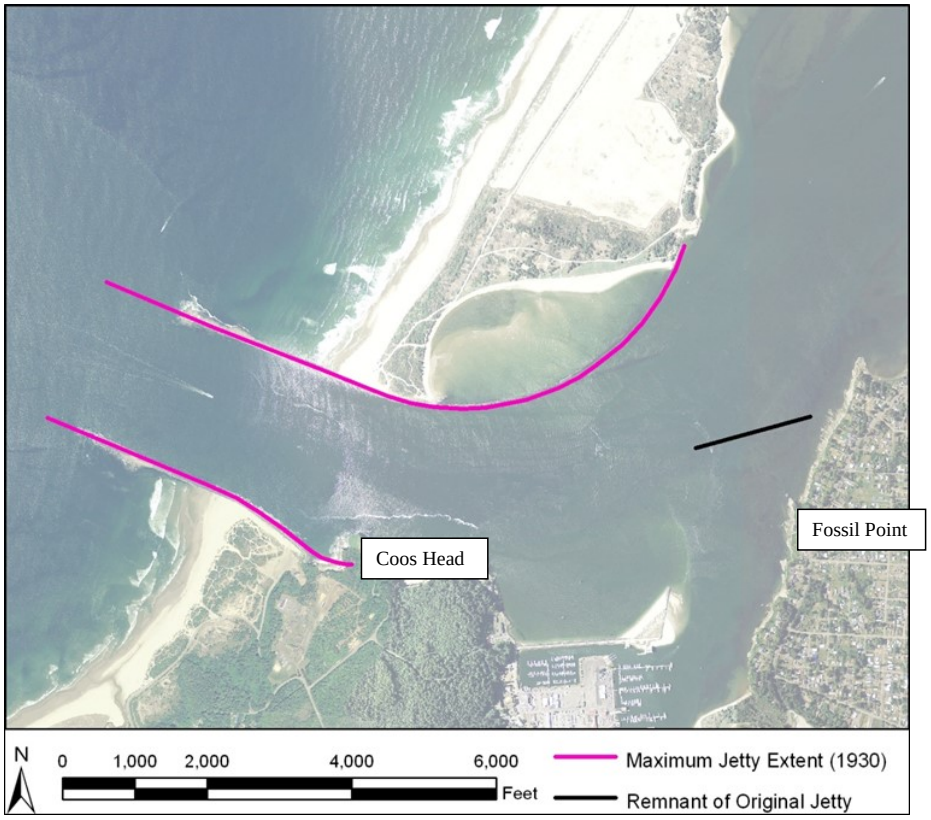

Figure 2-32
Maximum Extent of Coos Bay Jetties and Remnant of Original Jetty

The 1890 authorization provided for the construction of two rubble-mound jetties. The North Jetty was constructed first along the southern end of the North Spit, which was then a low shifting sand spit. Construction of the South Jetty did not begin until 1924. Figure 2-33 shows the jetty stationing currently used by the USACE, and which is used throughout this document. The relic structure attaching to the North Jetty at approximately Station 30+11 is the remains of a rail spur, rather than a jetty structure.

Figure 2-33
Coos Bay Jetty Stationing, 2009 Photograph

The North Jetty was originally constructed on a foundation of brush mattresses (Case 1983) and was authorized at 9,600 ft long. By 1894, the authorized project depth had been reached, although the jetty was still approximately 80 ft short of the authorized length (Chief of Engineers 1915). The jetty head was at Station 86+77 based on present-day stationing (Figure 2-33). The jetty crest elevation was slightly below MHW. The method of construction involved initial construction of a pile-supported tramway along the jetty alignment with rock placed from that tramway.

Between 1894 and 1901 the jetty was repeatedly damaged and rebuilt, particularly at its seaward end (Chief of Engineers 1915). Immediately after construction of the North Jetty, sand began to accumulate on its north side, forming the North Spit; the North Spit now extends well south of its pre-construction extent.

Although the authorized length of the jetty was 9,600 ft, it is not clear that this full length was ever achieved. Similarly, the authorized upstream end of the jetty is not well-defined. In 1922, restoration of the North Jetty to its full length was authorized, together with construction of the South Jetty (discussed further below). This was closely followed by another authorization in 1927, which covered "the extension of the jetties to such lengths as may be practicable within the estimate of the total cost of the jetties" (Chief of Engineers 1931). Restoration and extension of the North Jetty, including the construction of a concrete cap, was completed by 1931. At this point, the North Jetty was at its maximum extent, with its head at Station 95+07. Since that time, the head of the jetty has suffered continuous damage due to wave attack; the overall length of the jetty

has decreased, and the jetty has required repairs every 10 to 20 years, generally with increasing rock size and increased crest height. The North Jetty root is also in failed condition, with its crest generally at 0 to +4 ft MLLW. This portion of the jetty is relatively protected from waves, but is subject to erosion and undermining of the toe. Previous USACE (2012b) studies have noted that, "structural condition of Reach N1 is strongly affected by littoral processes."

Although the South Jetty was originally authorized in 1890, its construction did not begin until 1924. In 1922, the South Jetty was authorized at a length of 3,900 ft; in 1927, an additional authorization covered "the extension of the jetties to such lengths as may be practicable within the estimate of the total cost of the jetties" (Chief of Engineers 1931). Construction methods were similar to those used for the North Jetty. The jetty head was at approximately Station 41+60 by present-day stationing.

Between 1940 and 1941, the South Jetty was reconstructed as a composite concrete and rock structure; a cast-in-place monolithic concrete core was installed and protected by rock on both sides. The offshore limit of the jetty was constructed at Station 37+37. In the 1964 rehabilitation, 80 ft of concrete was broken up and removed down to MLLW. This concrete structure still acts as a jetty head in that it breaks the incoming waves; rock on the South Jetty is present at Station 34+23.

2.2.2.2 Present Condition

Presently, the USACE has initiated a three-year North Jetty Repair Major Maintenance project on April 1, 2023 and is expected to last until December 2025. The design elevations from the repair project (USACE 2021) were incorporated in the extreme waves modeling (Section 3.3).

The condition of the North Jetty varies along its length. Figure 2-34 illustrates its condition by showing the deficit between jetty elevations measured in 2009 and the design template; the deficit refers to the difference between the design elevation and the present elevation. This figure also shows the reach designation for the north jetty as defined in the Preliminary Major Maintenance Report (MMR) (USACE 2012b).

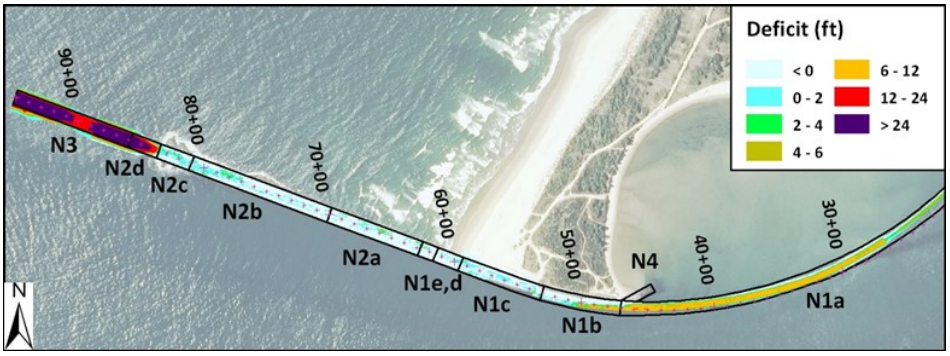

Figure 2-34
North Jetty Deficit in Elevation Compared to Design Template, with MMR Reach Designation

Reach N1a, the jetty root alongside the LSB, was originally constructed to support the trestle for jetty construction. It began to function as part of the jetty as the LSB formed. However, considered as part of a functioning jetty, it has failed. Its crest elevation is generally at MLLW (and never higher than +4 ft MLLW); Figure 2-35 shows this reach barely visible above the water at mid-tide. It may retain some function in dissipating wave energy towards LSB, thereby decreasing erosion of the bay. Figure 2-35 was taken from Reach N4, the hard point at LSB. This hard point was reconstructed in 2008 and is in good condition. This hard point provides a sill for the beach and has deterred seaward translation of the LSB (USACE 2012b).

Figure 2-35
Birds Perched on Relic Jetty Root, Water Level about +4 ft MLLW
(Photograph Taken from Hard Point (Reach N4 in Foreground), October 2010)

At the far offshore end of the North Jetty, Reach N2d and reaches further offshore (N3) have also failed. The crest elevation of Reach N2d is as low as -10 to -20 ft MLLW; at most, it functions to break waves that attack the present jetty head and to provide a barrier to sediment transport around the jetty. Neither Reach N2c nor N2d were designed as a jetty head – the most recent major repair, in 1989, stabilized the jetty head at Station 86+40, but this head has failed.

Reach N2c acts as the present jetty head; however, it is in poor condition and is receding at a rate between 10 and 20 ft per year. Figure 2-36 illustrates the field of displaced stone that surrounds this area.

Figure 2-36
Displaced Stone Adjacent to Reach N2c, Channel Side, October 2010

The intermediate reaches, N1b through N2b, are in fair to good condition with scalloping in places, but reasonably good structural stability.

Inshore of the current head, the South Jetty is in fair to good condition, as suggested by Figure 2-37. Similar to the North Jetty, the South Jetty is not at its original design length. Reach S3b is a combination of displaced rock and a partially demolished concrete core. The core is visible at low tide, as shown in Figure 2-38, Reach S3c, the original head, consists of the original concrete structure. The rock at S3a is in good condition, possibly due to the presence of the concrete head that dissipates incoming wave energy.

Other parts of the South Jetty are in reasonable condition and the Preliminary MMR does not recommend repairs to this jetty.

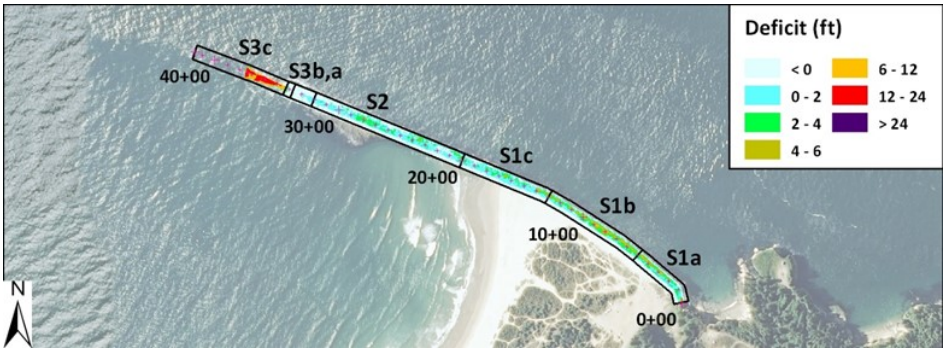

Figure 2-37
South Jetty Deficit in Elevation Compared to Design Template, with MMR Reach Designation

Figure 2-38
Demolished Concrete Core at Reach S3b: 2009, Low Tide

2.2.3 Dredging History

Sedimentation at Coos Bay has been influenced by the ongoing dredging of the channel by the USACE for both construction and maintenance. Ever since the navigation channel was first authorized, maintenance dredging quantities have been significant. Since the previous channel modification in 1998, the average O&M dredging in the Entrance Channel has been 660,000 cy/yr. This is very similar to the long-term average of 740,000 cy/yr (dating back to pre-1900). The rate has not increased in a consistent way as the channel width and depth have been increased.

Dr. Rosati (2014) provided the dredging data used in her analysis (1899 through 2005). M&N extended and further analyzed the data as follows:

- Where possible, M&N separated the dredging records into upstream maintenance (above RM 2.5), entrance maintenance, and new work.

- Between 1970 and 1976 the dredging records did not provide a breakdown according to area. However, the upstream entrance dredging was relatively consistent. This allowed an estimated split between the two areas to be made. The figures in this report assume that split to be correct, allowing the total entrance dredging in that period to be estimated. This period is shown as a gap in the data, with the subsequent years including this estimated amount.

The USACE Portland District and Coos Bay Field Office provided data to allow extension of the series between 2005 and 2014.

Rosati (2014) interprets the changes in dredging as resulting from the channel dimensions, as indicated in Figure 2-39. The channel dimensions shown in this figure refer to the Entrance Channel, not the overall channel dimensions. The channel width was not defined before 1914 – only the depth at the bar. From this data, Rosati concluded that shoaling grows when the width and depth of navigation channels increase, but the rate of growth is irregular.

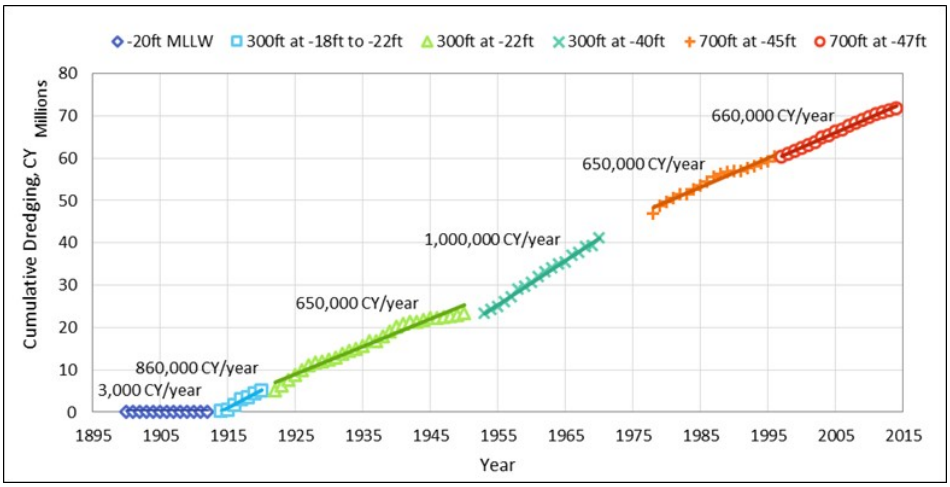

Figure 2-39
Maintenance Dredging in the Entrance Channel According to Entrance Channel Dimensions

The results do not show a simple progression of increased maintenance dredging rates with increased channel depths. The largest rates of maintenance dredging occurred with Entrance Channel dimensions of 300 ft width by 40 ft MLLW depth, with the second-largest at 300 ft width by 18 ft to 22 ft MLLW depth. In addition, the annual maintenance dredging decreased after 1974 (when the Entrance Channel was deepened to 45 ft MLLW and widened to 700 ft) and showed relatively little change after 1996 (deepening to 47 ft MLLW).

2.2.4 Material Placement

The U.S. Environmental Protection Agency (USEPA) designated three ODMDSs (ODMDS E, F, and H) off the Coos Bay entrance in 1977 for interim use until further study and final site designation could be completed (Figure 2-40). The need for ocean disposal sites was becoming increasingly important, as suitable upland sites for dredged material disposal were becoming less available (USEPA and USACE 1986).

The area in the vicinity of ODMDS E and F (1986) was selected for the placement of coarse-grained material dredged from below RM 12. The area in the vicinity of ODMDS H was selected for placement of fine-grained material dredged from above RM 12. Currently, material dredged during routine channel maintenance consists of sand and silt, which are placed at ODMDS F and H, respectively.

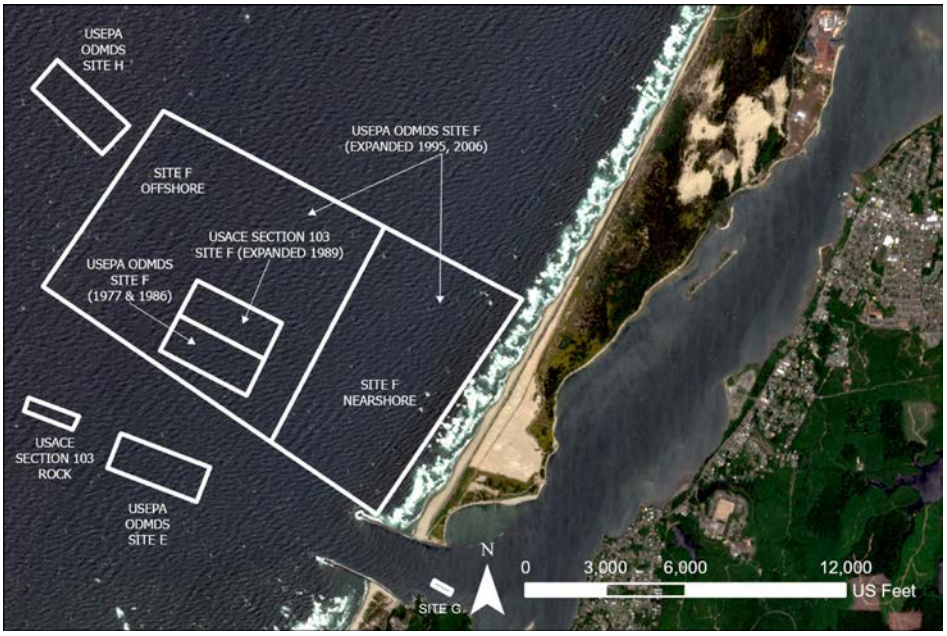

Figure 2-40
Location of the ODMDSs

2.2.4.1 Ocean Dredged Material Disposal Site E

ODMDS E is located approximately 1.5 mi southwest of the entrance to Coos Bay. The use of the site was limited to the placement of no more than 150,000 cy annually in 1987 due to mounding throughout the site and lower than predicted dispersion rates (USACE 2012a). The site has not been used since 1991 (except for 79,900 cy being placed in 2006) and there are currently no known plans to use the site. Bathymetric surveys show that the mounding has decreased since 1991, compared to the 1982 condition (USACE 2012a).

2.2.4.2 Ocean Dredged Material Disposal Site F

ODMDS F is located approximately 0.5 NM outside and west of the Coos Bay entrance. It is the largest of the Coos Bay ODMDSs and is used for the placement of clean sand dredged below RM 12 in the federal channel, other local USACE projects, and by appropriately permitted dredged material from non-USACE projects. ODMDS Site F (1986) has been expanded in past years (1989, 1995, and 2006) to accommodate annual maintenance dredging activities by the USACE and is currently 3,075 ac in area.

Mounding in the original USEPA interim ODMDS F (1977) was first observed with bathymetry surveys in 1982 (USACE 2012a). The 1989 expansion doubled the size of Site F, expanding it northwards. By 1994, a maximum of 15 ft of material had accumulated when compared to the 1982 survey, and mounding had also been observed in the expanded portion of ODMDS F. Since 1994 (with one exception in 2006), no material from the channel has been placed in the original ODMDS F area or the 1989 expansion area, and some of the mound has begun to erode. A survey in 2000 showed a 19-ft mound in the NW corner of the original site. By 2010, the mound had decreased to 10 to 11 ft compared to the 1982 baseline.

Water depth at ODMDS F varies between about 20 and 160 ft MLLW. Dispersion rates at depths greater than 60 ft MLLW are very slow (USEPA & USACE 2006). Management of ODMDS F distinguishes between nearshore and offshore portions, with the boundary between the two at a water depth of 60 ft MLLW. Current USACE maintenance dredging practices call for the maximum amount of material to be placed in the nearshore portion of Site F to support nourishment of the littoral environment. The offshore portion of ODMDS F is now used when weather and wave conditions do not allow dredging equipment to move into the shallower portions of ODMDS F, when more than one dredge is working, or to allow dispersion of material in the nearshore area. The maximum capacity of the site has never been studied or defined (Siipola 2011).

Dredged material placement in the ODMDS F nearshore area is controlled through use of a grid system to distribute dredged material and minimize mounding. Recent bathymetry of ODMDS F nearshore suggests that mounding is starting to occur (Siipola 2011). A September 2000 survey indicated a 1-ft to 5-ft increase in bottom height throughout the nearshore site when compared to an October 1995 survey. The trend of decreasing depth occurs throughout the nearshore portion of Site F, except in the very southeast corner of the site (USACE 2012a). Most of the build-up occurs along the shoreward portion of the site.

2.2.4.3 Ocean Dredged Material Disposal Site H

ODMDS H is a USEPA designated ODMDS used for the placement of finer-grained sand and silt materials from above RM 12 in the Coos Bay Navigation Channel. The site is located further offshore than ODMDS F at approximately 3.7 mi NW of the entrance to Coos Bay (outside of the territorial sea boundary). It is 3,600 ft by 1,450 ft with an area of 120 ac and the average water depth is 180 ft MLLW.

Since 1986, the site has been used to place over 6.7 mcy of material for an average annual amount of 375,000 cy/yr. A comparison between the 2010 and 1986 surveys show that some mounding does occur at this site (USACE 2012a). Placed material redistributes north and northeast of the site, and the movement of placed material can be identified outside the boundaries of the site.

3. DESIGN CONDITIONS

This section outlines the metocean conditions that drive the dynamics of the Coos Bay offshore area and the Entrance Channel. Coos Bay entrance area is subject to forces such as wind, tides, waves, and currents. Local winds generate sea waves. Far-off storms generate swell waves that propagate into the entrance. The waves mobilize sediment at the seabed, and currents carry the sediments along as sediment transport.

Numerical wave modeling is used to compare wave propagation under different conditions. This includes different channel bathymetry conditions as well as different offshore conditions (see the Dredged Material Disposal Sites Report – OIPCB 2017c). Ultimately, changes to wave climate are expected to play a significant role in understanding the effects of the 2023 PA.

3.1 Design Water Levels

- As noted in Section 2.1.3, various components contribute to the water levels observed at Coos Bay. These water levels were incorporated into various studies performed throughout the report, including navigation studies, simulation of estuarine and Entrance Channel hydrodynamics, sediment transport studies, wave modeling, and design of structures. Different water level components were used for these various studies as appropriate. This section describes the water levels used to drive the analyses described in the remainder of this report.
- *Extreme Wave Conditions*: Wave modeling to categorize extreme waves were based on offshore wave data from 79 measured storms. Offshore of the -150 ft MLLW contour, the observed surge was used to propagate the offshore wave towards Coos Bay. For depths less than 150 ft MLLW, four tidal conditions (MHHW, MLLW, MSL plus flood currents, and MSL plus ebb currents) were superimposed on the measured surge. These tidal conditions are equal probability, which allows them to be incorporated into a statistical extreme value analysis.
- It should be noted that there is no apparent correlation between storm intensity (wave heights) and observed surge at Charleston (Section 3.3.4). Therefore, it was not deemed appropriate to superimpose additional surge (i.e., beyond measured surge) on the tidal water levels.
- *Wave Analysis at ODMDS E and F (OIPCB 2017c)*: A three-month period containing both large storm waves and operational waves was identified for analysis of ODMDS E and F. This time period was selected because it includes both operational and extreme conditions. The observed water levels were used in the model for this period.
- *Design of Rock Apron*: Armor stone stability was considered for various tidal conditions, and it was found that the MLLW condition yielded the most conservative results.
- *Erosion at LSB*: Erosion at LSB is understood to result from wave propagation (Hays & Moritz 2003). Therefore, the results of the extreme wave analysis, together with general wave climate, are used to evaluate erosion at LSB.
- *Sediment Transport Modeling*: Water levels used for this analysis consisted of tides and surge. The tide predictions from Pacific Ocean database of the TPXO7.2 global inverse tide model (Egbert and Erofeeva 2002) developed by Oregon State University were used.

Water level predictions from the global ocean analysis and forecast of the E.U. Copernicus Marine Service program were superimposed on the tides to account for offshore surge.

3.1.1 Future Sea Level Change

It is recognized that changes in sea levels predicted in the future are likely to impact design conditions at Coos Bay. Various studies suggest that climate is changing and weather extremes are increasing in frequency. The USACE promotes that preparedness is more cost-effective than response and recovery, and improved resilience to more frequent but less extreme events should be considered as well as extreme events (Moritz 2016).

Future SLC was taken into consideration as part of the statistical water level combination analysis. The USACE guideline on breakwater and jetty design (1986) recommends that, "the economic design life of most breakwaters and jetties is 50 years." Therefore, a time horizon of 50 years (approximately by Year 2080) is selected for the consideration of the representative SLC in this study. As shown in Table 2-4, the USACE Intermediate curve projects sea level increases of 1.1 ft by 2080. The USACE high curve projects sea level increases of 3.2 ft by 2080. Therefore, the USACE High projection of +3.2 ft SLC is selected for this study. The selected sea level of 3.2 ft is a conservative assumption for Coos Bay, but not overly conservative compared to other higher projections available, e.g. NOAA 2012. In addition, the relative impact of 3.2 ft of raised water level was compared to infrastructure within the Coos Bay estuary system. If sea levels rise more than predicted, or even by the conservative amounts predicted, the whole of the Coos Bay system would be submerged and the State-wide impacts would be devastating. Therefore, the objective of selecting a value for this analysis was to be conservative without selecting a value where the impacts to the federal infrastructure are far outweighed by the regional effects. Detailed discussion of projected SLC is in Section 2.1.3.4. The SLR projections adopted for this modeling work are the same as the USACE's Coos Bay North Jetty Repair project (USACE 2019). An excerpt from the USACE's report is provided below.

Commented [QW1]: 10462088: Section 3.2.4, Sea Level Change: Provide a short explanation for why the USACE "High" RSLC scenario will be used to evaluate future water level conditions for this project, as opposed to using the "Low" or "Intermediate" RSLC scenarios.

(comment by Rod Moritz)

Commented [QW2R1]: Text added to address DrChecks20230929, Comment ID 10462088

"The life-cycle damage for random samples of historical storms was also performed taking into account three relative sea level change (SLC) scenarios. These scenarios are defined in ER 1100-2-8162 (USACE 2013). The curves for the USACE high, USACE intermediate, and USACE low scenarios result in increases in SWL of 0.33 ft, 0.87 ft and 2.59 ft feet respectively for the year 2070."

The evaluations on future SLC consisted of repeating the wave modeling for the 2023 PA condition performed for current no SLC condition and including 3.2 ft of SLR (see Section 3.3.7). The modeled SLC case was used to generate extreme wave heights, to assess how waves propagate through the inlet, and to perform a probabilistic assessment of stability at the North and South Jetties.

3.2 Design Currents

Currents are driven by a combination of winds, waves, and water levels. Depth-averaged currents in the Entrance Channel and offshore area were simulated for two purposes: firstly, maximum ebb and flood currents were used as input to the wave model described in Section 3.3; secondly, the change in currents in the Entrance Channel was evaluated and provided in Section 3.2.2.

Entrance currents were simulated with the MIKE-21 coupled Hydrodynamic (HD) and Spectral Wave (SW) module, which is used in isolation to simulate currents throughout Coos Bay offshore area and the Entrance Channel. This model was approved by USACE for this use.

Figure 3-1 illustrates the full estuary model domain and elevation. Details of various sources of elevation data are provided in Sub-Appendix 3, *Estuarine Dynamics*.

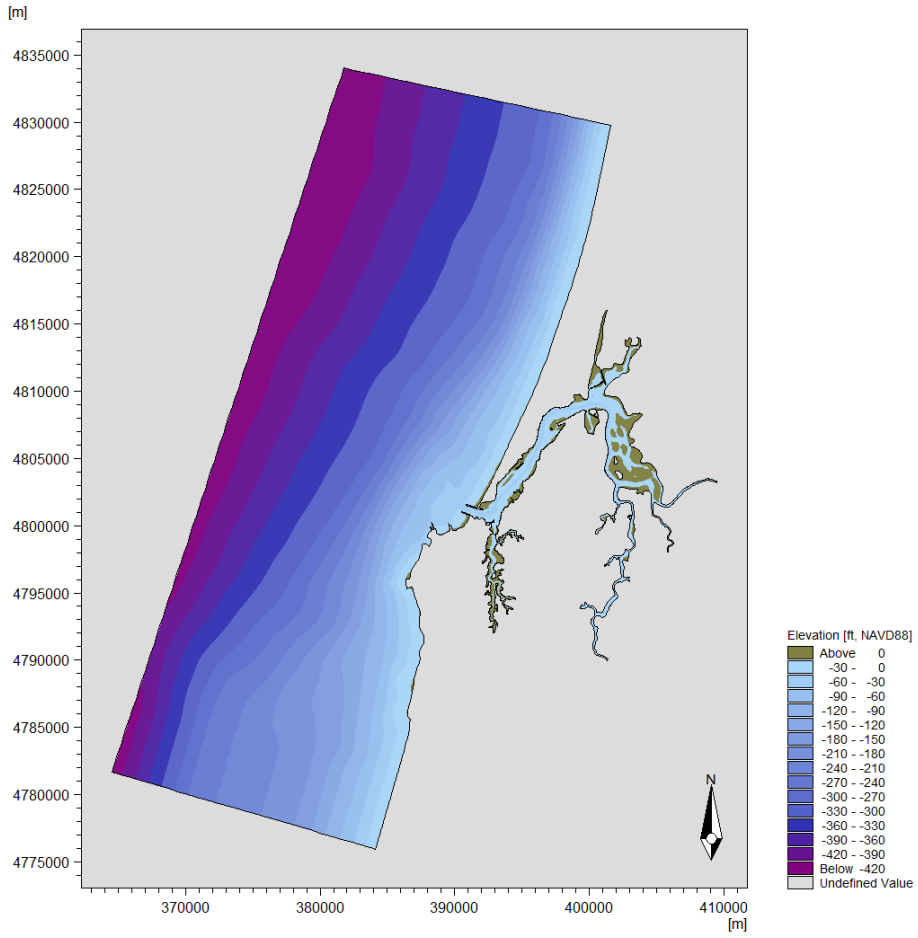

Figure 3-1
Full Estuary Model Domain and Elevation

3.2.1 Model Calibration

The following modeling effort of tides and currents calibration was originally documented in Coos Bay Jetties Preliminary Major Maintenance Report Appendix B, prepared for USACE in July 2012

(M&N, 2012). The review comments received from USACE were addressed in this final report, and no specific comment was related to this section (M&N, 2011).

3.2.1.1 Data Availability

The following data are available for tides and currents (Figure 3-2).

- NOAA has measured tidal elevations at Charleston, OR since 1970.
- David Evans & Associates, Inc. (DEA) used moored Acoustic Doppler Current Profilers (ADCP) to measure tidal elevations and currents at three locations from March 28 to April 23, 2010 (OIPCB 2010). Two of these locations are inside the estuary, while the third is offshore.
- NOAA measured tidal elevations and currents from September 15 through October 5, 1982. The tides and currents were measured at several locations throughout the estuary.

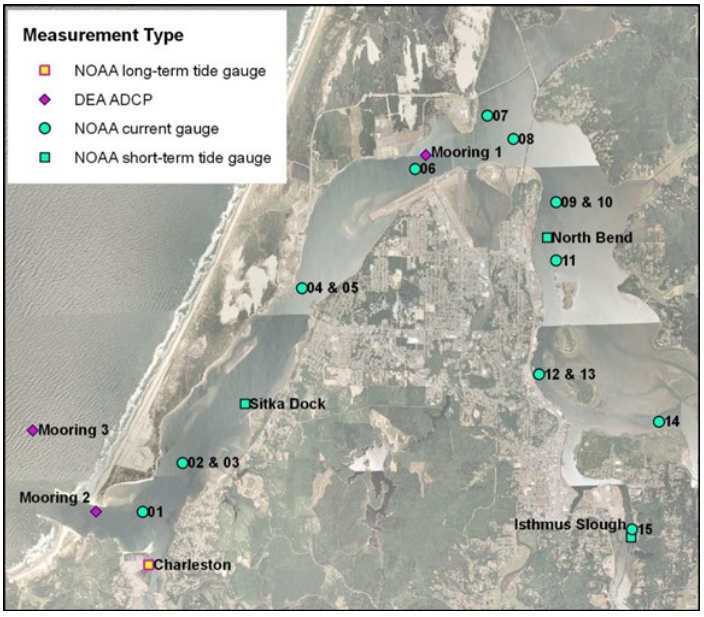

Figure 3-2
Locations of Measuring Stations

In Figure 3-3, the current speed comparisons between the model results and the current measurements by NOAA at Gauges 01 through 03 are presented. Other gauges located upstream of RM 3 are considered as estuarine and are discussed separately. The comparison plots indicate that measurements by NOAA gave significantly higher current velocities than the model results at NOAA current Gauge 01, moderately higher at Gauge 02 and lower currents than modeled results at Gauge 03. It is expected that the main reason is that the measurements by NOAA were

performed in 1982, using Aanderaa RCM4 rotary current meters, approximately 4.5 ft long with a 3-ft long vane that oriented the meter to the prevailing current direction. The speed was calculated by averaging the number of rotations of the rotor over a 10-minute interval; the direction was determined as an instantaneous value from the vane direction (NOAA/NOS 1999). As such, the current velocities were measured at a single point in the water column[5], while the model results are depth-averaged.

In contrast, the ADCP measurements by DEA provide a depth-average over most of the water column, and more closely match the quantity modeled.

A second possible reason relates to changes in the channel since the measurements were performed. Figure 3-4 illustrates the Entrance Channel cross-sections in September 1982 and in 2010 (the 1982 data are from dredging records and only provide bathymetry within and very close to the dredged channel). The hydrodynamic model mesh was developed from bathymetric surveys between 2007 and 2010. Since there are depth changes in the channel interannually as shown in Figure 3-4, using current measurements in 1982 to calibrate a model with 2010 bathymetric data is not a good option. It is also hard to expect the model results match the measurements. Therefore, DEA (2010) current measurements at Mooring 1 and Mooring 2 are a better data source for model calibration.

Hydrodynamic calibration is performed using elevation measurements by NOAA and the current measurements by DEA.

[5] *The depths of NOAA current gauges are: Gauge 01 - 30 ft above bottom, Gauge 12 - 20 ft above bottom at 12, Gauges 02, 04 and 09 - 15 ft above bottom, Gauges 03, 05, 06, 07, 08, 10, 11, 13, 14 and 15 - 5 ft above bottom. These current measurements were provided by NOAA Center for Operational Oceanographic Products and Services on June 14, 2010 via email communications.*

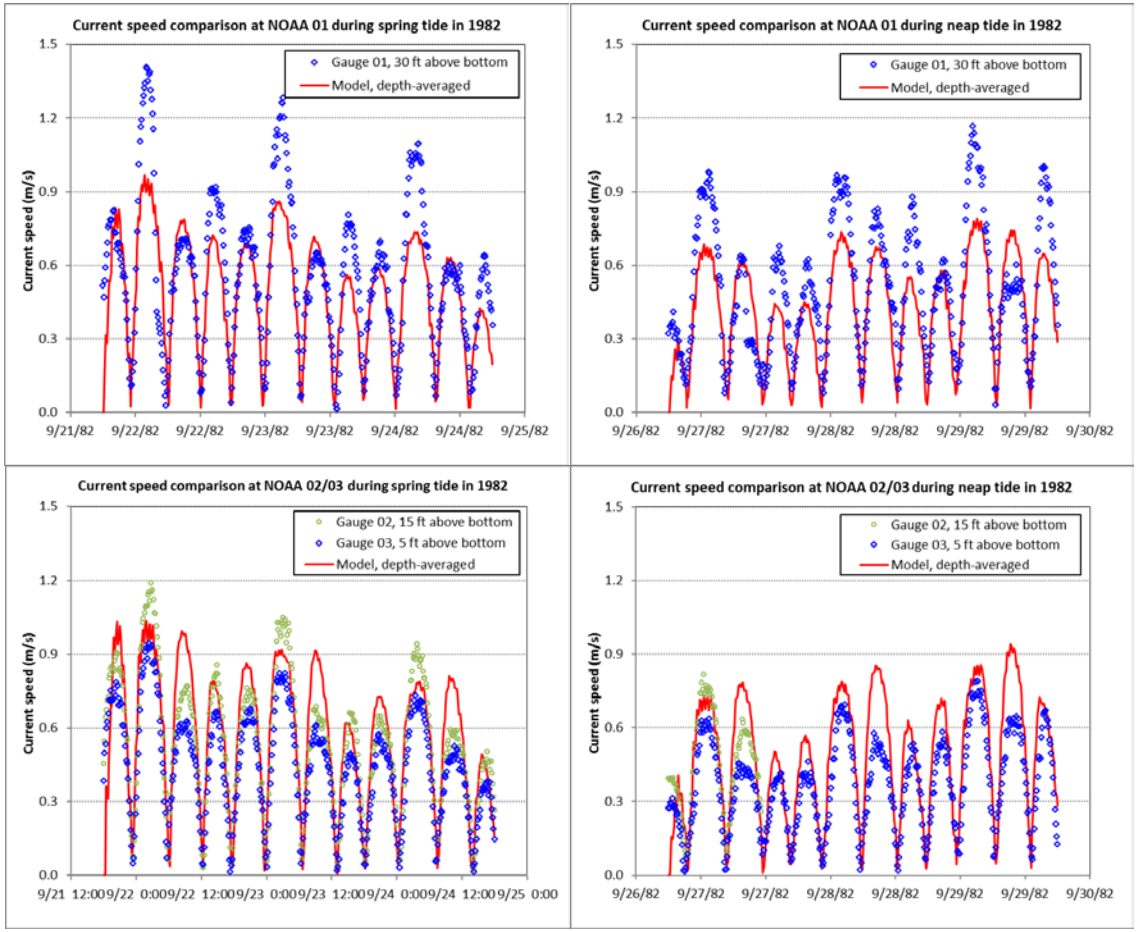

Figure 3-3
Current Speed Comparisons at NOAA Current Gauges 01 through 03

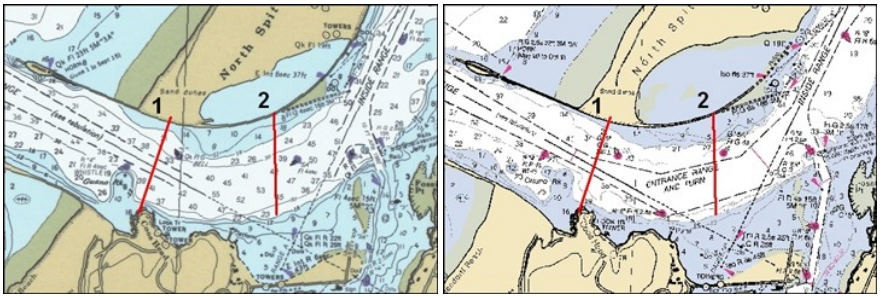

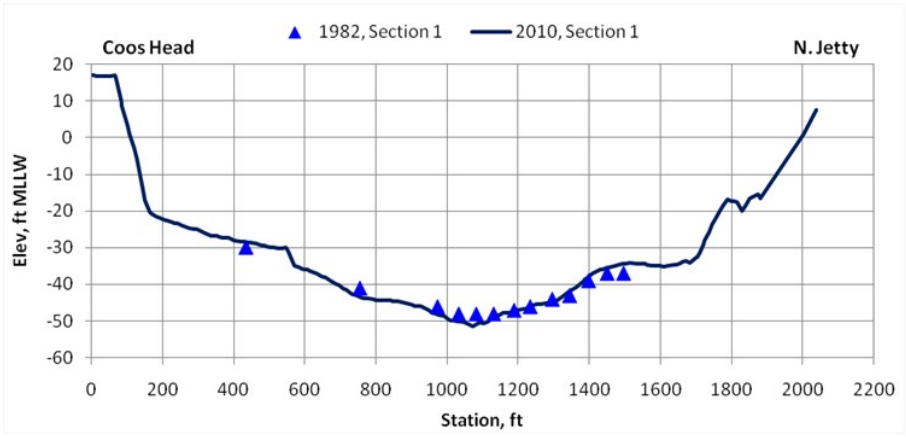

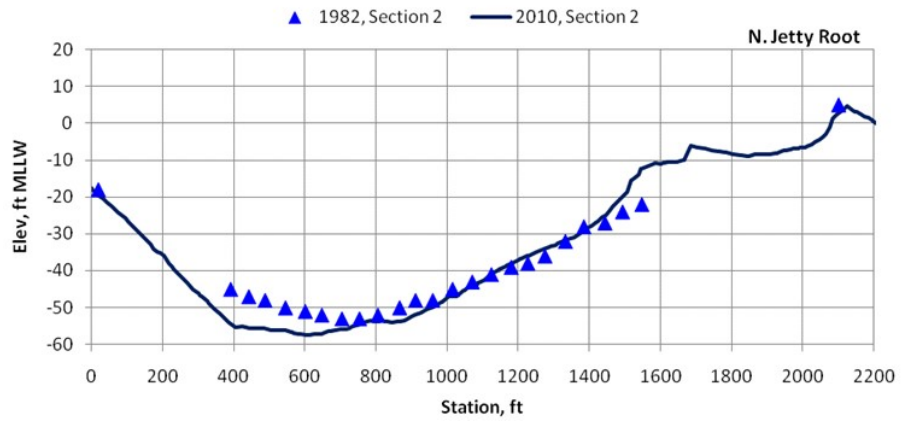

Figure 3-4
Entrance Channel Cross-Section in 1982 and 2010

3.2.1.2 Boundary Conditions

Boundary conditions for the hydrodynamic model are water levels and currents at the offshore boundary and freshwater inflows at the upstream boundaries.

The offshore water levels and currents were extracted from the OSU Tidal Data Inversion, specifically the TPXO8 global tidal solution with a resolution of 1/6° (Egbert & Erofeeva 2002).

The upstream freshwater inflows include the Coos River, the Haynes Inlet, the Kentuck & Willanch Sloughs, the Isthmus Slough, and the South Slough. Flows from the Coos River are based on discharge measured by Coos Watershed Association. For the sloughs, the runoff is estimated using rainfall-runoff analysis based on average seasonal precipitation (Black & Veatch 2006). These calculated values are based on monthly average precipitation for the same period. These discharges are much smaller than typical winter and spring discharges from the Coos River. The upstream freshwater boundary locations are presented in Figure 3-5. The time histories of freshwater inflows used in the model are provided in Figure 3-6.

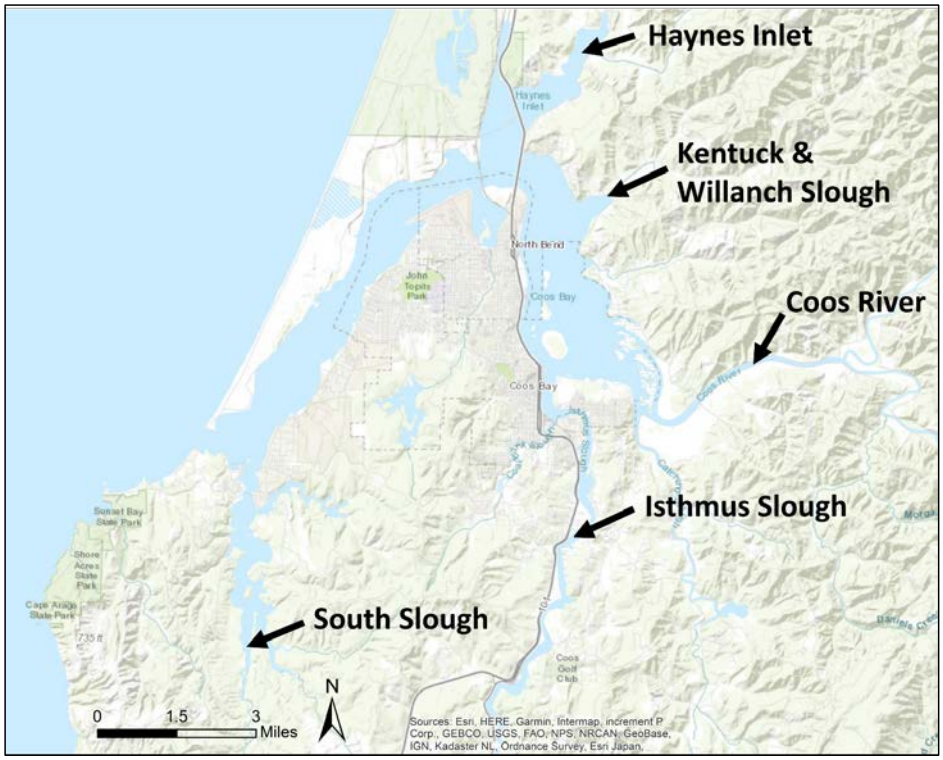

Figure 3-5
Upstream Freshwater Open Boundaries

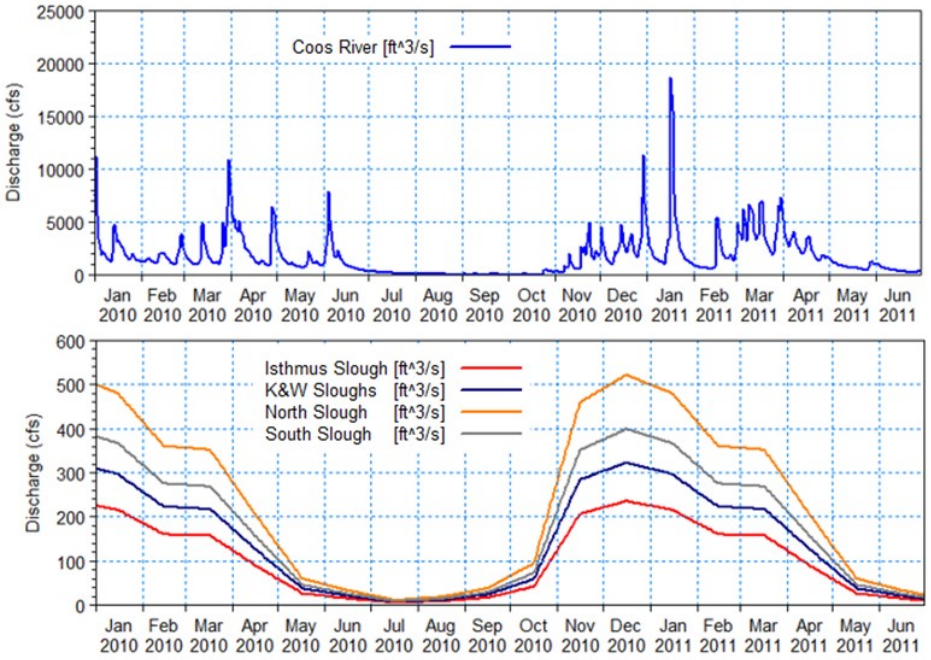

Figure 3-6
Upstream Freshwater Inflows from January 2010 to June 2011

3.2.1.3 Calibration Results

Figure 3-7 illustrates the observed and simulated currents during spring tide, as measured by DEA in March 2010 (DEA 2010). These comparisons are given at two locations – Mooring 2 between the jetties and Mooring 1 near the airport. The observed currents have been depth-averaged for this comparison.

At Mooring 2, the observed current matches the predicted current to within 25 percent. Deviations between the measured and modeled currents may be a result of wave effects. Except for one unusually high set of observed currents near the end of the set shown here, the fit between the observed and predicted currents at Mooring 1 is very close.

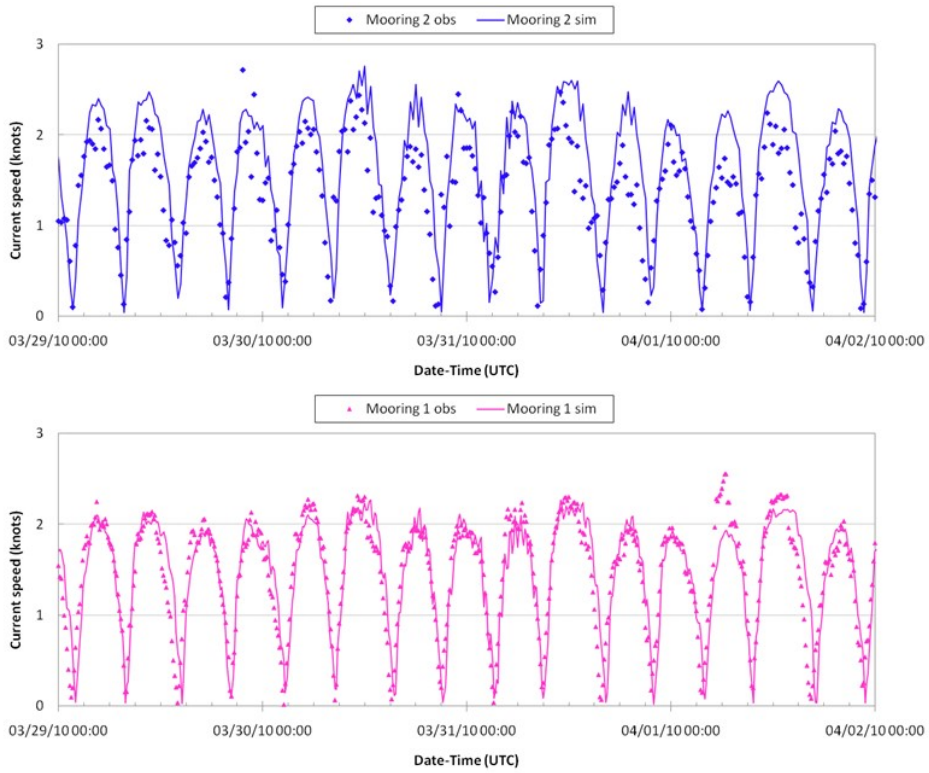

Figure 3-7
Observed and Simulated Current Measurements during Spring Tide

3.2.2 Results

Figure 3-8 and Figure 3-9 illustrate typical entrance currents for the Existing Conditions and the 2023 PA, respectively. Peak ebb tide, peak flood tide, and three high tide slack cases are shown. The reason for showing different high tide slack cases is to illustrate complex interactions between tides and waves at the entrance area. In some cases, there are essentially no currents; in others, the currents in the entrance can exceed 1 knot. Inside the LSB, tidal currents are small (e.g., less than 0.25 knots) throughout the tidal cycle.

Figure 3-10 illustrates the differences in current speed between the 2023 PA and the Existing Conditions. It shows that currents within the entrance channel are generally lower in the 2023 PA than in the Existing Conditions. Overall, the difference is less than 0.3 knots. Even the currents at the high tide slack Case 2 indicate an increase of 0.1 – 0.3 knots along the north jetty under the 2023 PA, the magnitude of current speed during the high tide slack is significantly lower than during ebb and flood tide. Therefore, this small increase in currents at high tide slack does not have the potential to cause erosion along the north jetty. In addition, no changes are noted in the LSB.

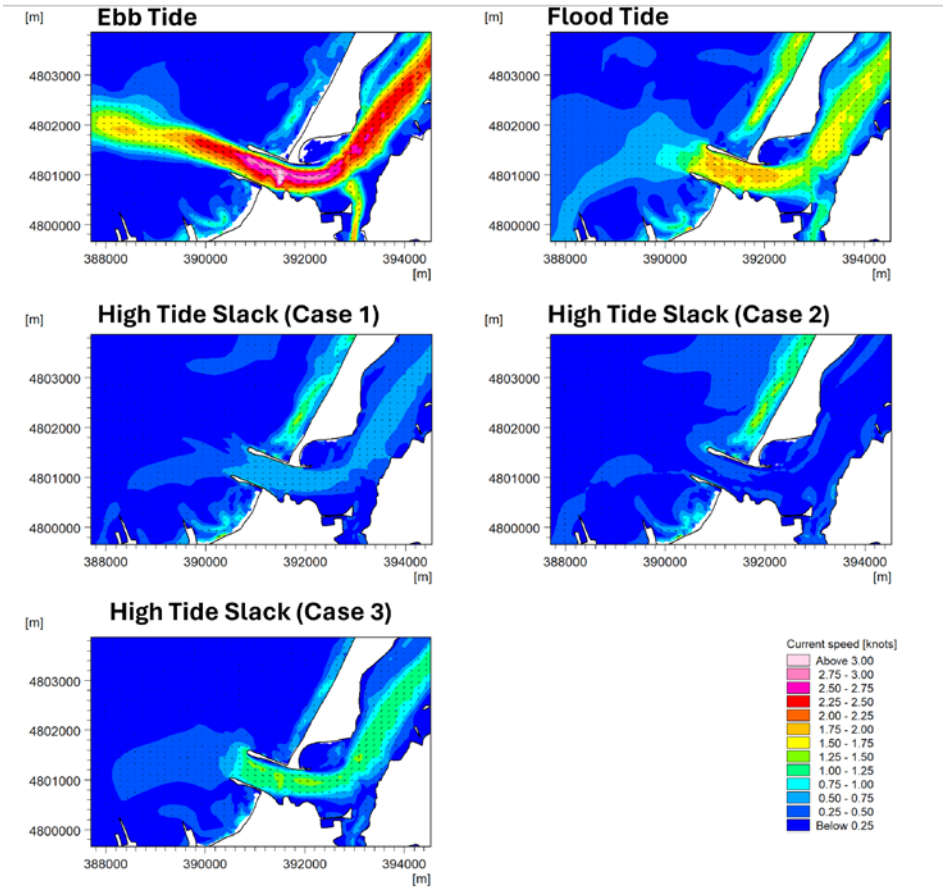

Figure 3-8
Entrance Currents throughout Tidal Cycle, Multiple High Tide Slack Cases Shown to Highlight Variability, Existing Conditions

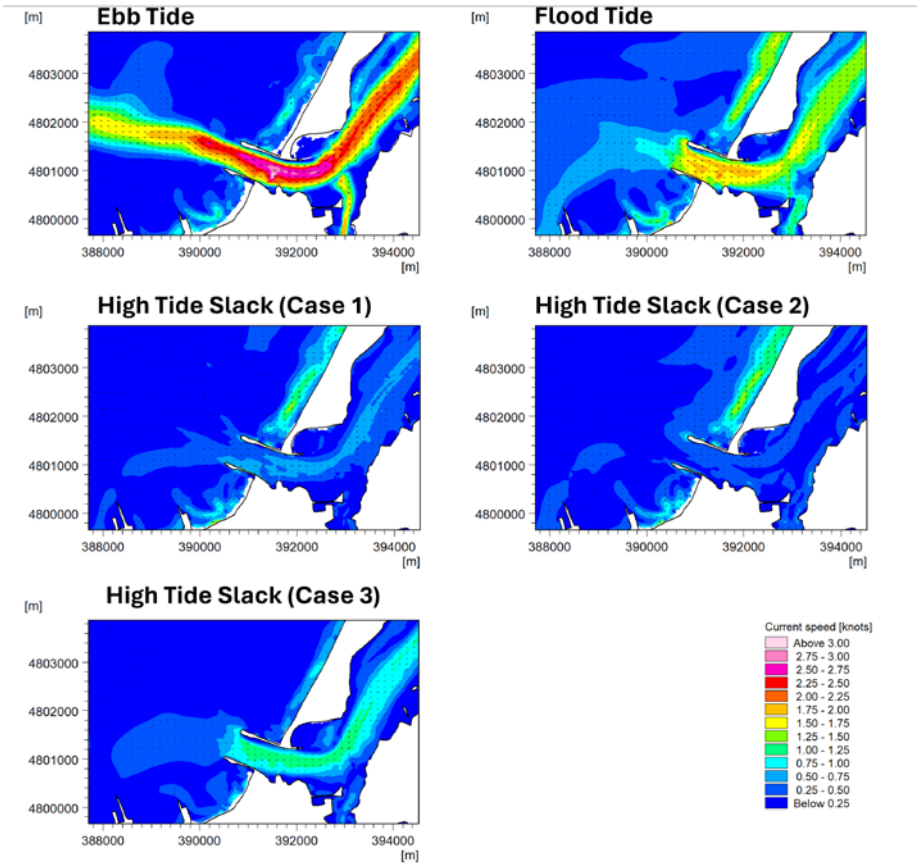

Figure 3-9
Entrance Currents throughout Tidal Cycle, Multiple High Tide Slack Cases Shown to Highlight Variability, 2023 PA

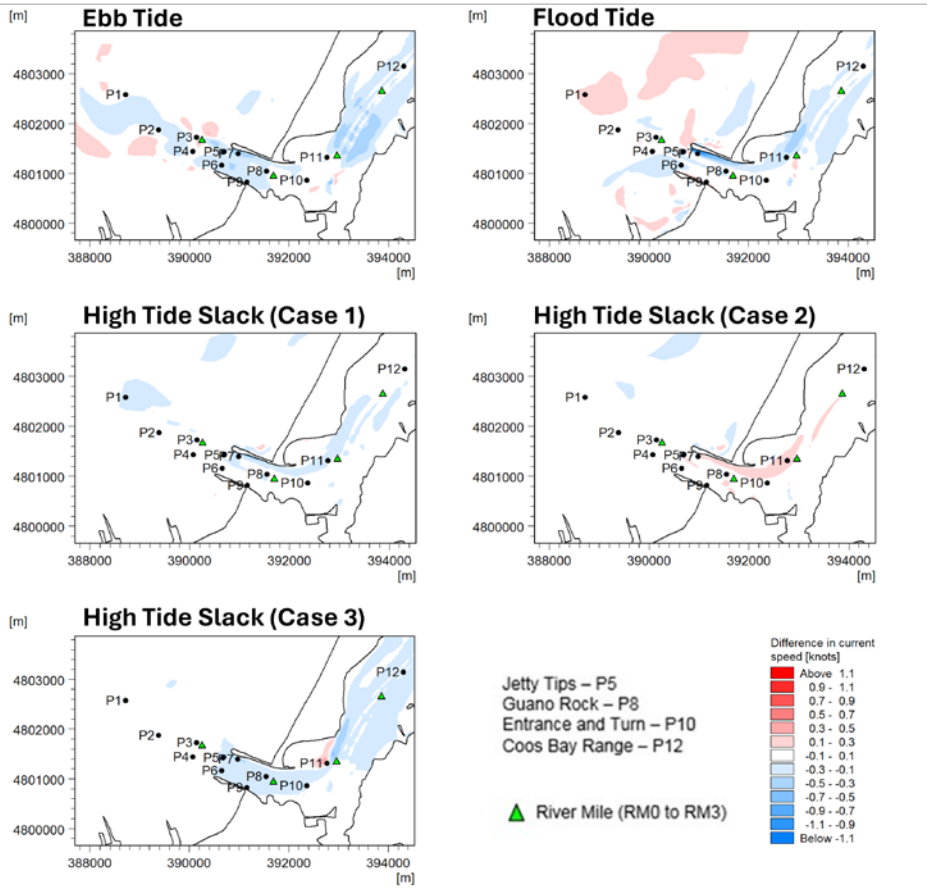

Figure 3-10
Difference Plots of Entrance Currents throughout Tidal Cycle (2023 PA minus Existing Conditions)

To illustrate current speed variations throughout the offshore and entrance area, 12 observation points were selected. Their locations, as well as the RM marks, are illustrated in Figure 3-10.

Figure 3-11 and Figure 3-12 show the percent of exceedance for current speeds at the 12 observation points under the Existing Conditions and the 2023 PA. The results indicate that the median current speed increases from the offshore locations (i.e., P1 though P4, less than 0.7 knots) to the entrance area between the jetty trunks (i.e., P5 through P9, 0.9 to 1.4 knots). The median speed then decreases into the inner channel (i.e., P10 through P12, 0.9 to 1.1 knots).

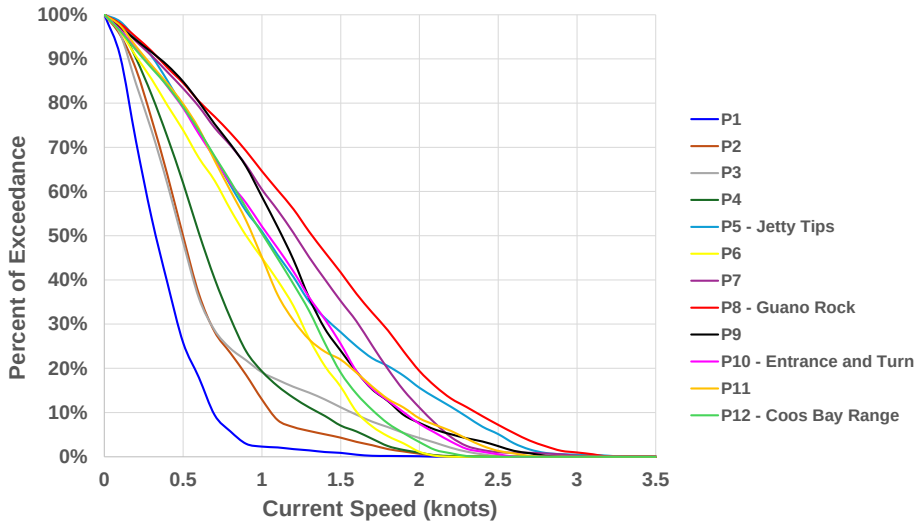

Figure 3-11
Percent of Exceedance of Current Speeds, Existing Conditions (Locations of P1 through P12 shown in Figure 3-10)

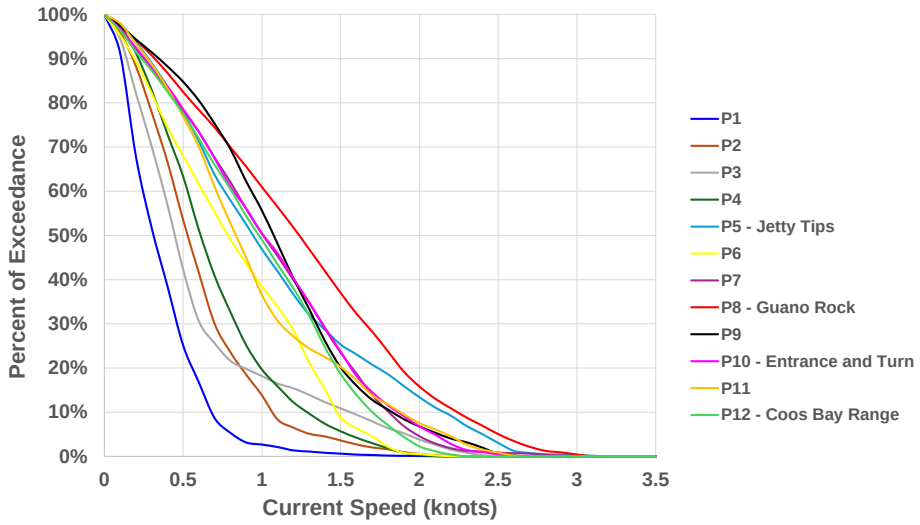

Figure 3-12
Percent of Exceedance of Current Speeds, 2023 PA (Locations of P1 through P12 shown in Figure 3-10)

Figure 3-13 and Figure 3-14 further compare the current speeds between the two scenarios. Except at P2 and P4, all other locations show a decrease in median current speed under the 2023 PA.

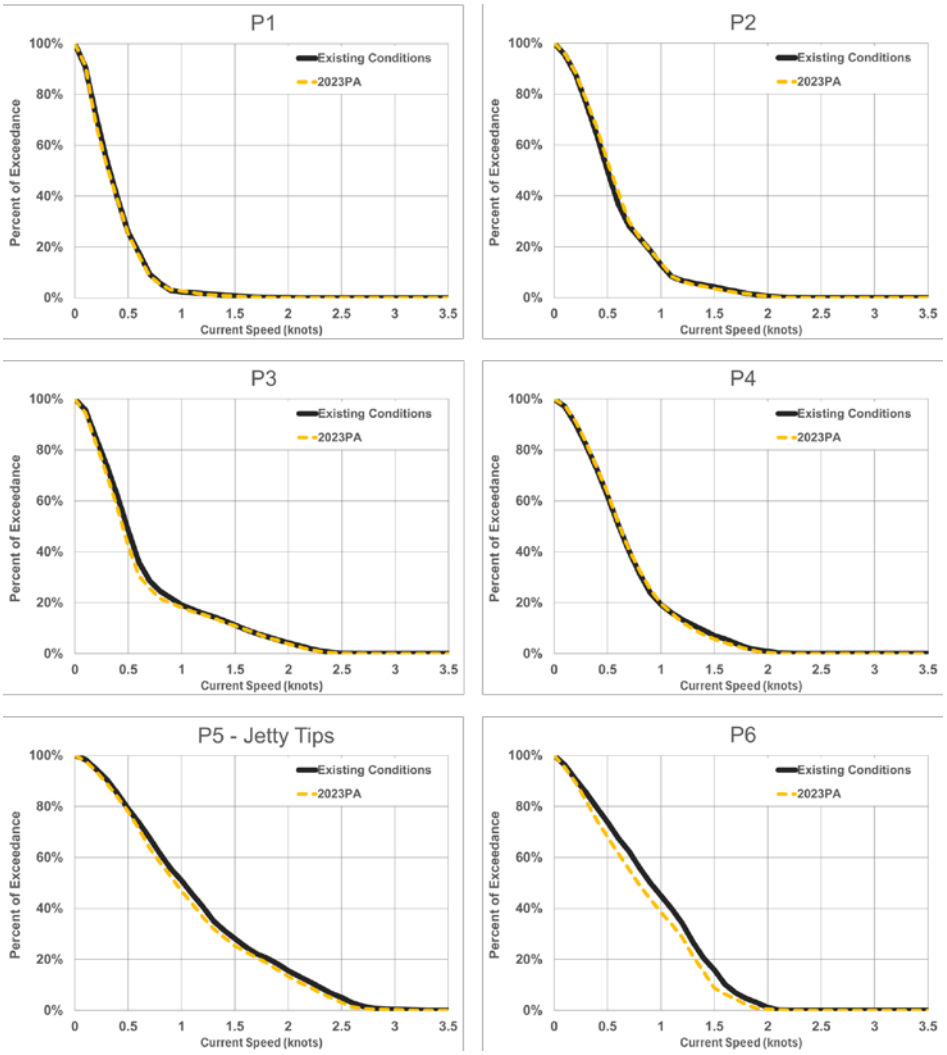

Figure 3-13
Comparison of Current Speeds: P1 through P6

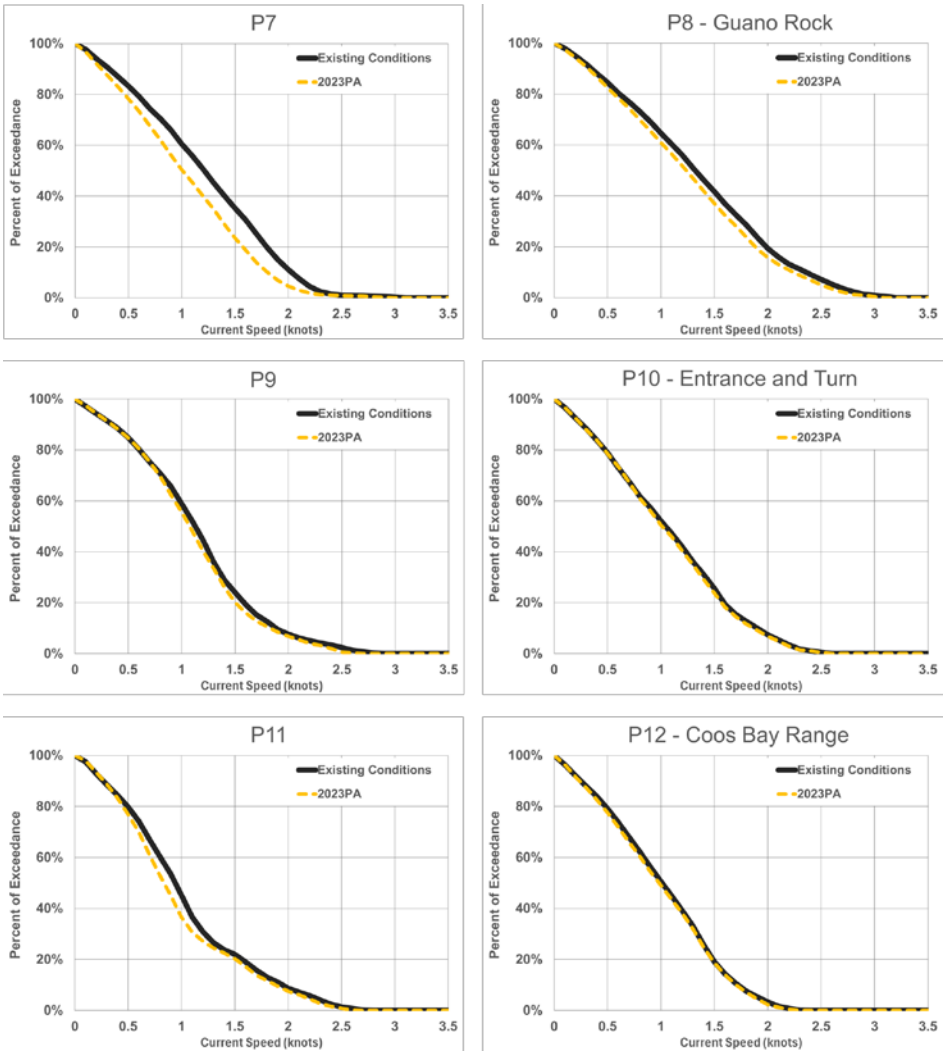

Figure 3-14
Comparison of Current Speeds between Model Scenarios: P7 through P12

Percent of exceedance for current speeds are summarized in Table 3-1 and Table 3-2 for the Existing Conditions and the 2023 PA, respectively. Each table lists the current speed that is exceeded 95, 75, 50 (i.e., the median value), 25, and 5 percent of the time. Table 3-3 presents the difference between the two model scenarios. Generally, the current speeds for the 2023 PA are

smaller than the Existing Conditions. Therefore, the 2023 PA is not expected to cause adverse impacts on channel morphology or jetty stability at the Coos Bay entrance area.

Table 3-1
Depth-Averaged Current Speeds, Existing Conditions

Percent of Exceedance	P1 (knots)	P2 (knots)	P3 (knots)	P4 (knots)	P5 - Jetty Tips (knots)	P6 (knots)
95%	0.07	0.11	0.11	0.14	0.19	0.12
75%	0.18	0.31	0.29	0.37	0.58	0.48
50%	0.32	0.50	0.49	0.61	1.01	0.90
25%	0.51	0.77	0.78	0.88	1.60	1.32
5%	0.82	1.41	1.93	1.64	2.50	1.78
Percent of Exceedance	**P7 (knots)**	**P8 - Guano Rock (knots)**	**P9 (knots)**	**P10 - Entrance and Turns (knots)**	**P11 (knots)**	**P12 - Coos Bay Range (knots)**
95%	0.17	0.20	0.18	0.14	0.16	0.13
75%	0.69	0.75	0.71	0.56	0.59	0.58
50%	1.21	1.32	1.13	1.04	0.94	1.01
25%	1.70	1.88	1.48	1.51	1.35	1.41
5%	2.19	2.62	2.21	2.13	2.24	1.91

Table 3-2
Depth-Averaged Current Speeds, 2023 PA

Percent of Exceedance	P1 (knots)	P2 (knots)	P3 (knots)	P4 (knots)	P5 - Jetty Tips (knots)	P6 (knots)
95%	0.08	0.11	0.10	0.15	0.17	0.11
75%	0.17	0.32	0.26	0.38	0.55	0.39
50%	0.31	0.53	0.45	0.61	0.95	0.79
25%	0.50	0.78	0.71	0.90	1.52	1.25
5%	0.81	1.32	1.92	1.55	2.40	1.68

Percent of Exceedance	P7 (knots)	P8 - Guano Rock (knots)	P9 (knots)	P10 - Entrance and Turns (knots)	P11 (knots)	P12 - Coos Bay Range (knots)
95%	0.13	0.18	0.18	0.14	0.16	0.13
75%	0.57	0.68	0.71	0.57	0.53	0.55
50%	1.01	1.24	1.08	1.01	0.84	0.98
25%	1.47	1.78	1.41	1.48	1.28	1.40
5%	1.98	2.50	2.13	2.10	2.17	1.87

Table 3-3
Difference in Depth-Averaged Current Speeds, 2023 PA Minus Existing Conditions

Percent of Exceedance	P1 (knots)	P2 (knots)	P3 (knots)	P4 (knots)	P5 - Jetty Tips (knots)	P6 (knots)
95%	0.00	0.01	-0.01	0.02	-0.02	-0.01
75%	-0.01	0.01	-0.03	0.01	-0.03	-0.09
50%	-0.01	0.03	-0.04	0.01	-0.06	-0.11
25%	0.00	0.00	-0.07	0.02	-0.08	-0.07
5%	-0.01	-0.09	-0.01	-0.09	-0.10	-0.10
Percent of Exceedance	**P7 (knots)**	**P8 - Guano Rock (knots)**	**P9 (knots)**	**P10 - Entrance and Turns (knots)**	**P11 (knots)**	**P12 - Coos Bay Range (knots)**
95%	-0.04	-0.02	0.00	0.00	0.01	-0.01
75%	-0.12	-0.07	0.00	0.00	-0.06	-0.03
50%	-0.20	-0.08	-0.05	-0.02	-0.11	-0.03
25%	-0.24	-0.10	-0.07	-0.03	-0.07	-0.01
5%	-0.21	-0.11	-0.08	-0.03	-0.07	-0.04

3.3 Extreme Waves

The study of extreme waves documents the potential effects of the navigation project on wave heights at the North and South Jetties, at the Charleston Breakwater, and within the Entrance Channel.

Numerical modeling of the offshore area and the Entrance Channel was used to quantify the effects of the proposed channel modification on wave propagation. This section presents the details of the numerical wave modeling study, including model methodology, setup, calibration, and results indicating how wave heights may change throughout the Coos Bay channel entrance under the Existing Conditions and the 2023 PA.

The purpose of this study is to identify how the 2023 PA effect wave propagation at Coos Bay. Therefore, the methodology assesses the propagation of measured offshore waves, instead of using artificial offshore conditions that correspond to extreme conditions. Offshore wave conditions include a wide range of wave heights, periods, and directions to investigate the full spectrum of wave propagation. Ultimately, the values presented herein are not recommended for design, but instead indicate how implementation of the proposed channels effect the wave climate.

3.3.1 Model Methodology

The numerical modeling analysis is composed of three steps. First, a set of wave conditions representing 79 storms events was selected from the available deep-water wave measurements for simulation. Second, a SW Model was developed to transform offshore storm conditions (wave spectra) for selected events to a depth of approximately 150 ft MLLW. Third, a high resolution BW Model was used to propagate waves from the computed spectra into the Coos Bay Entrance Channel. The BW Model incorporated the effects of water level and wave-current interactions, which can occur during storm events. From the modeling results, an extreme value analysis was performed to categorize extreme wave heights at the relevant locations at the Coos Bay entrance. The details of the selected storms and modeled scenarios are discussed in Section 3.3.4. The observations from offshore wave gauges (see Section 2.1.5) show the peak wave periods occur most frequently in the 6 to 16 second range. The waves with period less than 7 seconds have a low occurrence and do not lead to extreme conditions at the entrance jetties.

Commented [WQ3]: 10462086: Section 3.1, Bouss-2D model runs: Supplement the modeling plan to specify how waves have period shorter than 7 seconds will be addressed within the wave model.

(comment by Rod Moritz)

Commented [WQ4R3]: Response to DrChecks20230929 Comment ID 10462086.

Two different numerical models were used for this study:

- The SW Model was developed using the MIKE-21 Spectral Wave module by the Danish Hydraulic Institute (DHI 2016). The model is a third-generation spectral wind-wave model, and it is capable of simulating the growth, decay, and transformation of wind-generated waves and swells.
- The BW Model was developed using BOUSS-2D model by USACE (Nwogu & Demirbilek 2001). The model simulates the propagation and transformation of waves based on a time-domain solution of Boussinesq-type equations. Nearshore wave phenomena, such as wave shoaling, reflection, diffraction, wave breaking, wave-wave interaction, and wave-current interaction, are simulated. The BW Model is generally regarded as the best choice for high resolution detailed modeling of wave propagation in complex environments, which require accurate representation of non-linear wave-wave interactions, wave refraction over variable bathymetries, and diffraction around coastal structures.
- As noted above, models were approved by USACE for their respective uses.

3.3.2 Model Domain and Bathymetry

Two model domains were used in the wave analysis for the Coos Bay entrance. The MIKE-21 SW Model domain extends from depths of approximately 450 ft to the shoreline. The BOUSS-2D model domain starts at approximately 150 ft (45 m) contour line offshore and extends into Coos Bay to approximately RM 2.5 near Fossil Point.

The model bathymetry for both wave models was generated from the following sources:

- One-meter gridded Digital Terrain Model (DTM) created by DEA in the vicinity of the Coos Bay Federal Channel (OIPCB 2017d). The DTM is a composite of multiple existing data sets collected between 2007 and 2016. Figure 3-15 shows the data source of the DTM within the model domain. Both North Jetty and South Jetty have recent bathymetry data from the 2016 survey.
- At the North Jetty, the bathymetry from DTM was replaced by the design elevations from Coos Bay North Jetty Repair Major Maintenance project (USACE 2021).
- LSB and Charleston Marina are represented by the more recent USACE Lidar data from 2014.
- Within the dredged Entrance Channel, the bathymetry from DEA was supplemented by the navigation depths for two channel scenarios: 1) the Existing Conditions and 2) the 2023 PA. Advanced maintenance depth was added to the nominal depth for both scenarios. Detailed channel depths are provided in Section 1.4.
- Areas not covered by the DTM or the other sources named above, including the areas of the Pacific coast, offshore areas, and South Slough, are represented by data from nautical charts with interpretation aided by aerial photography.

The model domain includes a porosity layer around the North and south Jetties, commonly referred to as a “buffer zone”, this layer effectively dissipates wave energy similar to that of a rubble mound structure. The porosity layer is four nodes thick, consistent with typical modeling practice. In the vicinity of the jetties, the mesh spacing is approximately 50 ft; therefore, the porosity layer has a thickness of 200 ft.

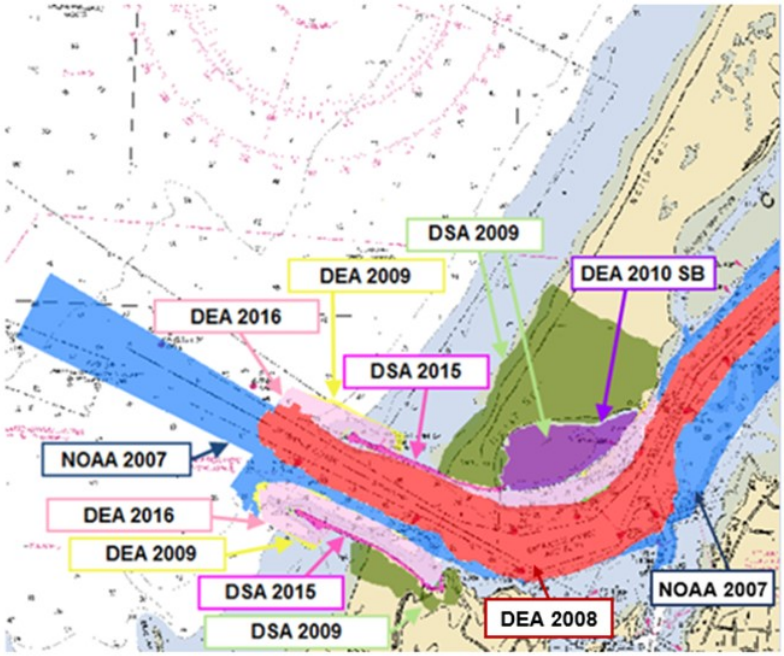

Figure 3-15
Data Sources Used for DTM

3.3.2.1 Offshore to Nearshore Spectral Wave Model

The MIKE-21 SW Model grid and bathymetry is shown in Figure 3-16. The model domain is similar to that used in the MMR (USACE 2012b), but further refined near the North and South Jetties. This flexible mesh has a total of 22,758 nodes and 43,497 elements. The model resolution varies from 1 km at offshore to a minimum of 15 m at the channel entrance. The yellow rectangle in Figure 3-16 shows the extent of the BW Model domain.

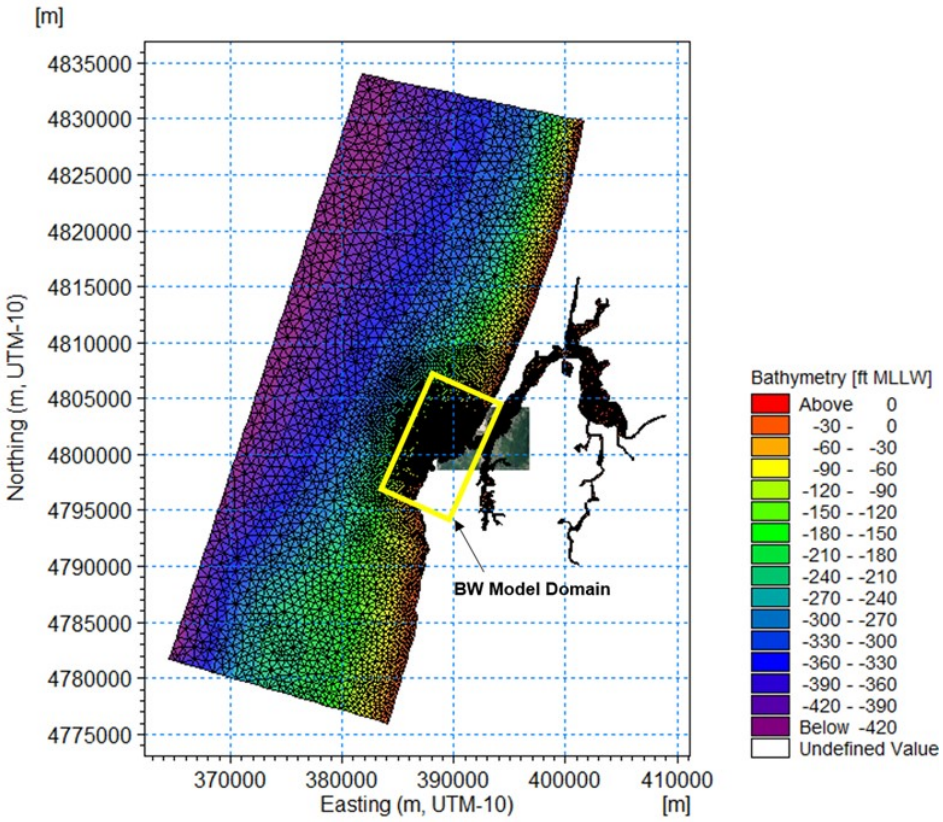

Figure 3-16
Offshore Spectral Wave Model Grid and Bathymetry

3.3.2.2 Channel Entrance BW Model

The BOUSS-2D model domain and bathymetry is shown in Figure 3-17. This local grid for the Coos Bay entrance is about 7.5 by 4.3 mi with 50-ft (15-m) grid resolution. The offshore boundary is parallel to the coastline and at a depth of 150 ft (45 m) MLLW. The grid covers the offshore area, including the jetties, and extends to the shorelines north and south of the jetties. The domain's along-shore extent is sufficient to propagate waves from all wave directions from southwest to northwest without adverse effects of the lateral boundaries. The Coos Bay estuary is included up to RM 2.5. LSB and the channel side of the Charleston Marina are also included in the domain.

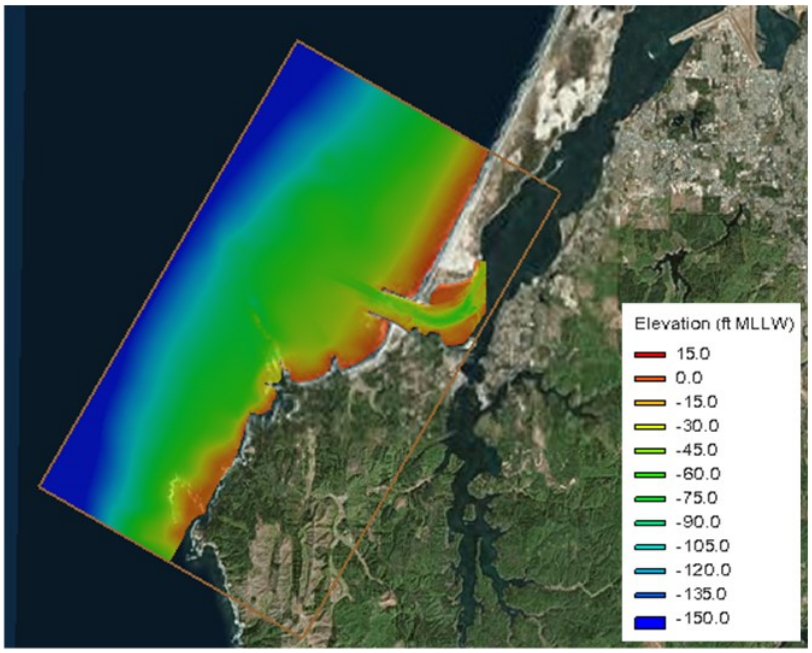

Figure 3-17
Entrance BOUSS-2D Model Domain and Bathymetry

Two model bathymetry variations were developed for the entrance wave modeling. Each grid represents one of the two following channel conditions:

- Existing Conditions
- 2023 PA

Table 3-4 lists the channel modifications that have been included in each model scenario. The difference between the Existing Conditions and the 2023 PA is the channel authorized depths. Both scenarios include the USACE North Jetty repair. Figure 3-18 presents a detailed view of the Entrance Channel for each model scenario. The differences among the scenarios are also illustrated in the figure.

Table 3-4
Differences in the Two Model Scenarios at the Entrance Area

Condition	Bathymetry	North Jetty Head	North Jetty Root	Log-spiral Bay
Existing Conditions	-37 ft MLLW FNC plus 1 ft AMD	USACE Repair	USACE Repair	Existing Bathymetry
2023 PA	-45 ft MLLW FNC plus 1 ft AMD	USACE Repair	USACE Repair	Existing Bathymetry

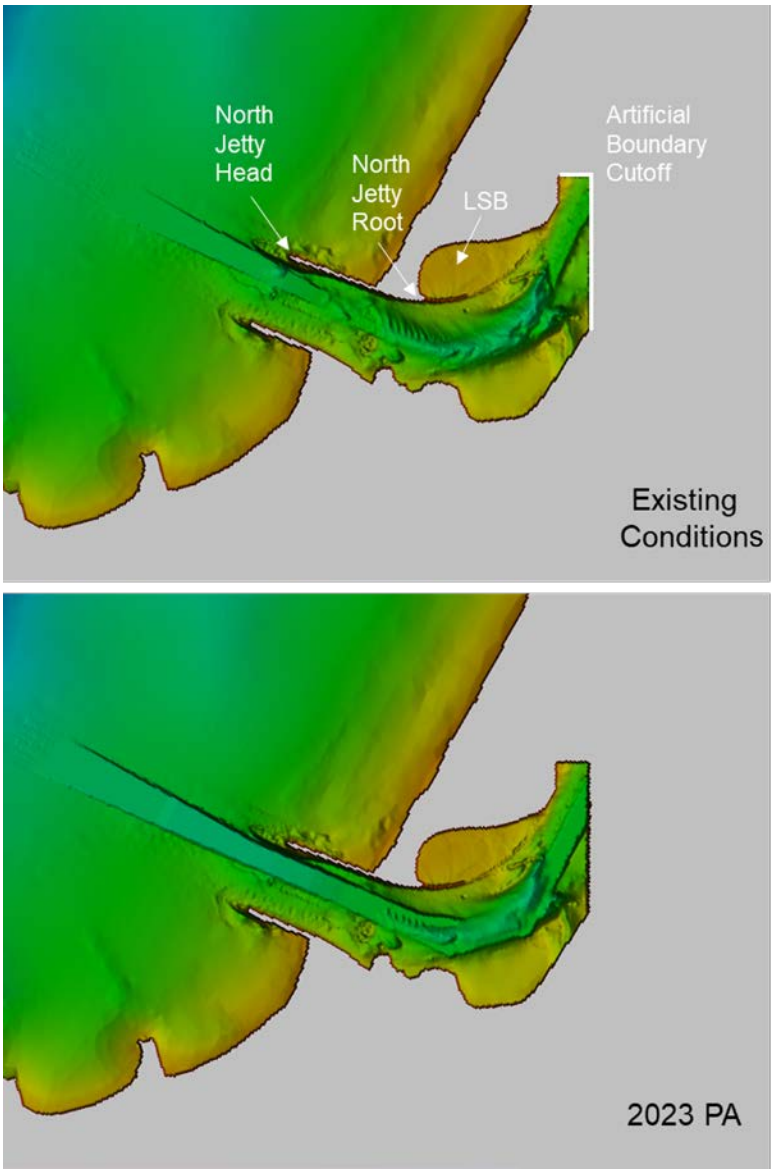

Figure 3-18
BOUSS-2D Wave Model Bathymetry at the Entrance

3.3.3 Model Calibration

The offshore model is forced by wave measurements at offshore CDIP Buoy 139p1, and measured winds from NDBC C-MAN station at Cape Arago (CARO3). Water levels that vary in time, but are constant over the domain, are applied in the model. Historical water level measurements from NOAA gauge at Charleston (Station 9432780) were used. Model parameters, such as wave breaking, white capping parameters, bottom roughness coefficient, and wind drag coefficient, were determined during the calibration process.

The offshore SW Model is calibrated based on DEA ADCP measurements during March and April 2010 (see Section 3.2.1). The offshore ADCP called "Mooring 3" is used for model calibration. A spring tide period is simulated from 3/28/2010 – 4/2/2010, while a neap tide period is represented by 4/5/2010 – 4/12/2010. The modeled waves at Mooring 3 are compared to the ADCP measurements during both periods; these comparisons are presented in Figure 3-19 and Figure 3-20. The measurements are shown in blue marks; the modeled results are shown in green lines; and the red dash lines show the modeling results from the preliminary MMR study (USACE 2012b). These figures demonstrate a good agreement between the SW Model and the measurements during neap tide period. The explanation to the under-estimation during spring tide period is: On March 31 and April 1, 2010, no corresponding high peaks found in offshore waves at model boundary. The offshore wave heights never exceed 5m during the two-day period, but 7 to 8 m waves were measured at Mooring 3. The peaks measured at Mooring 3 may be due to local wind effects at nearshore or false data in ADCP measurements. As the calibrated SW model was only used to force the BW model, such under-predictions possibly due to local effects would not have any impact to the modeled waves at the BW Model boundary.

The storm events used to determine impacts to the wave climate include offshore wave directions between 195°N and 330°N. The wave directions during the model calibration periods are within this range, so the calibration cases are considered valid for all directions.

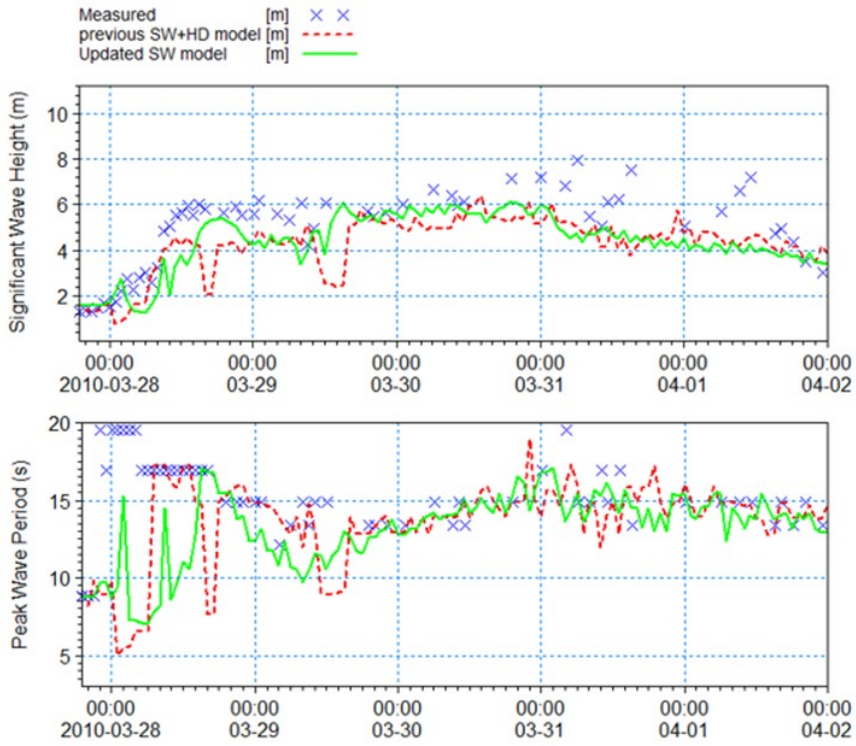

Figure 3-19
Modeled and Measured Waves at ADCP Mooring 3 during Spring Tide

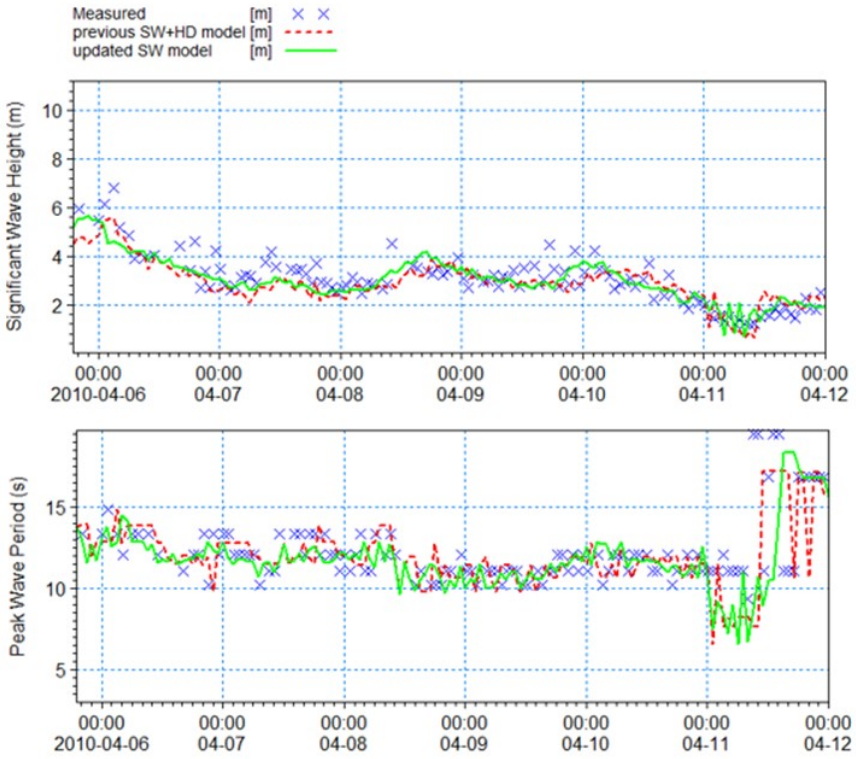

Figure 3-20
Modeled and Measured Waves at ADCP Mooring 3 during Neap Tide

The Boussinesq model is forced by time series of waves derived from wave spectra developed from the SW Model results, and it is verified with measurements at the two ADCPs - offshore Mooring 3 (offshore) and Mooring 2 (in the channel) – which can be seen in Figure 3-2. A number of BOUSS-2D runs with similar wave conditions as the measurements at Mooring 3 during neap tide were selected for calibration; the modeled waves at Mooring 2 were compared to the measurements at Mooring 2 for the for these same waves, effectively comparing the model's ability to transform waves from offshore to the Entrance Channel. Figure 3-21 shows that offshore waves with heights measured to be 3 to 4 m at Mooring 3 are transformed to wave heights of 1 m at Mooring 2. The observed wave periods were 10 to 14 seconds (shown within the green box). On the right, the resulted wave heights from BOUSS-2D at Mooring 2 match the 1 m height with little variation. Therefore, the BOUSS-2D entrance wave model is considered reasonable.

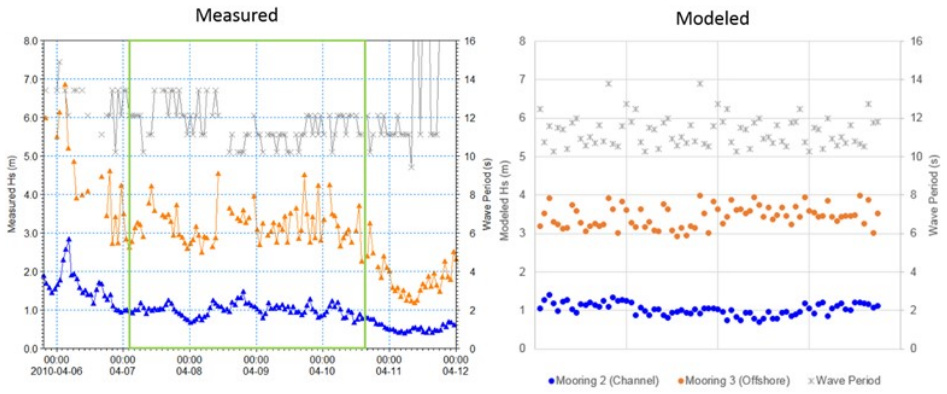

Figure 3-21
Comparison of Wave Transformation between Mooring 3 (Offshore) and Mooring 2 (Channel) for Measurements and BOUSS-2D Model

3.3.4 Model Scenarios and Setup

3.3.4.1 Selection of Storm Events

Storms are identified from the combined time series of CDIP buoys offshore of Coos Bay (see Figure 3-22). The CDIP buoys appear to be more suitable for characterizing waves at Coos Bay than the Port Orford NDBC buoys, based on water depth and proximity. Storms were selected as events having the largest 0.05 percent of significant wave heights at the buoy. A total of 79 storm events were selected from the available CDIP wave measurements (2005 to 2016). Eight events are from CDIP Buoy 126p1 and 71 events are from CDIP Buoy 139p1. The storm event with highest waves occurred on December 10, 2015 with a significant wave height of 37 ft (11.3 m) from the west (270°N). The incoming wave direction of the 79 storms ranges from 330°N (northwesterly) to 195°N (southwesterly); peak wave periods vary from 10 seconds to 20 seconds. As noted above, the selection of offshore storm waves covers a wide range of offshore wave characteristics in order to assess the effects of the 2023 PA on wave propagation under various conditions. Figure 3-23 presents percentage occurrence of all measured waves versus only the storm waves at CDIP Buoy 139p1. The prevailing wave directions are from the west through NW, whereas the largest storm waves tend to come from the SSW, west, and WNW directions.

Table 3-5 tabulates the offshore wave conditions of the 79 storm events, including time, significant wave height, peak period, mean wave direction, and surge. The representative wave conditions under MHHW at BOUSS-2D model boundary are included as well.

The 79 storms representing offshore wave conditions were identified from 11-year measurements. In the BOUSS-2D wave model, each storm has been simulated with four tidal conditions: MLLW, MHHW, MSL with maximum ebb currents, and MSL with maximum flood currents. Assuming equal probability of the four tidal conditions and same offshore statistics over long period of time, the combined equivalent duration of observations for the total modeled 316 storms is approximated as 44 years. This approach was based on USACE evaluation of the Mouth of the Columbia River (MCR) Jetty System (USACE 2012c) and recommended by USACE for use on this project. As

discussed in Section 3.3.5, this duration is used to estimate return periods of evaluation. By using a synthetic record of 44 years, the maximum wave heights of the simulated wave heights will nearly reflect a 50-year wave height. Since a 50-year wave height is specified by USACE design documents, showing the effects of such a storm provides an adequate level of conservatism for assessment of physical effects associated with project alternatives. Moreover, this approach is acceptable for this effort, which aims to estimate how the project would alter the existing wave conditions versus design of new infrastructure.

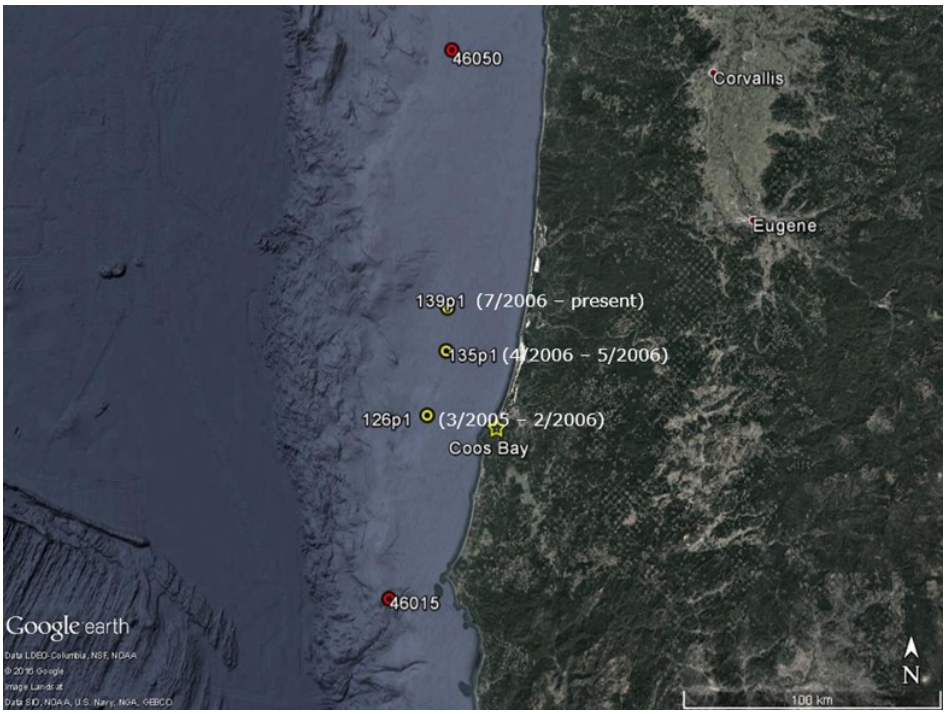

Figure 3-22
Locations of CDIP Buoys near Coos Bay

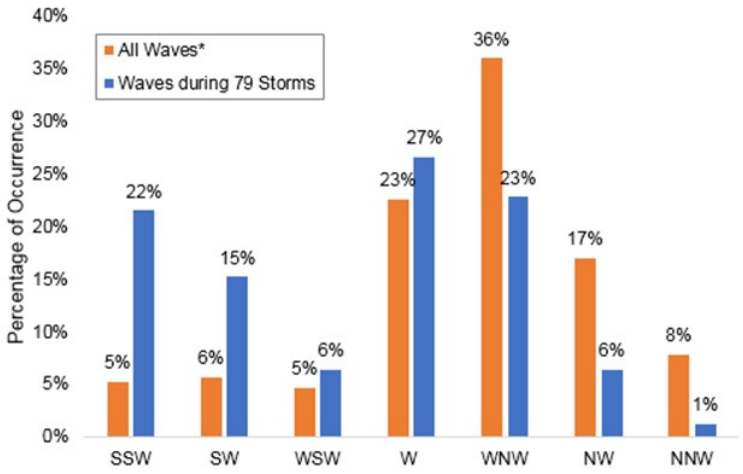

Figure 3-23
Offshore Wave Direction Distribution

Table 3-5
Wave Conditions of 79 Selected Storms (2005 – 2016)

Storm Peak Time	Offshore				BOUSS-2D Boundary		
	Hs[1] (ft)	Tp[2] (s)	MWD[3] (°N)	Surge (ft)	Hs (ft)	Tp (s)	MWD (°N)
03/20/2005 06:59 PM	21.6	11.1	229	1.8	16.8	12.5	244
12/21/2005 03:58 AM	24.1	16.7	232	1.5	17.7	17.1	253
12/27/2005 12:58 PM	25.7	20.0	279	1.6	22.4	20.2	264
12/28/2005 05:58 AM	24.9	18.2	293	2.1	19.9	16.1	264
12/30/2005 08:58 AM	28.0	10.5	220	2.6	22.9	11.1	251
01/01/2006 03:58 PM	25.7	10.5	204	2.9	18.6	10.8	237
01/04/2006 06:28 AM	28.6	18.2	273	1.7	25.5	18.2	278
01/05/2006 08:28 PM	24.8	14.3	246	1.9	20.7	14.7	261
11/13/2006 03:34 AM	32.7	11.8	200	1.4	22.1	11.6	237

Storm Peak Time	Offshore				BOUSS-2D Boundary		
	Hs[1] (ft)	Tp[2] (s)	MWD[3] (°N)	Surge (ft)	Hs (ft)	Tp (s)	MWD (°N)
11/16/2006 02:04 AM	23.4	9.9	217	1.2	18.3	10.3	240
12/12/2006 12:36 AM	25.6	15.4	286	1.8	23.6	15.3	273
12/14/2006 02:06 AM	28.5	16.7	279	1.3	25.7	17.2	282
12/14/2006 11:06 PM	24.1	14.3	276	1.7	20.7	14.4	253
12/21/2006 01:36 PM	25.2	15.4	273	1.3	23.2	15.4	272
12/27/2006 07:06 PM	24.1	12.5	315	1.5	21.7	12.7	315
02/27/2007 01:35 PM	24.6	13.3	288	1.7	22.0	12.8	280
03/27/2007 12:35 PM	24.9	13.3	294	1.0	22.7	13.7	296
10/18/2007 02:33 PM	23.0	9.9	197	1.1	17.3	11.5	241
11/12/2007 07:33 PM	26.3	10.5	215	0.6	21.8	11.2	251
12/03/2007 01:03 PM	34.0	14.3	207	1.8	23.8	14.0	238
01/05/2008 06:03 AM	30.8	16.7	248	2.6	26.2	16.9	259
01/08/2008 02:03 PM	23.5	11.8	203	1.9	17.8	11.4	233
01/09/2008 09:33 PM	23.3	16.7	295	1.4	21.2	15.7	293
01/30/2008 08:02 PM	23.0	16.7	321	1.0	21.0	15.6	300
02/01/2008 09:02 AM	27.1	18.2	291	1.4	24.7	17.8	293
12/13/2008 11:25 AM	27.5	13.3	304	1.0	25.0	13.1	306
12/25/2008 08:55 PM	26.9	16.7	310	1.5	24.8	16.8	301
02/11/2009 02:25 PM	22.6	15.4	288	1.4	19.6	15.5	285
11/06/2009 08:10 PM	22.9	16.7	289	0.5	21.2	16.9	285

Storm Peak Time	Offshore				BOUSS-2D Boundary		
	Hs[1] (ft)	Tp[2] (s)	MWD[3] (°N)	Surge (ft)	Hs (ft)	Tp (s)	MWD (°N)
11/07/2009 02:10 PM	22.6	18.2	289	0.7	20.6	17.4	289
11/17/2009 07:10 AM	29.1	11.8	233	0.8	23.7	11.6	249
11/22/2009 07:10 AM	26.3	9.9	204	1.1	18.3	10.4	233
01/02/2010 01:40 AM	22.9	16.7	272	1.5	21.1	16.0	270
01/12/2010 05:10 AM	22.6	11.8	234	1.6	18.0	11.8	246
01/18/2010 08:40 AM	27.3	14.3	244	2.4	23.0	13.8	251
01/25/2010 01:40 PM	27.0	16.7	271	1.9	25.2	17.0	267
02/13/2010 01:10 PM	27.4	16.7	262	1.2	23.7	16.7	274
02/14/2010 09:10 AM	24.8	18.2	280	1.4	21.7	18.4	274
03/12/2010 07:40 AM	26.7	16.7	292	1.9	21.8	16.9	268
03/17/2010 01:10 AM	23.5	15.4	271	0.9	20.7	15.0	271
03/29/2010 01:10 PM	22.7	11.8	248	1.7	17.9	12.0	252
04/03/2010 05:40 AM	25.1	14.3	302	1.5	23.0	14.7	291
10/25/2010 07:40 AM	26.6	15.4	278	1.0	23.8	15.4	277
11/02/2010 08:10 AM	22.4	18.2	282	0.6	21.0	18.7	283
11/23/2010 08:40 AM	22.6	12.5	330	0.4	20.8	12.3	319
11/30/2010 09:10 PM	23.7	10.5	221	0.4	17.5	10.9	242
02/14/2011 07:10 PM	23.2	10.5	202	1.1	16.7	10.6	232
02/28/2011 04:40 PM	24.4	9.9	238	1.1	20.3	9.8	265
03/02/2011 12:40 PM	24.0	11.1	206	1.5	17.6	11.0	230

Storm Peak Time	Offshore				BOUSS-2D Boundary		
	Hs[1] (ft)	Tp[2] (s)	MWD[3] (°N)	Surge (ft)	Hs (ft)	Tp (s)	MWD (°N)
03/14/2011 07:10 PM	25.8	15.4	261	1.2	23.2	15.1	264
11/22/2011 05:54 AM	22.6	10.5	201	0.6	17.0	10.7	235
11/23/2011 04:54 AM	23.5	9.9	223	1.3	18.5	11.6	243
11/30/2011 02:54 PM	23.8	14.3	299	-0.4	22.8	14.2	297
01/18/2012 03:54 PM	26.5	11.1	198	1.2	18.3	10.8	231
01/22/2012 05:54 PM	25.8	9.9	198	1.8	18.5	13.8	247
02/18/2012 07:24 PM	22.5	15.4	296	0.5	20.0	15.0	294
02/25/2012 08:24 PM	25.1	14.3	296	0.4	22.6	14.3	298
03/12/2012 09:54 PM	32.1	11.8	206	1.8	24.2	11.8	247
11/19/2012 10:22 PM	27.7	10.5	212	1.2	20.5	10.7	240
12/04/2012 10:22 AM	25.9	11.1	195	1.8	17.8	10.5	230
12/17/2012 12:22 PM	27.0	13.3	281	1.8	25.7	13.3	280
12/20/2012 06:52 AM	28.5	11.8	229	1.7	20.9	11.6	240
01/12/2014 05:22 AM	31.5	16.7	284	0.9	29.2	16.5	279
04/20/2014 07:29 AM	23.4	14.3	279	0.6	21.1	14.8	282
10/25/2014 06:59 PM	28.5	12.5	206	1.6	17.9	12.8	241
12/10/2014 08:29 PM	23.6	15.4	272	2.1	17.6	14.9	257
12/11/2014 09:59 PM	30.2	13.3	227	2.4	22.5	13.0	244
12/20/2014 12:59 PM	23.0	16.7	281	1.7	19.6	16.7	277
02/06/2015 10:59 AM	22.4	11.8	198	2.2	15.0	11.8	233

Storm Peak Time	Offshore				BOUSS-2D Boundary		
	Hs[1] (ft)	Tp[2] (s)	MWD[3] (°N)	Surge (ft)	Hs (ft)	Tp (s)	MWD (°N)
12/06/2015 03:05 AM	23.0	11.8	218	1.6	17.4	11.8	236
12/07/2015 07:35 AM	28.4	16.7	270	1.7	23.8	17.1	264
12/10/2015 09:05 PM	37.0	18.2	271	2.8	33.8	18.4	277
12/13/2015 10:05 AM	24.0	14.3	292	2.0	22.0	14.8	289
12/14/2015 12:35 PM	23.5	13.3	296	1.7	21.7	12.7	306
12/21/2015 09:05 PM	24.4	11.1	278	2.5	20.7	11.5	276
12/23/2015 11:35 PM	27.0	15.4	306	2.3	25.5	15.1	299
03/10/2016 03:35 AM	27.0	9.9	202	1.9	19.7	10.8	241
03/13/2016 05:05 PM	24.7	14.3	268	3.0	21.5	14.1	264
04/14/2016 04:35 PM	24.4	14.3	271	1.8	21.4	14.5	271

1 – significant wave height;

2 – peak wave period;

3 – mean wave direction at peak period from North.

3.3.4.2 Water Levels

In the SW Model, each storm was simulated at three water levels: MHHW, MSL, and MLLW.

In the BOUSS-2D model, four simulations were performed for each storm. The four conditions included: 1) tidal water level at MHHW with observed storm surge; 2) tidal water level at MLLW with observed storm surge; 3) tidal water level at MSL with observed storm surge and peak ebb current; and 4) tidal water level at MSL with observed storm surge and peak flood current.

Storm surge/non-tidal residual water level values were derived from the measured water levels at Charleston (NOAA Station 9432780) for each storm. Storm surge was determined as the maximum residual water level within an 18-hour window (12 hours before and 6 hours after the storm peak). There is not a strong correlation between significant wave height and surge values (see Figure 3-24 – correlation coefficient is only 0.34). In fact, residual water levels can be negative when wind is blowing from northern directions during the storm. Due to this lack of correlation, the various storms were modeled with their measured residual water level – therefore, the wave modeling considered a broad range of residual water levels.

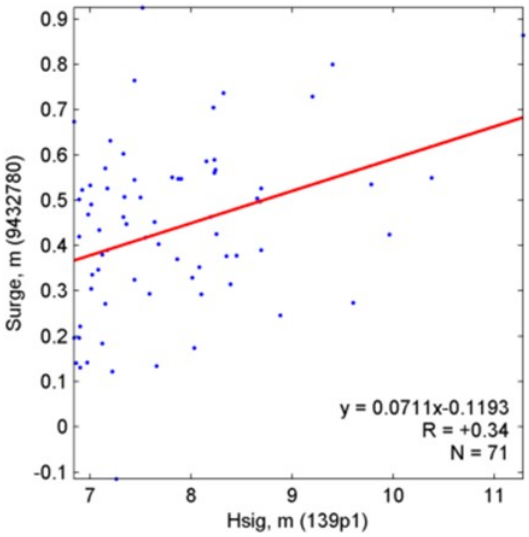

Figure 3-24
Correlation between Measured Storm Surge and Significant Wave Height

Figure 3-25 includes the measured surges of all 79 storms computed from the historical measurements at Charleston (NOAA Station ID 9432780) from 2005 to 2016. The surges vary from -0.4 ft (-0.1 m) up to around 3 ft (0.9 m). Each surge is added to high/middle/low tide levels and applied to its corresponding storm event.

Future SLC were also considered in the modeled water levels. The SLC impacts to the wave conditions at the jetty entrance are evaluated in Section 3.3.7.

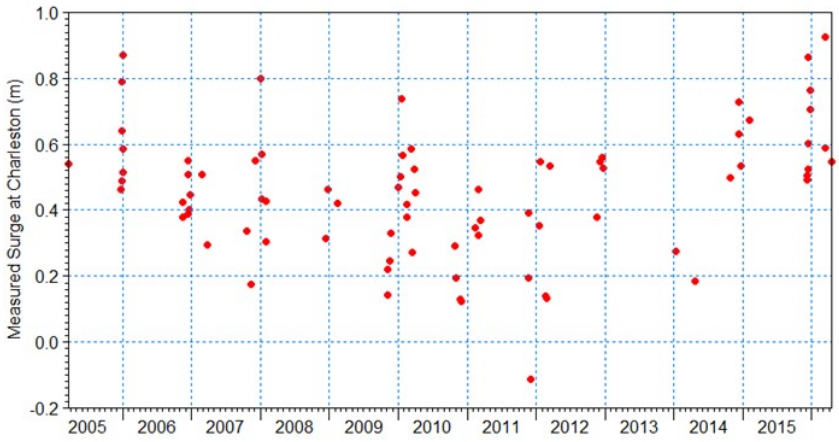

Figure 3-25
Measured Surges at Charleston (NOAA Station ID 9432780)

3.3.4.3 Currents

Model results indicate that maximum flood and ebb tidal currents generally occur close to mid-tide level. These currents are obtained from the regional hydrodynamic model (Section 3.2). Typical tide conditions were simulated for a full month to cover a neap-spring cycle. The period of August 2009 was chosen as the typical month because its computed tidal datums are close to the long-term NOAA tidal datums at Charleston (Table 3-6).

Figure 3-26 shows the modeled currents in the Entrance Channel. Larger tidal currents occur during spring tides. Both conditions show current velocities above 2 knots (3.4 ft/s) at Mooring 2. The selected tidal phases for the maximum tidal flood and ebb currents are circled in the figure. These are purely tidal currents without effect of freshwater inflows. Because significant freshwater discharges may not necessarily coincide with the peak of the storms, their effects are not included in this wave study. Effects of wind- and wave-induced currents are not included as well.

The spatial variation of the current fields associated with the maximum flood and ebb conditions are included in Figure 3-27. As expected, currents in the Entrance Channel are stronger due to the sudden change of flow restrictions. Tidal current speeds decrease dramatically in the open ocean just outside the Entrance Channel. These two tidal current fields were applied as model boundary conditions associated with the mid-tide level.

Commented [WQ5]: 10462087: Section 3.2.2 Currents (and Section 3.2.3 Water Levels): Supplement the modelling report to specify that the correct tidal phase for tide stage and associated tidal current will be imposed as needed for wave model boundary conditions.

(comment by Rod Moritz)

Commented [WQ6R5]: Revised texts to respond to DrChecks20230929 Comment ID10462087.

Table 3-6
Comparison of Tidal Datums for the Typical Period

Datum	Charleston, Long-term	Annual, 2009	August 2009
MHHW (ft)	7.62	7.61	7.59
MHW (ft)	6.96	6.87	6.80
MLW (ft)	1.27	1.27	1.27
MLLW (ft)	0.00	-0.09	-0.01

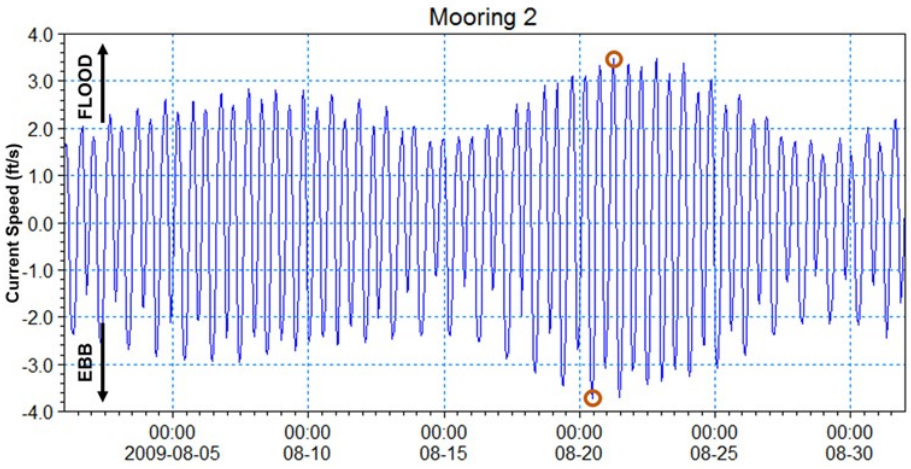

Figure 3-26
Simulated Tidal Currents at the Inlet (Mooring 2) for the Typical Period
(The selected max ebb and flood current moments are marked with circles)

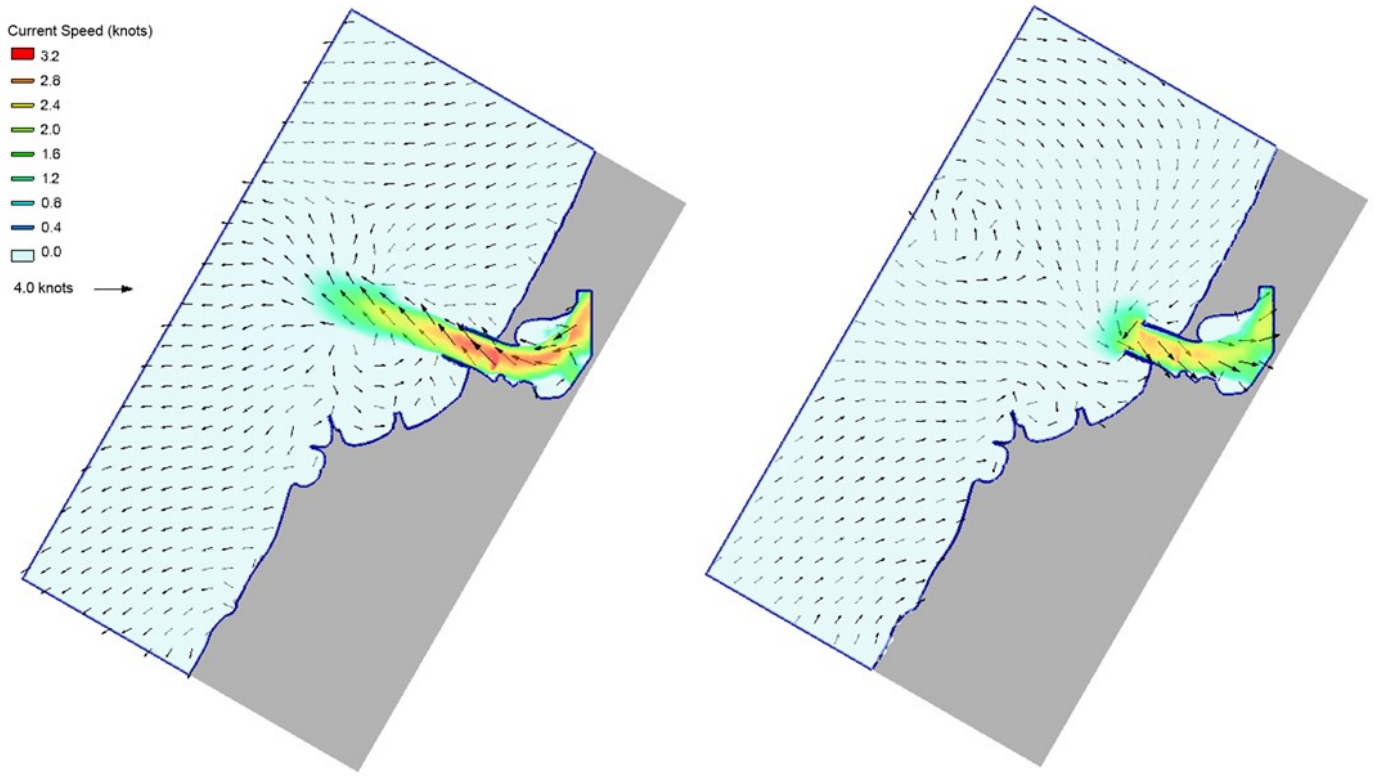

Figure 3-27
Maximum Flood (Left) and Ebb (Right) Current Fields Applied in the BOUSS-2D Model

3.3.4.4 Wave Boundary Conditions

Directional spectra of storm waves were output from the MIKE-21 SW Model at the -150 ft MLLW contour and used to force the BOUSS-2D wave model. Forcing the model with directional spectra instead of bulk parameters (such as significant wave height, mean wave direction, and peak period) ensures accurate representation of storm wave field. Figure 3-28 shows plots of wave spectra for four sample storms representing waves from the southwest, west, NW, and storms with a dual-peaked directional spectrum. The offshore incoming wave directions for the 79 storms range from 195°N to 330°N. The peak wave periods are between 10 seconds and 20 seconds. The wave spectra from MIKE-21 SW Model are output on a logarithmic frequency interval and was re-interpolated to uniform frequency bins and then adjusted to achieve equivalent total wave energy in BOUSS-2D.

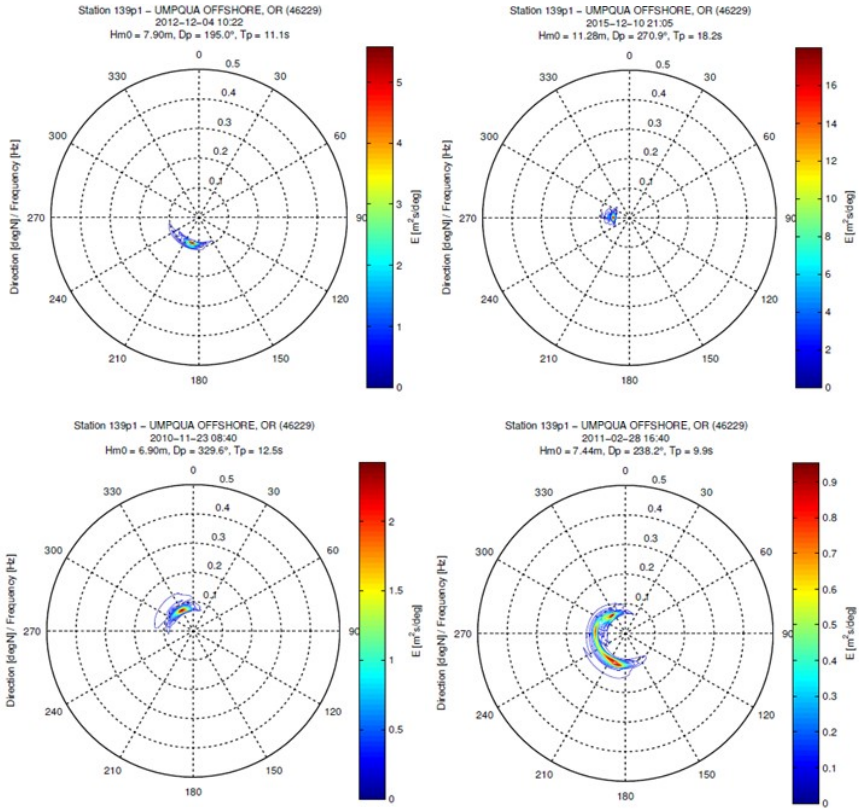

Figure 3-28
Directional Spectra of Storm Peaks at the Boussinesq Model Boundary (Upper Left – Storm 60 Southwesterly Waves; Upper Right – Storm 72 Westerly Waves; Lower Left – Storm 45 Northwesterly Waves; and Lower Right – Storms with dual peaks)

3.3.4.5 Model Scenarios

This section summarizes the modeled scenarios.

Offshore Spectral Wave Model

The offshore SW Model simulated a total of 79 storms with variations of tidal levels (MLLW, MSL, and MHHW) plus observed surges. To provide boundary conditions for the BW Model, the directional wave spectrum from each model run was output at a depth of approximately 150 ft MLLW (45 m), representing the BOUSS-2D model boundary.

Entrance Boussinesq Wave Model

As described above, the BW Model was run under low/middle/high tide levels combined with storm-specific surges and tidal currents (i.e., the tidal water level/currents were superimposed onto the measured residual water level as described in Section 3.3.4.2). Each selected storm was simulated with the following four scenarios:

- High tide (MHHW) with storm surge and without currents;
- Middle tide (MSL) with storm surge and with maximum flood currents;
- Middle tide (MSL) with storm surge and with maximum ebb currents; and
- Low tide (MLLW) with storm surge and without currents.

This methodology provides multiple options for design needs. Results from runs at lower water levels would be more appropriate for sediment transport evaluation; extreme waves may be driven by higher water levels. For the subsequent extreme wave height analysis described below, the multiple tidal scenarios for each storm are considered to have equal probability.

With the combination of two model bathymetry conditions (as in Figure 3-18) and four water levels/ current conditions, the total number of Boussinesq wave simulations is 2x4x79=632. Each bathymetry condition has 4x79=316 storm peaks simulated. This provides a base for the extreme value analysis on the wave conditions. As described in Section 3.3.2, the Existing Conditions and the 2023 PA have different channel authorized depths.

Besides the above simulations, additional tests on infragravity (IG) waves were conducted to evaluate whether IG waves play a significant role here and need to be considered during the estimation of extreme waves. It was determined that IG waves could be excluded from the final set of wave simulations; a discussion on IG waves is included in Section 3.3.5.

3.3.5 Boussinesq Model Results

This section describes the results of the wave modeling. The general trend is that deepening and extending of the Entrance Channel increases refraction of incoming waves. The deeper channel has longer side slopes, resulting in increased refraction under the 2023 PA as waves refract from the deeper channel towards the shallower side slopes. For waves from the south through the west, this tends to focus more energy at the South Jetty head. For waves from the NW and NNW, this tends to focus more energy at the North Jetty head. The channel daylight location also extends further seaward beyond the jetties due to the greater dredge depth. Therefore, the refraction begins further offshore, and can shift wave energy away from the ocean entrance. This is particularly true for storms from the WNW direction, which travel approximately parallel to the entrance. A more detailed look is provided below.

Wave modeling results are detailed by considering significant wave heights at extraction points shown in Figure 3-29 and Figure 3-30. The yellow dots represent the data extraction points. The locations along the jetties are approximately 400 ft away from the jetties. The 400-ft distance was determined to avoid impacts from model absorption/porosity layer in BOUSS-2D while remaining within one to two wave lengths from the structure. The presence of the absorption layer is not anticipated to affect the comparison between conditions. Wave heights at the output location are not affected by the porosity layer and therefore a relative comparison between project conditions is valid. The offshore extent of the extraction locations, S2 and R7, are located offshore of the authorized jetty lengths. Figure 3-30 shows a larger area view with all locations, including offshore points and those along the northern adjacent shoreline. A total of 54 points are selected and they are separated into ten sub-areas:

- North Jetty—N1 to N15;
- South Jetty—S1 to S8;
- North Jetty Extension (covering the authorized length of North Jetty)—R1 to R7;
- Charleston Marina—CM1 to CM4;
- Middle of Channel—C1 to C2;
- Inner-Channel—I1 to I5;
- Pacific Coast—Nearshore 1 to Nearshore 4;
- Bastendorff Beach—Nearshore 5 to Nearshore 7;
- Offshore—Offshore 1 to Offshore 3; and
- Log-spiral Bay—L1 to L3.

Figure 3-29
Extraction Locations near the Entrance

Figure 3-30
Zoom-out View of All 54 Extraction Locations

At each location, two sets of plots have been developed: cumulative distribution plots and directional plots. The cumulative distribution plots were developed by rank-ordering the wave heights and presenting them in terms of the cumulative distribution. An example is shown in Figure 3-31. Cumulative distribution plots show the data in terms of their percentile ranking. For example, the 0.9 value on the x-axis corresponds to the 90th percentile wave height. These plots are useful to analyze wave heights – for example, they can answer the question of how often a 20 ft wave can be expected at each point during the various project conditions. Because this is based on 44 years of data, the wave height for x = 1 corresponds to nearly the 50-year wave. Plots showing the portion of the distribution from 0.9 to 1.0 are also shown to provide more precision for the largest 10 percent of waves (Figure 3-32).

Model results are also summarized by the directional plots. An example is shown in Figure 3-33. For these plots, waves are ordered along the x-axis by the offshore wave direction, and the width of each directional band corresponds to the number of storm waves from this direction. A different plot has been created for each tidal condition simulated (MLLW, MSL w/ Ebb, MSL w/ Flood, and MHHW). Figure 3-33 shows the MHHW condition, which generally corresponds to the largest waves. The purpose of these plots was to show which directional/tidal wave conditions showed changes in wave heights at each extraction point.

It should be noted that these plots include wave height thresholds. These are the thresholds at which waves may threaten the stability of the jetty armor stone. The significance of these thresholds and the method for determining these thresholds is presented in Section 6.

The analysis does not include an extreme value analysis that would typically be used for design. Instead, the analysis provides an assessment of how the 2023 PA would affect the propagation of actual, measured waves.

Cumulative distribution and directional plots for each extraction point are provided in Attachment A.

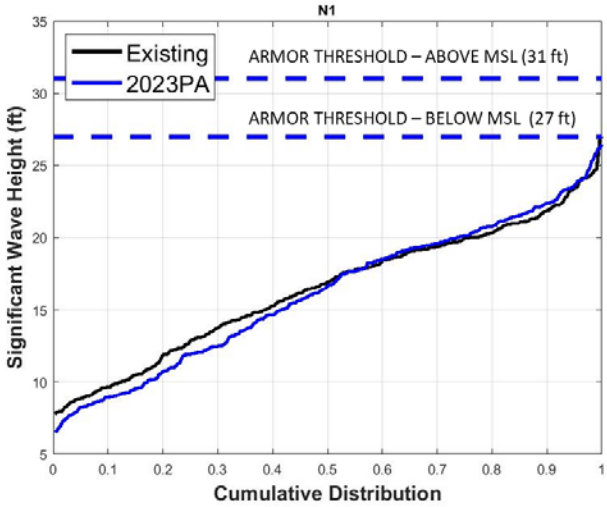

Figure 3-31
Example Plot, Cumulative Distribution of Significant Wave Height at N1

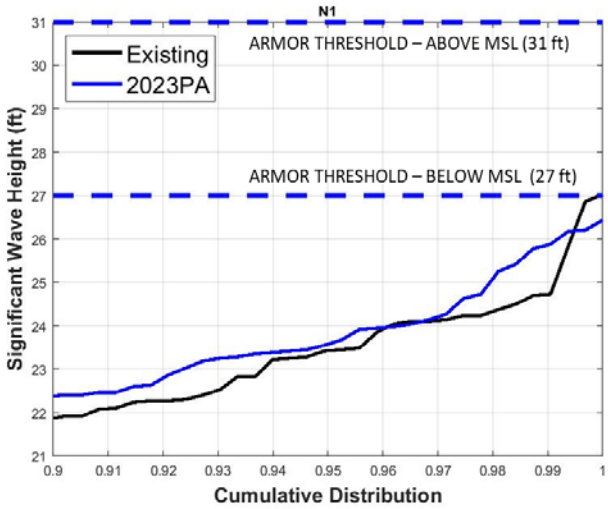

Figure 3-32
Example Plot, Cumulative Distribution of Significant Wave Height at N1 (Largest 10% of Waves)

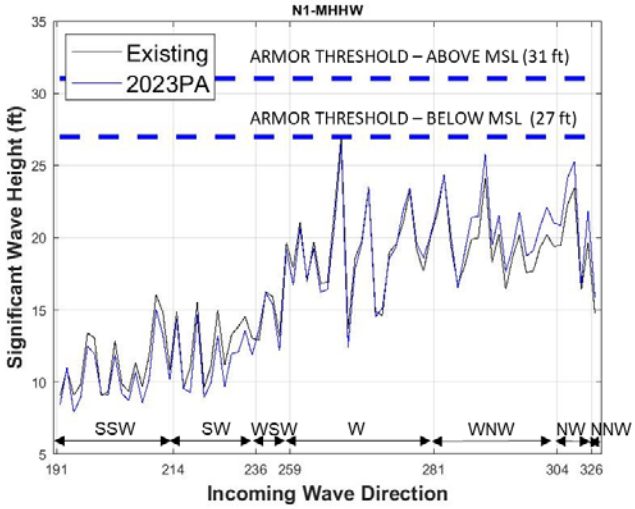

Figure 3-33
Wave Direction Plot for Waves at MHHW at N1

The subsections (Section 3.3.5.1 to 3.3.5.10) below discuss the dynamics of wave propagation at ten sub-areas within the inlet. These sections focus only on wave heights and changes under the various conditions; effects to jetties are discussed in Section 6.

3.3.5.1 North Jetty – N1 to N15

Significant wave height cumulative distribution plots along the North Jetty are presented in Figure 3-34 through Figure 3-49. N1 through N3 represent the North Jetty head, N4 though N7 represent the jetty trunk, and N8 through N15 represent the jetty root.

At the jetty head, the wave heights are expected to decrease at points N2 and N3. At N1, the largest of the storm waves are expected to increase. Figure 3-35 shows the 10 percent of largest waves at this point. N1 also shows an approximate 0.5 ft increase in significant wave height under the 2023 PA relative to the Existing Conditions – the extension of the jetty head increases wave focusing. At N1, waves from the west through NNW tend to increase in wave height; the increase in waves at N1 coupled with the decrease in wave heights at N2 and N3 is likely a result of the increased refraction under the 2023 PA. As the waves begin to refract further offshore, some of the wave energy that was previously directed toward N2 is now observed at N1. At N2, waves from the NW and NNW sectors tend to increase in height, while waves from the west and WNW decrease in height or stay the same. All waves at N3 decrease in height.

Overall, the waves at N2 are larger than the waves at N1, corresponding to the most energetic west and WNW sectors. As a result, armor stone stability is governed by the wave climate at N2. Ultimately, the decreased wave heights at N2 are expected to improve stability of the North Jetty head; this is discussed in Section 6.

There is a substantial decrease in wave height between N2 and N3. The reasons for this decrease are wave retraction and wave shoaling. At the Coos Bay inlet, wave refraction causes wave energy from the channel to the adjacent areas; since N3 is located close to the channel, a significant portion of the offshore wave energy has refracted to the adjacent areas before reaching this point. The effect of refraction on reduced wave heights within the channel can be seen in Figure 3-94, which shows the lowest wave heights within the channel, and the largest wave heights immediately adjacent to the channel. Similarly, Figure 3-95 shows how the effect is amplified under the 2023 PA, reducing wave heights along the North Jetty. The second reason for the difference in wave heights between N2 and N3 is shoaling. N2 is located above the relic jetty head, waves propagating towards the north jetty head are amplified through focusing at the jetty head and shoaling at the relic jetty head. These predictions are consistent with the results of the 2017 jetty inspection (USACE 2017), which found major damage to the North Jetty head, and minor damage in only limited areas of the North Jetty Trunk. This damage pattern confirms that waves at N2 are in fact much larger than at N3.

Throughout the jetty trunk (N4 through N7), the wave heights consistently (for all offshore wave directions) decrease under the 2023 PA relative to the Existing Conditions. This is likely a function of the increased wave refraction offshore. At the western portion of the jetty root (N8 through N11), the wave heights are decreased under the 2023 PA relative to the Existing Conditions, similar to observations at the jetty trunk.

The results at N12 through N15 show the same trend that the 2023 PA has lower wave heights than the Existing Conditions. At N14, the significant wave heights under the 2023 PA are consistently lower than 1.5 ft. At N15, all wave heights under the PA are below 1 ft.

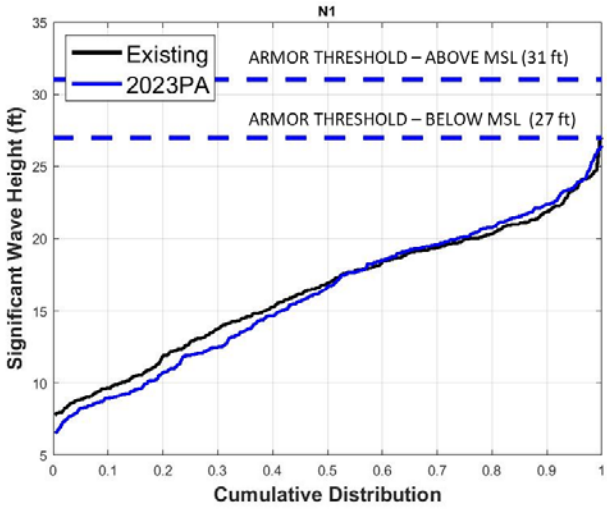

Figure 3-34
Cumulative Distribution of Significant Wave Height at N1

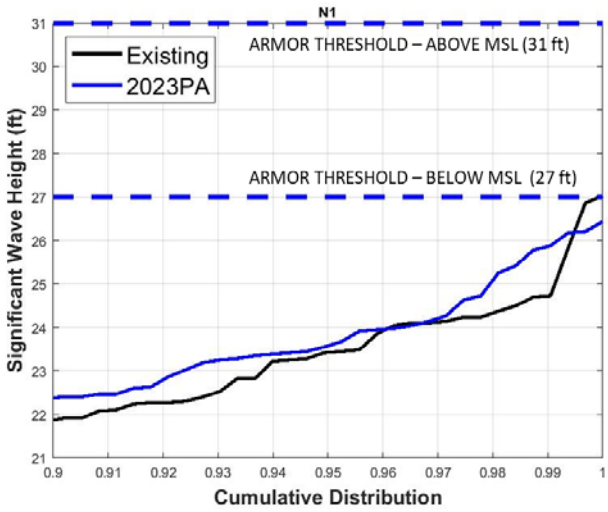

Figure 3-35
Cumulative Distribution of Significant Wave Height at N1 (Largest 10% of Waves)

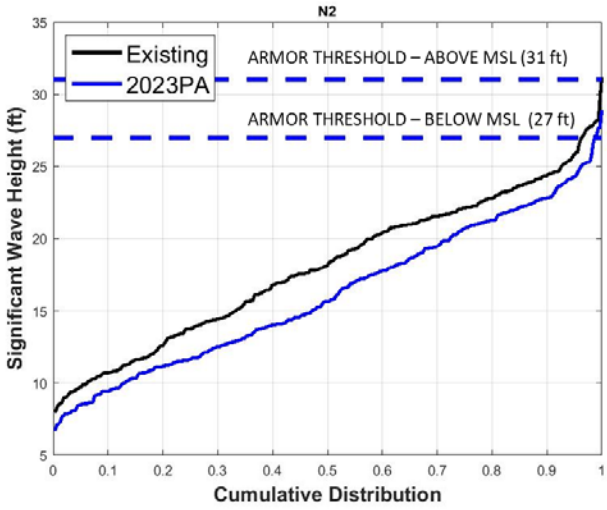

Figure 3-36
Cumulative Distribution of Significant Wave Height at N2

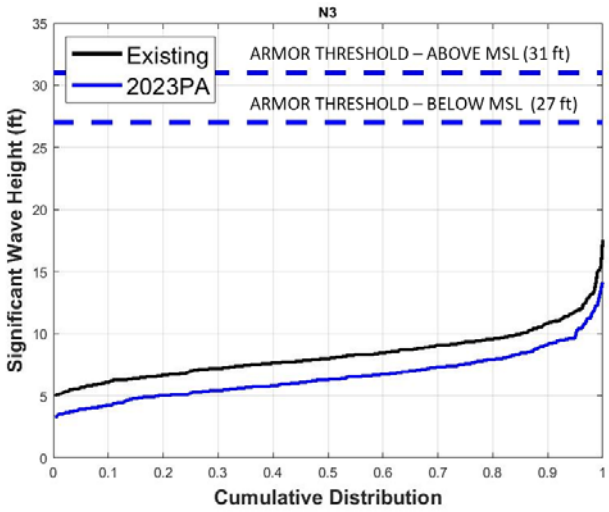

Figure 3-37
Cumulative Distribution of Significant Wave Height at N3

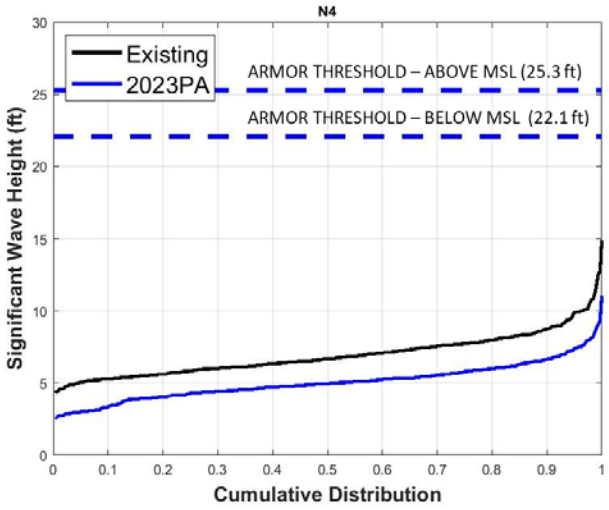

Figure 3-38
Cumulative Distribution of Significant Wave Height at N4

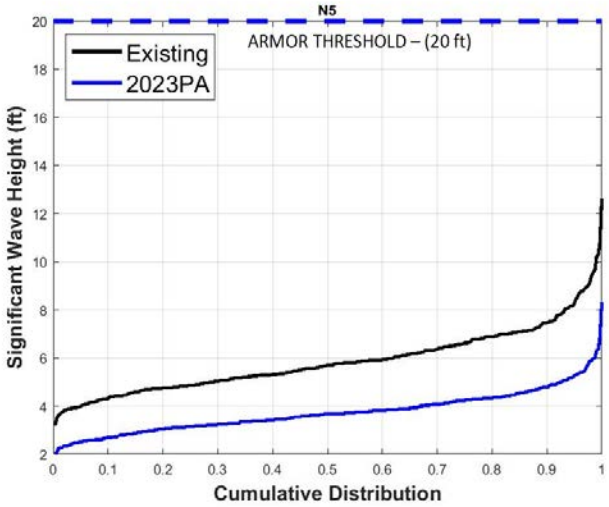

Figure 3-39
Cumulative Distribution of Significant Wave Height at N5

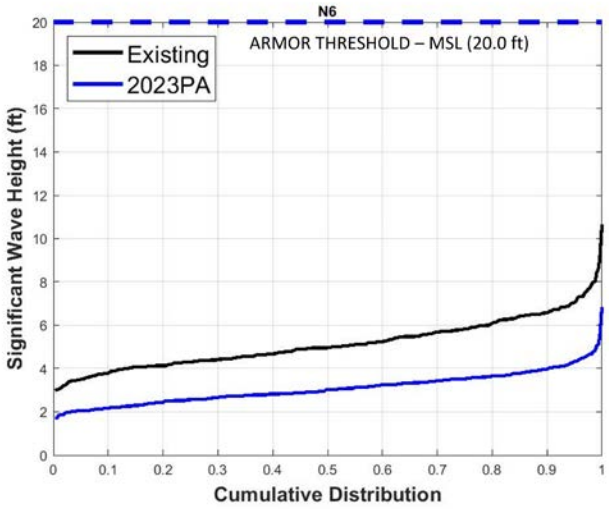

Figure 3-40
Cumulative Distribution of Significant Wave Height at N6

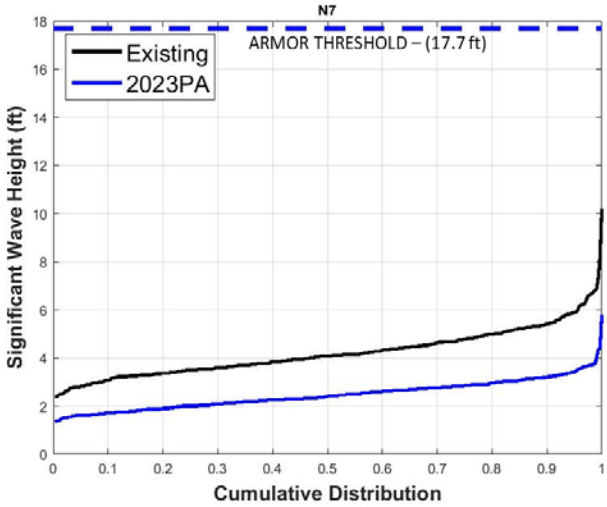

Figure 3-41
Cumulative Distribution of Significant Wave Height at N7

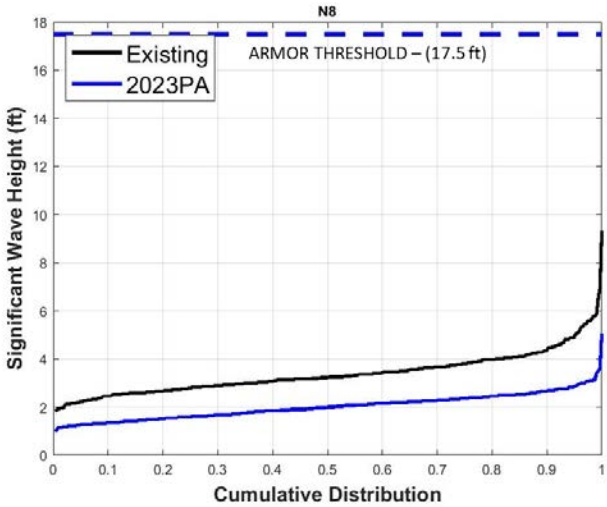

Figure 3-42
Cumulative Distribution of Significant Wave Height at N8

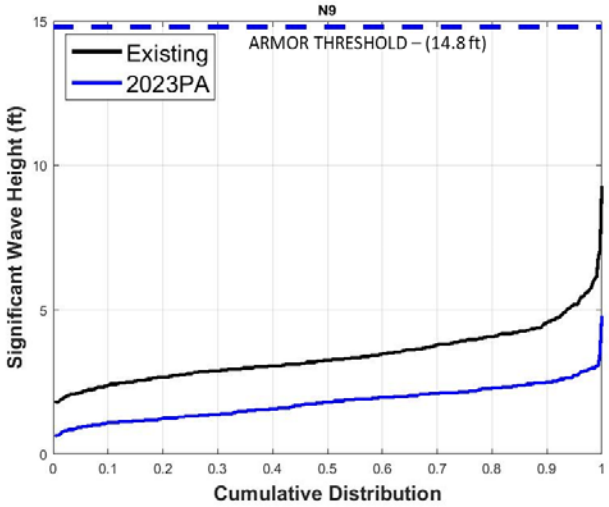

Figure 3-43
Cumulative Distribution of Significant Wave Height at N9

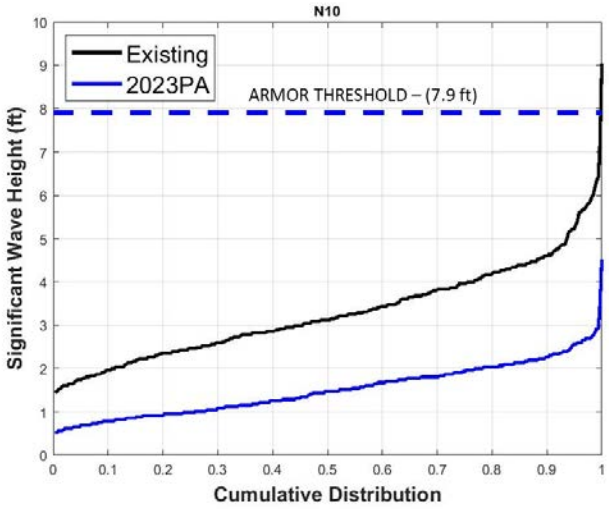

Figure 3-44
Cumulative Distribution of Significant Wave Height at N10

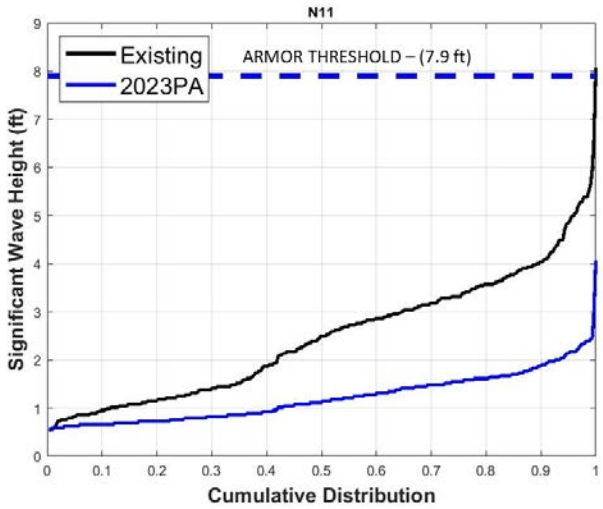

Figure 3-45
Cumulative Distribution of Significant Wave Height at N11

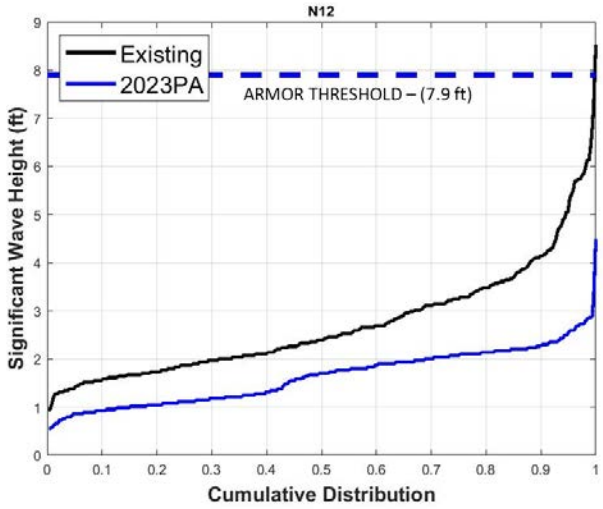

Figure 3-46
Cumulative Distribution of Significant Wave Height at N12

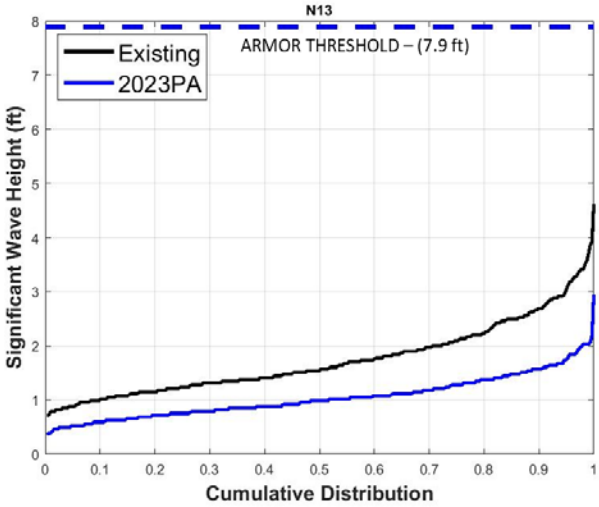

Figure 3-47
Cumulative Distribution of Significant Wave Height at N13

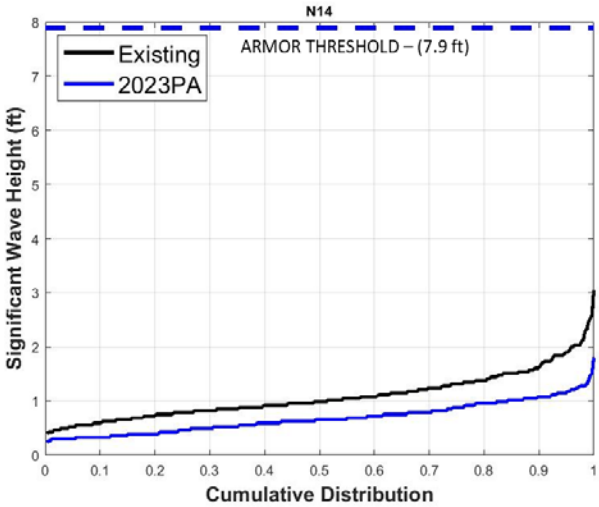

Figure 3-48
Cumulative Distribution of Significant Wave Height at N14

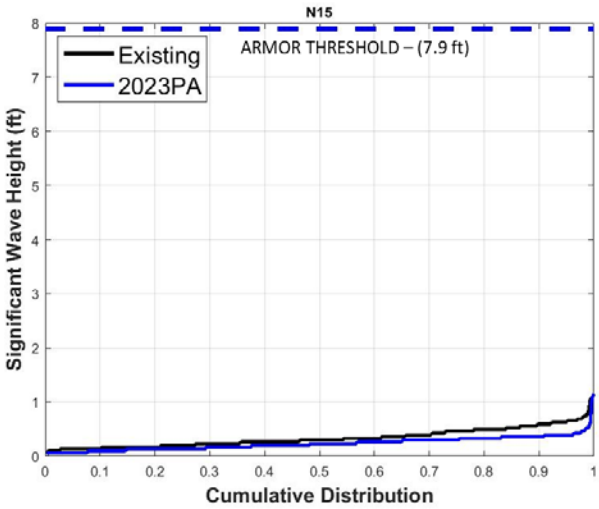

Figure 3-49
Cumulative Distribution of Significant Wave Height at N15

3.3.5.2 South Jetty – S1 to S8

Significant wave height cumulative distribution plots along the South Jetty are presented in Figure 3-50 through Figure 3-58. Points S1 through S3 describe the wave climate at the Jetty Head. The largest waves are encountered at S3, corresponding to the waves from the west. At S1, the largest 50 percent of wave heights are equivalent under both project conditions, while the smallest half of waves are up to 1.5 ft larger under the PA than the Existing Conditions. However, these waves are beneath the threshold for armor stone stability and will not lead to jetty recession, as discussed in Section 6. At S2, the median waves (20^{th} percentile to 85^{th} percentile) decrease under the PA relative to the Existing Conditions, while the largest waves increase by less than 1.0 ft. A similar trend can be seen at S3, where the 20^{th} to the 95^{th} percentile decrease under the PA; the increases in wave heights are less than one foot (Figure 3-53). The implications of this increase for jetty stability are discussed in Section 6.

At the jetty head, waves from the SSW though west tend to increase in height, while waves from the WNW through NNW tend to decrease in height. Since waves from west are the largest at the jetty heads, the increase in wave heights from this sector drives the increase in extreme wave heights.

Points S4 though S8 describe the wave climate at the jetty trunk. For all of these stations, the wave heights decrease under the PA relative to the Existing Conditions for the 35^{th} percentile and higher, reducing any risk to the jetty. The wave distribution that exceeds stability thresholds decreases in wave height. The decrease in wave height is due to wave energy focusing at the jetty head. The implications for jetty stability are discussed in Section 6.

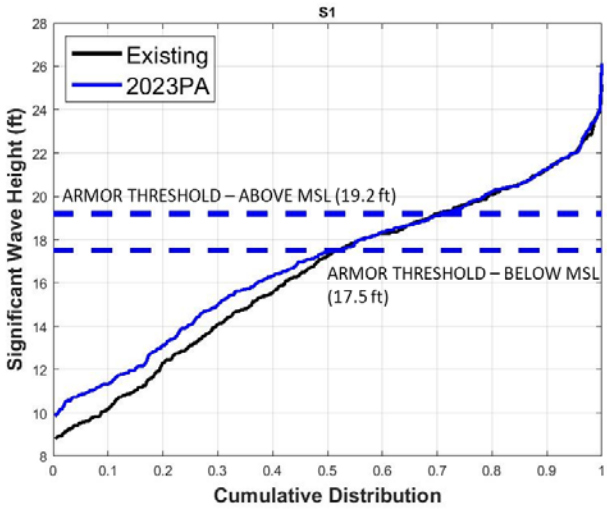

Figure 3-50
Cumulative Distribution of Significant Wave Height at S1

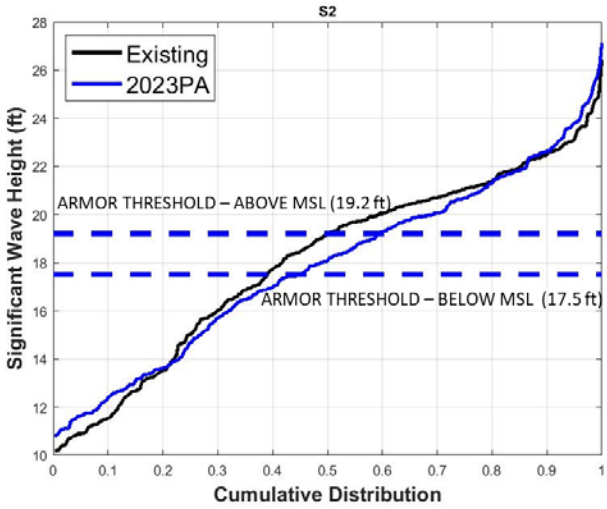

Figure 3-51
Cumulative Distribution of Significant Wave Height at S2

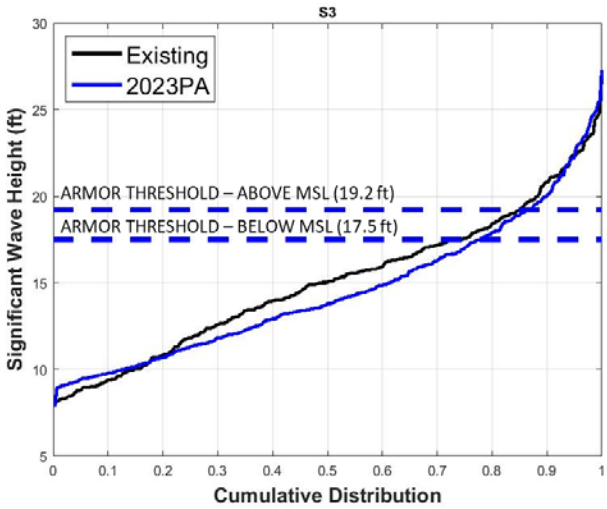

Figure 3-52
Cumulative Distribution of Significant Wave Height at S3

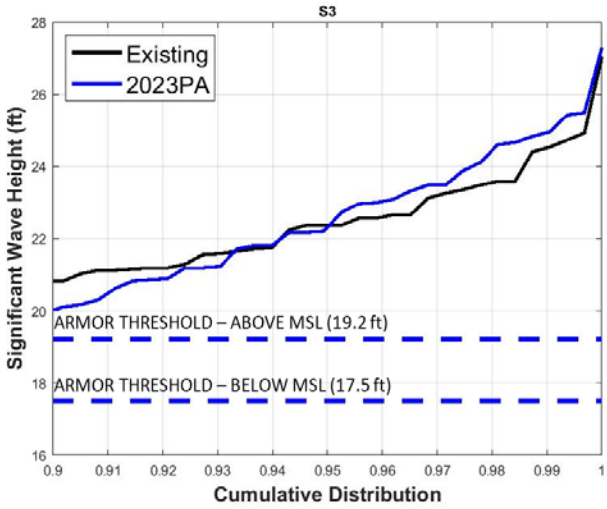

Figure 3-53
Cumulative Distribution of Significant Wave Height at S3 (Largest 10% of Waves)

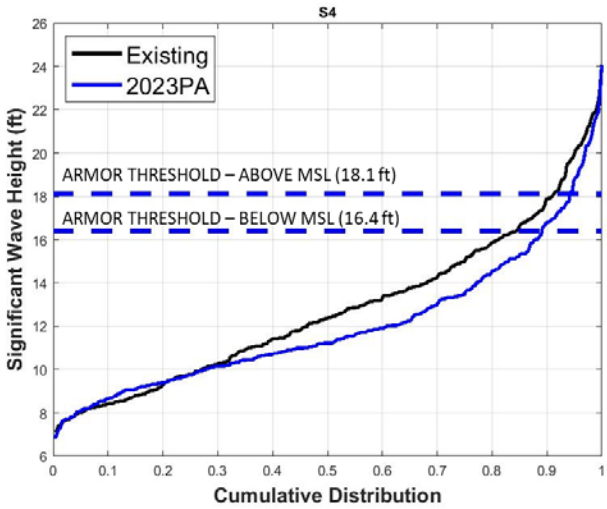

Figure 3-54
Cumulative Distribution of Significant Wave Height at S4

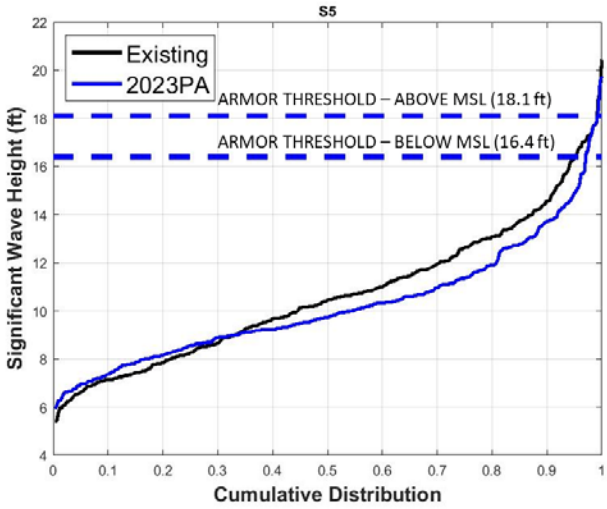

Figure 3-55
Cumulative Distribution of Significant Wave Height at S5

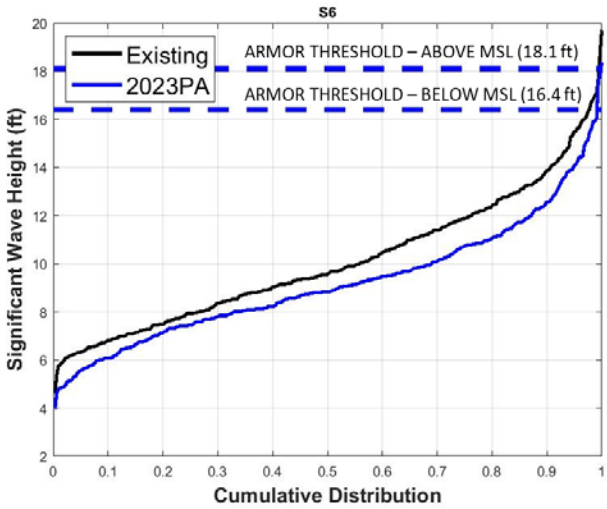

Figure 3-56
Cumulative Distribution of Significant Wave Height at S6

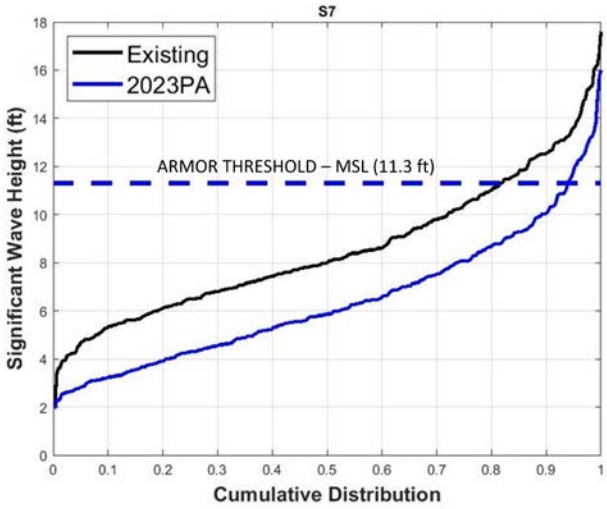

Figure 3-57
Cumulative Distribution of Significant Wave Height at S7

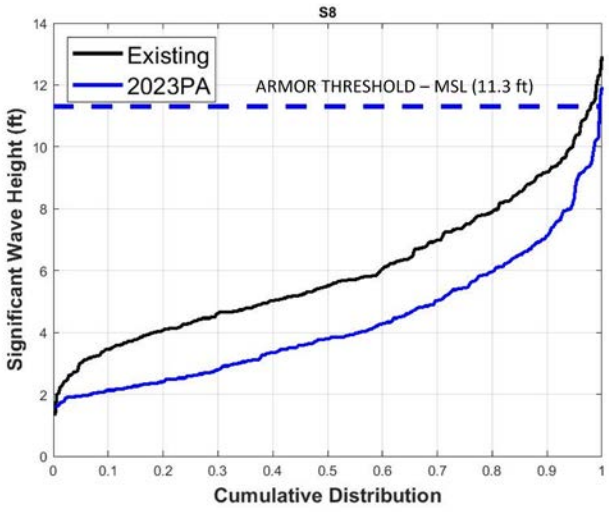

Figure 3-58
Cumulative Distribution of Significant Wave Height at S8

3.3.5.3 North Jetty Extension – R1 to R7

Significant wave height cumulative distribution plots offshore of the North Jetty are presented in Figure 3-59 through Figure 3-65. At R2, R3, and R5 through R7, the wave heights decrease under the 2023 PA relative to the Existing Conditions throughout the distribution. At R1 and R4, the largest 40-50 percent of waves increase in height by up to 1 ft (although the extreme 1 percent of waves do not change). These two points are directly offshore of N1; the same conditions that cause the increase in wave heights at N1 (Section 3.3.5.1) similarly drive this increase. These wave points are offshore of the North Jetty; effects to the jetty head are based on N1 through N3.

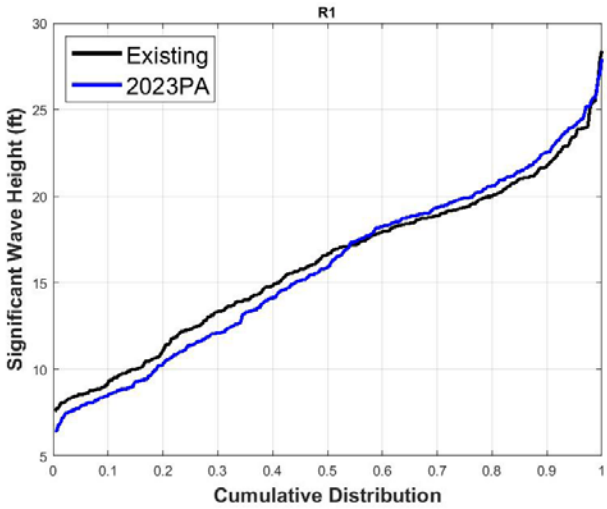

Figure 3-59
Cumulative Distribution of Significant Wave Height at R1

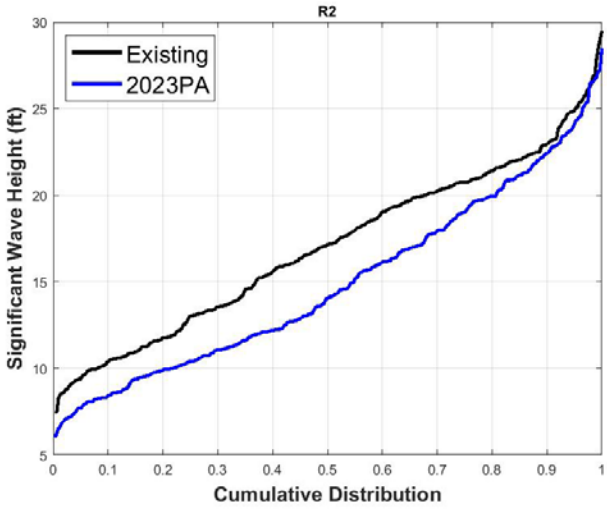

Figure 3-60
Cumulative Distribution of Significant Wave Height at R2

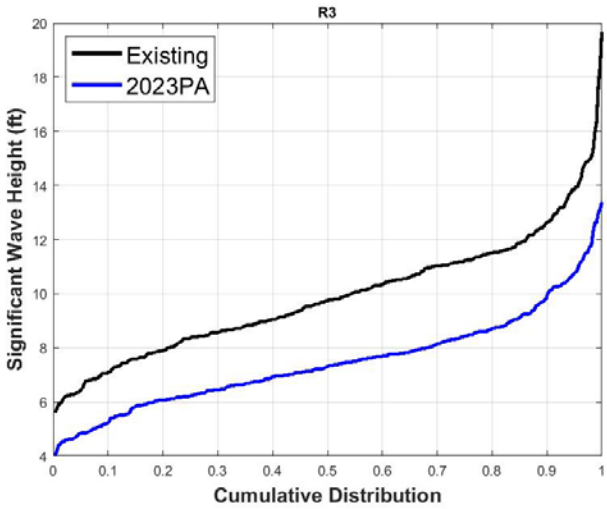

Figure 3-61
Cumulative Distribution of Significant Wave Height at R3

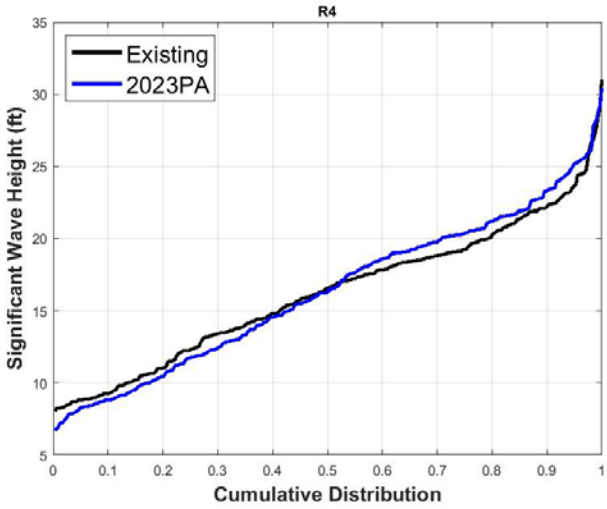

Figure 3-62
Cumulative Distribution of Significant Wave Height at R4

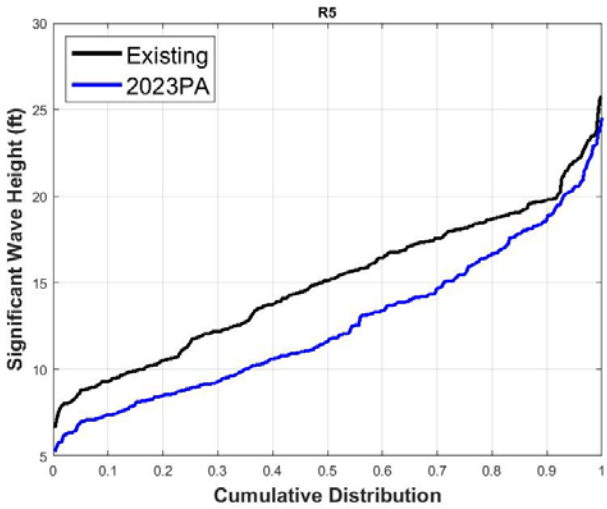

Figure 3-63
Cumulative Distribution of Significant Wave Height at R5

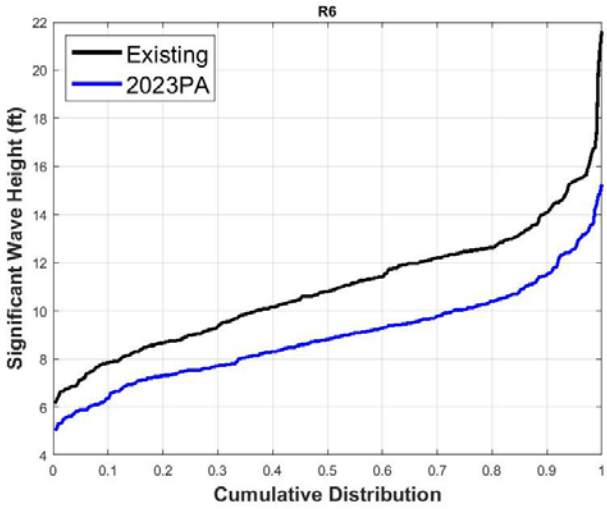

Figure 3-64
Cumulative Distribution of Significant Wave Height at R6

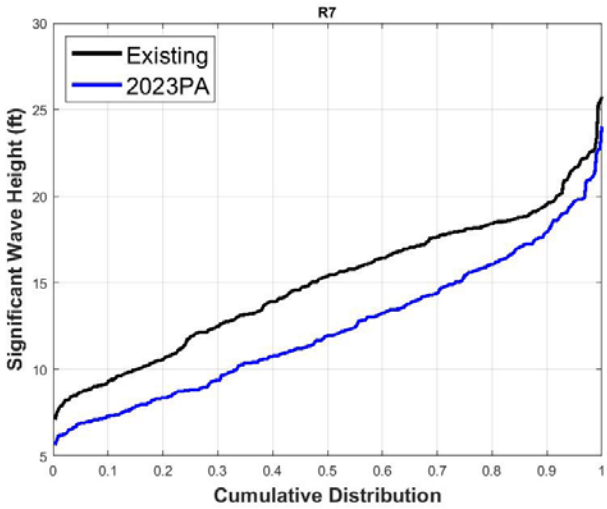

Figure 3-65
Cumulative Distribution of Significant Wave Height at R7

3.3.5.4 Charleston Marina – CM1 to CM4

Significant wave height cumulative distribution plots in the vicinity of the Charleston Marina are presented in Figure 3-66 through Figure 3-69. As these plots show, the wave heights are expected to decrease throughout the distribution at all locations. Wave heights decrease from waves from all offshore directions. No negative effects to the Charleston Breakwater are expected.

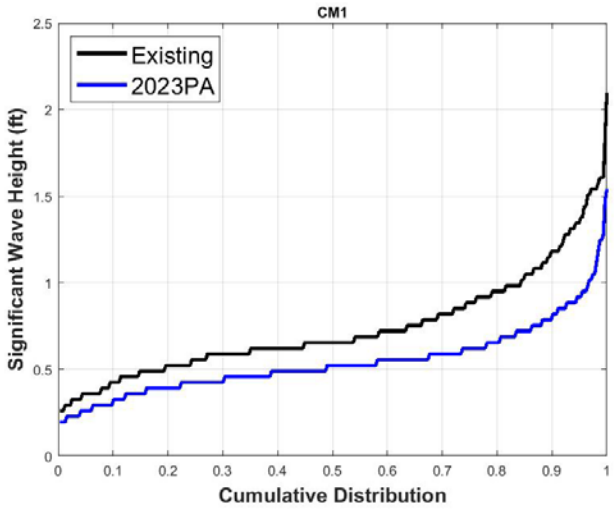

Figure 3-66
Cumulative Distribution of Significant Wave Height at CM1

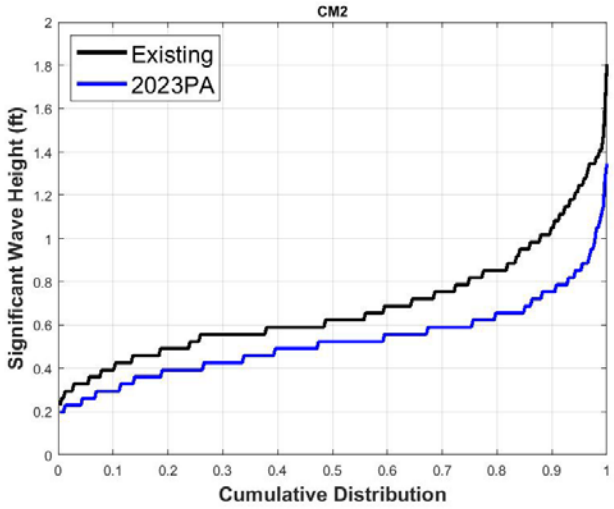

Figure 3-67
Cumulative Distribution of Significant Wave Height at CM2

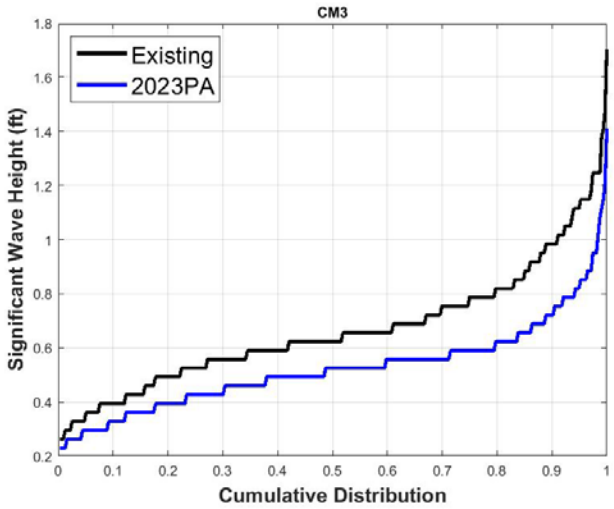

Figure 3-68
Cumulative Distribution of Significant Wave Height at CM3

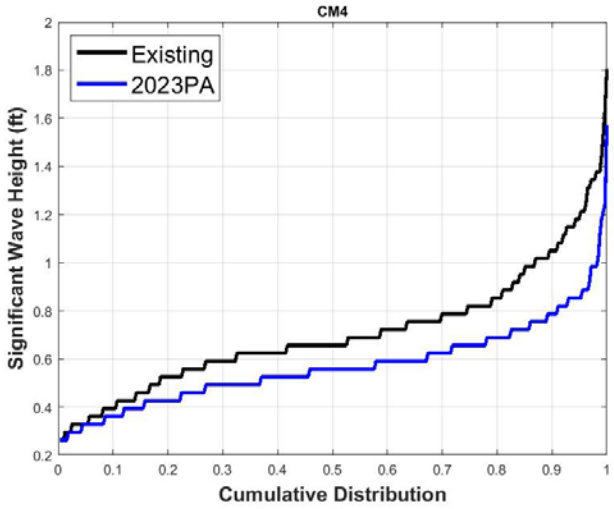

Figure 3-69
Cumulative Distribution of Significant Wave Height at CM4

3.3.5.5 Middle of Channel – C1 to C2

Significant wave height cumulative distribution plots in the channel center are presented in Figure 3-70 and Figure 3-71. Wave heights in the throat of the channel are expected to decease under the 2023 PA relative to the Existing Conditions. At C1, the decrease in wave heights is up to 0.75 ft, indicating an improvement to navigation. At C2, the decrease is up to 0.2 ft. At C2, little wave energy penetrates into the channel – all but the top 2 percent of storm waves have a significant wave height of less than 1 ft under all conditions. At C1 and C2, waves from all directions decrease in wave height.

The decrease in wave height reflects the general trend of less wave energy penetrating into the channel.

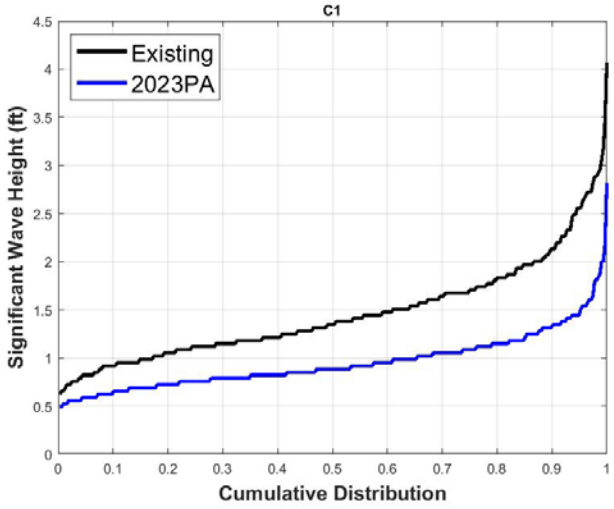

Figure 3-70
Cumulative Distribution of Significant Wave Height at C1

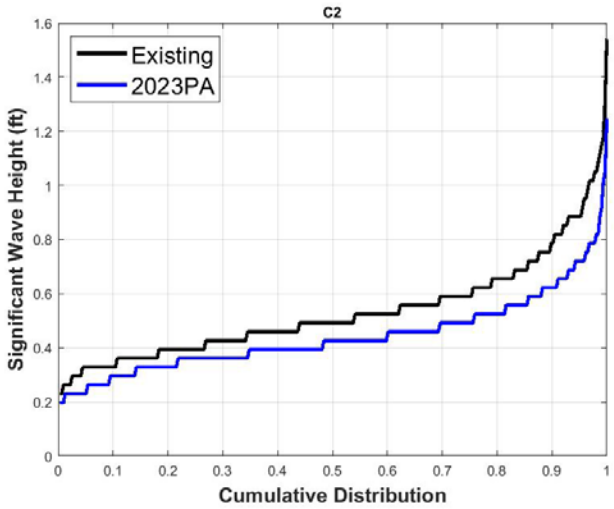

Figure 3-71
Cumulative Distribution of Significant Wave Height at C2

3.3.5.6 Inner-Channel – I1 to I5

Significant wave height cumulative distribution plots near the limit of the model boundary are presented Figure 3-72 through Figure 3-76. As these plots show, wave heights are small at these locations; at each point, less than 3 percent of waves have a significant wave height greater than 1 ft. Moreover, waves from all directions decrease in wave height under the 2023 PA relative to the Existing Conditions. The difference is up to 0.25 ft. Upstream of these locations, any change to wave heights is expected to be less than 0.25 ft.

Commented [WQ7]: Comment #A-4-8 (Dr. Checks 8071912)

Commented [WQ8R7]: No NED condition in this study.

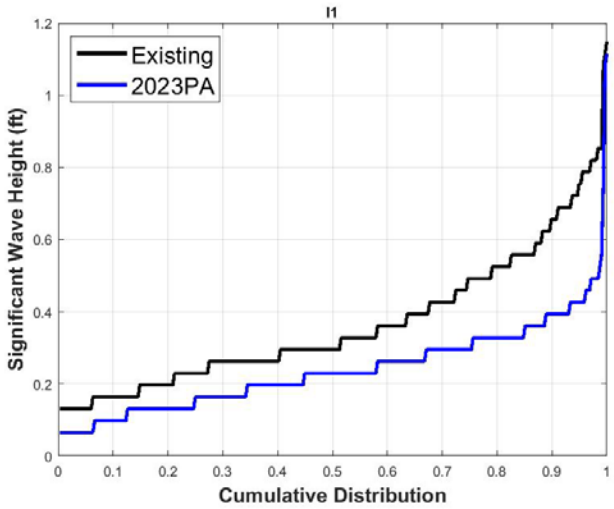

Figure 3-72
Cumulative Distribution of Significant Wave Height at I1

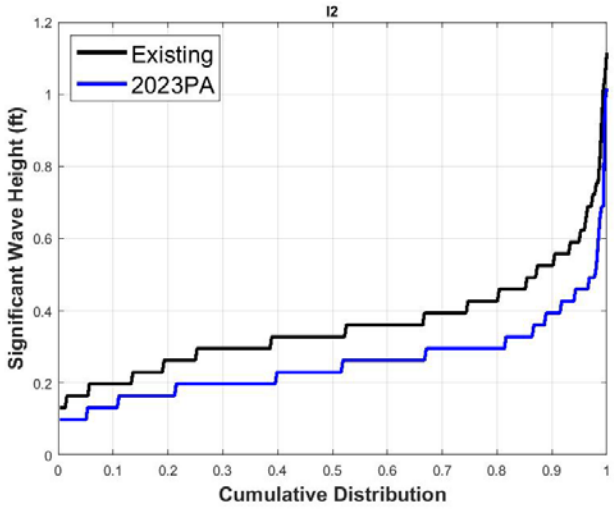

Figure 3-73
Cumulative Distribution of Significant Wave Height at I2

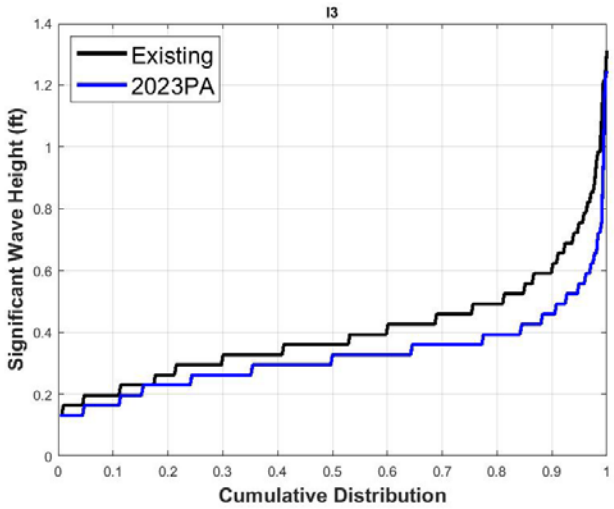

Figure 3-74
Cumulative Distribution of Significant Wave Height at I3

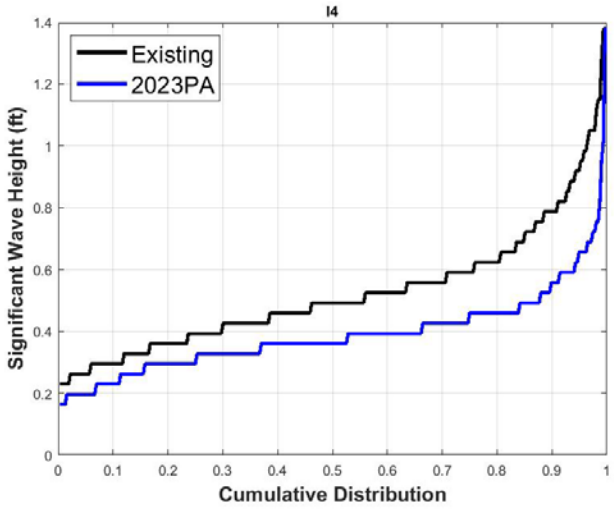

Figure 3-75
Cumulative Distribution of Significant Wave Height at I4

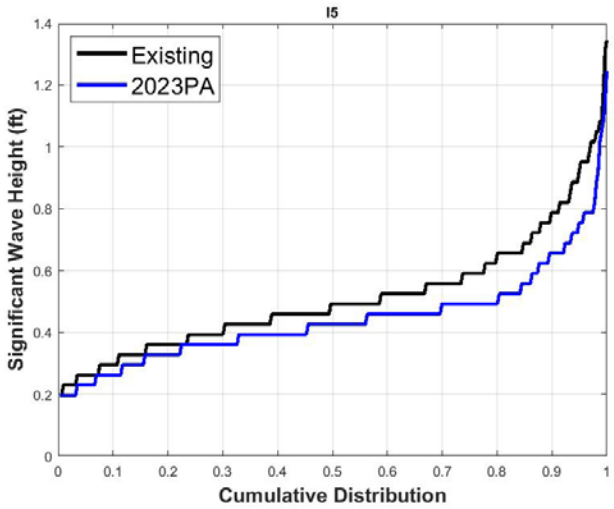

Figure 3-76
Cumulative Distribution of Significant Wave Height at I5

3.3.5.7 Pacific Coast – Nearshore 1 to Nearshore 4

Significant wave height cumulative distribution plots along the Pacific coast north of the North Jetty are presented in Figure 3-77 through Figure 3-80. Nearshore 1 is located offshore of the neck of LSB. At this point, the 2023 PA results in a 0.1-0.3 ft increase throughout the distribution above 25th percentile (with increases as high as 0.5 ft at the 75th and 96th percentiles). The increases occur for waves occurring from all offshore directions. The implications on sedimentation and shoreline stability are discussed in Section 5. At Nearshore 2, the increase of waves under the 2023 PA is less than 0.2 ft. At Nearshore 3 and Nearshore 4, the change in significant wave heights between the two conditions reduces to less than 0.05 ft.

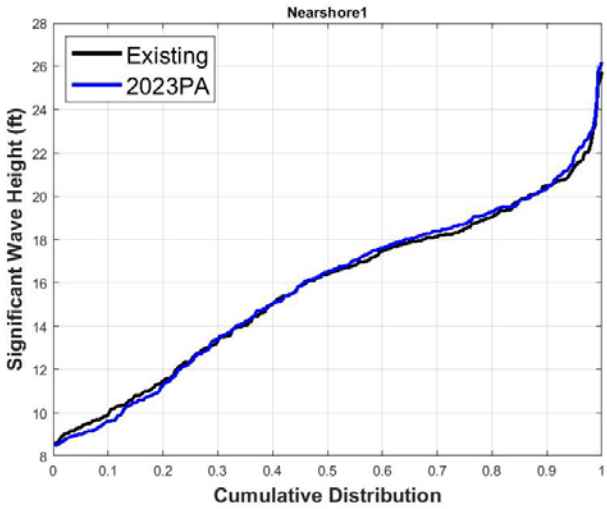

Figure 3-77
Cumulative Distribution of Significant Wave Height at Nearshore 1

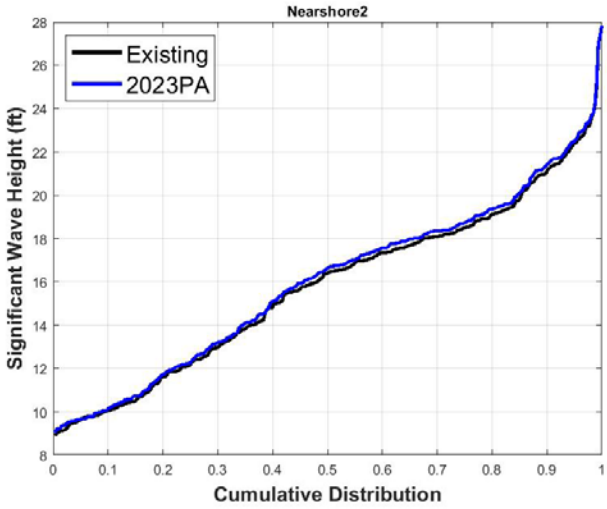

Figure 3-78
Cumulative Distribution of Significant Wave Height at Nearshore 2

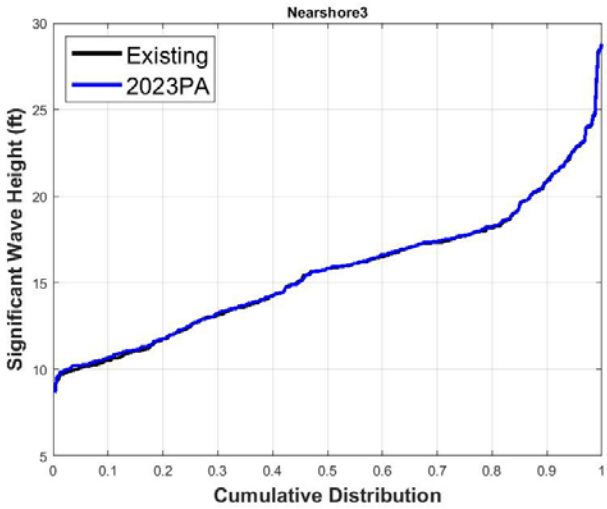

Figure 3-79
Cumulative Distribution of Significant Wave Height at Nearshore 3

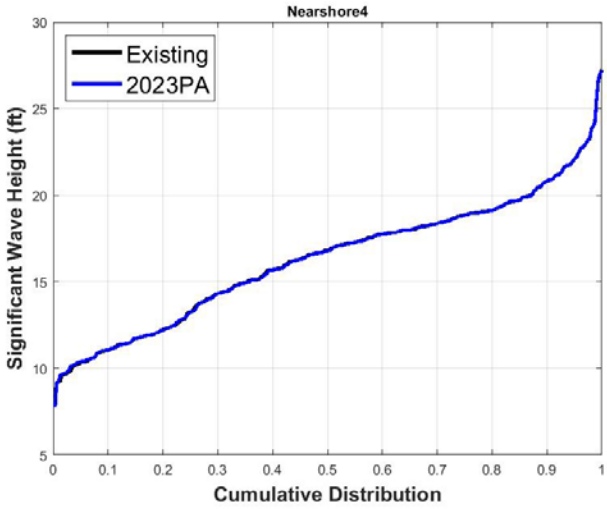

Figure 3-80
Cumulative Distribution of Significant Wave Height at Nearshore 4

3.3.5.8 Bastendorff Beach – Nearshore 5 to Nearshore 7

Significant wave height cumulative distribution plots at Bastendorff Beach are presented in Figure 3-81 through Figure 3-83. As these plots show, wave heights along Bastendorff Beach do not change as a result of the project.

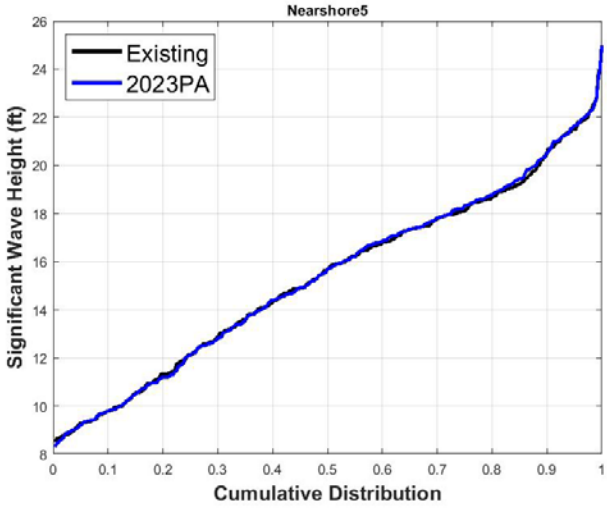

Figure 3-81
Cumulative Distribution of Significant Wave Height at Nearshore 5

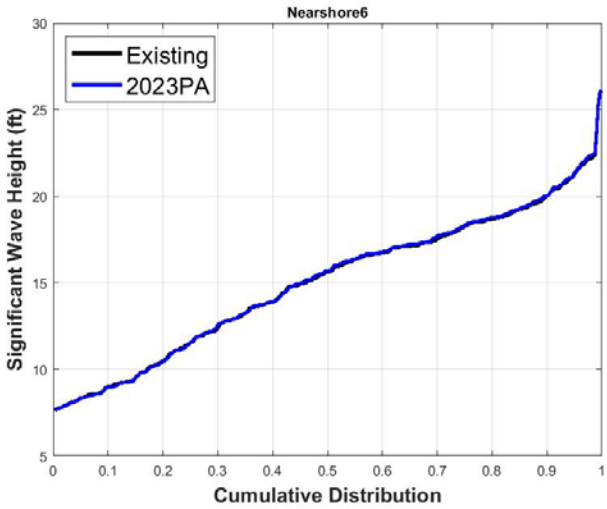

Figure 3-82
Cumulative Distribution of Significant Wave Height at Nearshore 6

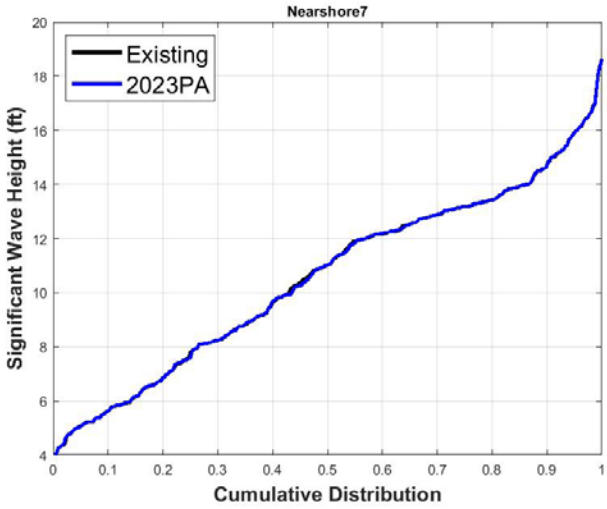

Figure 3-83
Cumulative Distribution of Significant Wave Height at Nearshore 7

3.3.5.9 Offshore – Offshore 1 to Offshore 3

Significant wave height cumulative distribution plots offshore of the Entrance Channel are presented in Figure 3-84 through Figure 3-86. As these plots show, wave heights offshore do not change as a result of the project.

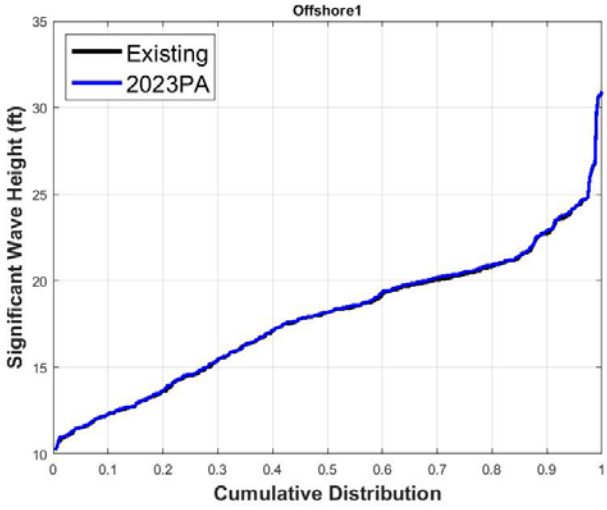

Figure 3-84
Cumulative Distribution of Significant Wave Height at Offshore 1

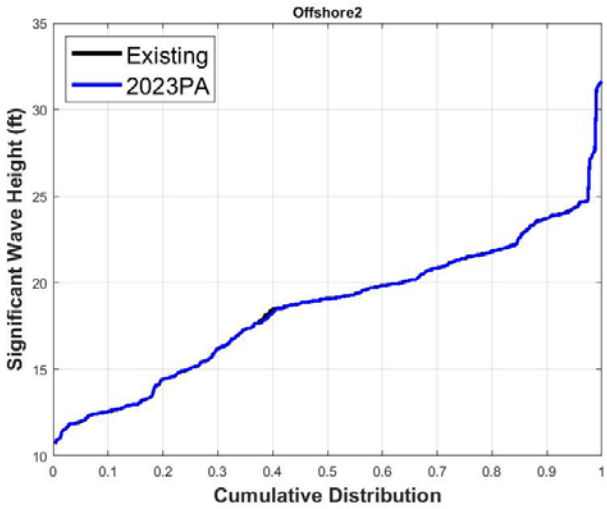

Figure 3-85
Cumulative Distribution of Significant Wave Height at Offshore 2

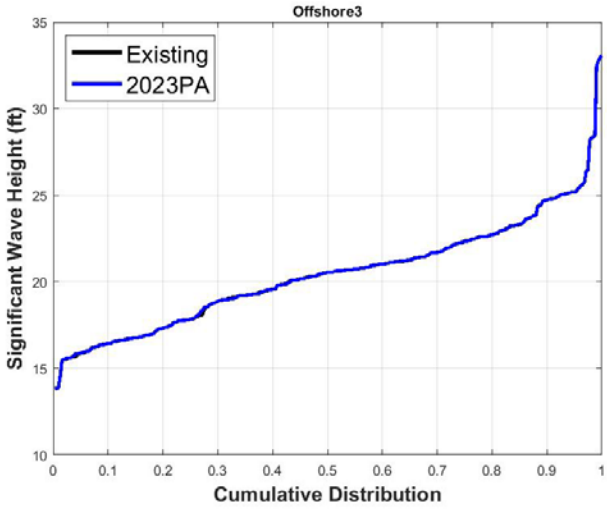

Figure 3-86
Cumulative Distribution of Significant Wave Height at Offshore 3

3.3.5.10 Log-spiral Bay – L1 to L3

Significant wave height cumulative distribution plots in LSB are presented in Figure 3-87 through Figure 3-89. As noted in Hays and Moritz (2003), the headland of the bay is located where the root of the jetty meets the unmaintained remnant jetty. This point is shown in Figure 3-90; this figure also shows wave crests within the bay, which appear to be traveling northwards. Figure 3-91 shows modeled wave crests, which are consistent with the wave crests in Figure 3-90. This figure indicates that waves diffract around the headland, causing erosion throughout the Bay.

The exceedance curves at L1 and L3 have a similar shape, indicating that waves possibly propagate from L1 to L3. Based on the wave crest analysis, waves propagate from N9 and N10 to LSB points L1 and then to L3. Since waves at N9 and N10 are smaller under the 2023 PA than under the Existing Conditions, they are also smaller at the L1 and L3 locations.

At L2, the shape of the wave plot is similar to that of N11 and N12 (Figure 3-45 and Figure 3-46), indicating that waves propagate from N11/N12 to L2; this is consistent with the wave crest analysis (Figure 3-91). Therefore, the decrease in wave heights is due to the increased offshore refraction that reduces the wave energy at N11 and N12.

Ultimately, the reduction in wave heights suggests the potential for decreased erosion at LSB.

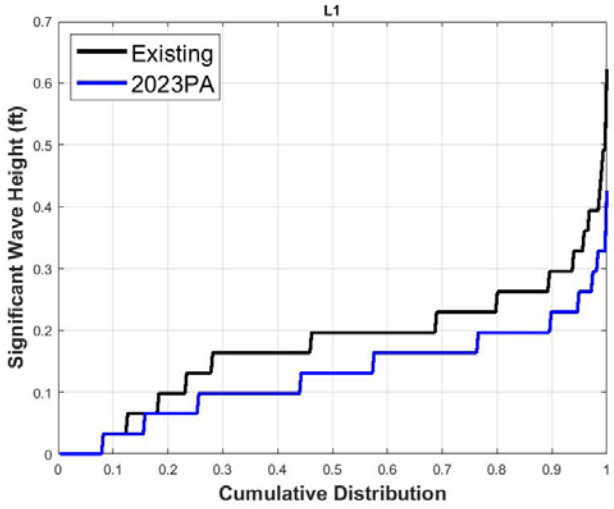

Figure 3-87
Cumulative Distribution of Significant Wave Height at L1

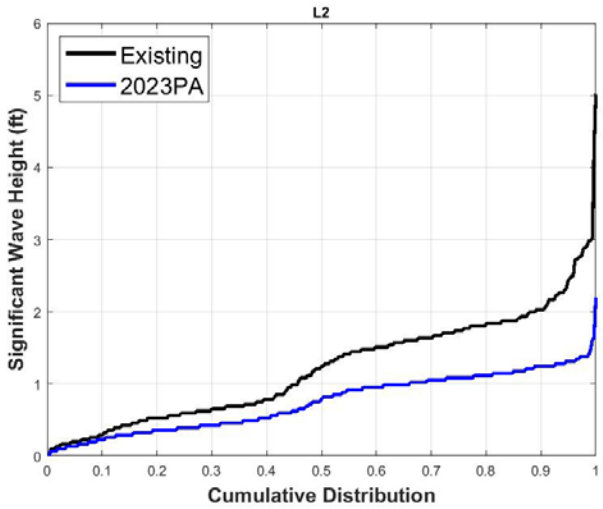

Figure 3-88
Cumulative Distribution of Significant Wave Height at L2

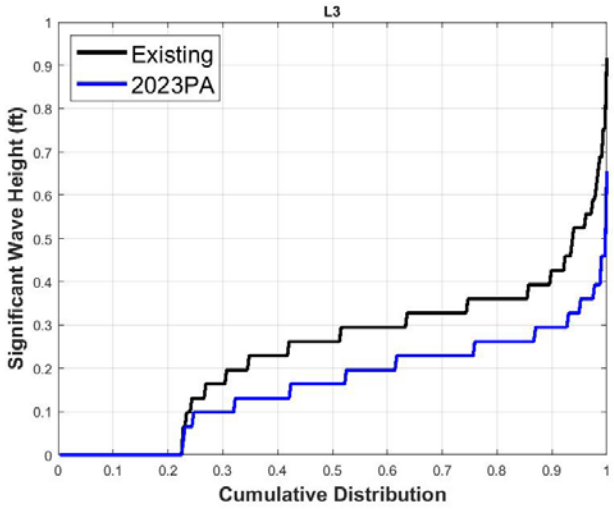

Figure 3-89
Cumulative Distribution of Significant Wave Height at L3

Figure 3-90
Wave Points and Headland Location at LSB

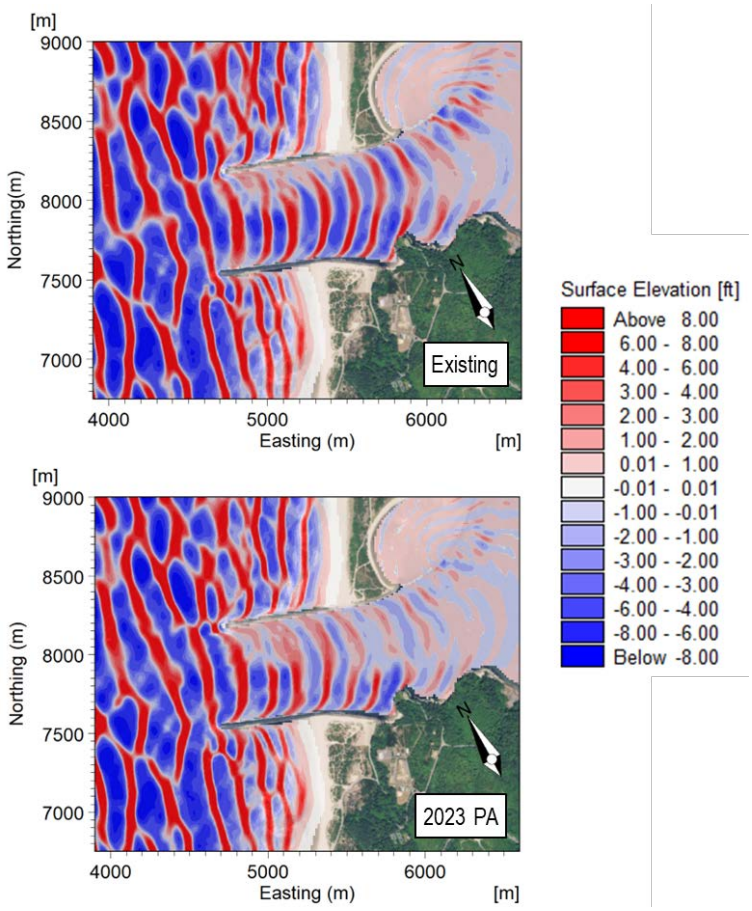

Figure 3-91
Graphic Illustration of Wave Crests at the Entrance for the Existing Conditions and the 2023 PA under MHHW

3.3.5.11 Analysis of Illustrative Individual Storm Events

This section provides detailed graphics that show the modeling results from three example storms presented in Table 3-7. These three storms were selected as illustrative examples for the following reasons:

- Storm #72 has the highest wave height among the 79 storms and from the approach direction is approximately due west (271 deg);
- Storm #60 has the most south-westerly approach direction among the 79 storms (195 deg); and
- Storm #45 has the most north-westerly approach direction (320 deg).

Storm #60 and Storm #45 are the southerly-most and northerly-most storms, making them directional extremes and not necessarily representative of the majority of incoming wave conditions. Hence, the results of the cumulative distribution will differ from the individual results of these three storms. Moreover, it should be noted that these storms are not the largest from the northwest and southwest directions. However, these storms illustrate the full range of wave heights and directions. For reference, the entrance channel is oriented towards the west-northwest (approximately 290 deg).

Table 3-7
Example Storms

Incoming Wave Direction		**Southwest**	**West**	**Northwest**
Storm No.		**Storm #60[2]**	**Storm #72[1]**	**Storm #45[2]**
Conditions at Offshore[3]	Significant Wave Height (ft)	25.9	37.0	22.6
	Peak Wave Period (s)	11.1	18.2	12.5
	Mean Wave Direction (°N)	195	271	330
	Surge (ft)	1.80	2.83	0.43
Conditions at BOUSS-2D Boundary[4]	Significant Wave Height (ft)	17.7	33.7	20.7
	Peak Wave Period (s)	10.5	18.4	12.3
	Mean Wave Direction (°N)	230	277	319

[1] Storm 72 has the highest wave height among the 79 storms.

[2] Storm 45 has the most north-westerly incoming direction; Storm 60 has the most south-westerly incoming direction.

[3] Wave conditions during storm peaks at offshore CDIP.

[4] Wave conditions at BOUSS-2D model offshore boundary (at a depth of 150 ft MLLW).

Figure 3-92 through Figure 3-97 illustrate the significant wave heights of three selected storms under the four simulated tidal cases for the Existing Conditions and the 2023 PA. Wave heights generally increase in the vicinity of the South Jetty head, where the bathymetry is much shallower than the navigation channel. This is due to refraction of the waves over the side slopes towards shallower water. In other locations, wave heights generally decrease.

For the three storms, the MHHW condition shows the highest waves at the jetties and Entrance Channel. MLLW conditions yield the lowest wave heights. Differences in wave heights are also observed between MSL with flood currents and MSL with ebb currents. Ebb currents cause an increase of the wave heights relative to flood currents.

These figures are particularly illustrative in demonstrating wave propagation at Coos Bay. For all of the storms, the waves tend to focus on the jetty heads. Within the entrance channel, the largest wave heights propagate along the North Jetty, and propagate into LSB just upstream of the LSB headland depicted in Figure 3-90. This further justifies using wave heights at N9 and N10 to assess potential changes to erosion within LSB. Finally, it should be noted that the various results are self-similar; across all incoming wave directions, they show similar behavior, even if the wave heights change between the project conditions.

These figures, particularly Figure 3-94, illustrate the refraction along the channel. Offshore of the jetties, this figure shows wave heights consistently lower in the channel than outside of the channel. Moreover, the highest observed wave heights occur directly adjacent to the channel. This phenomenon explains why the wave heights are drastically larger at extraction point N2 relative to N3.

The differences in significant wave height between the 2023 PA and the Existing Conditions for all three storms are illustrated in Figure 3-98, Figure 3-99, and Figure 3-100. Waves from southwest to west sectors (Storm #60 and Storm #72) tend to show an increase in wave heights at the South Jetty head, and a decrease in wave heights at the North Jetty. This effect is caused by wave refraction over the southern side slope of the deeper channel. Conversely, waves from the northwestern direction (Storm #45) show increased wave heights at the North Jetty and decreased wave heights at the South Jetty. For all cases, wave heights upstream of RM 1 are expected to decrease. This implies less wave propagation to the Charleston Breakwater, LSB, and the eastern shoreline of Coos Bay.

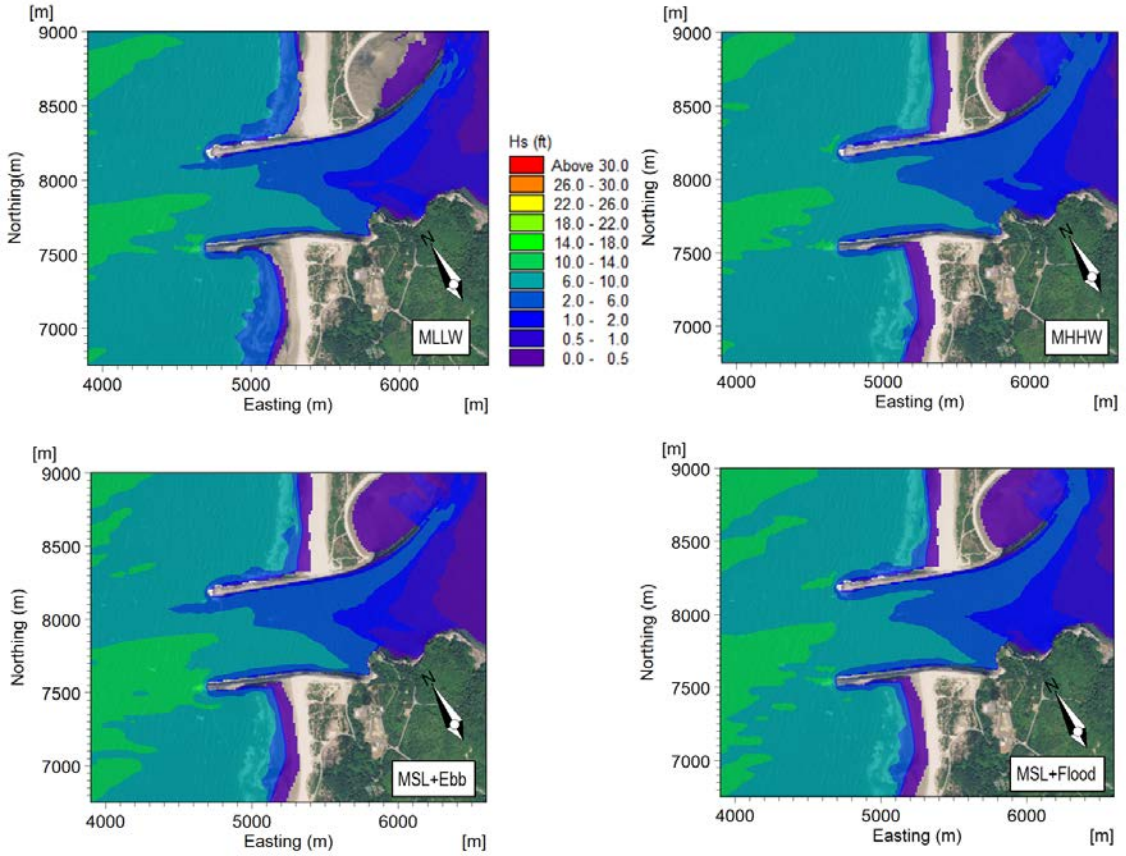

Figure 3-92
South-western Storm #60: Significant Wave Height with Varied Water Levels – Existing Conditions (Wave Direction = 195°; Offshore Hs = 25.9 ft; Peak Wave Period = 11.1 s; Surge = 1.8 ft)

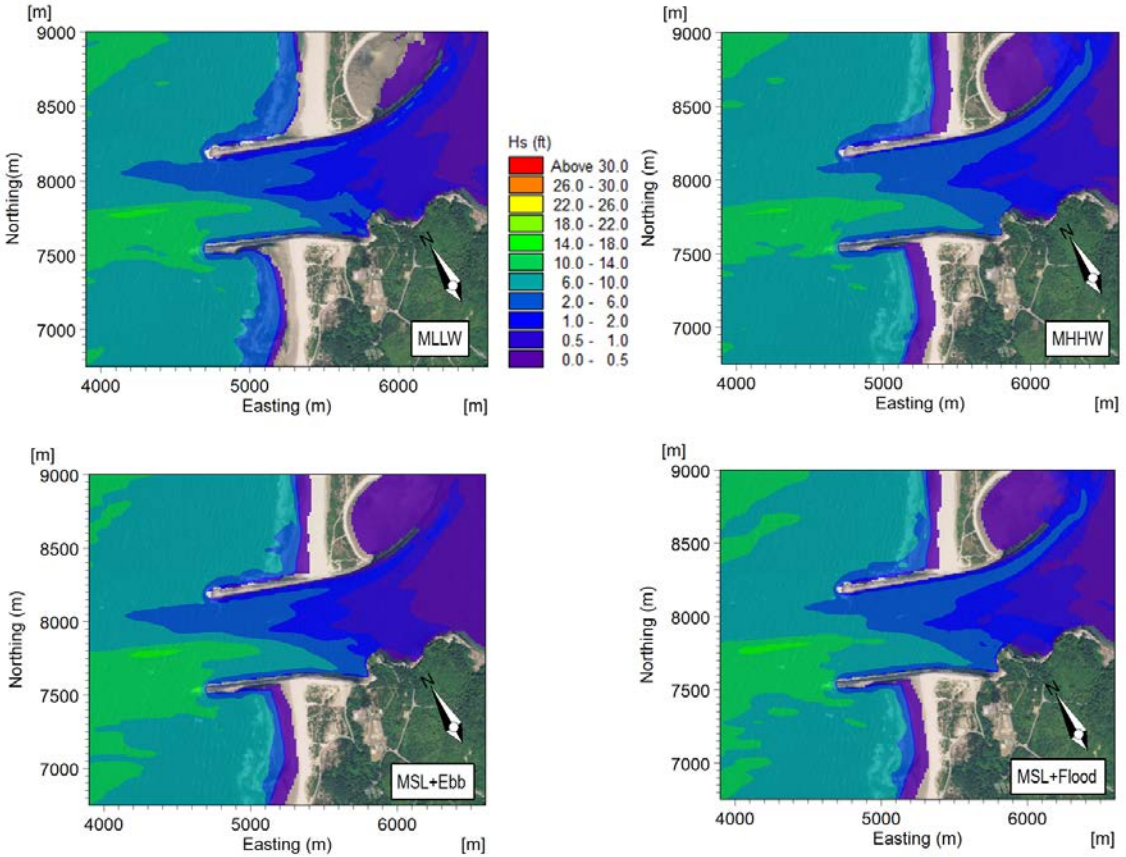

Figure 3-93
South-western Storm #60: Significant Wave Height with Varied Water Levels – 2023 PA (Wave Direction = 195°; Offshore Hs = 25.9 ft; Peak Wave Period = 11.1 s; Surge = 1.8 ft)

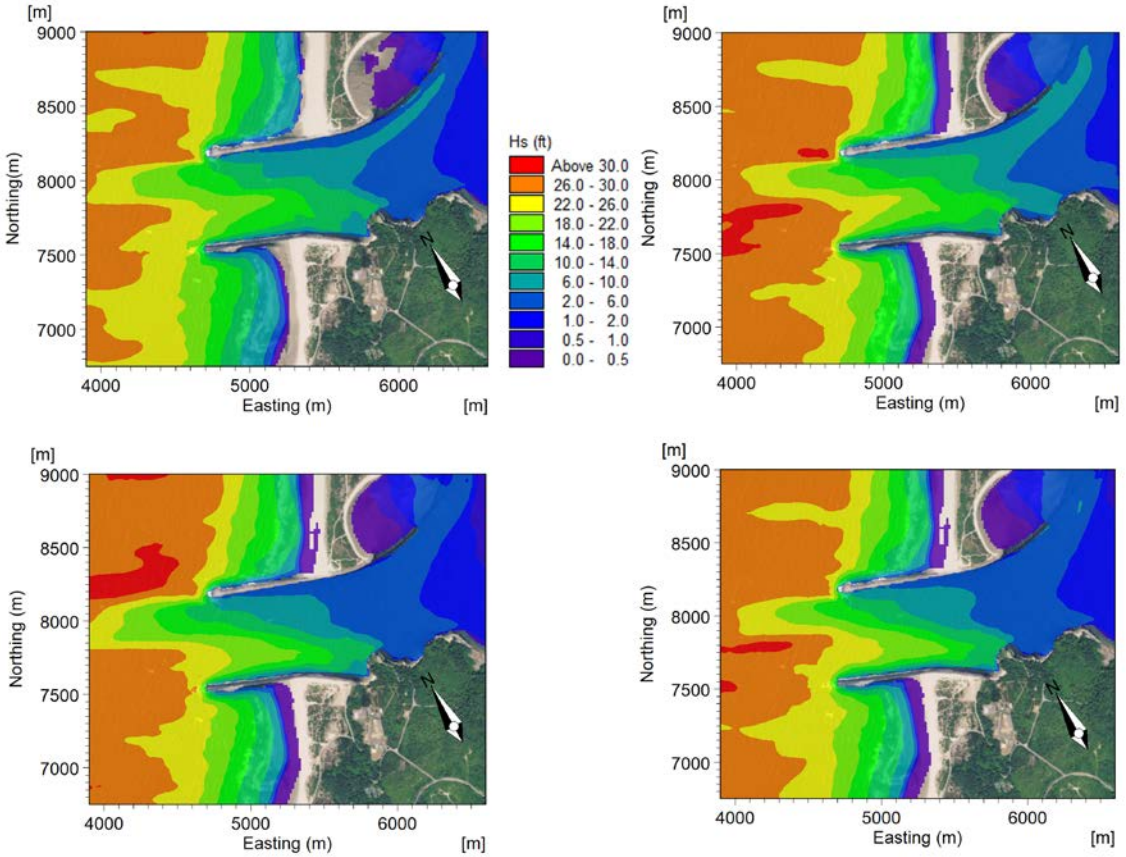

Figure 3-94
Western Storm #72: Significant Wave Height with Varied Water Levels - Existing Conditions (Wave Direction = 271°; Offshore Hs = 37.0 ft; Peak Wave Period = 18.2 s; Surge = 2.8 ft)

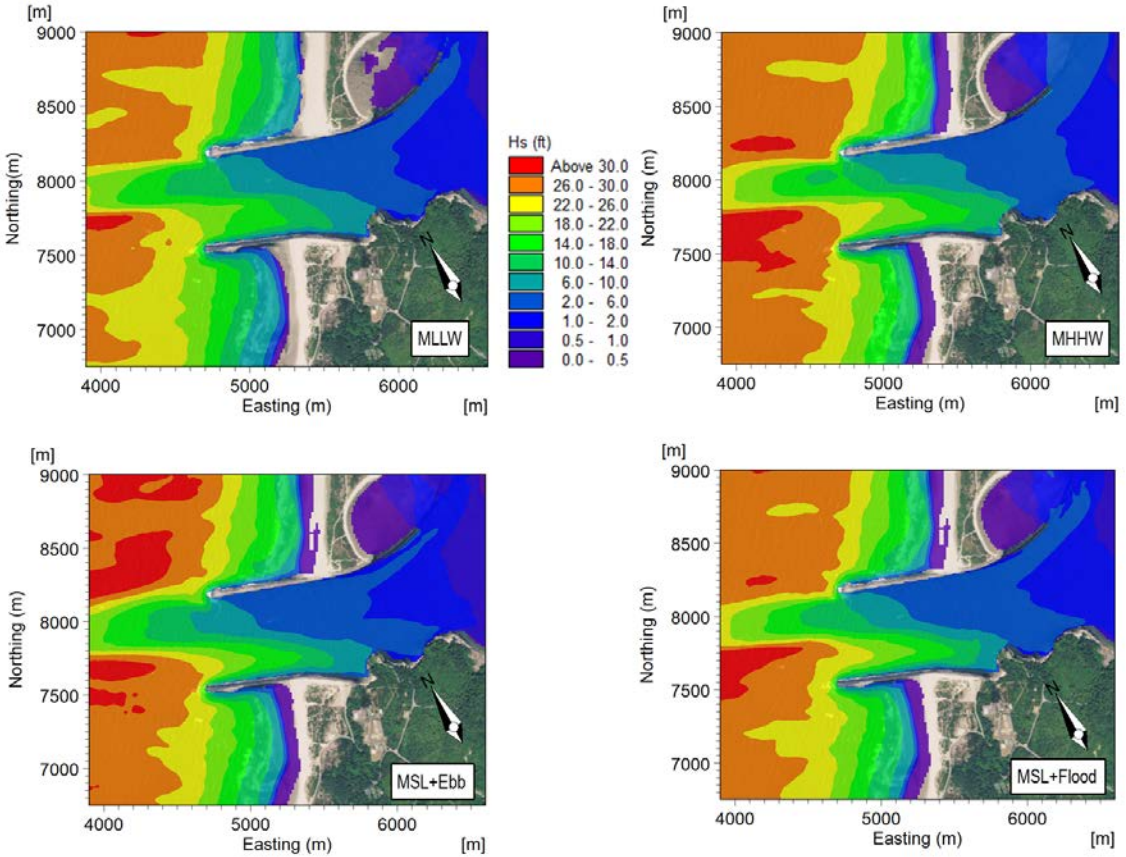

Figure 3-95
Western Storm #72: Significant Wave Height with Varied Water Levels – 2023 PA (Wave Direction = 271°; Offshore Hs = 37.0 ft; Peak Wave Period = 18.2 s; Surge = 2.8 ft)

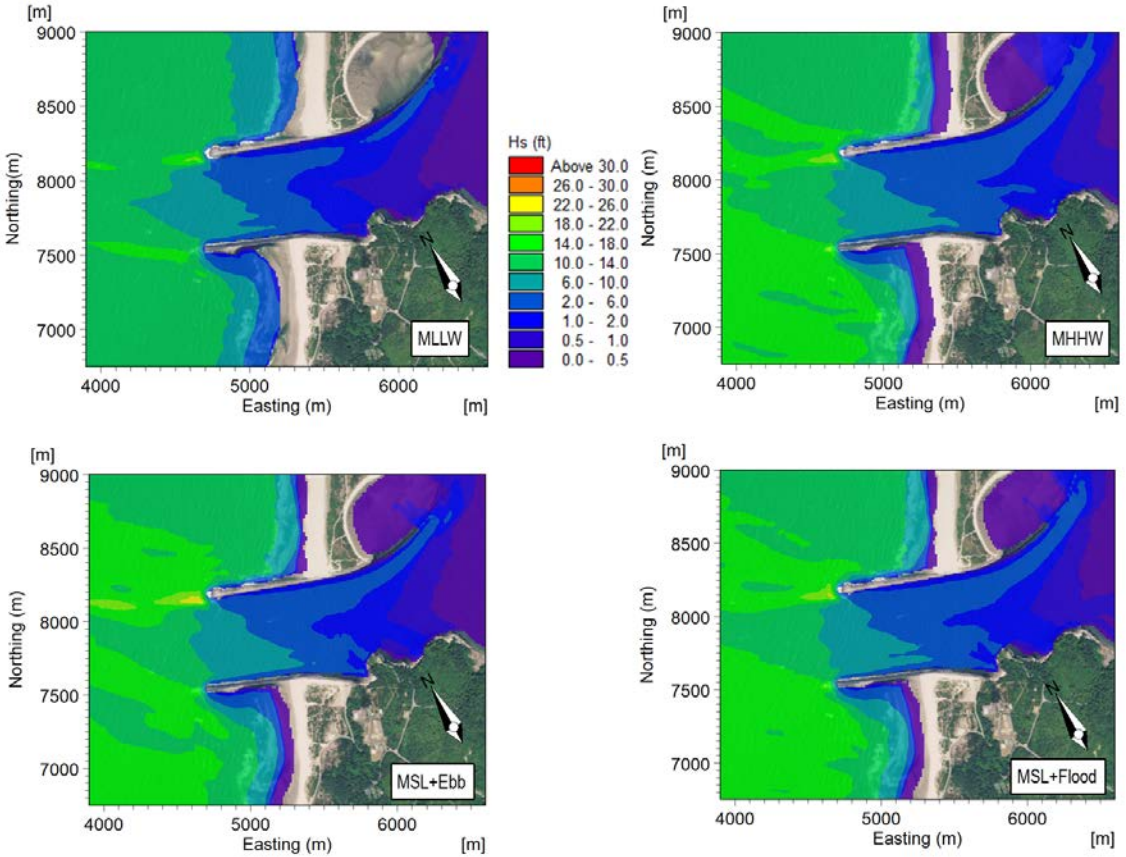

Figure 3-96
North-western Storm #45: Significant Wave Height with Varied Water Levels – Existing Conditions (Wave Direction = 330°; Offshore Hs = 22.6 ft; Peak Wave Period = 12.5 s; Surge = 0.4 ft)

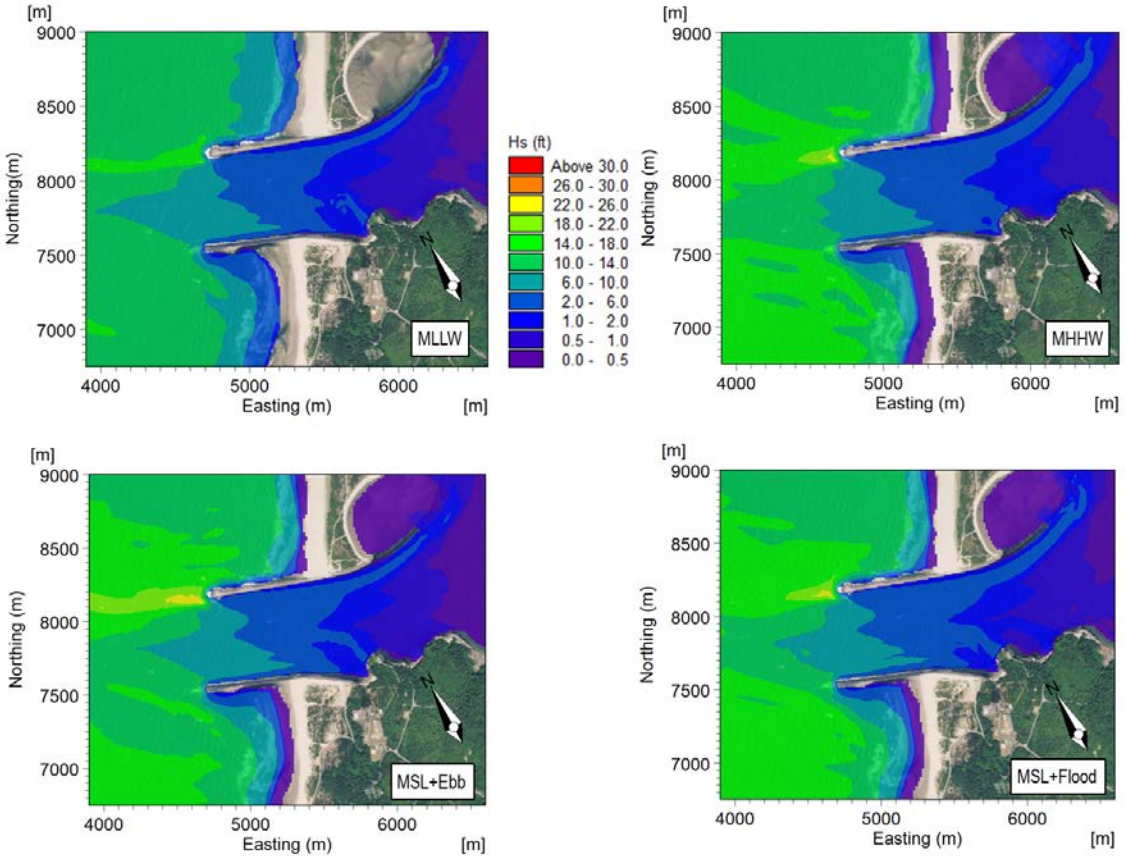

Figure 3-97
North-western Storm #45: Significant Wave Height with Varied Water Levels – 2023 PA (Wave Direction = 330°; Offshore Hs = 22.6 ft; Peak Wave Period = 12.5 s; Surge = 0.4 ft)

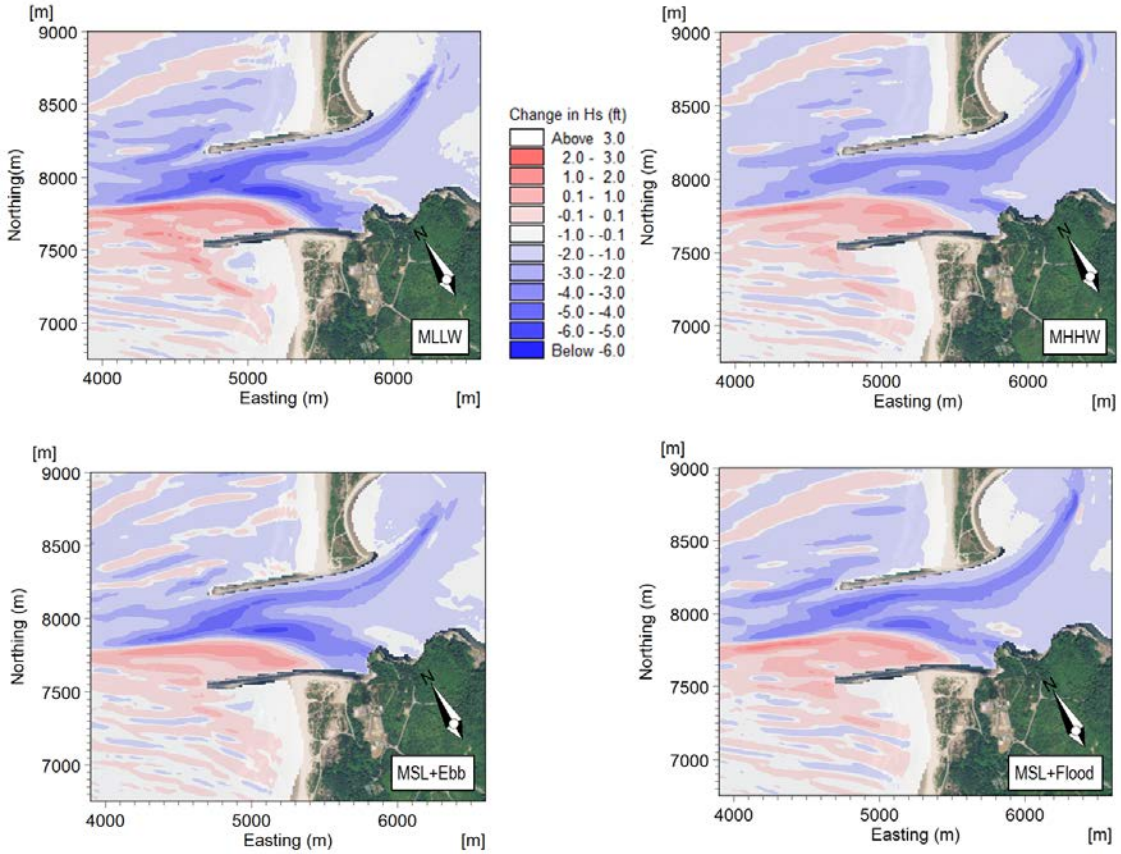

Figure 3-98
South-western Storm #60: Change in Significant Wave Height of 2023 PA (Existing Conditions as Base Case) (Wave Direction = 195°; Offshore Hs = 25.9 ft; Peak Wave Period = 11.1 s; Surge = 1.8 ft)

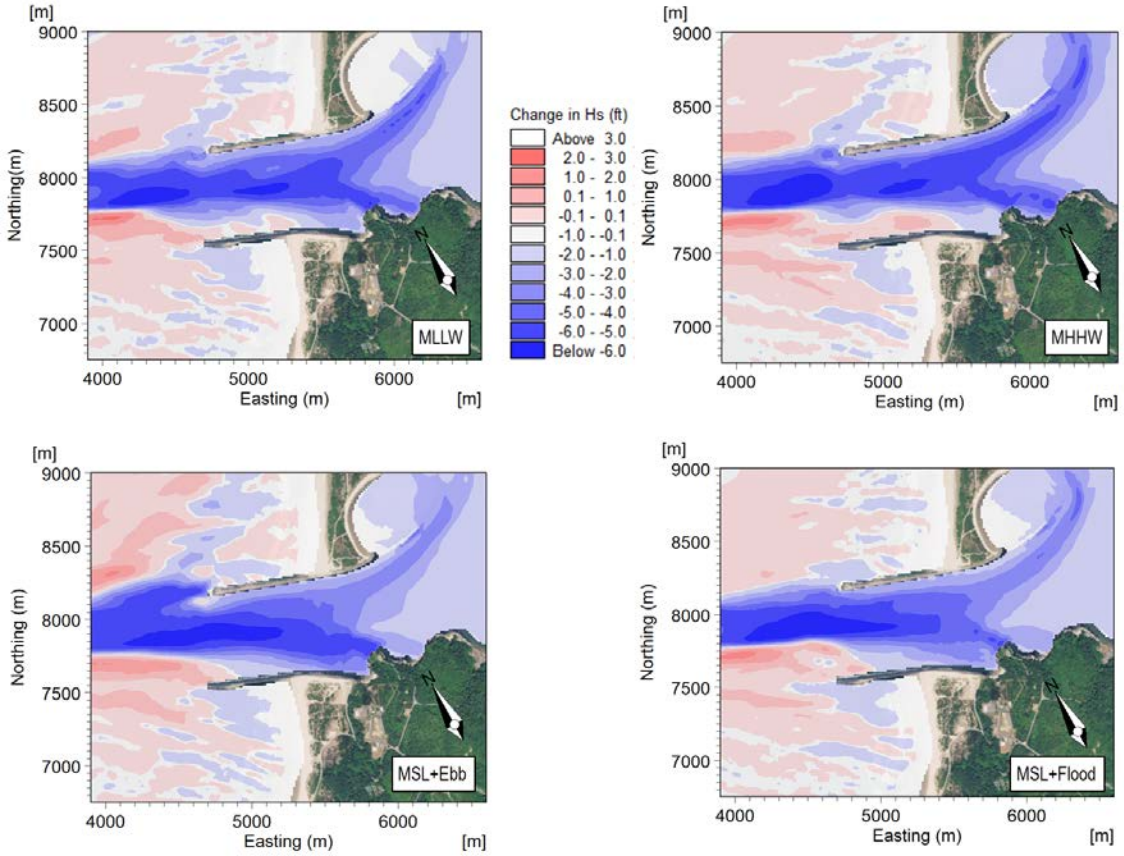

Figure 3-99
Western Storm #72: Change in Significant Wave Height of 2023 PA (Existing Conditions as Base Case)
(Wave Direction = 271°; Offshore Hs = 37.0 ft; Peak Wave Period = 18.2 s; Surge = 2.8 ft)

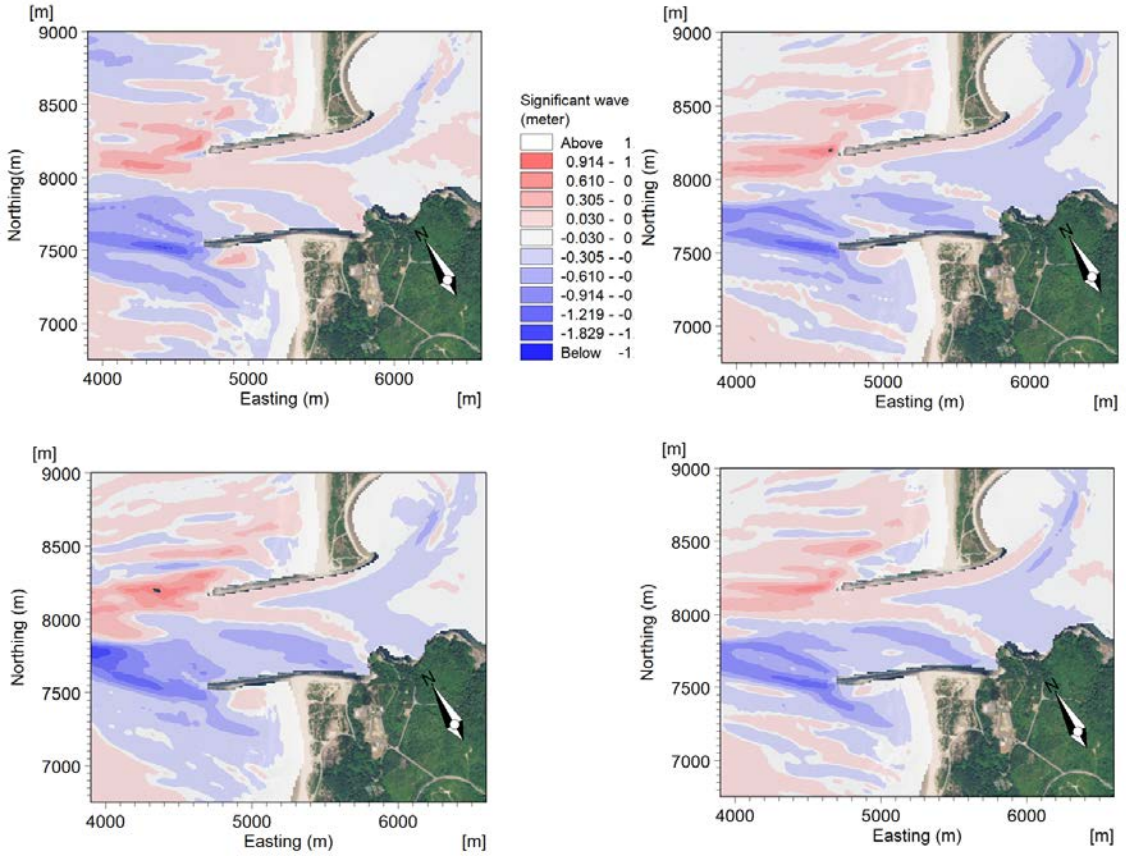

Figure 3-100
North-western Storm #45: Change in Significant Wave Height of 2023 PA (Existing Conditions as Base Case)
(Wave Direction = 330°; Offshore Hs = 22.6 ft; Peak Wave Period = 12.5 s; Surge = 0.4 ft)

It should be noted that the difference plots in Figure 3-98 through Figure 3-100 do show some increases in wave heights under the 2023 PA at certain locations, which appears to contradict the cumulative distribution plots in Figure 3-34 through Figure 3-58. To understand this difference, it should be reiterated that the three storms for which difference plots were generated are directional extremes and not representative of the majority of storms.

In addition, it should be noted that each storm may exhibit a different percentile ranking within the cumulative distribution between the Existing Conditions and the 2023 PA. This fact is exemplified in Figure 3-101. This figure shows cumulative distribution plots at N2 for the four tidal levels, with stars corresponding to Storm 45. As this figure shows, Storm 45 does increase in height at N2 as a result of the 2023 PA. Under MHHW, for example, the significant wave height increases from 19 ft (53^{th} percentile) to 22 ft (82^{th} percentile). Under the PA condition, the northerly direction of the waves focuses more energy on the North Jetty head, and thus the wave height of this storm increases relative to other storms. Considering all storms, however, there is a cumulative decrease in wave energy at this point.

The fact that the wave heights for this storm correspond to different portions of the distribution is illustrative of how the results of the difference plots and the cumulative distribution plots are consistent, despite showing apparently different results. Ultimately, the cumulative distribution plots summarize wave heights for a broad range of storm conditions, not only the directional extremes.

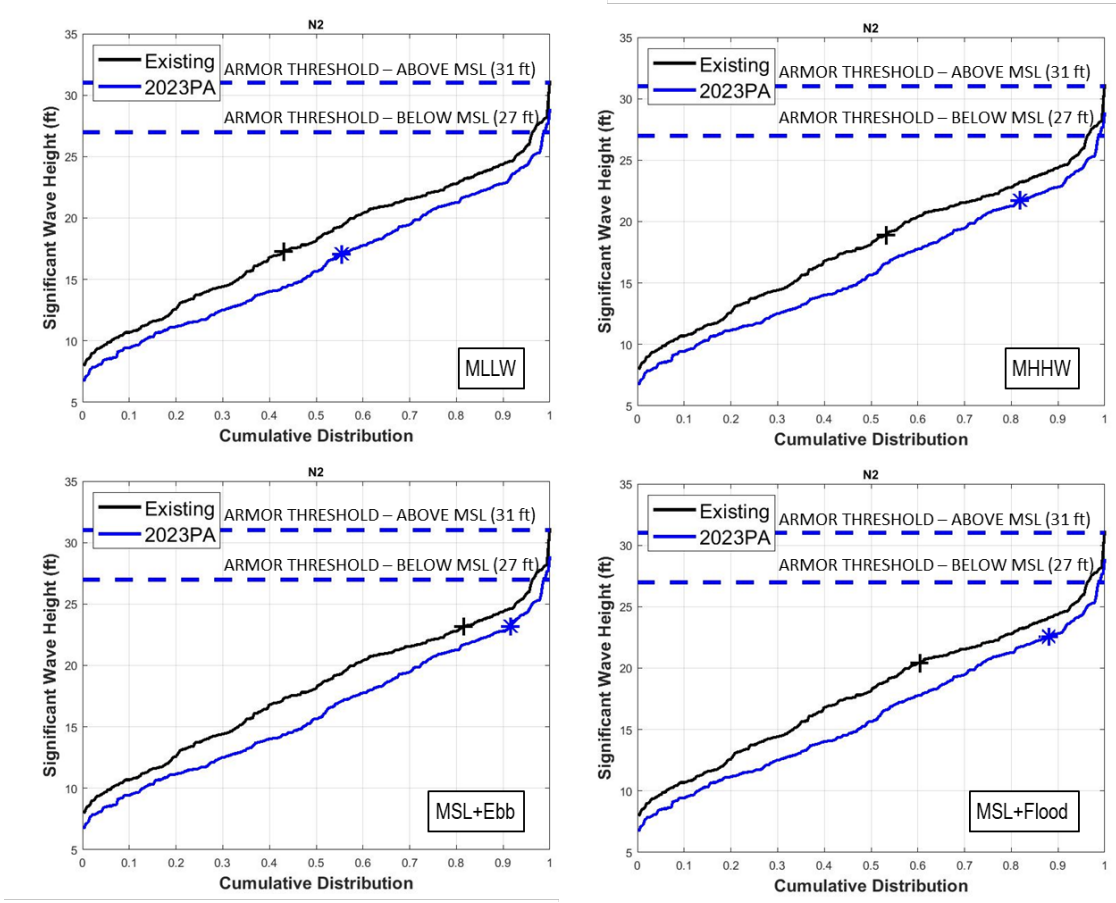

Figure 3-101
Cumulative Distribution Plots Showing the Position of Storm 45

3.3.5.12 Discussion of Extreme Wave from the NW and NNW Sectors at the North Jetty Head

Discussions with USACE staff (Moritz 2018) indicate that waves from the NW and NNW sectors can be especially damaging to coastal infrastructure such as the North Jetty.

Wave simulations were performed for 24 storms from the NW and NNW sectors, with offshore wave directions ranging from 304°N (northwesterly) to 330°N (north-northwesterly). The results of these simulations are summarized in Table 3-8. This table includes the offshore direction and wave height at the North Jetty head under the Existing Conditions and the 2023 PA, and the percent change in wave height. Overall, only 13 of these 24 storms (54 percent) increased in wave height at the North Jetty head. However, for the ten largest storms (i.e., those with the most potential to cause damage), seven result in a decrease in wave height, with the percentage of the decrease exceeding the percentage of the increase. This table is based on the wave extraction point N2 because the largest waves were encountered at point and, therefore, it is critical for jetty stability.

Table 3-8
Simulation of Storms from NW and NNW Directions

Storm Number	Offshore Direction (°N)	North Jetty Wave Height (ft), Existing Conditions	North Jetty Wave Height (ft), 2023 PA	% Change in Height
185	310	29.8	27.7	-7%
106	310	28.0	28.9	3%
264	310	27.5	27.1	-2%
234	306	28.2	24.8	-12%
182	321	26.9	25.3	-6%
313	306	25.8	25.3	-2%
155	306	25.9	26.6	2%
184	304	26.0	25.0	-4%
261	321	25.2	24.4	-3%
103	321	24.6	25.7	4%
27	310	24.5	24.6	0%
173	315	23.9	24.1	1%
76	306	23.7	23.5	-1%
263	304	23.3	24.0	3%
203	330	23.2	23.2	0%
24	321	23.0	22.9	-1%
105	304	22.8	25.1	10%
252	315	21.0	23.1	10%
282	330	20.5	22.6	11%
26	304	21.1	22.2	5%
94	315	19.9	22.8	15%

Storm Number	Offshore Direction (°N)	North Jetty Wave Height (ft), Existing Conditions	North Jetty Wave Height (ft), 2023 PA	% Change in Height
15	315	19.6	21.3	8%
124	330	18.9	21.8	15%
45	330	17.3	17.1	-1%

3.3.5.13 Discussion on Effect of Infragravity Waves

The possibility that infragravity (IG) waves can impact wave propagation at Coos Bay was also investigated. IG transients are generated by nonlinear interactions between gravity waves. IG contributes to the total water level and produces enhanced runup and erosion during storm events. As the water level increases at the crest of the IG wave, depth-limited storm waves can be larger. No data/measurements of IG waves at Coos Bay is available; however, to evaluate their potential effect, the approach used at the MCR by the USACE (Moritz & Moritz 2007) is adopted here. An IG wave spectrum was approximated using a set of parameters from the MCR study. The spectrum was added to the original storm wave spectra with expanded frequency range and resolution. The IG components used to generate the spectra are listed below:

- Significant Wave Height = 2 m;
- Peak Wave Period = 160 s;
- Mean Wave Direction = 290°N; and
- Directional Spreading Deviation = 45°.

A directional spreading of 45 degrees is used when applying the IG component, so the IG waves appear more as a random field. The modeled storms have different intensities, which most likely will result in different magnitudes of IG waves. However, this modeling analysis is done with the same IG parameters.

The BOUSS-2D model ran for three representative storms at MHHW plus surge levels with the existing bathymetry. These three storms correspond to northwest, west, and southwest incoming wave events separately. The Coos Bay Entrance Channel is oriented toward the WNW. The detailed metocean conditions of each of these representative storms are listed in Table 3-7; it should be noted that storms listed in this table do not correspond to the largest storm from these respective directions.

The results from with IG wave runs were compared to those without IG waves. Post-processing was based on the frequency range less than 0.03 Hz, so the energy associated with the IG component was removed before computing significant wave heights (as H_{m0}). Table 3-9 and Table 3-10 list the modeled wave heights at North Jetty and South Jetty points (N1 to N15 and S1 to S8) for both with and without IG waves and the difference (delta) between the two. The tables show that including IG waves could either increase or decrease the waves along the North Jetty. The change of waves varies by individual storms. By keeping the wave frequency band ($f<0.03$ Hz) consistent for with and without IG waves, the results of waves at the North Jetty do not show any trend in wave height change. Measurements of IG waves at the project site during and after project implementation is recommended to assess if there are project related effects on IG wave energy in and outside of the inlet as these related to environmental effects.

Table 3-9
Comparison of Modeled Significant Wave Heights at North Jetty Points (Existing Bathymetry)

Point Name	Storm #72			Storm #45			Storm #60		
	w/o IG (ft)	w/ IG (ft)	Delta* (ft)	w/o IG (ft)	w/ IG (ft)	Delta* (ft)	w/o IG (ft)	w/ IG (ft)	Delta* (ft)
N1	26.5	25.8	-0.7	14.9	15.3	0.4	9.0	10.0	1.0
N2	31.7	29.6	-2.1	19.2	19.3	0.0	9.4	11.2	1.9
N3	17.1	17.0	-0.1	9.3	9.9	0.7	8.3	8.5	0.2
N4	14.3	14.4	0.1	7.2	7.4	0.2	7.9	7.8	-0.1
N5	12.1	12.4	0.2	5.2	5.1	-0.1	6.9	6.9	0.0
N6	10.4	10.5	0.1	4.7	4.6	-0.2	6.4	6.4	0.0
N7	9.7	9.5	-0.2	3.8	4.0	0.1	5.3	5.4	0.0
N8	8.8	8.7	-0.1	3.1	3.2	0.1	4.2	4.1	-0.1
N9	9.0	8.8	-0.2	3.2	3.3	0.1	4.3	4.3	0.0
N10	8.8	8.6	-0.3	3.4	3.5	0.1	4.5	4.5	0.0
N11	7.7	7.8	0.1	2.8	3.0	0.1	3.8	3.9	0.1
N12	7.8	8.5	0.7	1.8	2.2	0.4	3.1	3.5	0.4
N13	4.3	4.4	0.1	1.8	1.7	-0.1	2.6	2.3	-0.2
N14	2.8	3.0	0.1	1.2	1.2	0.0	1.8	1.6	-0.2
N15	0.9	1.0	0.1	0.5	0.4	-0.1	0.6	0.6	-0.1

* Wave height increase due to IG wave components shown in orange font, decrease shown in blue font.

Table 3-10
Comparison of Modeled Significant Wave Heights at South Jetty Points (Existing Bathymetry)

	Storm #72	Storm #45	Storm #60

Point Name	w/o IG (ft)	w/ IG (ft)	Delta* (ft)	w/o IG (ft)	w/ IG (ft)	Delta* (ft)	w/o IG (ft)	w/ IG (ft)	Delta* (ft)
S1	24.1	23.5	-0.5	15.4	16.3	0.8	8.8	10.7	1.9
S2	25.9	25.3	-0.6	16.1	16.0	0.0	9.7	11.5	1.8
S3	27.4	25.4	-2.0	10.6	11.8	1.2	8.9	10.3	1.5
S4	23.0	21.4	-1.7	8.8	9.7	0.9	7.8	9.0	1.2
S5	18.8	16.9	-1.9	7.7	9.0	1.2	6.5	8.0	1.5
S6	17.9	16.0	-1.9	6.4	8.0	1.6	7.0	7.9	1.0
S7	17.1	15.6	-1.5	4.0	5.5	1.6	7.8	8.2	0.4
S8	12.9	12.4	-0.5	2.4	3.8	1.4	5.6	5.8	0.2

* Wave height increase due to IG wave components shown in orange font, decrease shown in blue font.

3.3.6 Expected Extreme Waves for Storm Conditions

The extreme wave heights are evaluated at the toe of slope (for the jetty crest and trunk) and approximately 400 ft from the jetty tips along the jetty alignment. Figure 3-102 illustrates the significant wave heights for 50-year return period along the North and South Jetties from the head to the trunk for the Existing Conditions and the 2023 PA. It should be noted that the Existing Conditions markers are sometimes located directly beneath the 2023 PA markers. The best-fit and 95 percent confidence 50-year significant wave heights at the jetty heads are summarized in Table 3-11. The 50-year return period waves at the North Jetty head (N2) decrease from 30.9 ft under the Existing Conditions to 29.1 ft under the 2023 PA. At the South Jetty head (S3), the 50-year wave increases from 26.7 ft (Existing Conditions) to 27.7 ft (2023 PA).

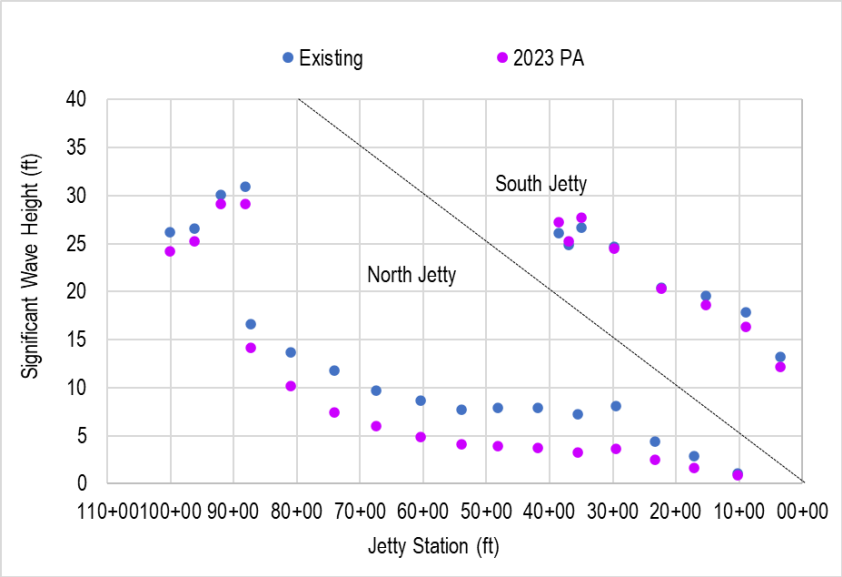

Figure 3-102
50-year Return Period Significant Wave Heights along the Trunk and at the Head of North Jetty and South Jetty for the Existing Conditions and 2023 PA

Table 3-11
50-year Return Period Significant Wave Heights at North and South Jetty Head

Location	North Jetty[1]		South Jetty[2]	
	Best-fit	95% non-exceedance	Best-fit	95% non-exceedance
Existing Conditions	30.9	33.3	26.7	28.8
2023 PA	29.1	31.3	27.7	30.5

[1] The highest waves among the North Jetty points at N2 are presented.
[2] The highest waves among the South Jetty points at S3 are presented.

In summary, the conclusions and recommendations from the wave modeling are:

- Extreme wave conditions along the North and South Jetties are established by simulating multiple storm events combining different water levels and tidal currents. The trends presented above represent a statistical analysis comprising 316 data points.
- Under northern and northwestern wave conditions, the extreme wave heights at North Jetty head would increase due to the deepening associated with the 2023 PA channel. Under western and southwestern waves, the waves at North Jetty head would decrease with deeper

channels. The majority of storm events are from western and southwestern directions, and these storms appear to dominate the extremes analysis, such that the statistical analysis shows decreased extreme waves with the 2023 PA.

- The 50-year return period waves at the North Jetty head (N2) decrease from 30.9 ft under the Existing Conditions to 29.1 ft under the 2023 PA.
- The 50-year return period waves at the South Jetty head (S3) increase from 26.7 ft (Existing Conditions) to 27.7 ft (2023 PA).
- Propagation of extreme waves into the estuary is expected to decrease.

3.3.7 SLC Impacts on Extreme Waves

The same modeling methodology as presented in the previous Section 3.3.1 was adopted in the SLC impact study. The modeled scenarios included elevated water levels that were deemed to represent SLC scenarios. The selected representative SLC value of +3.2 ft is discussed in Section 3.1.1. The four water level and tidal current conditions applied for each storm are:

- MHHW with storm surge and SLC;
- MLLW with storm surge and SLC;
- Max ebb current at MSL with storm surge and SLC; and
- Max flood current at MSL with storm surge and SLC.

The model domain and grid setup are both consistent with what has been discussed in Section 3.3.2. It is assumed that the wave condition changes due to SLR at the BOUSS-2D model boundary are negligible, since the offshore MIKE-21 bathymetry is sufficiently deep that wave propagation is not affected by the 3.2 ft increase in water level. Thus, the MIKE-21 SW model does not need to be re-ran for this supplemental study. Two channel scenarios (Existing Conditions and 2023 PA) were analyzed and compared. Modeling of the two scenarios with and without SLC is to illustrate the differences between pre- and post-project conditions due to SLC.

3.3.7.1 Results of Extreme Waves under Storm Conditions

Extreme wave conditions along the North and South Jetties, at the Charleston Breakwater and Log Spiral Bay are established by extreme value analyses at the selected locations shown in Figure 3-30. Figure 3-103 illustrates the significant wave heights for 50-year return period along the North and South Jetties from the head to the trunk for the Existing Conditions without SLC, the Existing Conditions with SLC, the 2023 PA without SLC, and the 2023 PA with SLC. Extreme wave heights were calculated based on the POT method (Goda 2010). The figure clearly shows the wave heights along the jetties with the jetty station values on the x-axis. However, it can be difficult to see the differences among the four alternative scenarios (i.e., Existing Conditions, 2023 PA, with and without SLC) at some locations. Therefore, separate bar charts for the North and South Jetty presenting the wave heights and the differences due to SLC are provided. In Figure 3-104 and Figure 3-105, the 50-year waves without SLC from Existing Conditions are in blue bars, and runs without SLC from the 2023 PA are in pink. The increases in wave heights due to SLC are shown in the additional red outlined bars on top of the colored bars. Both the Existing Conditions and the 2023 PA experience higher waves along the North and South Jetties with rising sea levels, with an increase up to 2.1 ft. The wave height increases due to SLC are larger at the South Jetty locations than those at North Jetty. This is because the depths along the South Jetty are shallower than those along the North Jetty. The federal navigation channel does not sit in the middle of the entrance, it

is closer to the North Jetty. The rising of sea level affects the depth-controlled wave breaking, and shallower locations are impacted more than the deeper ones.

Table 3-12 lists the 50-year extreme wave heights at the key infrastructure (e.g., the North and South Jetty) of four simulated alternatives. The wave height differences between with and without SLC are also listed in the table. The 50-year return period waves with future sea level (+3.2 ft) at the North Jetty head decrease from 32.0 ft under the Existing Conditions with SLC to 30.7 ft under the 2023 PA with SLC. The wave decrease between the Existing Conditions and the 2023 PA are 1.8 ft for no SLC and 1.3 ft for with SLC, respectively. The 50-year return period waves with future sea level (+3.2 ft) at the South Jetty head increase from 27.8 ft (Existing Conditions with SLC) to 29.3 ft (2023 PA with SLC). The wave decrease between the Existing Conditions and the 2023 PA are 1.1 ft for no SLC and 1.5 ft for with SLC, respectively. According to the 50-year waves with SLC, slightly less decrease of waves at North Jetty and more increase of waves at South Jetty under deepen channel condition of the 2023 PA.

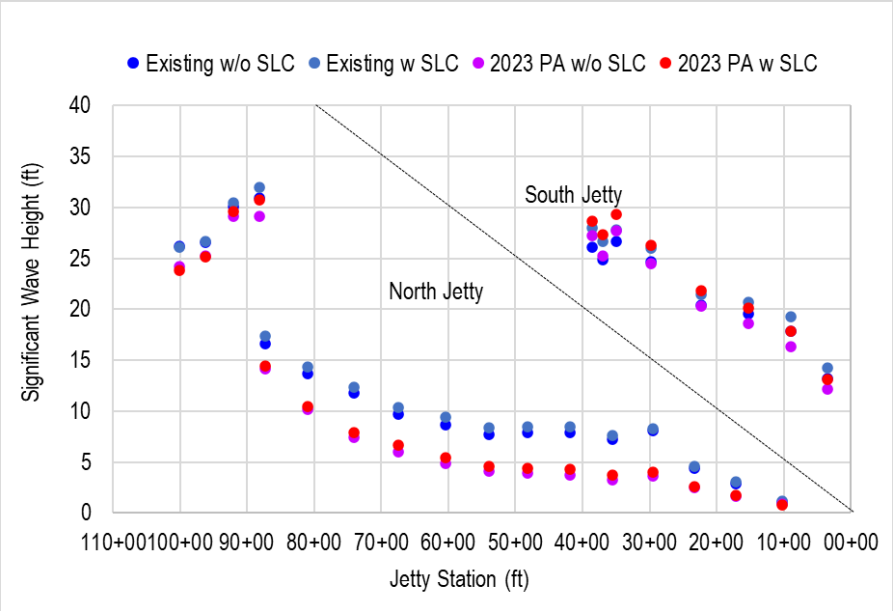

Figure 3-103
50-year Return Period Significant Wave Heights along the Trunk and at the Head of North Jetty and South Jetty for the Existing Conditions and the 2023 PA (w and w/o SLC)

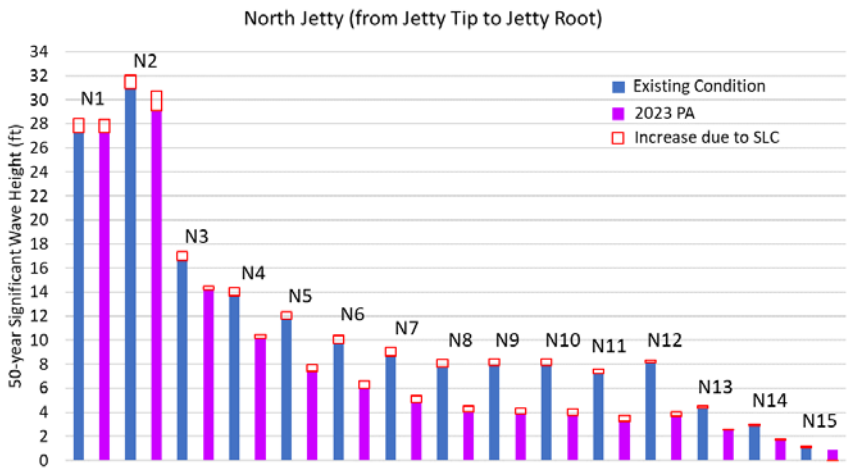

Figure 3-104
Bar Chart of 50-year Extreme Waves at the North Jetty (Location N1 to N15)

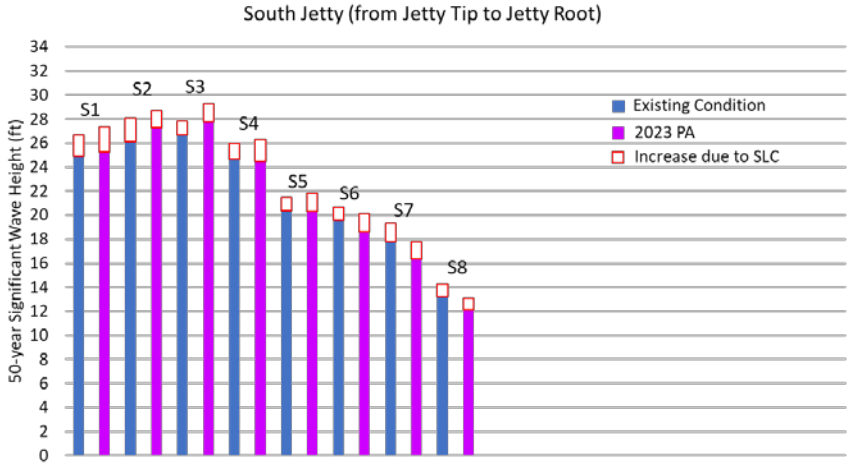

Figure 3-105
Bar Chart of 50-year Extreme Waves at the South Jetty (Location S1 to S8)

Table 3-12
50-year Extreme Wave Heights (Hs in ft) at the Extraction Locations (w/o SLC and w SLC)

Location	w/o SLC			w +3.2' SLC		
	Existing Conditions	2023 PA	Difference[1]	Existing Conditions	2023 PA	Difference
North Jetty (N2)	30.9	29.1	-1.8	32.0	30.7	-1.3
South Jetty (S3)	26.7	27.7	1.1	27.8	29.3	1.5
Log Spiral Bay (L2)	4.2	1.8	-2.4	6.3	3.0	-3.3
Charleston Marina (CM1)	2.0	1.5	-0.5	2.2	1.8	-0.4
Channel Center (C1)	3.8	2.4	-1.4	4.1	2.8	-1.3
Nearshore Beach (Nearshore3)	29.1	29.1	0.0	29.7	29.8	0.1
Offshore (Offshore1)	31.1	33.1	2.0	31.1	33.4	2.2

[1] Significant wave height difference of the 2023 PA from the Existing Conditions.

After analyses of the modeled results, the following conclusions can be made:

- Extreme wave conditions along the North and South Jetties are established by simulating multiple storm events combining different tidal levels, storm surges, tidal currents and a representative SLC by 2080.
- Under northern and northwestern waves, the extreme wave heights at the North Jetty head would increase due to the deepening associated with the 2023 PA channels. Under western and southwestern waves, the waves at the North Jetty head would decrease with the deeper channel. The majority of storm events are from western and southwestern directions, and these storms appear to dominate the extremes analysis such that the statistical analysis shows decreased extreme waves under the 2023 PA condition. This is consistent with what was concluded in without SLC scenarios between the Existing Conditions and the 2023 PA.
- Compared to without SLC scenarios, the increase in wave height occurred over the entire entrance including the jetties, the navigation channel, Charleston Marina and the Log-Spiral Bay with SLR. During the propagation of waves into the entrance, the wave height increases due to SLC are bigger at South Jetty than those at North Jetty.

- The 50-year return period waves with future sea level (+3.2 ft) at the North Jetty head decrease from 32.0 ft under the Existing Conditions to 30.7 ft under the 2023 PA. The wave decrease between the Existing Conditions and the 2023 PA are 1.8 ft for without SLR and 1.3 ft for with SLC, respectively.
- The 50-year return period waves with SLC (+3.2 ft) at the South Jetty head increase from 27.8 ft (Existing Conditions) to 29.3 ft (2023 PA). The wave decrease between the Existing Conditions and the 2023 PA are 1.1 ft for no SLC and 1.5 ft for with SLC, respectively.
- According to the 50-year waves with SLC, slightly less decrease of waves at North Jetty and more increase of waves at South Jetty under the 2023 PA deepened channel condition occurs.

4. VESSEL MOTION DUE TO WAVES

This section outlines the evaluation of wave-induced vessel motion in the Entrance Channel. Vessel motions in waves are governed by the interactions of a complex set of parameters to include:

1. Vessel length, breadth, draft, and displacement
2. Metacentric height and cargo loading
3. Vessel speed and direction
4. Wave encounter frequency
5. Wave encounter direction
6. Channel depth and banks

The modeling of these interactions is not trivial and often benefits from validation of models by independent methods. EM 1110-2-1613 (USACE 2006) identifies the problem with a lack of specific data for ship motion prediction validation in shallow water conditions. The EM presents three methods of analysis for final design: 1) analytical using theoretical calculation tools; 2) experimentally with scale models; or 3) direct full-scale measurements of transiting ships. For development of the vessel response in the Coos Bay Entrance Channel, analytical tools have been applied using numerical modeling software.

The vertical response of vessels to waves was evaluated using ANSYS-AQWA, a program that is designed to evaluate the dynamic response of floating bodies (e.g., vessels) to waves. While a typical application of the program may be for mooring analysis, the program is capable of simulating the encounter frequency of waves when the vessel is underway, providing a technical basis for estimating vessel response while underway.

4.1 Software – ANSYS-AQWA

AQWA is a suite of programs comprising a diffraction/radiation analysis program, a hydrostatic solver, and frequency and time domain analysis programs. The hydrodynamic diffraction program is a frequency domain solver utilized for developing the primary hydrodynamic parameters required for undertaking complex motions and response analyses. These include wave forces, interference or diffraction effects, and body-induced radiation terms. Response transfer functions, referred to as response amplitude operators (RAOs), are also produced. Computation of the second-order wave forces via the full quadratic transfer function matrices permits use over a wide range of water depths. While primarily used for mooring analysis, AQWA can be used for assessing a constrained vessel response in spectral waves. Run in time domain simulations, time series of spectral waves may be applied in conjunction with defined directional spreading.

4.2 Design Vessels

The project design vessels include a large forest products bulker and Containership. The selected design vessel for the wave response analysis was a post-Panamax Containership, representative of the longest vessel likely to visit Coos Bay under the PA Condition. The primary analysis for vessel excursions is based Containership. A sensitivity analysis is used to compare the response of the container ship to the response of the bulker and illustrate differences that could be the subject of further study (see sensitivity analysis in Section 4.6). Table 4-1 shows the vessel particulars for the Post-Panamax Containership *Kalina*.

Table 4-1
Vessel Particulars for Post-Panamax Containership Kalina

Parameter	Operating Draft
Length Overall (LOA)	1200.8 ft (366 m)
Beam	168 ft (51.2 m)
Operating Draft	45 ft (13.7 m)

4.3 Wave Conditions

Waves as far upstream as Guano Rock can have a substantial effect on the ability of vessels to transit the entrance under varying wave conditions. The risk that vertical motion induced by waves might cause the vessel to bottom out is particularly significant with the hard, rocky bottom of the channel near Guano Rock. The wave response simulations were performed based on wave statistics at four different points in the channel:

- Guano Rock
- Jetty Tips
- RM 0
- RM -1

The wave climate used for this study is based on the wave modeling presented elsewhere in this study (e.g., Section 3.3). To reduce the computational burden on the analysis, approximately 50% of the offshore wave conditions were identified as “calms” (below ~2.5ft Hs) and were excluded from the analysis. The remaining wave conditions (51.7% of all wave states) were used as the basis for the vertical vessel motion analysis.

The wave conditions retained for analysis were propagated from offshore to the project using a spectral wave model. Joint histograms of wave height and period for these conditions are presented in Figure 4-1 and Figure 4-2 for the four locations used in this analysis. Note that these histograms only account for 51.7% of the data, with the remaining data points considered as “calm” with no vertical vessel motion analyzed.

For each non-zero cell in each joint histogram, vessel response simulations were performed in AQWA assuming a mean wave direction coincident with the vessel path and a second wave heading that was 15 degrees oblique to the vessel track. With this method, wave direction was not included as a statistical variable, but is accounted for in that two wave headings were analyzed for each wave condition and the most conservative result was reported to represent that wave height and period combination.

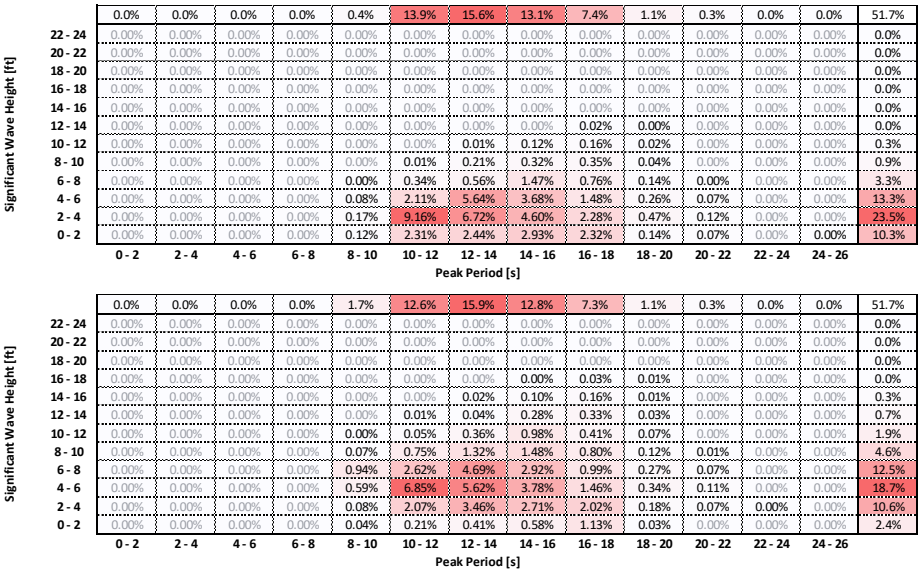

Figure 4-1
Joint Histogram of Wave Conditions at Guano Rock (top) and Jetty Tips (bottom)

Figure 4-2
Joint Histogram of Wave Conditions at RM 0 (top) and RM -1 (bottom)

4.4 Operating Conditions

Because container ships can operate at the design operating draft in both inbound and outbound paths, the design container ship was simulated in both directions. As observed in the vessel simulation study (see Sub Appendix 7), the speed of the vessel varies along the path and is different for inbound and outbound directions. Typical transit speeds at each point in the channel were obtained from the vessel simulation results and are summarized in Table 4-2.

Table 4-2
Typical Transit Speeds for Containership Kalina

Location	Typical Speeds [knots]	
	Inbound	Outbound
Guano Rock	6 – 8	7 – 9
Jetty Tips	7.9 – 9.5	11 – 13
RM 0	8 – 10	12 – 14
RM -1	8 – 10	12 – 14

The goal of this modeling effort was strictly to evaluate vertical vessel motion due to waves. Therefore, a simple bathymetry was defined, with the vessel traveling in a straight line through open water with a specified depth. Representative depths were defined for each location based on preliminary channel design. The depth simulated in the model for the Jetty Tips and further offshore (RM 0 and RM -1) was 62 ft. This accounts for a 57 ft channel with 5 ft tidal assist. The water depth simulated at Guano Rock was 50 ft, which corresponds to a 45 ft channel with 5 ft tidal assist.

AQWA simulations (Figure 4-3) were prepared to evaluate the response of the design vessel at each of the four channel locations, for the design wave conditions (Figure 4-1 and Figure 4-2). The vertical response of each wave condition at each location was considered with the vessel transiting inbound and outbound, each direction at two different speeds (reflecting the ranges shown in Table 4-2).

Each simulation was run for a duration of 3 hours and the average of the six maximum negative excursions was used as the statistic for reporting. This represents a mean estimate of the maximum negative excursion over a 30-minute period.

With between 40 and 72 wave height and period combinations considered for each location, two different wave headings, two different vessel speeds, and two different transit directions, a total of approximately 2,000 AQWA simulations were completed to simulate vertical vessel motions for this study.

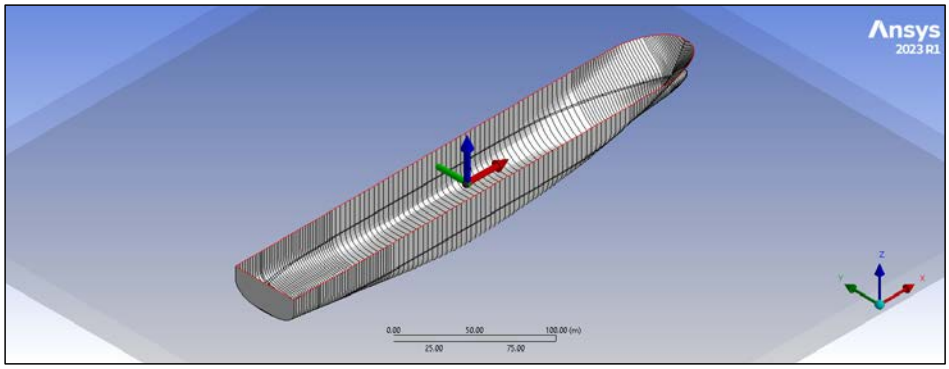

Figure 4-3
AQWA Container Model

4.5 Analysis Results

Figure 4-4 shows the vertical motion due to waves calculated for the PA. Only 52% of waves were simulated at the four locations with the assumption that the remaining wave conditions result in calms with negligible vertical motion effects. The histogram indicates wave shoaling as waves progress from the deeper waters at RM-1 to the shallower depths at Guano Rock, which is identified by the increased number of lower wave excursions at Guano Rock. The histogram is positively skewed, with a long right-hand tail. This indicates that while most vertical excursion values are smaller in nature, there are wave excursions exceeding 15-feet at the offshore locations (RM -1 and RM 0). Vessel excursions at the Jetty Tips did not exceed 14-feet, while the max excursion at Guano Rock did not exceed 10-feet.

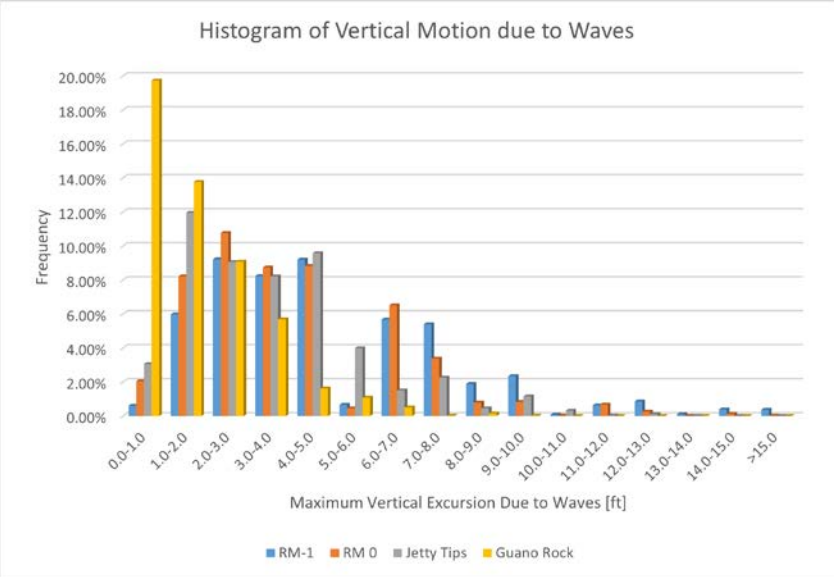

Figure 4-4
Histogram of Vertical Motion due to Waves

Figure 4-5 depicts the percent exceedance of various vertical motion thresholds that could be used for design. The graph shows how increasing the motion allowance in each location would affect the percent of the time that vessels could safely pass. Table 4-3 provides same data in tabular form. The shading within the table indicates the ability to transit based on the following categories:

- **RED** = less than 85% availability
- **ORANGE** = 85% to 90% availability
- **GREEN** = 90% to 95% availability
- **BLUE** = greater than 95% availability

These categories reflect a subjective classification of channel availability, but with the understanding that container ports require a high-degree or operability in order to maintain the scheduled routes.

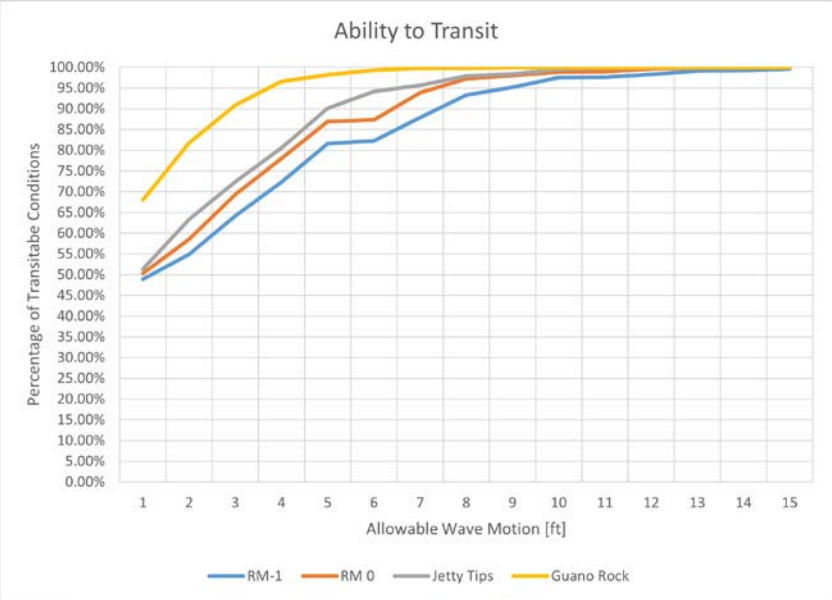

Figure 4-5
Ability to Transit at Various Wave Locations

Table 4-3
Percent of the Time That Vessels Can Transit Each Point

Allowable Wave Motion (ft)	RM - 1	RM 0	Jetty Tips	Guano Rock
1	48.9%	50.4%	51.4%	68.0%
2	54.9%	58.6%	63.3%	81.8%
3	64.1%	69.3%	72.4%	90.9%
4	72.4%	78.1%	80.6%	96.6%
5	81.6%	86.9%	90.2%	98.2%
6	82.2%	87.4%	94.2%	99.3%
7	87.9%	93.9%	95.7%	99.8%
8	93.3%	97.3%	97.9%	99.8%
9	95.2%	98.1%	98.4%	100.0%
10	97.6%	98.9%	99.5%	100.0%
11	97.6%	98.9%	99.8%	100.0%
12	98.3%	99.6%	99.9%	100.0%

These vertical vessel motion statistics were incorporated into the design channel depth analysis (See Section 6.6 in the Main Engineering Appendix Report). Additionally, the resulting channel availability will be incorporated into a comprehensive terminal downtime analysis (as part of the terminal design) that will also account for fog, extreme winds and the ability of pilots to board the vessels to determine the terminal's overall operational availability.

4.6 Model Validation and Sensitivity Test

According to EM 1110-2-1613 (USACE 2006), the use of analytical tools for predicting vertical vessel motions in shallow, exposed waterways are an area of active development with few data for validation. However, within EM 1110-2-1613 itself, results are presented from studies at the MCR as collected by Portland District over two years in the late 1970s. Based on those studies, maximum ship motion for waves of 6-12 ft high are expected to be approximately two times the significant wave height. This result is higher than the ratio of maximum vessel excursion to wave height for AQWA simulations in this study, which are generally less than 1.0. A reasonable explanation for this difference is that the vessels studied 40 years ago would have been smaller than the large Containership examined for the present study and would have likely been much more responsive to the waves.

As a sensitivity analysis, the AQWA simulations for the design container ship were compared to analogous simulations for an 820 ft bulker. This vessel is smaller than the container ship and would be expected to respond more to the wave excitation (if the logic provided in the preceding paragraph holds true). Table 4-4 provides the vessel parameters and Table 4-5 provides the results.

Table 4-4
Vessel Model Parameter Comparison - Container Ship and Bulker

Parameter	Container Ship	Bulker
Length Overall (LOA)	1200.8 ft	820.2 ft
Beam	168 ft	141 ft
Operating Draft	45 ft	39.4 ft

Table 4-5
Comparison Container Ship to Bulker Wave Response

Comparison Case No.	Peak Wave Period [s]	Sig. Wave Height [ft]	Wave Dir Relative to Course [deg]	Maximum Negative Amplitude [ft]	
				Container Ship	Bulker
1	9	15	4	2.7	5.9
2	9	15	10	2.5	5.3
3	9	12	15	2.0	4.6
4	12	12	4	4.0	6.4
5	12	12	10	5.1	5.8
6	12	9	15	4.2	4.2
7	15	6	15	5.4	5.4
8	18	4	15	2.8	5.9

Commented [JS9]: A-4-12 Bulker Sensitivity

Commented [JS10R9]: Analysis has been revised and included in Main Engineering Appendix Report Section 6.6

5. SEDIMENTATION

Analysis of sedimentation patterns at Coos Bay was performed to quantify:

- Material transported along the adjacent coastline;
- The potential for this material to be deposited within the channel; and
- The short- and long-term fate of the dredged material.

This section describes the sediment transport patterns near the navigation channel and associated ocean disposal sites within the larger context of the larger Coos littoral cell.

5.1 Background

This section provides an overview of the historic observations of sediment transport at Coos Bay. This is based on the information contained in the 1994 Environmental Impact Statement (EIS) (USACE 1994).

Coos Bay lies at the southern boundary of the Coos littoral cell, which extends for 90 kilometers from Cape Arago to Heceta Head (Figure 5-1). This littoral cell is the largest on the Oregon coast. Except for the headlands at both ends of the cell, the entire coastline consists of beach fronting sand dunes. Three major river systems enter the cell. From south to north these are the Coos River, the Umpqua River (which is the largest and provides the major source of sediment to the cell), and the Siuslaw River. Mineral assemblages of the Umpqua River correlate with the littoral sand mineralogy, which indicates that the primary source of sand within the cell is from the Umpqua River. Various sedimentological studies based upon sand mineralogy have suggested an offshore limit of modern sand movement at 60 ft depth, while others push this limit out to over 100 ft. The Coos River is situated at the southern boundary of the Coos littoral cell, adjacent to Cape Arago. Material dredged from the lower Coos Bay channel is similar, relative to local beach sands.

The EIS (USACE 1994) referenced two zones of sand transport: inner and outer, based on wave conditions. The inner littoral zone is the area of significant year-round transport, both alongshore and onshore-offshore, by breaking waves. The outer shoal zone is affected by large wave conditions and is limited to onshore-offshore transport. In general, winter storms erode and transport sand offshore and summer swell moves sand onshore. Comparison of aerial photographs along the Oregon coast shows a dramatic increase in width of the surf zone during the winter.

The limiting depth for strong longshore transport is proposed to vary from 28 ft in summer to 50 ft in winter on the Oregon coast. At depths less than 50 ft, coarse-grained sediments experience strong onshore and longshore transport during most of the year. At depths greater than 150 ft, coarse-grained sediments are little influenced by waves and currents strong enough to cause significant movement (i.e., depths greater than 150 ft are non-dispersive). The area between 50 and 150 ft is progressively influenced by waves and currents sufficiently strong enough to cause movement with decreasing depth.

Figure 5-1
Extents of Coos Littoral Cell

5.2 Observed Vegetation Line Change

The anthropogenic changes within Coos Bay have had a significant impact on sedimentation patterns. The construction of the North Jetty resulted in the formation of a well-defined North Spit in a sandy shoal that had been previously migrated along the coastline. Similarly, the construction of the South Jetty retained sand behand Coos Head and Cape Arago in the location that is presently Bastendorff Beach (immediately south of the South Jetty).

Accretion of the North Spit continued until about 1944, when the fully-develop spit began to erode; erosion occurred from both the seaward (beach) side as well as from the interior (LSB). This section investigates the use of aerial imagery and topographic data to quantify sedimentation patterns.

5.2.1 Long-Term Overview

The entrance to Coos Bay and surrounding areas is characterized by substantial sediment transport, significant human intervention, and a very energetic wave and current environment. The original

nearshore bathymetry, prior to construction of any of the jetties, is shown in Figure 5-2. This original bathymetry exhibits a nearshore shoal, oriented northward, that has almost no relationship to the present nearshore bathymetry.

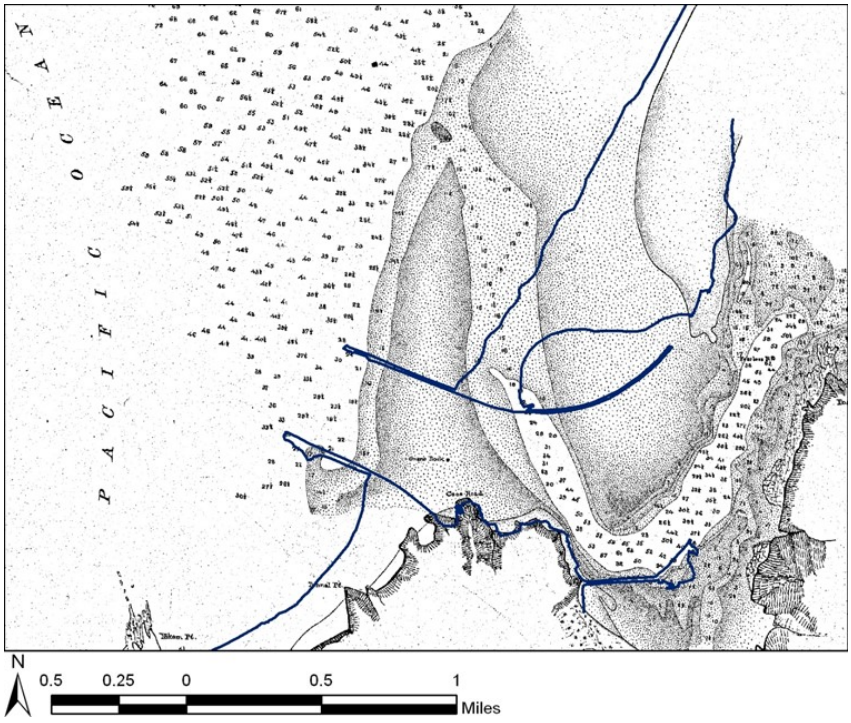

Figure 5-2
Original Nearshore Bathymetry: 1879 Survey

Before jetty construction, the nautical chart indicates a shifting spit to the north and rocky headland with little beach to the south. The North Jetty was constructed from 1891 to 1895 and the South Jetty from 1924 to 1928. Figure 5-3 illustrates the changes of long-term vegetation line at Coos Bay, that is, since construction of the jetties. The dune line is a reasonable proxy for the vegetation line. In the figure, the blue line illustrates the dune line from the 1865 nautical chart, which reflects entrance conditions before either jetty was constructed. The pink and purple lines are vegetation lines from the 1944 and 2019 aerial photographs, respectively.

By 1944, the vegetation line along the Pacific coast was approximately in its current position. Bastendorff Beach had formed as a pocket beach between the South Jetty and the rocky Cape Arago to the south. The vegetation line at the north end of Bastendorff Beach was close to its present-day condition, but elsewhere it was still 400 to 700 ft inshore of its present position. The Pacific shoreline of the North Spit had essentially stabilized by 1944. LSB had just begun to form at the root of the North Jetty.

Between 1944 and the present time, the most significant changes are the formation and growth of LSB and ongoing accretion of the south part of Bastendorff Beach.

The following points illustrate the large sediment quantities and large inertia in the system:

- The North Spit accreted by more than 300 ac on the ocean side in response to construction of the North Jetty. This corresponds to approximately 30 mcy, based on an active profile of 60 ft, from a dune top at +20 ft MLLW to the limit of the nearshore zone at -40 ft MLLW. The North Spit accreted for approximately 50 to 60 years, from construction of the North Jetty at the end of the 19th century until the maximum extent was reached in the 1950s. Since that time through 2019, it has generally been receding.
- Bastendorff Beach accreted by approximately 80 ac, or approximately 8 mcy. This beach is either stable or still accreting 70 years after construction of the South Jetty.
- More than 100 mcy of material has been dredged from Coos Bay since the end of the 19th century, excluding material from above RM 12 (dredging upstream of this removes fine material that is of fluvial rather than marine origin).

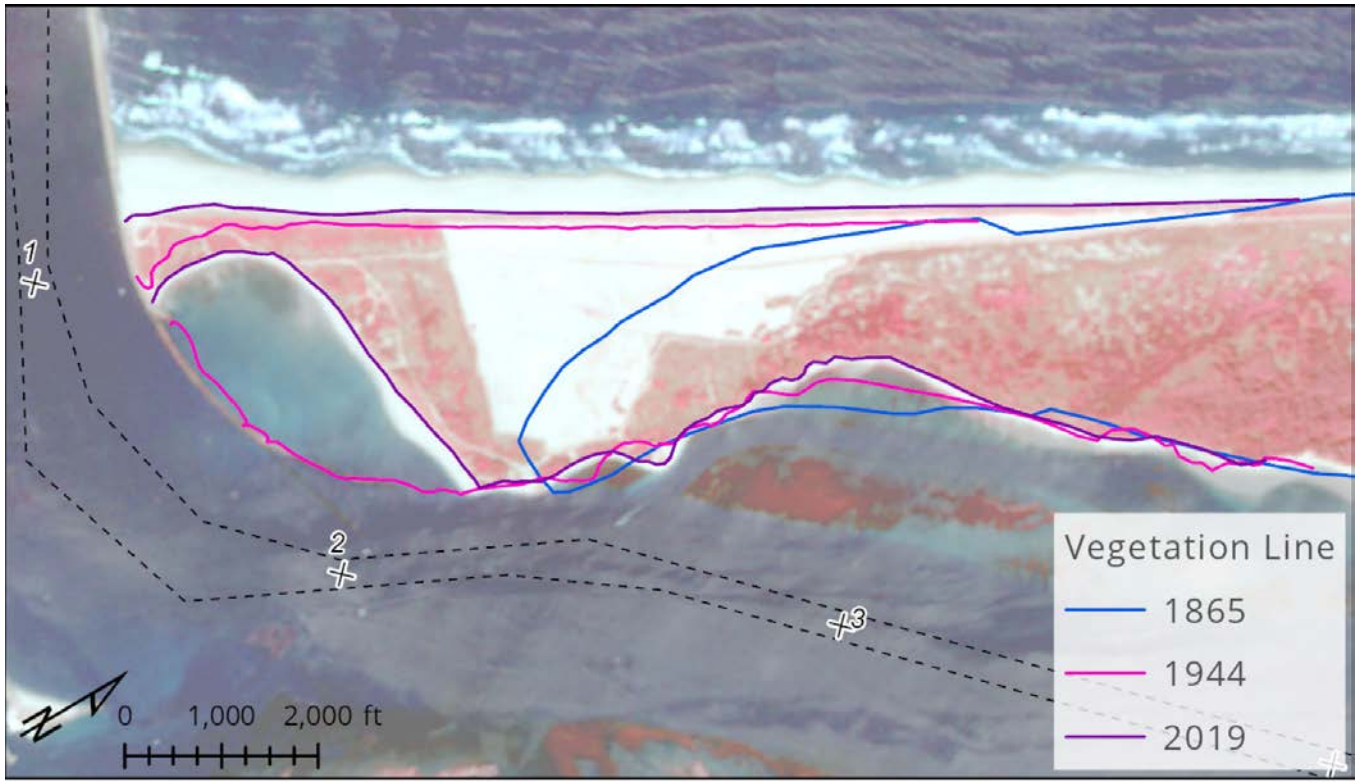

Figure 5-3
Long-Term Vegetation Line Change at Coos Bay, OR. Chart / Photograph Dates 1865, 1944, and 2019

5.2.2 Pacific Coast

Eighteen aerial images, listed in Table 5-1, were acquired and geo-referenced by M&N. The two photographs from the National Agriculture Imagery Program (NAIP) were provided as orthorectified data files. The photographs from the USACE had been scanned from 9”×9” black and white or color contact prints and were rectified for this work. One earlier (1939) data set was available but could not be satisfactorily rectified because of the small area of coverage and lack of registration points.

Table 5-1
Aerial Photographs Used in Vegetation Line Change Analysis

Photo Date	Source	Photo Date	Source
05/11/2016	NOAA	9/15/1983	USACE
06/10/2012	NOAA	4/15/1980	USACE
6/17/2009	NAIP	8/27/1978	USACE
2/15/2008	USACE	5/10/1973	USACE
12/10/2005 *	USACE	10/16/1971	USACE
7/17/2005	NAIP	8/29/1968	USACE
6/19/2002	USACE	7/28/1959 †	USACE
8/8/1995	USACE	7/29/1956	USACE
11/2/1989	USACE	5/15/1944	USACE

Notes:

* This image is not used because the errors in geo-referencing are similar to the size of changes since the earlier, higher quality photograph.

† This image is not used because it only covers a small area of shoreline.

Most of the photographs were geo-referenced using registration points from the orthorectified 2009 NAIP photograph. This photograph has very high resolution and covers the full area of interest. For photographs after 1971, persistent features could be identified to geo-reference the image. Supplementary registration points were identified on the 1971 photograph and used in geo-referencing the earlier photographs.

The analysis focuses on the vegetation line, which marks the edge of the dune. The wetted bound line (which is sometimes used as a proxy for the high tide line) is not used here. On the open Oregon coast, wave conditions are so variable and can be so energetic that a dramatic difference (as much as 600 ft) in the position of the wetted bound line can simply reflect wave activity, not the shoreline position. Furthermore, the dune vegetation line is consistently present along the Coos Bay North Spit shoreline and typically extends to a scarp face that varies in height, which can obscure what would be otherwise noted as a wetted bound for an open beach slope.

Studying the movement of the vegetation line indicates that the North Spit underwent erosion in the period after the accretional period described above. This erosion is episodic and not necessarily consistent along the North Spit. However, it appears that erosion on the North Spit started near the North Jetty and has propagated northward.

Figure 5-4 shows the position of the vegetation line along the Pacific coast of the North Spit for the period 1944 through 2016 (the dune line is estimated from the 1890 nautical chart). The figure also shows transect lines used to quantify the change in position of the vegetation line.

Commented [CT11]: A-4-16: First paragraph refers to "shoreline change" being the focus of the evaluation. Text needs to specify what is meant by "shoreline" in this evaluation. Given more than 6' of tidal amplitude, shoreline is too imprecise a term. Consider asserting that the shoreline analysis compares changes to a lines portraying the extent of the "mean high water."

Commented [CT12R11]: The analysis focuses on the vegetation line, which marks the edge of the dune.

Figure 5-4
Vegetation Line Change along the North Spit: from 1944 to 2016

Within 2,000 ft of the North Jetty, the vegetation line accreted dramatically between 1944 and 1956 and the line was erosional between 1956 and 2009 at a rate of 5.1 ft/year. During the earlier time period, dredge and disposal records were not meticulously kept and there is no known evidence of upland disposal on the North Spit that would cause this accretion. Other potential reasons for this vegetation line change can be inferred from the Coos Bay Jetties Major Maintenance Report, Appendix B: Coastal Engineering (USACE 2012b). Similar sediment accumulation behind the jetty is seen at other nearby locations. The Siuslaw North Jetty also experienced rapid accretion after the jetty was constructed and again after the jetty was lengthened. The Coos Bay North Jetty head has been eroding and receding since its original construction. The jetty length may have reached a tipping point in 1956 and, this; combined with a reduced sediment

load from changes in upstream practices, could account for the vegetation line changes near the North Jetty.

Further from the jetty (2,000-6,500 ft), there was relatively less accretion before 1956 and less erosion after 1956, indicating that this region may not be affected by the jetty to the same extent.

Vegetation line change has been relatively stable from 2009-2016. The USACE changed their practices for offshore placement of material dredged from the channel entrance after 2005: the material is now placed in the nearshore with the goal of retaining sand within the littoral system. The timing of this practice corresponds to the period during which the vegetation line recession has appeared to decelerate. This reduction in vegetation line erosion also may be attributable to a dune revegetation project in 2008-2009, or relatively short-term wave conditions. Another potential impact to the vegetation line, may be the dispersion of a 1 mcy mound located in ODMDS E. The majority of the dispersion occurred from 1994 – 2006.

5.2.3 Log-Spiral Bay

5.2.3.1 General Trends

The LSB at the root of the North Jetty has been enlarging since 1939 (Hays & Moritz 2003). Its evolution, based on the aerial photography described above, is illustrated in Figure 5-5.

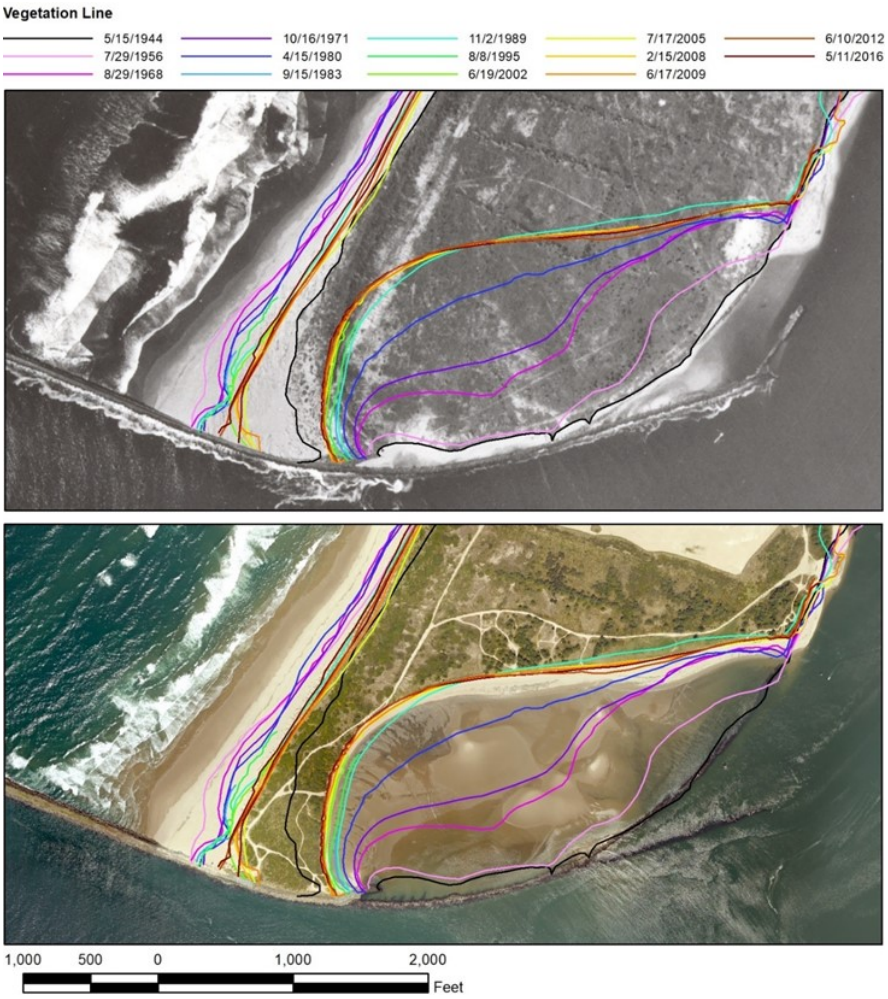

Figure 5-5
Evolution of Log-Spiral Bay since 1944
(Upper Photograph: 1944. Lower Photograph: 2016)

The bay has a classic LSB formation. Waves that propagate into the navigation channel diffract around the hard point of the structure, over the failed portion of the North Jetty. This diffraction, together with refraction within the bay, gives rise to wave crests that are parallel to the shoreline in the equilibrium condition.

South of the jetty root are the remains of a trestle that previously supported a rail spur; an associated dock is visible in the 1944 photograph (Figure 5-5). Crest elevations at the structure are generally

in the range of -6 ft MLLW to +2 ft MLLW. Figure 5-6 illustrates the bathymetry in and around the bay. Portions of the bay are elevated above MLLW (i.e., these areas dry out at low tide).

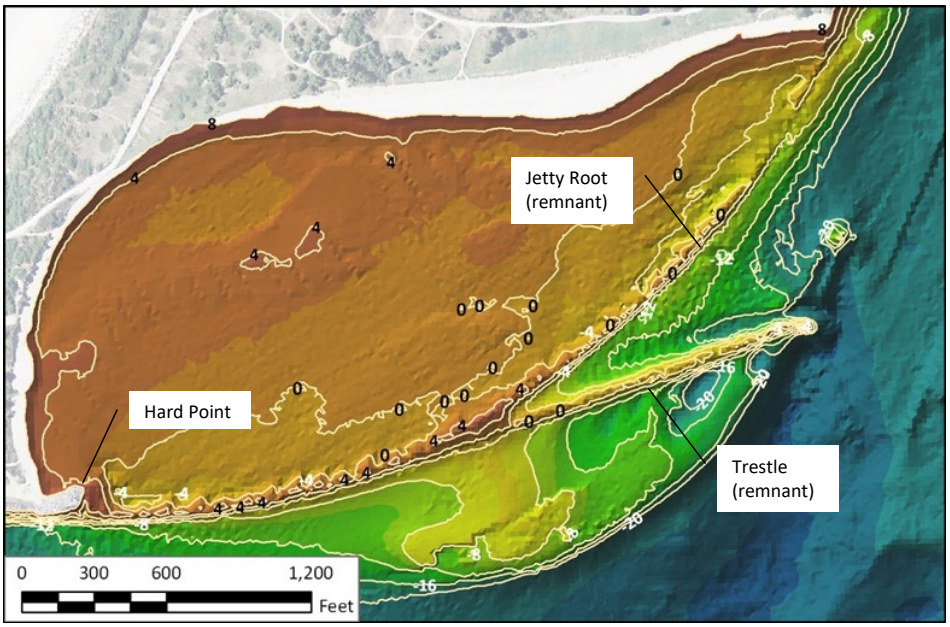

Figure 5-6
LSB Bathymetry: Elevations in ft, MLLW

The inner vegetation line of the North Spit began to erode at the far upstream end of the North Jetty, near the present upstream limit of LSB, immediately after the North Jetty was constructed. This initial erosion may have resulted from current rather than wave activity and did not produce the classic log-spiral shape. Once wave activity began to propagate through or over the jetty root in the early 1940s, wave action became dominant and the bay began to erode towards its present shape.

A hard point, indicated in Figure 5-6, was constructed in 1939-1940 and reconstructed in 2008. The reason for its original construction was not known. However, it has deterred seaward translation of the LSB; this is the reason for its recent reconstruction.

The growth of the log-spiral continued through 1990, after which the bay appears to have stabilized. Figure 5-7 shows historical vegetation lines at LSB. The figure also shows two section lines, one along the North Jetty and one along the "neck," or narrowest point, of LSB. Figure 5-8 plots the recession of the Pacific coast and the LSB vegetation lines at each of these locations. Along the North Jetty, the LSB vegetation line eroded through 2005, after which it has been constrained at the hard point. The Pacific coast vegetation line eroded at a slow rate (~2.5 ft/year) until 1995, and appeared to rapidly recede from 1995 through 2002; it can be speculated that this rapid recession may be due to the strong 1997/1998 El Niño, which caused significant erosion and a runnel effect immediately adjacent to the North Jetty (it did not appear to have such a dramatic

impact at the neck). It has slightly recovered since 2010. At the neck, both sides showed significant erosion through 1990, after which they appeared to stabilize. The recreational road along the west side of LSB has been relocated since 1989 (the date of this photograph) and is again being threatened by erosion.

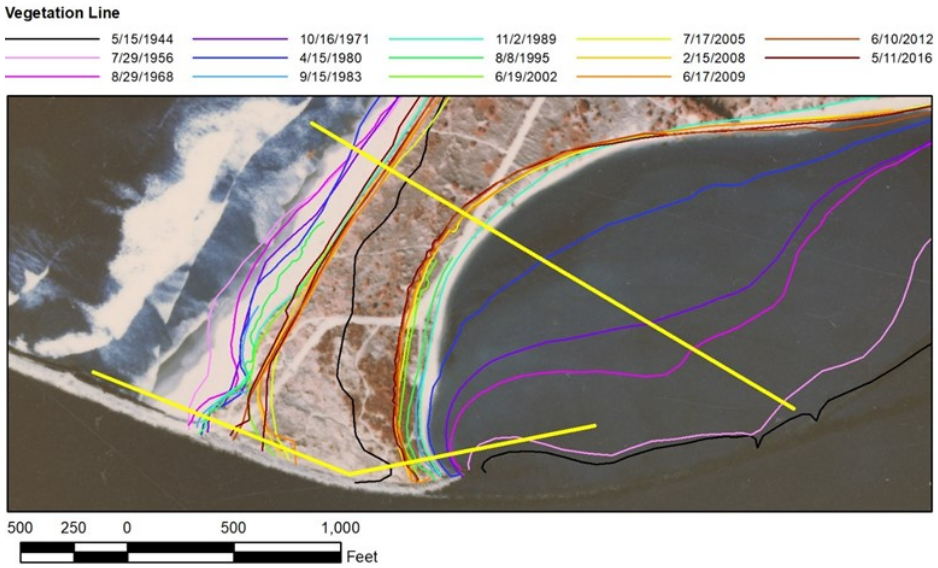

Figure 5-7
Recent Narrowing of the North Spit with Transect Locations, Photograph Date: 1989

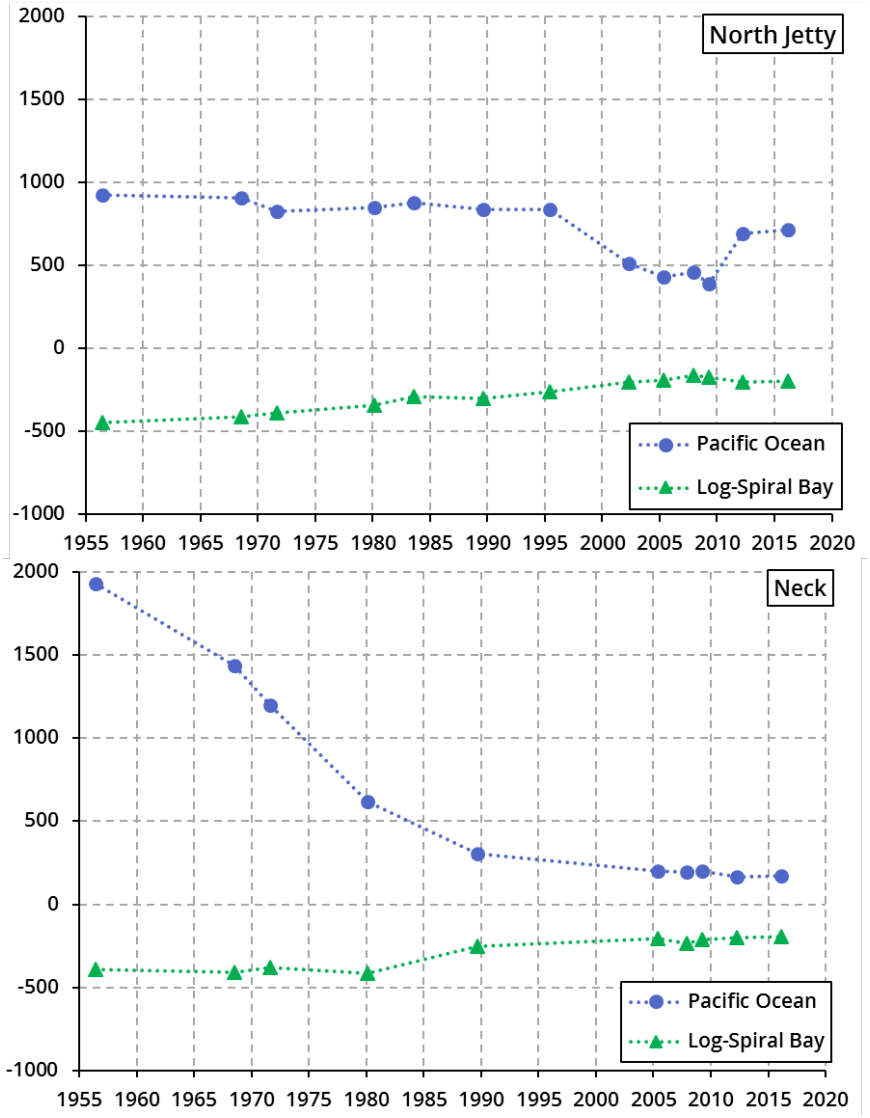

Figure 5-8
Locations of the Pacific Coast and LSB Vegetation Lines

5.2.3.2 Discussion

The past behavior of LSB can be summarized as follows:

- The North Spit has been subject to erosion from the channel side since the North Jetty was first constructed. This erosion started from the upstream end of the jetty root, around Station 07+00, and gradually propagated downstream.
- By the 1940s, this erosion had reached the present hard point (around Station 47+00). The jetty root had degraded to the point that some wave activity was now able to reach the sandy spit. This began formation of a classic LSB. The jetty root has continued to degrade since that time.
- The bay increased in size at a consistent rate until approximately 1990, at which point the erosion rate slowed down.
- The hard point, constructed in 1939-1940 and reconstructed in 2008, has ameliorated seaward translation of LSB.

It has been hypothesized (Hays & Moritz 2003) that this erosion is the result of reduced sediment supply and enhanced wave propagation. The numerical wave model described in Section 3.3 has been configured to extract wave data from within the bay. This section quantifies the changes to the wave climate as a result of deepening, and how that change may change the rate at which sediment is mobilized.

5.2.4 Channel Shoaling

As noted in Section 2.2.3, significant quantities of sediment are dredged from the Entrance Channel annually. Generally, USACE performs pre- and post-dredge surveys for each dredging event. These surveys can be digitized using GIS software and compared (i.e., comparing a pre-dredge to a post-dredge survey) to indicate where shoaling occurs within the Entrance Channel.

At present, two distinct shoals form in the entrance area. Figure 5-9 illustrates the shoals, showing the dredging depths in 2007 and 2009. The outer shoal is the traditional ebb shoal and lies between 1,000 and 2,000 ft of the jetty tips; the second is just inside the jetty tips. Typically, the outer shoal collects more material on the southern side (and dredging to the south of the navigation channel is authorized for this reason); the 2007 illustration is more typical than the 2009 illustration in this way.

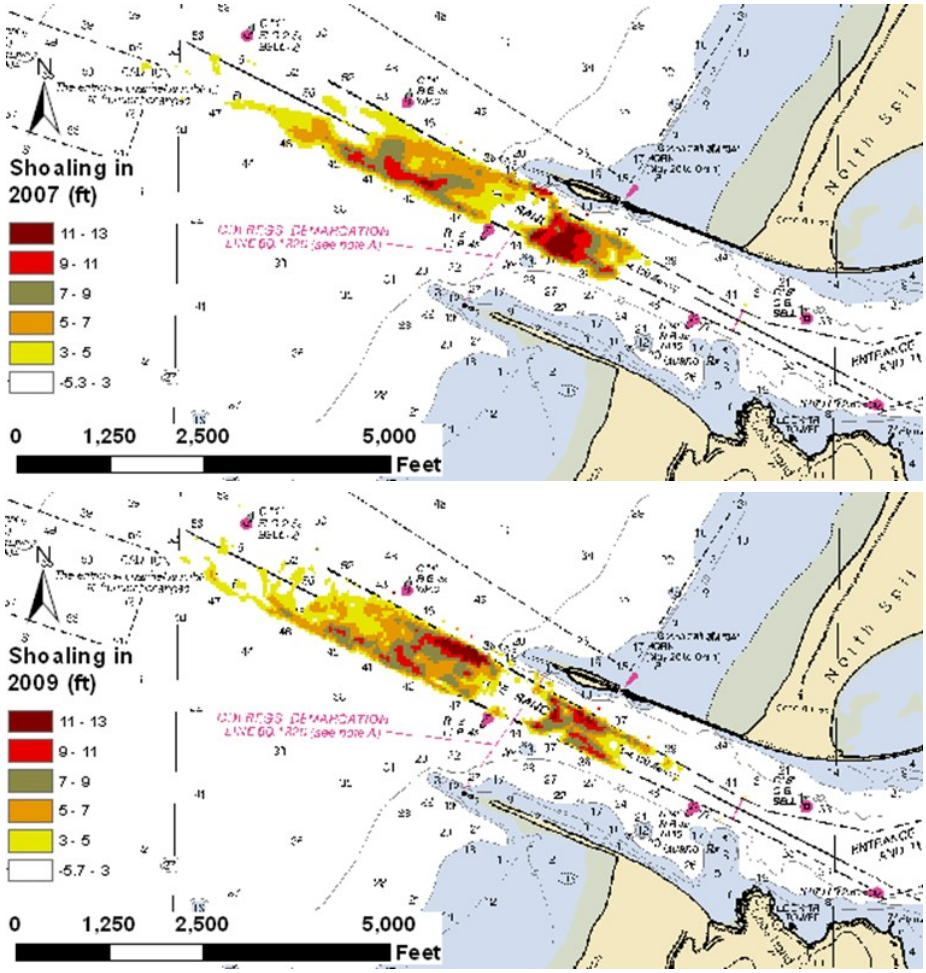

Figure 5-9
Channel Dredging with Apparent Overall Transport Directions, Upper: 2007; Lower: 2009

Shoaling volumes on the south and north sides of the channel were analyzed from 2000-2010 (these years were selected because selected dredging dates were provided). This comparison indicates that the long-term trend is for 61 percent of shoaling to occur on the south side of the channel, while 39 percent of the shoaling occurs on the north side of the channel. This indicates that 61 percent of the gross longshore transport is northward, near the navigation channel.

5.3 Conceptual Sediment Budget

A sediment budget is an accounting of sediment gains and losses, or sources and sinks, within a specified control volume (cell), or a series of connecting cells, over a given period. Sediment budgets can provide a conceptual and qualitative model of sediment transport pathways in coastal systems, as well as a framework for understanding complex coastal systems and their responses to coastal engineering projects.

This work updates the sediment budget developed by USACE (2012b). New data were analyzed over two time periods to refine the understanding of sedimentation in the study area. The study area extends from Cape Arago (the southern boundary) to 2.6 mi north of the inlet (Figure 5-14) and offshore to a depth of approximately 150 ft MLLW. These boundaries were determined by available survey data and the limits of sediment transport (Section 5.3.2). The analysis herein considers two sediment budgets. The first sediment budget considers the entire offshore area as one cell, for the purpose of quantifying the general behavior of the area. The other sediment budget consists of three control areas: one south of the Entrance Channel, one located at the Entrance Channel, and one located north of the Entrance Channel. This more detailed budget provides additional specificity on the transport of sediment around the Entrance Channel.

5.3.1 Estimating Longshore Sediment Transport

A preliminary step in understanding the sediment transport in the vicinity of Coos Bay was to use various empirical relationships to estimate the potential wave-driven longshore transport (LST). Three equations were selected; each of these calculate the LST in the surf zone:

- CERC (USACE 2002): The CERC formula can be used to calculate the potential LST based on incident wave energy. Inputs to the formula include significant wave height (at breaking) and wave direction. This equation is valid for median grain sizes of 0.2 to 0.6 mm, and beach slopes of 0.01 to 0.1 (note that the measured bathymetry at Coos Bay is 0.01). Wang et al. (2002) estimates that this equation overpredicts LST by 239 percent and 578 percent for spilling and plunging waves, respectively, based on measurements in a large-scale sediment transport facility. Van Rijn (2002) compared results of this equation to measured LST rates and found that it yields LST rates that are slightly too large (factor 2) for spilling waves, and much too large (factor 5) for plunging waves.
- The Kamphuis equation, presented in Smith et al. (2003), is an empirical equation based on a re-examination of field data that incorporates wave peak period, grain size, and nearshore beach slope in addition to the parameters required for CERC. Wang et al. (2002) found this analysis to slightly under-predict LST by about 30 percent and 24 percent for spilling and plunging waves, respectively. Based on the set of waves analyzed by Van Rijn (2002), this equation under-predicts (factor 1.5) LST in large waves, and overpredicts (factor 3) LST for small wave conditions.
- Van Rijn (2002) developed a sand transport equation based on seven data sets from the USA and the Netherlands. This equation incorporates tidal current in addition to the parameters used in the Kamphuis equation.

For all the equations described above, wave data (significant wave height, direction, peak period) was based on the directional offshore data from CDIP Buoy 139p1 (Section 2.1.5). Offshore wave conditions were converted to breaking wave conditions according to the dissipation and breaking model presented in the scientific documentation for MIKE LITPACK (irregular wave model of

Battjes and Janssen 1978). This calculation uses an offshore beach slope of 0.01, measured from offshore bathymetry.

The shoreline orientation (the entire shoreline near Coos Bay) was measured from aerial imagery to be 290 degrees. Incoming waves were adjusted by this value such that 0 degrees represented shore-perpendicular, negative angles represented south-bound transport, and positive angles represented north-bound transport. Any incoming waves originating from less than -90 degrees or more than +90 degrees were discarded.

The median grain size was assumed to be 0.2 mm, consistent with sediments sampling near the ODMDSs (USACE 2012a). The nearshore slope was measured to be 0.016, which was measured from the 2014 NWP LiDAR bathymetry.

Average LST was calculated for each year within the record, and for the total period of record (2006-2016). This analysis defines one year as the period from September through August, consistent with the storm season; for example, 2013 refers to September 1, 2012 through August 31, 2013. For each time period considered, the waves were segmented into a joint-probability matrix that determined the percent occurrence of each wave direction, significant wave height, and peak wave period combination.

The estimated LST for each year and each method can be seen in Table 5-2. As this table shows, the net LST may range from 0.6 to 2.5 mcy/year (to the north). It should be noted that these equations calculate the *potential* LST rate. This assumes an infinite supply of sediment and idealized conditions conducive to sediment transport (i.e., lack of jetties or other infrastructure that limits LST). As a result, these equations tend to overpredict LST. Assuming that the CERC equation overpredicts LST by a factor of 2 and that the Kamphuis (Smith et al. 2003) under-predicts LST by a factor of 1.5 in large wave climates (such as Coos Bay), it may be reasonable to assume that the net LST on a shoreline without shore-perpendicular structures is on the order of 1 mcy/year (to the north). At the inlet, LST is further limited by the presence of the two jetties.

The results also indicate that 60-65 percent of the gross transport is expected to be northwards. This is consistent with the directionality presented in other literature (Section 5.1) and by the observed shoaling patterns (Section 5.2.4). Therefore, it may be reasonable to assume that the ratio of gross northward to southward LST is on the order of 3:2 to 2:1.

Figure 5-10 shows the gross LST rate from 2007-2016. As this chart shows, the LST rate varies proportionally throughout the various equations, with Kamphuis consistently predicting about 50 percent of CERC, and Van Rijn predicting about 150 percent of CERC. This figure also shows that the LST rate was likely fairly constant from 2007-2014, and spiked in 2015 (i.e., 2015 brought stronger and more southerly waves than the previous years).

Table 5-2
Calculated Potential LST Rates at Coos Bay (mcy/year)

Period	CERC, 2002				Kamphuis, 1991 (as presented in Smith et al. 2003)				Van Rijn, 2002			
	Northward Transport	Southward Transport	Gross Transport	Net Transport	Northward Transport	Southward Transport	Gross Transport	Net Transport	Northward Transport	Southward Transport	Gross Transport	Net Transport
Aug 2006 - Sept 2007	3.37	2.23	5.61	1.14	1.42	1.22	2.65	0.20	4.80	3.73	8.53	1.07
Aug 2007 - Sept 2008	3.71	2.92	6.63	0.78	1.57	1.52	3.09	0.04	6.12	4.67	10.79	1.45
Aug 2008 - Sept 2009	2.18	3.21	5.40	-1.03	0.92	1.44	2.36	-0.52	2.50	5.12	7.62	-2.61
Aug 2009 - Sept 2010	6.37	1.97	8.35	4.40	2.64	1.20	3.83	1.44	9.95	3.55	13.51	6.40
Aug 2010 - Sept 2011	4.53	2.37	6.90	2.15	1.76	1.18	2.94	0.59	6.08	3.56	9.64	2.51
Aug 2011 - Sept 2012	4.64	1.74	6.38	2.90	1.93	1.12	3.04	0.81	6.61	3.27	9.88	3.34
Aug 2012 - Sept 2013	2.76	2.25	5.00	0.51	1.21	1.25	2.46	-0.04	3.50	3.53	7.03	-0.03
Aug 2013 - Sept 2014	2.91	1.78	4.69	1.12	1.32	0.96	2.28	0.36	3.90	2.58	6.48	1.32
Aug 2014 - Sept 2015	3.88	1.35	5.23	2.52	1.73	0.74	2.46	0.99	5.04	1.87	6.92	3.17
Aug 2015 - Sept 2016	7.42	2.45	9.87	4.97	3.19	1.35	4.54	1.84	12.99	4.25	17.24	8.74
Average	4.18	2.23	6.40	1.95	1.77	1.20	2.96	0.57	6.15	3.61	9.76	2.54

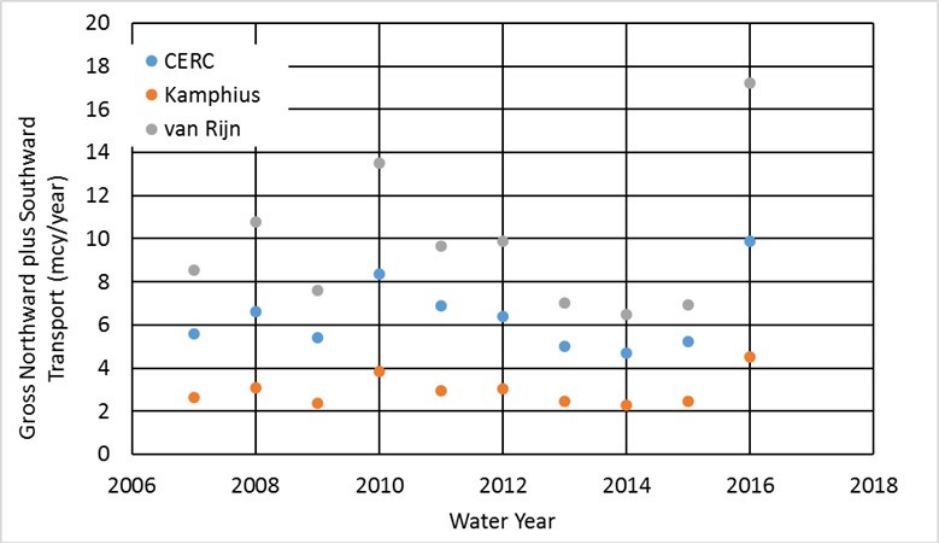

Figure 5-10
Estimated LST, 2007-2016

5.3.2 Formulating a Sediment Budget

A sediment budget is a tool used to estimate relative sources, sinks, and pathways of sediment. Essentially, it is a way of accounting for how sediment moves within a domain. This tool has been developed for Coos Bay to quantify the general sedimentation trends in the offshore area. A sediment budget has been developed over two distinct time periods: 1994 to 2006 (Period 1) and 2006 to 2014 (Period 2). The data used for these time periods are presented in Table 5-3 and Figure 5-11. These time periods were selected due to available survey data and because the behavior of the area south of the Entrance Channel differs during these two periods. At the start of Period 1, ODMDS E contains a mound of about 1 mcy (OIPCB 2017c), that disperses over the course of Period 1. The ODMDS is stable from 2006 onwards (i.e., during Period 2). These time periods also differ by the season in which the surveys were measured. Period 1 begins in the summer and ends in the fall, while Period 2 begins in the fall and ends in the summer. The wave climate differs slightly between these two periods; therefore, the volume changes observed reflect seasonal variation in addition to long-term transport. It would have been ideal to use survey data measured during the same season; however, such data was not available.

Table 5-3
Survey Data Used for Sediment Budget

Period	Offshore Survey (Start)	Offshore Survey (End)	Channel Survey (Start)	Channel Survey (End)
Period 1	7/23/1994	10/2/2006	7/22/1994	9/18/2006
Period 2	10/2/2006	6/23/2014	9/18/2006	6/12/2014

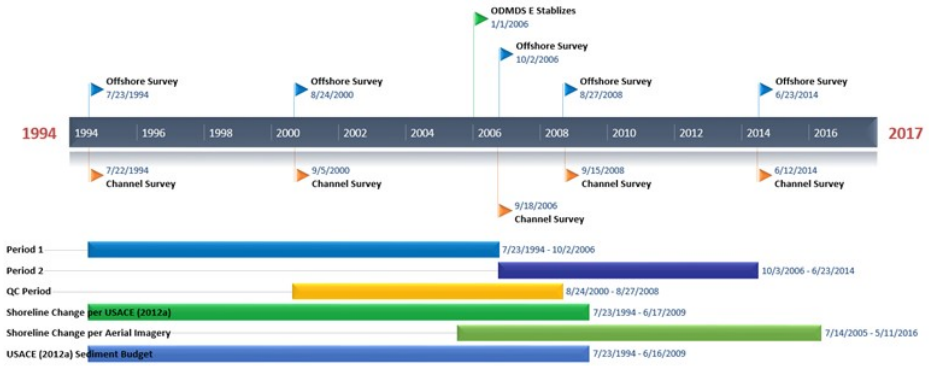

Figure 5-11
Sediment Budget Data Timeline

The sediment budget developed for Coos Bay includes several cells and is based on the following balance (i.e., this balance is applied to each cell):

$$\sum Q_{source} - \sum Q_{sink} + P - D = \Delta V + Residual$$

ΔV = net volume change within cell

P = volume of material placed within a cell

D = volume of material dredged from a cell

Q_{source} = net longshore sediment transport into a cell

Q_{sink} = net longshore sediment transports out of a cell

Residual = Volume of sediment transported into or out of a cell that is not described by any of the processes above.

5.3.2.1 Volume Change

The net volume change within each cell was calculated by comparing triangular irregular network surfaces generated from the USACE surveys listed in Table 5-3 and Figure 5-11. The 1994 survey

was selected because it represents one of the earliest surveys available. The 2006 survey was selected because it represents the beginning of placement in ODMDS F Offshore. In addition, it represents a condition in which there was relatively little mounding in ODMDS E and F, and they both appear relatively stable (USACE 2012a). The 2014 survey was selected because it was the most recent survey provided by USACE. Therefore, it represents the longest amount of time over which operational conditions could be examined.

The volume change observed during Period 1 and Period 2 can be seen in Figure 5-12 and Figure 5-13, respectively; the control volumes used in the sediment budget (see below) have been superimposed on the volume changes. The offshore surveys do not cover the entire Entrance Channel; therefore, Entrance Channel surveys taken as close to the date as the offshore survey as possible was appended to the surface.

As these figures show, the study area is accretional over both time periods. Possible causes for the wide variation in observed volumes can be speculated. It might be the result of the strong 1997–1998 El Niño,[6] other large meteorological events, or a discrepancy/bias in the survey data. Other studies have also pointed to a large inter-annual variability in the beach profiles at the Oregon coast (Komar 1992) and an intra-annual variability in the MSL that is exacerbated during periods of El Niño events (Ruggiero et al. 2012), which might contribute to the large variability among surveys if this effect is not correctly considered during data collection and comparison of the surveys. It is also possible that there is a datum inconsistency or other error in the vertical data. As explained below, a residual is included in the sediment budget to reduce the impact of the wide variation in sediment volumes.

[6] *It has been reported by Komar (1992) and others that during strong El Niño years, both wave direction and magnitude change from the typical year, which could produce different sediment transport regimes in some areas of the Oregon coast.*

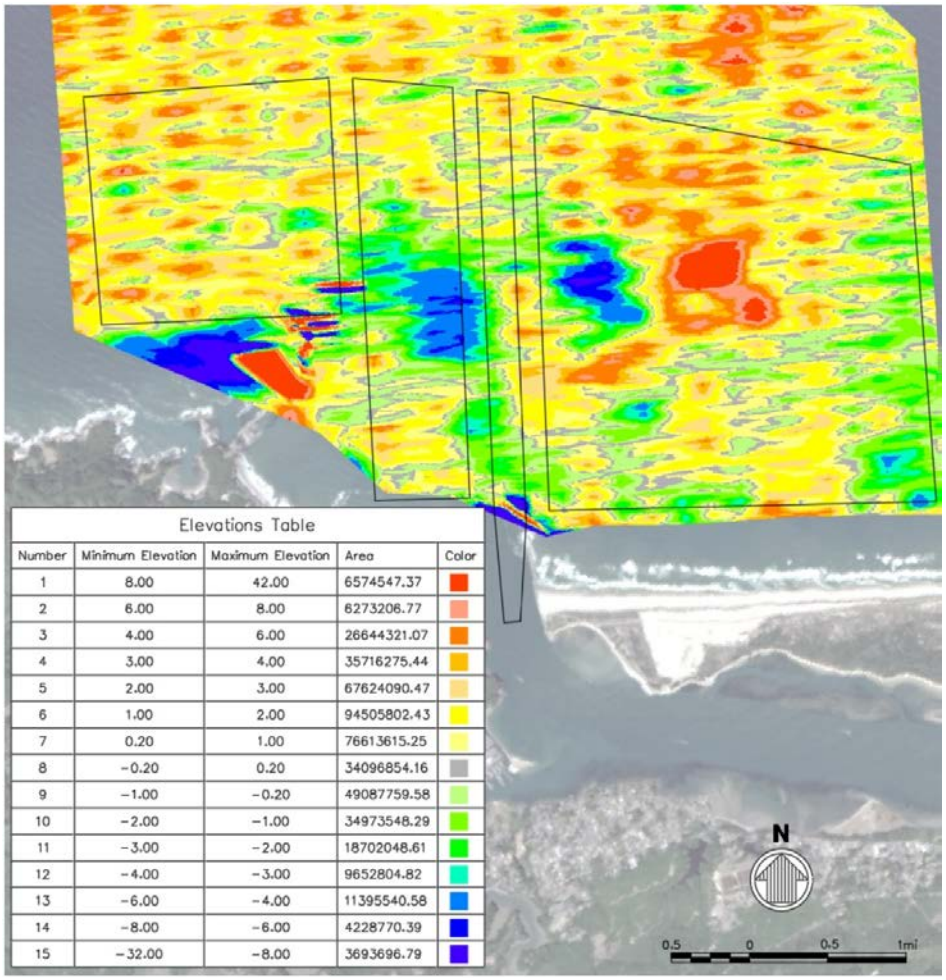

Elevations Table

Number	Minimum Elevation	Maximum Elevation	Area	Color
1	8.00	42.00	6574547.37	
2	6.00	8.00	6273206.77	
3	4.00	6.00	26644321.07	
4	3.00	4.00	35716275.44	
5	2.00	3.00	67624090.47	
6	1.00	2.00	94505802.43	
7	0.20	1.00	76613615.25	
8	−0.20	0.20	34096854.16	
9	−1.00	−0.20	49087759.58	
10	−2.00	−1.00	34973548.29	
11	−3.00	−2.00	18702048.61	
12	−4.00	−3.00	9652804.82	
13	−6.00	−4.00	11395540.58	
14	−8.00	−6.00	4228770.39	
15	−32.00	−8.00	3693696.79	

Figure 5-12
Volume Change Measured during Period 1 (7/23/1994-10/2/2006)

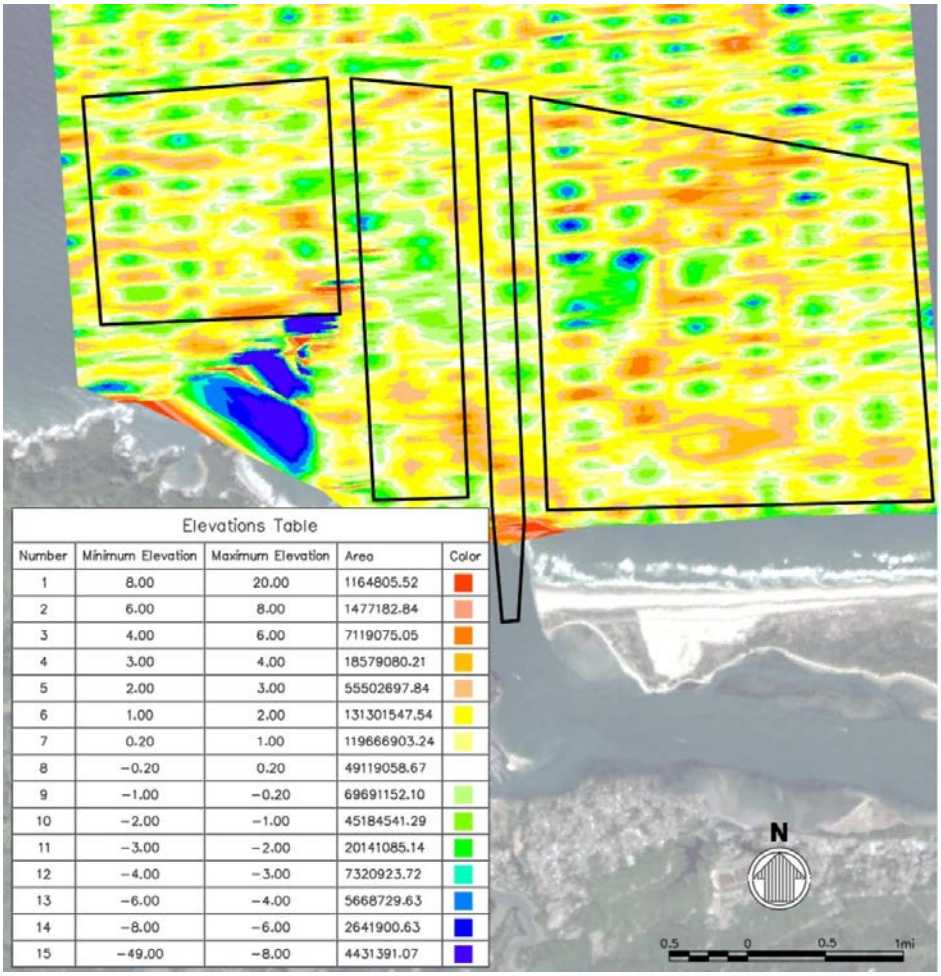

Elevations Table

Number	Minimum Elevation	Maximum Elevation	Area	Color
1	8.00	20.00	1164805.52	
2	6.00	8.00	1477182.84	
3	4.00	6.00	7119075.05	
4	3.00	4.00	18579080.21	
5	2.00	3.00	55502697.84	
6	1.00	2.00	131301547.54	
7	0.20	1.00	119666903.24	
8	−0.20	0.20	49119058.67	
9	−1.00	−0.20	69691152.10	
10	−2.00	−1.00	45184541.29	
11	−3.00	−2.00	20141085.14	
12	−4.00	−3.00	7320923.72	
13	−6.00	−4.00	5668729.63	
14	−8.00	−6.00	2641900.63	
15	−49.00	−8.00	4431391.07	

Figure 5-13
Volume Change Measured during Period 2 (10/2/2006-6/23/2014)

The two surveys that were used to determine volume change did not have any data shallower than 30 ft MLLW. Therefore, the volume change in the breaker zone (i.e., landward of -30 ft MLLW) for Period 1 was based on the analysis of historical shoreline data presented in USACE (2012b); this document indicates the shoreline change results in a volume change of 50,000 cy/yr (erosion) through 2010 (see Table 5-5). For Period 2, the shoreline change was estimated by the area of dune retreat measured from aerial images from 2016 and 2005 (Table 5-1), as these dates matched the survey dates most closely. Volume changes based on shoreline movement was normalized to an annual rate. A comparison of the shorelines can be seen in Figure 5-4.

5.3.2.2 Material Placement

As described in Section 2.2.4, material dredged from the Entrance Channel and the Inner Channel (through RM 12) is generally placed in ODMDS F. Table 5-4 shows the approximate annual volume dredged from the Entrance Channel and placed in ODMDS F; the volume placed exceeds the volume dredged because material dredged from other portions of the channel is also placed in ODMDS F. Most dredging occurs in September; therefore, less than 15,000 cy is included in the sediment budget for 2014 (June 2014 survey date).

Table 5-4
Approximate Volume of Material Dredged and Material Placed

Year	Quantity Dredged (cy)	Quantity Placed (cy)
1994	566,204	722,300
1995	567,215	686,600
1996	1,008,000	1,760,100
1997	536,969	609,400
1998	771,000	965,900
1999	565,837	774,600
2000	777,256	903,800
2001	568,069	789,100
2002	663,000	1,313,900
2003	662,916	768,000
2004	394,431	425,800
2005	777,472	564,000
2006	333,366	487,500
2007	888,865	1,021,105
2008	622,007	782,173

Year	Quantity Dredged (cy)	Quantity Placed (cy)
2009	777,472	938,898
2010	598,906	690,875
2011	645,847	813,743
2012	532,384	637,879
2013	364,343	608,007
2014	0	14,899

5.3.2.3 Dredged Material

Historic Entrance Channel dredging has been provided as far back as 1992 (Section 2.2.3). The Entrance Channel is generally dredged in August through September; therefore, dredging is assumed to occur on September 1 of each year for establishing a sediment budget. Dredging is not included in 2014 for Period 2, because the 2014 survey takes place before this date. Table 5-4 shows the annual dredging volumes included in the sediment budget.

5.3.2.4 Sources and Sinks

The sources and sinks were estimated from previous USACE studies, as discussed in Section 5.1. This literature indicates that the Coos River is not a source of sediment to the offshore area (USACE 2012b). Similarly, the offshore boundaries of the control volumes are defined to be so deep that cross-shore transport is likely negligible. Therefore, there are no expected sources and sinks to the study area besides LST. LST at the southern boundary is limited by Cape Arago.

5.3.2.5 Residual

As noted in Section 5.1, LST is expected to be marginal in depths greater than 60 ft. In addition, cross-shore transport is not expected to occur across the 150-ft contour. The residual during Period 1 and Period 2 was calculated as the observed volume change from 1994-2014 at a cell immediately offshore of Cape Arago, ranging in depth from 60 ft MLLW to 150 MLLW, and bound by the cape at the shoreward portion of the cell; based on published literature, sediment transport in this area is expected to be minimal. This cell is named the “Far South Cell” in Figure 5-14 and Figure 5-15. Any volume change noted in this cell may be a result of inconsistent datums during surveys or may be due to other processes that are not well understood. The residual is calculated based on the observed volume change in this cell and normalized for the area of the respective cell.

Periods 1 and 2 were both accretional; the long-term residual was deemed appropriate for use within each period because of the similar behavior of each period.

5.3.2.6 Control Volumes (Cells)

The locations of the sediment budget cells were determined based on literature describing sediment transport along the shoreline fronting Coos Bay. As described in Section 5.1, sediment transport is limited to depths of 150 ft, and LST is generally limited to 60 ft. Therefore, the cells of the 1-cell and 3-cell sediment budgets extend from the dune to a depth of 150 ft.

To the south, the sediment budget is bordered by Cape Arago, which defines the southern boundary of the littoral cell; sediment transport is limited across this boundary. On the north, the sediment budget is bound by the extent of the survey data.

The cell from which the residual is determined is called the "Far South Cell," consistent with the sediment budget developed by USACE (2012b). The 1-cell sediment budget encompasses the entire boundary of the budget; it is presented in Figure 5-14, along with the Far South Cell.

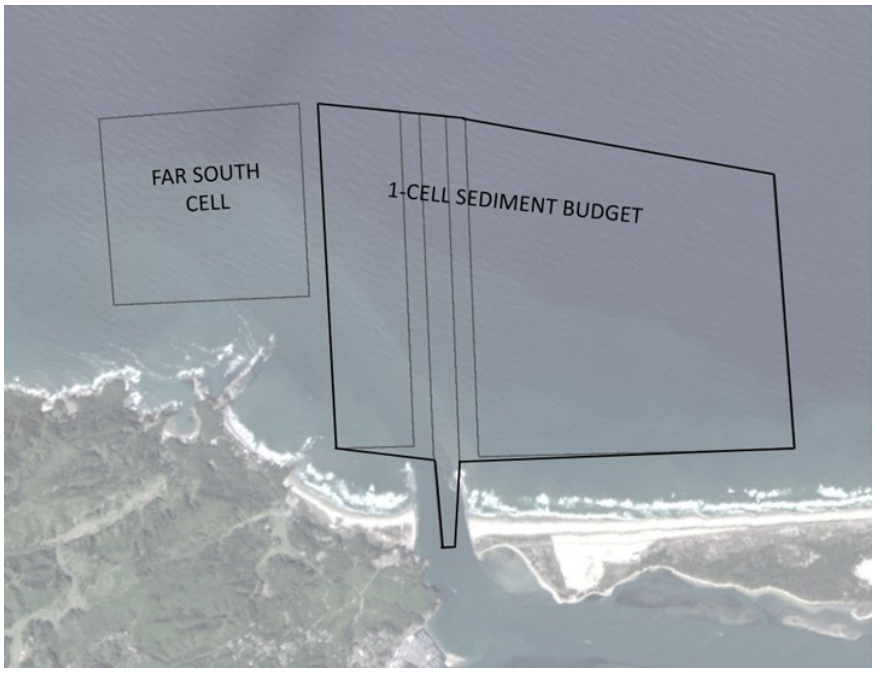

Figure 5-14
1-Cell Sediment Budget and Far South Cell

The 3-cell sediment budget is presented in Figure 5-15; the new cells are located south of the inlet (Cell 1), at the inlet (Cell 2), and north of the inlet (Cell 3). For this exercise, the cell north of the inlet represents ODMDS F (69 percent of this area consists of ODMDS F). The purpose of this configuration is to compare the volume change in this cell with placement volume.

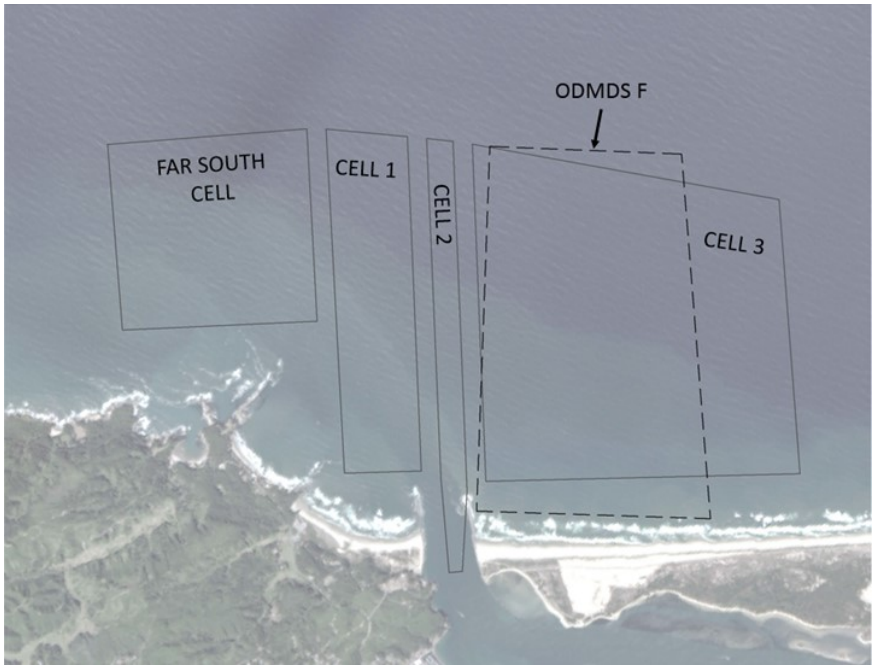

Figure 5-15
3-Cell Sediment Budget and Far South Cell

5.3.3 Existing Sediment Budget

The 1-cell sediment budget incorporates volume change, shoreline change, dredge volume, and material placement throughout the entire domain. The results of this analysis for both periods can be seen in Table 5-5 and Table 5-6. In these tables, the "Total Volume Change" refers to the net change in measured volume through the cell, while the "Net LST" is the difference in LST within the domain (a negative value indicates that more LST leaves the cell than enters). As these tables show, the long-term behavior of this area is accretional; the total volume change is positive. For Period 1 and Period 2, the residual is positive, while the sources-sinks is negative. This implies that there is a large and unknown source of sediment into the area, and a net LST out of the area. It should also be noted that placement exceeds dredging.

Table 5-5
Sediment Budget: 1 Cell, Period 1 (cy/year)

Cell	Bathymetry Change	Shoreline Change	Total Volume Change	Dredging	Placement	Residual	Net LST
1	403,000	-50,000	353,000	670,000	880,000	856,000	-721,000

Table 5-6
Sediment Budget: 1 Cell, Period 2 (cy/year)

Cell	Bathymetry Change	Shoreline Change	Total Volume Change	Dredging	Placement	Residual	Net LST
1	988,000	-11,000	977,000	575,000	715,000	863,000	-26,000

The 1-cell budget indicates that this is an accretional area. This is consistent with the previous findings of the USACE (2012b). However, as noted above, this may be due to large inter-annual variability or datum inconsistencies during surveys. Comparing the far-right column of Table 5-5 and Table 5-6 shows a significant difference in the net LST between the two periods; much more sediment leaves the site during Period 1 than during Period 2. This is attributable to several factors, such as the initial bathymetry (including the mound at ODMDS E), the higher placement rate, or seasonal differences. These factors are considered in more detail below.

The 3-cell sediment budget investigates the transport patterns within the entire control area. Specifically, it calculates the volume change within each of the cells presented in Figure 5-15 and estimates the LST at the boundary of each cell, as well as the sediment bypassing around the inlet.

The process for estimating LST at the boundary of each cell is described below. The notation is given as L_{XY}, meaning LST from Cell X into Cell Y (Cell O refers to outside of the boundary). L_{13} indicates sediment bypassing.

Assumptions are given as follows:

- As described in Section 5.2.4, approximately 60 percent of channel shoaling collects at the southern portion of the channel; this calculation assumes that sediment originates from Cell 1. Therefore, L_{12} is greater than L_{32} by 50 percent.
- Similarly, the general direction of the net LST is to the north (Section 5.3.1). The quantity of sediment traveling northward is 50 percent greater than southward. Therefore, sediment bypassing is assumed to move sediment from Cell 1 to Cell 3.
- The percentage of sediment that bypasses the channel is given by the trapping ratio calculation presented by Kraus & Larson (2001); based on this method, 68 percent of the LST is trapped by the inlet (32 percent of LST bypasses).

Using these assumptions, the following equations are used to calculate LST:

$$L_{32} = \frac{2}{5}(\Delta_2 + D_2 + R_2)$$

$$L_{12} = \frac{3}{2}L_{32}$$

$$L_{31} = 0.47(L_{12} - L_{32})$$

$$L_{3O} = P_3 + R_3 + L_{31} - L_{32} - \Delta_3$$

$$L_{O1} = \Delta_1 + L_{12} + L_{13} - R_1 - P1$$

where R is the residual in each cell, P is placement, and D is dredging.

The results of the 3-cell sediment budget for the various time periods are presented in Table 5-7 and Table 5-8; these results are shown as LST values in Figure 5-16 and Figure 5-17. In general, LST increases from south to north. This may be due to Cape Arago limiting transport from the south, combined with the fact that sediment is deposited north of the channel and travels northward (making Cell 3 sediment rich). Sediment enters the navigation channel from both directions and is removed by annual dredging.

Table 5-7
Sediment Budget: 3 Cells, Period 1 (cy/yr, except where noted)

Cell	Area (sq ft)	Bathymetry Change	Shoreline Change	Total Volume Change	Dredging	Placement	Residual	Net LST
1	56,496,000	-86,000	0	-86,000	0	7,000	180,000	-273,000
2	24,390,000	-45,000	0	-45,000	671,000	0	78,000	548,000
3	187,795,000	534, 000	-50,000	484,000	0	883,000	598,000	-997,000

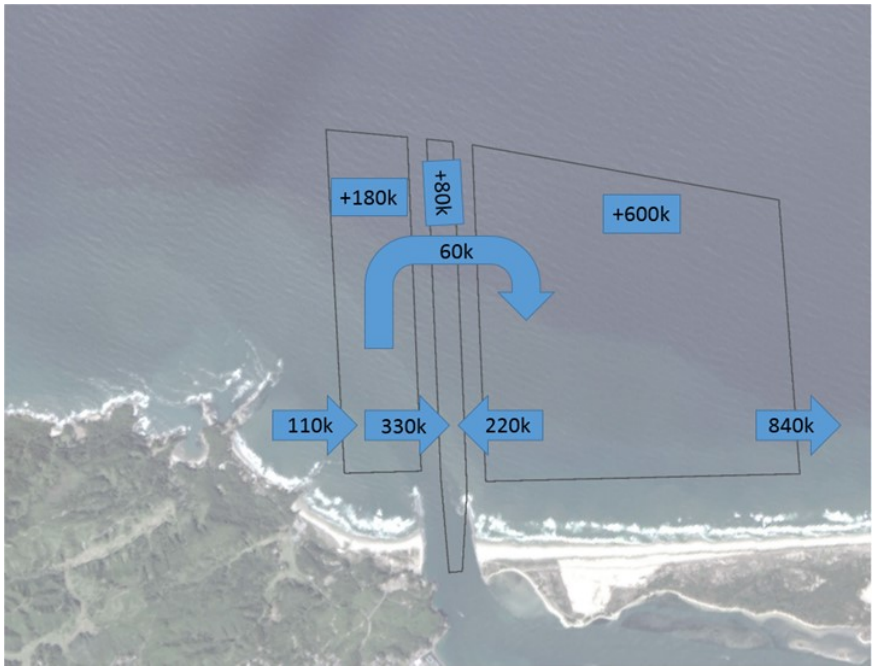

Figure 5-16
LST (arrows) and Residual (boxes) Estimated from Period 1 Sediment Budget

Table 5-8
Sediment Budget: 3 Cells, Period 2 (cy/yr, except where noted)

Cell	Area (sq ft)	Bathymetry Change	Shoreline Change	Total Volume Change	Dredging	Placement	Residual	Net LST
1	59,149,000	127,000	0	127,000	0	0	188,000	-61,000
2	24,823,000	123,000	0	123,000	575,000	0	79,000	619,000
3	187,100,000	738,000	-11,000	727,000	0	715,000	596,000	-584,000

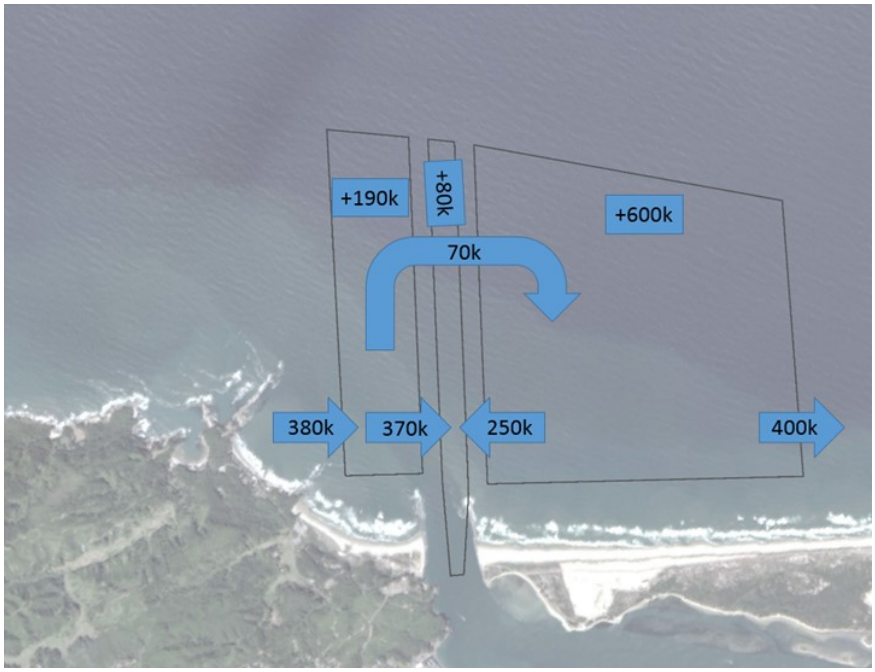

Figure 5-17
LST (arrows) and Residual (boxes) Estimated from Period 2 Sediment Budget

During Period 1, LST from the south into Cell 1 is much lower than during the other period. There are two possible explanations for this. Firstly, sediment is dispersing from the historic mound at ODMDS E, at approximately 90,000 cy/yr. This may result in some southward transport. Secondly, the calculated sediment transport rate may be a reflection of seasonal variation. During the summer, waves tend to be more northerly, causing sediment to accumulate south of hard points such as Cape Arago. Therefore, the initial survey may have been seasonally sediment-rich, and the volume change underestimates the long-term trend. Underestimating the accretion here would lower the calculated transport into the cell.

During Period 2, the opposite occurs. The final survey shows seasonal accumulation north of the North Jetty, overestimating the accretion that occurs during this period. The calculated transport out of Cell 3 may underestimate the actual transport.

The results of this analysis can be used to estimate typical LST rates in the offshore and Entrance Channel. The data presented above indicate that LST into this domain from the south may range from 200-400 cy/yr. LST is lowest along this boundary due to the presence of Cape Arago. LST from Cell 1 into Cell 2 is on the order of 300-400 cy/yr. The transport from Cell 3 into Cell 2 is on the order of 200-250 cy/yr. The transport from Cell 3 to the north may range from 700,000-900,000 cy/yr. About 60,000 cy of sediment bypasses the channel each year. The mean values of these transport rates are presented in Figure 5-18.

Not only do these numbers reflect the LST that was estimated from the two time periods, they also reflect the observed behavior of the channel and the shoreline. Combined with the observed residual into Cell 1, this cell remains relatively stable, consistent with long-term observations. The average shoaling in Cell 2 is approximately 660,000 cy, which is approximately equal to the average annual dredging rate. In Cell 3, transport out of the cell is roughly equivalent to material placement.

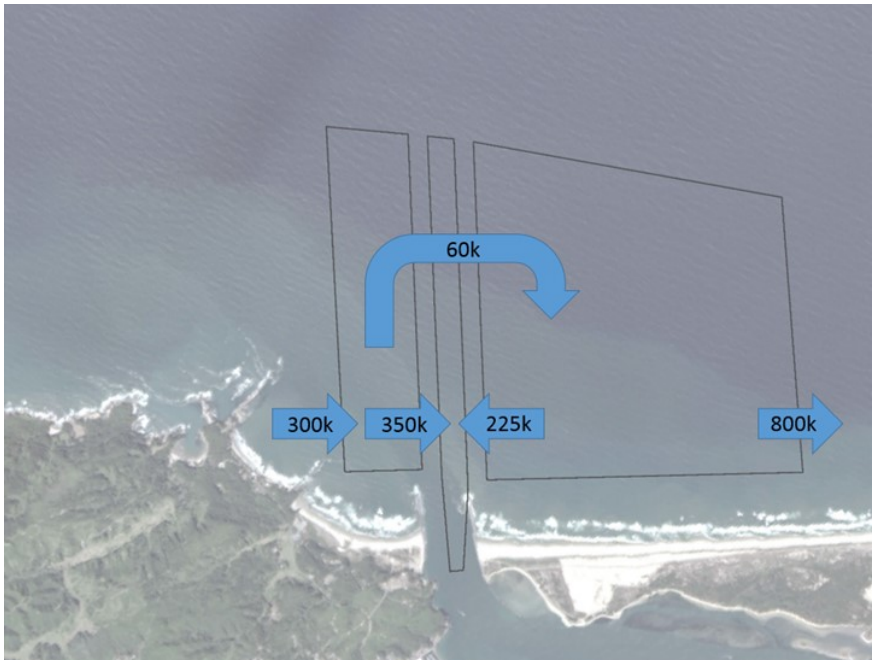

Figure 5-18
Average Estimated LST Rates

The numbers above represent the net transport from one cell to another. However, these values can also be used to calculate the gross transport out of each cell, in each direction. Using the top three equations listed above, the gross transport out of Cell 1 to the north may be on the range of 440,000-590,000 cy/yr. Similarly, the gross transport out of Cell 2 to the south may be on the range of 290,000-370,000 cy/yr.

Figure 5-18 does not include the residual. The residual was introduced to balance the budget and account for the errors introduced by the survey. While additional sediment may enter the southern cell to balance the budget, the source of this sediment is unknown and is not included here. The northern cell is balanced by placement of dredge material.

The results of the sediment budget developed from survey data is corroborated by the U.S. Army Corps of Engineers (USACE) tracer study and numerical modeling conducted in 2017 and 2018. The USACE study focused on sediment transport specifically from the nearshore portion of

ODMDS F site. The USACE study results demonstrated sediment transported northward from ODMDS F site propelled by southerly winds. Initially, tracer results detected sediments moving towards the inlet, with some tracers identified in the navigation channel. However, further sampling suggested that not all this material remained in the channel. Strong ebb tides carried a portion offshore. The overall trend for material disposed in Site F (North of the North Jetty) is northward, especially during time periods of high energy currents and large waves, which namely occurs during the winter months.

5.3.4 2023 PA Sediment Budget

No long-term sources or sinks of sediment are expected to emerge under the implementation of the 2023 PA. In addition, the transport patterns along the coastline are not expected to change significantly. As a result of the wider, deeper channel, the channel trapping efficiency is expected to increase, meaning that a greater proportion of LST may be trapped in the channel; as a result, channel shoaling may increase while sediment bypassing may decrease. This does not have significant implications for the 1-cell budget, as the entire area was incorporated into the one cell. The 3-cell sediment budget will be impacted in that L_{12} and L_{32} will increase while L_{13} decreases. The trapping efficiency calculation by Kraus & Larson (2001) indicate that the trapping efficiency for the 2023 PA would be 76 percent (versus 68 percent today).

Certain elements of the 3-cell sediment budget were re-calculated to reflect the change in sediment trapping. The net transport from Cell 1 to the north (440,000-590,000 cy/yr) and the net transport from Cell 3 to the south (290,000-370,000 cy/yr) are assumed to remain constant. However, with the revised trapping value for trapping efficiency, the values of L_{12} and L_{32} are expected to change. Under the 2023 PA, L_{12} may range from 340,000-450,000 cy/yr, and L_{32} may range from 225,000-280,000 cy/yr. Channel bypassing is expected to decrease to 45,000 cy/yr. Dredging is expected to increase from the current 660,000 cy/yr to 725,000 cy/yr (a 65,000 cy/yr, or 10 percent, increase). The expected transport rates between the various cells can be seen in Figure 5-19.

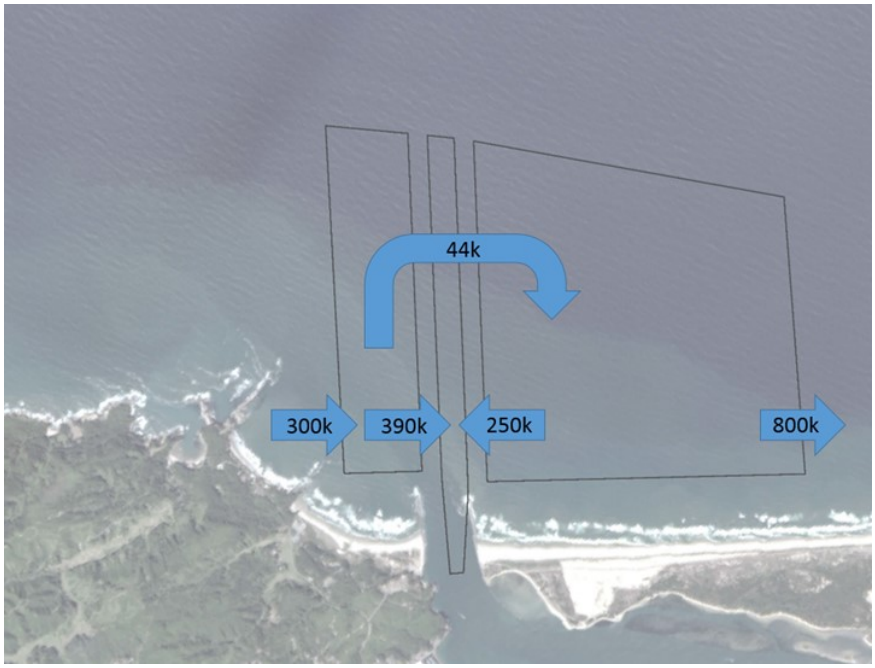

Figure 5-19
Estimated LST Rates under the 2023 PA

5.3.5 Conclusions

The sediment budget exercise provides a conceptual and qualitative model of sediment transport pathways in the nearshore zone. Key conclusions of the sediment budget are:

- Net longshore transport is to the north, with bi-directional gross transport.
- Sediment enters the navigation channel from the both directions, with a majority coming from the south.
- Cape Arago, 2.5 mi south of the inlet, restricts sediment transport from the south. This limits the quantity of sediment that can reach the inlet.
- The results of the sediment budget developed from survey data is corroborated by the U.S. Army Corps of Engineers (USACE) tracer study and numerical modeling conducted in 2017 and 2018. The USACE study focused on sediment transport specifically from the nearshore portion of ODMDS F site. The overall trend for material disposed in Site F (North of the North Jetty) is northward, especially during time periods of high energy currents and large waves, which namely occurs during the winter months.
- The 2023 PA would increase the channel trapping efficiency by 8 percent (from 68 percent efficiency to 76 percent efficiency) relative to the Existing Conditions.

Ultimately, this analysis shows that the availability of sediment is limited by the adjacent headland to the South and that widening and deepening the channel has a small effect on the channel's trapping efficiency. Therefore, dredging the 2023 PA would be expected to increase channel shoaling by 65,000 cy/yr.

5.4 Sediment Transport Modeling

The following sections provide an overview of the Coastal Modeling System (CMS) modeling framework used to assess sedimentation in the Entrance Channel and offshore area. This discussion includes the model setup, calibration, and validation results, followed by model projections for the Existing Conditions and the 2023 PA.

CMS is a numerical model capable of simulating relevant hydrodynamic and sediment transport processes in tidal inlets and coastal areas. It is a product of the Coastal Inlets Research Program administered by the USACE. CMS is composed of two coupled models: (1) CMS-Flow (Buttolph et al. 2006; Wu et al. 2010; Sanchez et al. 2011a; Sanchez et al. 2011b), and (2) CMS-Wave (Lin et al. 2008; Lin et al. 2011). The CMS model was selected for this application because it is the USACE-preferred model for sediment transport.

CMS-Flow is a finite-volume, depth-averaged model that can calculate water surface elevations, currents, sediment transport, and morphological change (Camenen & Larson 2007). CMS-Flow can be coupled with CMS-Wave (which calculates spectral wave propagation with wave refraction, diffraction, reflection, shoaling, and breaking) and thus incorporate wave-driven sediment transport processes. The sediment transport model within CMS-Flow includes various formulations for simulating bedload and suspended modes of transport, settling, and deposition for sediments classified as sands (particle diameters greater than 0.063 mm). Short-term and long-term morphological changes can also be calculated using an approach that relies on morphological scaling factors (Lesser 2009). The combination of tidal hydrodynamics and waves makes the CMS modeling framework suitable for sand transport and morphological studies in coastal environments and tidal inlets such as Coos Bay.

The CMS model setup used for this study, for the most part, is derived from a CMS application developed by USACE-Engineer Research and Development Center (ERDC) and shared with OIPCB. The model framework consists of a hydrodynamic model, a wave model, and a sediment transport model. The hydrodynamic and wave model components used in this study are identical to the application developed by USACE-ERDC. As part of this study, the hydrodynamic and wave model were applied to different time periods, and its performance evaluated against measurements. The parameterization of both models was not changed as part of this process. In contrast, a new sediment transport model setup and parameterization was developed to calibrate and reproduce sedimentation volumes measured in the inlet channel. Therefore, the overall model application presented herein represents a refinement of the application developed by USACE-ERDC. The setup and validation of the hydrodynamic and wave model, and the setup and calibration of the sediment transport model are described in subsequent sections.

5.4.1 Hydrodynamic and Wave Model

As mentioned previously, the hydrodynamic and wave model components used in this study are identical to the application developed by USACE-ERDC. This section presents a brief overview of the computational grid, model bathymetry, boundary conditions, parameterization, and results.

A limited validation based on measured data on water levels, currents, and wave characteristics is also presented.

5.4.1.1 Model Grid

The Coos Bay CMS model grid is based on the grid setup received from USACE-ERDC. The setup includes two separate grids of similar spatial extent to run CMS-Flow and CMS-Wave. The CMS-Flow grid, shown in Figure 5-20, extends about 19 km (12 mi) offshore from the coastline, and includes the Coos Bay Estuary. The CMS-Flow setup uses a telescoping rectilinear grid with five different levels of resolution ranging from 320 m (1,050 ft) offshore to 20 m (66 ft) at the Coos Bay inlet and in the Entrance Channel. The CMS-Wave setup shown in Figure 5-21, also over the same spatial extent as the CMS-Flow grid, uses a rectilinear grid with variable resolution, with a maximum resolution of about 20 m (66 ft) along the shoreline and parallel to the inlet. This allows the representation of wave processes and resulting sediment dynamics in areas most important for the morphological processes at the inlet location.

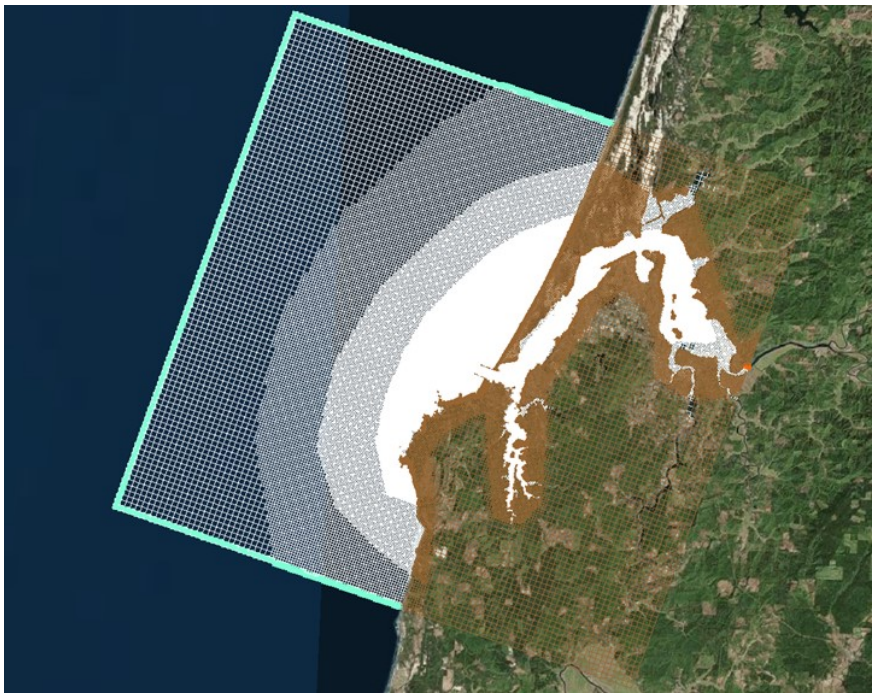

Figure 5-20
Overview of Coos Bay CMS-Flow Model Grid

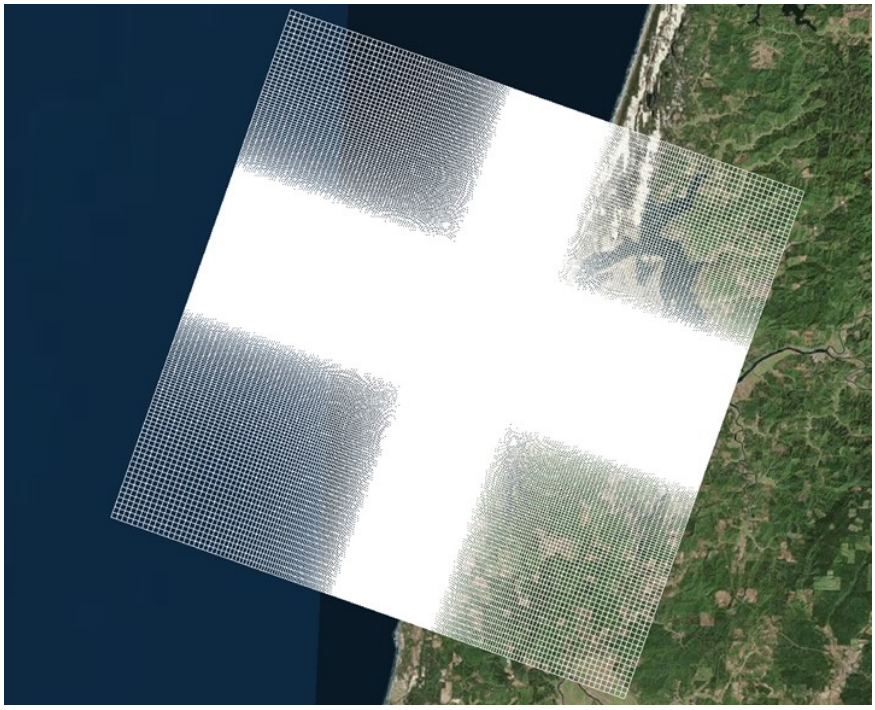

Figure 5-21
Coos Bay CMS-Wave Model Grid

5.4.1.2 Model Bathymetry

The Coos Bay CMS model includes the grid bathymetry developed by USACE-ERDC, which combined data from multiple sources. Data from NOAA National Geodetic Data Center (NGDC) and USACE Portland District surveys were used to develop the nearshore and offshore model bathymetry. In addition, single-beam bathymetric transects collected by Oregon State University (OSU) and LiDAR topo-bathymetry were used to define the model depths within the bay. Figure 5-22 shows the overview of the model bathymetry. Depths range from about 120 m (395 ft) offshore, to less than 10 m (33 ft) with respect to MSL along the coastline and in the sub-tidal shallows within Coos Bay. The interpolated bathymetry near the Entrance Channel on the flow and wave grid are shown in Figure 5-23 and Figure 5-24, respectively. Both Figure 5-23 and Figure 5-24 show that the grid resolution is sufficient to represent longitudinal and lateral variations in bathymetry within the navigation channel, with multiple grid cells representing the channel cross-section at any given location.

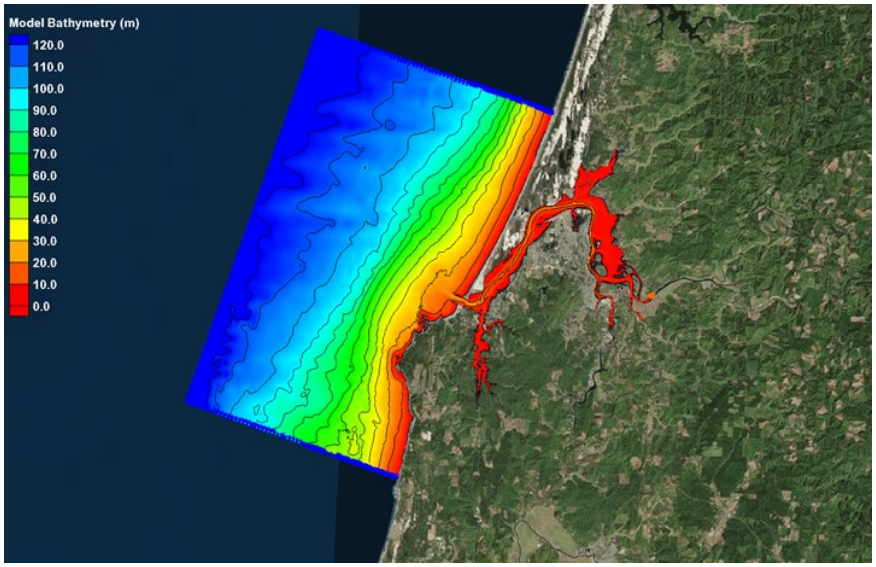

Figure 5-22
Overview of CMS Model Bathymetry

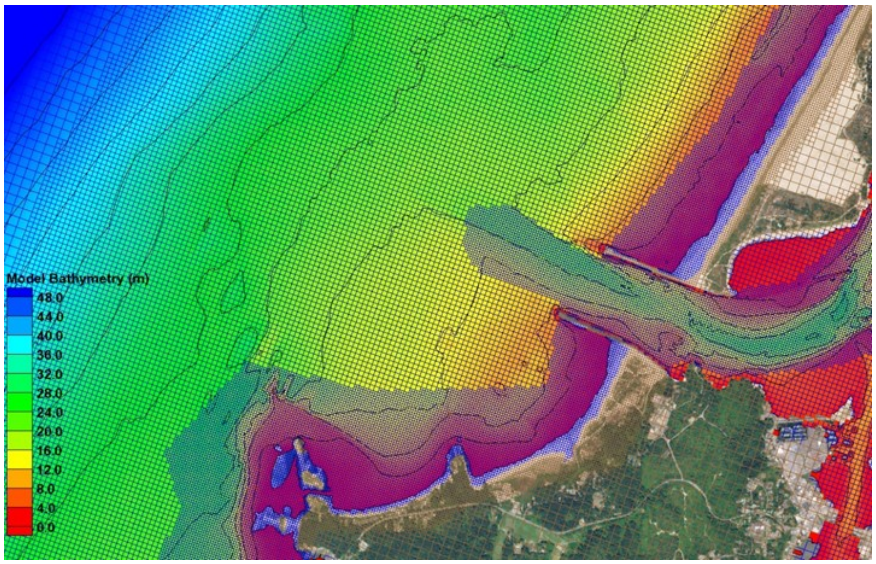

Figure 5-23
CMS-Flow Grid and Bathymetry near Entrance Channel

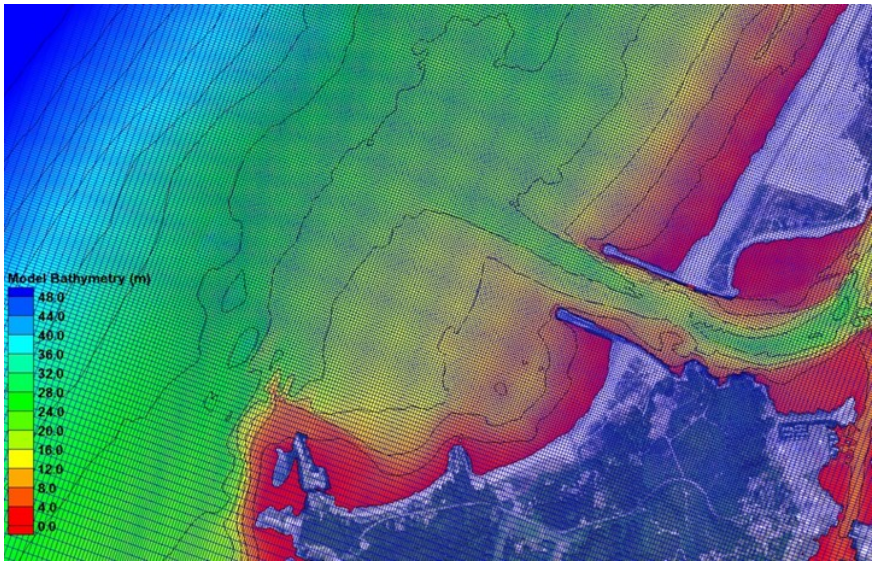

Figure 5-24
CMS-Wave Grid and Bathymetry near Entrance Channel

5.4.1.3 Model Parameters

The hydrodynamic and wave model parameters, as developed by USACE-ERDC and calibrated to water-level and current data from 2014, were used in the Coos Bay CMS model application presented herein. The hydrodynamic and wave parameters used in the model are shown in Table 5-9. An implicit time-stepping scheme with a 600-second time-step was used. A spatially variable Manning's n roughness, shown in Figure 5-25, was used.

Table 5-9
Hydrodynamic/Wave Model Parameters used in the Coos Bay CMS Model

Model Parameter	Value
Bottom Eddy Viscosity	0.067 m^2/s
Horizontal Eddy Viscosity	0.2 m^2/s
Wave Eddy Viscosity	0.5 m^2/s
Turbulence Model	Subgrid
Wave-current Mean Stress formulation	Quadratic
Wave Bottom Friction coefficient	0.65

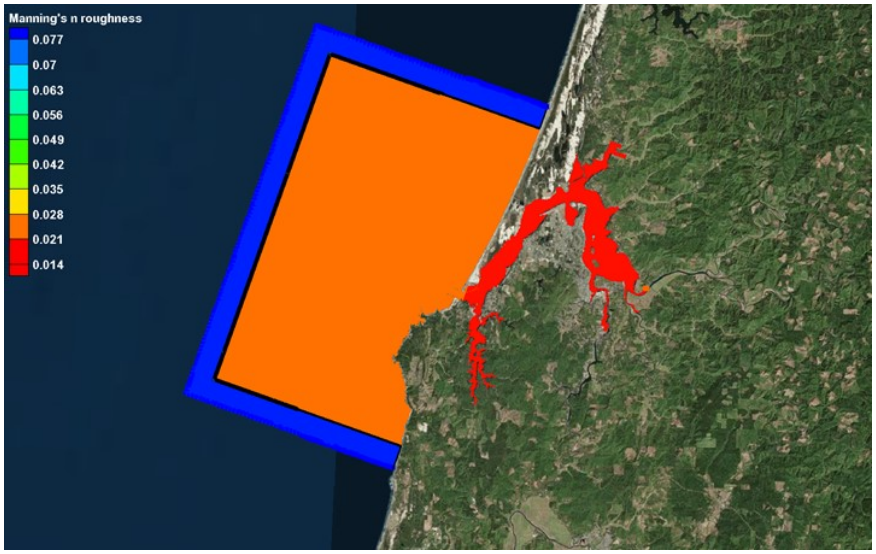

Figure 5-25
Map of Manning's n Roughness used in the Model

5.4.1.4 Hydrodynamic Boundary Conditions

The model application developed by the USACE-ERDC was calibrated to data collected in 2014. The application presented in this report utilizes additional hydrodynamic measurements available from 2010 in the vicinity of the inlet to assess model performance in the study's focus area as a

validation exercise. Therefore, model boundary conditions were developed as appropriate for the period in 2010 when model-data comparisons are performed. The water level and wave boundary conditions for the present application were developed as described below.

5.4.1.5 Water Levels

Predicted tides and surge were used to define the boundary condition for the CMS-Flow model at the offshore boundaries. The tide predictions from Pacific Ocean database of the TPXO7.2 global inverse tide model (Egbert & Erofeeva 2002) developed by OSU were used. In addition, water level predictions from the global ocean analysis and forecast of the E.U. Copernicus Marine Service program were superimposed on the tides to account for offshore surge. Due to numerical stability issues in initial test runs using a spatially-varying water level boundary condition, a spatially-uniform water level was used at the offshore boundaries.

5.4.1.6 Waves

The CMS-Wave model was forced at the offshore boundary using directional wave data from NDBC buoy CDIP139p1 (Section 2.1.5). A JONSWAP spectrum based on the wave parameters from the buoy was used as the offshore forcing spectrum. Locally generated wind-waves were not simulated; hence, no wind forcing was applied to the wave-model.

5.4.1.7 Hydrodynamic Model Validation

The hydrodynamic and wave model setup, which includes the grids, bathymetries, bottom roughness, and other physical parameters in the model, were developed and calibrated by USACE-ERDC to water-level and current data within the estuary at RM 7 from June - July 2014 collected by the University of Oregon. The USACE-ERDC hydrodynamic and wave models were further validated by USACE-ERDC to current and wave measurements collected offshore of the North Jetty of Coos Bay inlet from September 2015 to March 2016, and to velocity transects across the inlet measured using ship-board ADCP during September to October 2016. For the application presented in this report, additional current and wave measurements available from 2010 in the vicinity of the inlet were utilized to assess model performance in the study's focus area as a validation exercise.

Water level and current data in the area of interest were obtained from two ADCP gages deployed near the inlet for a period of about one month from March 27 to April 23, 2010 (Section 3.2.1.1). Wave data was collected at the same locations.

Figure 5-26 shows the comparison of model-predicted and measured water levels and currents at the ADCP 2 location. The model performs reasonably well in reproducing the water level at this location – the tidal range, as well as high-water and low-water levels as calculated by the model are comparable to measured values. However, tidal currents tend to be somewhat under-predicted by the model, seen most notably in lower peak flood and peak ebb velocities calculated by the model as compared to measured values. The flow at this location represents predominantly the tidal inflows and outflows, both of which are dependent on the tidal prism of Coos Bay, and it is not significantly influenced by upstream river discharge. Since the size of the Coos Bay estuary, and therefore the tidal prism of the system, is well represented in the model, the apparent bias between model and data for currents may be an artifact of either the ADCP location or the representation of local bathymetry at this location in the model. The ADCP is located just outside the edge of the channel and close to the channel bend where relatively sharp bathymetric changes occur, and the currents could, therefore, be especially sensitive to local bathymetry and geometry.

In addition, it is also possible that the depth at the ADCP location is overestimated in the model representation, leading to the under-prediction of currents by the model. A scatter-plot of the measured and model-calculated current components along the cardinal directions, shown in Figure 5-27, shows a reasonable correspondence between the two, with model-calculated directions somewhat different from the measurements, likely reflecting small-scale spatial variability not captured by the model due to limitations of grid resolution.

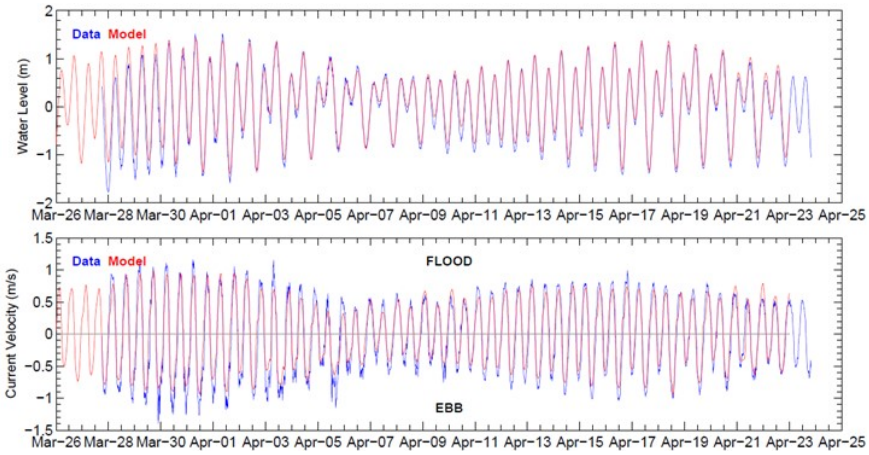

Figure 5-26
Comparison of Time-series of Water Levels and Currents at ADCP 2

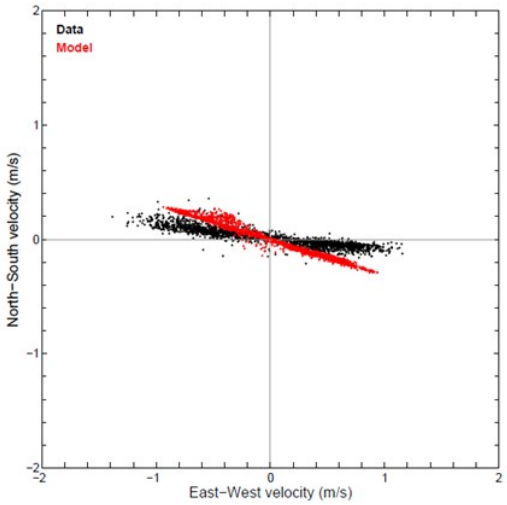

Figure 5-27
Scatter-plot of N-S and E-W Velocity Components from Model and Data at ADCP 2

The CMS-Wave model performance at the ADCP 2 location, shown in Figure 5-28, shows that while model performance is mostly consistent with data during the latter part of the validation period, the model appears to significantly under-predict wave heights during the first half of the deployment. However, there appears to be a lot of unexplained scatter in the wave height signal recorded at this location during this half of the deployment, as evidenced by large changes in reported wave height within unreasonably short intervals of 1 or 2 hours, which suggests that measurements during this period might possibly be contaminated. Another possible reason for this variance might be the instrument's proximity to the jetty. In contrast, during the latter part of the deployment, when there is less scatter in the measured signal, the model does well in reproducing the measured wave heights. The wave periods and directions also closely resemble the data. It should be reiterated that the CMS hydrodynamic and wave models were calibrated and validated as described above and used for the comparison in Figure 5-28.

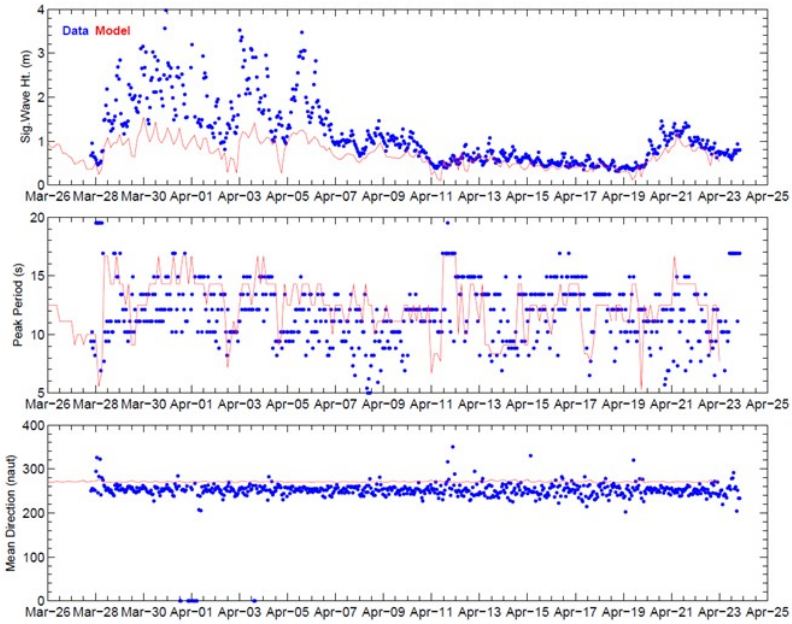

Figure 5-28
Comparison of Time-series of Wave Heights and Periods at ADCP 2

Model results for water-level and currents at ADCP 3 are shown relative to data in Figure 5-29 and Figure 5-30. The model performs reasonably well in reproducing the water level at this location – the tidal range, as well as high-water and low-water levels as calculated by the model are comparable to measured values. It is, however, noted that during the latter part of the validation period the model tends to over-predict both high- and low-water levels by about 25 cm (0.8 ft). Review of the along-shore and cross-shore currents shows that, in general, the model reproduces the along-shore component during the first half of the validation period well. During the second half of the validation period, the model generally tends to under-predict current magnitudes even

though the net direction of transport (towards the south) is generally consistent with the data. This may likely be an artifact associated with the use of spatially uniform tide boundary conditions, which prevents the correct representation of geostrophic currents driven by the variations in water levels along the boundary. Review of maps of currents calculated by the model in the coastal zone shows the formation of large-scale eddies. Unfortunately, the limited ADCP data available in this zone precludes a thorough assessment of model performance in this regard.

A scatter-plot of the measured and model-calculated current components along the cardinal directions, shown in Figure 5-30, shows a reasonable correspondence between the two – the currents are mostly directly parallel to the shoreline (roughly running from the north-east to south-west). The model tends to under-predict currents directed towards the south, likely associated with the specification of spatially uniform water levels along the boundary.

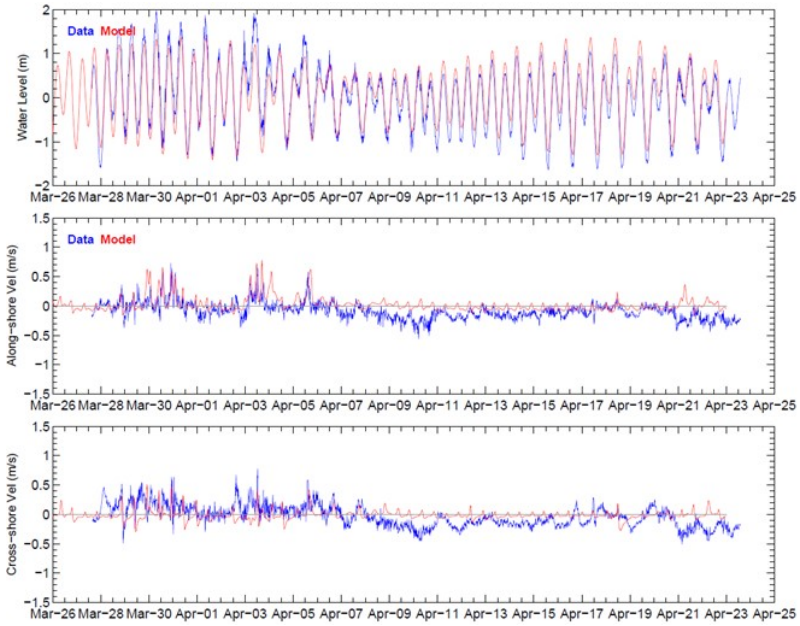

Figure 5-29
Comparison of Time-series of Water Levels and Currents at ADCP 3

Figure 5-31 shows the model-data comparison of waves at the ADCP 3 location. The model results show a good correspondence with data during most of the validation period. The wave heights during the two offshore storm events occurring during the first half of the deployment are somewhat under-predicted by the model. This may be an artifact of data used to define the wave model boundary conditions, with the measurements from a location about 35 mi away from the boundary of the wave model. Nonetheless, wave periods and directions are well-reproduced by the model. It should be reiterated that the CMS hydrodynamic and wave models were calibrated and validated as described above and used for the comparison in Figure 5-31.

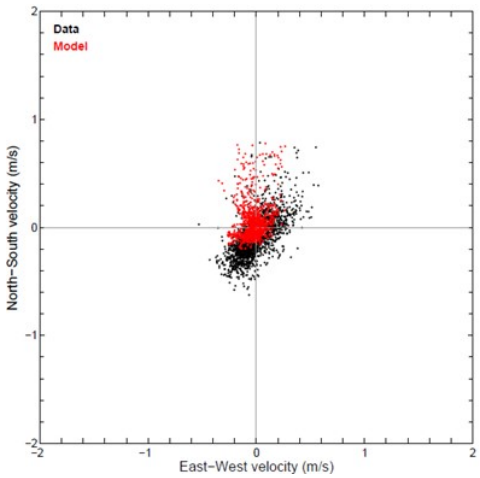

Figure 5-30
Scatter-plot of N-S and E-W Velocity Components from Model and Data at ADCP 3

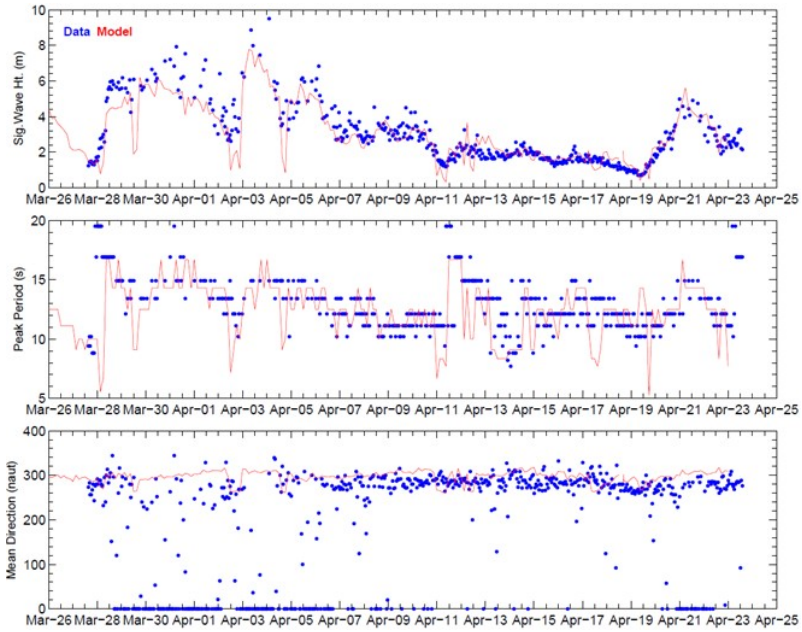

Figure 5-31
Comparison of Time-series of Wave Heights and Periods at ADCP 3

5.4.2 Morphological Model

Following the validation of the hydrodynamic and wave models, the USACE-ERDC CMS model was applied to a period with measurements of post-dredge sedimentation volume in the Coos Bay entrance channel. The USACE-ERDC CMS model results for sedimentation volume were compared to measurements to assess model performance and the modeled patterns and magnitudes of sedimentation were found to be inconsistent with measurements. Therefore, in the present study, a different morphological model setup and parameterization was developed, calibrated, and validated before application to various future channel dredging and management scenarios. This section of the report describes the setup, parameterization, and calibration of the revised CMS morphological model.

5.4.2.1 Sediment Transport Formulation and Inputs

The morphological model setup consists of defining a number of sediment inputs – number and size of sediment classes, number of bed layers, grain size distribution in the bed, rock outcrops, boundary conditions, and the formulation for resuspension and bedload transport used by the model.

Sediment grain-size distribution data for the Coos Bay area is available from the U.S. Geological Survey (USGS) usSEABED database (Reid et al. 2006). This dataset includes surficial bed sediment data from grab samples and from virtual sampling such as from seafloor photographs. Figure 5-32 shows a map of locations for which surficial bed grain size distribution and average grain-size data exists. Based on the available data, average fractions for four different grain sizes were included in the CMS model. The model was initialized with these surficial sediment size fractions applied uniformly over the entire domain.

In addition, multiple bed layering was implemented in the model to simulate increased bed-strength with depth, which would mostly be achieved in the model through sediment coarsening. Table 5-10 shows the grain-size distribution used in the model over each model bed-layer, and the respective layer thickness. It should be noted that the vertical variation in grain size distribution has a relatively small impact on overall model results for sedimentation within the Coos Bay inlet. The fall velocity and critical shear stress for each grain-size was calculated within the model based on the Soulsby (1997) formulation. The model calculates the sorting of bed sediments using the mixing or active layer concept (Wu 1991). The thickness of the mixing layer, which acts as an interface for exchange of bed sediments with the water column, is specified as a user input. During erosion, the mixing layer loses sediments to the water column, which is then replenished by depleting sediments from the first bed layer below the mixing layer. During sediment deposition, the water-column sediment gets deposited to the mixing layer, which then transfers the additional mass to the underlying bed layer, keeping the thickness of the mixing layer constant. Variations in the size of the particles eroded and/or deposited in a given location thus lead to changes in the grain size distribution in the bed over spatial and temporal scales.

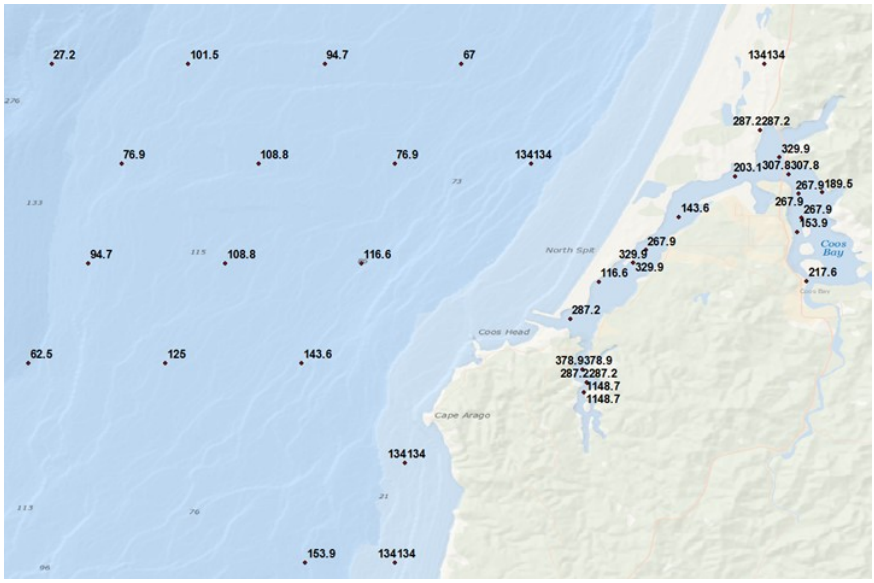

Figure 5-32
Map Showing Locations of Available USGS Grain-size Data in Coos Bay and the Average Grain Size (Microns) at Each Location

Table 5-10
Model Initial Grain-size Fractions Over Each of 10 Model Bed-layers

Layer #	Thick (m)	Class 1 (0.03 mm) fraction	Class 2 (0.15 mm) fraction	Class 3 (0.35 mm) fraction	Class 4 (0.8 mm) fraction
1	0.05	0.17	0.05	0.77	0.01
2	0.05	0.17	0.05	0.77	0.01
3	0.1	0.1	0.1	0.79	0.01
4	0.1	0.1	0.1	0.79	0.01
5	0.1	0.0	0.1	0.8	0.1
6	0.1	0.0	0.1	0.8	0.1
7	0.5	0.0	0.0	0.6	0.4

Layer #	Thick (m)	Class 1 (0.03 mm) fraction	Class 2 (0.15 mm) fraction	Class 3 (0.35 mm) fraction	Class 4 (0.8 mm) fraction
8	0.5	0.0	0.0	0.6	0.4
9	0.5	0.0	0.0	0.6	0.4
10	0.5	0.0	0.0	0.6	0.4

The depth of the rock layer input to the model is shown in Figure 5-33. It should be noted that the depth to rock layer shown in the figure is relative to the sediment bed. The bed elevation in the CMS model is in turn based on the bathymetry from 1999 that was used in the model calibration to long-term observed annual average sedimentation. Changes in bed elevation over time could lead to change in the relative depth of the rock layer, and so this model assumption may not necessarily contradict the recent data.

Known rock outcrops in the Coos Bay area include Guano Rock in the Entrance Channel, Baltimore Rock near Gregory Point south of the inlet, and relics or other rock in the immediate vicinity of the jetties. These areas were included in the model as a hard-bottom layer, i.e., non-erodible. Outside the channel limits, there is little available data describing the bedrock relative to model bathymetry. Therefore, the presence or lack of rock in these areas was estimated from adjacent areas. Initial simulations omitted the presence of rock in the Entrance Channel, and the results showed significant unrealistic erosion adjacent to the North and South Jetties (up to 10 ft/yr), areas that are not known to substantially erode. Therefore, at-bed or near-bed rock layers were assumed over most of the area adjacent to the Entrance Channel to limit the model erosion in these areas. Without these assumptions, the model may overestimate the magnitude of predicted sedimentation in the navigation channel (with these assumptions, the model was able to reproduce measured shoaling, in fulfilling the primary purpose for the CMS model simulations). It should be noted that upstream of LSB, no bedrock is included in the model, since CMS model results are not considered in this area.

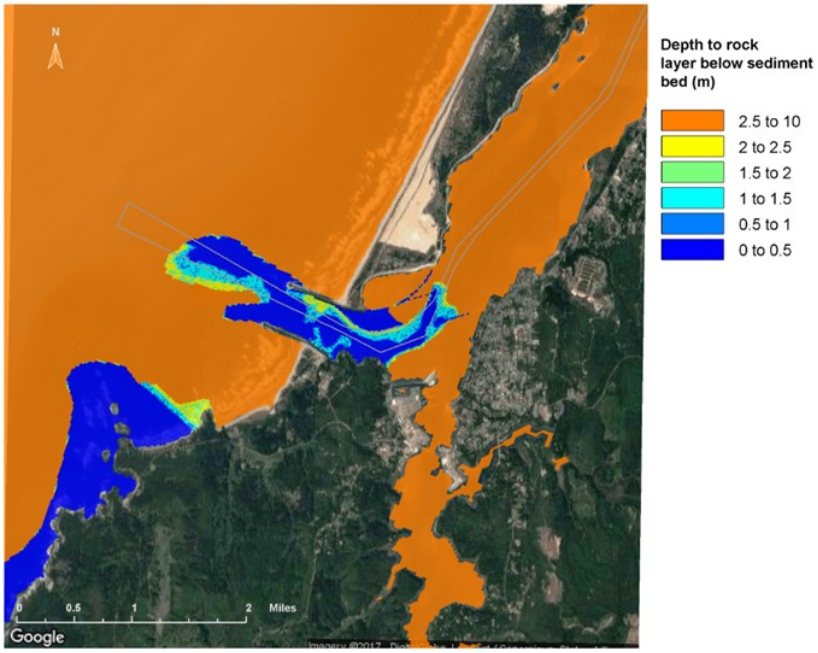

Figure 5-33
Depth to Rock Layer below Surface of Sediment Bed

Commented [CT13]: USACE 10462090: This figure appears to indicate that the sand-sediment layer is less than 0.5 m thick within the Inlet entrance where present O&M dredging addresses shoaling that 1-3 m thick. Ensure that this figure is appropriate for using as an erodible sediment BC for the Coos Bay CMS model.

Commented [CT14R13]: Added
"The depth to rock layer shown in the figure is relative to the sediment bed. The bed elevation in the CMS model is in turn based on the bathymetry from 1999 that was used in the model calibration to long-term observed annual average sedimentation. Changes in bed elevation over time could lead to change in the relative depth of the rock layer, and so this model assumption may not necessarily contradict the recent data."

Offshore boundary conditions for suspended load and bedload were defined using the equilibrium sediment concentration approach. In this approach, the sediment concentrations at the boundaries were set equal to the equilibrium concentration at inflow cells, where the equilibrium concentration is calculated as the steady-state total sediment concentration for a given instantaneous shear stress. This determines the suspended and bedload sediment fluxes entering the CMS model domain with the incoming currents. For currents directed outward of the model domain, a zero-concentration gradient condition is applied by the model.

Finally, the transport formulation used by the model was defined on the basis of several tests. Suspended sediment and bedload transport were modeled in CMS using the non-equilibrium total load approach, which implements a combined equation for suspended and bed-load transport. Using this approach, multiple formulations for calculating near-bed sediment concentration or capacity are available for use within CMS. Following sensitivity tests with different formulations, the Watanabe (1987) formulation was selected for the present model as best suited to produce realistic morphological change patterns and magnitudes.

5.4.2.2 Calibration Metric

The data used to develop the calibration metric for the morphological model comes from periodic bathymetric surveys of the entrance available from the USACE. Some of these include surveys conducted before and after maintenance dredging of the Entrance Channel.

Model calibration was performed in a manner that recognizes the fact that the boundary conditions were based on the entire wave record. Therefore, the modified morphological model used the average annualized sedimentation near the Entrance Channel, calculated from historical bathymetric survey data, for calibration.

Calibration of the model also incorporated USACE comments that the portion of the channel offshore of the jetty tips may behave differently than the area between the jetties. In order to best reproduce the behavior in this area, calibration focused on the area offshore of the jetty tips.

The gross volume of sedimentation offshore of the jetty tips was computed as an annual rate based on historical survey data from pre- and post-dredge surveys; this data was used as a calibration target. Figure 5-34 shows the observed sedimentation over an average 9-month period, with the calibration target shown in the diagonally shaded area. The annualized average gross sedimentation within the calibration target area was calculated to be approximately 360,000 cy/yr. Table 5-11 shows the annualized sedimentation calculated from available survey data for each year that data was available. It should be noted that the measured annual average sedimentation within the entire Entrance Channel is 680,000 cy/yr, slightly higher than the annual average dredging in this area.

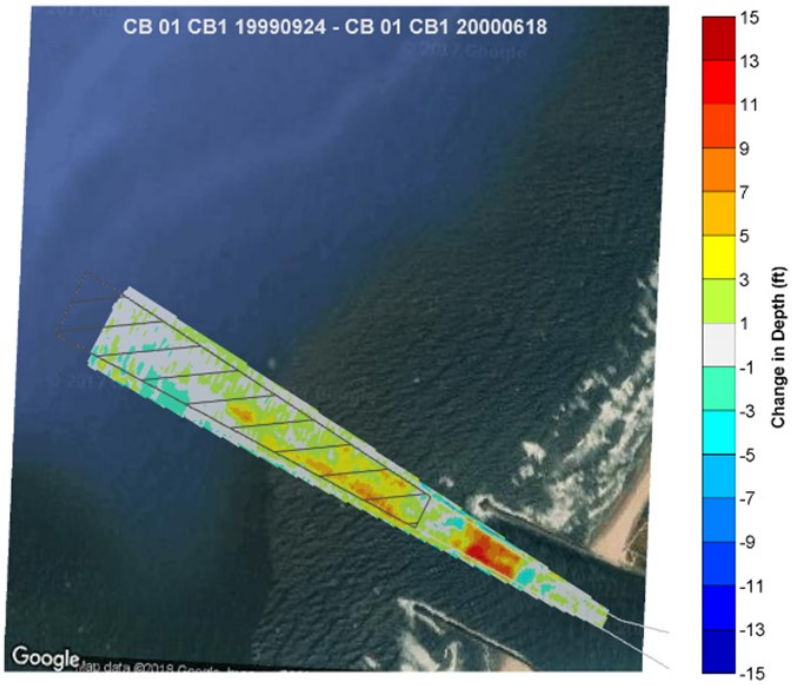

Figure 5-34
Entrance Channel Sedimentation Based on Bathymetric Survey Data (09/24/1999 to 6/18/2000), Showing Focus Area for Model Calibration

Table 5-11
Measured Annualized Sedimentation in Model Calibration Target Area

Period	Post-dredge Survey Date	Pre-dredge Survey Date	Annualized Sedimentation (cy/yr)
1999-2000	1999/9/24	2000/6/18	416,300
2000-2001	2000/9/05	2001/8/14	207,200
2001-2002	2001/8/30	2002/5/20	568,400
2002-2003	2002/9/09	2003/8/13	310,900
2004-2005	2004/9/08	2005/5/04	240,500
2005-2006	2005/8/19	2006/8/22	195,500
2006-2007	2006/9/18	2007/8/03	530,100
2007-2008	2007/9/24	2008/8/18	294,800
2008-2009	2008/9/08	2009/8/12	459,100
Average			358,089

5.4.2.3 Modeling Approach for Calibration

In order to simulate long-term morphological changes with reasonable computational times, a boundary condition reduction and morphological acceleration factors (MorFac) approach was applied (Lesser 2009). The tide and wave boundary conditions over the 7-month period were schematized so that selected representative tide and wave conditions were simulated to represent the wave climate over the entire period. The 7-month wave climate of the calibration period was schematized into 14 representative wave conditions. The morphological changes calculated by the model over these individual conditions were multiplied by input MorFacs in order to simulate the overall change over the 7-month interval representing the calibration period.

5.4.2.4 Schematization of Tide Boundary Condition

The tide boundary condition for the 7-month calibration period was schematized such that the complex time-series of water levels is replaced with a single semi-diurnal tide following Latteux (1995). The schematized tide was chosen such that the residual sediment transport in one tidal cycle is similar to the residual transport in one complete spring-neap cycle. The overall tide was reduced to a combination of two astronomical tidal components M_2 and C_1, where amplitude of $C_1 = (2O_1K_1)^{0.5}$. According to Hoitink et al. (2003), the interaction of the M_2 component with the diurnal O_1 and K_1 components can be expected to be the dominant factor in determining the residual transport as long as these diurnal components are significant, which is true for most of the

west coast of the U.S. A comparison of the measured tide over a spring-neap tidal cycle, and the reduced tide used at the model boundary is shown in Figure 5-35.

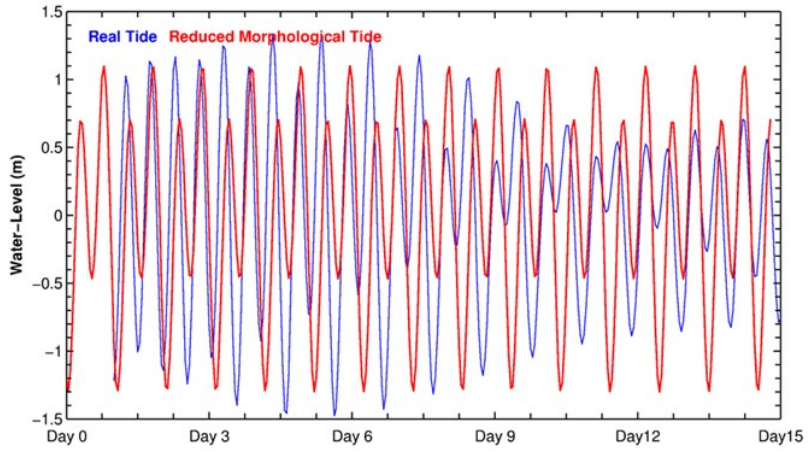

Figure 5-35
Comparison of the Morphological Tide to the Tidal Water Levels Over a Spring-Neap Cycle

5.4.2.5 Schematization of Wave Boundary Conditions

A schematized tide and wave boundary condition was used in the morphological model to efficiently simulate the long-term morphological behavior. Developing this type of boundary condition entails selecting representative wave conditions to characterize the entire period of record. Each of the representative wave condition bins is described by a significant wave height, wave period, and direction. Each bin was used to force the model for an average 24-hour tidal period, in sequence. The observed bed changes for each model time-step were scaled up using a MorFac specific to each representative wave condition to estimate the bed changes associated with the wave condition over the course of a year. Therefore, the wave boundary conditions were schematized to capture the wave conditions that have the most significant effect on sedimentation, MorFacs were selected based on the relative occurrence of the specific wave condition.

The alternate approach used herein was to select representative wave conditions based on the morphological impact along with the probability of occurrence of each offshore wave bin – where the morphological impact is quantified by the magnitude of sedimentation at the Entrance Channel. That is, the wave bins were selected based on their potential to drive sediment transport.

Since the CMS model allows for the specification of only one MorFac over the length of a single model run, the different selected wave conditions with the corresponding MorFacs were set up separately. The different wave conditions were then run sequentially using the hot start file from the end of the preceding wave condition to obtain a continuous simulation. The wave conditions in the sequence were ordered from the smallest wave heights to the largest wave heights to approximate the wave climate from roughly summer to winter and spring, which typically see the largest wave activity. The wave conditions were also ordered to minimize the change in wave

height or direction between successive cases to minimize the shock to the system due to a sudden change in either.

The wave climate schematization is updated based on wave data at Station 139p1 (2006-2016). Figure 5-36 shows the combined probability distribution of each wave condition. The collective wave observations at this location are divided into wave-height bins of 0.5 meter and directional bins of 30-degree widths, and the probability of occurrence of wave conditions corresponding to each bin is illustrated. This figure is normalized, such that the numeric value is directly equivalent to the probability of occurrence.

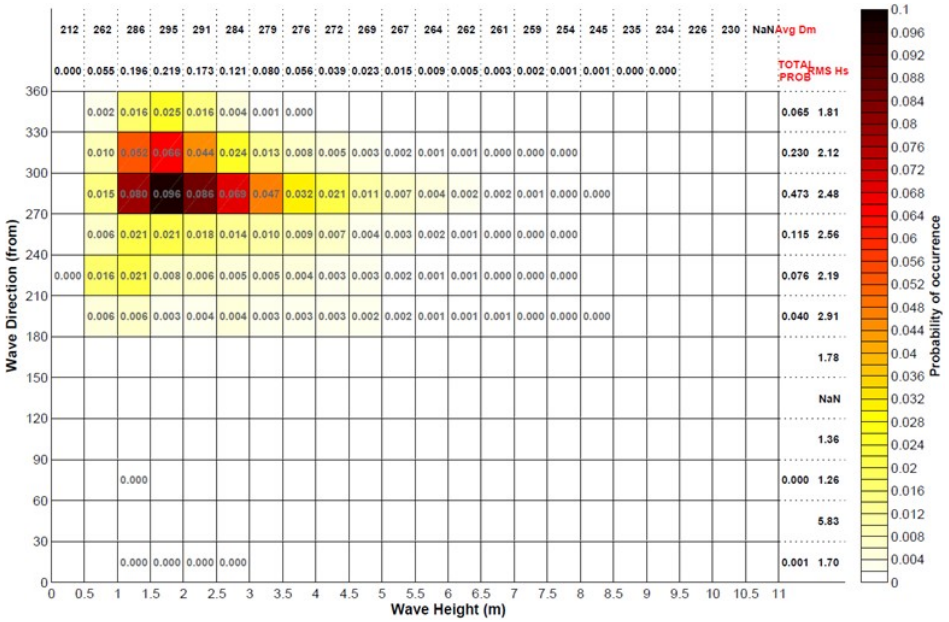

Figure 5-36
Probability Distribution of Wave Conditions at NDBC Buoy 139p1 for Model Boundary

The morphological impact of each wave condition was estimated by simulating wave conditions corresponding to each bin for which waves occur. Therefore, a total of 117 steady state simulations were performed. For each bin, the wave height was defined as the root-mean-square of all wave height observations within the bin, the wave direction was defined as the mean value of all waves within the bin, and the simulated period defined by the modal peak period of the observed wave conditions within the bin. For each simulation, the impact on sedimentation was recorded. Figure 5-37 shows the relative impact on sedimentation for all cases, assuming a constant simulation period. Cells with no data indicate that no such waves occurred in that bin. This figure is normalized to show how certain bins compare to others in their morphological impact. Figure 5-37 shows that waves from 260 degrees (west) result in the most significant morphological change, followed by waves from 285 degrees (WNW).

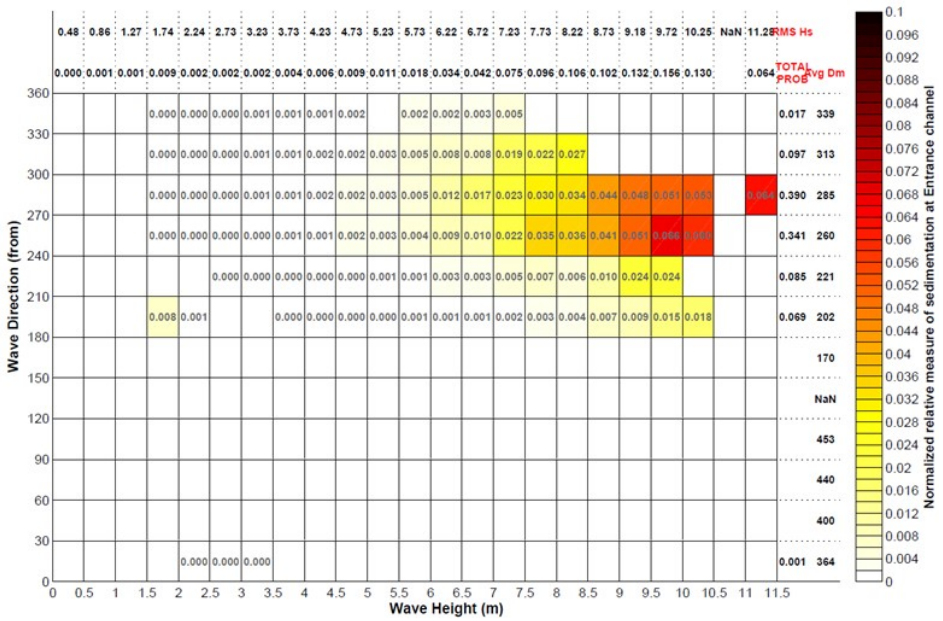

Figure 5-37
Normalized Relative Height of Each Wave Bin Based on Impact to Sedimentation

The set of representative wave conditions was selected based on the morphological impact of each wave condition (Figure 5-37) as well as the frequency of occurrence of that wave condition (Figure 5-36). Figure 5-38 shows relative effect of each wave condition on sedimentation, which is the product of the morphological impact and the frequency of occurrence.

The representative wave conditions used in the final model aggregated the small bins into larger blocks, also shown in Figure 5-38. Wave characteristics were developed for each of these blocks based on the root-mean square wave height, the average wave direction, and the modal peak period. The characteristics of the representative wave conditions can be seen in Table 5-12. This table also includes the annual probability of occurrence for each wave condition, which is based on the data in Figure 5-36. Finally, Table 5-12 includes the MorFac used in the long-term simulations, which was calculated as the annual probability of occurrence multiplied by 365 to determine the number of days the wave condition would occur in each year. As noted above, the total impact to sedimentation was calculated by simulating the representative wave condition for a 24-hour morphological tide, and then multiplying the resultant sedimentation by the MorFac.

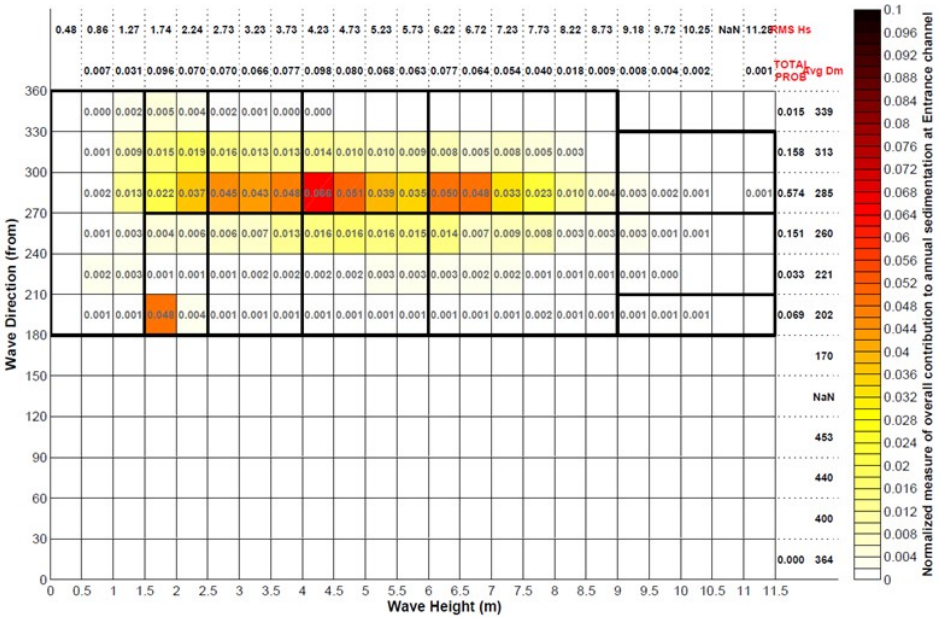

Figure 5-38
Normalized Measure of Contribution to Annual Entrance Channel Sedimentation from Each Wave Condition

Table 5-12
Representative Wave Conditions Used for Simulation of Average 1-year Morphology

ID	Significant Wave Height (m)	Mean Wave Direction (deg N)	Peak Period (s)	Probability of Annual Occurrence*	MorFac
1	1.90	228	9.40	0.0670	24.60
2	3.31	228	9.80	0.0660	24.30
3	5.01	228	11.2	0.0370	13.30
4	7.25	226	12.8	0.0070	2.40
5	1.14	269	10.7	0.1440	52.50

ID	Significant Wave Height (m)	Mean Wave Direction (deg N)	Peak Period (s)	Probability of Annual Occurrence*	MorFac
6	1.99	317	9.10	0.3810	139.20
7	3.10	314	10.70	0.2280	83.10
8	4.67	311	12.50	0.0620	22.50
9	6.82	311	13.40	0.0080	2.80
10	9.57	277	17.10	0.0003	0.10
11	9.46	248	16.20	0.0002	0.06
12	9.65	201	13.50	0.0002	0.06

*Corresponding to set of wave conditions represented by respective selected condition

5.4.2.6 Morphological Model Calibration

The model was calibrated by adjusting the suspended load and the bedload scaling factors that multiply the transport capacity calculated by the Watanabe (1987) sediment transport formulation. The CMS User Manual recommends scale factor values within the range of 0.2 and 5, with a scale factor of 5 being the one chosen as the calibrated value for this application. The final set of sediment transport parameters used in the model is shown in Table 5-13.

Table 5-13
Calibrated Sediment Transport Model Parameters

Sediment Transport Parameter	Value
Transport Formula	Watanabe
Concentration Profile	Rouse
A-Coefficient (Watanabe formula)	0.15
Sediment Density	2650 kg/m^3
Sediment Porosity	0.4
Adaptation Length (constant)	20 m
Bed-Slope Coefficient	0.1

Sediment Transport Parameter	Value
Suspended Load Scale Factor	5.0
Bed-Load Scale Factor	5.0

The results of the calibrated model can be seen in Figure 5-39. This figure shows the measured change in bathymetry from 1999 through 2000 (a typical year based on the shoaling volume) and the modeled bathymetry change under the schematized boundary condition that represents the waves with the highest potential to drive sedimentation. The gross volume of sedimentation within the calibration area was calculated to be 370,000 cy/yr, which compares very well to the measured sedimentation rate of 360,000 cy/yr. The model appears to reproduce the longitudinal trend in sedimentation observed in data, with relatively significant sedimentation along the southern edge of the channel outside the area between the jetties and along the northern edge of the channel near the tip of the North Jetty. The predicted total sedimentation in the Entrance Channel was simulated to be 700,000 cy/yr, which matches closely with the measured average annualized sedimentation of 680,000 cy/yr. Therefore, this model is able to reproduce the observed shoaling well, both in the calibration area offshore of the jetties and within the entire Entrance Channel. The shoaling rate of 700,000 cy/yr represents the modeled shoaling under the Existing Conditions.

There are no specific codes or standards for assessing performance of morphological models in terms of simulation of observations (goodness-of-fit between model predictions and measurements). However, review of recent[7] and similar[8] modeling studies confirmed that performance of the model is within the standard of practice to quantitatively compare alternatives.

[7] *Williams& Esteves (2017) stated that "a model predicting the dredged volumes to within 50% of the measured rates is normally deemed to be satisfactory for most practical applications".*
[8] *ERDC (2018) modeling study, not for a 204/408 project, matched the observed sedimentation patterns within an order of magnitude.*

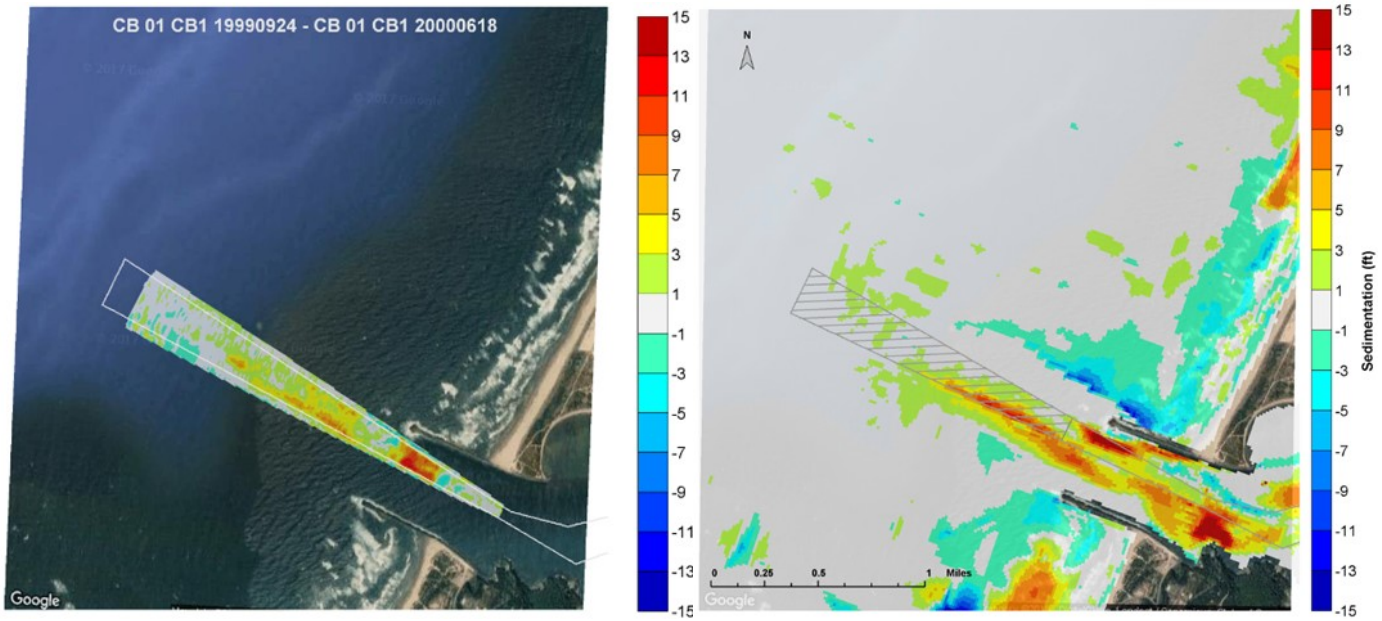

Figure 5-39
Comparison of Observed Bathymetry Change in a Typical Year (Left) and Modeled Sedimentation under Annual Average Wave Climate (Right)

To provide a comparison of net sediment transport pathways with other sources, the model-predicted suspended sediment transport vectors during the calibration period are shown in Figure 5-40. Seaward of the jetties, the net direction of sediment transport appears to be from south to north, which is consistent with other long-shore sediment transport studies (USACE 2012b and Section 5.3.1) of this area. A significant percentage of the sediments transported along this pathway get deposited in the Entrance Channel.

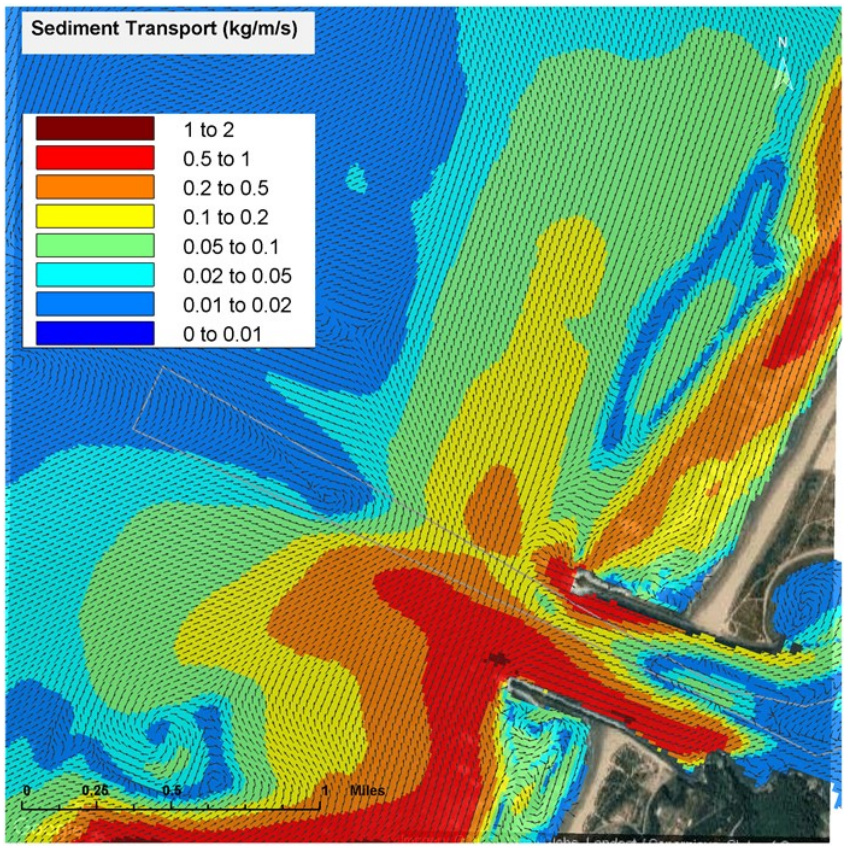

Figure 5-40
Model-Simulated Net Sediment Transport Vectors for September 2009 to April 2010 Calibration Period

5.4.2.7 Summary

The CMS model application for the Coos Bay inlet morphology study was developed using a prior USACE-ERDC CMS application as a starting point. The model was subsequently refined and calibrated to reproduce the measured sedimentation volume from 1999-2009. The model

reasonably reproduced the measured sedimentation volumes and the spatial pattern of sedimentation.

5.4.3 Simulation of Future Channel Conditions

The hydrodynamic, wave, and morphological models were applied to evaluate sedimentation volumes under various future channel conditions and management scenarios. Each of the future channel conditions was evaluated by simulating the morphological change with the calibrated CMS sediment-transport model with an average one-year climate following construction of the dredged channel. The modeling approach with the reduced boundary conditions, as applied for the calibration simulations, was used for these projection scenarios to obtain model results within reasonable computational time.

5.4.3.1 Projection Scenarios

The following scenarios, which are described in further detail in the following sections, were simulated with the calibrated morphological model:

- Calibration Condition: The dredged channel condition prior to the Coos Bay Jetty repairs was simulated as documented in Section 5.4.2.6.
- Existing Conditions: This scenario assumes no new capital dredging of the Coos Bay navigation channel and includes design elevations from the Coos Bay North Jetty Repair Major Maintenance project (USACE 2021).
- 2023 PA: This is the Proposed Alteration, which includes a dredged Entrance Channel and the North Jetty repair.

The modeled conditions are summarized in Table 5-14.

Table 5-14
Modeled Conditions for Sediment Transport Modeling

Condition	Bathymetry	South Jetty	North Jetty Head	North Jetty Root
Calibration	September 24, 1999	No Change	No change – Jetty head at 83+00 (2012 MMR)	No Change
Existing Conditions	-52 ft MLLW near RM 0; -38 ft MLLW at RM 1	No Change	North Jetty repair (USACE 2021)	North Jetty repair (USACE 2021)
2023 PA	-63 ft MLLW near RM 0; -46 ft MLLW at RM 1	No Change	North Jetty repair (USACE 2021)	North Jetty repair (USACE 2021)

5.4.3.2 Projection Boundary Conditions

The production model runs were forced with the same boundary conditions used for calibration (i.e., the annual average wave climate from 2006-2016). These are presented in Figure 5-39 and Table 5-12.

5.4.3.3 Simulation of Existing Conditions

The Existing Conditions scenario was simulated to provide a baseline estimate of future sedimentation in the absence of any channel deepening project. The Existing Conditions scenario is similar to the calibration scenario presented in the preceding section, except that it includes the North Jetty repair. The updates include extension of the North Jetty head by 125 ft, with the reconstructed jetty head placed on the pre-existing relic stone.

The degree of average annual sedimentation under the Existing Conditions can be seen in Figure 5-41. The annual shoaling is modeled to be 707,000 cy/yr, or 7,000 cy/yr more than under the calibration condition, with a similar spatial distribution to the calibration (Figure 5-39). The increase may be due to the increased jetty length, which limits longshore currents carrying sediment from the south and increases deposition. Overall, however, this is only a 1 percent increase above the calibration condition.

An illustration of a type of complexity involved in morphological modeling is the high-shoaling area indicated by the model adjacent to the North Jetty in Figure 5-41. In reality, this is a scour area formed by a 3D phenomenon in which flood currents overtop the relic jetty, splashing into the seabed and eroding the material just south of North Jetty. However, since this 3D process cannot be simulated by a 2D model such as CMS, the model predicts shoaling. The historical scouring in this area is expected to continue under the existing and future PA conditions.

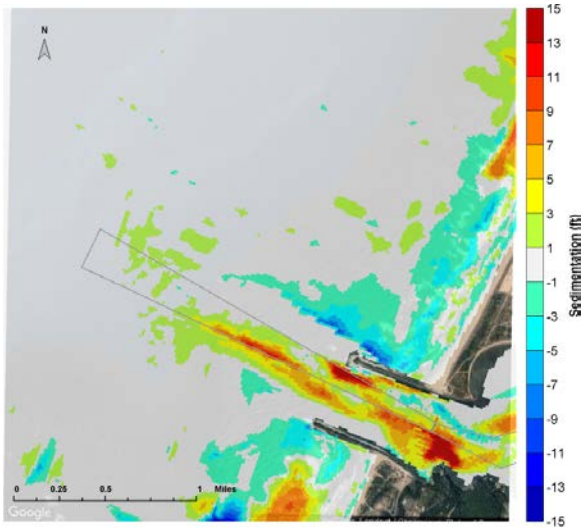

Figure 5-41
Modeled Annual Sedimentation under Existing Conditions

5.4.3.4 Simulation of 2023 PA

As noted above, the 2023 PA simulation includes the jetty repair plus channel modification. A complete description of the channel condition can be found in Section 1.4. The modeled sedimentation pattern for the 2023 PA is shown in Figure 5-42, both with *constructed condition* and *future equilibrium* side slopes. These slope conditions are described Sub-Appendix 6 - *Channel Side Slope Analysis* and summarized by RM in Table 4-10 of that document. The modeled sedimentation for the 2023 PA downstream of River Mile 1 is 1,348,000 cy/yr and 1,015,000 cy/yr for constructed and future equilibrium side slopes, respectively. Spatially, sedimentation patterns under the 2023 PA are similar to the Existing Conditions, with a large shoal just south of the North Jetty head and another shoal along the southern edge of the channel. Under the 2023 PA, these shoals contain more sediment than under other conditions.

The result based on future equilibrium side slopes – 1, 015,000 cy/yr – is used to estimate long-term O&M because it does not include the shoaling associated with side slope equilibration. Therefore, the 2023 PA represents a 308,000 cy/yr increase over the Existing Conditions.

The erosional trends in the vicinity of the North Jetty root seen in Figure 5-41 can also be seen in Figure 5-42, generally indicating that the 2023 PA will have a limited effect on erosion in this area.

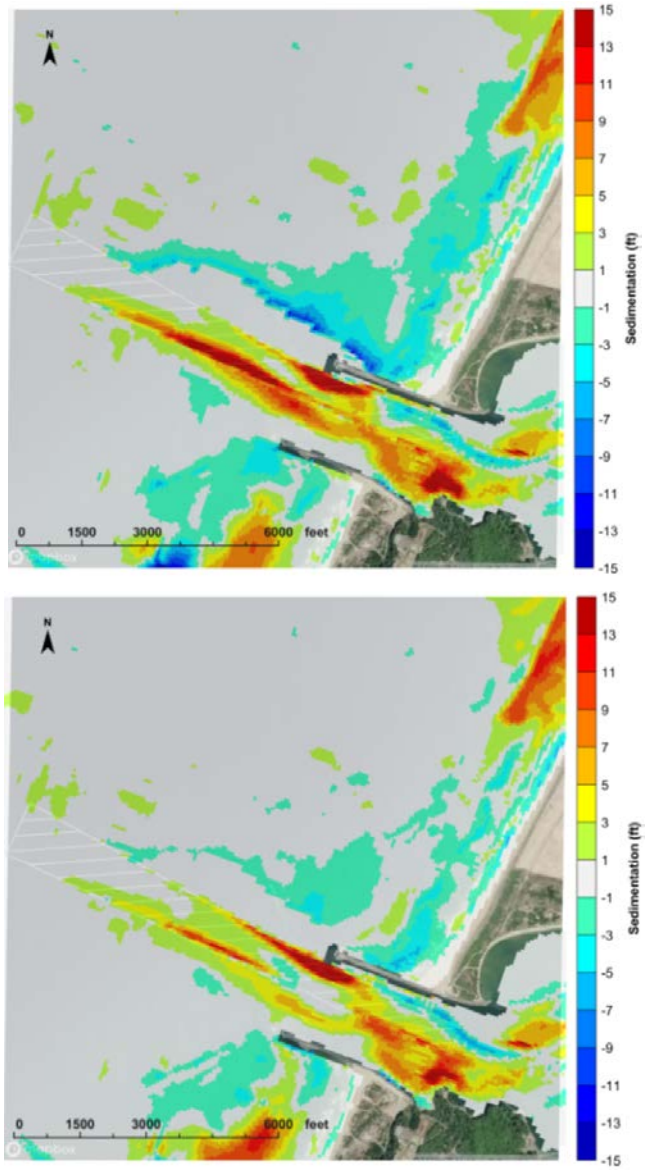

Figure 5-42
Modeled Annual Average Sedimentation under the 2023 PA (Top: Constructed Side Slopes; Bottom: Future Equilibrium Side Slopes)

5.4.3.5 Comparison of Sedimentation Rate under Different Scenarios

Table 5-15 shows the estimated annual average sedimentation volumes in the entrance channel and up to RM 2.5 for the various project scenarios described above. The 2023 PA simulations that include the equilibrated channel represent a better estimate for the long-term shoaling of the channel (as it is expected that side slopes will equilibrate over this time period). The results for the reach between RM 1 and RM 2.5 appear to be driven at least partly by marginally higher deposition in the deeper areas in the simulation with equilibrium side-slopes, which may not translate to a requirement for additional O&M dredging.

Table 5-15
Comparison of Annual Sedimentation under Different Project Scenarios

		Existing Conditions	2023 PA with Construction Side Slopes	2023 PA with Equilibrium Side Slopes
RM -1 to 1	Net Sedimentation (cy)	707,000	1,348,000	1,015,000
	Change Relative to Existing Conditions (cy/yr)		+641,000	+308,000
RM 1 to 2.5	Net Sedimentation (cy)	291,000	299,000	342,000
	Change Relative to Existing Conditions (cy/yr)		+8,000	+51,000

The difference between shoaling under the Existing Conditions and the 2023 PA with future equilibrium side slopes between RM -1 and RM 1 is approximately 308,000 cy/yr. Model results (Figure 5-42) show that sedimentation in the channel is largely driven by the channel footprint. Under the 2023 PA, the shoaling extends further offshore, and hence it traps some longshore transport material as well. However, as sedimentological studies have suggested an offshore limit of longshore transport decreases at -60 ft MLLW (USACE 1994), only a portion of this offshore extent traps sediment.

5.4.3.6 Sedimentation at LSB

CMS model results can also be used to examine sedimentation trends at LSB. Figure 5-43 shows annual sedimentation plots in the vicinity of LSB through RM 2.5. As these plots show, the model predicts erosion at the base of the jetty root. However, this erosion is similar under both future with project conditions. A difference plot is shown in Figure 5-44.

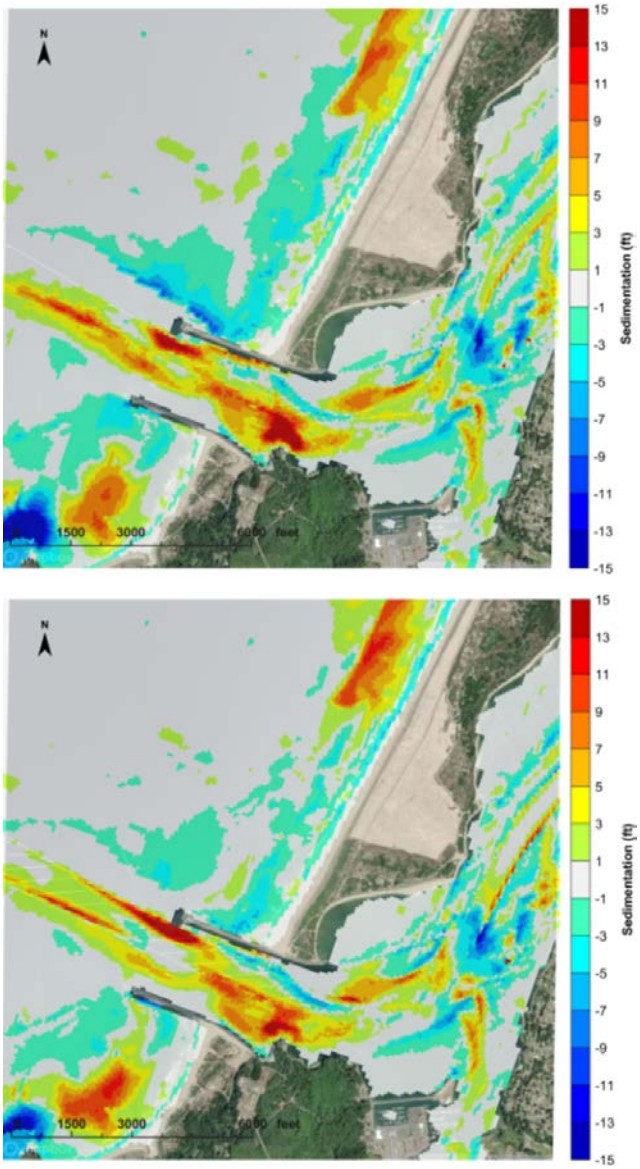

Figure 5-43
Sedimentation at LSB (Top: Existing Conditions, Bottom: 2023 PA with Future Equilibrium Side Slopes)

5.4.3.7 Limitations of Sedimentation Modeling Results for Future Channel Conditions

The sedimentation modeling results presented in Figure 5-41 through Figure 5-44 illustrate the degree of average annual sedimentation in the offshore and ocean entrance channel areas that are the focus area of this sub-appendix and the CMS morphological model analyses. In contrast to the figures presented in Section 5.4.2.6 illustrating the model calibration and the Existing Conditions results, the figures illustrating future projection scenarios show qualitative degrees of erosion and deposition. Even with the careful development of model inputs, boundary conditions and the simulation approach, and the high degree of agreement of the calibrated model with measured shoaling volumes, estimating annual erosion and deposition with a sediment transport model involves significant uncertainty. The physical processes are complex and the forcing conditions are subject to wide variations year to year, and it is not feasible to capture all of the complexity and variability in a reasonable scope of modeling for this type of project. Given the successful calibration described above, the morphological modeling program is sufficient to provide qualitative comparisons of the likely annual erosion and deposition trends and magnitudes within the offshore and ocean entrance area. The color scales in Figure 5-41 through Figure 5-44 illustrate the relative magnitudes of annual deposition and erosion expected across this sub-appendix focus area for each of the considered project scenarios and are the direct output from the numerical model. The quantitative modeled results provided in the text and in the figures for the future PA scenario are still intended to facilitate a relative qualitative comparison of scenarios with respect the Existing Conditions.

Commented [MO15]: A-4-28, A-4-24, A-4-25 (Dr. Checks 8071912) and DCC ID 8070856

Commented [SJ16R15]: Need concurrence

Commented [MD17R15]: Moved this section here where it seems more appropriate (from 5.4.3.3)

5.4.4 Conclusions

A calibrated and validated CMS model has been developed and applied for modeling existing and future morphological changes at the Coos Bay inlet. The model builds upon the original model application to Coos Bay developed by USACE-ERDC. The model consists of linked models for the hydrodynamics, waves, sediment transport, and morphological changes within Coos Bay and the adjacent coastal zone. The setup and parameterization of the hydrodynamic and wave models are the same as established by USACE-ERDC, with the exception of the boundary conditions. The hydrodynamic and wave model performance was further validated against water level, current, and wave measurements in the vicinity of the Coos Bay inlet.

The sediment transport and morphological model was refined in several respects and calibrated against measured sedimentation within the Coos Bay inlet. The model performs reasonably well in reproducing the net sedimentation volumes and spatial patterns. The model also reproduces the along-channel patterns of accumulation.

The calibrated morphological model was used to simulate an average year under the Existing Conditions and the 2023 PA. The results of these simulations were used to estimate future O&M in the Entrance Channel. The model predicts an increase in sedimentation of approximately 308,000 cy/yr under the 2023 PA relative to the Existing Conditions. The construction of the proposed channel does not significantly affect the predicted sediment transport pathways, as the sediment travels from south of the inlet across the dredged channel in front of the inlet, the larger depth gradient from the channel deepening leads to significant sediment deposition along the channel edge.

Ultimately, the projected increase in shoaling exceeds the increase projected by the sediment budget (Section 5.3). Examining Figure 5-42 shows that much of the sediment that fills in the channel is sourced from erosion of the adjacent areas – north of North Jetty (ODMDS F) and south of the South Jetty. The fact that sediment ODMDS F is a major source of sediment to the system would support the conclusion in Section 5.3.5 that the potential sediment available to shoal in the channel is limited (in this case, it is limited by the amount of sediment placed in ODMDS F). Therefore, it is reasonable that sedimentation only increases by the estimated 308,000 cy/yr under the 2023 PA.

The sediment transport analysis was also used to evaluate the stability of the Pacific shoreline, LSB, and the foundation of the jetties. As Figure 5-42 shows, erosion under the 2023 PA is not expected along the Pacific shorelines, along the south side of the South Jetty tip, the north side of the North Jetty trunk, and along the North Jetty root near LSB. The area between the rock apron on the south side of the North Jetty trunk is depositional, as is the north side of the South Jetty trunk.

To consider the effect of erosion, a difference plot to compare shoaling under the 2023 PA minus the Existing Conditions is presented in Figure 5-44; in this figure, green and red colors represent more shoaling under the 2023 PA relative to the Existing Conditions, and blue colors represent more erosion under the 2023 PA. In addition, in areas where the bottom substrate is rock and would not be subject to erosion, the difference plot could still show blue colors if the area experiences less deposition under the 2023 PA (e.g., near Guano Rock). As a result, they will not show up in Figure 5-45, where the actual erosional potential was considered.

As this plot shows, there is effectively no change in shoaling between the 2023 PA and the Existing Conditions along the Pacific shoreline nor within LSB. Along the South Jetty, sedimentation increases. Sedimentation decreases along a portion of the North Jetty root (blue shaded area landward of the jetty head). As shown in Figure 5-42, this area is still depositional under the 2023 PA and therefore no additional protection is required. There is also an area with net negative sedimentation adjacent to the North Jetty trunk. This area goes from being net depositional under the Existing Conditions (Figure 5-41) to net erosional under the 2023 PA (Figure 5-42). As a result, a rock apron is recommended in this area (North Jetty Station 56+50 to 71+90) to protect the foundation of the North Jetty trunk.

Commented [CT18]: A-4-26: Revise explanation to state that although the results depict the model results, the text needs to state that this area of the inlet is rock and would not be expected to erode (or has less erosion potential than FWOP).

Commented [CT19R18]: Added text.

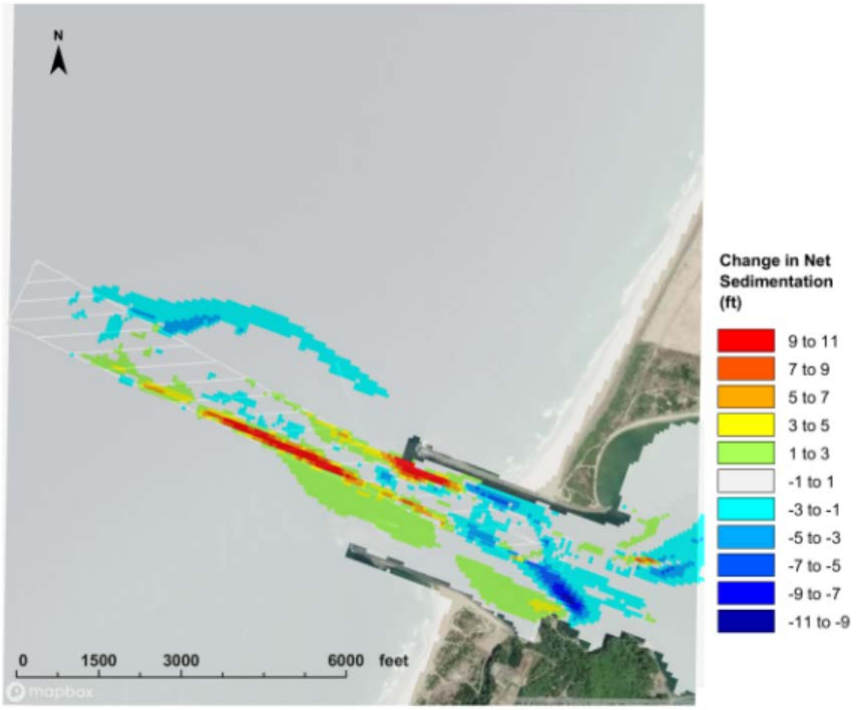

Figure 5-44
Comparison of Sedimentation between the 2023 PA with Future Equilibrium Side Slopes and the Existing Conditions

The erosional potential under the 2023 PA with equilibrium side slopes compared to the Existing conditions is shown in Figure 5-45. The erosional potential was computed as follows:

- If computation cell is erosional in the 2023 PA, then show negative value (erosion) from the 2023 PA.
- If computation cell is depositional in the 2023 PA, but erosional in the Existing Conditions, then show positive value (deposition) from the 2023 PA.
- If computational cell is depositional in both the Existing Conditions and the 2023 PA, then show "no value".

Therefore, Figure 5-45 can be used to identify the areas which remain or become erosional under the 2023 PA compared to the Existing Conditions. The values represent computed annual sedimentation or erosion under the 2023 PA, but ignore the areas, where the model predicts deposition under both conditions. Based on the presented results, areas which under the 2023 PA may remain or become erosional are along the North Jetty trunk (Area A), jetty structures along the LSB (Area B, north and south), and Charleston Harbor breakwater (Area C).

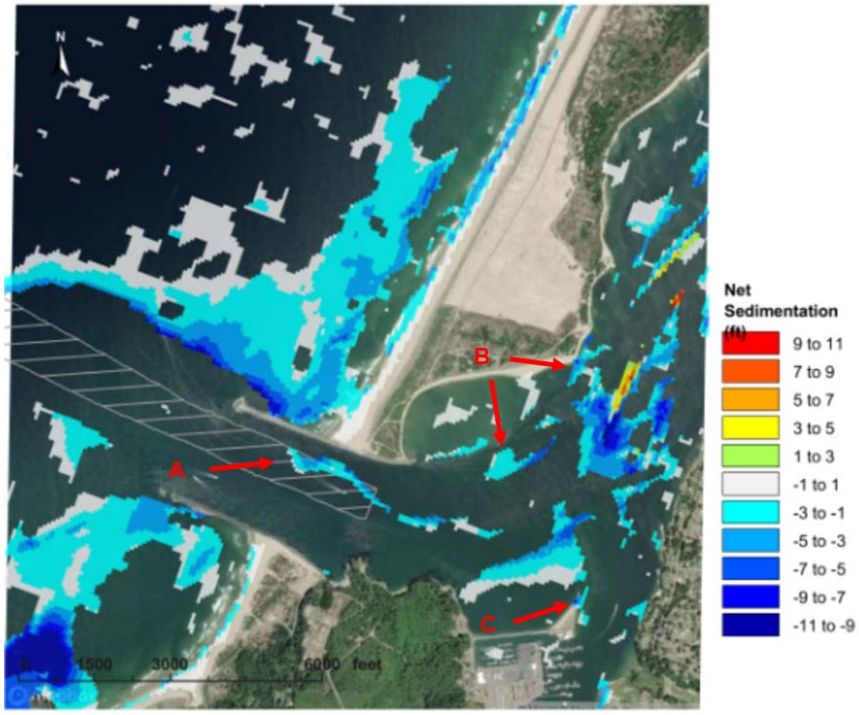

Figure 5-45
Erosional Potential under the 2023 PA with Future Equilibrium Side Slopes compared to the Existing Conditions

Additional detail on the proposed jetty toe protection is provided in Section 6.2.

Two areas within the Entrance Channel show high increases in sedimentation: along the southern boundary of the offshore channel and adjacent to the North Jetty head. The increase in shoaling along the southern boundary of the channel results from relocation of the offshore portion of the channel. As shown in Sheet C-101, (Sub-Appendix 8 - *Drawings*), the channel limits are shifted south in this area. Therefore, the shoaling along this channel boundary similarly shifts south; hence, Figure 5-44 shows an increase in shoaling along the 2023 PA channel boundary, and a reduction in shoaling north of this. The other area of high increased shoaling, adjacent to the North Jetty, is an artifact of the CMS model and is discussed in Section 5.4.3.3.

5.5 Shoaling Estimates

This report presents two techniques that were used to estimate future shoaling rates at Coos Bay: a conceptual sediment budget and CMS modeling. The CMS modeling is generally accepted as a more reliable tool to quantify changes to sedimentation at inlets. It predicted higher shoaling rates, therefore presenting a possibly more conservative estimate of future O&M dredging requirements.

Long-term O&M dredge rates are calculated by defining the baseline condition and adding the incremental increase in shoaling; the result is presented in Table 5-16. The baseline dredging rate for before the USACE jetty repairs (calibration condition) is 660,000 cy/yr, as reported in Section 2.2.3. This number is the actual volume of sediment that is dredged from the channel from 1998-2014. As the actual, reported dredge volume, this number reflects channel shoaling, dredging budget, equipment availability, and weather conditions. Under the 2023 PA, shoaling is expected to change; however, it is not clear how those other factors may change.

For the Existing Conditions, sediment transport modeling indicates that shoaling is higher by approximately 7,000 cy/yr. Thus, 667,000 cy/yr is used to define the baseline Existing Conditions dredging. The expected increase in shoaling based on sediment transport modeling is 308,000 cy/year up to RM 1 and an additional 51,000 cy/year between RM 1 and 2.5 for the 2023 PA. This amounts to a total increase of 359,000 cy/year with the 2023 PA.

Table 5-16
Expected Dredge Volumes for Model Scenarios

Estimate	Calibration Condition (Historical)	Projected Entrance Channel Dredging in cy/yr	
		Existing Conditions	2023 PA
Expected Value	660,000	667,000	1,026,000

It should be noted that these represent annual average conditions – shoaling may be more or less in any given year. Historically, the standard deviation is approximately 170,000 cy/yr, or 26 percent of the mean. Applying this percentage of the mean, under the 2023 PA, the standard deviation would be approximately 266,000 cy/year; this corresponds to an expected future O&M range of between 760,000 cy/year and 1,290,000 cy/yr.

5.6 Effect of Non-Erodible Bottom on Sedimentation Results

Figure 5-46 (from ERDC, 2018) shows median sediment size data in the vicinity of the entrance channel. The median sediment size in the scour area south of the North Jetty relic is greater than 0.5 mm with over 30% of sediments coarser than 0.7 mm. Also, it is noticeable that sediment sizes inside the entrance are coarser than at the beach. Therefore, excessive scour in the model near the North Jetty relic could be attributed to setting fine sediment size in this area of the model. Similarly, the model shows erosion around the South Jetty head, which is inconsistent with historical observations.

The CMS model includes rock (non-erodible) layer inputs based on known rock outcrops with the initialized model bathymetry. As Section 5.4.2.1 states: “rock outcrops in the Coos Bay area include Guano Rock in the Entrance Channel, Baltimore Rock near Gregory Point south of the inlet, and relics or other rock in the immediate vicinity of the jetties. These areas were included in the model as a hard-bottom layer, i.e., non-erodible. Outside the channel limits, there is little available data describing the bedrock relative to model bathymetry. Therefore, the presence or lack of rock in these areas was estimated from adjacent areas. Initial simulations omitted the presence of rock in the Entrance Channel, and the results showed significant unrealistic erosion adjacent to the North and South Jetties (up to 10 ft/yr), areas that are not known to substantially erode.

Therefore, at-bed or near-bed rock layers were assumed over most of the area adjacent to the Entrance Channel to limit the model erosion in these areas. Without these assumptions, the model may overestimate the magnitude of predicted sedimentation in the navigation channel (with these assumptions, the model was able to reproduce measured shoaling, in fulfilling the primary purpose for the CMS model simulations). The revised depth of the rock layer input to the model is shown in Figure 5-33. It should be noted that upstream of LSB, no bedrock is included in the model, since CMS model results are not considered in this area."

The depth of the non-erodible bottom input to the model is shown in Figure 5-47 (left). The location of non-erodible layers as computed from the 2017 DEA measurements are shown in Figure 5-47 (right). The comparison shows that data available to construct the non-erodible area from measurements did not cover the entire model domain and some assumptions were necessary to setup the model.

The model results (Figure 5-48) show no scour around the North Jetty relic (due to the application of non-erodible bottom), and only limited deposition in the scour area south of the relic. The following observations can be made:

- The assumption of non-erodible bottom helps limit the scour on the end and north side of the North Jetty Relic. The application of non-erodible bottom in this location was justified based on a higher stability of seabed in this area, which can be observed from available bathymetric surveys compared to the model results. Such stability can also be due to the presence of coarser sediment material; however, more accurate sediment size distribution data is not available.

- The area to the north of entrance channel is not erosional in the model. The only potential impact of the non-erodible bottom in this area would be to provide less sediment available material for erosion. However, since the models show no erosion in this location, it would not be expected to contribute to sedimentation in the channel as a sediment source. Other processes would not be affected.

- The assumed rock layer input in the model helps limit excessive erosion around the South Jetty head. Similar to the North Jetty head area, this area is expected to be stable in the model simulations of long-term conditions. Also, there is no data available in this area on sediment sizes.

- The assumption of non-erodible bottom at the location of rock coast next to Cape Arago limits the influx of sediments from around the South Jetty head which might otherwise contribute to overestimation of sedimentation at the entrance.

- Other areas: Sedimentation in other areas was not affected by the application of non-erodible bottom. Areas inside the channel are depositional in the model and had sufficient sediment availability for sediment transport formulation.

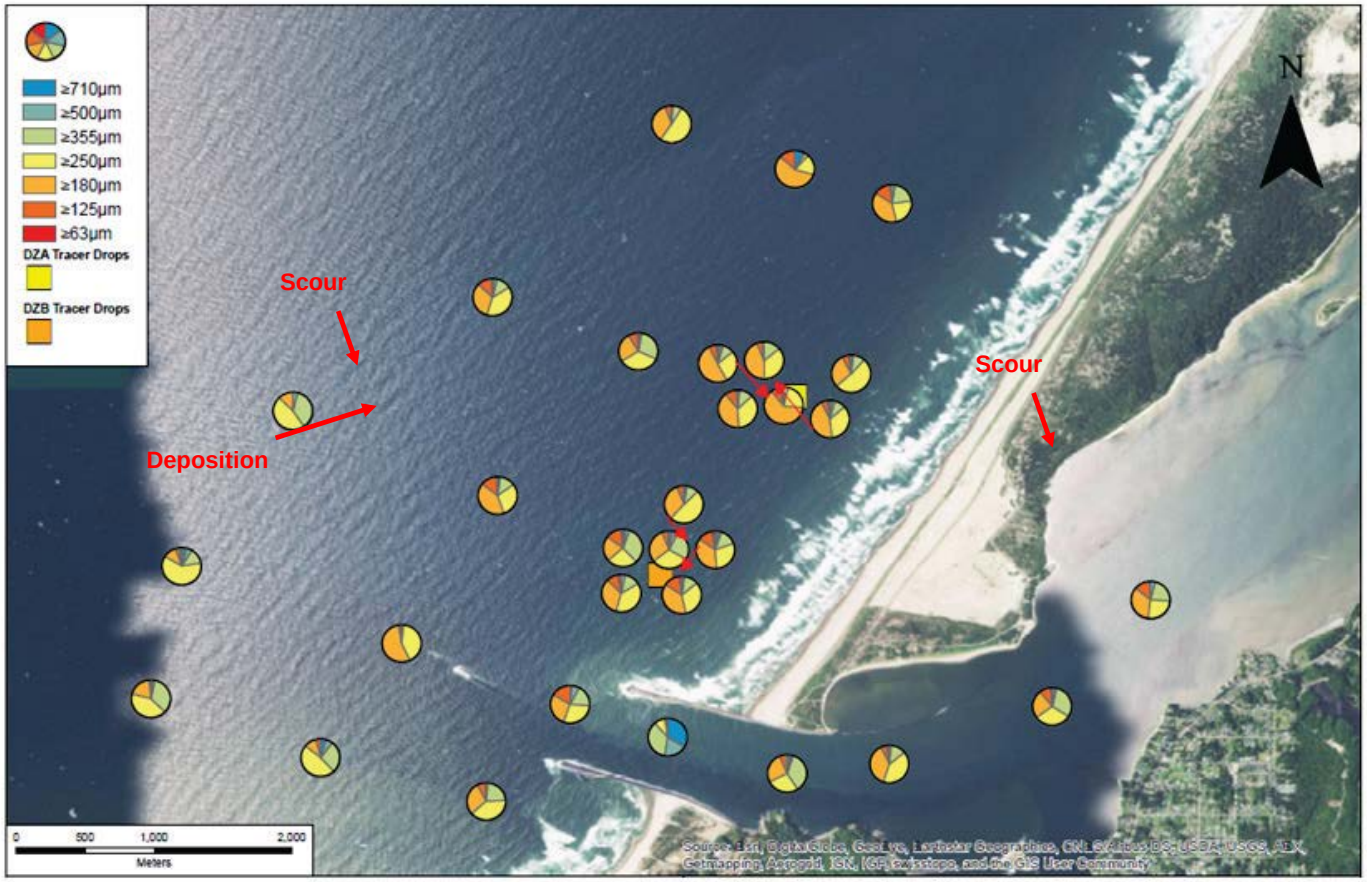

Figure 5-46
Background particle size data for grab samples collected from the study area (September 18, 2015) (Figure 3-8 from ERDC, 2018)

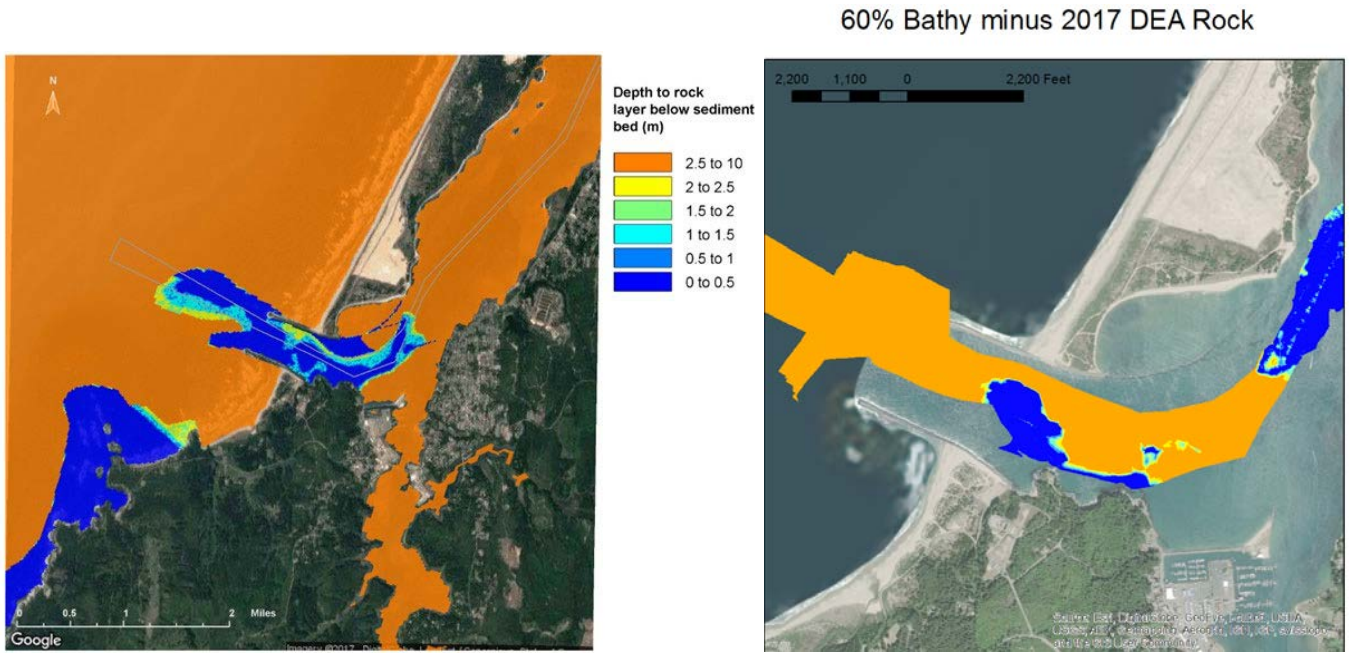

Figure 5-47
Left — Depth to Rock Layer below Surface of Sediment Bed in 2019 Model (same as Figure 5-33).
Right — Estimated Sediment Thickness based on the Difference between Bathymetry and 2017 DEA Measurements

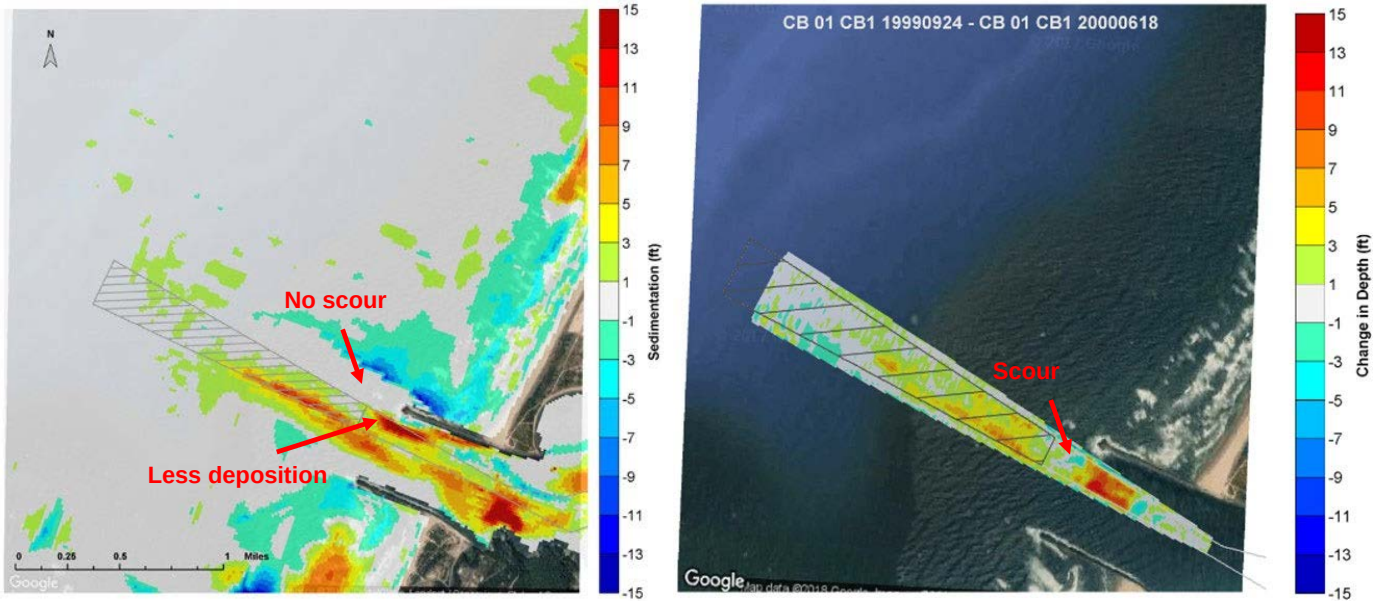

Figure 5-48
Comparison of Modeled Sedimentation under Annual Average Wave Climate with CMS Model (Left) (same as Figure 5-39) and Observed Bathymetry Change in a Typical Year (Right)

5.7 Qualitative Assessment of Entrance Channel Erosion and Risks for Structures

As discussed in Section 5.4, the primary purpose of application of the CMS sediment transport model was predicting changes in the Entrance Channel sedimentation and maintenance dredging associated with the 2023 PA. As further addressed in Section 5.4.3.7, estimating annual erosion and deposition with a sediment transport model involves significant uncertainty. A good model calibration using historic data was achieved. The model performance was improved through adjustment of the non-erodible bottom boundary layer. This adjustment could potentially limit scour predictions. To qualitatively assess areas of potential erosion associated with future with-project conditions, model results were analyzed.

The model results show increased potential for scour near the North Jetty trunk compared to the Existing Conditions results. Similarly, the simulation with equilibrated channel side slopes shows relatively higher erosion, compared to the simulation with construction slopes.

Based on the qualitative assessment, the following conclusions can be made:

- Areas around the North Jetty head show a high potential for erosion under all modeled conditions. Under future channel modifications, this erosional potential may increase even more. However, since the model configurations did not include accurate sediment characteristics in these areas (just as the models were configured to use finer sediment sizes than present in the area), the predicted magnitude of erosion may be overestimated by the models. Since the risks to the North Jetty head and relic are high, the project included the rock apron to protect the structure toe slope.
- Areas along the North Jetty trunk inside the entrance are prone to erosion under all modeled conditions. Simulations with future channel modifications indicated that erosion potential may increase. Since the risks to the North Jetty trunk are high, the project included the rock apron to protect the structure toe slope.
- Areas around the South Jetty head and trunk show potential for erosion under all modeled conditions. From the qualitative comparison, it appears that the risks to the structure under future channel modification conditions may be comparable to the Existing Conditions. Therefore, the project does not include additional measures to minimize the erosion potential, but these are the areas of potential concern and will be included into the Risk Management Plan.
- As shown in Figure 5-45, area along the jetty structure south and north of the LSB are the areas of potential concern due to erosional potential under future conditions. These areas will be included into the Risk Management Plan.
- As shown in Figure 5-45, area along the Charleston Harbor breakwater is the area of potential concern due to erosional potential under future conditions. This area will be included into the Risk Management Plan.

Given the qualitative nature of the assessment and limitations of the modeling tools, potential areas of concern and risk are addressed in the Risk Management Plan discussed in Section 8 of this sub-appendix and in the *Engineering Appendix* Section 11.

5.8 Comparison to Other Channels

This section investigates maintenance dredging requirements at other FNCs in the Pacific Northwest that extend beyond their respective jetties to provide insight as to how extending the 2023 PA beyond the jetty tips may impact maintenance dredging. It should be noted that the Coos Bay Entrance Channel already extends beyond the jetty tips; maintenance is performed to RM -0.55, while the jetty tips are located at RM 0.3. However, the 2023 PA does propose to extend the channel further offshore.

This section draws on data compiled by Dr. Rosati (2003) on four channels: Grays Harbor Outer Bar Channel, MCR, Yaquina Bay, and Siuslaw River. The location of the channels relative to the jetty tips are based on navigation charts from the NOAA site (NOAA 2017b). Moreover, this section uses maintenance dredging records to approximate shoaling, since these records are more readily available. Over the long-term, this is acceptable because long-term O&M will adapt to shoaling patterns to maintain a navigable channel.

5.8.1 Grays Harbor Outer Bar Channel

Dredge records at Grays Harbor Outer Bar channel extend back to 1920, when the channel was 500 ft wide by 24 ft deep. In 1927 the channel was expanded to 1,500 ft wide by 36 ft deep, and around 1991 it was modified to 1,000 ft wide by 46 ft deep. The original jetties suffered rapid deterioration after construction and were repaired in 1940-1942 (present and historic lengths are unknown).

The dredging rates in Grays Harbor Outer Bar Channel are presented in Figure 5-49. As this figure shows, the dredging rate was the highest for the 36-ft deep, 1,500-ft wide channel. Based on the data presented in this chart, it appears that the construction of new jetties in 1940-1942 reduced the need for maintenance dredging in the 36-ft deep channel; after initial jetty construction, the channel was self-maintaining and required little to no maintenance dredging. Dredging became necessary again in 1990; this may be due to deterioration of the jetty or the channel deepening (which extended further offshore), or both.

While the authorized channel extends well beyond the jetties, inspecting pre-dredge surveys from the past two years (USACE 2017a) indicates that dredging is limited to areas within the jetty tips. Therefore, the increase in dredging noticed in 1990 may be attributable to one or a combination of three factors: changes to the hydrodynamics, increased channel trapping efficiency, or recession of the jetty heads. The first factor reflects the assumption that a deeper channel may reduce channel velocities over the bar, thereby increasing shoaling. The second factor reflects the fact that the deeper channel may have the potential to trap sediment in areas where the natural depth is greater than 36 ft and less than 46 ft, such as the offshore bar. Investigating the adjacent bathymetry and the depth of the channel shoals indicate that the natural depth of the present shoaling location is deeper than 36 ft. Thus, the offshore bar was not deep enough to impact this bar prior to 1991. The third factor hypothesizes that the jetties have been receding and allow more material to circumvent the jetty tips and settle into the channel.

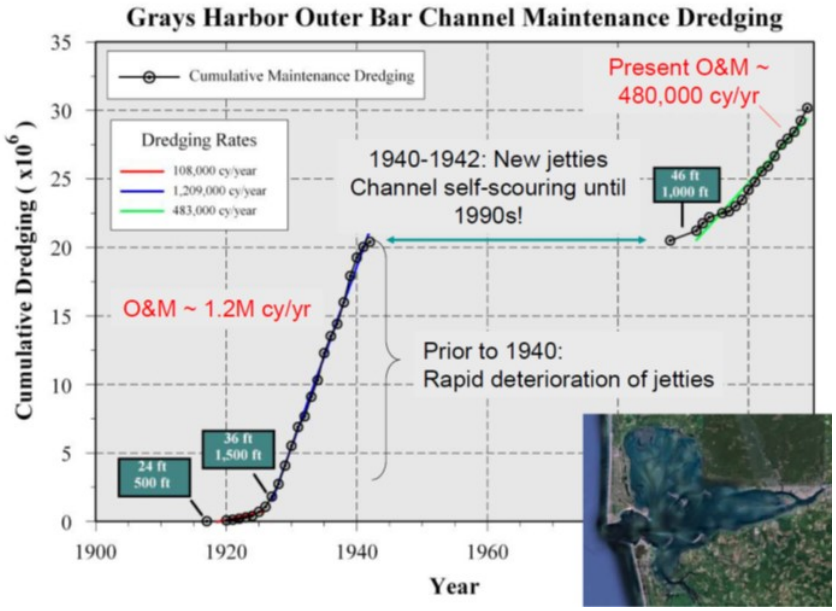

Figure 5-49
Historic Dredging Rates at Grays Harbor Outer Bar Channel

A detailed history of the jetties and the shoaling patterns prior to 1940 would be necessary to determine why the 1940-1942 jetty reconstruction removed the requirement for maintenance dredging. However, because all shoaling occurs between the jetties, it does not appear that extending the channel beyond the jetty tips is the key factor for the presently required level of maintenance dredging.

5.8.2 Mouth of the Columbia River

Dredge records at the MCR extend back to 1910 (initial channel and jetty dimensions are unknown). In 1954 the channel was expanded to 2,640 ft wide by 48 ft deep, and around 1982 it was modified to 2,000 ft wide by 55 ft deep. No information on the histories of the jetties have been provided.

Historic dredging rates at MCR are presented in Figure 5-50. Maintenance dredging appears to have increased proportional to channel depth. While Figure 5-50 shows average dredging rates associated with each channel dimension, it appears that the present dredging rate was achieved in 1972, about 10 years before the most recent channel deepening. Therefore, the increased dredging may be attributable to an external factor (such as funding, equipment used, or increased sedimentation from upstream).

The present channel extends 3 mi offshore of the jetty tips (and has historically extended beyond the jetty tips); channel surveys indicate that shoaling occurs both within the jetties, as well as beyond the jetty tips. The Columbia River transports a large quantity of sediment that continuously

moves around offshore. The increase in dredging may be a result of the increased trapping efficiency of the deeper channel.

The fact that channel dredging appears to have occurred 10 years prior to modification indicates that some other factor besides the channel offshore extent drives shoaling. Therefore, it should not be concluded that the location of the jetty tips relative to the end of the jetties solely impact historical dredging rates.

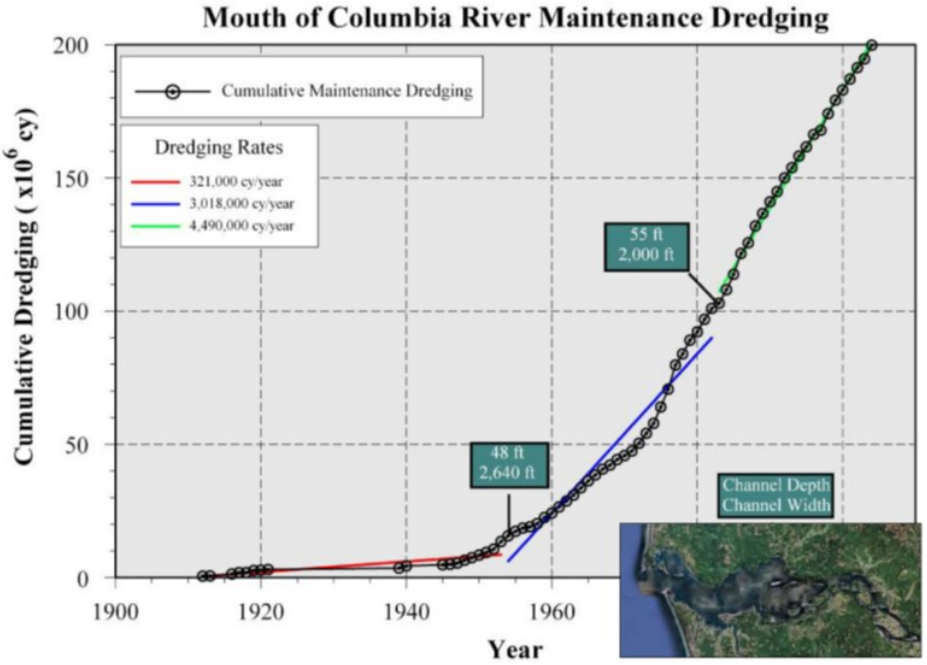

Figure 5-50
Historic Dredging Rates at Mouth of the Columbia River

5.8.3 Yaquina Bay

Dredge records at Yaquina Bay extend back to 1929, when the channel was 20 ft deep and 200 ft wide. In 1958 the channel was expanded to 40 ft deep by 400 ft wide. The jetties were extended in 1969 (historic lengths are unknown). The authorized channel extends 0.5 mi offshore of the jetties, with a natural bar (depth of less than 20 ft) just offshore of the jetty tips.

Historic dredging rates at Yaquina Bay are presented in Figure 5-51. As the figure shows, dredging increased after the channel was expanded. Interestingly, the increase in dredging peaked immediately after the jetties were extended. Dredging rates were the highest from 1970 to 1980, immediately after jetty lengthening; this increased dredging may have been a result of short-term changes to sedimentation as a response to the new structures, or due to side slope equilibration. Since that time, the dredging rate appears to have decreased to pre-1960 levels.

At Yaquina Bay, the background depth offshore of the jetty tips (excluding the bar) is generally greater than 30 ft. Therefore, the increase in dredging noted after 1980 (relative to pre-1970 levels) may be due to the offshore extent of the channel. Dredging appears to occur both within the jetties and at the bar. There is no information indicating the location of dredging prior to channel expansion.

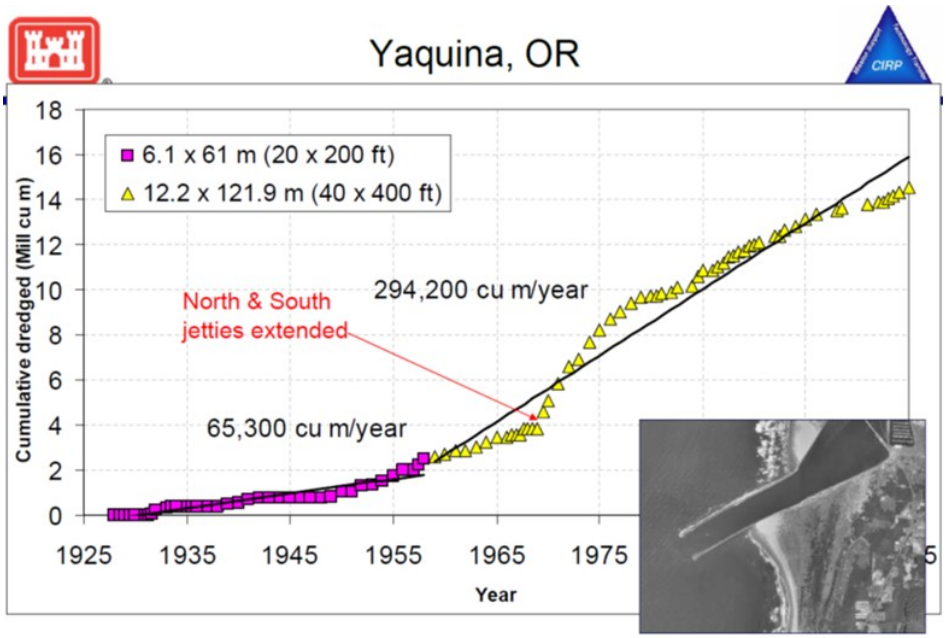

Figure 5-51
Historic Dredging Rates at Yaquina Bay

5.8.4 Siuslaw River

Dredge records at Siuslaw River date back to 1928. Maintenance dredging began in 1955, when the channel was 12 ft deep by 200 ft wide. In 1970, the channel was extended to 17 ft deep by 250 ft wide. Spurs were added to the jetties in 1982. The navigation channel does not extend offshore of the jetties. With the exception of the bar just offshore of the jetties, the natural depth outside of the jetties is greater than 17 ft.

Historic dredging rates at Siuslaw River are presented in Figure 5-52. Dredging appears to have been relatively consistent, with a slight increase after channel expansion, followed by a slight decreased in response to the construction of jetty spurs. The increase in dredging associated with the wider, deeper channel may be a result of increased channel trapping efficiency at the bar. After the spurs were constructed, sediment transport around the jetties, and sediment transport from the beach to the bar, was limited. At Siuslaw River, it is reasonable to conclude that maintenance dredging depends on the channel trapping efficiency and the ability of sand to circumvent the jetties and reach the offshore bar.

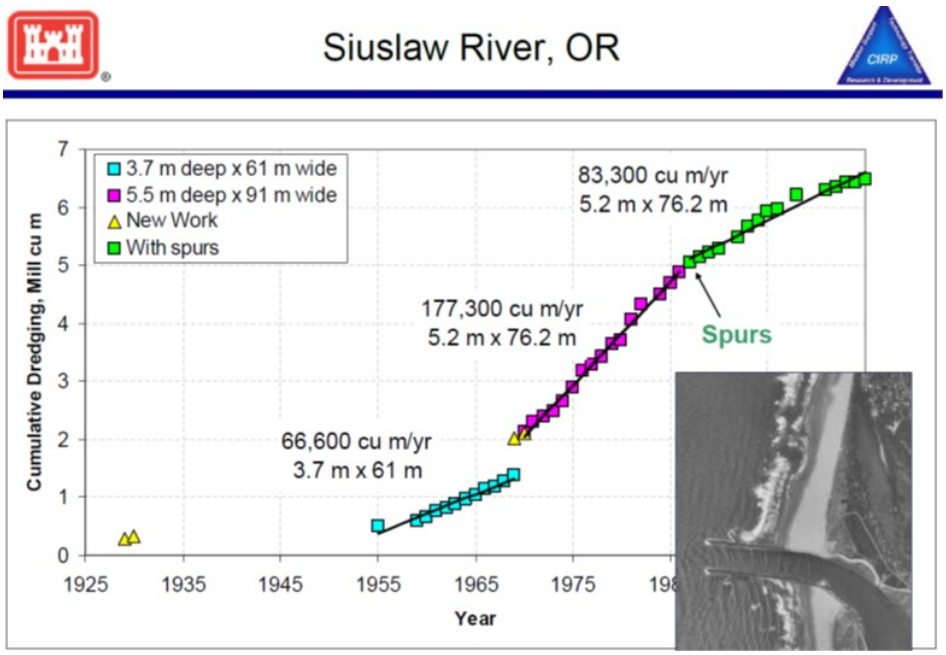

Figure 5-52
Historic Dredging Rates at Siuslaw River

5.8.5 Results

Historical dredging data and navigation charts is available for four channels in the Pacific Northwest. The results at each channel are summarized below:

- At the Grays Harbor Outer Bar Channel, maintenance dredging was temporarily ceased after jetty reconstruction, and resumed after the channel was deepened in the location of the Outer Bar. Shoaling occurs between the jetties, and the mechanism controlling shoaling cannot be determined from the data available.
- At the MCR, the channel historically extends offshore of the jetty tips. Maintenance dredging appears to increase with channel trapping efficiency and is also correlated with an unknown external factor.
- At Yaquina Bay, offshore dredging has been relatively constant, with a temporary increase in response to jetty construction and the associated changes to sedimentation.
- At the Siuslaw River, maintenance dredging appears to be proportional to the channel trapping efficiency and the ability of sediment to circumvent the jetties.
- At Coos Bay, maintenance dredging appears to have been constant over time. Overall, there is no evidence to support that extending a navigation channel beyond the jetties causes an increase in shoaling.

These five channels show that the rate of channel shoaling depends most on sediment supply, channel trapping efficiency, and hydrodynamics. In channels such as the MCR and Siuslaw River where sediment is rapidly sourced by the river and by adjacent beaches, channel trapping efficiency directly affects channel shoaling. At the Grays Harbor Outer Bar and Yaquina Bay, the hydrodynamics appear to drive shoaling. At the Grays Harbor Outer Bar, when jetties maintained a self-scouring environment throughout the channel, no shoaling was observed. At Yaquina Bay, temporary increases in sedimentation appeared to correlate to changes in hydrodynamics as a result of jetty construction. As seen at the Siuslaw River, the jetty configuration can limit shoaling to the extent that it limits the supply of sediment to the bar or channel. For example, constructing jetty spurs decreased shoaling by limiting the quantity of sediment that was able to circumvent the jetties.

5.8.6 Conclusions

At Coos Bay, channel shoaling appears to be controlled by sediment availability. As the channel has become a more efficient sediment trap, a corresponding increase in channel shoaling has not occurred. From a hydrodynamics perspective, the channel may not be able to maintain itself, since there is a channel constriction at Guano Rock, limiting channel velocities in the entrance channel.

While the channel presently extends beyond the jetty tips, it may not have always done so. Prior to 1952, the authorized channel was less than 24 ft deep. During this time, the channel may have been within the jetty tips. Even during this period, the dredging rate was higher than it is today, indicating the sediment's ability to circumvent the jetties and settle into the channel. The fact that the shoaling rate has been so constant, despite the relatively constant hydrodynamics and the increasing trapping efficiency, may indicate that sediment availability is the key factor in controlling sedimentation in the channel. The presence of Cape Arago immediately to the south may also be responsible for limiting sediment transport to the channel.

Ultimately, there is no evidence to suggest that extending the channel further beyond the jetty tips would be responsible for increased shoaling in the channel. Increasing the length of the jetty might limit the amount of sediment that circumvents the jetties and approach channel; however, the sediment that is able to circumvent the jetties is likely to be deposited at some location within the channel – either between the jetties or on the bar – regardless of the channel footprint.

6. COOS BAY JETTIES

Armor stone on the South Jetty head is sheltered by a concrete monolith that extends 300 ft offshore of the structure at MLLW, which appears to dissipate a portion of the incoming wave energy. The armor stone at the South Jetty head is presently in fair condition (USACE 2012b). The USACE 2017b report notes the ongoing deterioration of the North Jetty head. The head has been receding since the last repair in 1989. The current North Jetty head is located at Station 82+86; the rate of retreat has been slowing in recent years, and only 5 ft of recession was noted from 2016-2017 (compared to 17 ft/year from 1994-2011 as noted in USACE 2012b). Presently, the USACE has initiated a three-year North Jetty Repair Major Maintenance project on April 1, 2023, and it is expected to last until December 2025.

The effects of the project alternatives on the jetties were estimated using the Hudson equation to estimate changes to armor stone stability, based on predicted changes in wave conditions as presented in Section 3.3.5. This analysis is detailed in this section. The assessment of the jetty foundations due to changes in sedimentation patterns are discussed in Section 5.7. Analysis of the stability of the Charleston Breakwater is not included since the wave heights are expected to decrease at the breakwater, as shown in Section 3.3.5.4.

The changes to the wave climate form the basis for this assessment. The distribution of wave heights at the jetties was analyzed for the fifteen "N" and eight "S" points as shown in Figure 3-29. The distribution of wave heights at each point can be seen in Figure 3-34 through Figure 3-58. These wave plots, plus additional plots that show only the largest 10 percent of waves, and wave height distribution by direction, are included in Attachment A.

6.1 Armor Stability

6.1.1 Approach

Armor stone stability on the North and South Jetties was evaluated by determining a wave threshold (called the "armor threshold" in Figure 3-34 through Figure 3-58) corresponding to the initiation of damage under the Hudson equation (U.S. Army Coastal Engineering Research Center 1977). Typically, the Hudson equation is used to calculate armor stone size based on wave height, armor stone slope, stability coefficient K_D, and armor stone density. The assessment performed for the existing jetties uses the Hudson equation to calculate the wave damage threshold based on armor stone size. Where rock placement differed above MSL than below MSL, a threshold was calculated for both above and below MSL based on different appropriate stability coefficient. The armor stone above MSL was repaired using selective placement, and therefore a larger stability coefficient is assumed for armor above MSL.

The input data to the Hudson formula are the jetty conditions – the armor stone size, jetty slope, armor stone density, and K_D parameter. All of these data were provided by USACE. Table 6-1 and Table 6-2 summarize the input data and calculated wave height thresholds for the North and South Jetties, respectively.

Table 6-1
Wave Threshold Calculation for Armor Stone Stability, North Jetty

Location (Model Output)	Description	Jetty Condition	KD	Armor size (tons)	Cot(θ)	Density (pcf)	Calculated Wave Damage Threshold (ft)
N1, above MSL	North Jetty head	Repaired, using selective placement	6	33	2.5	175	31.0
N1, below MSL	North Jetty head	Repaired	4	33	2.5	175	27.0
N2, above MSL	North Jetty head	Repaired, using selective placement	6	33	2.5	175	31.0
N2, below MSL	North Jetty head	Repaired	4	33	2.5	175	27.0
N3, above MSL	North Jetty head	Repaired, using selective placement	6	33	2.5	175	31.0
N3, below MSL	North Jetty head	Repaired	4	33	2.5	175	27.0
N4, above MSL	North Jetty trunk	Repaired, using selective placement	6	25	2	170	25.3

Location (Model Output)	Description	Jetty Condition	KD	Armor size (tons)	Cot(θ)	Density (pcf)	Calculated Wave Damage Threshold (ft)
N4, below MSL	North Jetty trunk	Repaired	4	25	2	170	22.1
N5	North jetty trunk	Repaired, using selective placement	5	15	2	170	20.0
N6	North jetty trunk	Repaired, using selective placement	5	15	2	170	20.0
N7	North jetty root	No repair – assume random placement	4	13	2	170	17.7
N8	North jetty root	Repaired, using selective placement	5	10	2	170	17.5
N9	North jetty root	Repaired, using selective placement	5	8	1.5	170	14.8
N10	North jetty root	failed	2.5	4	1.5	150	7.9
N11	North jetty root	failed	2.5	4	1.5	150	7.9

Location (Model Output)	Description	Jetty Condition	KD	Armor size (tons)	Cot(θ)	Density (pcf)	Calculated Wave Damage Threshold (ft)
N12	North jetty root	failed	2.5	4	1.5	150	7.9
N13	North jetty root	failed	2.5	4	1.5	150	7.9
N14	North jetty root	failed	2.5	4	1.5	150	7.9
N15	North jetty root	failed	2.5	4	1.5	150	7.9

Table 6-2
Wave Threshold Calculation for Armor Stone Stability, South Jetty

Location (Model Output)	Description	Jetty Condition	KD	Armor size (tons)	Cot(θ)	Density (pcf)	Calculated Wave Damage Threshold (ft)
S1, above MSL	South jetty head	Slumping of armor stone – assume random placement	3	22	2	170	19.2
S1, below MSL	South jetty head	Slumping of armor stone – assume random placement	3	22	1.5	170	17.5
S2, above MSL	South jetty head	Slumping of armor stone –	3	22	2	170	19.2

Location (Model Output)	Description	Jetty Condition	KD	Armor size (tons)	Cot(θ)	Density (pcf)	Calculated Wave Damage Threshold (ft)
		assume random placement					
S2, below MSL	South jetty head	Slumping of armor stone – assume random placement	3	22	1.5	170	17.5
S3, above MSL	South jetty head	Slumping of armor stone – assume random placement	3	22	2	170	19.2
S3, below MSL	South jetty head	Slumping of armor stone – assume random placement	3	22	1.5	170	17.5
S4, above MSL	South Jetty trunk	Good condition – assume selective placement	5	11	2	170	18.1
S4, below MSL	South Jetty trunk	Good condition – assume selective placement	5	11	1.5	170	16.4
S5, above MSL	South Jetty trunk	Good condition – assume selective placement	5	11	2	170	18.1

Location (Model Output)	Description	Jetty Condition	KD	Armor size (tons)	Cot(θ)	Density (pcf)	Calculated Wave Damage Threshold (ft)
S5, below MSL	South Jetty trunk	Good condition – assume selective placement	5	11	1.5	170	16.4
S6, above MSL	South Jetty trunk	Good condition – assume selective placement	5	11	2	170	18.1
S6, below MSL	South Jetty trunk	Good condition – assume selective placement	5	11	1.5	170	16.4
S7	South Jetty root	Minor scallops – assume selective placement and slope of 2	5	4.5	2	150	11.3
S8	South Jetty root	Minor scallops – assume selective placement and slope of 2	5	4.5	2	150	11.3

6.1.2 Results

The key results for the armor stone stability analysis consist of calculating the design armor sizes for the 2023 PA relative to the Existing Conditions. Design armor size was calculated based on the wave height corresponding to the 95th percentile ranking determined from the cumulative distribution plots included in Attachment A. This wave height criterion is based on current USACE design practice. The calculation is as follows (using North Jetty location N1 as an example):

1. For the Existing Conditions, calculate the 95th percentile wave height. For example, for North Jetty location N1 (Figure 3-34), the wave height is 23.5 ft at the 95th percentile. Plots for all other jetty locations are included in Attachment A.
2. Calculate the wave height under the 2023 PA that corresponds to the same 95th percentile ranking (for location N1, the wave height is 23.7 ft).
3. Calculate the required armor stone sizes for the wave heights for both the Existing Conditions and the 2023 PA (for location N1 below MSL, it would be 21.6 tons for the Existing Conditions and 22.3 tons for the 2023 PA, an increase of 0.7 tons, or +3.0 percent).

The results of this analysis, for all wave extraction points at the jetties, are presented in Table 6-3. The effect on jetty stability is based on guidance from *The Rock Manual* (CIRIA 2007) which states that, for the Hudson equation, an 8% increase in wave heights is expected to result in an incremental increase in damage to a rubble mound structure. Because armor stone size is proportional to the cube of the wave height, an 8% increase in wave heights corresponds to a 26% increase in stone size. OIPCB will use this as a metric to consider augmenting the jetty stone size.

Table 6-3 shows the results of the jetty stone stability analysis. For each extraction point, the table includes the wave threshold for armor stability, the 95th percentile wave heights under the Existing Conditions and the 2023 PA, the percent change in wave height, the required armor stone sizes corresponding to 95th percentile wave heights, and the percent change in armor stone size.

It can be seen from Table 6-3 that the 95th percentile wave heights under the Existing Conditions and the 2023 PA exceed the corresponding armor stone stability thresholds at the South Jetty head (S1 through S4) and part of the South Jetty root (S7). At these locations, jetty damage is likely due to wave effects. However, along the entire North Jetty and part of the South Jetty (S5, S6 and S8), the 95th percentile wave heights are consistently below the wave thresholds under both model scenarios. This indicates that wave attack may not be the primary contributor of damage to this portion of the jetty. In Section 5.7, it is noted that sedimentation patterns are erosive near the foundation of the North Jetty root, which has likely caused the damage to this portion of the jetty. This is consistent with the assertion by USACE (2012b) that, "structural condition of Reach N1 is strongly affected by littoral processes."

Table 6-3 generally shows a decrease in wave height resulting from the 2023 PA. The largest percent increase in wave height occurs at extraction location S2, where the wave height increases by 2.4% (i.e., significantly lower than 8%). Therefore, an increase in damage is not expected per the *Rock Manual* design guidance. At the North Jetty, the 95th percentile wave heights are all below the wave thresholds. In addition, the 95th percentile wave heights decrease under the 2023 PA, which results in decreases of required armor sizes for all North Jetty locations except at N1. Therefore, the 2023 PA is not expected to result in any increased damage to the jetties.

Table 6-3
Results of Wave Analyses at the Jetties

Location (Model Output)	Wave Threshold (ft)	Hs at 95th percentile under Existing (ft)	Hs at 95th percentile under 2023 PA (ft)	Percent Change in Wave Height	Required Armor Stone Size at 95th Percentile Hs under Existing (tons)	Required Armor Stone Size at 95th Percentile Hs under 2023 PA (tons)	Percent Change in Armor Stone Size
N1, above MSL	31	23.46*	23.69*	1.0%	14.4	14.9	3.0%
N1, below MSL	27	23.46*	23.69*	1.0%	21.6	22.3	3.0%
N2, above MSL	31	25.95*	24.34*	-6.2%	19.5	16.1	-17.5%
N2, below MSL	27	25.95*	24.34*	-6.2%	29.3	24.2	-17.5%
N3, above MSL	31	11.84*	10.2*	-13.9%	1.9	1.2	-36.1%
N3, below MSL	27	11.84*	10.2*	-13.9%	2.8	1.8	-36.1%
N4, above MSL	25.3	9.91*	7.38*	-25.5%	1.5	0.6	-58.7%
N4, below MSL	22.1	9.91*	7.38*	-25.5%	2.3	0.9	-58.7%
N5	20	8.43*	5.28*	-37.4%	1.1	0.3	-75.4%
N6	20	7.12*	4.33*	-39.2%	0.7	0.2	-77.5%
N7	17.7	5.91*	3.44*	-41.8%	0.5	0.1	-80.3%
N8	17.5	5.05*	2.89*	-42.8%	0.2	< 0.1	-81.3%
N9	14.8	5.18*	2.72*	-47.5%	0.3	0.1	-85.5%
N10	7.9	5.31*	2.56*	-51.8%	1.2	0.1	-88.8%
N11	7.9	4.89*	2.17*	-55.6%	1.0	0.1	-91.3%
N12	7.9	5.35*	2.59*	-51.6%	1.3	0.1	-88.7%
N13	7.9	3.12*	1.77*	-43.3%	0.3	< 0.1	-81.7%
N14	7.9	1.90*	1.18*	-37.9%	0.1	< 0.1	-76.0%
N15	7.9	0.66*	0.39*	-40.9%	< 0.1	< 0.1	-79.4%
S1, above MSL	19.2	22.01	22.01	0.0%	33.2	33.2	0.0%

Location (Model Output)	Wave Threshold (ft)	Hs at 95th percentile under Existing (ft)	Hs at 95th percentile under 2023 PA (ft)	Percent Change in Wave Height	Required Armor Stone Size at 95th Percentile Hs under Existing (tons)	Required Armor Stone Size at 95th Percentile Hs under 2023 PA (tons)	Percent Change in Armor Stone Size
S1, below MSL	17.5	22.01	22.01	0.0%	44.3	44.3	0.0%
S2, above MSL	19.2	23.29	23.85	2.4%	39.4	42.3	7.4%
S2, below MSL	17.5	23.29	23.85	2.4%	52.5	56.4	7.4%
S3, above MSL	19.2	22.38	22.74	1.6%	34.9	36.6	4.9%
S3, below MSL	17.5	22.38	22.74	1.6%	46.6	48.8	4.9%
S4, above MSL	18.1	20.18	18.90	-6.3%	15.4	12.6	-17.8%
S4, below MSL	16.4	20.18	18.90	-6.3%	20.5	16.8	-17.8%
S5, above MSL	18.1	16.37*	14.96*	-8.6%	8.2	6.3	-23.7%
S5, below MSL	16.4	16.37*	14.96*	-8.6%	10.9	8.3	-23.7%
S6, above MSL	18.1	15.49*	14.11*	-8.9%	6.9	5.3	-24.4%
S6, below MSL	16.4	15.49*	14.11*	-8.9%	9.3	7.0	-24.4%
S7	11.3	13.68	12.04	-12.0%	7.9	5.4	-31.8%
S8	11.3	10.37*	8.83*	-14.9%	3.4	2.1	-38.3%

Note: The 95th percentile Hs is marked with * when it is smaller than the wave threshold.

6.2 Toe Stability

The entrance sedimentation result (see Section 5.4.4) indicates the potential for erosional behavior from North Jetty Station 56+50 to 71+90 under the 2023 PA. Additional research into this area, described below, confirms the recommendation for added toe protection.

The erosion in this area appears to result from the morphological response to the complex current conditions, which is represented by the meander pattern throughout the Entrance Channel. This phenomenon exists under the Existing Conditions and is anticipated to be further exaggerated by the 2023 PA. Figure 6-1 shows the modeled sedimentation under the Existing Conditions (same as the top panel of Figure 5-43) as well as a black line indicating the approximate meander pattern within the Entrance Channel.

Ebb tides emerge from the Entrance Turn into the Entrance Channel where Guano Rock restricts currents along the southern side of the Entrance Channel and encourages flow to go toward the

northern side of the channel next to the North Jetty. At this location, the currents encounter the jetty (the relic jetty starts to widen at this location as well) and meander towards the middle of the channel, causing a shoal to form at the North Jetty head. Offshore of the jetties, the ebb flows encounter the longshore transport with a net northerly direction, which causes velocities to be reduced, making the southern channel toe a primary depositional area.

The modeling for the Existing Conditions shows that this meander pattern already exists. Widening the channel closer to the North Jetty under the 2023 PA increases the hydraulic efficiency near the North Jetty, causing the meander to come closer to the North Jetty; thus, more erosion is predicted by the model. Figure 6-2 illustrates this potentially increased meander under the 2023 PA. The model result shows a higher erosion potential under the 2023 PA along the North Jetty in RM 0.7–1.0. In addition, Figure 6-3 shows an increase in the maximum ebb current velocity near the North Jetty trunk under the 2023 PA.

Toe protection under the 2023 PA for the North Jetty should be designed for up to 10 feet of erosion depth. Section 6.10 of the Engineering Appendix includes the design of toe protection.

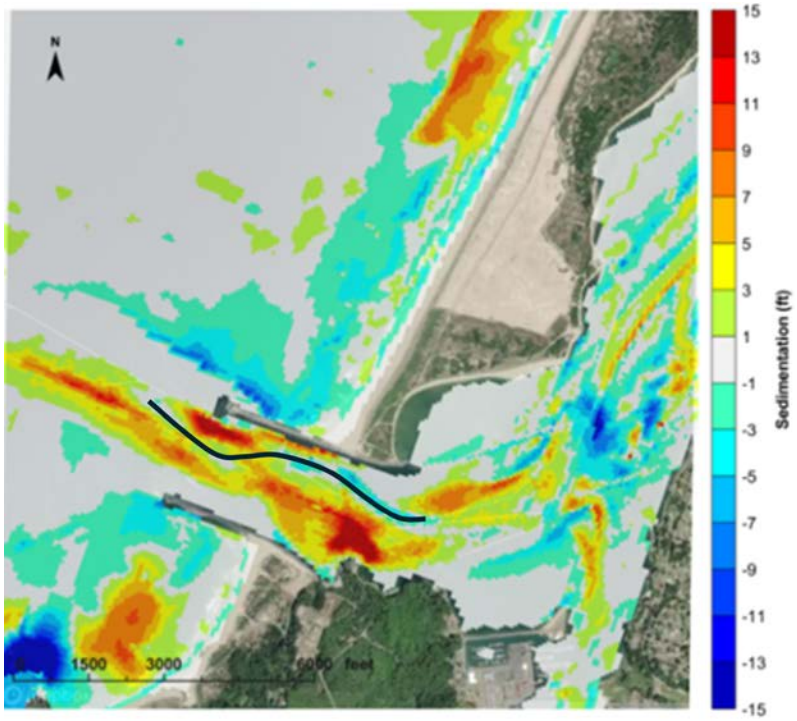

Figure 6-1
Entrance Sedimentation for Existing Conditions (Current Meander Shown in Solid Black Line)

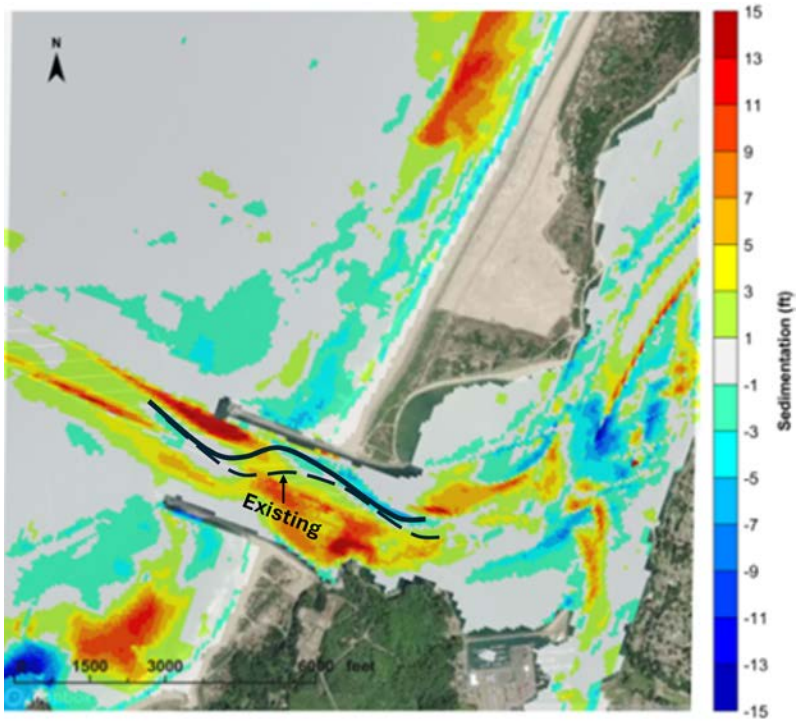

Figure 6-2
Entrance Sedimentation for 2023 PA (Current Meander Shown in Solid Black Line)

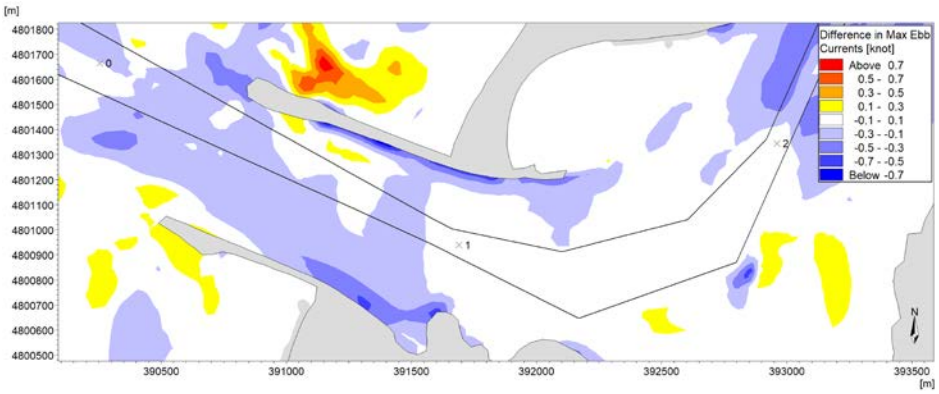

Figure 6-3
Difference in Maximum Ebb Currents at the Entrance Channel

There is evidence that this morphological pattern already exists. The hill shade imagery of the existing North Jetty bathymetry shows some scour at the base from stations 32+50 through 42+50 (Figure 6-4), as well as the modeled shoals from stations 25+00 to 30+00 and upstream of 47+50 (note: stationing in this figure refers to channel stationing, not North Jetty stationing – channel Station 32+50 through 42+50 is within North Jetty Station 56+50 to 71+90).

Moreover, bathymetry surveys from USACE show large shoals along the southern boundary of the channel. This suggests that these conditions sedimentation patterns are realistic and the modeled potential for erosion is viable. It should be noted that while the model may not accurately predict the rate of erosion, the long term the scour may develop to some extent.

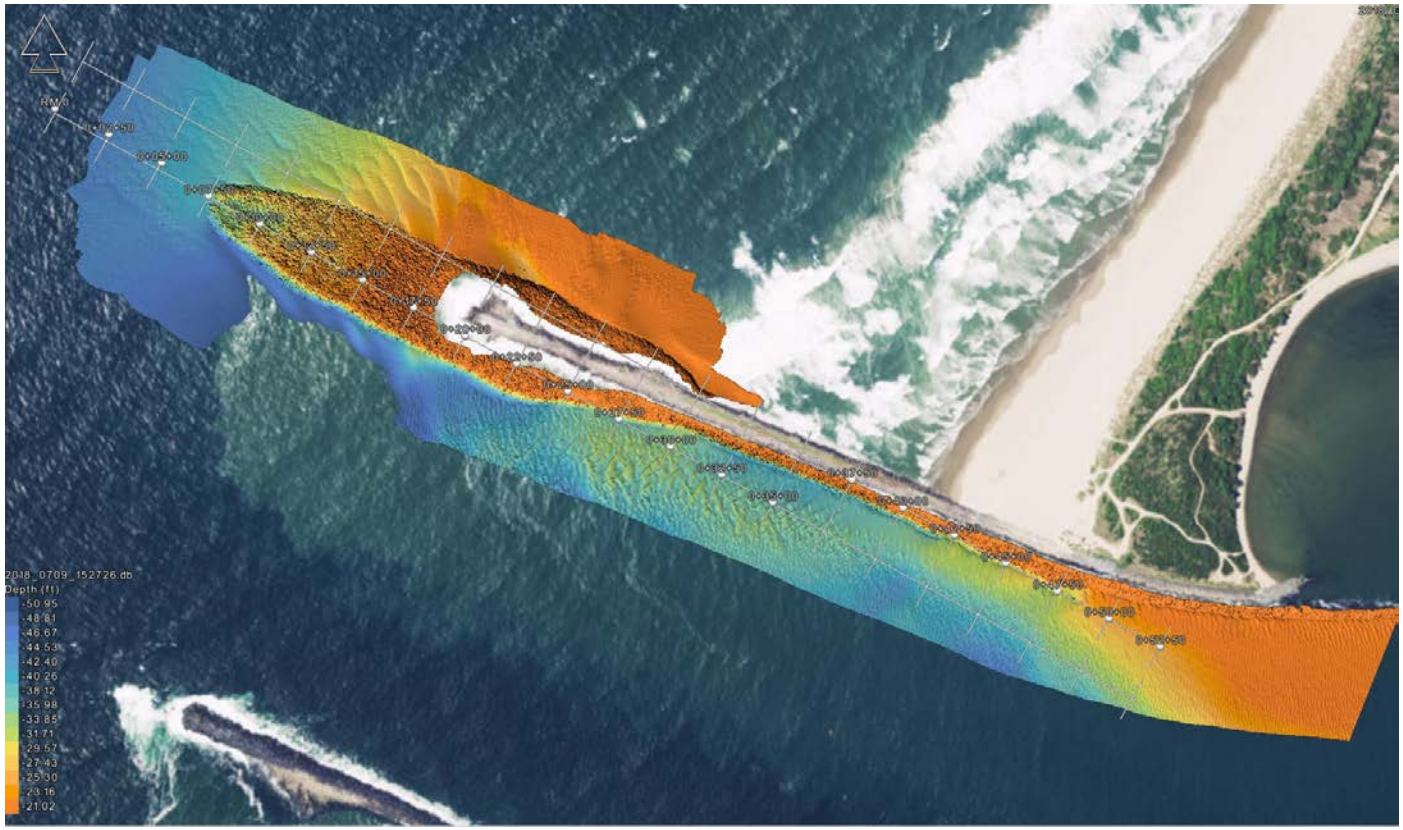

Figure 6-4
Hill shade Image of Bathymetry Along the North Jetty

7. TSUNAMI

This section summarizes the modeling performed to predict the changes in the propagation of a hypothetical tsunami from the Cascadia Subduction Zone (CSZ) into Coos Bay under the Existing Condition and the 2023 PA.

7.1 Tsunami Hazard in Oregon

Historically, tsunami strikes on the Oregon coast have been most notably the result of tectonic activity in far-field subduction zones in Alaska and the Aleutian Islands, Japan, Kuril Islands (Russia), and Chile. The 1964 Prince William Sound tsunami has been the most devastating far-field tsunami on record along the Oregon coast (Witter et al. 2011).

The hazard posed by a typical far-field tsunami is somewhat constrained by the energy dissipation that occurs as the tsunami travels long distances to reach the U.S. west coast. Far-field tsunamis also allow time for tsunami alerts to be issued in a timely manner, thus reducing the risk of human casualties.

However, tsunamis triggered by nearfield sources can cause great damage to the coast and increase the risk for human casualties because the reduced distance from the source to the point of impact drastically shortens evacuation times. For most of the U.S. west coast, the CSZ is the most significant nearfield tsunami source. The CSZ extends for over 600 mi from Cape Mendocino, California to Northern Vancouver Island. The CSZ is the result of the convergence of the North American Plate and the Juan de Fuca Plate, with the latter subducting under the former at a rate of about 1.5 inches (in.) per year (Figure 7-1). Large amounts of energy build up over time due to locking of the two tectonic plates, causing the North American Plate to bulge up. Eventually, rupture of the locked zone occurs and the North American Plate snaps westward, causing subsidence of the continental shelf and displacing the waters of the Pacific Ocean to create a tsunami (DOGAMI 2012).

Geologic records indicate that at least 19 major ruptures of the full length of the CSZ have occurred in the past 10,000 years, with earthquake magnitudes between 8.9 and 9.2 and a median time interval of 490 years. The last to occur took place on January 27, 1700, as determined from sand deposits on land. According to a study published by the USGS in 2008, there is a 10 percent probability that a CSZ earthquake of magnitude 8-9 will occur over the next 30 years (DOGAMI 2012).

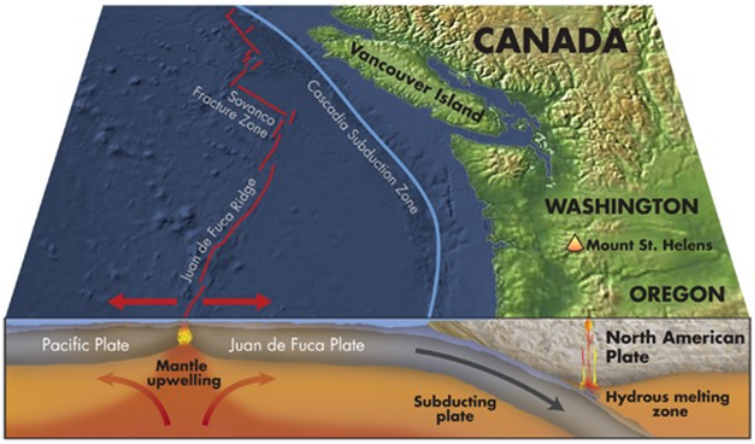

Figure 7-1
Tectonics in the CSZ

7.1.1 DOGAMI Work on Tsunami Hazard

The Oregon Department of Geology and Mineral Industries (DOGAMI) has been responsible for mapping tsunami hazards along the Oregon coast since 1994. Recognizing the tsunami generation potential of the CSZ, DOGAMI has created a new generation of tsunami inundation maps for the Oregon coast based on the result of modeling of a number of hypothetical, yet plausible, coseismic conditions.

7.1.1.1 Tsunami Scenarios

The DOGAMI tsunami inundation maps show the inundation caused by five hypothetical tsunami events labeled SM (small), M (medium), L (large), XL (extra-large), and XXL (extra-extra-large) to represent relative earthquake magnitude. These scenarios were defined based on analysis of the age and mass of 19 turbidites (i.e., sediment deposited by a turbidity current) along the CSZ margin. From these samples, the time interval between CSZ events and their earthquake magnitude were inferred. All five tsunami scenarios assume the full rupture of the CSZ, but vary the amount of slip experienced by the North American Plate as well as the influence of amplifying effects caused by activation of a splay fault (Witter et al. 2011). Table 7-1 summarizes the general characteristics of the five tsunamis that comprise the DOGAMI tsunami scenarios.

Table 7-1
DOGAMI Tsunami Scenarios (DOGAMI 2012)

Earthquake Size	Average Slip Range (ft)	Maximum Slip Range (ft)	Time to Accumulate Slip (years)	Earthquake Magnitude
XXL	59 to 72	118 to 144	1,200	~9.1
XL	56 to 72	115 to 144	1,050 to 1,200	~9.1
L	36 to 49	72 to 98	650 to 800	~9.0
M	23 to 30	46 to 62	425 to 525	~8.9
SM	13 to 16	30 to 36	275 to 300	~8.7

The 19 historical turbidites span a time period of 10,000 years and are indicative of events involving the rupture of the full length of the CSZ. According to Witter et al. (2011), the distribution of the earthquake size of these 19 events is: 5 SM, 10 M, 3 L, and 1 XL. The XXL event simply represents the upper limit of slip accumulation in the inter-event time range indicated by the turbidites. Using this information, a return period can be computed for each of the earthquake sizes, as shown in Table 7-2. Return periods are computed based on the annual chance of an event of given magnitude or larger (i.e., including each row above the row of interest).

Table 7-2
Return Period Estimated by M&N for DOGAMI Tsunami Scenarios

Earthquake Size	Number of Events in 10,000 Year Turbidite Record	Return Period, years
XXL	0	>10,000
XL	1	10,000
L	3	2,500
M	10	714
SM	5	526

Furthermore, Witter at al. (2011) accounted for the uncertainty in the up-dip limit of coseismic rupture for each earthquake size by evaluating three rupture model geometries for each earthquake size (e.g., L1, L2, and L3). Index "1" events correspond to events that involve simultaneous rupture of a splay fault, which amplifies the size of the triggered tsunami and grants them greater inundation potential. Index "2" events correspond to shallow buried rupture slip, and index "3"

events correspond to deep buried rupture slip. It is understood that the DOGAMI tsunami inundation maps are based on the results of the index "1" events for each of the five scenarios.

7.1.1.2 Tsunami Modeling

Senate Bill 379 (1995) instructed DOGAMI to establish the area of expected tsunami inundation based on scientific evidence and tsunami modeling in order to prohibit the construction of new essential and special occupancy structures in this tsunami inundation zone, (Priest, 1995). DOGAMI used the Semi-implicit Eulerian-Lagrangian Finite Element (SELFE) hydrodynamic model (Zhang & Baptista 2008) to simulate tsunami generation, propagation, and inundation. Although the model can support three dimensions, the tsunami modeling was carried out in two horizontal dimensions (Witter at al. 2011). The tsunami simulations were carried out using a pre-event tide level equal to MHHW, which is 6.79 ft (2.07 m) above NAVD88 according to the tide gauge at Port Orford, Oregon. The tide station is operated by the NOAA.

Maps showing inundation lines published by DOGAMI are presented in Figure 7-2 through Figure 7-5; these figures are available in higher resolution on DOGAMI's website. The inundation line depicted by the XXL rupture scenario is physically mapped throughout Coos Bay.

Based on DOGAMI's work, a tsunami generated by the XXL rupture scenario would inundate nearly the entirety of the North Spit. Tsunami would not propagate up the Lower Coos Bay so much as overtop the North Spit and continue into the Upper Bay. This is important to note; essentially, the project improvements are not significant in governing tsunami propagation into the Upper Bay under this scenario.

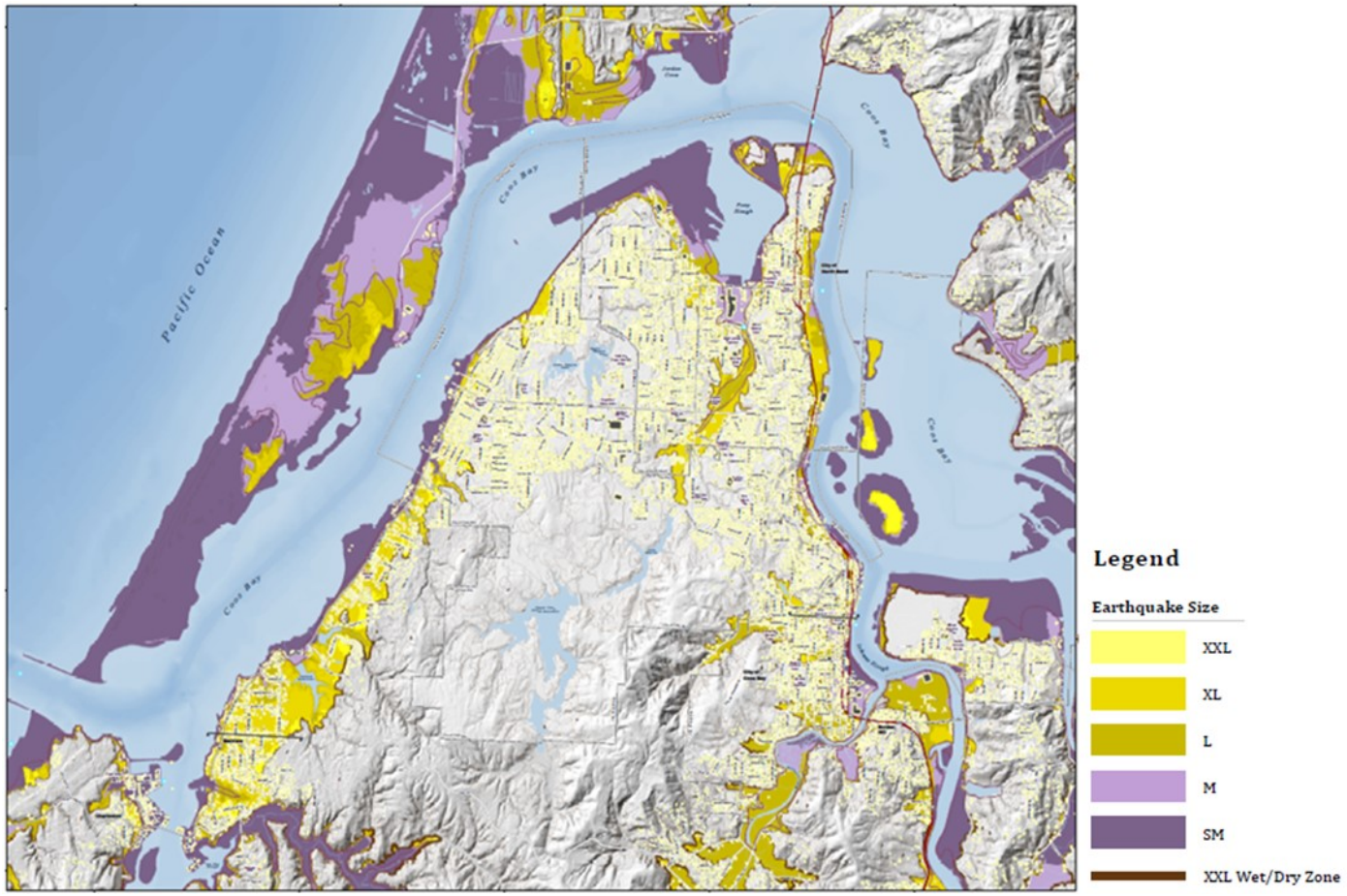

Figure 7-2
DOGAMI Inundation Map for Coos Bay/North Bend

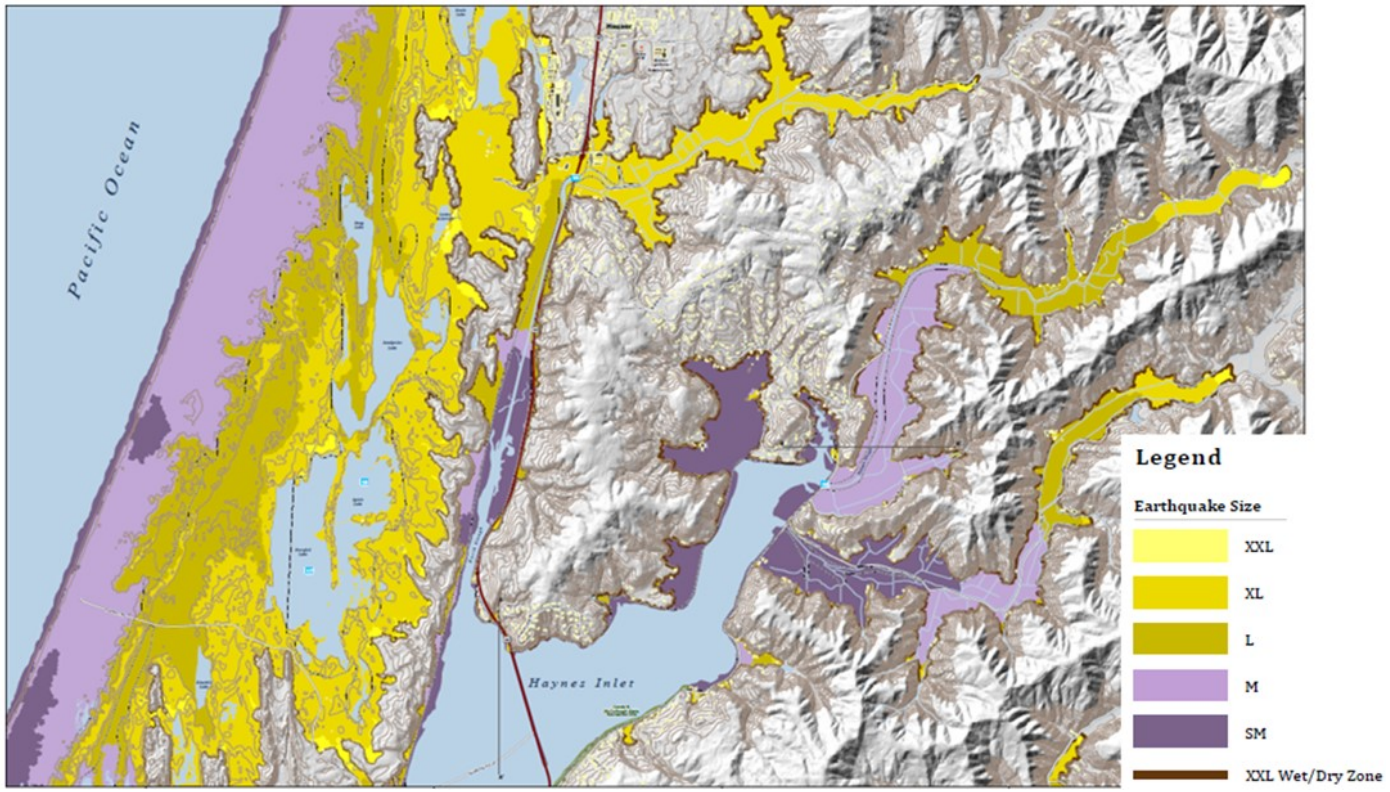

Figure 7-3
DOGAMI Inundation Map for Haynes Inlet

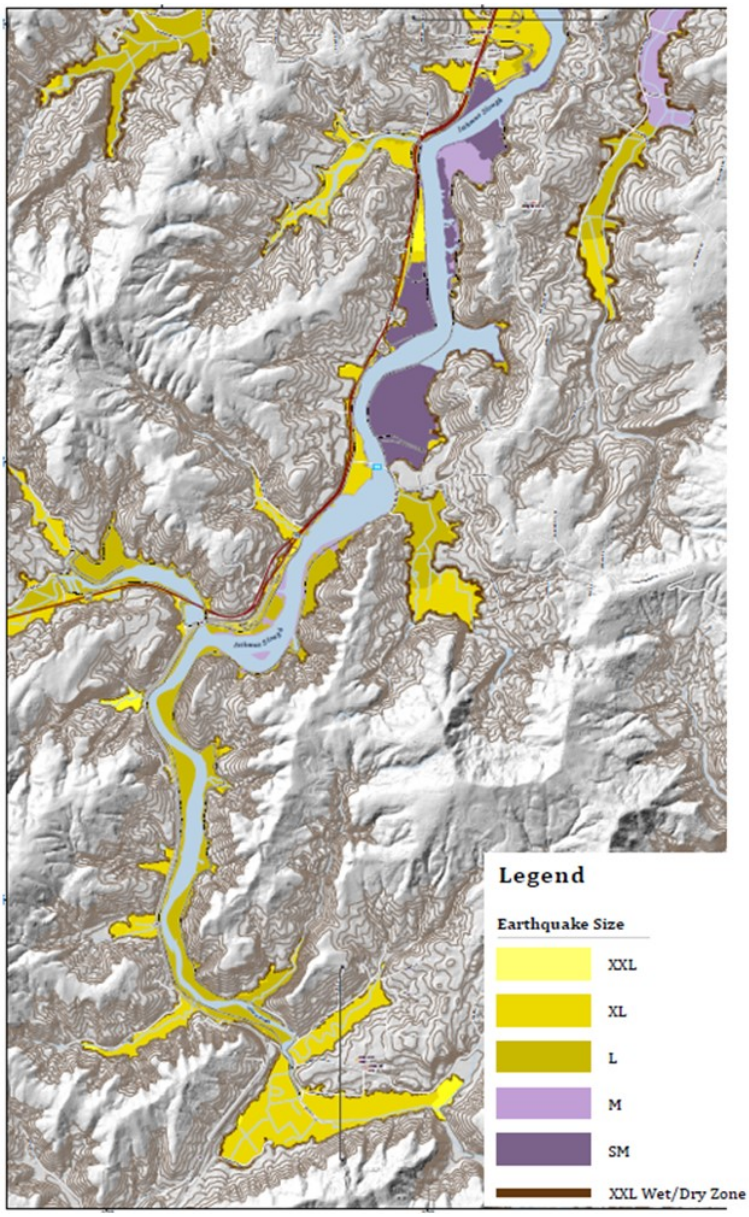

Figure 7-4
DOGAMI Inundation Map for Isthmus Slough

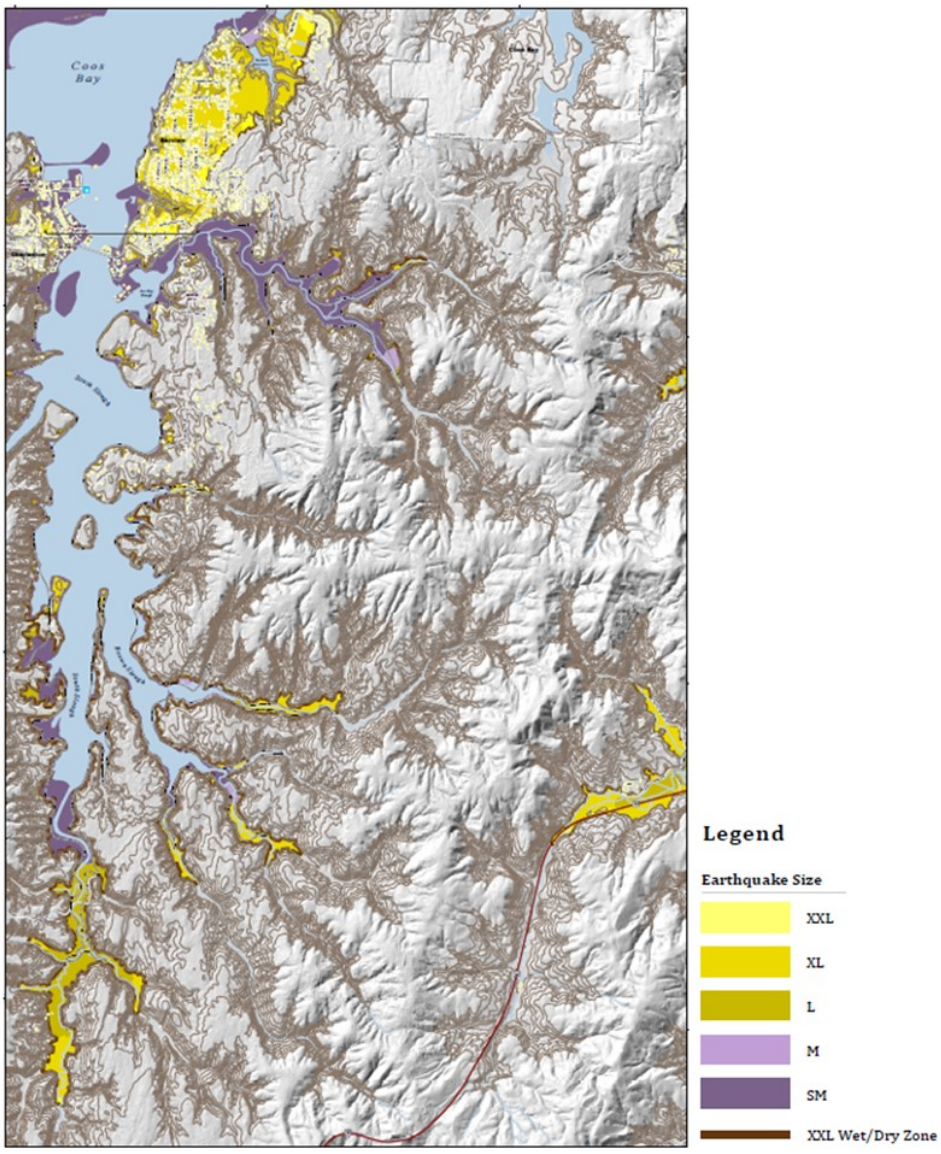

Figure 7-5
DOGAMI Inundation Map for South Slough

7.2 Tsunami Modeling

Tsunami Scenario XXL1 was selected to assess the impact of the different channel configurations on tsunami propagation in Coos Bay, with the aid of the MIKE-21 model suite developed by DHI. The modeling was carried out using two MIKE-21 hydrodynamic models, as described in subsequent sections. Scenario XXL1 was chosen because it is denoted around Coos Bay, where it represents "tsunami inundation" information made available to the public. This scenario is also the most conservative and would amplify the effects of tsunami propagation imposed by the different project scenarios.

MIKE-21 is an appropriate model to simulate tsunami in this environment and was approved by USACE for one-time use in this analysis. No such approval has been granted for SELFE. The model details and one-time approval that was obtained through the Corps of Engineers model approval process prior to application of the MIKE-21 model are presented in Section 3.3. The results differ from DOGAMI's model. Aside from model selection, three primary sources of differences are:

- Friction: Friction is omitted from the runup calculation used in DOGAMI's model. However, the MIKE-21 model does include friction in the runup, making its results less conservative (especially in upstream portions of the bay).
- Input Topography/Bathymetry: DOGAMI's elevations are based on bathymetry and topography from NOAA (2009); moreover, DOGMAI modified their input bathymetry based on their judgement. The MIKE-21 model is based on DEA (2016) bathymetry in the channel, and publicly available topography otherwise. (Section 7.2.3)
- Results Presentation: DOGAMI represent model output that have been manipulated from engineering judgement. MIKE-21 output is strictly model output in order to show any changes in physical phenomena.

7.2.1 Regional Model

Modeling of tsunami generation and propagation was carried out using a MIKE-21 FM HD model that covers the CSZ offshore of Coos Bay. The extent of this model allows for the modeling of tsunami generation at the CSZ by incorporation of the DOGAMI ground surface deformation maps. This model will be herein referred to as the regional model. The primary purpose of the regional model is to model tsunami generation and provide surface elevations to force the offshore boundary of a local, high resolution model.

Along the coast, the regional model extends from Cape Mendocino, California to the Oregon–Washington border (Figure 7-6). Topography is included in the Coos Bay area to model runup and inundation and minimize reflection of the tsunami from the shoreline towards the location of the local model offshore boundary.

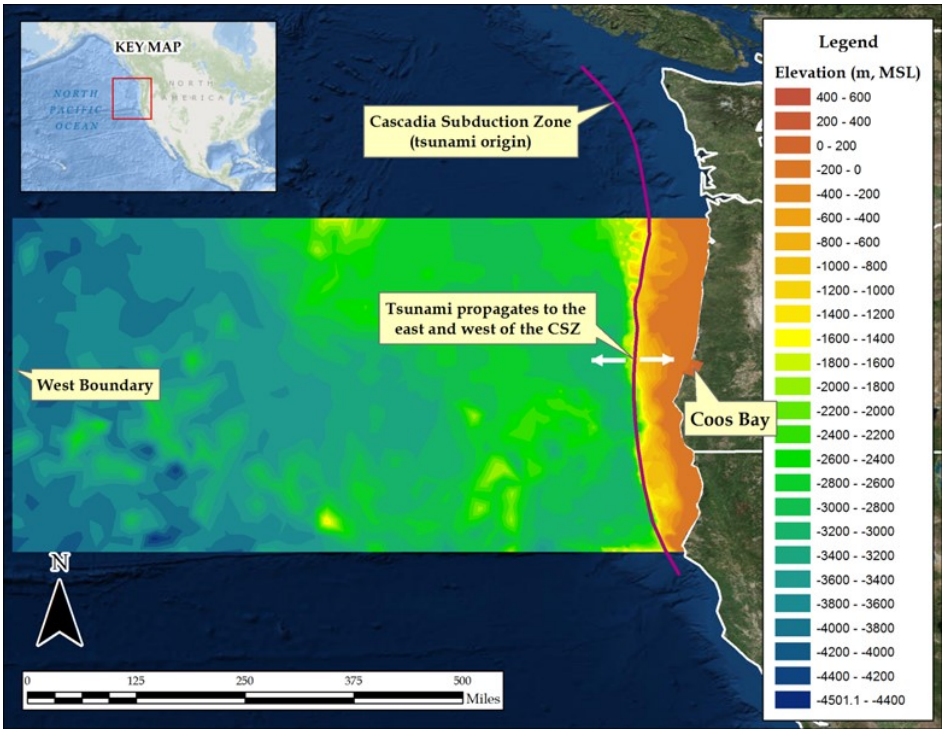

Figure 7-6
Regional MIKE-21 FM HD Model Domain

The resolution of the triangular elements in the regional model gradually increases from offshore to onshore east of the CSZ. West of the CSZ, the elements are coarse at 20-40 km (12-25 mi) in size. The purpose of this portion of the model is to allow the tsunami wave propagating away from the U.S. west coast to attenuate, through the use of artificially high roughness, before it is reflected from the west model boundary. Along the CSZ, the elements are about 2-3 km (1.2-1.9 mi) in size. In the Coos Bay channel, the elements are approximately ~100 ft (30 m) in size. In total, the mesh has approximately 1.6 million elements.

Even though the regional model has high resolution at the site to model runup and inundation, it was found that flooding and drying parameters had to be considerably relaxed to prevent model instabilities. This limitation affects the accuracy with which runup can be resolved in the regional model. Therefore, the regional model results were used to force a high resolution, structured grid local model, as described in the following section.

7.2.2 Local Model

The local model is a MIKE-21 structured grid Hydrodynamic Model covering Coos Bay (Figure 7-7). It has a uniform resolution of 9 m (30 ft). The shore-parallel offshore boundary is forced with results from the regional model; thus, the local model is used to model tsunami propagation into Coos Bay at high resolution and accuracy due to better stability during computation of tsunami inundation of dry areas.

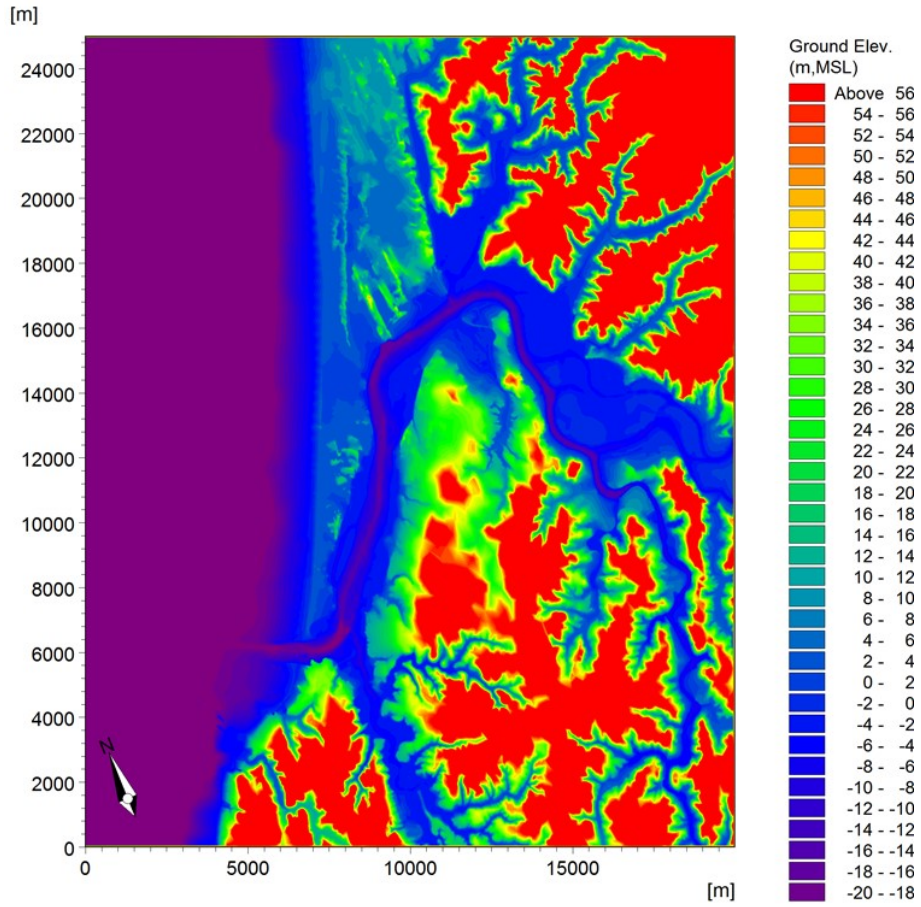

Figure 7-7
Local MIKE-21 Structured Grid Hydrodynamic Model Domain

7.2.3 Model Setup

7.2.3.1 Ground Elevations

The datasets used to generate ground elevations for the existing conditions model are listed below. A uniform Manning bottom roughness of 1/32 (Manning's "n") was assumed, based on guidance from the DHI Hydrodynamic Module manual (DHI 2016).

- C-Map bathymetry for the Pacific Ocean, including areas offshore of Coos Bay and Coos Bay itself. C-Map is a worldwide catalog of nautical charts developed by Jeppesen (DHI 2016).
- Coos Bay channel bathymetry from DTM by DEA in 2016, a composite of multiple existing data sets collected between 2007 and 2016 (OIPCB 2017d).
- USGS National Elevation Dataset data for all areas above MSL in Coos Bay (USGS 2013). It was used for the inundation modeling above MSL, as a supplemental dataset of USACE 2014 LiDAR.

The relationship between tidal and vertical datums used to adjust the various datasets was obtained from NOAA tide station 9432780 Charleston, Oregon, located near the Coos Bay jetties. Table 2-1 presents the datums at this location. All ground elevation surfaces used in the modeling are referenced to MSL.

7.2.3.2 Ground Uplift and Subsidence

The DOGAMI seafloor deformation grid for tsunami XXL1 was used to incorporate the uplift and subsidence associated with the seismic event into the ground elevation surfaces. Figure 7-8 shows a surface created from the deformation grid available from DOGAMI for Scenario XXL1.

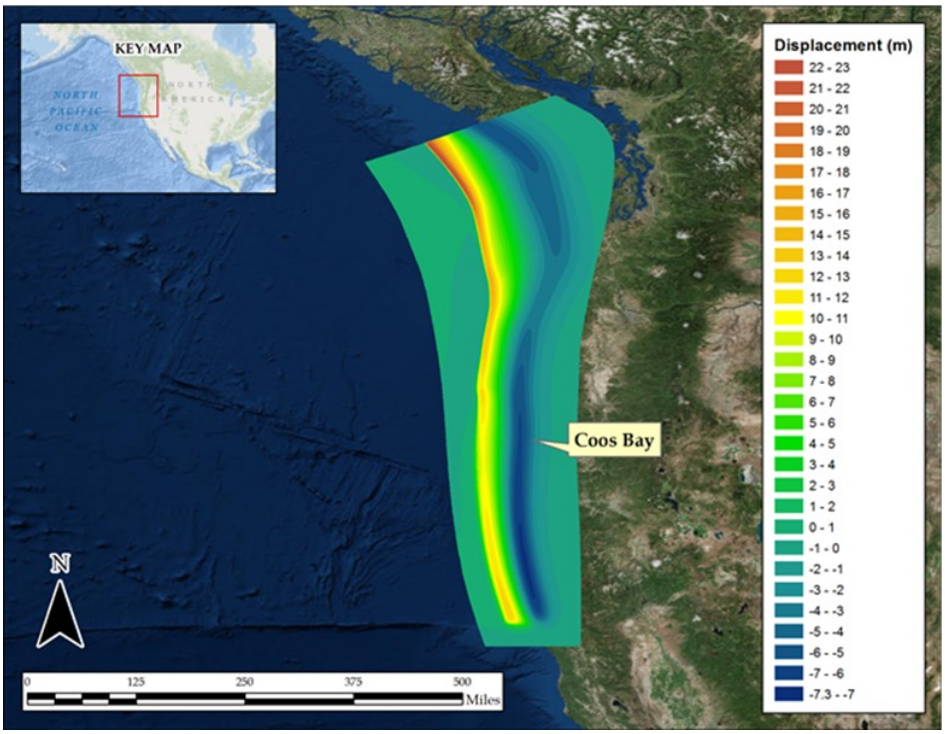

Figure 7-8
Seafloor Deformation for Scenario XXL1

7.2.3.3 Initial Surface Elevation

The DOGAMI ground deformation grid for tsunami XXL1 was also used to define the initial water surface elevation conditions at the beginning of the simulation. This assumption is widely accepted in the scientific community for the case of coseismic tsunami where the extent of the seismic source is very large in comparison to the water depth and the seafloor deformation happens quickly and impulsively (Jiang & LeBlond 1992; Cecioni & Bellotti 2010). Therefore, the hydrodynamic model was not used to model the exact moment of rupture, but to model the surface elevation conditions immediately after the rupture.

The spatially-varying water level was applied on top of the pre-event tidal level, which was set at MHHW (3.35 ft above MSL), consistent with DOGAMI's simulations.

7.2.4 Model Validation

The regional and local models were validated for Scenario L1 by comparing the time series of the surface elevation and current velocities against DOGAMI model results available at the locations shown in Figure 7-9. The comparison showed a good agreement between the two models for surface elevations of the leading waves. A comparison of water levels for select points within the

channel are presented in Figure 7-10 through Figure 7-12. As these figures show, the heights of the primary wave (which drives inundation) differ by less than 0.5 ft between the two models. Considering the fundamental differences in configuration and numerical schemes of both models, this comparison was deemed satisfactory and supportive of the adopted modeling methodology.

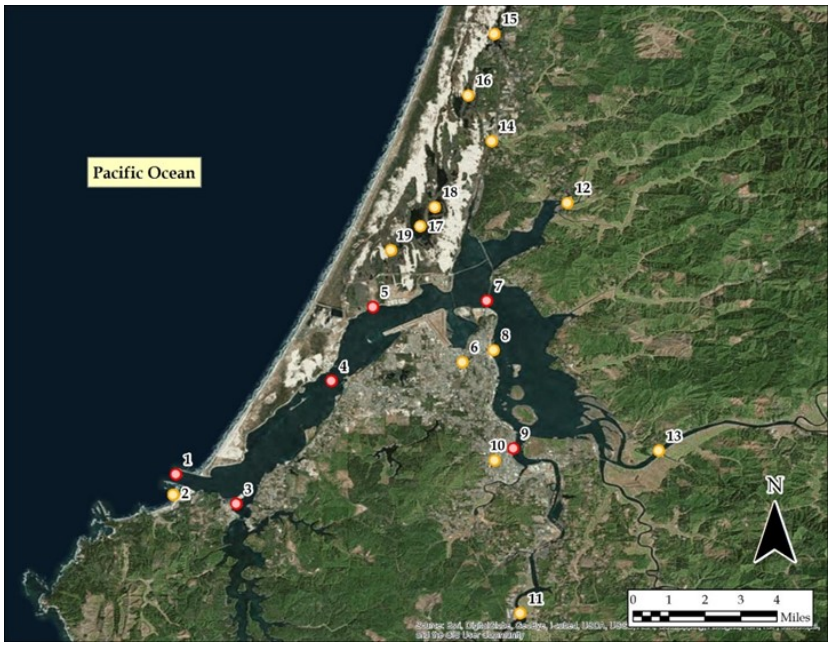

Figure 7-9
DOGAMI Stations with Selected Stations for Analysis of Results Shown in Red

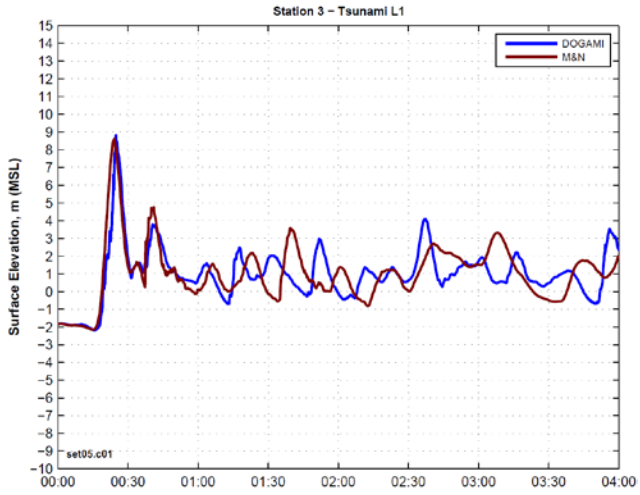

Figure 7-10
Water Level Comparison of DOGAMI and MIKE-21 (M&N) Models at Station 3

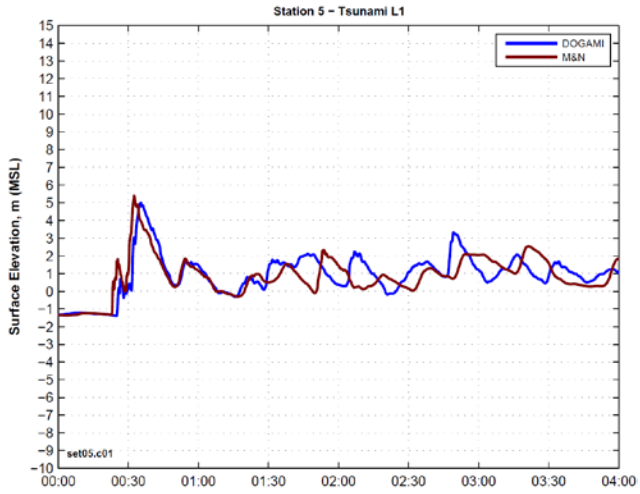

Figure 7-11
Water Level Comparison of DOGAMI and MIKE-21 (M&N) Models at Station 5

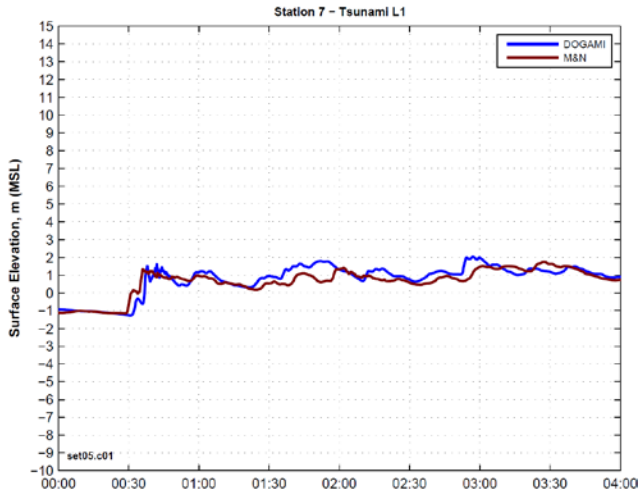

Figure 7-12
Water Level Comparison of DOGAMI and MIKE-21 (M&N) Models at Station 7

7.3 Results

The results are presented as tsunami inundation lines for the two model scenarios (the Existing Condition and the 2023 PA) as a result of the XXL1 scenario tsunami. The lines represent the maximum extent to which tsunami runup is achieved throughout the entire simulation period.

It should be noted that the purpose of this study is not to verify or reproduce the tsunami inundation maps published by DOGAMI, but to produce independent tsunami inundation lines for the purpose of examining the difference in tsunami inundation lines between the Existing Condition and the 2023 PA. The DOGAMI tsunami inundation maps are the official maps for the State of Oregon for land use, evacuation, etc. The results of this study can only be used to interpret how channel modification may influence the physics of tsunami propagation.

Two sets of inundation maps are presented. The first compare the DOGAMI inundation line for the XXL1 scenario with the Existing Condition. These maps can be seen in Figure 7-13 through Figure 7-16. Some general similarities are observed; the large tsunami wave completely overtops the North Spit, inundating this area and then propagating into the Upper Bay. Low-lying areas in the Upper Bay may be at risk of inundation.

A key difference between the DOGAMI and the MIKE-21 results is that the DOGAMI results predict more inundation than the MIKE-21 results. The key driver for this is the use of friction. The DOGAMI model neglected friction in the runup calculates to produce results that were sufficiently conservative given the nature of tsunami vulnerability. On the contrary, the MIKE-21 results do include friction in the runup calculations, with friction factors based on land use patterns. A second difference between the two models is the input bathymetry; the DOGAMI model is based on a NOAA 2009 dataset, while the MIKE-21 model is based on the DEA dataset, described in Sub-appendix 2, *Geophysical Report*.

It is also noted that MIKE-21 model domain does not extend as far into the tributaries and sloughs of Coos Bay as the DOGAMI model. As a result, the inundation lines produced from the MIKE-21 model results are truncated within tributaries and sloughs according to the limits of the model domain.

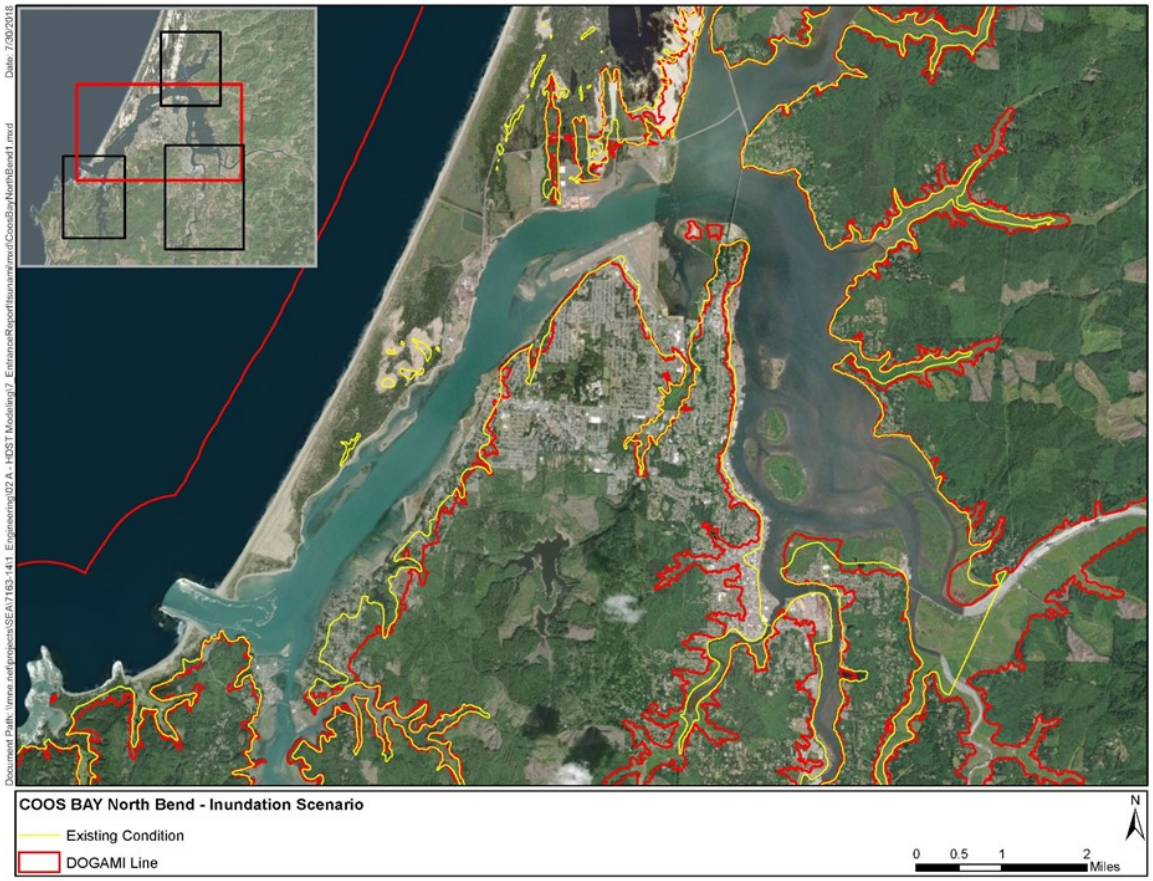

Figure 7-13
Comparison of DOGAMI XXL1 Inundation Line and MIKE-21 Existing Condition Simulation - North Bend and Coos Bay

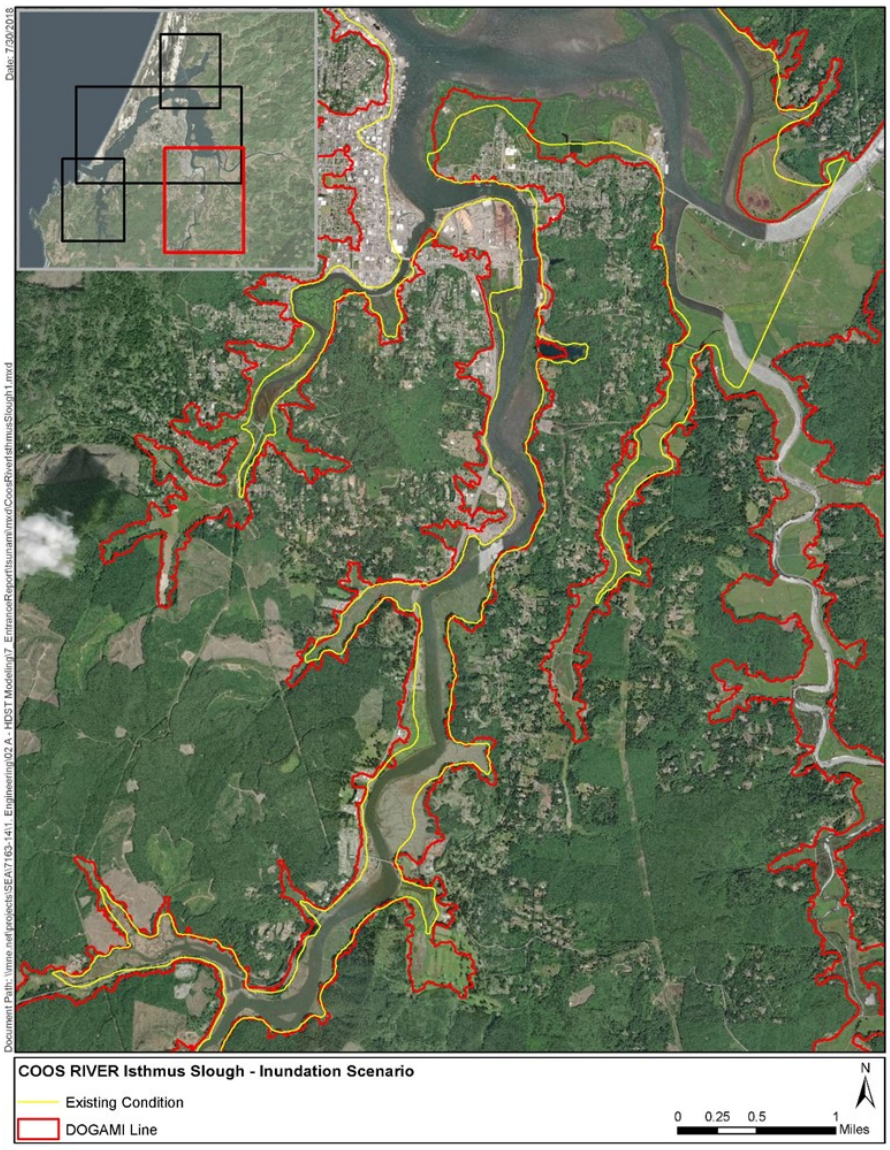

Figure 7-14
Comparison of DOGAMI XXL1 Inundation Line and MIKE-21 Existing Condition Simulation – Isthmus Slough

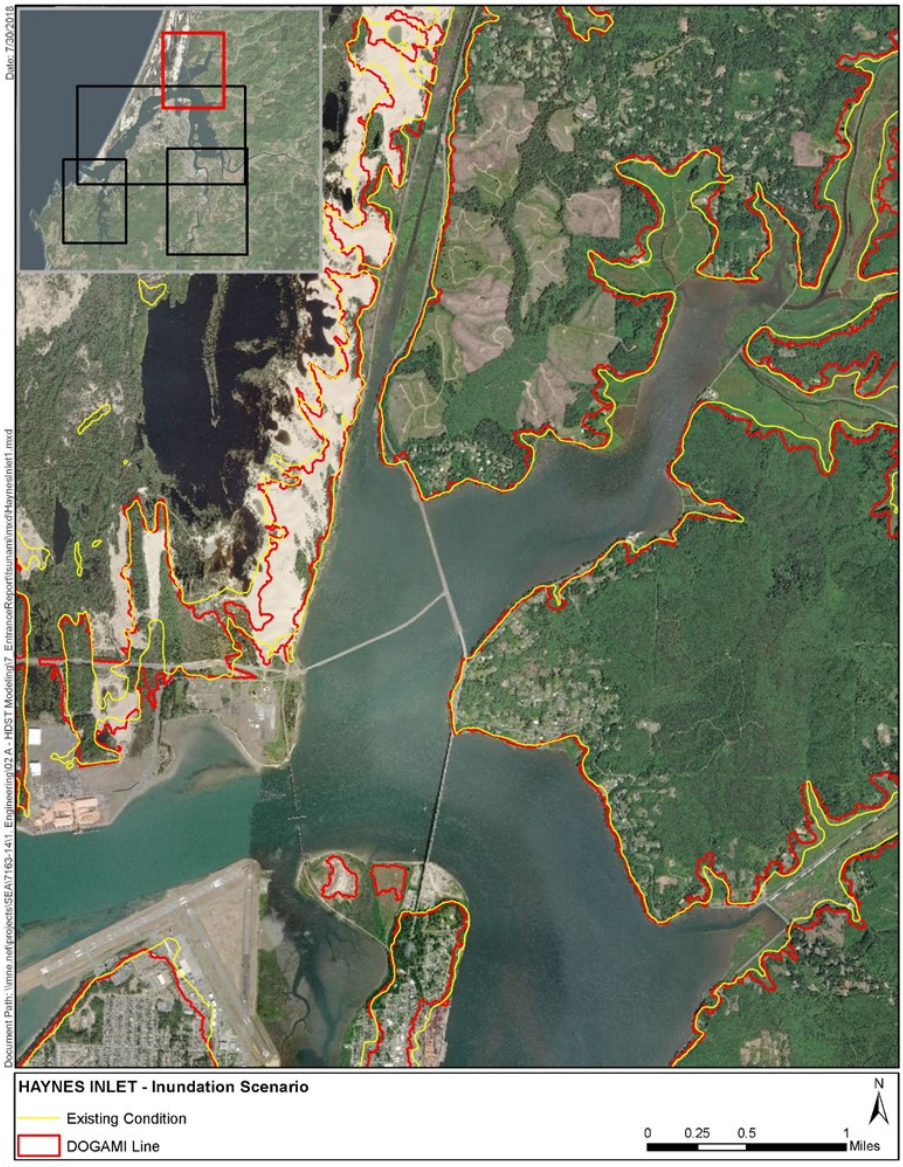

Figure 7-15
Comparison of DOGAMI XXL1 Inundation Line and MIKE-21 Existing Condition Simulation – Haynes Inlet

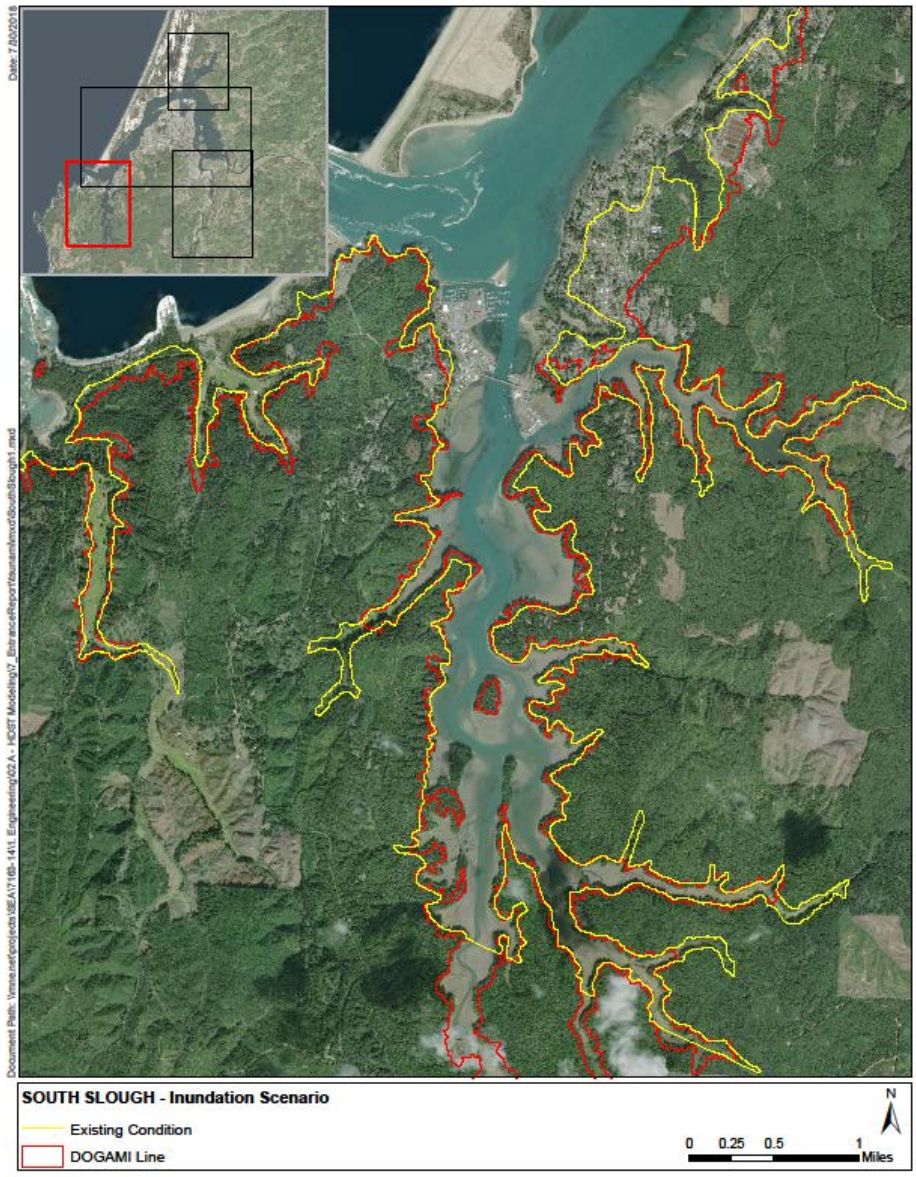

Figure 7-16
Comparison of DOGAMI XXL1 Inundation Line and MIKE-21 Existing Condition Simulation – South Slough

The effects of the 2023 PA on tsunami propagation can be seen in Figure 7-17 through Figure 7-20. These maps show nearly no changes between the Existing Condition and the 2023 PA. Therefore, the project improvements do not affect tsunami runup along the shorelines within Coos Bay.

Figure 7-17
Comparison of Tsunami Inundation Under 2023 PA - North Bend and Coos Bay

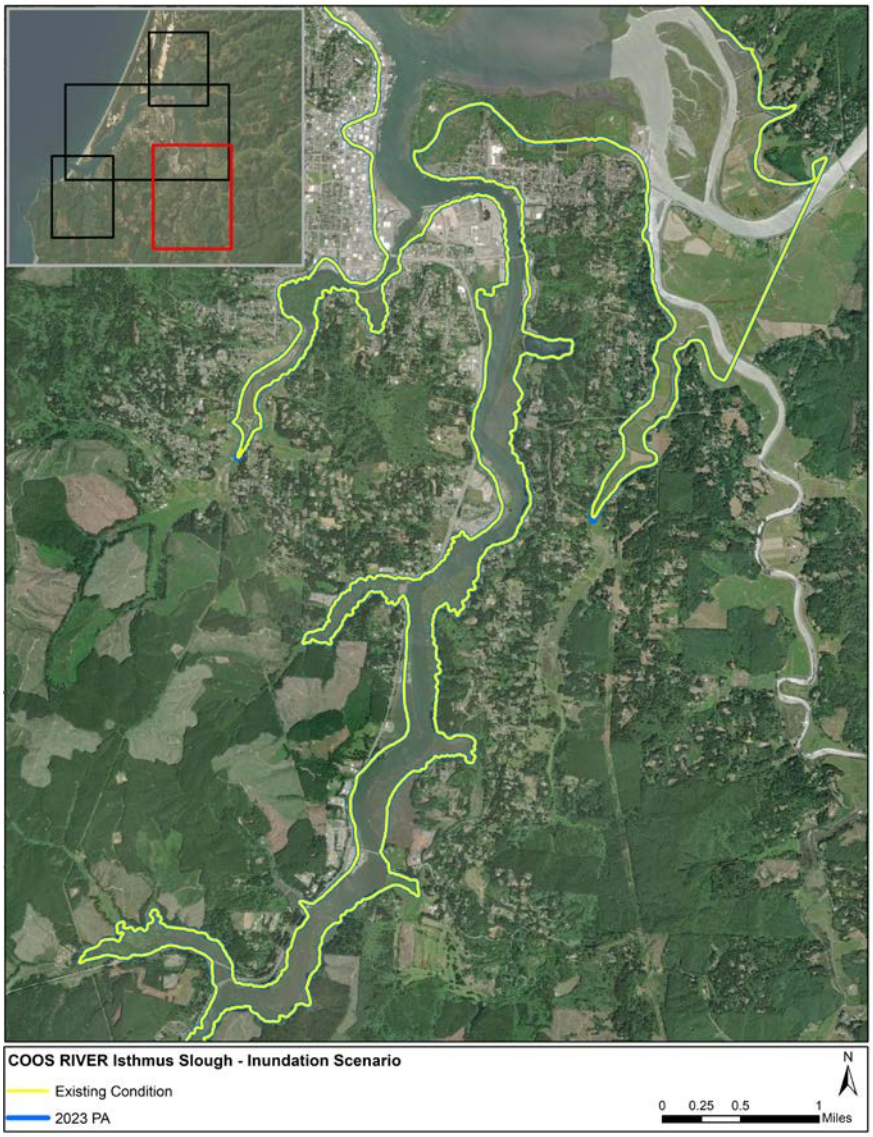

Figure 7-18
Comparison of Tsunami Inundation Under 2023 PA – Isthmus Slough

Figure 7-19
Comparison of Tsunami Inundation Under 2023 PA – Haynes Inlet

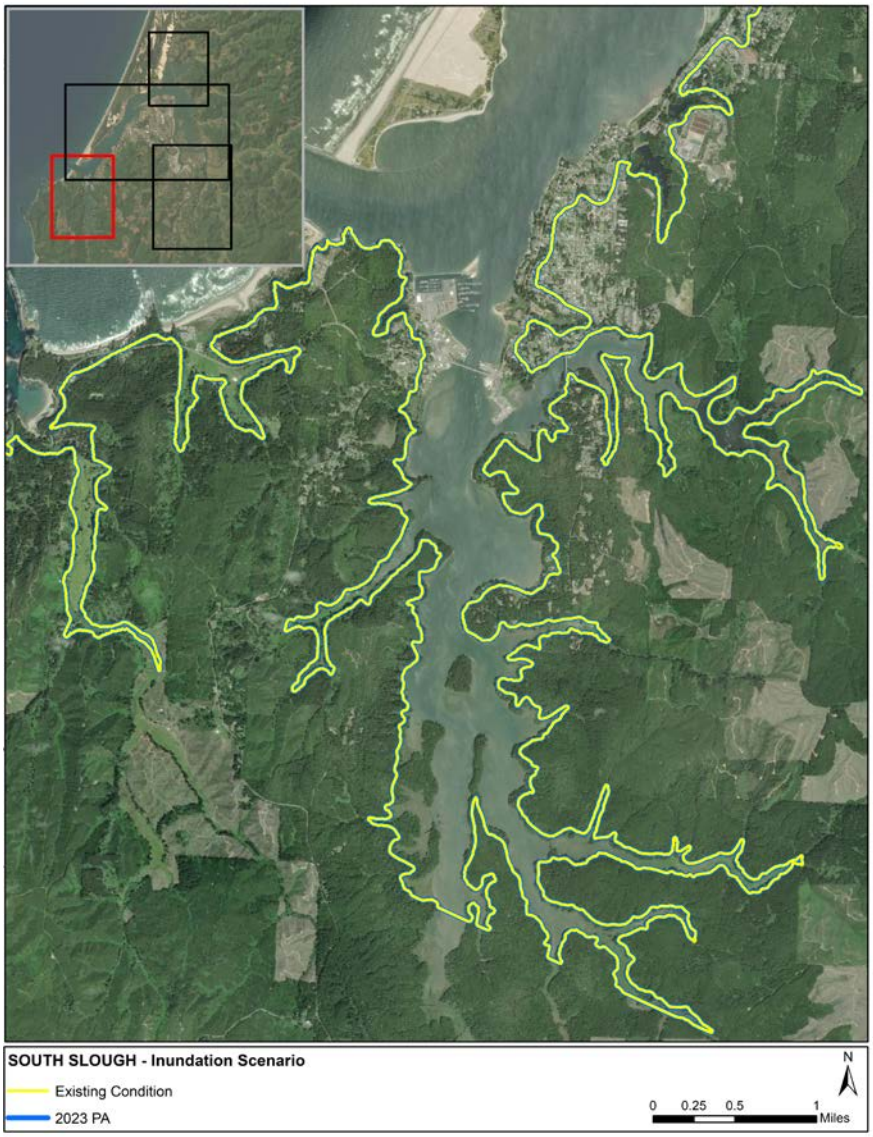

Figure 7-20
Comparison of Tsunami Inundation Under 2023 PA – South Slough

7.4 Conclusions

Tsunamis originating from seismic activity in the CSZ represent the most prominent nearfield threat to Coos Bay. DOGAMI has developed and modeled a number of hypothetical events involving the full rupture of this subduction zone to create tsunami inundation maps for the coast of Oregon. DOGAMI has marked inundation lines corresponding to the XXL scenario in the vicinity of Coos Bay. This same scenario was modeled to examine the impact that the project improvements would have on tsunami propagation in Coos Bay.

The results of the simulations indicate that there are nearly no changes between the Existing Condition and the 2023 PA. Therefore, the project improvements do not affect tsunami runup along the shorelines within Coos Bay. These results indicate that the deeper, wider channel does not affect tsunami propagation within Coos Bay. There are two reasons for this conclusion. The first is based on the conclusion from the Sub-appendix 3, *Estuarine Dynamics*, that the existing channel is hydraulically "efficient" and flows are not limited by side slope and bottom friction. As a result, increasing the cross-sectional area does enable greater flow rates. The second reason for this conclusion is that the changes in the nominal channel depth are not significant compared to the tsunami wavelength and, therefore, does not affect how the wave propagates.

As seen in both the DOGAMI and MIKE-21 results, the tsunami wave completely overtops the North Spit, after which it continues to propagate into the Upper Bay. Therefore, channel modifications in the lower bay have limited effect on the propagation of the wave.

8. RISK MANAGEMENT PLAN

Results of the investigations described in this Section 204(f)/408 Report, in the opinion of the OIPCB, show that all project effects on infrastructure and the natural environment have been managed and are minor and manageable. The Corps of Engineers, through their Section 408 and 404 reviews, will make the Federal determination whether the Proposed Alteration is environmentally acceptable and consistent with Federal policy. As is the case with the implementation of any navigation improvement project in such a dynamic physical environment and within an important and ecologically valuable estuary, there will be inherent residual risk and uncertainty associated project implementation. As such, Risk management will be a critical element of the project.

This sub-appendix describes analyses that were used to influence the design of the project and to assess any physical effects associated with the project in the Entrance Channel downstream of RM 2.5, where the dynamics are dominated by waves and currents. Project elements located downstream of RM 2.5 include the jetties, Charleston Breakwater, the Entrance Channel, the Entrance Turn, Charleston Marina, and Log-spiral Bay (LSB). Note that potential impacts to physical infrastructure related to the FWP conditions addressed in this sub-appendix relate to wave and current-driven hydrodynamics and littoral sediment transport processes. Potential impacts to physical infrastructure related to side slope equilibration of the deeper and wider FWP navigation channel are addressed in *Sub-Appendix 6 – Channel Side Slope Analysis*.

Throughout the development of the Section 204(f)/408 Report, potential areas of residual risk regarding the potential for impacts within the Coos Bay Entrance Channel area have been identified. While these potential impacts will be further evaluated in the EIS process, preliminary elements of risk identified as warranting quantitative risk management plan are summarized in Table 8-1.

Table 8-1
Risk Management Elements Related to Offshore and Ocean Entrance Dynamics Analyses

Issue or Concern	Primary Monitoring	Monitoring Tools	Frequency and Duration of Monitoring	Trigger(S) for Action	Possible Response Actions
North and South Jetty Stability	Bathymetric surveys	Bathymetric surveys to establish baseline Existing Conditions variability	Annually – 5-year period post construction. Periodic following major storm events.	Erosion beyond predicted limits and / or in close proximity to jetty structure	Temporarily suspend dredging operations; Add or enhance rock apron
Other Infrastructure Stability including LSB and Charleston Breakwater	Bathymetric surveys	Bathymetric surveys to establish baseline Existing Conditions variability	Annually – 5-year period post construction. Periodic following major storm events.	Erosion beyond predicted limits and / or in close proximity to jetty structure	Temporarily suspend dredging operations; Add or enhance rock apron or other protective measures

The Risk Management Plan will be developed based on USACE Risk Management guidance.

9. REFERENCES

Battjes, J.A. and Janssen, J.P.F.M. 1978. Energy Loss and Set-up due to Breaking of Random Waves: Coastal Engineering, pp 569-587.

Black & Veatch. 2006. Jordan Cove LNG Terminal, Coos Bay, Oregon. Sedimentation Study. Prepared by Moffatt & Nichol (M&N). May.

Buttolph, A.M., Reed, C.W., Kraus, N.C., Ono, N., Larson, M., Camenen, B., Hanson, H.,Wamsley, T., and Zundel, A.K. 2006. Two-dimensional depth-averaged circulation model CMS-M2D: Version 3.0, Report 2: Sediment transport and morphology change. Tech. Rep. ERDC/CHL TR-06-9, U.S. Army Engineer Research and Development Center, Coastal and Hydraulic Engineering, Vicksburg, MS.Case, G.B. 1983. The History of the Port of Coos Bay, 1852 – 1952. Thesis Presented to Graduate School of Pan American University, Edinburg, TX.

Camenen, B., and Larson, M. 2007. A unified sediment transport formula-tion for coastal inlet application. Technical report ERDC/CHL CR-07-1, US Army Engineer Research and Development Center, Vicksburg, MS.

Case, G.B. 1983. The History of the Port of Coos Bay, 1852 – 1952. Thesis Presented to Graduate School of Pan American University, Edinburg, TX.

Cecioni, C. and Bellotti, G. 2010. "Modeling tsunamis generated by submerged landslides using depth integrated equations." Applied Ocean Research 32, 343-350.

Chief of Engineers. 1915. A Historical Summary giving the Scope of Previous Projects for the Improvement of Certain Rivers and Harbors. Appendix to the Annual Report of the Chief of Engineers.

___. 1924. Report upon the Improvement of Rivers and Harbors in the Portland, Oreg. District. Extract from the Annual Report of the Chief of Engineers.

___. 1926. Report upon the Improvement of Rivers and Harbors in the Portland, Oreg. District. Extract from the Annual Report of the Chief of Engineers.

___. 1927. Report upon the Improvement of Rivers and Harbors in the Portland, Oreg. District. Extract from the Annual Report of the Chief of Engineers.

___. 1931. Report upon the Improvement of Rivers and Harbors in the Portland, Oreg. District. Extract from the Annual Report of the Chief of Engineers.

CIRIA. 2007. The Rock Manual: The use of rock in hydraulic engineering (2nd edition). CIRIA C683.

Coastal Engineering Research Center (CERC). Shore Protection Manual. Department of Defence, Department of the Army, Coastal Engineering Research Center.

Danish Hydraulic Institute (DHI). 2016. "MIKE-21 Flow Model FM." Hydrodynamic Module User Guide.

___. 2016. DHI C-MAP, worldwide digital nautical charts by Jeppesen. <https://www.mikepoweredbydhi.com/products/mike-c-map>.

David Evans and Associates (DEA). 2010. Current and Wave Monitoring Survey Results, March – April 2010, Coos Channel Modifications Project Coos Bay, OR. May.

Earle, M.D, K. E. Steele, K.E, and D.W.C. Wang. 1999. Use of advanced directional wave spectra analysis methods, Ocean Engineering, Volume 26, Issue 12, December 1999, Pages 1421–1434.

Egbert, G.D., and Erofeeva, S.Y. 2002. Efficient Inverse Modeling of Barotropic Ocean Tides. J. Atmos. Oceanic Technology, 19, 183204.

Goda Y., 2010. Random Seas and Design of Maritime Structures. 3rd Edition. Volume 33. Advanced Series on Ocean Engineering.

Hancock, et al. 1981. Coos Bay Offshore Disposal Site Investigation Interim Report Phase I. Oregon State University, Corvallis, OR.: U.S. Army Corps of Engineers, Portland District.

Hays, J. R. and H. R. Moritz. 2003. Evolution of Sediment Issues at Coos Bay, US Army Corps of Engineers, Portland District. Preceedings from 10th International Workshop on Wave hindcasting and Forecasting and Coastal Hazard Symposium, Hawaii, November.

Hoitink, A., Hoekstra, P., & van Maren, D. 2003. Flow asymmetry associated with astronomical tides: Implications for the residual transport of sediment. J. Geophysical Research, 108(C10) , 3315.

Komar, P.D. 1992. Ocean processes and hazards along the Oregon Coast. Oregon geology, volume 54, number 1, January.

Kraus, N.C. and Larson, M. 2001. Mathematical Model for Rapid Estimation of Infilling and Sand Bypassing at Inlet Entrance Channels. ERDC/CHL CHETN-IV-35.

Jiang, L. and LeBlond, P.H. 1992. "The Coupling of a Submarine Slide and the Surface Waves which it Generates." Journal of Geophysical Research, Vol. 97(C8), 12, 731 – 12, 744.

Latteux, B. 1995. Techniques for long-term morphological simulations under tidal action. Marine Geology 126 , 87-242.

Lesser, G. 2009. An approach to medium-term coastal morphological modeling. PhD thesis, UNESCO-IHE & Delft University of Technology, Delft: CRC Press/Balkema. ISBN 978-0-415-55668-2.

Lin, L., Demirbilek, Z., Mase, H., Zheng, J., and Yamada, F. 2008. CMS-Wave: a nearshore spectral wave processes model for coastal inlets and navigation projects. Tech. Report ERDC/CHL TR-08-13. Vicksburg, MS: U.S. Army Engineer Research and Development Center.

Lin, L., Demirbilek, Z., and Mase, H. 2011. Recent capabilities of CMS-Wave: A coastal wave model for inlets and navigation projects. Journal of Coastal Research, Special Issue 59, 7-14.

Moffatt & Nichol (M&N). 2008. Oregon Gateway Marine Terminal Aeolian Transport at Port Stockpile Site. Memorandum. Prepared for David Evans & Associates.

___. 2011. "Coos Bay Jetties Preliminary Major Maintenance Report, Appendix B Coastal Engineering." Comment Matrix to 60% and pre-90% submittal. Prepared for U.S. Army Corps of Engineers, Portland District.

___. 2012. "Coos Bay Jetties Preliminary Major Maintenance Report, Appendix B Coastal Engineering." Final Report, Prepared for U.S. Army Corps of Engineers, Portland District. July 2012.

___. 2016. "Tsunami Modeling." Rev C. Prepared for Jordan Cove LNG.

Moritz, Hans R. 2016. "Future Sea level change adaptive approach for rubblemound structures at Mouth of Columbia River." CWG Vicksburg-MS. November 17.

___. 2018. OIPCB-USACE Portland Monthly Meeting.

Moritz, H. R. and Moritz, H. P. 2007. Assessing Extreme Storm Intensity by Combining Storm Power with Surge, Oregon. District, U.S. Army Corps of Engineers, Portland District.

National Data Buoy Center (NDBC). 2015. National Data Buoy Center. Viewed online at <http://www.ndbc.noaa.gov/>.

National Ocean and Atmospheric Administration (NOAA). Global Sea Level Rise Scenarios for the United States National Climate Assessment. Publication available at <https://scenarios.globalchange.gov/sites/default/files/NOAA_SLR_r3_0.pdf>

___2014. Chart 18587, U. S. Department of Commerce, National Oceanic and Atmospheric Administration, National Ocean Service, Coast Survey. Last Correction 3/26/2014. <http://www.charts.noaa.gov/OnLineViewer/18587.shtml>

___. 2015. Mean Sea Level Trend: 9432780, Charleston, Oregon. Available online at: <http://tidesandcurrents.noaa.gov/sltrends/sltrends_station.shtml?stnid=9432780>

___. 2017. Extreme Water Levels: 9432780 Charleston, OR. Available online at <http://tidesandcurrents.noaa.gov/est/est_station.shtml?stnid=9432780>.

___. 2017b. Chart Downloader for NOAA RNC. <http://www.charts.noaa.gov/RNCs/RNCsIndv.shtml> accessed May 24, 2017.

National Oceanic and Oceanographic Administration (NOAA), National Ocean Service (NOS). 1999. Assessment of the National Ocean Service's Tidal Current Program. NOAA Technical Report NOS CO-OPS 022. Available online at <http://tidesandcurrents.noaa.gov/publications/techrpt22.pdf>.

Nwogu, O. and Demirbilek, Z. 2001.BOUSS-2D: A Boussinesq Wave Model for Coastal Regions and Harbors. ERDC/CHL TR-01-25:September.

Oregon Department of Geology and Mineral Industries (DOGAMI). 2012. "Local Source (Cascadia Subduction Zone) Tsunami Inundation Map, Coos Bay – North Bend, Oregon."

Oregon International Port of Coos Bay (OIPCB). 2010. Coos Bay Channel Modifications Project. Current and Wave Monitoring Survey Results. Prepared by David Evans & Associates (DEA): May.

___. 2015. Oregon International Port of Coos Bay, Oregon Section 204(f)/406 Report: 30% Design Documentation Report. Prepared by Moffatt & Nichol: February.

___. 2016. Oregon International Port of Coos Bay, Oregon Section 204(f)/406 Report: Full Ship Simulation Report. Prepared by Moffatt & Nichol: October.

___. 2017. Coos Bay, OR Section 204(f) Channel Modification Project 60% Engineering Design Report. Prepared by Moffatt & Nichol.

___. 2019. Engineering Appendix A: Design Documentation Report. Oregon International Port of Coos Bay Proposed Section 204(f)/408 Channel Modification Project. October 2019.

PIANC. 2014. Harbour Approach Channels Design Guidelines. Report no 121-2014.

Reid, J.A., Reid, J.M., Jenkins, C.J., Zimmermann, M., Williams, S.J., and Field, M.E. 2006. usSEABED: Pacific Coast (California, Oregon, Washington) offshore surficial-sediment data release. U.S. Geological Survey Data Series 182, version 1.0. Online at http://pubs.usgs.gov/ds/2006/182/

Rosati, J.D. 2003. Shoaling in Navigation Channels.

___. 2014. RE: Historical dredging records for Coos Bay? (UNCLASSIFIED). E-mail to Susan Tonkin: May 5.

Ruggiero, P. et al. 2012. National Assessment of Shoreline Change: Historical Shoreline Change Along the Pacific Northwest Coast, Open-File Report 2012–1007, U.S. Department of the Interior and U.S. Geological Survey.

Sánchez, A., Wu, W. Rosati, J.D., Demirbilek, Z. Li, L., Rosati, J., Thomas, R., Reed, C., Watts, I., and Brown, M. 2011a. Validation of the Coastal Modeling System: Report III, Hydrodynamics. ERDC/CHL-TR-11-10, US Army Engineer Research and Development Center, Coastal and Hydraulics Laboratory, Vicksburg, MS.

___. 2011b. Validation of the Coastal Modeling System: Report IV, Sediment Transport and Morphology Change. ERDC/CHL-TR-11-10, US Army Engineer Re-search and Development Center, Coastal and Hydraulics Laboratory, Vicksburg, MS.

SHN. 2007. Sediment Sampling and Analysis Report, Oregon Gateway Marine Terminal, Coos Bay, Oregon. Prepared for The Port of Coos Bay and Jordan Cove Energy.

Siipola, M. 2011. Personal Communication. Telephone call with Mark Siipola, USACE, Portland District with M. Schwertner, Moffatt & Nichol, October 20.

Smith, E.R. et al. 2003. Evaluation of the CERC Formula Using Large-Scale Laboratory Data. University of South Florida Scholar Commons.

Soulsby, R.L. 1997. Dynamics of marine sands. Thomas Telford, London.

U.S. Army Coastal Engineering Research Center. 1977. Shore Protection Manual.

U.S. Army Corps of Engineers (USACE). 1940. Reconstruction of South Jetty Concrete Breakwater and Terminal. Drawing CB-1-309/2.

___. 1986. Design of Breakwaters and Jetties. EM 1110-2-2904: August 8.

___. 1994. Coos Bay, Oregon Navigation Improvements: Final Feasibility Report and Environmental Impact Statement: January.

___. 2002. Coastal Engineering Manual (CEM), Engineer Manual (EM) 1110-2-1100, U.S. Army Corps of Engineers, Washington, D.C. (6 volumes).

___. 2006. Hydraulic Design of Deep-Draft Navigation Projects. EM 1110-2-1613: May 31.

___.2005. Coos Bay Sediment Quality Evaluation Report. Prepared by Tim Sherman.

___.2012a. Coos Bay Dredged Material Report. February.

___.2012b. Coos Bay Jetties Perliminary Major Maintenance Report Appendix B: Coastal Engineering. Prepared by Moffatt & Nichol: July.

___. 2012c. Columbia River at the Mouth, Oregon and Washington Major Rehabilitation of the Jetty System at the Mouth of the Columbia River. Final Report.

___. 2013. Encorporated Sea Level Change in Civil Works Programs. ER 1100-2-8162: December 31.

___. 2014. Procedures to Evaluate Sea Level Change: Impacts, Responses and Adaptation. Technical Letter No. 1100-2-1

___. 2017a. Survey & Mapping Hydrographic Surveys. < http://navigation.usace.army.mil/Survey/Hydro#state=WA#channel=CENWS_GH_01_ENT> accessed May 24, 2017.

___. 2017b. Coos Bay North and South Jetty Site Inspections, 24-25 July 2017. Memorandum for Record.

___. 2019. Coos Bay North Jetty Major Maintenance DDR. Appendix C – North Jetty Head Stabilization Repair Assessment Report.

___. 2021. Coos Bay North Jetty Repair Major Maintenance Design Drawings. July 26, 2021.

U.S. Army Engineer Research and Development Center (ERDC). 2018. "Field Measurements, Sediment Tracer Study, and Numerical Modeling at Coos Bay Inlet, Oregon", Final Report, June 2018.

U.S. Environmental Protection Agency (USEPA) Region X and U.S. Army Corps of Engineers (USACE) – Portland District. 1986. Coos Bay, Oregon. Dredged Material Disposal Site Designation. Final Environmental Impact Statement.

USEPA & USACE. 2006. Final Site Management/Monitoring Plan. Coos Bay, Oregon Site E, Site F, and Site H.

U.S. Geological Survey (USGS). 2013. USGS National Elevation Dataset (NED) 1/3 arc-second digital elevation models collection. <https://catalog.data.gov/dataset/usgs-ned-n44w125-1-3-arc-second-2013-1-x-1-degree-img>.U.S. Environmental Protection Agency (USEPA) Region X and US Army Corps of Engineers (USACE), Portland District. 1986. Coos Bay, Oregon. Dredged Material Disposal Site Designation. Final Environmental Impact Statement.

___.2006. Coos Bay, Oregon. Dredged Material Disposal Site Designation. Final Environmental Impact Statement.

Van Rijn., L.C. 2002. Longshore Sand Transport.

Wang, P. Ebersole, B.A., and Smith, E.R. 2002. Longshore Sand Transport – Initial Results from Large-Scale Sediment Transport Facility. ERDC/CHL CHETN-II-46.

Watanabe, A. 1987. 3-dimensional numerical model of beach evolution. Proceedings Coastal Sediments '87, 802-817.

Williams, J.J., and L.S. Esteves (2017) "Guidance on Setup, Calibration, and Validation of Hydrodynamic, Wave, and Sediment Models for Shelf Seas and Estuaries", Advances in Civil Engineering, Volume 2017, Article ID 5251902, 25 pages, https://doi.org/ 10.1155/2017/5251902.

Witter, R.C., Zhang, Y., Wang, K., Priest, G.R., Goldfinger, C., Stimley, L.L., English, J.T., and Ferro, P.A. 2011. "Simulating Tsunami Inundation at Bandon, Coos County, Oregon, Using Hypothetical Cascadia and Alaska Earthquake Scenarios." Oregon Department of Geology and Mineral Industries, Special Paper 43.

Wu, W. 1991. The study and application of 1-D, horizontal 2-D and their nesting mathematical models for sediment transport. PhD dissertation: Wuhan University of Hydraulic and Electrical Engineering, Wuhan, China.

Wu, W., Sánchez, A., and Mingliang, Z. 2010. An implicit 2-D depth-averaged finite-volume model of flow and sediment transport in coastal waters. Proceeding of the International Conference on Coastal Engineering.

Zhang, Y.L. and Baptista, A.M. 2008. “SELFE: A semi-implicit Eulerian-Lagrangian finite-element model for cross-scale ocean circulation.” Ocean Modelling, 21(3-4),71 – 96.

ATTACHMENT A

Modeled Waves At North and South Jetties

A.1 WAVE PLOTS AT N1

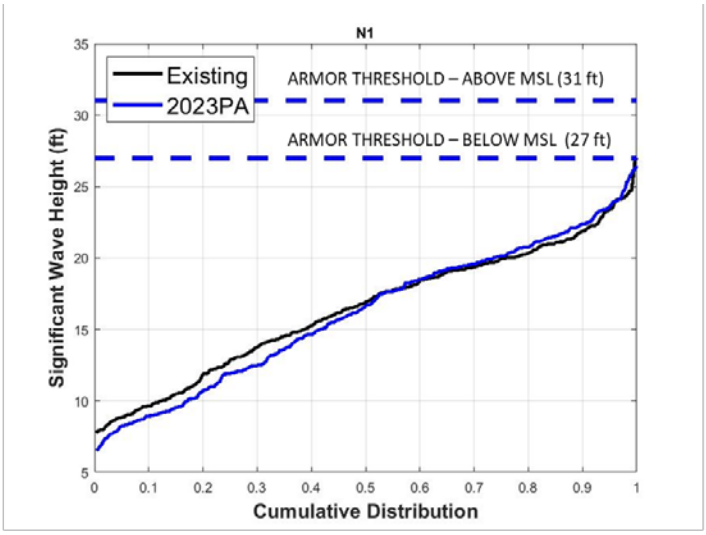

Figure A-1: Cumulative Distribution Wave Plot at N1

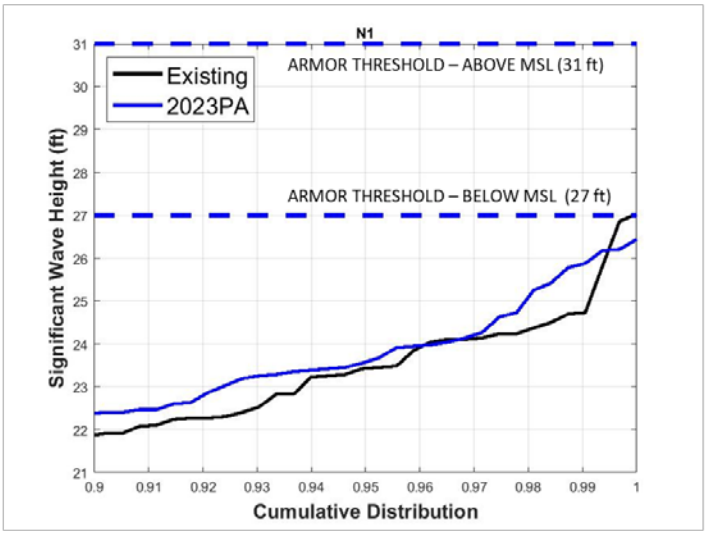

Figure A-2: Cumulative Distribution Wave Plot at N1 (Largest 10% of Waves)

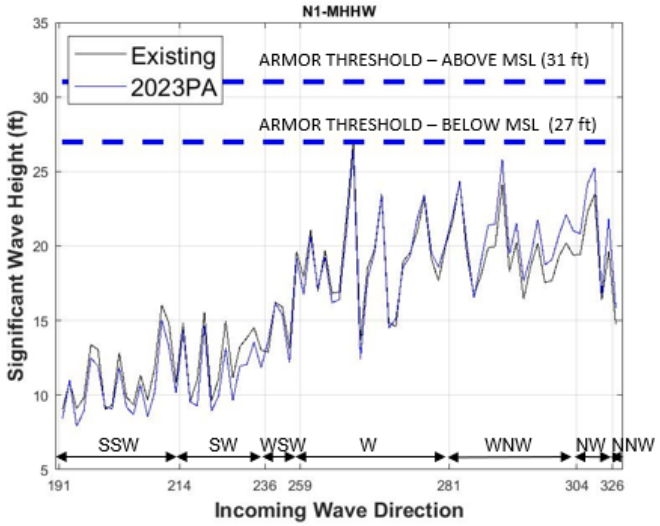

Figure A-3: Wave Direction Plot for Waves at MHHW at N1

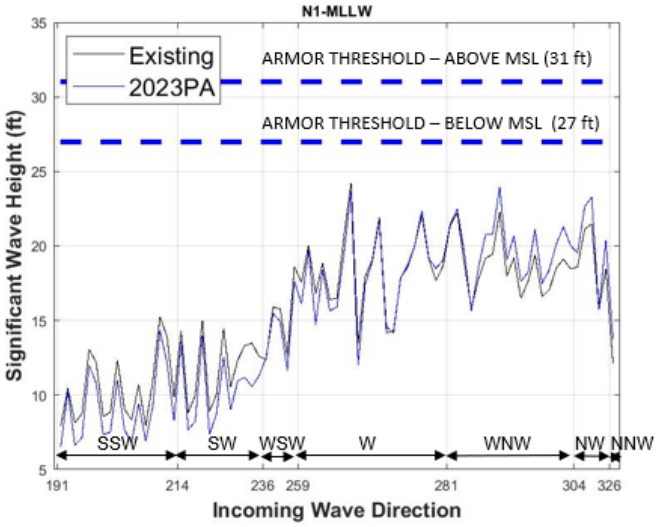

Figure A-4: Wave Direction Plot for Waves at MLLW at N1

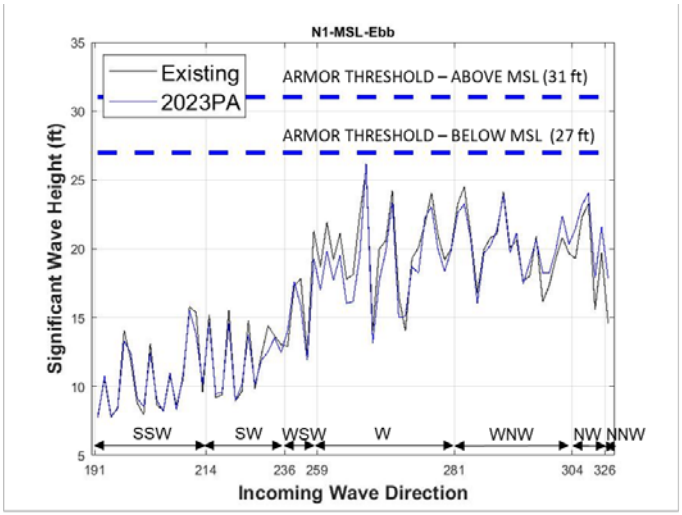

Figure A-5: Wave Direction Plot for Waves at MSL-Ebb at N1

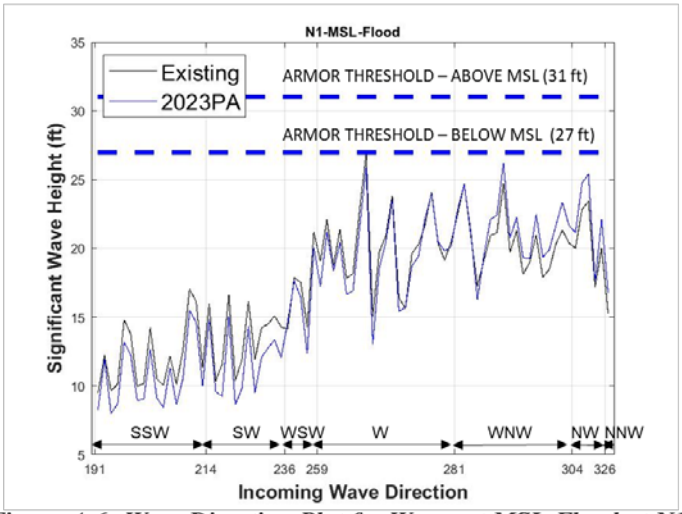

Figure A-6: Wave Direction Plot for Waves at MSL-Flood at N1

A.2 WAVE PLOTS AT N2

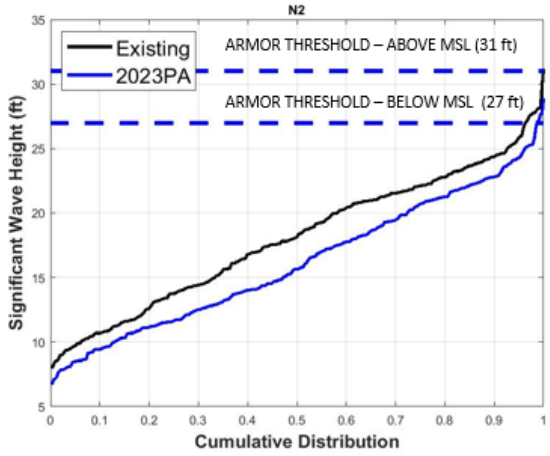

Figure A-7: Cumulative Distribution Wave Plot at N2

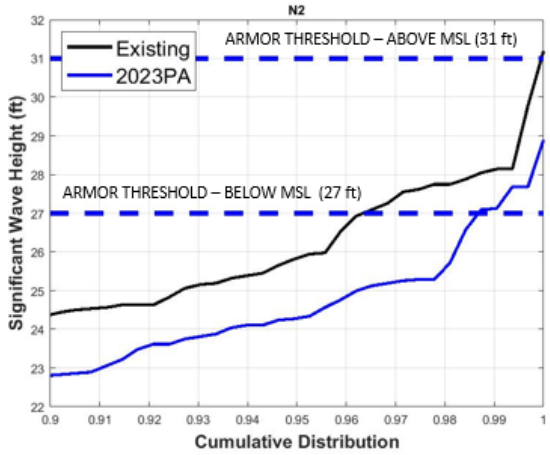

Figure A-8: Cumulative Distribution Wave Plot at N2 (Largest 10% of Waves)

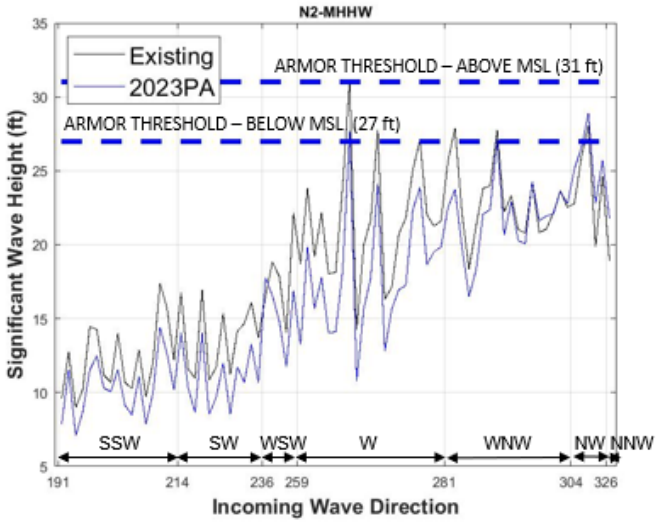

Figure A-9: Wave Direction Plot for Waves at MHHW at N2

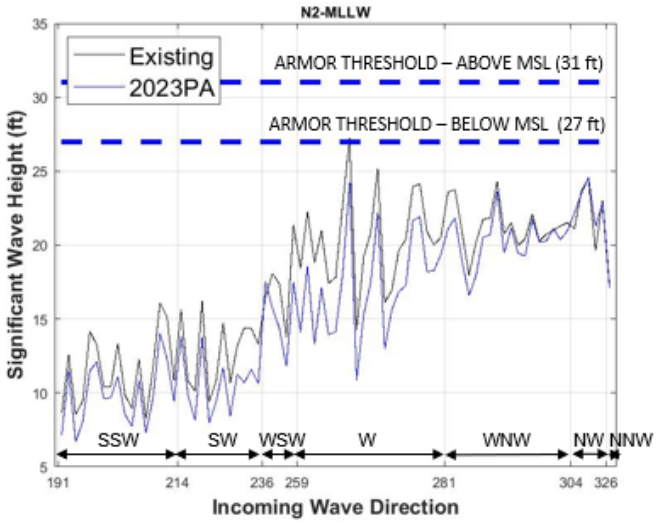

Figure A-10: Wave Direction Plot for Waves MLLW at N2

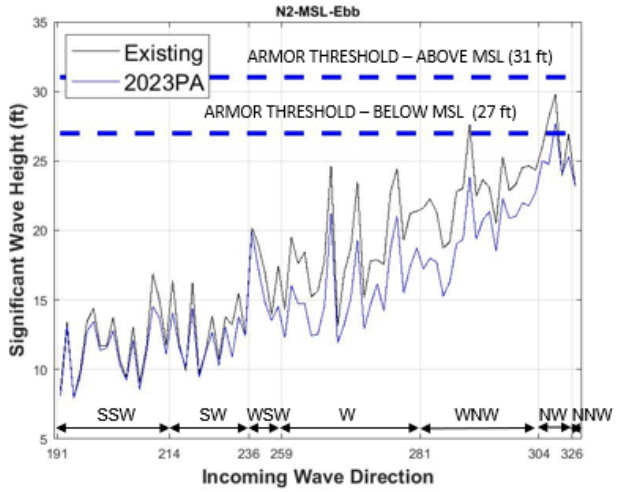

Figure A-11: Wave Direction Plot for Waves at MSL-Ebb at N2

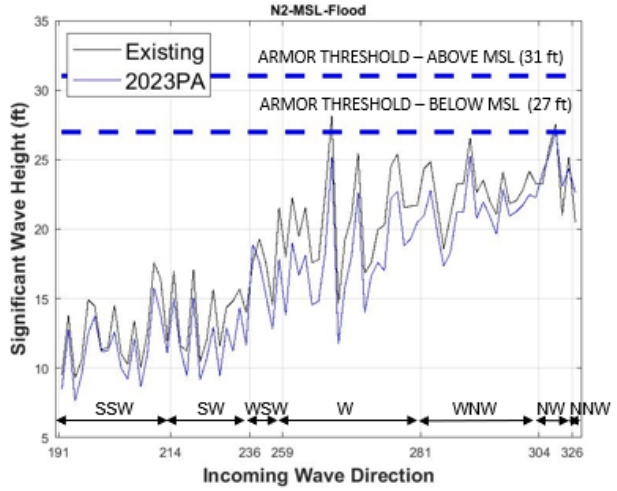

Figure A-12: Wave Direction Plot for Waves at MSL-Flood at N2

A.3 WAVE PLOTS AT N3

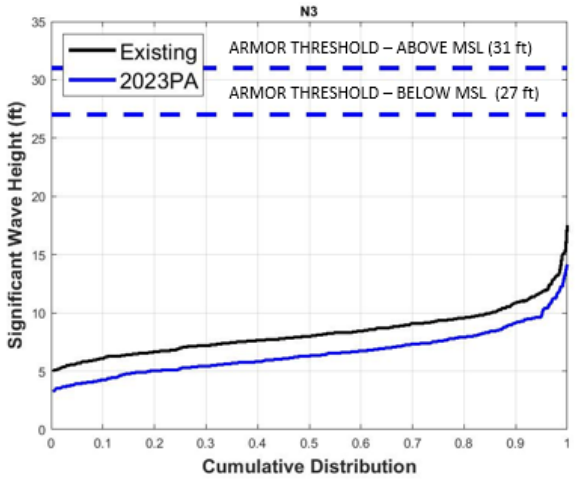

Figure A-13: Cumulative Distribution Wave Plot at N3

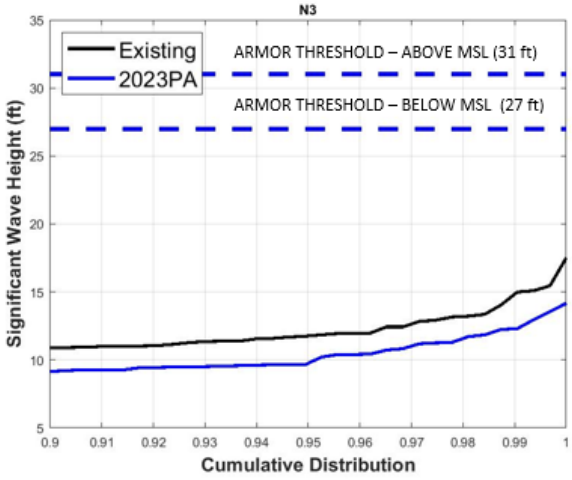

Figure A-14: Cumulative Distribution Wave Plot at N3 (Largest 10% of Waves)

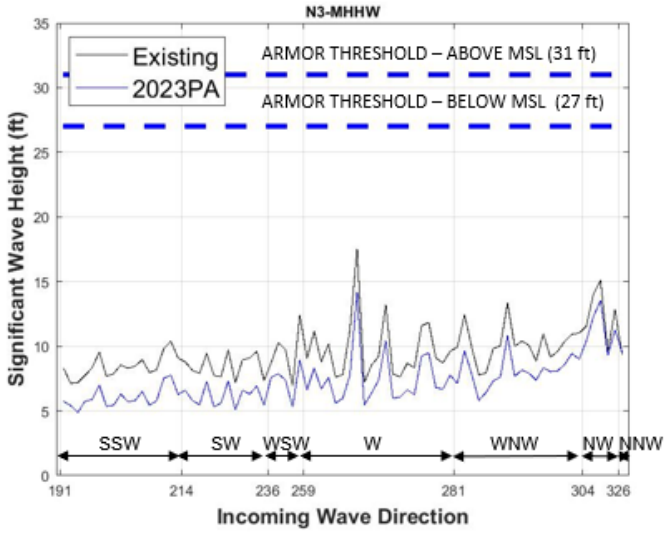

Figure A-15: Wave Direction Plot for Waves at MHHW at N3

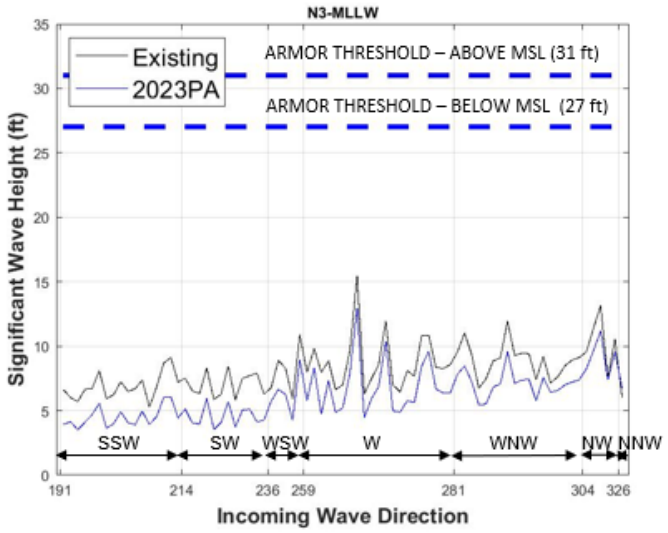

Figure A-16: Wave Direction Plot for Waves MLLW at N3

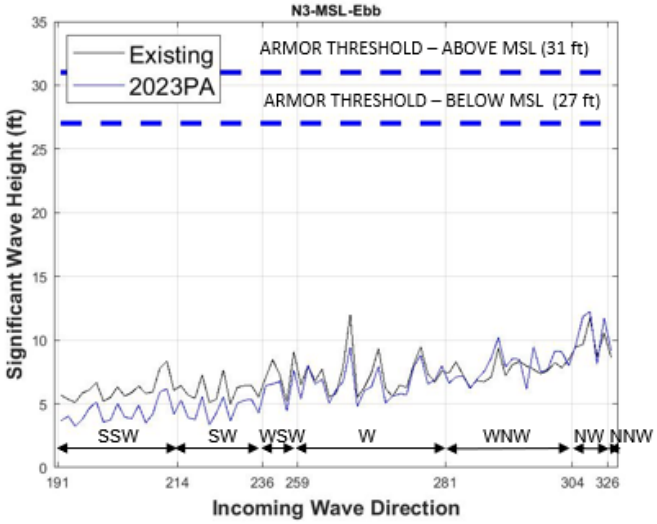

Figure A-17: Wave Direction Plot for Waves at MSL-Ebb at N3

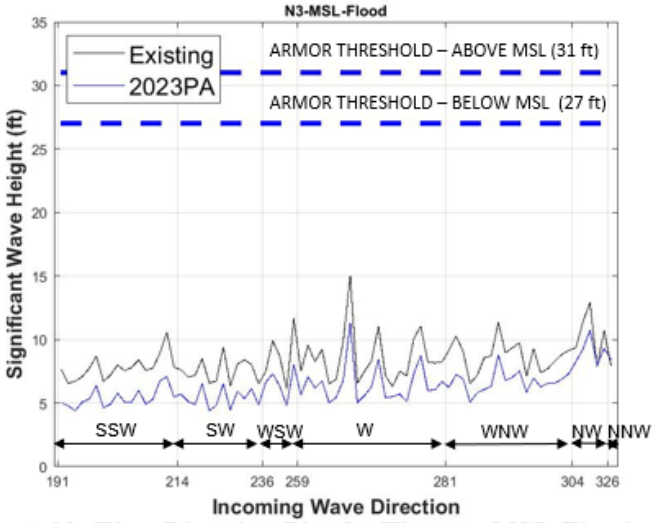

Figure A-18: Wave Direction Plot for Waves at MSL-Flood at N3

A.4 WAVE PLOTS AT N4

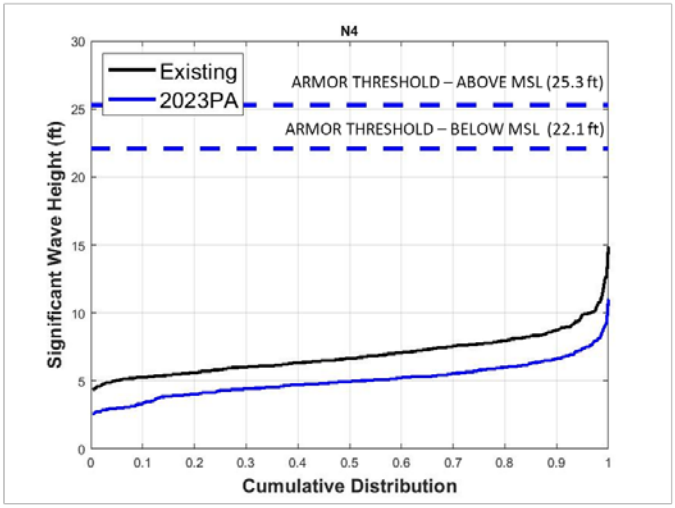

Figure A-19: Cumulative Distribution Wave Plot at N4

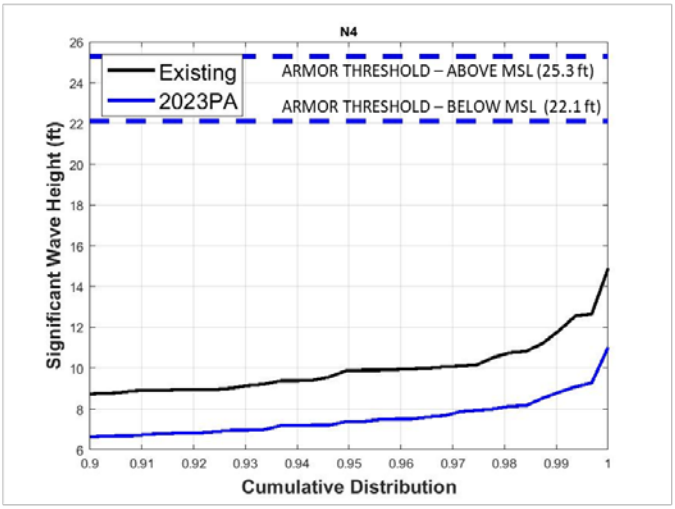

Figure A-20: Cumulative Distribution Wave Plot at N4 (Largest 10% of Waves)

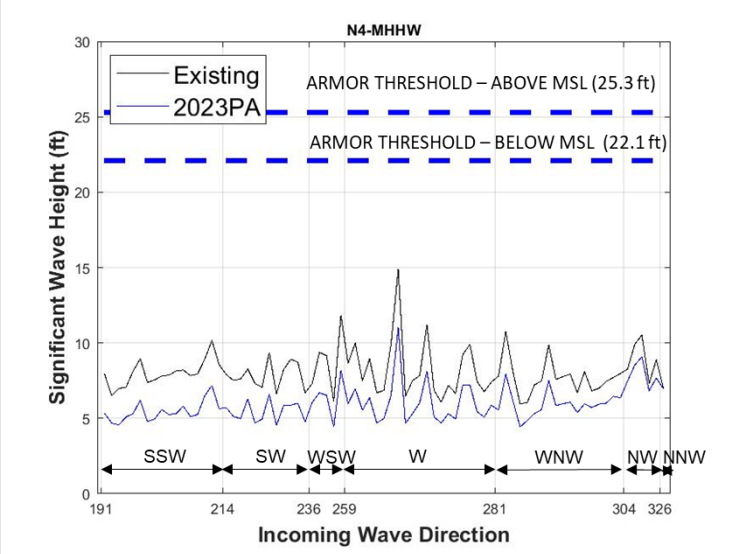

Figure A-21: Wave Direction Plot for Waves at MHHW at N4

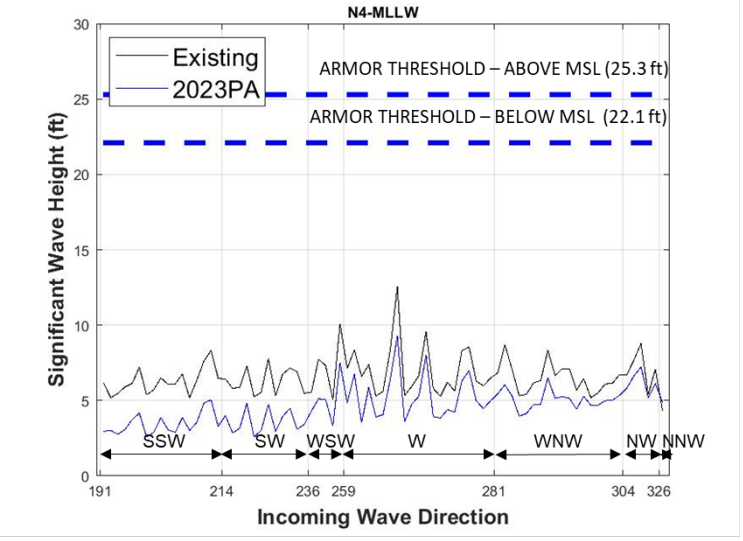

Figure A-22: Wave Direction Plot for Waves MLLW at N4

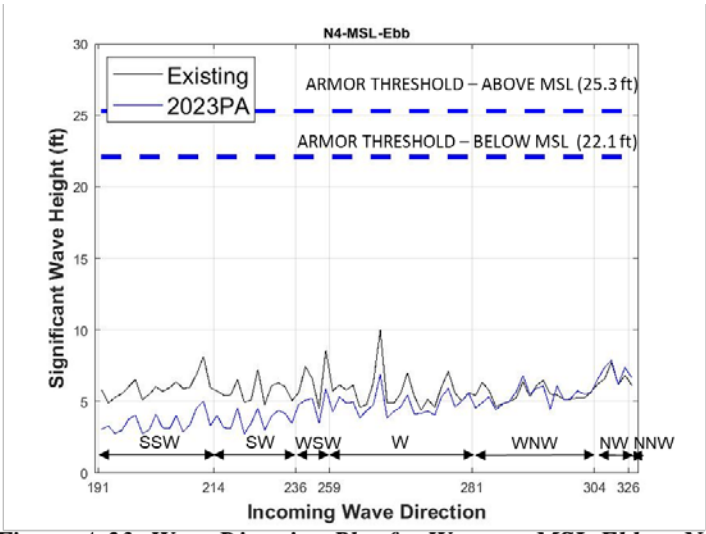

Figure A-23: Wave Direction Plot for Waves at MSL-Ebb at N4

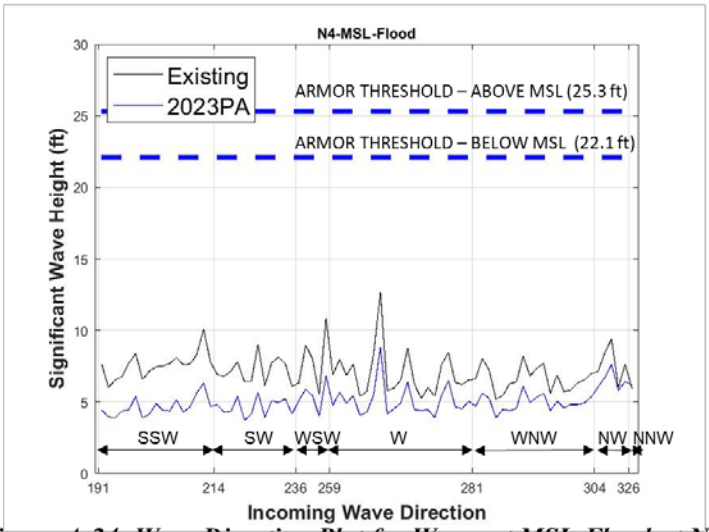

Figure A-24: Wave Direction Plot for Waves at MSL-Flood at N4

A.5 WAVE PLOTS AT N5

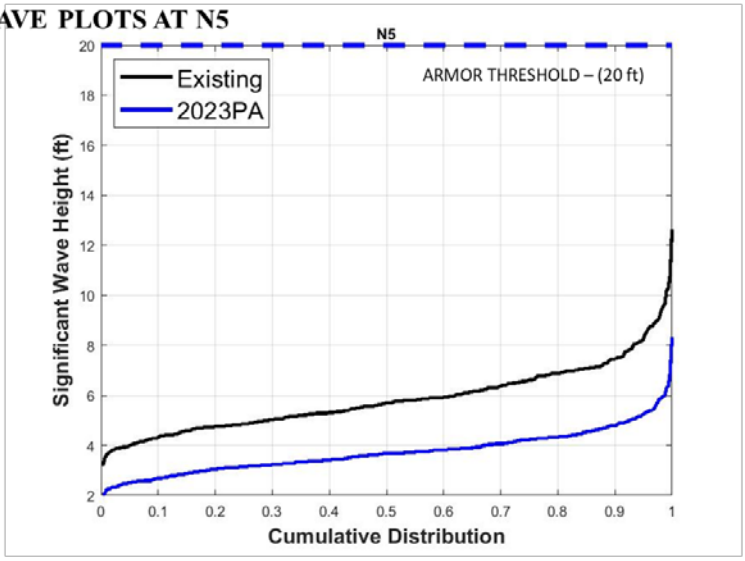

Figure A-25: Cumulative Distribution Wave Plot at N5

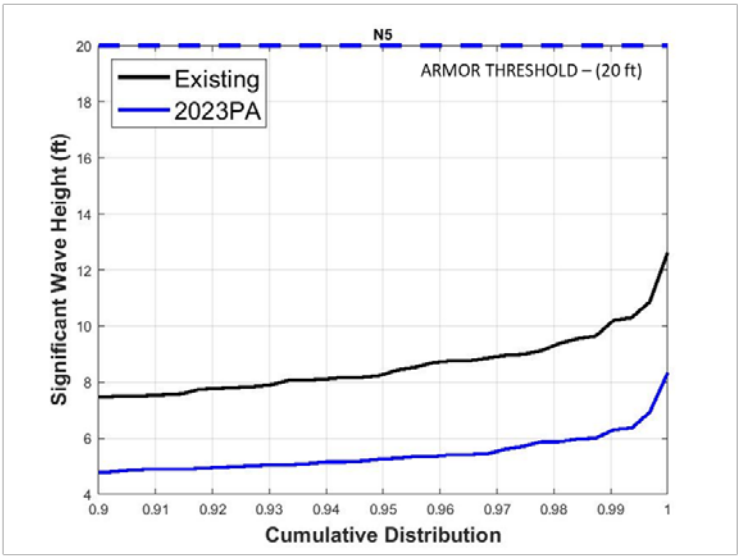

Figure A-26: Cumulative Distribution Wave Plot at N5 (Largest 10% of Waves)

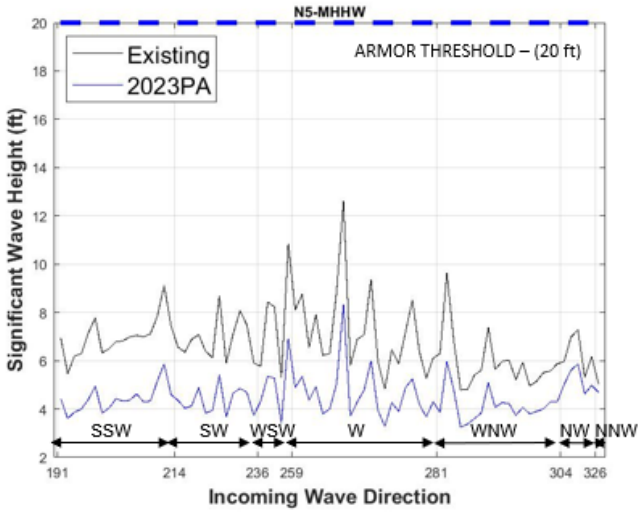

Figure A-27: Wave Direction Plot for Waves at MHHW at N5

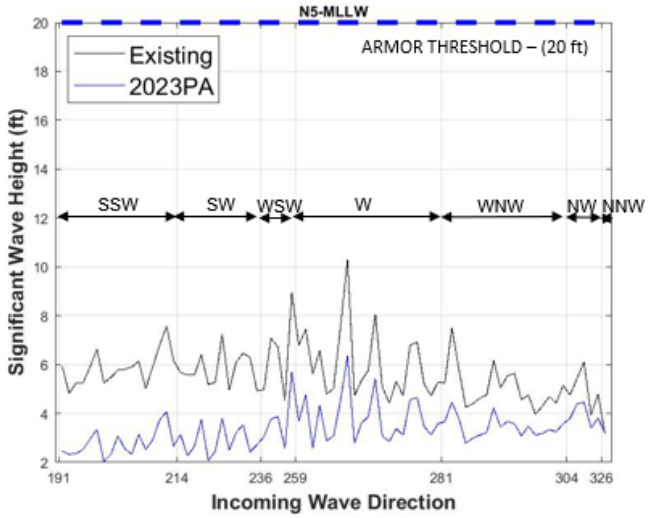

Figure A-28: Wave Direction Plot for Waves MLLW at N5

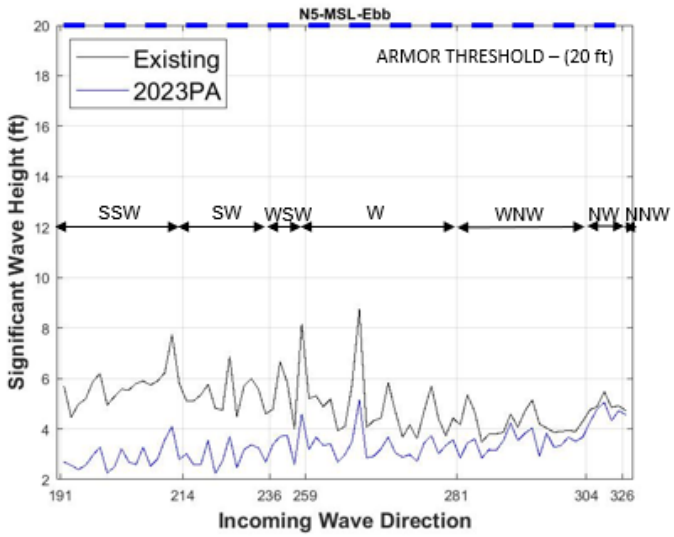

Figure A-29: Wave Direction Plot for Waves at MSL-Ebb at N5

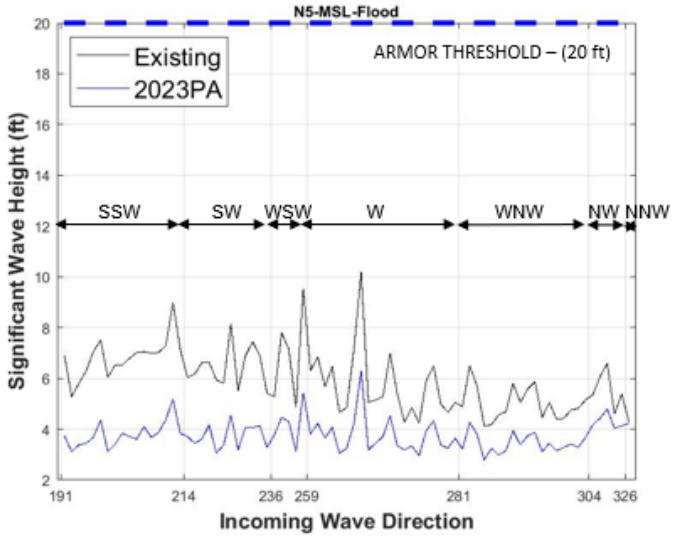

Figure A-30: Wave Direction Plot for Waves at MSL-Flood at N5

A.6 WAVE PLOTS AT N6

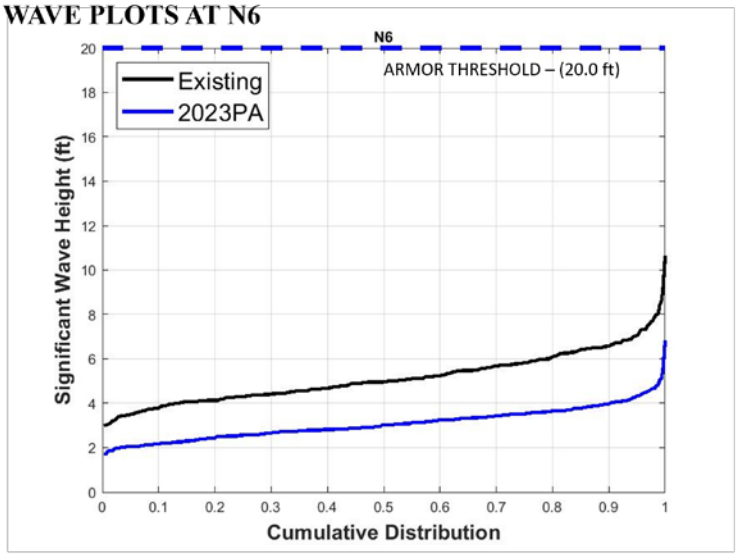

Figure A-31: Cumulative Distribution Wave Plot at N6

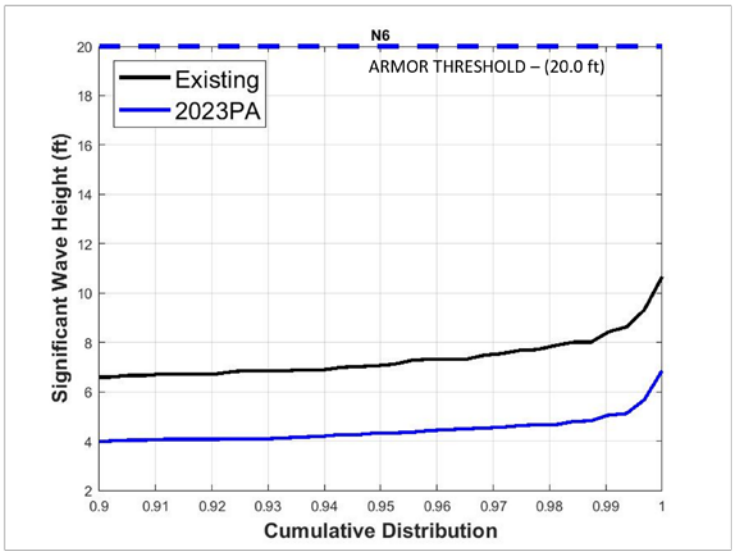

Figure A-32: Cumulative Distribution Wave Plot at N6 (Largest 10% of Waves)

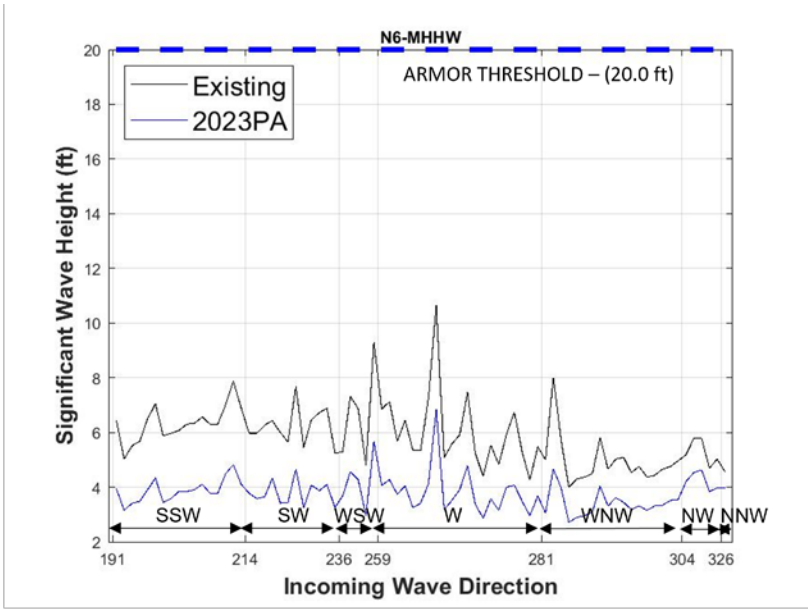

Figure A-33: Wave Direction Plot for Waves at MHHW at N6

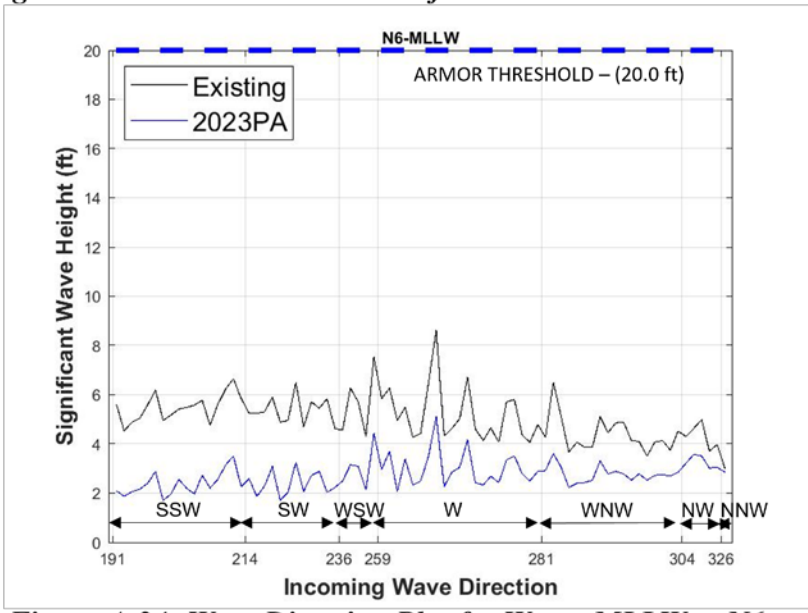

Figure A-34: Wave Direction Plot for Waves MLLW at N6

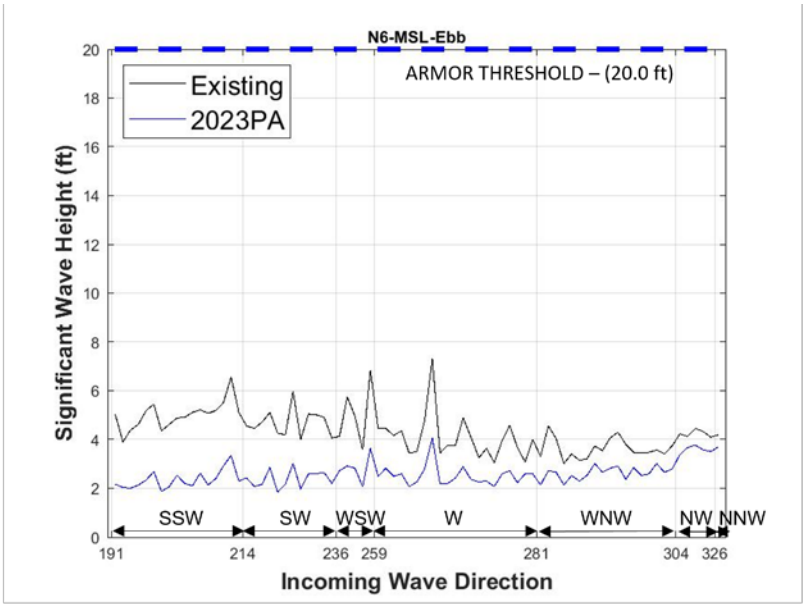

Figure A-35: Wave Direction Plot for Waves at MSL-Ebb at N6

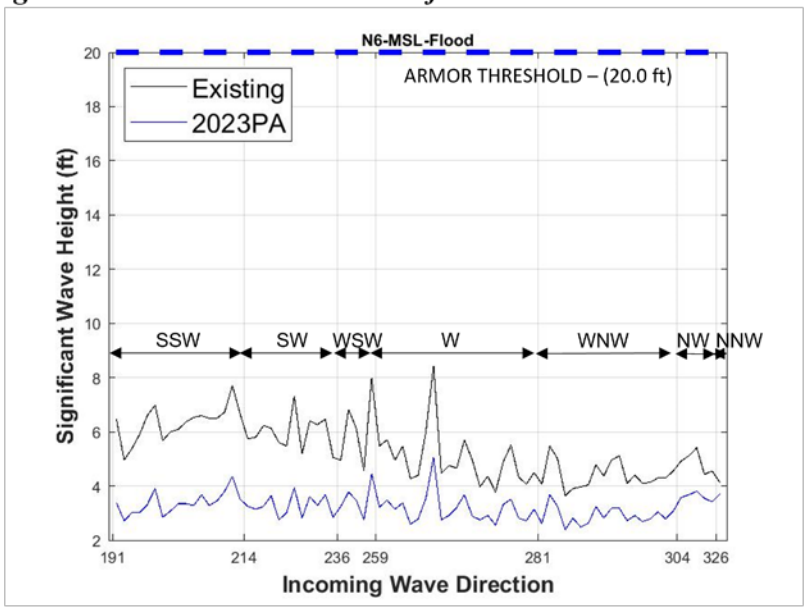

Figure A-36: Wave Direction Plot for Waves at MSL-Flood at N6

A.7 WAVE PLOTS AT N7

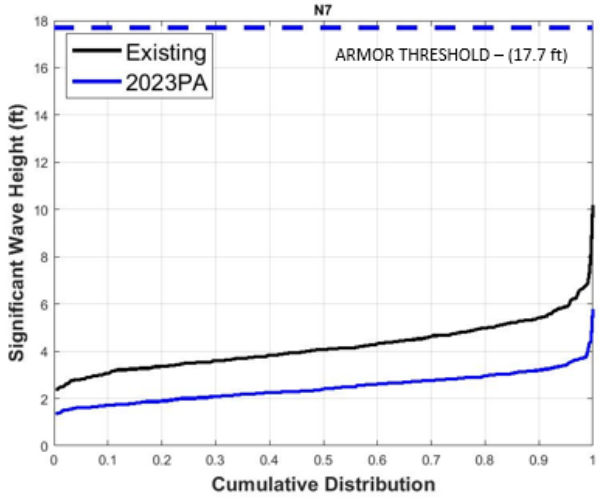

Figure A-37: Cumulative Distribution Wave Plot at N7

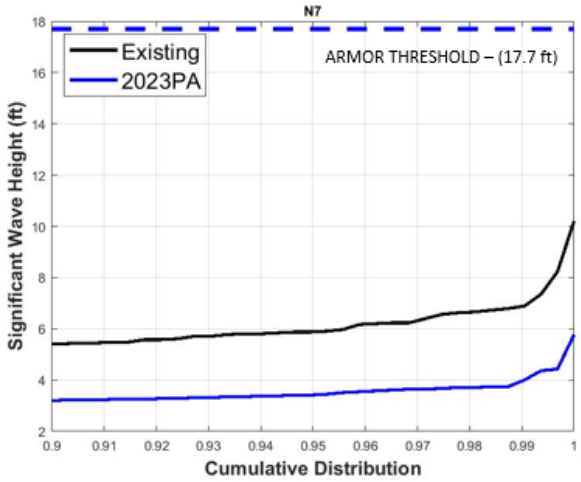

Figure A-38: Cumulative Distribution Wave Plot at N7 (Largest 10% of Waves)

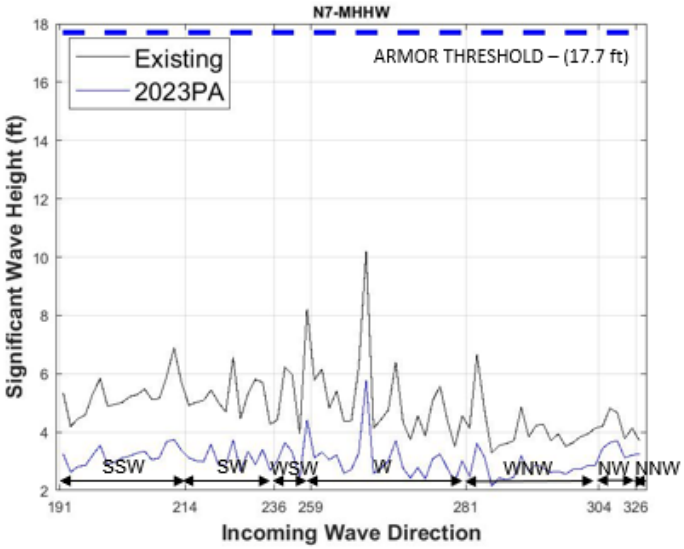

Figure A-39: Wave Direction Plot for Waves at MHHW at N7

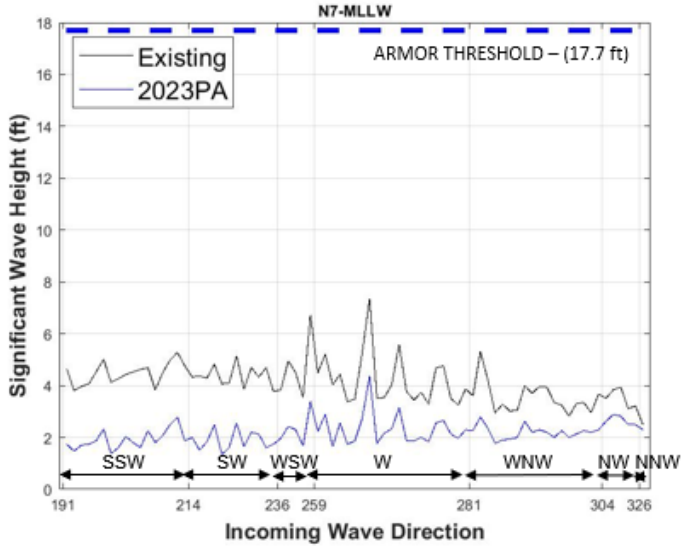

Figure A-40: Wave Direction Plot for Waves MLLW at N7

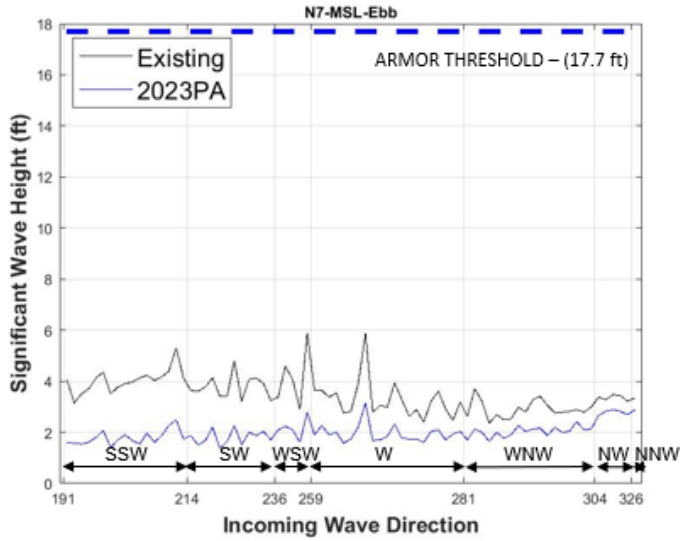

Figure A-41: Wave Direction Plot for Waves at MSL-Ebb at N7

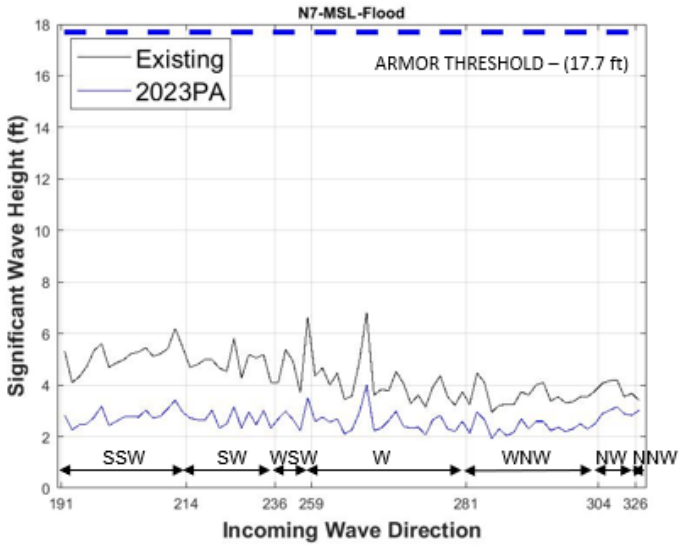

Figure A-42: Wave Direction Plot for Waves at MSL-Flood at N7

A.8 WAVE PLOTS AT N8

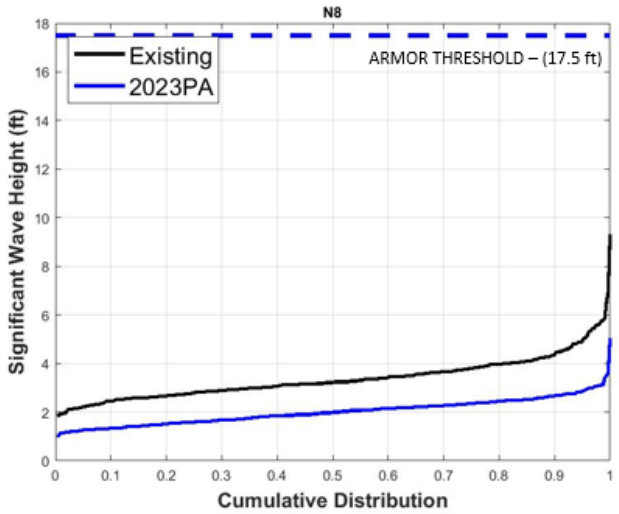

Figure A-43: Cumulative Distribution Wave Plot at N8

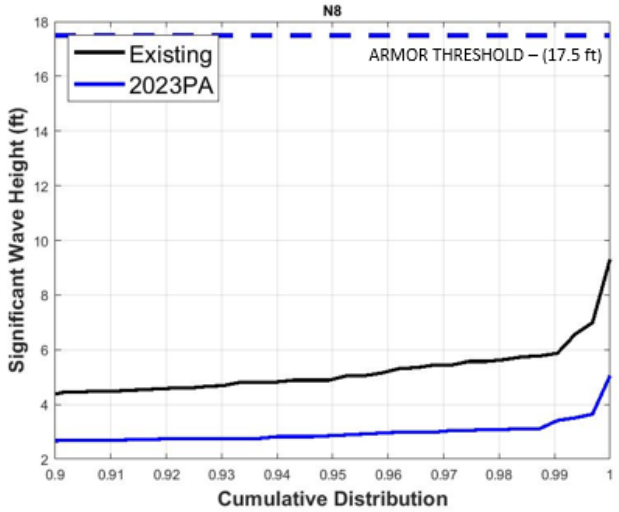

Figure A-44: Cumulative Distribution Wave Plot at N8 (Largest 10% of Waves)

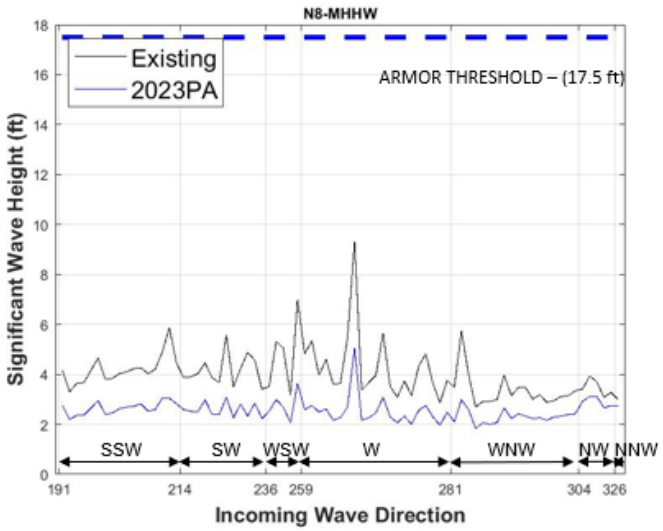

Figure A-45: Wave Direction Plot for Waves at MHHW at N8

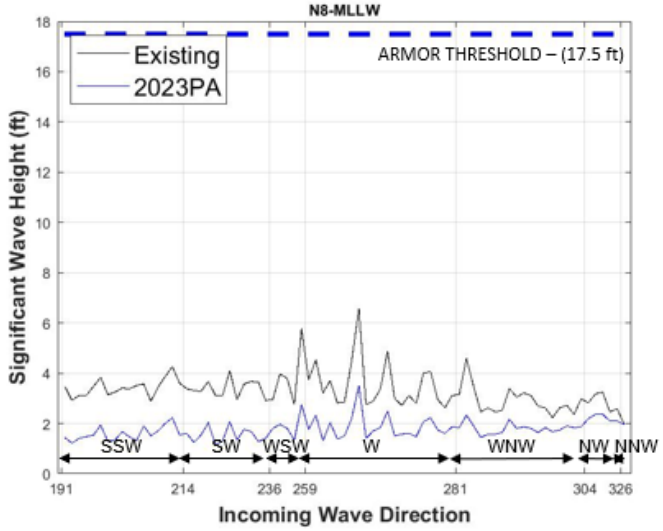

Figure A-46: Wave Direction Plot for Waves MLLW at N8

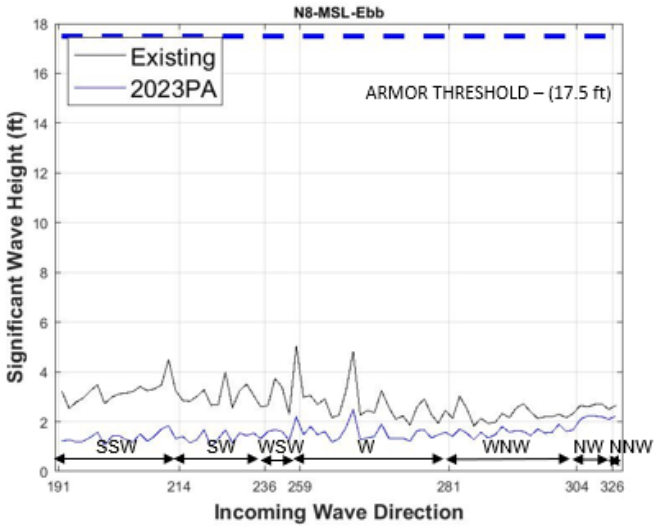

Figure A-47: Wave Direction Plot for Waves at MSL-Ebb at N8

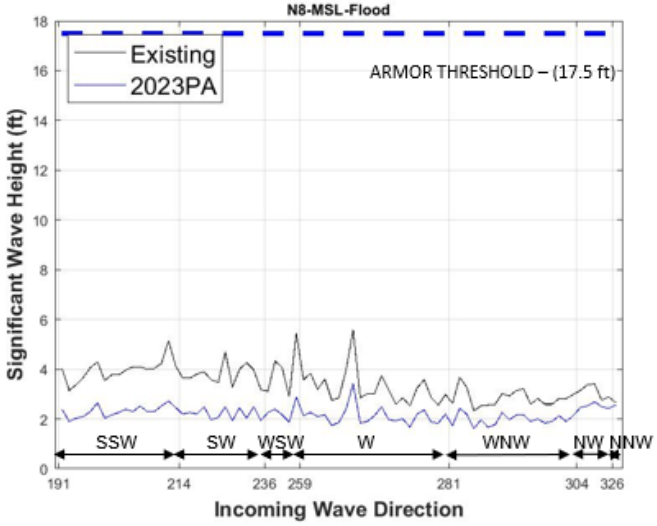

Figure A-48: Wave Direction Plot for Waves at MSL-Flood at N8

A.9 WAVE PLOTS AT N9

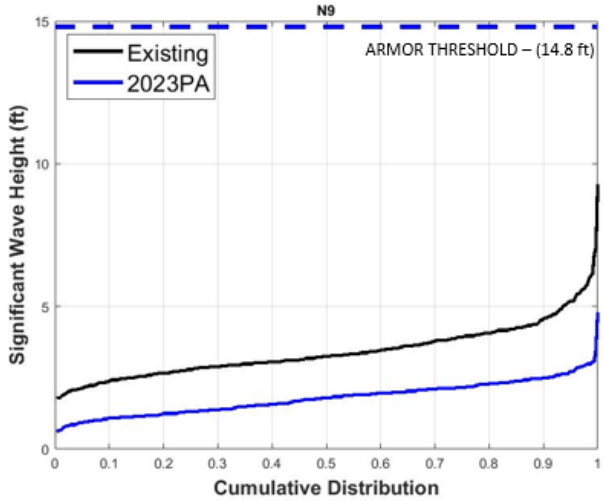

Figure A-49: Cumulative Distribution Wave Plot at N9

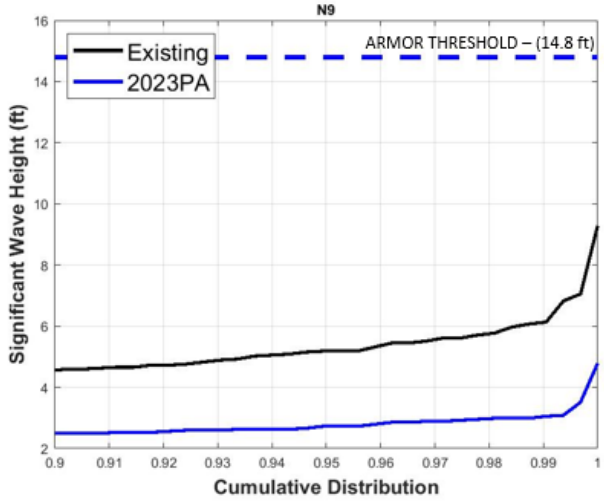

Figure A-50: Cumulative Distribution Wave Plot at N9 (Largest 10% of Waves)

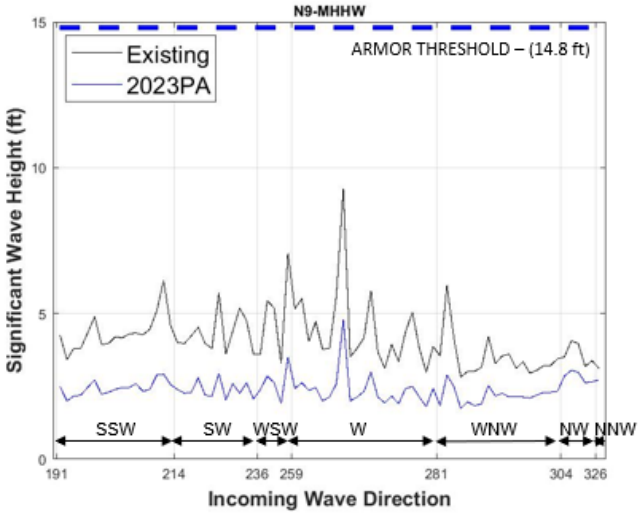

Figure A-51: Wave Direction Plot for Waves at MHHW at N9

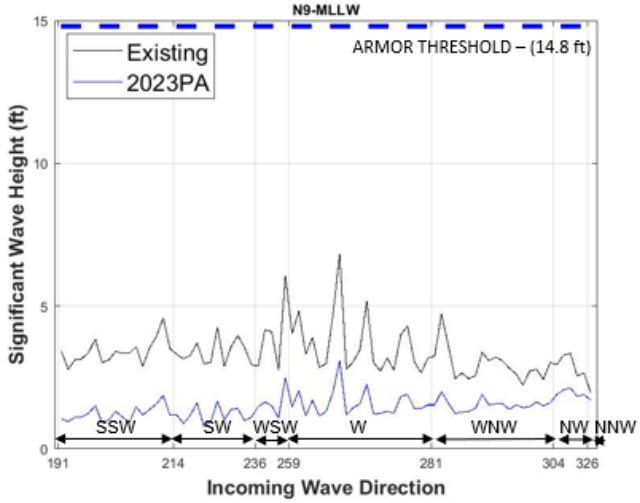

Figure A-52: Wave Direction Plot for Waves MLLW at N9

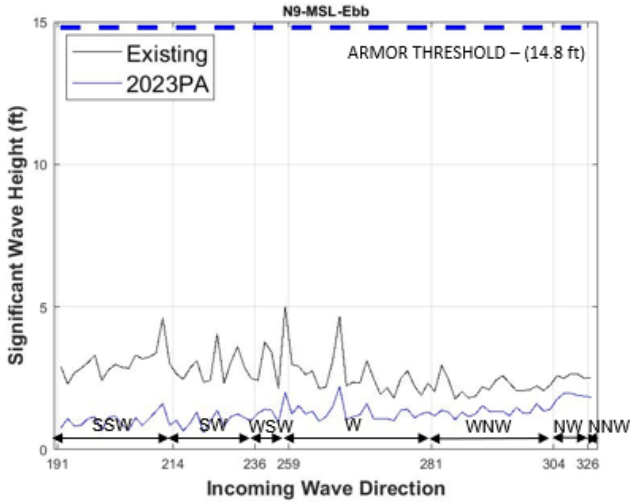

Figure A-53: Wave Direction Plot for Waves at MSL-Ebb at N9

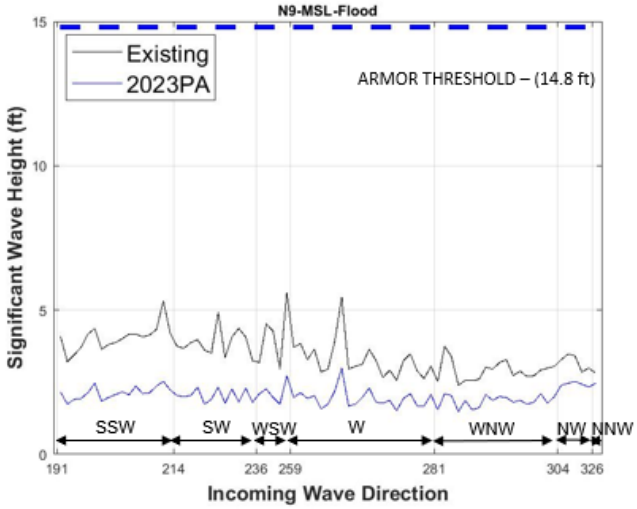

Figure A-54: Wave Direction Plot for Waves at MSL-Flood at N9

A.10 WAVE PLOTS AT N10

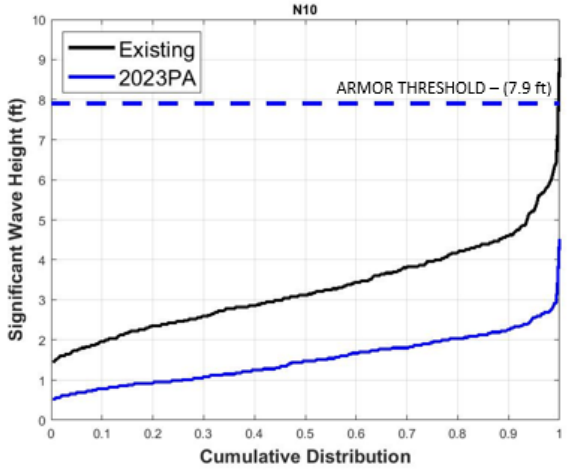

Figure A-55: Cumulative Distribution Wave Plot at N10

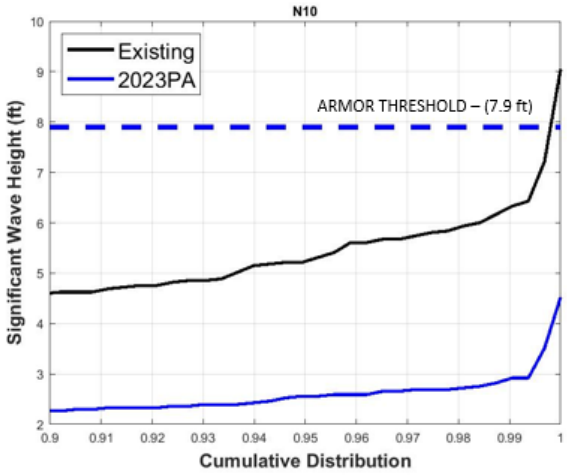

Figure A-56: Cumulative Distribution Wave Plot at N10 (Largest 10% of Waves)

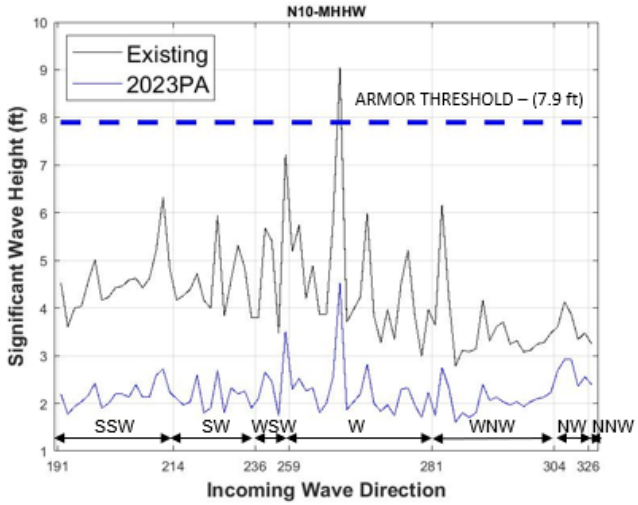

Figure A-57: Wave Direction Plot for Waves at MHHW at N10

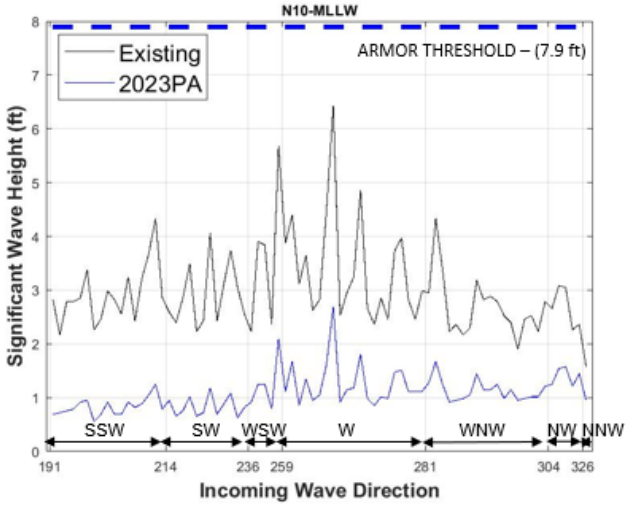

Figure A-58: Wave Direction Plot for Waves MLLW at N10

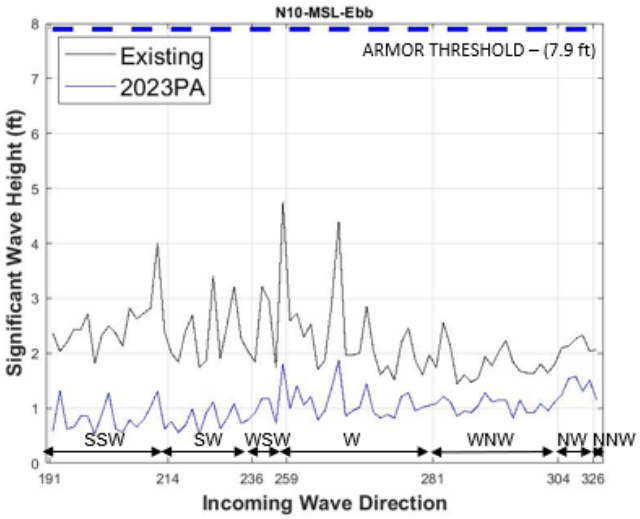

Figure A-59: Wave Direction Plot for Waves at MSL-Ebb at N10

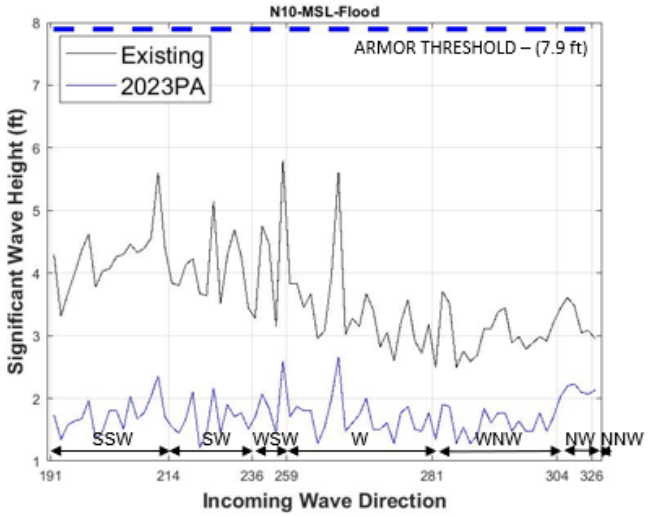

Figure A-60: Wave Direction Plot for Waves at MSL-Flood at N10

A.11 WAVE PLOTS AT N11

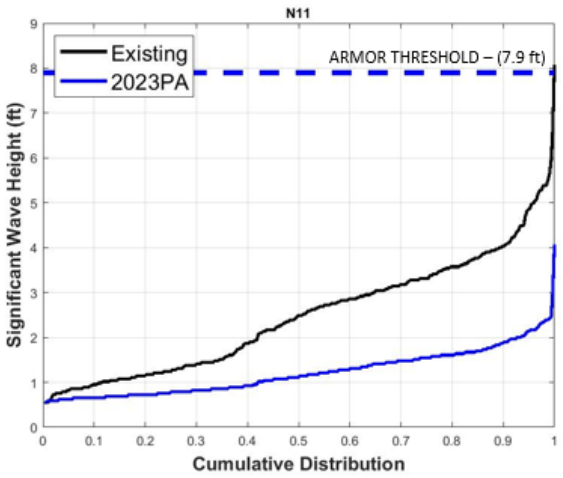

Figure A-61: Cumulative Distribution Wave Plot at N11

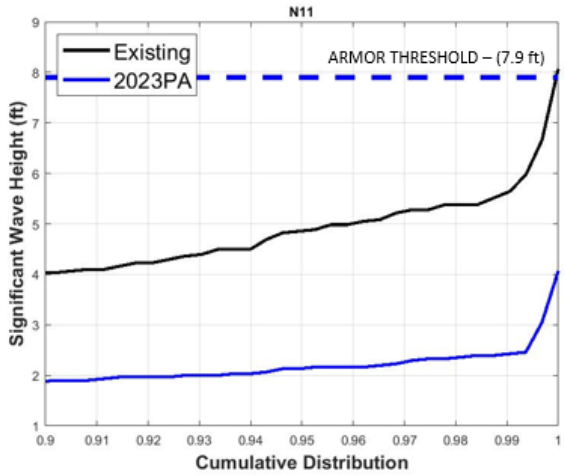

Figure A-62: Cumulative Distribution Wave Plot at N11 (Largest 10% of Waves)

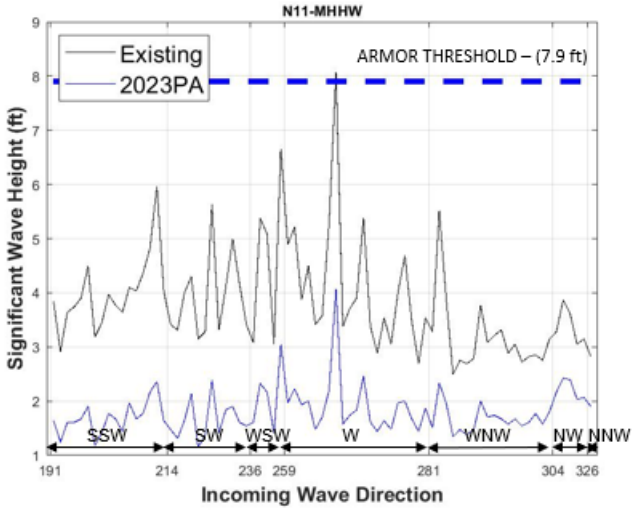

Figure A-63: Wave Direction Plot for Waves at MHHW at N11

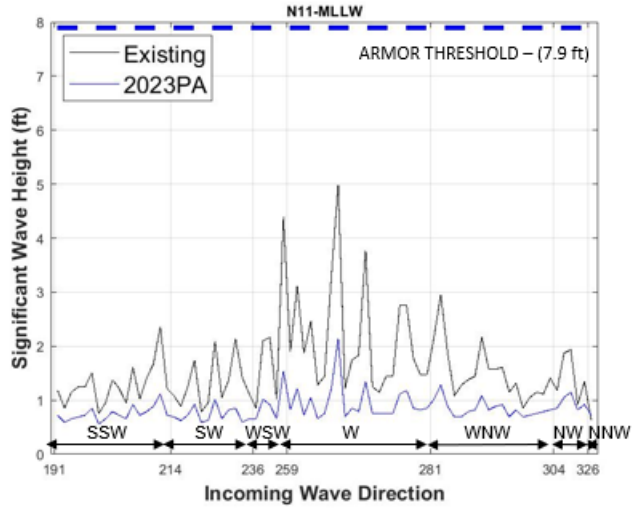

Figure A-64: Wave Direction Plot for Waves MLLW at N11

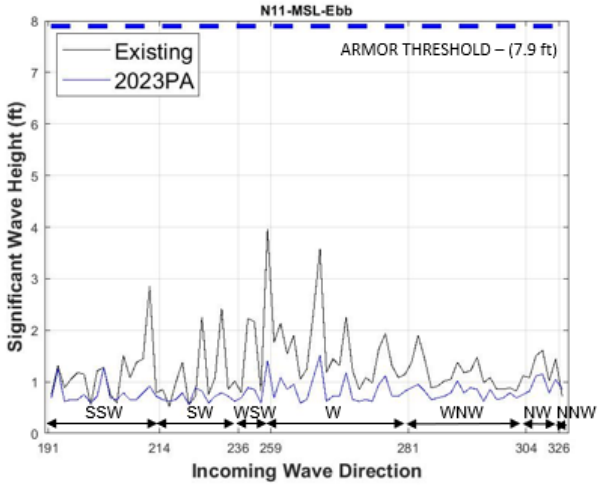

Figure A-65: Wave Direction Plot for Waves at MSL-Ebb at N11

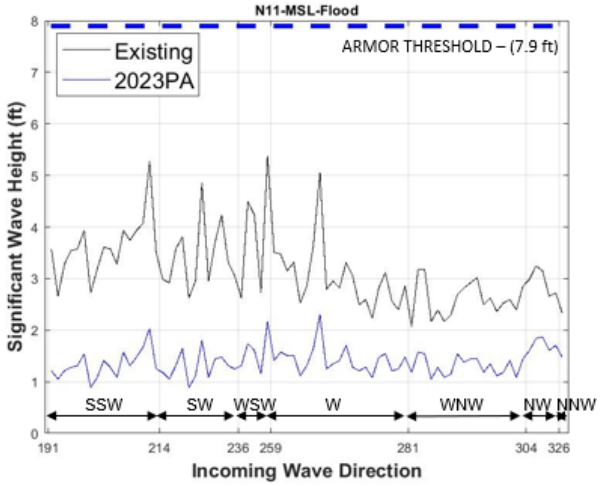

Figure A-66: Wave Direction Plot for Waves at MSL-Flood at N11

A.12 WAVE PLOTS AT N12

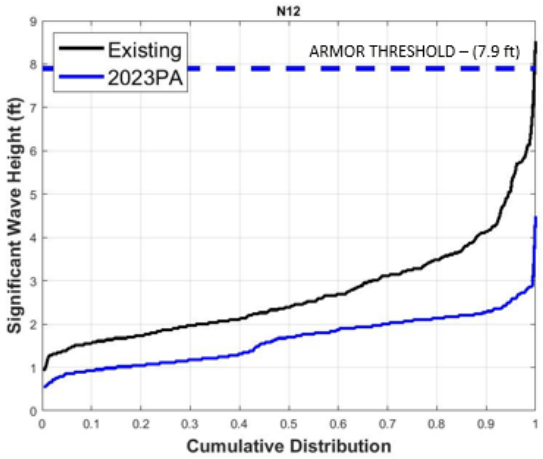

Figure A-67: Cumulative Distribution Wave Plot at N12

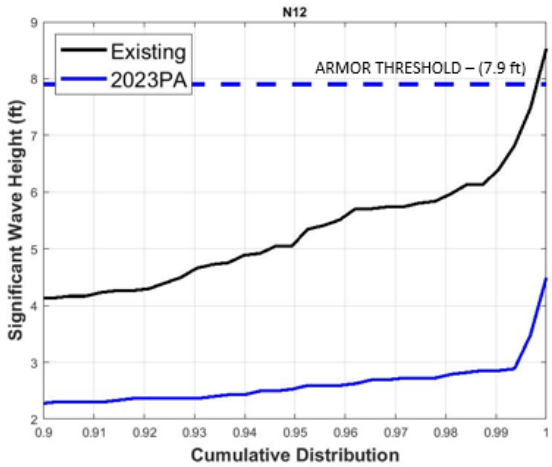

Figure A-68: Cumulative Distribution Wave Plot at N12 (Largest 10% of Waves)

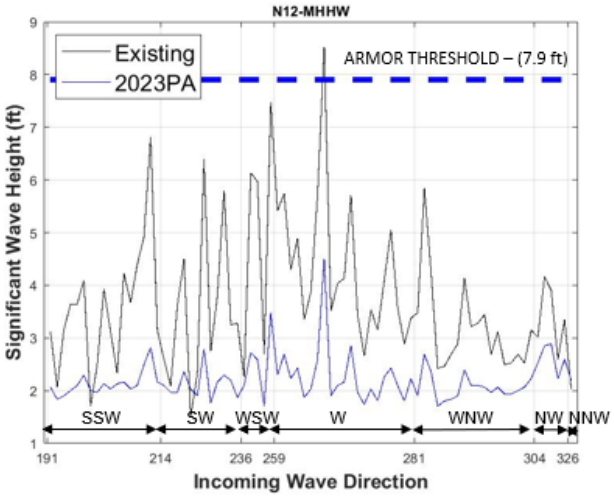

Figure A-69: Wave Direction Plot for Waves at MHHW at N12

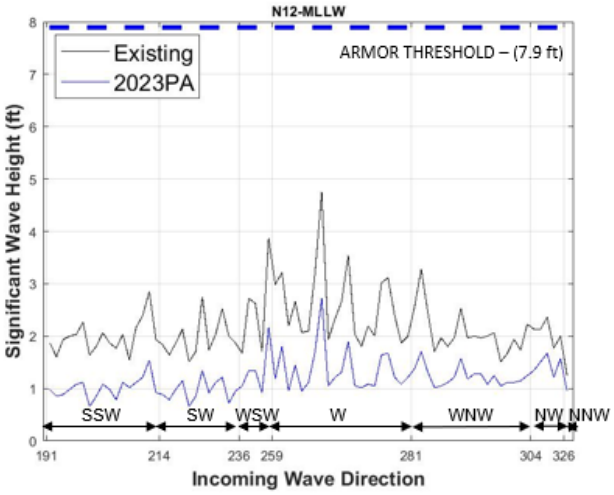

Figure A-70: Wave Direction Plot for Waves MLLW at N12

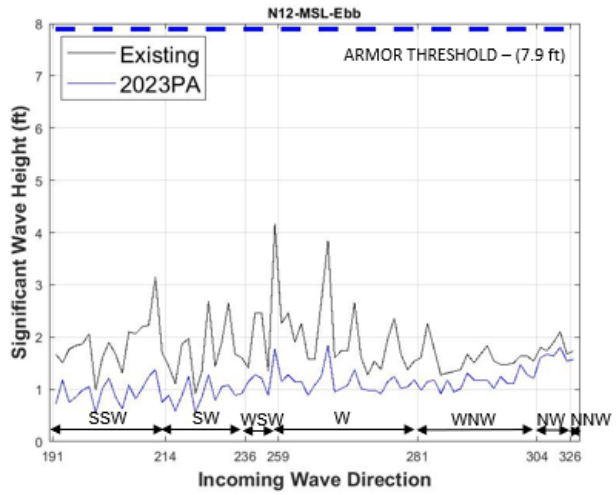

Figure A-71: Wave Direction Plot for Waves at MSL-Ebb at N12

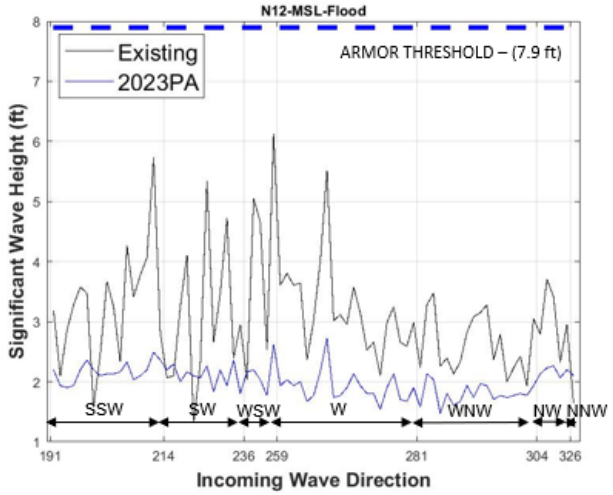

Figure A-72: Wave Direction Plot for Waves at MSL-Flood at N12

A.13 WAVE PLOTS AT N13

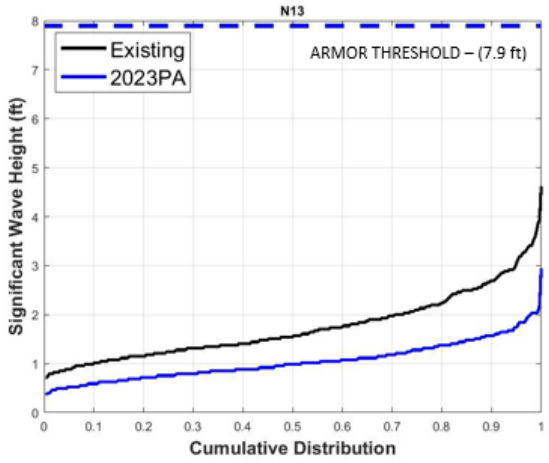

Figure A-73: Cumulative Distribution Wave Plot at N13

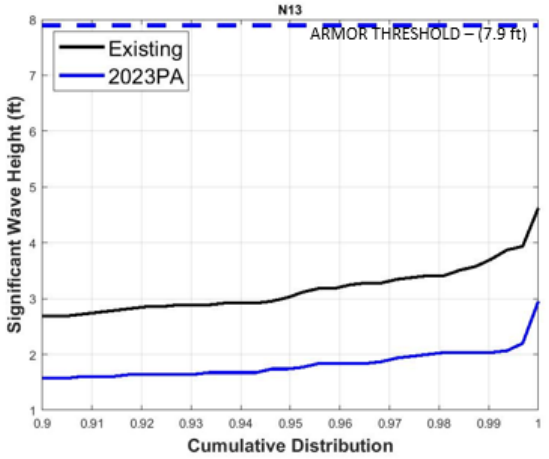

Figure A-74: Cumulative Distribution Wave Plot at N13 (Largest 10% of Waves)

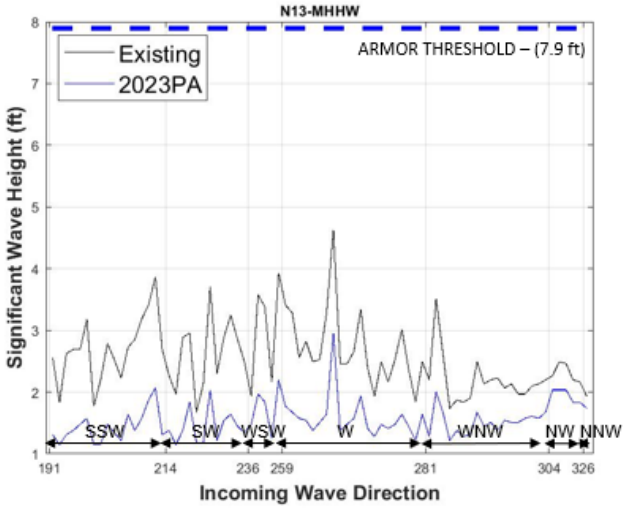

Figure A-75: Wave Direction Plot for Waves at MHHW at N13

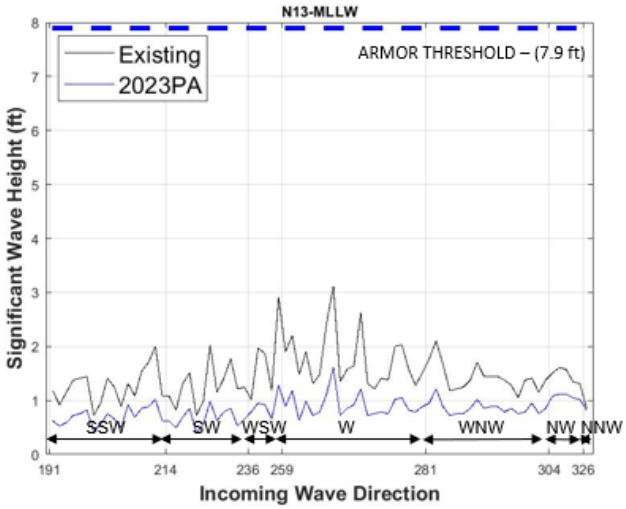

Figure A-76: Wave Direction Plot for Waves MLLW at N13

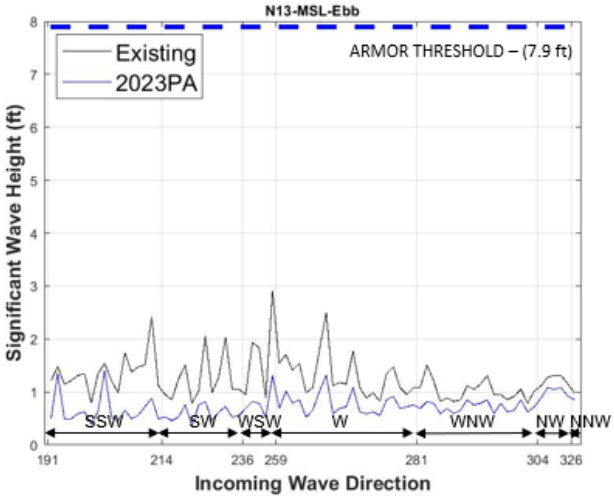

Figure A-77: Wave Direction Plot for Waves at MSL-Ebb at N13

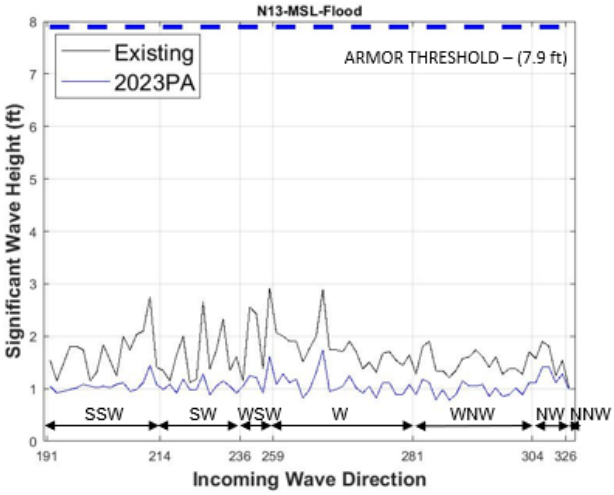

Figure A-78: Wave Direction Plot for Waves at MSL-Flood at N13

A.14 WAVE PLOTS AT N14

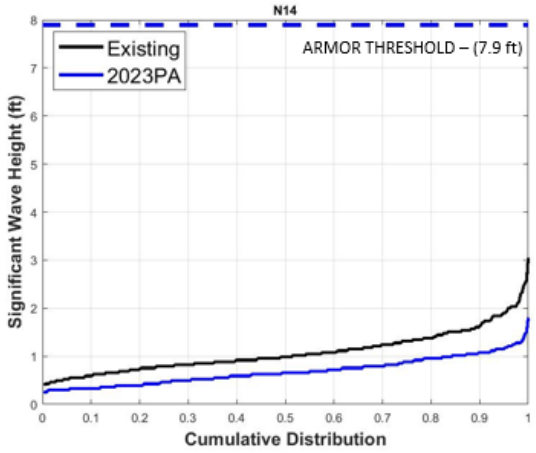

Figure A-79: Cumulative Distribution Wave Plot at N14

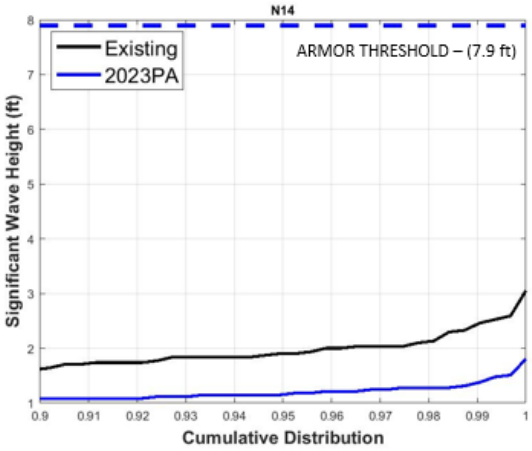

Figure A-80: Cumulative Distribution Wave Plot at N14 (Largest 10% of Waves)

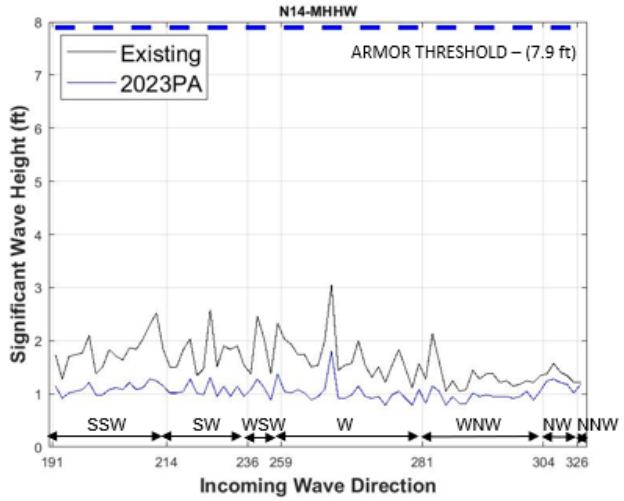

Figure A-81: Wave Direction Plot for Waves at MHHW at N14

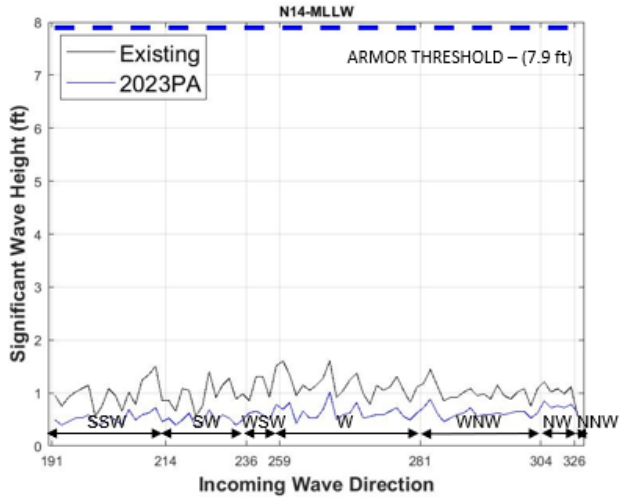

Figure A-82: Wave Direction Plot for Waves MLLW at N14

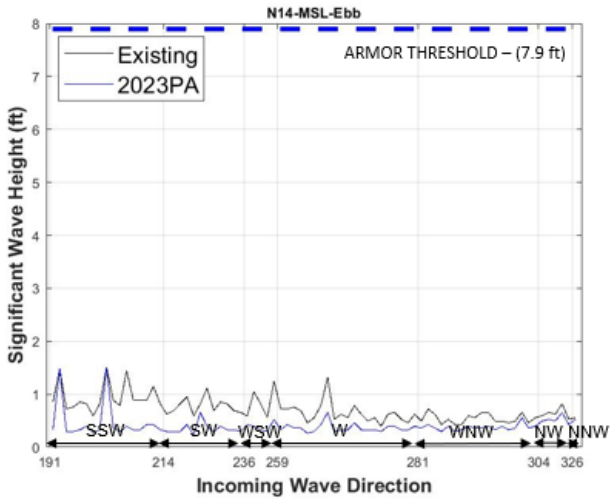

Figure A-83: Wave Direction Plot for Waves at MSL-Ebb at N14

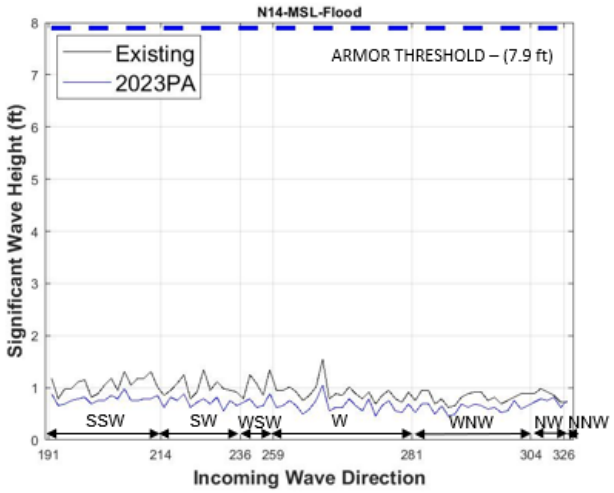

Figure A-84: Wave Direction Plot for Waves at MSL-Flood at N14

A.15 WAVE PLOTS AT N15

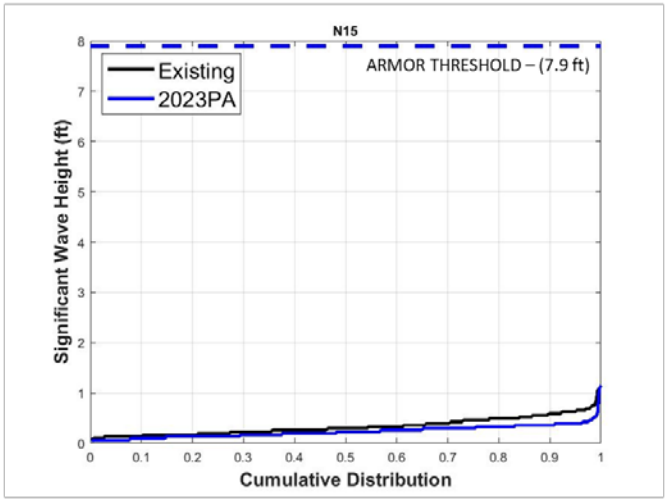

Figure A-85: Cumulative Distribution Wave Plot at N15

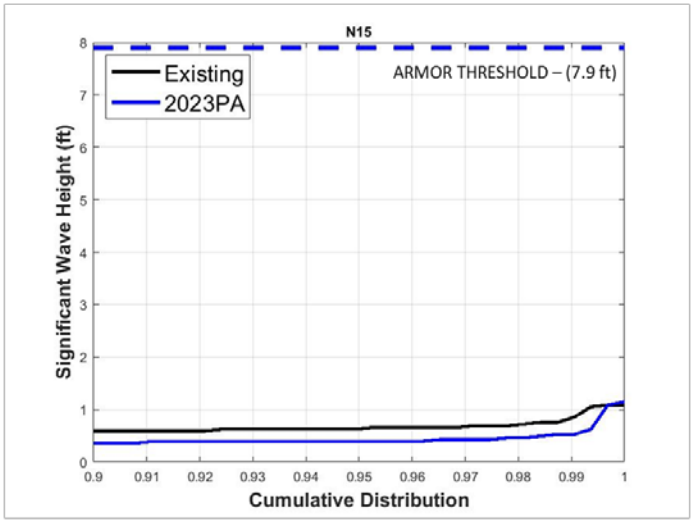

Figure A-86: Cumulative Distribution Wave Plot at N15 (Largest 10% of Waves)

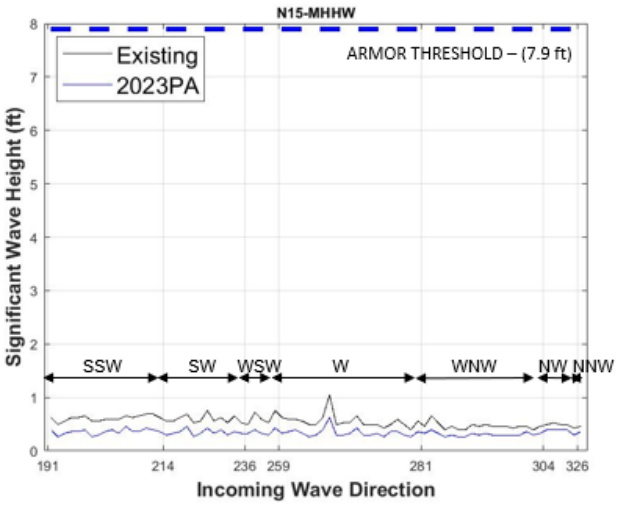

Figure A-87: Wave Direction Plot for Waves at MHHW at N15

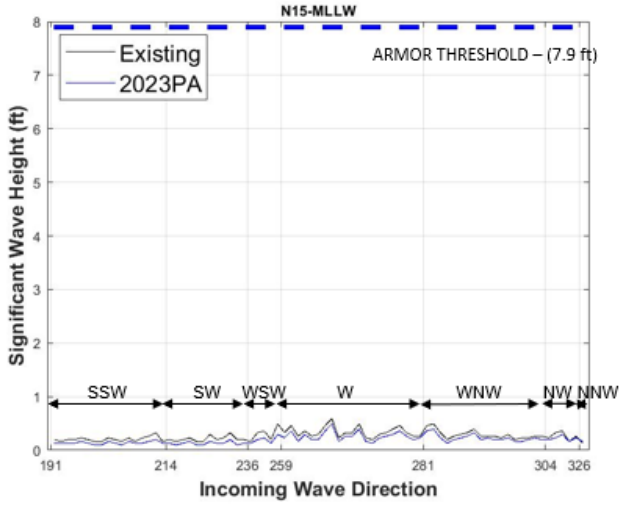

Figure A-88: Wave Direction Plot for Waves MLLW at N15

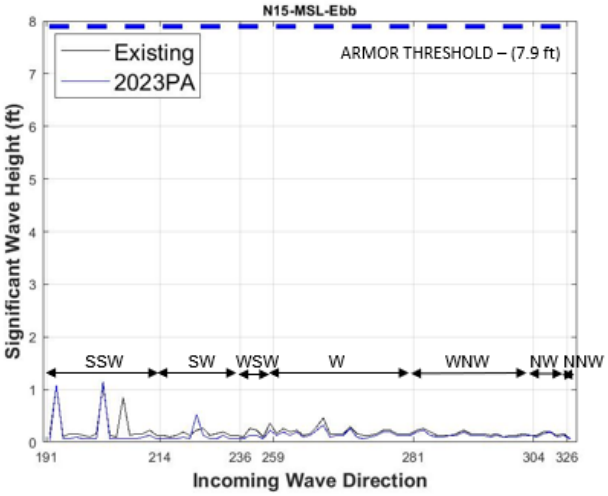

Figure A-89: Wave Direction Plot for Waves at MSL-Ebb at N15

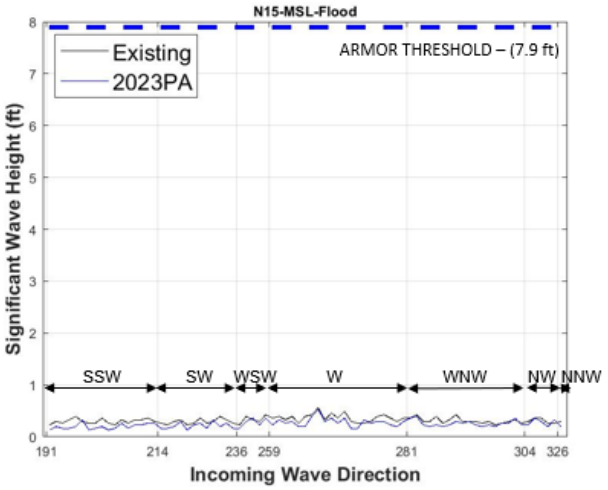

Figure A-90: Wave Direction Plot for Waves at MSL-Flood at N15

A.16 WAVE PLOTS AT S1

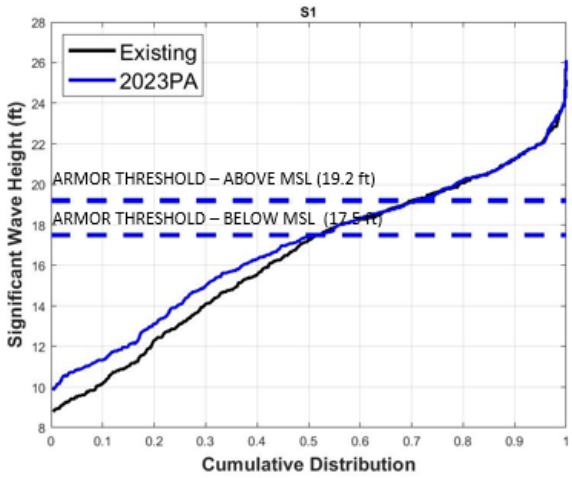

Figure A-91: Cumulative Distribution Wave Plot at S1

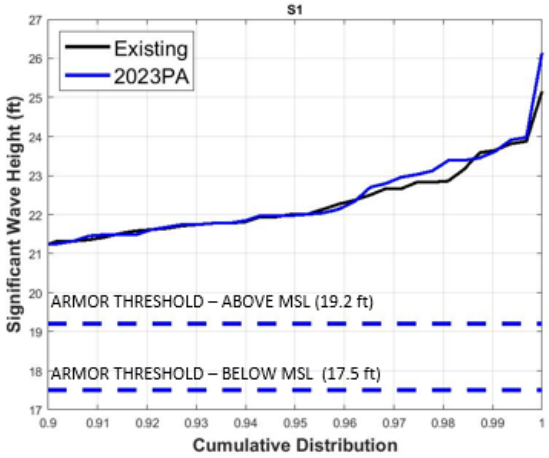

Figure A-92: Cumulative Distribution Wave Plot at S1 (Largest 10% of Waves)

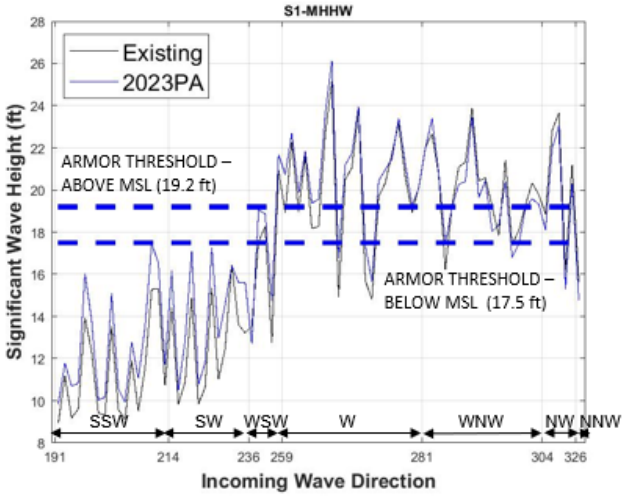

Figure A-93: Wave Direction Plot for Waves at MHHW at S1

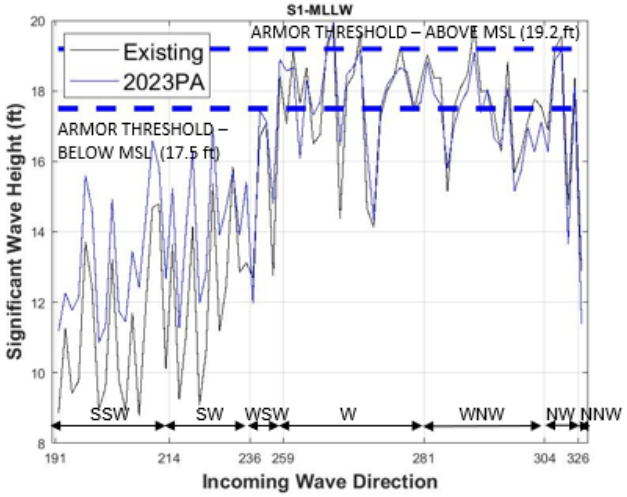

Figure A-94: Wave Direction Plot for Waves MLLW at S1

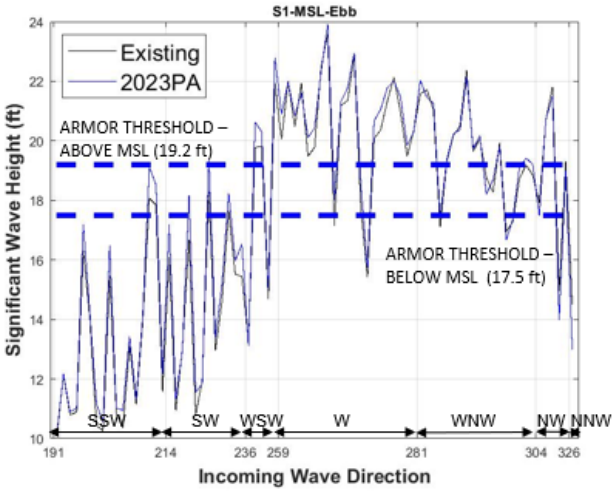

Figure A-95: Wave Direction Plot for Waves at MSL-Ebb at S1

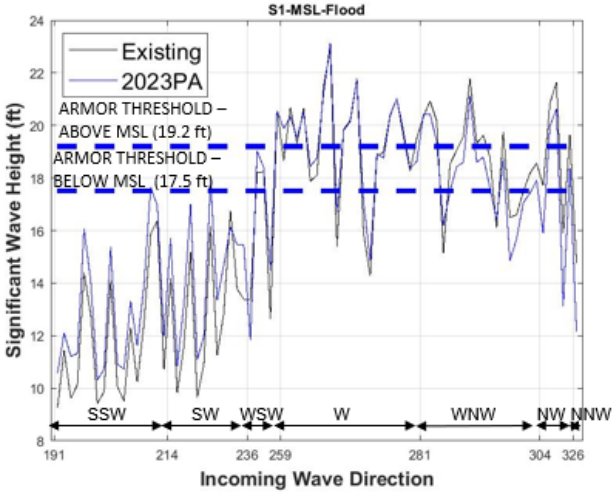

Figure A-96: Wave Direction Plot for Waves at MSL-Flood at S1

A.17 WAVE PLOTS AT S2

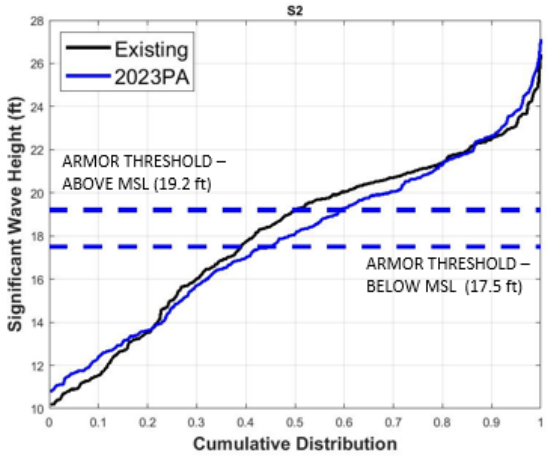

Figure A-97: Cumulative Distribution Wave Plot at S2

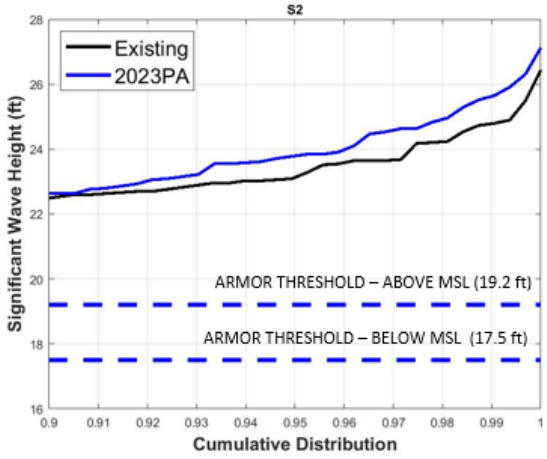

Figure A-98: Cumulative Distribution Wave Plot at S2 (Largest 10% of Waves)

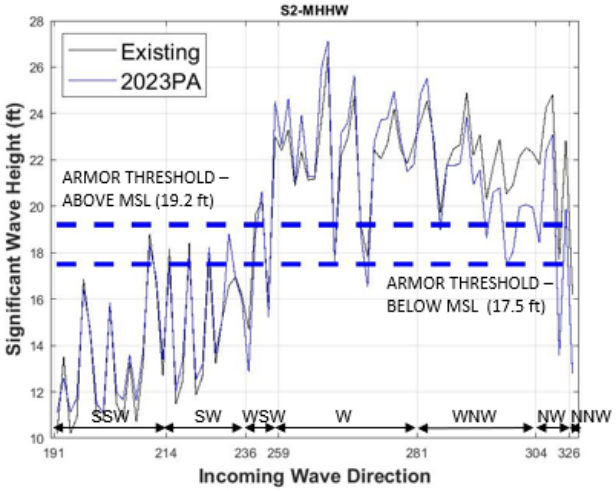

Figure A-99: Wave Direction Plot for Waves at MHHW at S2

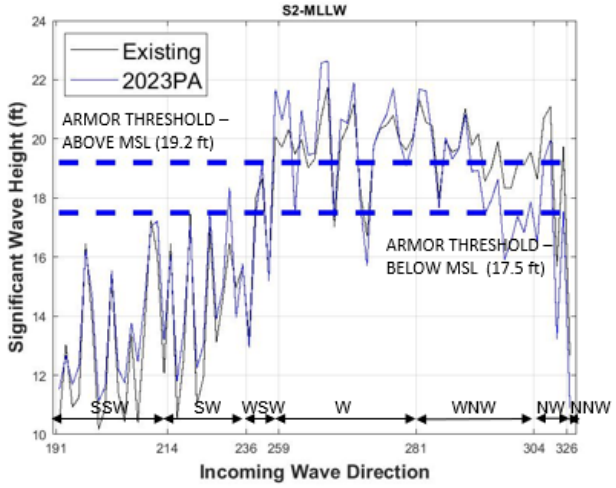

Figure A-100: Wave Direction Plot for Waves MLLW at S2

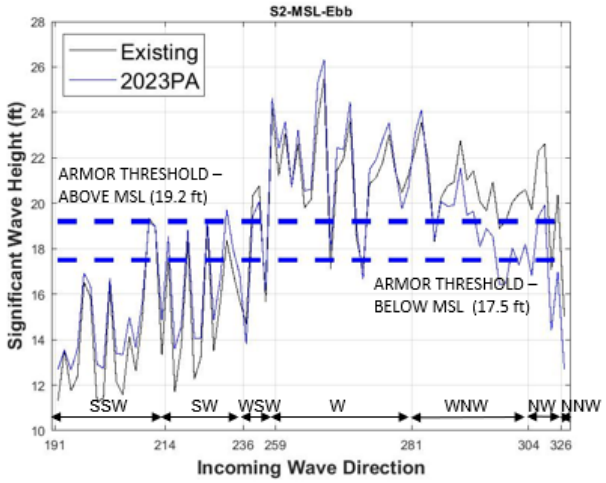

Figure A-101: Wave Direction Plot for Waves at MSL-Ebb at S2

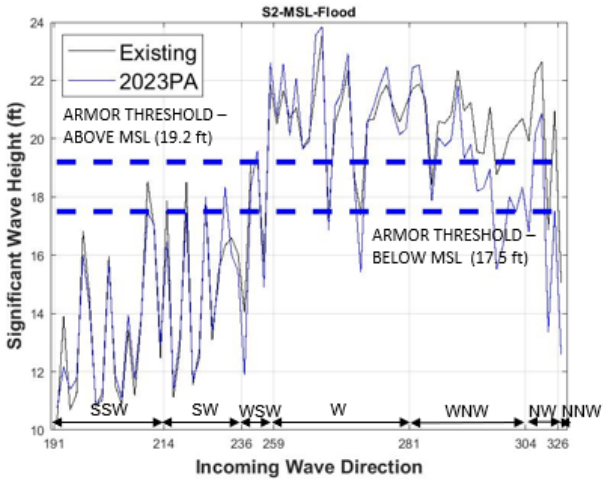

Figure A-102: Wave Direction Plot for Waves at MSL-Flood at S2

A.18 WAVE PLOTS AT S3

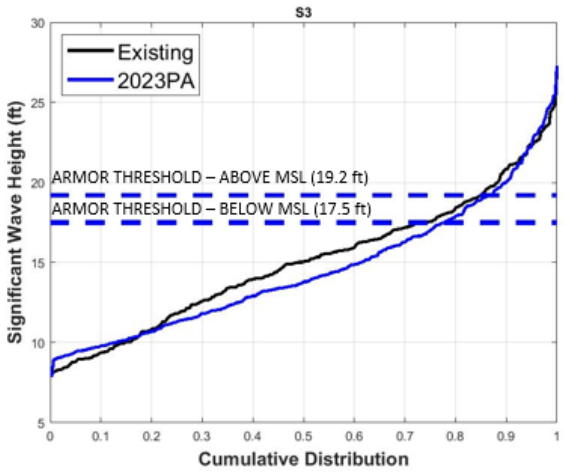

Figure A-103: Cumulative Distribution Wave Plot at S3

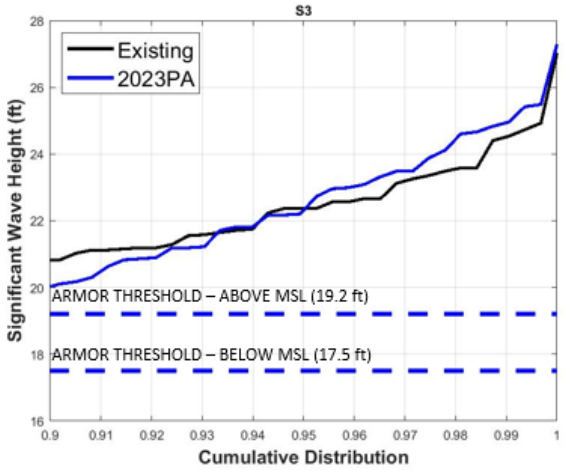

Figure A-104: Cumulative Distribution Wave Plot at S3 (Largest 10% of Waves)

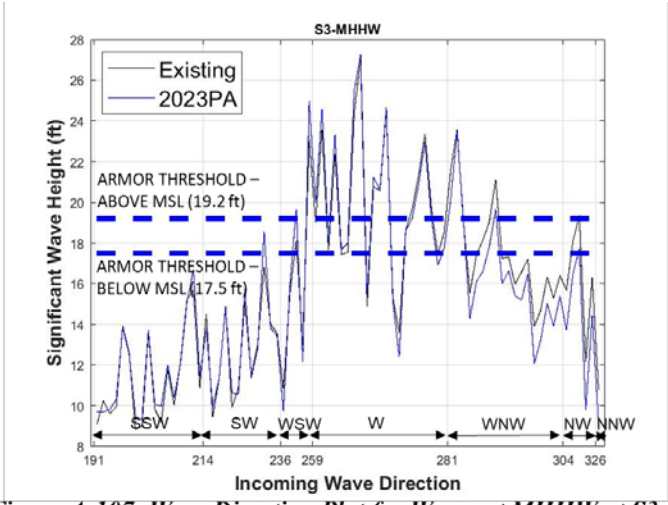

Figure A-107: Wave Direction Plot for Waves at MHHW at S3

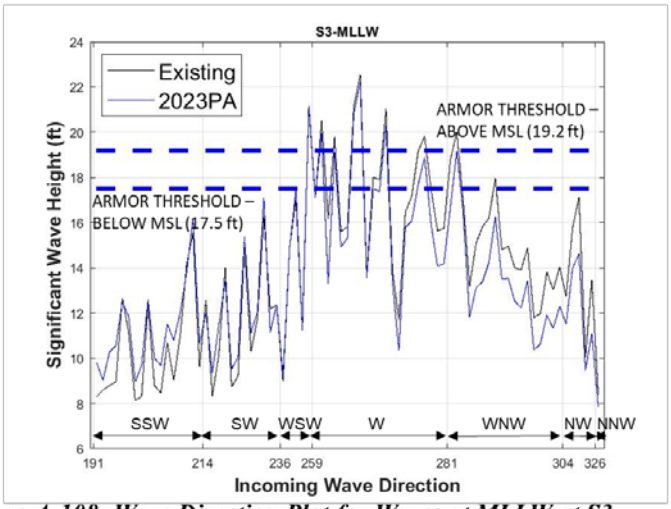

Figure A-108: Wave Direction Plot for Waves at MLLW at S3

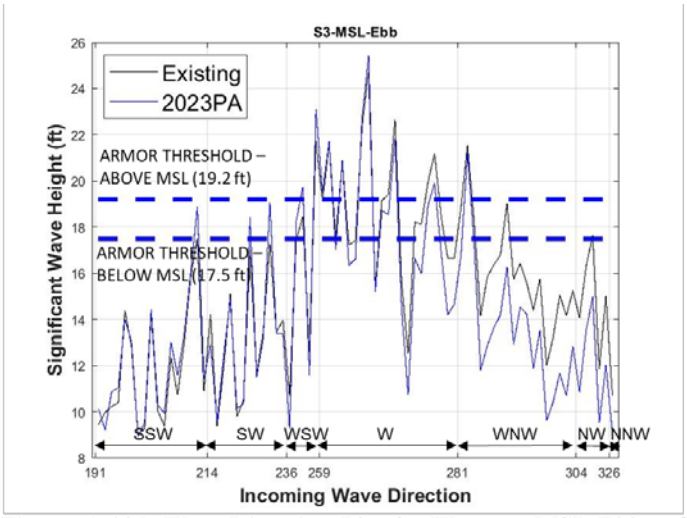

Figure A-105: Wave Direction Plot for Waves at MSL-Ebb at S3

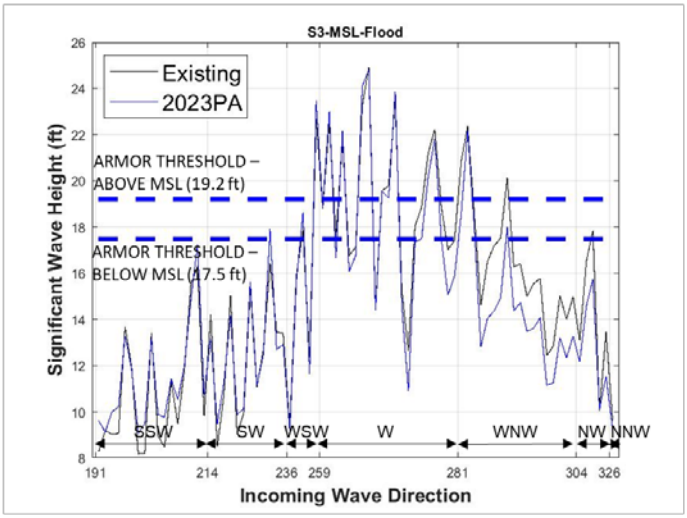

Figure A-106: Wave Direction Plot for Waves MSL-Flood at S3

A.19 WAVE PLOTS AT S4

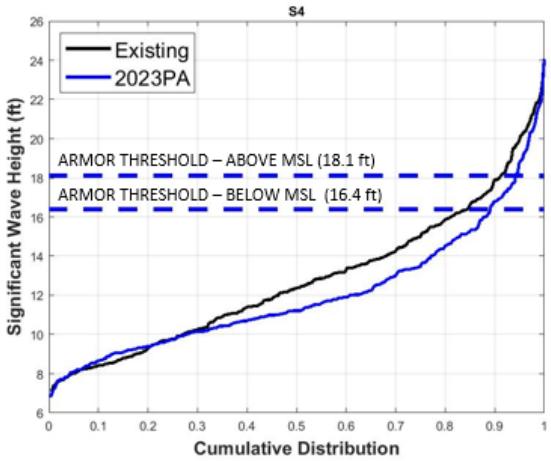

Figure A-109: Cumulative Distribution Wave Plot at S4

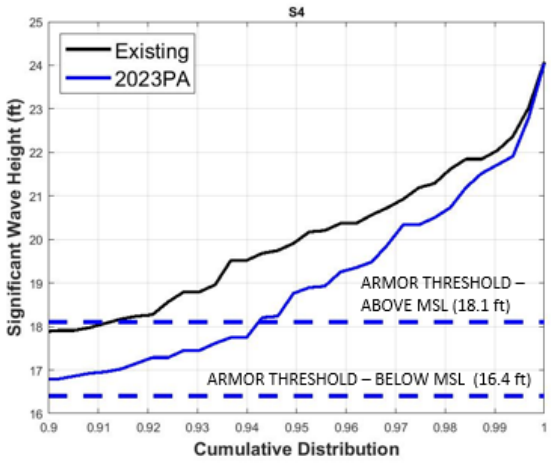

Figure A-110: Cumulative Distribution Wave Plot at S4 (Largest 10% of Waves)

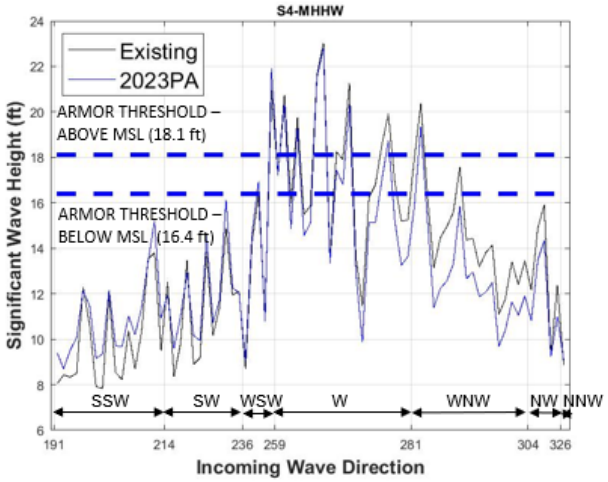

Figure A-111: Wave Direction Plot for Waves at MHHW at S4

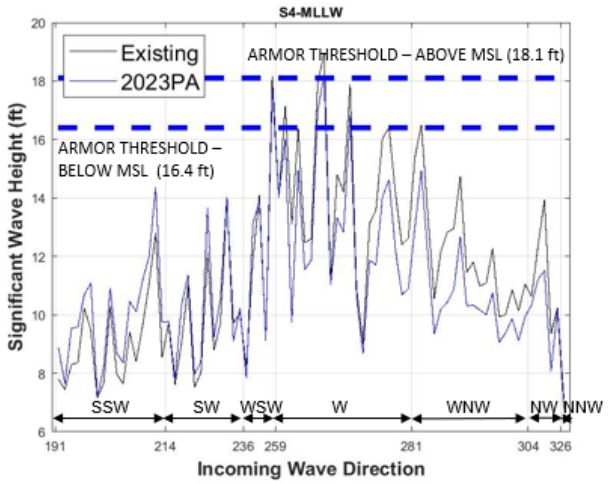

Figure A-112: Wave Direction Plot for Waves MLLW at S4

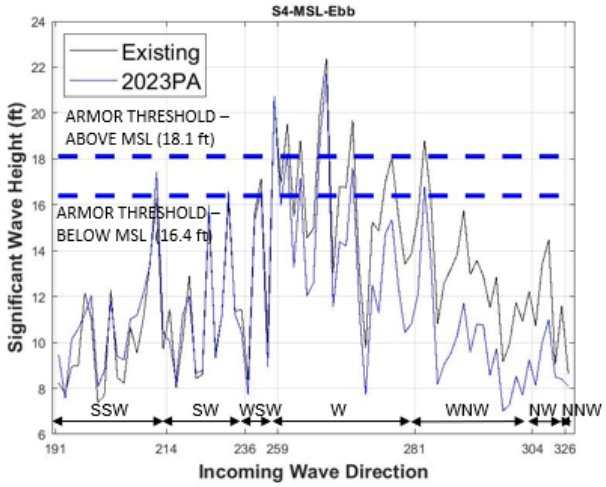

Figure A-113: Wave Direction Plot for Waves at MSL-Ebb at S4

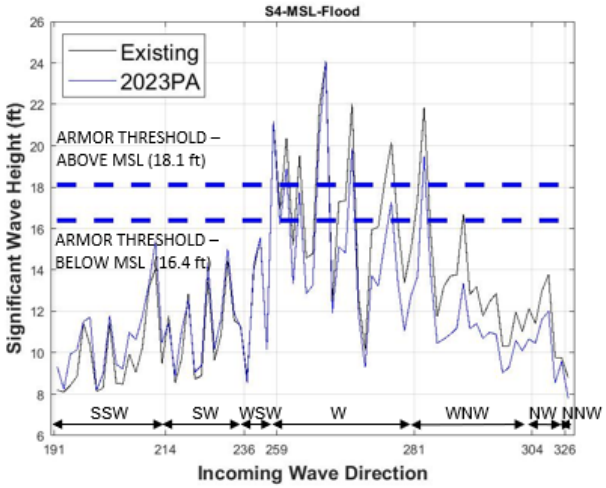

Figure A-114: Wave Direction Plot for Waves at MSL-Flood at S4

A.20 WAVE PLOTS AT S5

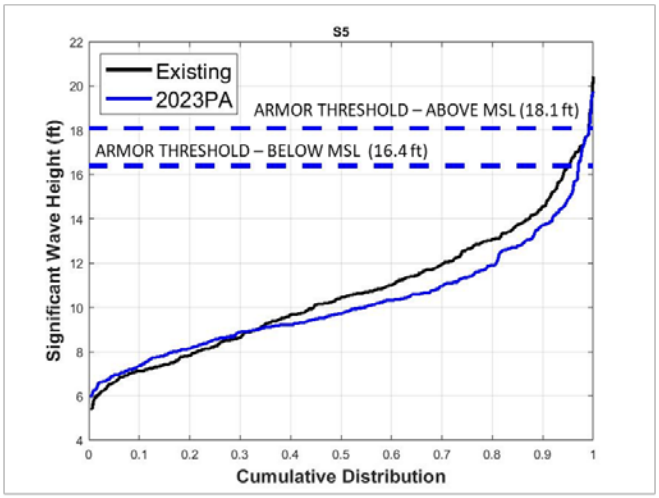

Figure A-115: Cumulative Distribution Wave Plot at S5

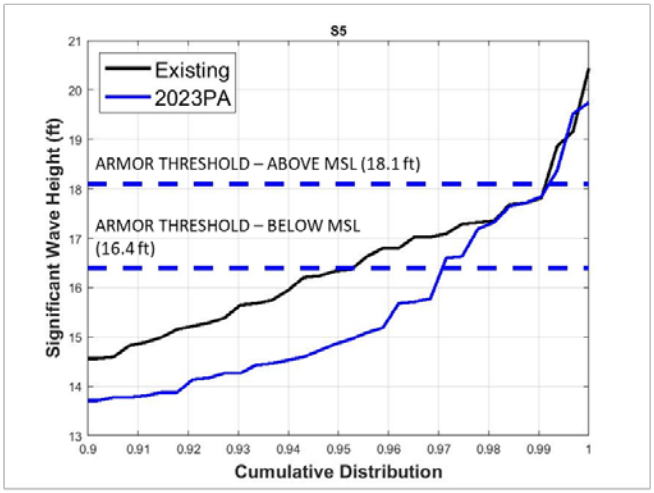

Figure A-116: Cumulative Distribution Wave Plot at S5 (Largest 10% of Waves)

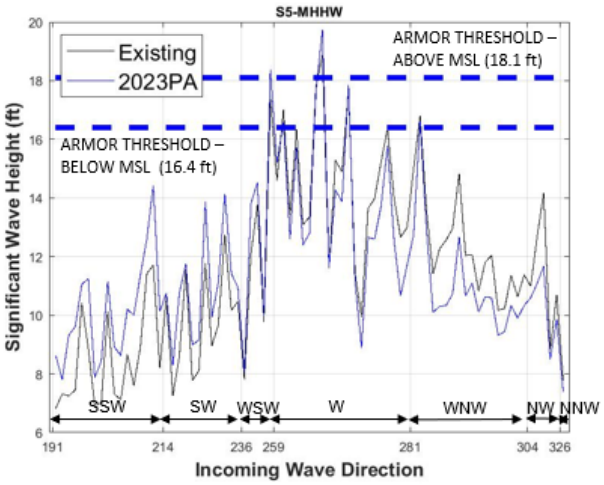

Figure A-117: Wave Direction Plot for Waves at MHHW at S5

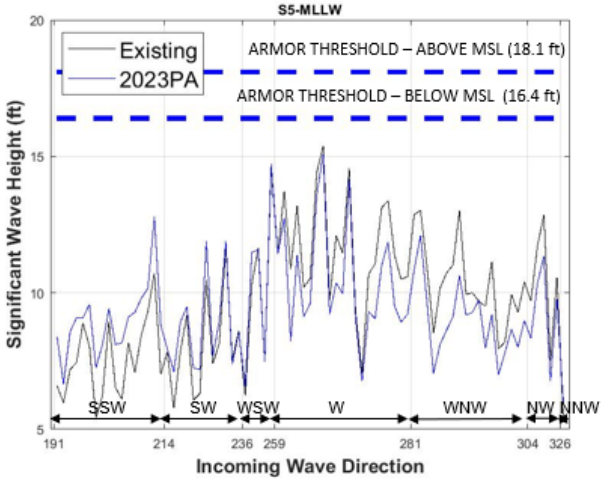

Figure A-118: Wave Direction Plot for Waves MLLW at S5

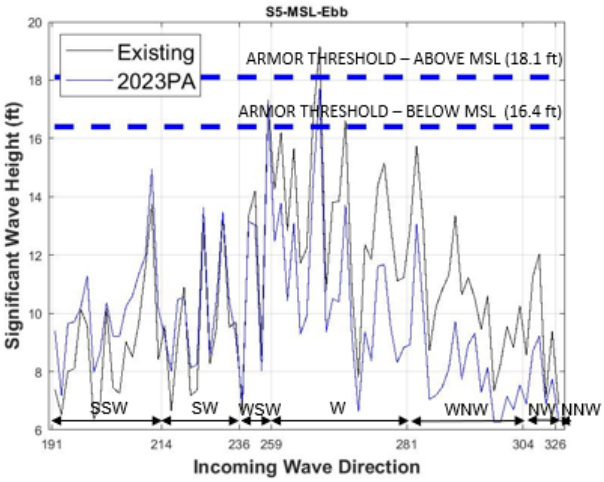

Figure A-119: Wave Direction Plot for Waves at MSL-Ebb at S5

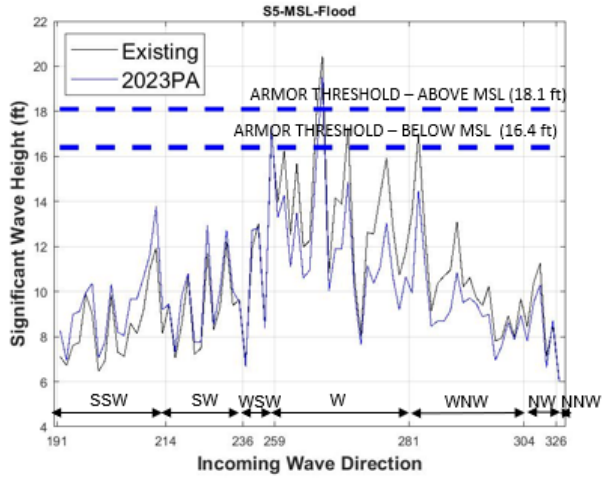

Figure A-120: Wave Direction Plot for Waves at MSL-Flood at S5

A.21 WAVE PLOTS AT S6

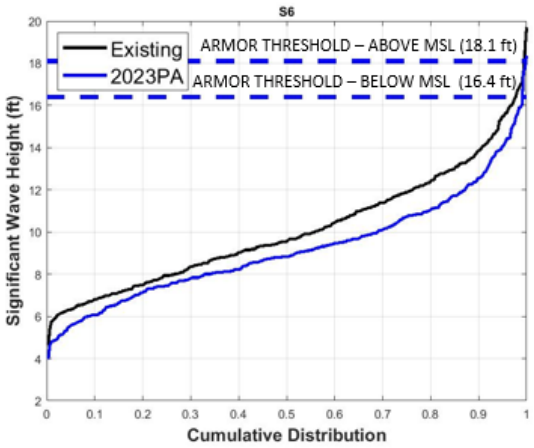

Figure A-121: Cumulative Distribution Wave Plot at S6

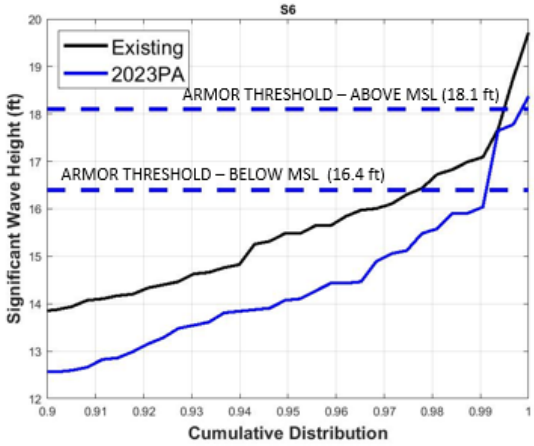

Figure A-122: Cumulative Distribution Wave Plot at S6 (Largest 10% of Waves)

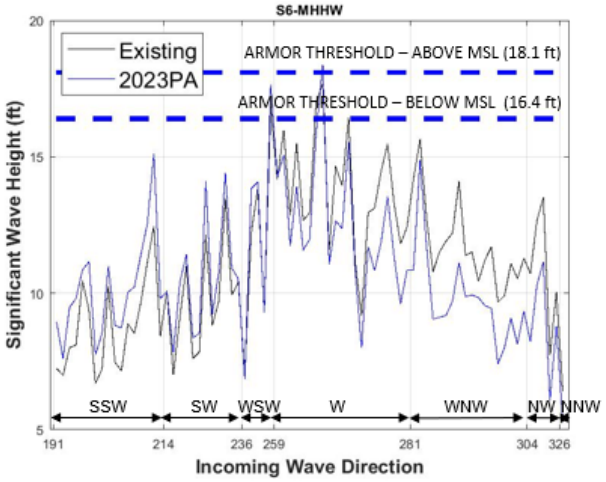

Figure A-123: Wave Direction Plot for Waves at MHHW at S6

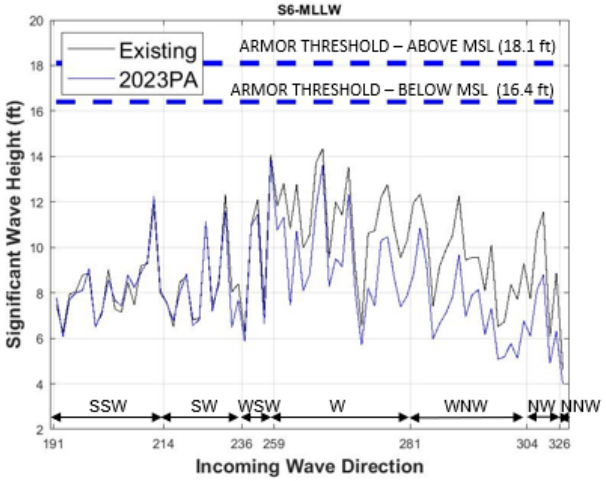

Figure A-124: Wave Direction Plot for Waves MLLW at S6

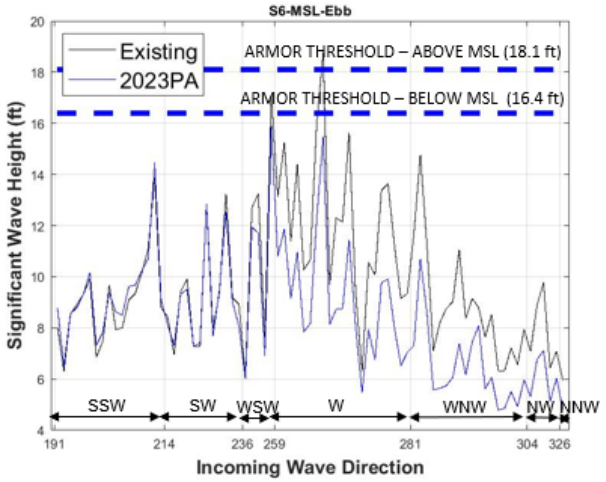

Figure A-125: Wave Direction Plot for Waves at MSL-Ebb at S6

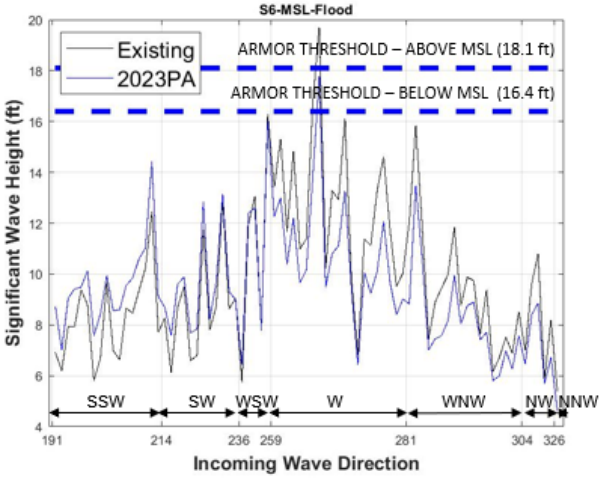

Figure A-126: Wave Direction Plot for Waves at MSL-Flood at S6

A.22 WAVE PLOTS AT S7

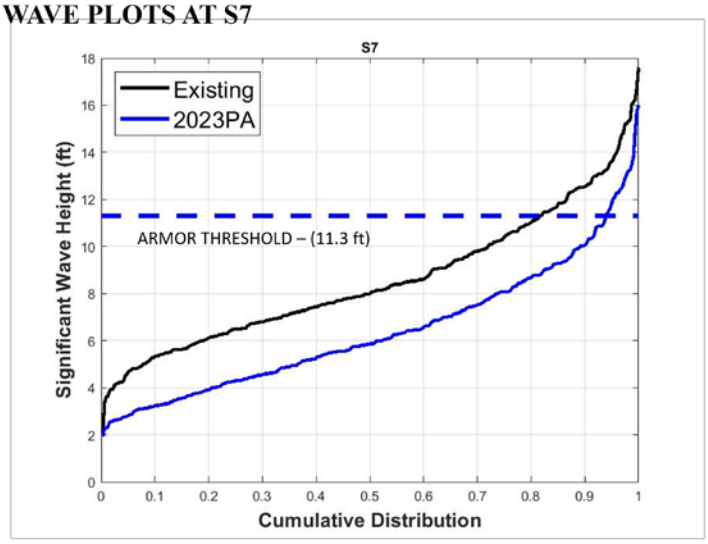

Figure A-127: Cumulative Distribution Wave Plot at S7

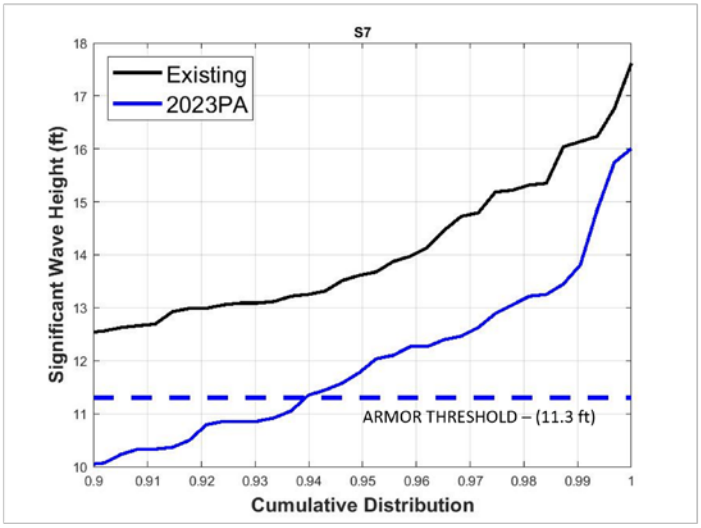

Figure A-128: Cumulative Distribution Wave Plot at S7 (Largest 10% of Waves)

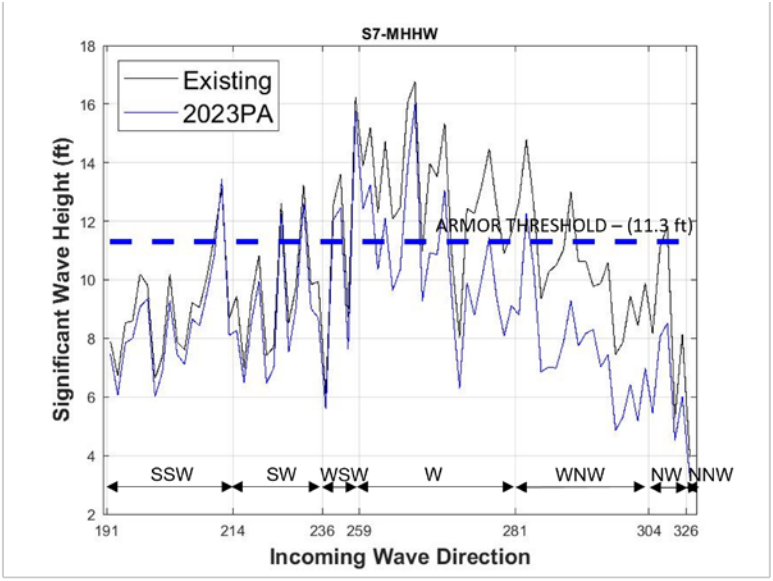

Figure A-129: Wave Direction Plot for Waves at MHHW at S7

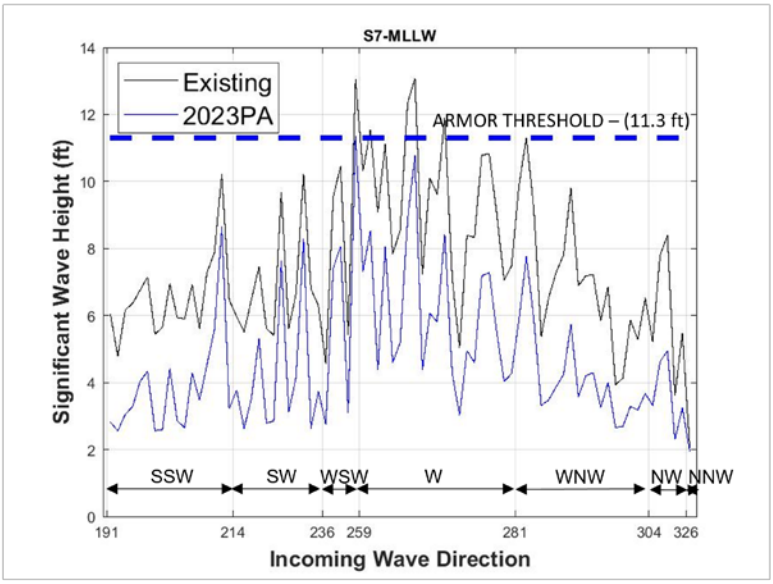

Figure A-130: Wave Direction Plot for Waves MLLW at S7

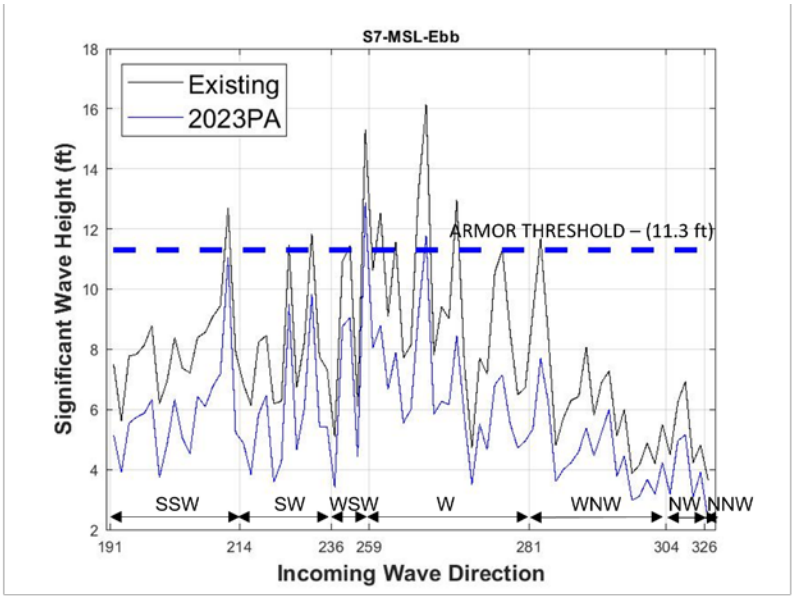

Figure A-131: Wave Direction Plot for Waves at MSL-Ebb at S7

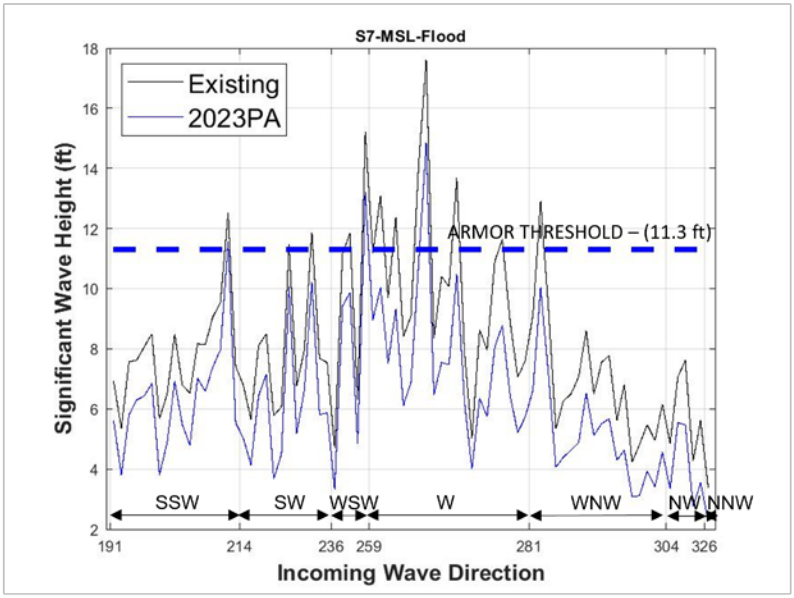

Figure A-132: Wave Direction Plot for Waves at MSL-Flood at S7

A.23 WAVE PLOTS AT S8

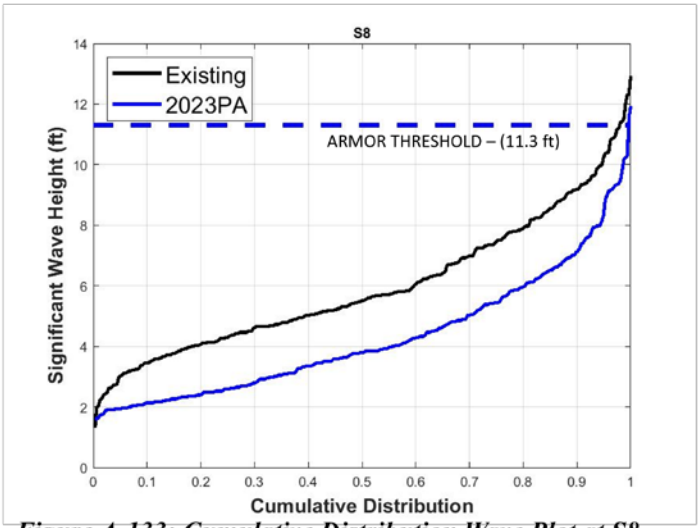

Figure A-133: Cumulative Distribution Wave Plot at S8

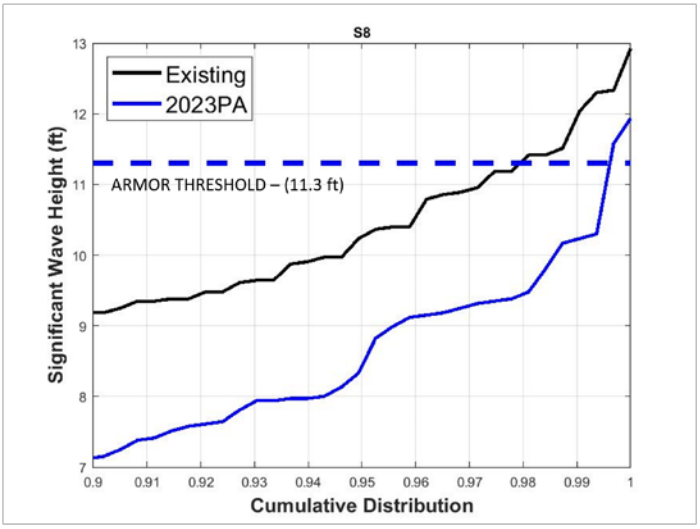

Figure A-134: Cumulative Distribution Wave Plot at S8 (Largest 10% of Waves)

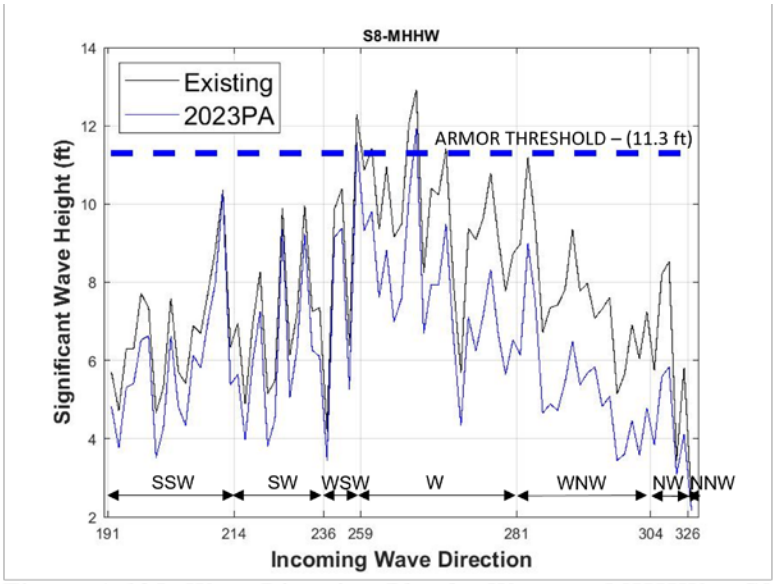

Figure A-135: Wave Direction Plot for Waves at MHHW at S8

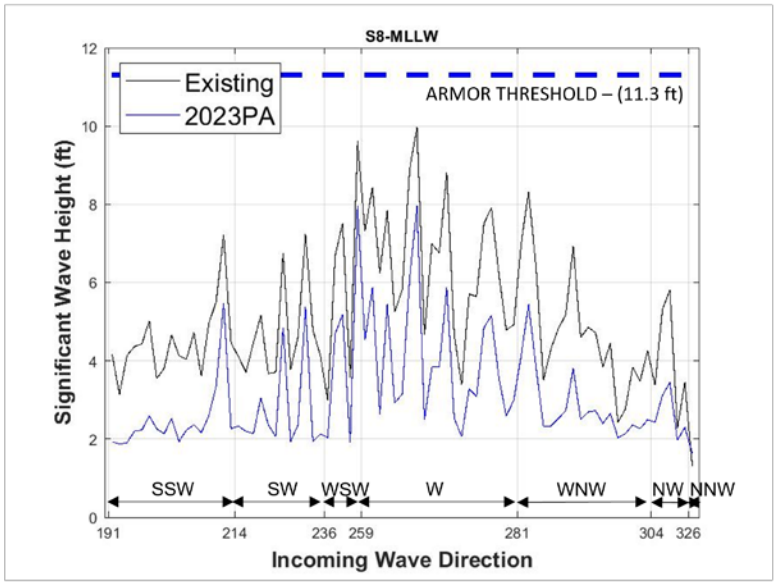

Figure A-136: Wave Direction Plot for Waves MLLW at S8

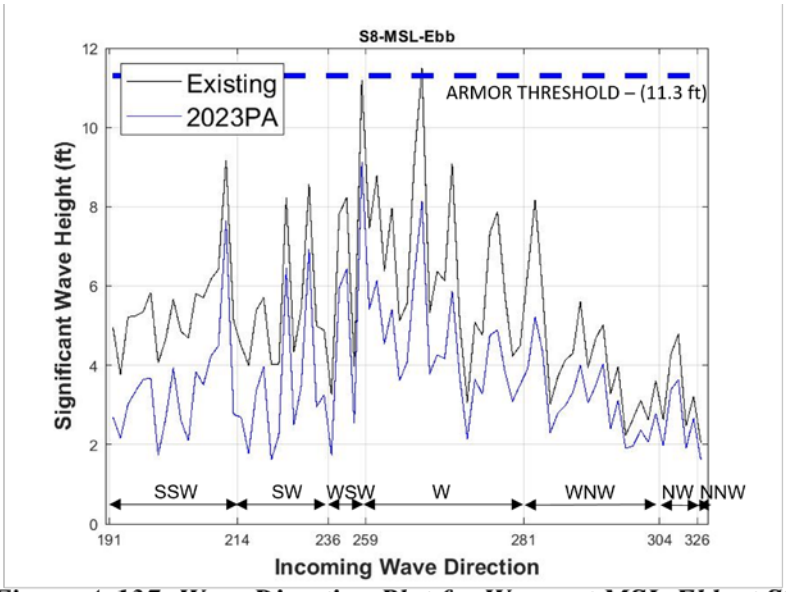

Figure A-137: Wave Direction Plot for Waves at MSL-Ebb at S8

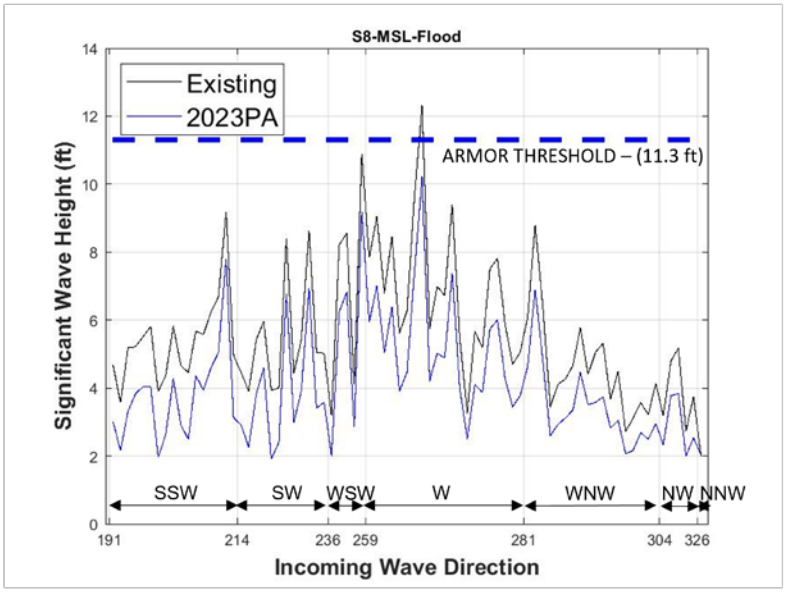

Figure A-138: Wave Direction Plot for Waves at MSL-Flood at S8

A.24 WAVE PLOTS AT C1

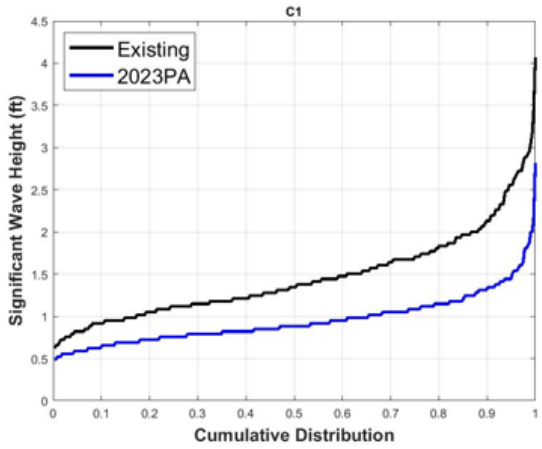

Figure A-139: Cumulative Distribution Wave Plot at C1

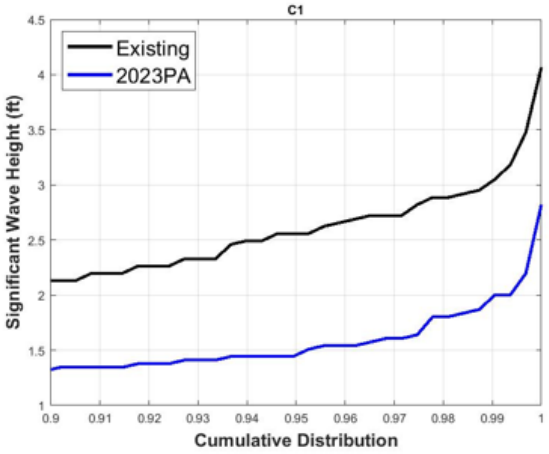

Figure A-140: Cumulative Distribution Wave Plot at C1 (Largest 10% of Waves)

A.25 WAVE PLOTS AT C2

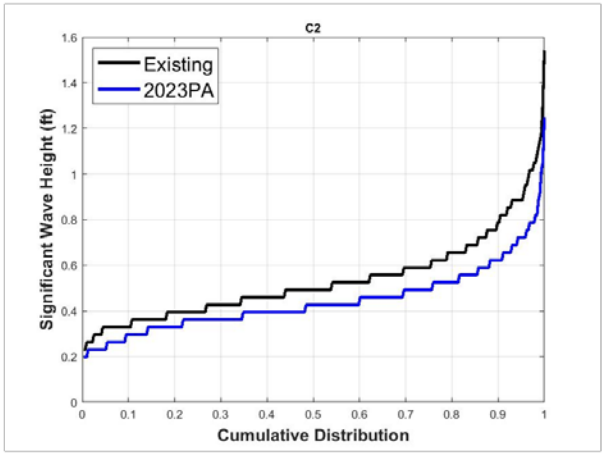

Figure A-141: Cumulative Distribution Wave Plot at C2

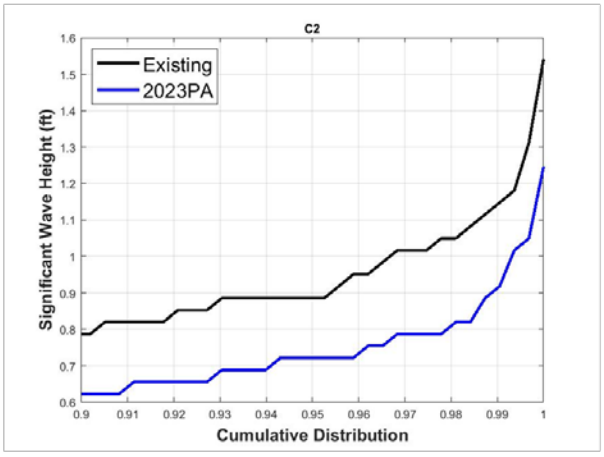

Figure A-142: Cumulative Distribution Wave Plot at C2 (Largest 10% of Waves)

A.26 WAVE PLOTS AT CM1

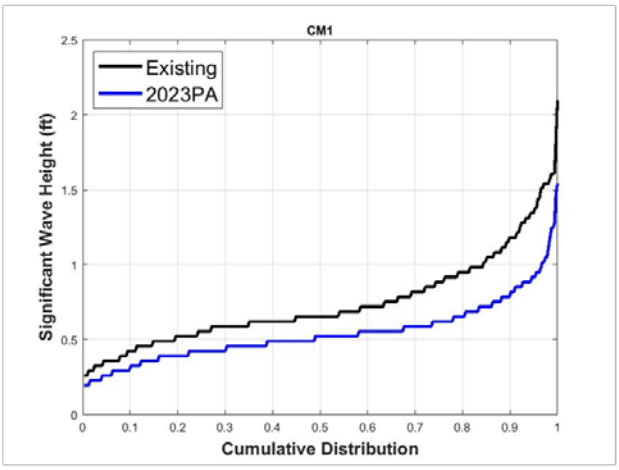

Figure A-143: Cumulative Distribution Wave Plot at CM1

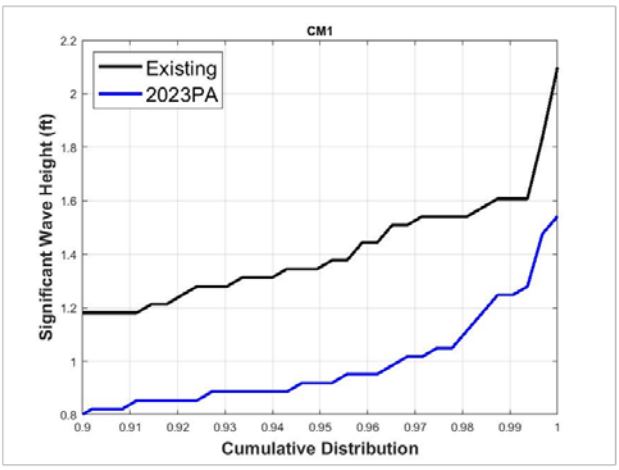

Figure A-144: Cumulative Distribution Wave Plot at CM1 (Largest 10% of Waves)

A.27 WAVE PLOTS AT CM2

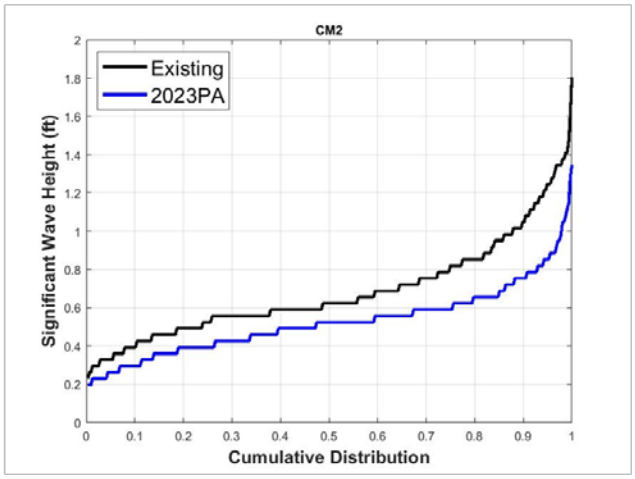

Figure A-145: Cumulative Distribution Wave Plot at CM2

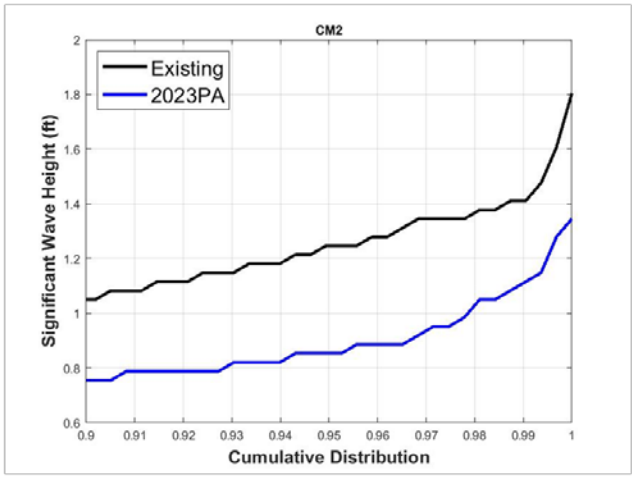

Figure A-146: Cumulative Distribution Wave Plot at CM2 (Largest 10% of Waves)

A.28 WAVE PLOTS AT CM3

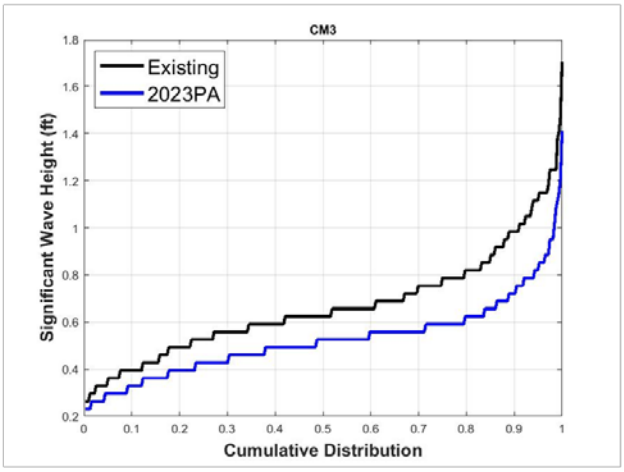

Figure A-147: Cumulative Distribution Wave Plot at CM3

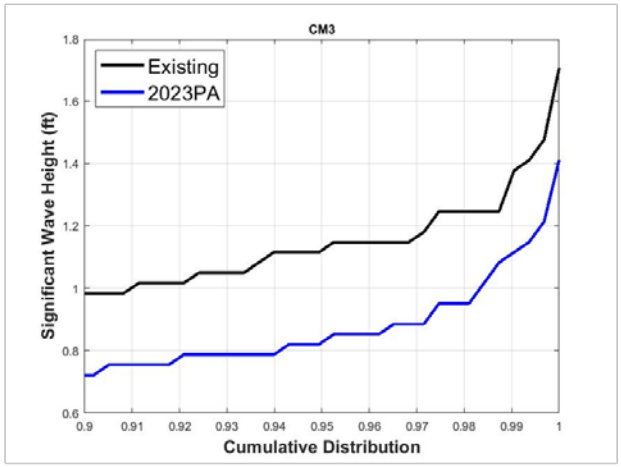

Figure A-148: Cumulative Distribution Wave Plot at CM3 (Largest 10% of Waves)

A.29 WAVE PLOTS AT CM4

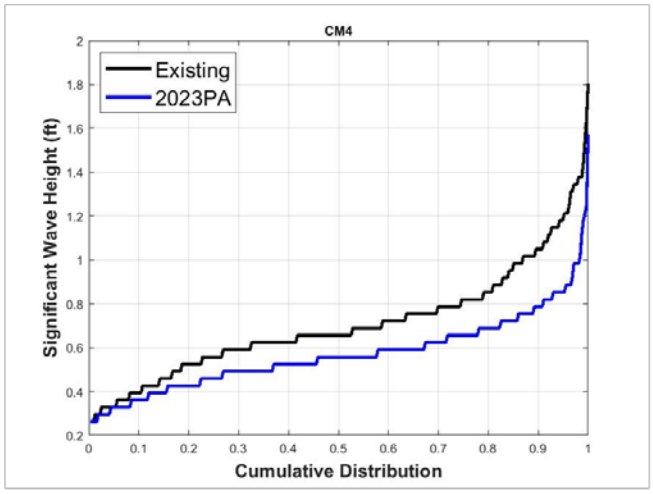

Figure A-149: Cumulative Distribution Wave Plot at CM4

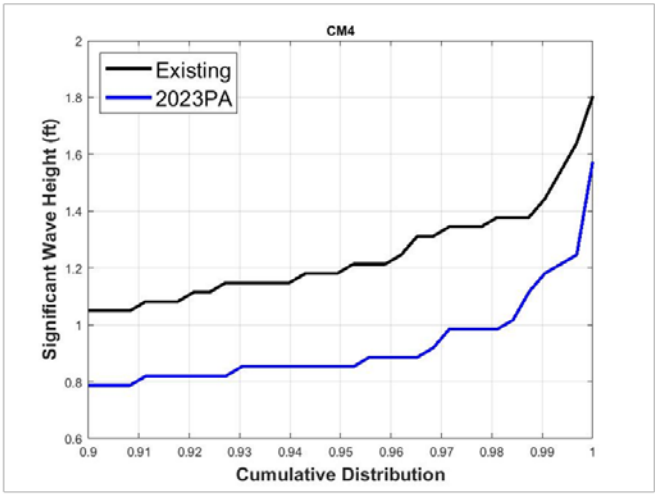

Figure A-150: Cumulative Distribution Wave Plot at CM4 (Largest 10% of Waves)

A.30 WAVE PLOTS AT I1

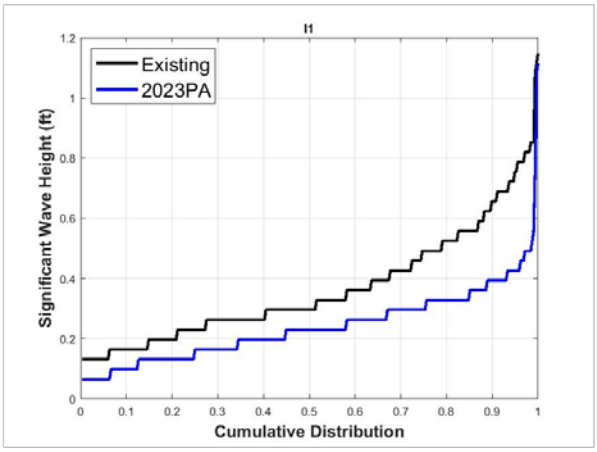

Figure A-151: Cumulative Distribution Wave Plot at I1

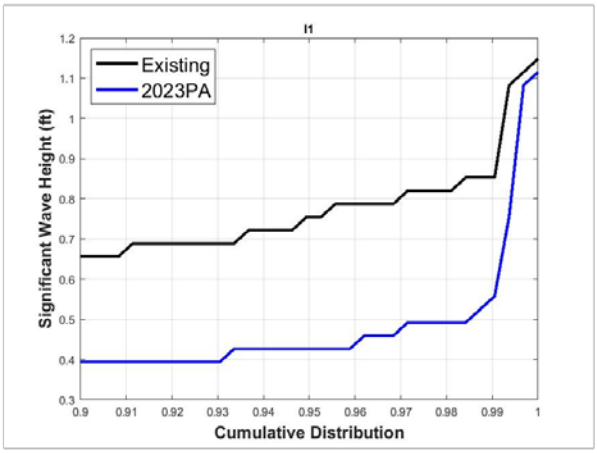

Figure A-152: Cumulative Distribution Wave Plot at I1 (Largest 10% of Waves)

A.31 WAVE PLOTS AT I2

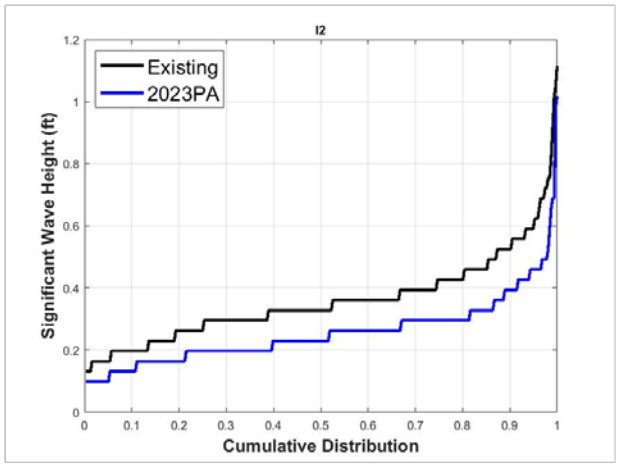

Figure A-153: Cumulative Distribution Wave Plot at I2

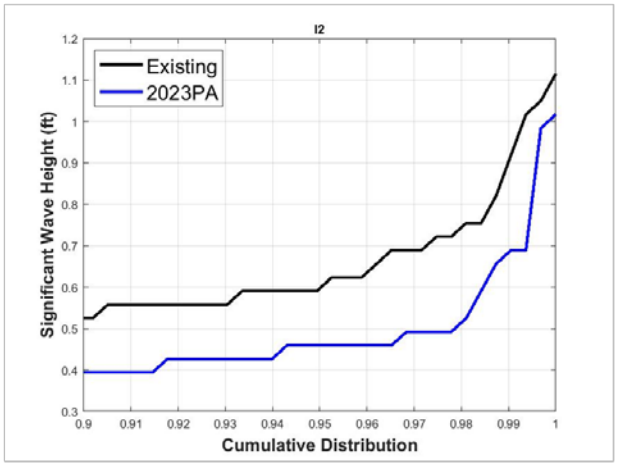

Figure A-154: Cumulative Distribution Wave Plot at I2 (Largest 10% of Waves)

A.32 WAVE PLOTS AT I3

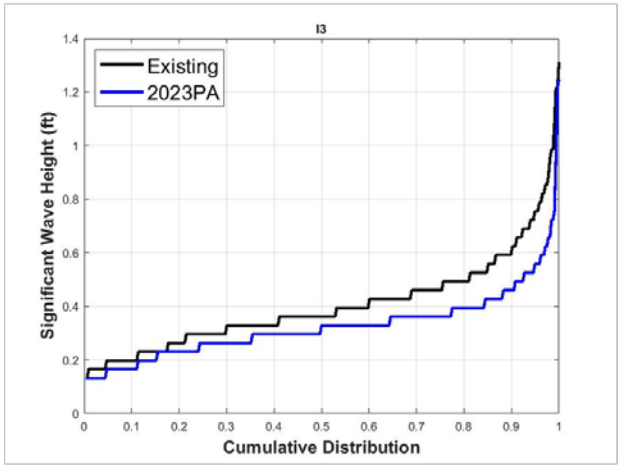

Figure A-155: Cumulative Distribution Wave Plot at I3

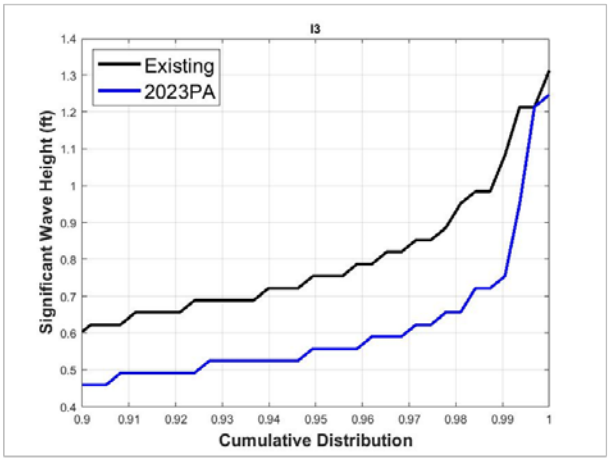

Figure A-156: Cumulative Distribution Wave Plot at I3 (Largest 10% of Waves)

A.33 WAVE PLOTS AT I4

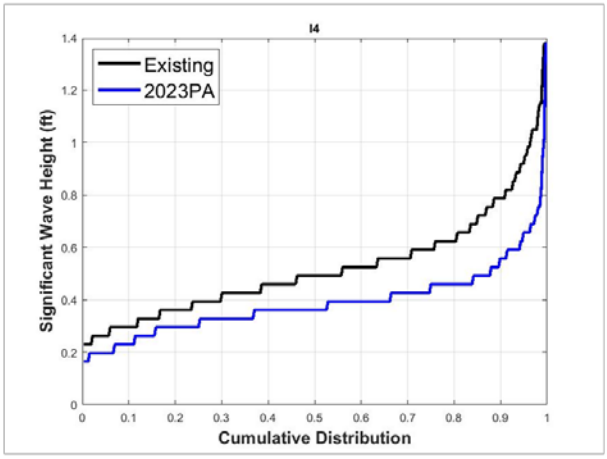

Figure A-157: Cumulative Distribution Wave Plot at I4

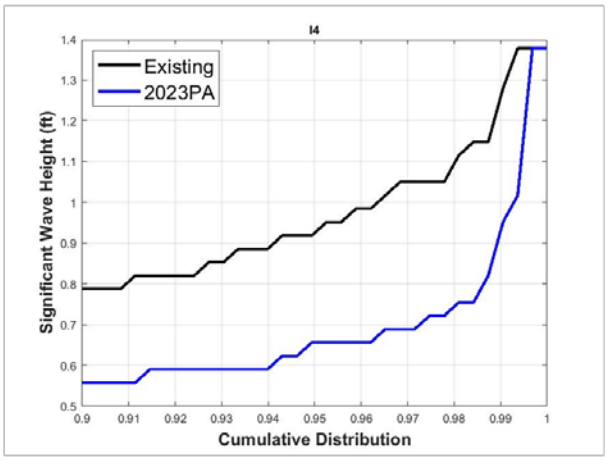

Figure A-158: Cumulative Distribution Wave Plot at I4 (Largest 10% of Waves)

A.34 WAVE PLOTS AT I5

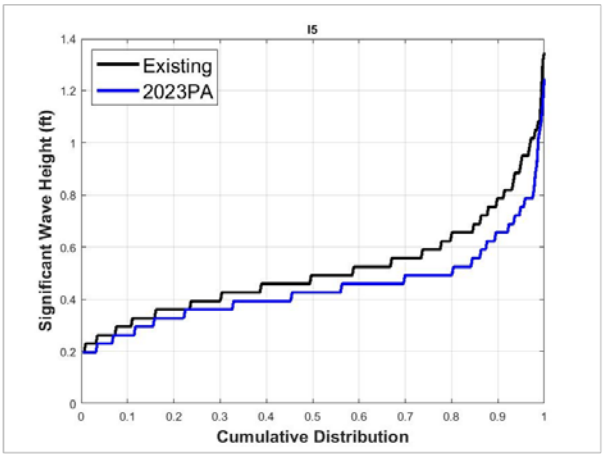

Figure A-159: Cumulative Distribution Wave Plot at I5

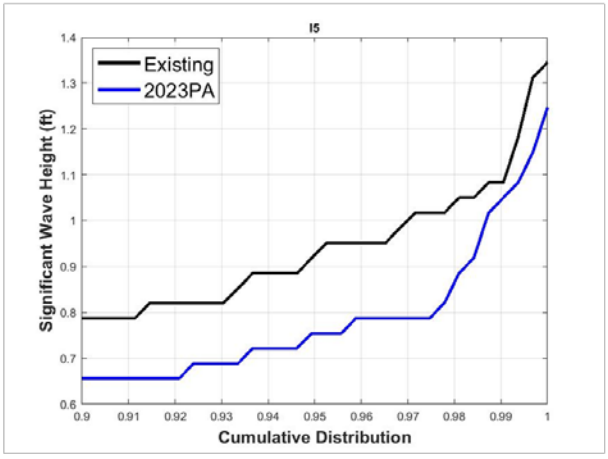

Figure A-160: Cumulative Distribution Wave Plot at I5 (Largest 10% of Waves)

A.35 WAVE PLOTS AT Nearshore1

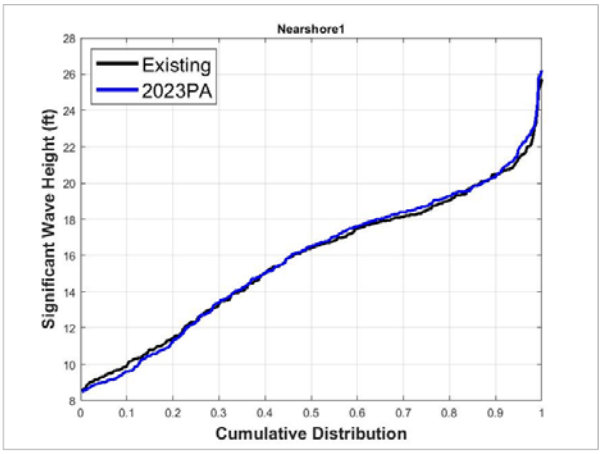

Figure A-161: Cumulative Distribution Wave Plot at Nearshore1

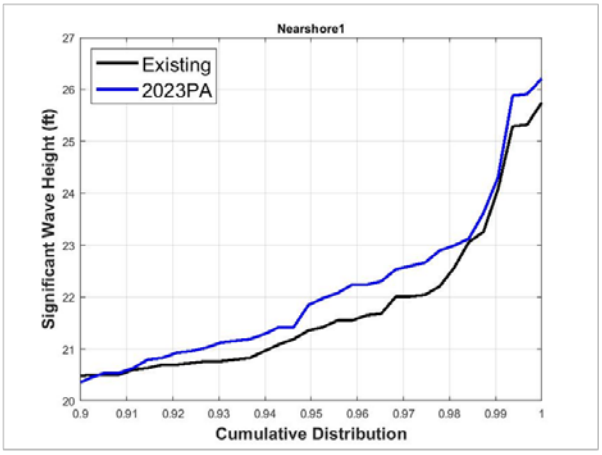

Figure A-162: Cumulative Distribution Wave Plot at Nearshore1 (Largest 10% of Waves)

A.36 WAVE PLOTS AT Nearshore2

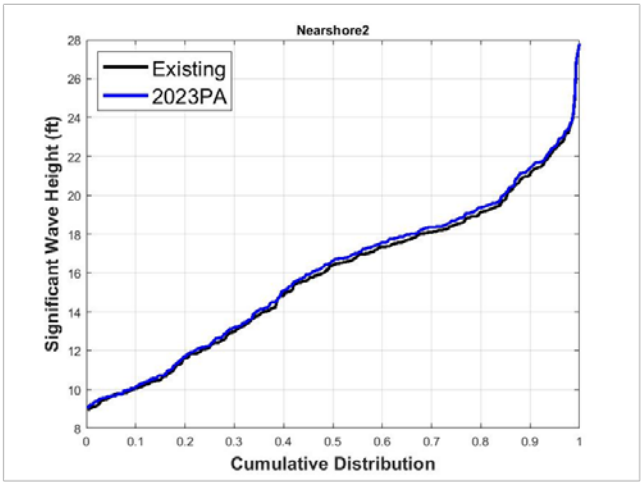

Figure A-163: Cumulative Distribution Wave Plot at Nearshore2

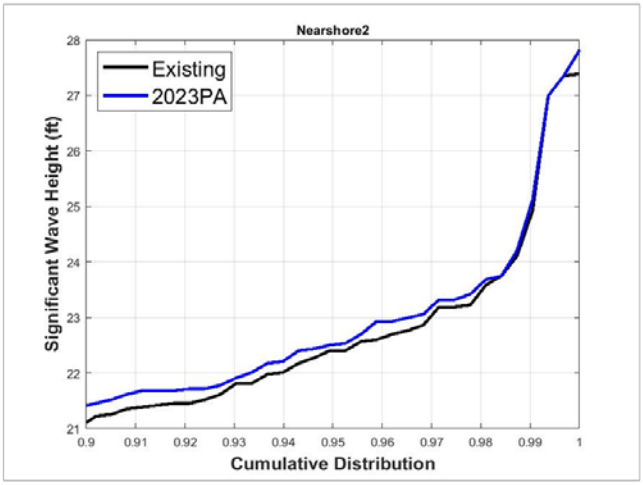

Figure A-164: Cumulative Distribution Wave Plot at Nearshore2 (Largest 10% of Waves)

A.37 WAVE PLOTS AT Nearshore3

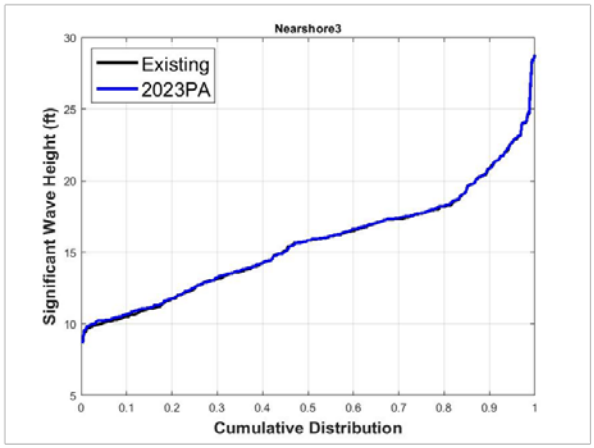

Figure A-165: Cumulative Distribution Wave Plot at Nearshore3

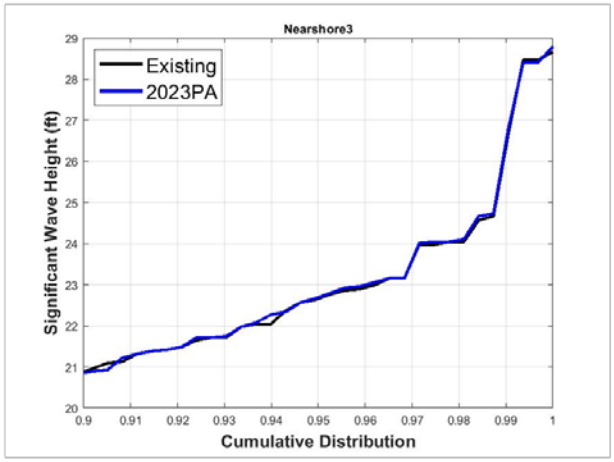

Figure A-166: Cumulative Distribution Wave Plot at Nearshore3 (Largest 10% of Waves)

A.38 WAVE PLOTS AT Nearshore4

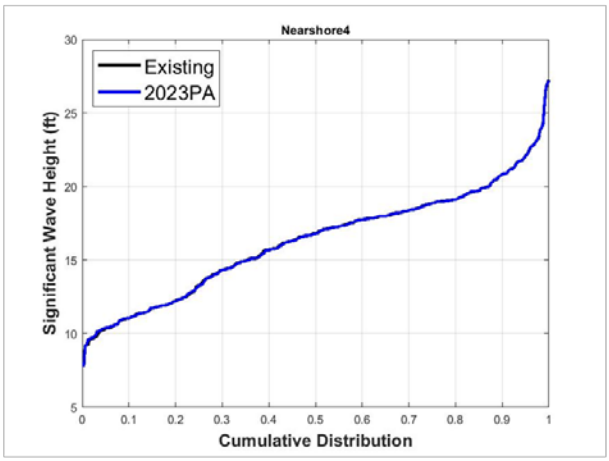

Figure A-167: Cumulative Distribution Wave Plot at Nearshore4

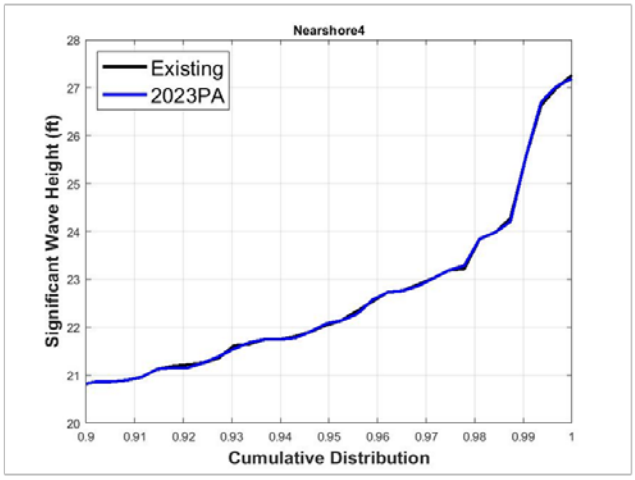

Figure A-168: Cumulative Distribution Wave Plot at Nearshore4 (Largest 10% of Waves)

A.39 WAVE PLOTS AT Nearshore5

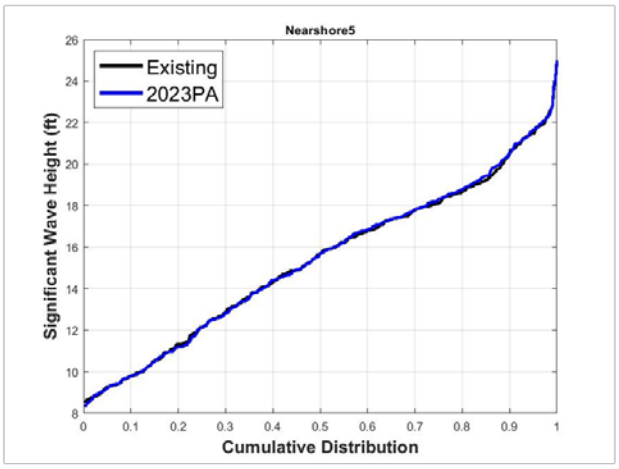

Figure A-169: Cumulative Distribution Wave Plot at Nearshore5

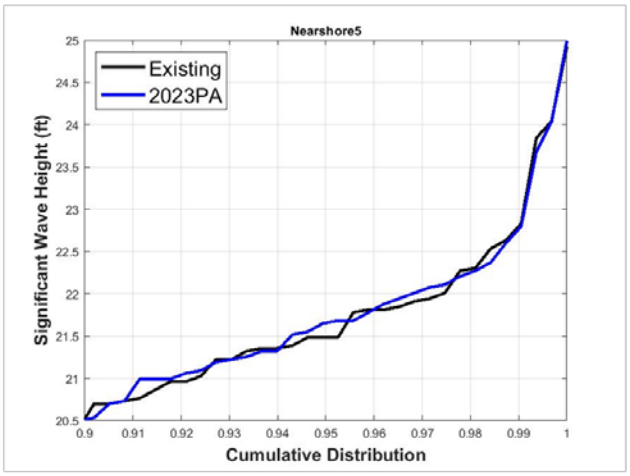

Figure A-170: Cumulative Distribution Wave Plot at Nearshore5 (Largest 10% of Waves)

A.40 WAVE PLOTS AT Nearshore6

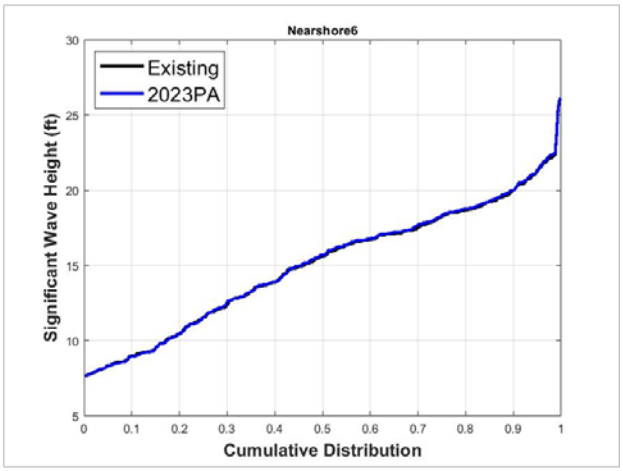

Figure A-171: Cumulative Distribution Wave Plot at Nearshore6

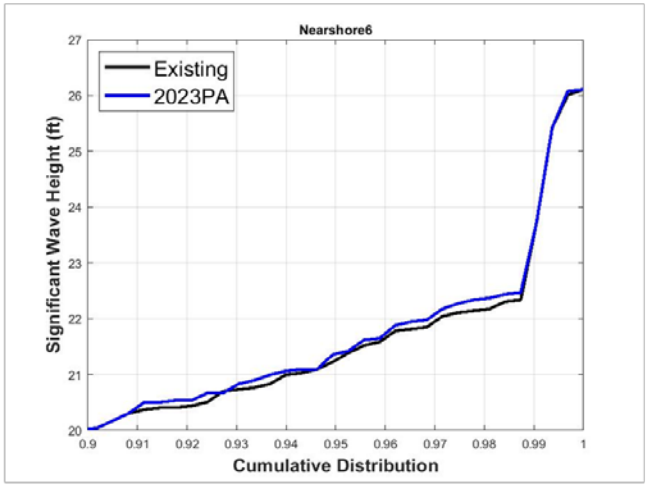

Figure A-172: Cumulative Distribution Wave Plot at Nearshore6 (Largest 10% of Waves)

A.41 WAVE PLOTS AT Nearshore7

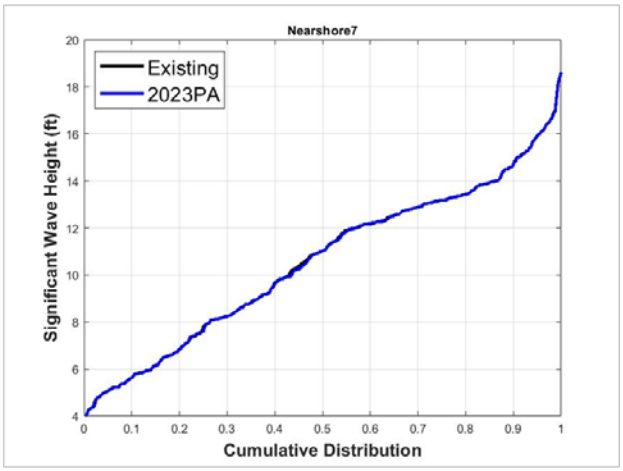

Figure A-173: Cumulative Distribution Wave Plot at Nearshore7

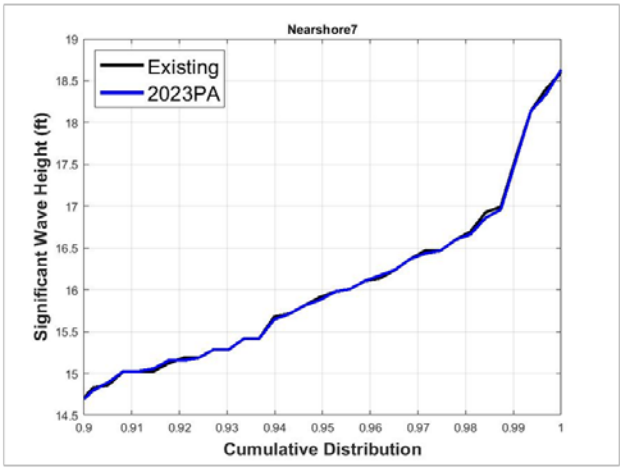

Figure A-174: Cumulative Distribution Wave Plot at Nearshore7 (Largest 10% of Waves)

A.42 WAVE PLOTS AT Offshore1

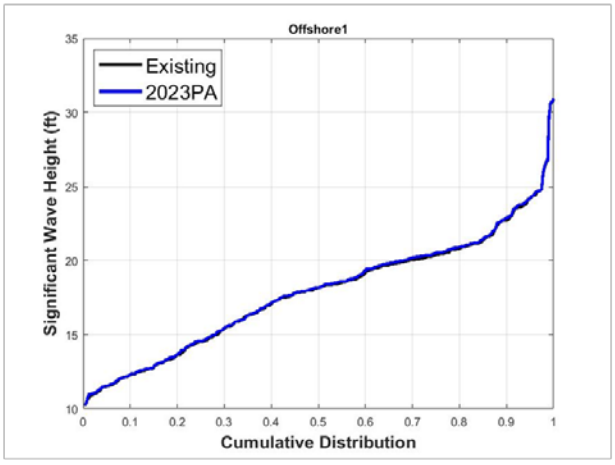

Figure A-175: Cumulative Distribution Wave Plot at Offshore1

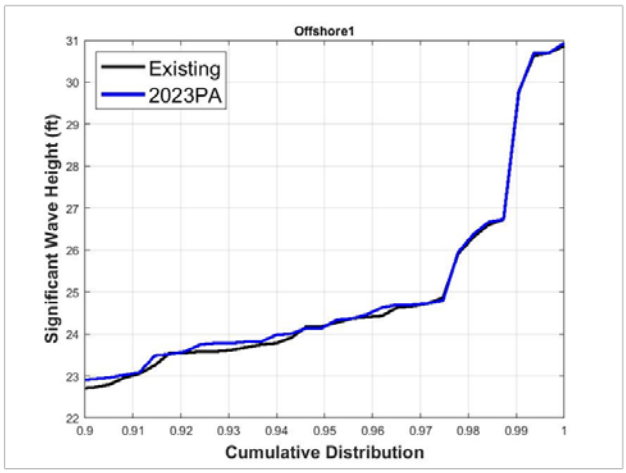

Figure A-176: Cumulative Distribution Wave Plot at Offshore1 (Largest 10% of Waves)

A.43 WAVE PLOTS AT Offshore2

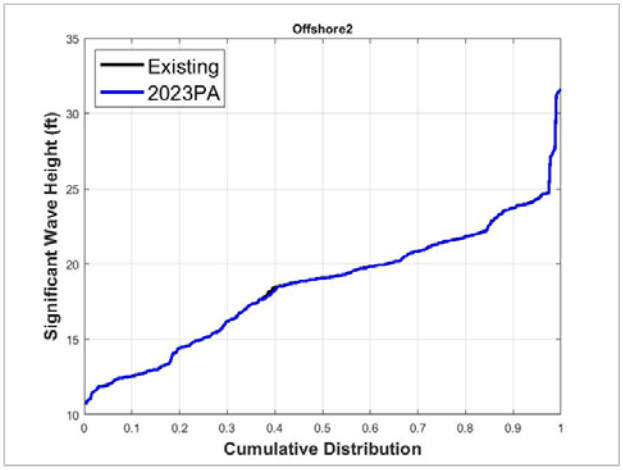

Figure A-177: Cumulative Distribution Wave Plot at Offshore2

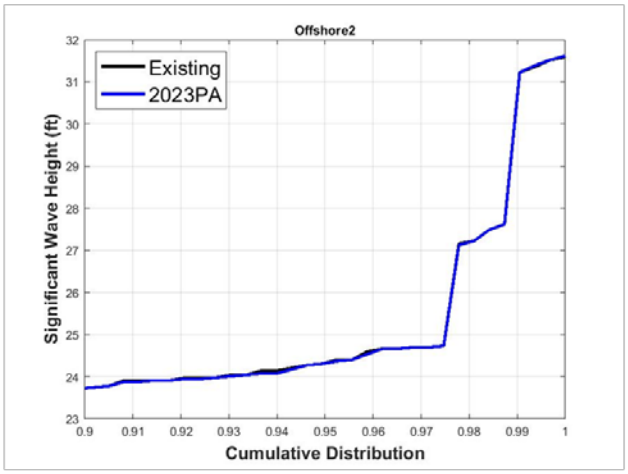

Figure A-178: Cumulative Distribution Wave Plot at Offshore2 (Largest 10% of Waves)

A.44 WAVE PLOTS AT Offshore3

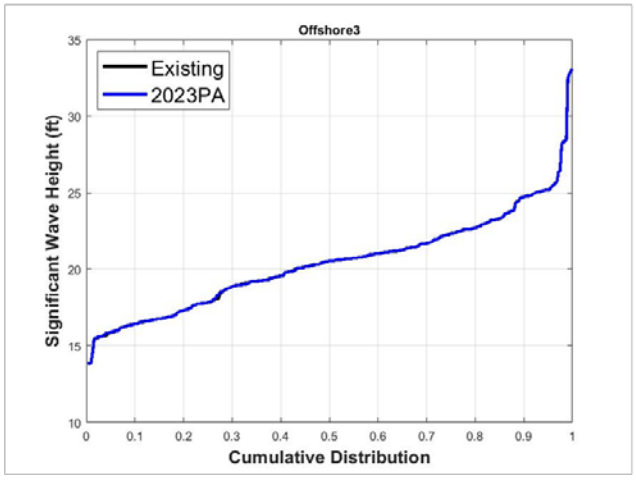

Figure A-179: Cumulative Distribution Wave Plot at Offshore3

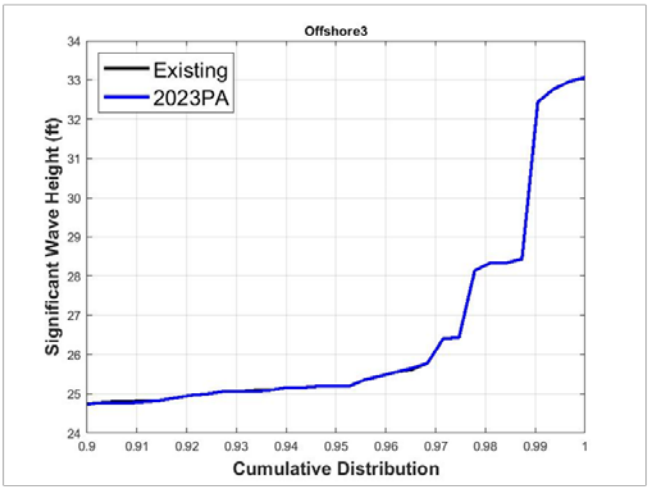

Figure A-180: Cumulative Distribution Wave Plot at Offshore3 (Largest 10% of Waves)

A.45 WAVE PLOTS AT R1

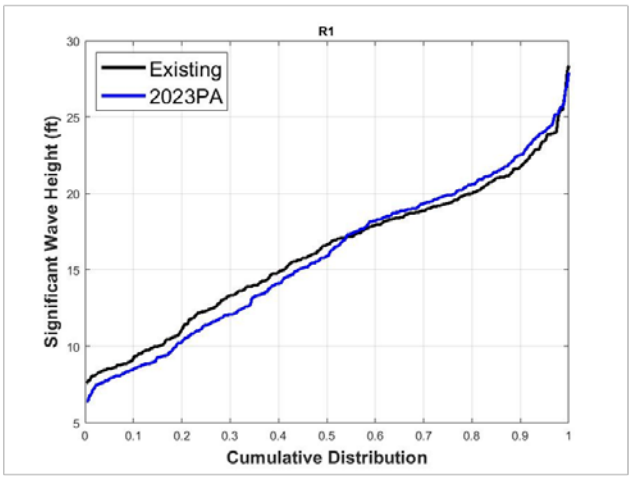

Figure A-181: Cumulative Distribution Wave Plot at R1

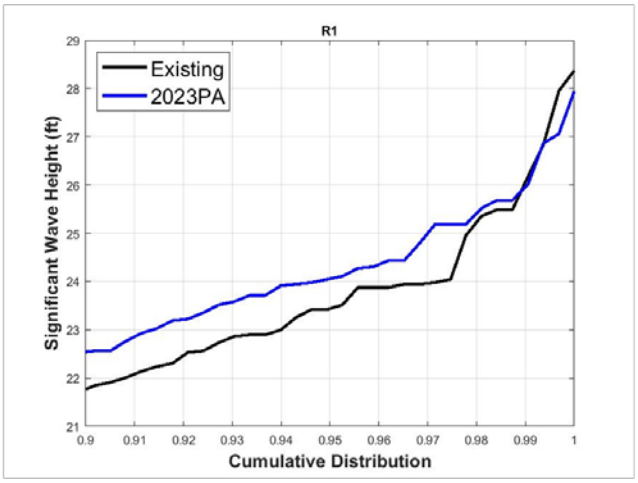

Figure A-182: Cumulative Distribution Wave Plot at R1 (Largest 10% of Waves)

A.46 WAVE PLOTS AT R2

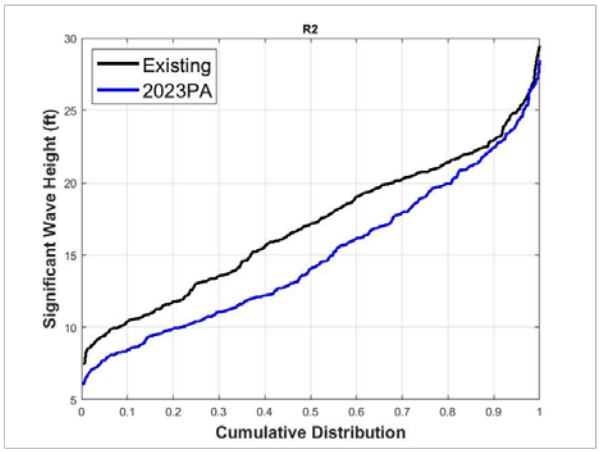

Figure A-183: Cumulative Distribution Wave Plot at R2

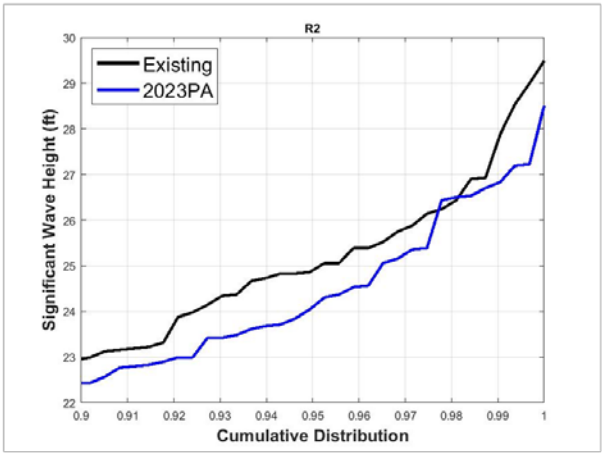

Figure A-184: Cumulative Distribution Wave Plot at R2 (Largest 10% of Waves)

A.47 WAVE PLOTS AT R3

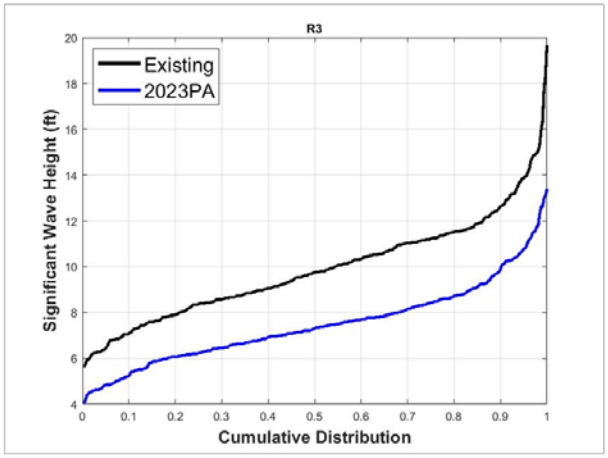

Figure A-185: Cumulative Distribution Wave Plot at R3

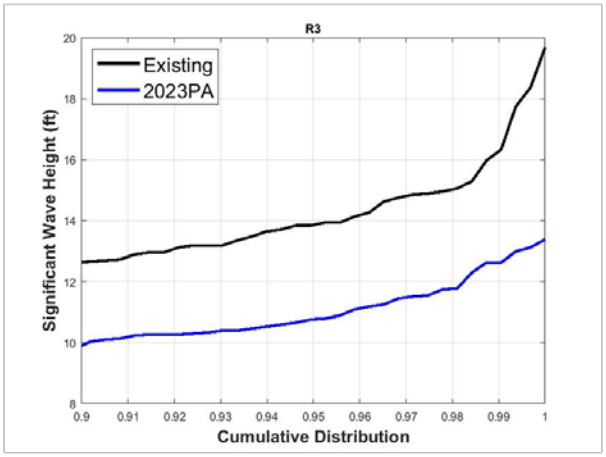

Figure A-186: Cumulative Distribution Wave Plot at R3 (Largest 10% of Waves)

A.48 WAVE PLOTS AT R4

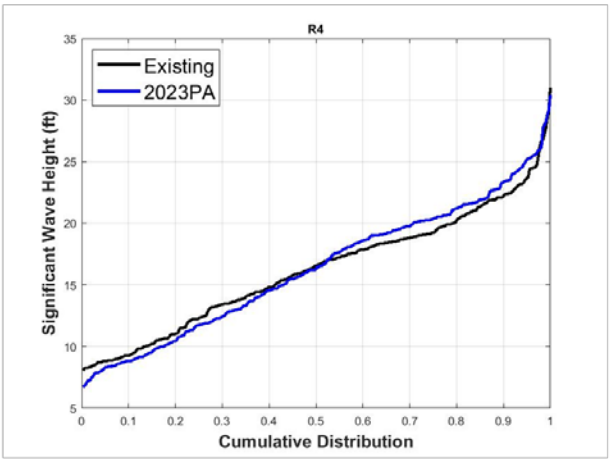

Figure A-187: Cumulative Distribution Wave Plot at R4

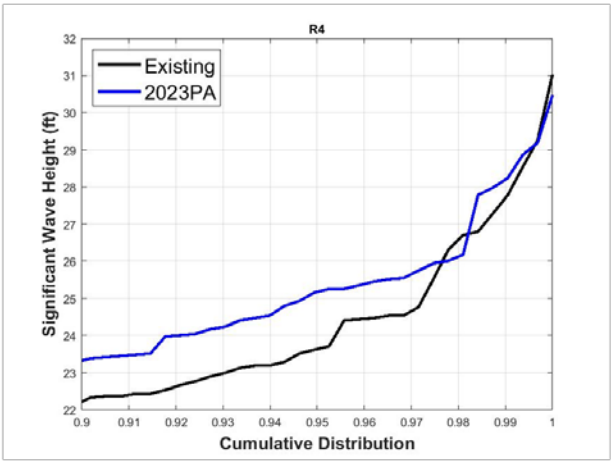

Figure A-188: Cumulative Distribution Wave Plot at R4 (Largest 10% of Waves)

A.49 WAVE PLOTS AT R5

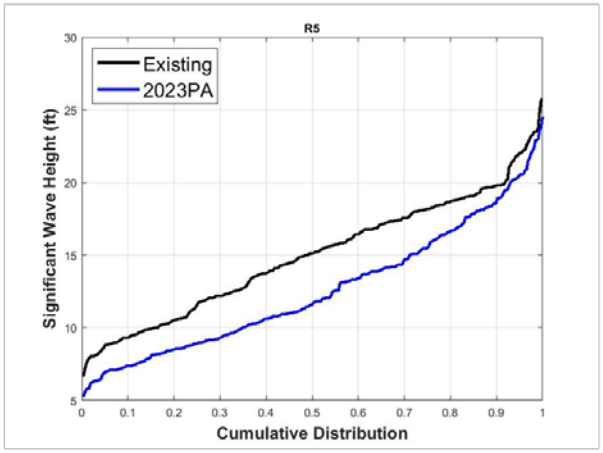

Figure A-189: Cumulative Distribution Wave Plot at R5

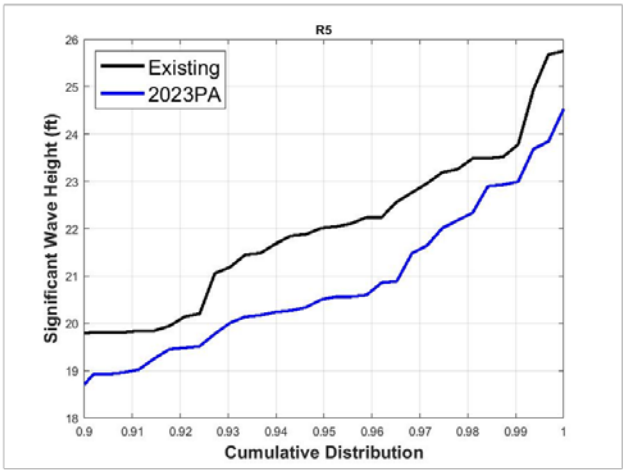

Figure A-190: Cumulative Distribution Wave Plot at R5 (Largest 10% of Waves)

A.50 WAVE PLOTS AT R6

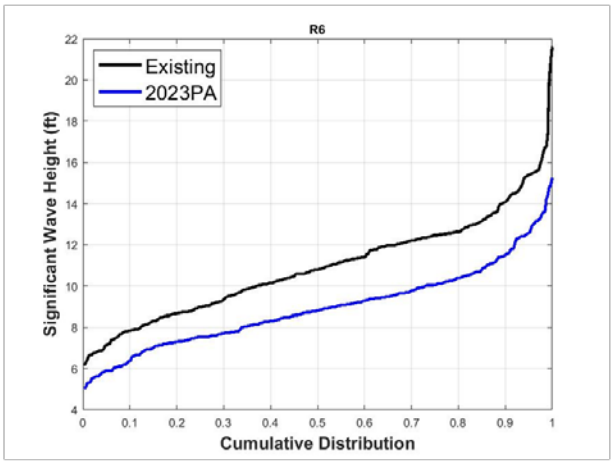

Figure A-191: Cumulative Distribution Wave Plot at R6

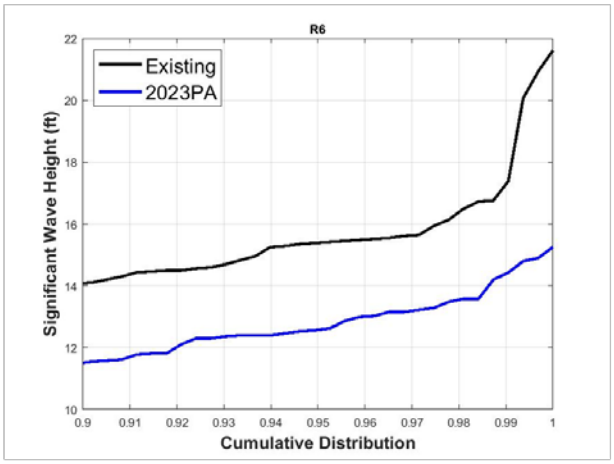

Figure A-192: Cumulative Distribution Wave Plot at R6 (Largest 10% of Waves)

A.51 WAVE PLOTS AT R7

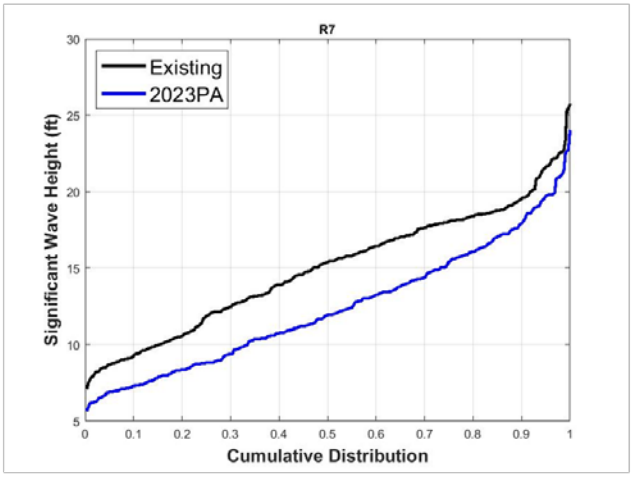

Figure A-193: Cumulative Distribution Wave Plot at R7

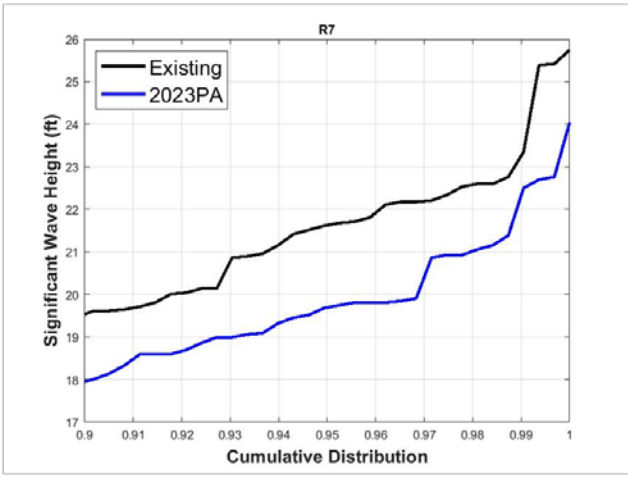

Figure A-194: Cumulative Distribution Wave Plot at R7 (Largest 10% of Waves)

A.52 WAVE PLOTS AT LOG-SPIRAL BAY L1-L3

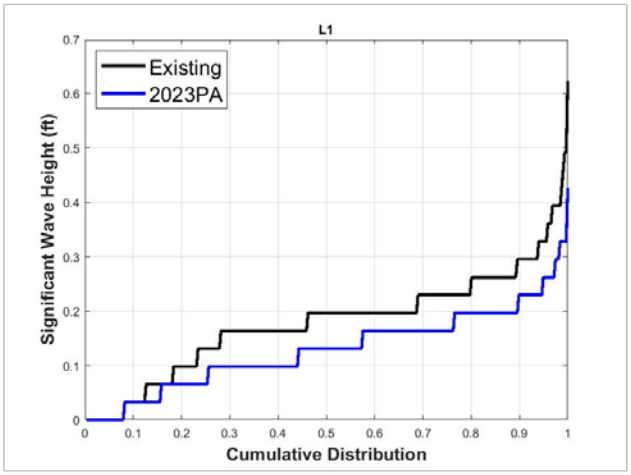

Figure A-195: Cumulative Distribution Wave Plot at L1

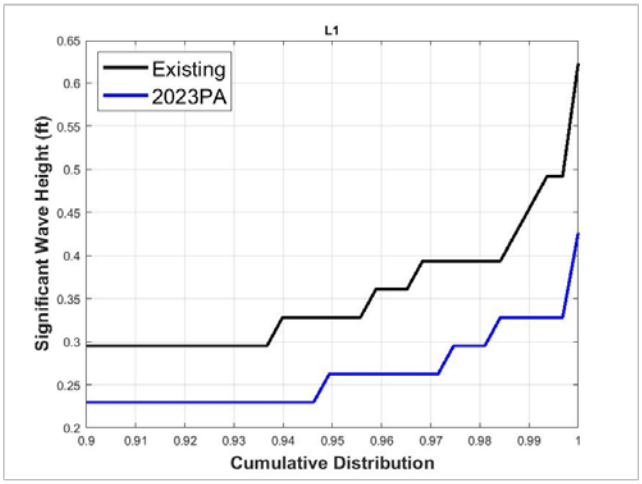

Figure A-196: Cumulative Distribution Wave Plot at L1 (Largest 10% of Waves)

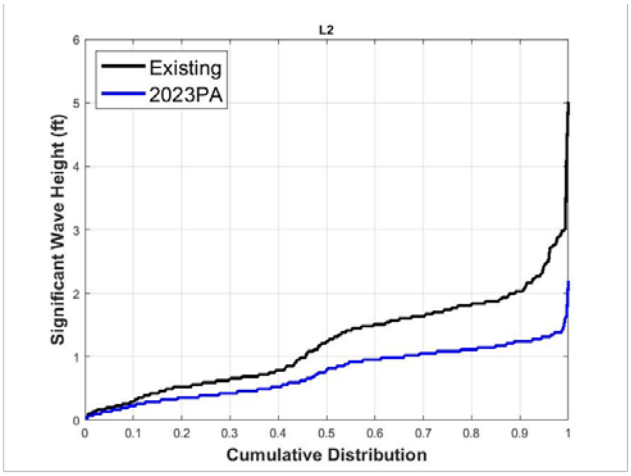

Figure A-197: Cumulative Distribution Wave Plot at L2

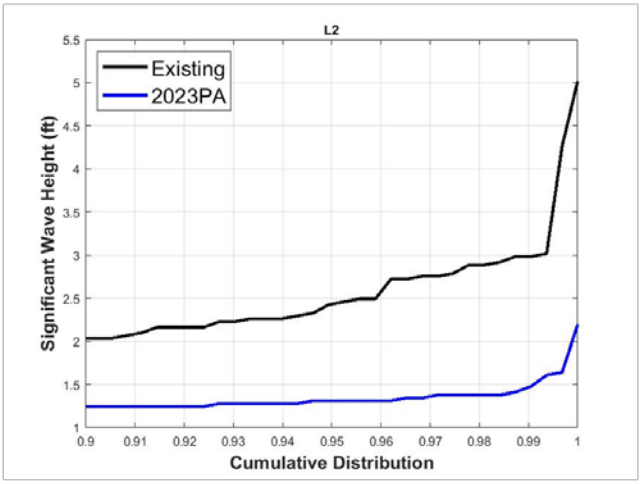

Figure A-198: Cumulative Distribution Wave Plot at L2 (Largest 10% of Waves)

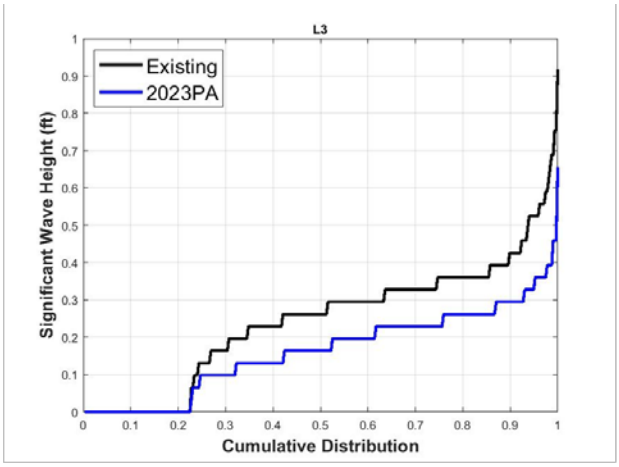

Figure A-199: Cumulative Distribution Wave Plot at L3

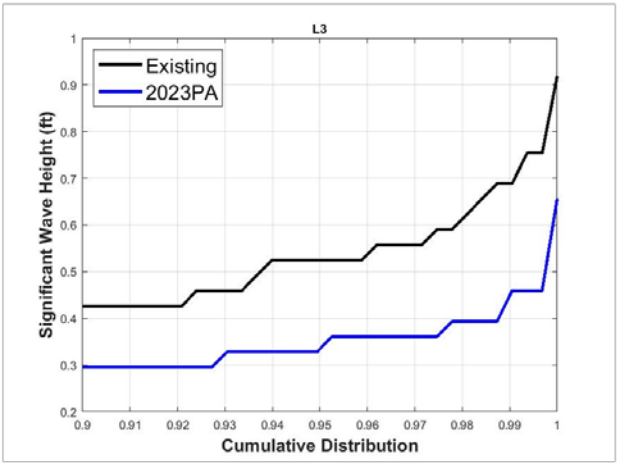

Figure A-200: Cumulative Distribution Wave Plot at L3 (Largest 10% of Waves)

ATTACHMENT B

Extreme Waves at North and South Jetties

NORTH JETTY – BY HEIGHT

Table B-1: Wave heights at the North Jetty, under the Existing Condition and 2023 PA, organized by wave direction (from south to north). Grey: wave heights decrease under the PA; White: wave heights increase under the PA.

Storm Number	Offshore Direction		Nearshore Wave Height (ft)		Change in ... (%)	
	°N	Cardinal Direction	Existing	2023 PA	Wave Height	Wave Energy
60	195	SSW	8.6	7.1	-17%	-32%
139	195	SSW	9.6	7.9	-18%	-33%
218	195	SSW	8.5	8.1	-5%	-10%
297	195	SSW	9.5	8.5	-11%	-21%
18	197	SSW	12.6	11.5	-9%	-17%
97	197	SSW	12.7	11.5	-9%	-18%
176	197	SSW	13.4	13.1	-3%	-5%
255	197	SSW	13.8	12.8	-7%	-14%
54	198	SSW	9.4	8.1	-15%	-27%
55	198	SSW	14.2	11.5	-19%	-34%
69	198	SSW	8.5	6.7	-22%	-39%
133	198	SSW	10.2	8.7	-15%	-28%
134	198	SSW	14.5	11.5	-20%	-37%
148	198	SSW	9.0	7.1	-21%	-38%
212	198	SSW	9.9	9.6	-4%	-7%
213	198	SSW	13.4	12.7	-5%	-10%
227	198	SSW	7.9	7.9	0%	0%
291	198	SSW	10.6	9.5	-10%	-19%
292	198	SSW	14.9	12.5	-16%	-30%
306	198	SSW	9.3	7.7	-17%	-32%
9	200	SSW	13.3	12.1	-9%	-17%
88	200	SSW	14.3	12.5	-13%	-23%
167	200	SSW	14.4	13.4	-7%	-13%
246	200	SSW	14.5	13.7	-5%	-10%
51	201	SSW	10.4	9.6	-8%	-15%
130	201	SSW	11.2	10.3	-8%	-15%
209	201	SSW	11.7	11.4	-3%	-5%
288	201	SSW	11.3	11.2	-1%	-2%
47	202	SSW	10.4	9.7	-7%	-14%
77	202	SSW	13.4	11.1	-17%	-31%
126	202	SSW	10.7	10.1	-6%	-11%
156	202	SSW	14.0	11.5	-18%	-32%

205	202	SSW	11.7	11.5	-1%	-3%
235	202	SSW	13.8	12.8	-7%	-14%
284	202	SSW	11.5	11.2	-2%	-4%
314	202	SSW	14.5	12.6	-13%	-25%
22	203	SSW	9.9	8.6	-13%	-25%
101	203	SSW	10.7	9.1	-15%	-27%
180	203	SSW	10.7	10.3	-3%	-7%
259	203	SSW	11.0	10.0	-9%	-18%
6	204	SSW	12.3	10.8	-12%	-22%
32	204	SSW	9.0	7.7	-14%	-25%
85	204	SSW	12.9	11.1	-14%	-26%
111	204	SSW	10.3	8.5	-17%	-31%
164	204	SSW	13.1	12.1	-7%	-14%
190	204	SSW	9.4	9.2	-2%	-3%
243	204	SSW	13.4	12.1	-9%	-18%
269	204	SSW	10.3	9.2	-10%	-19%
49	206	SSW	8.3	7.3	-12%	-22%
58	206	SSW	16.1	14.0	-13%	-24%
65	206	SSW	11.7	9.7	-17%	-31%
128	206	SSW	9.7	7.9	-19%	-34%
137	206	SSW	17.4	14.4	-17%	-31%
144	206	SSW	12.0	10.0	-17%	-32%
207	206	SSW	9.1	8.6	-5%	-10%
216	206	SSW	16.8	14.5	-14%	-25%
223	206	SSW	11.5	11.2	-3%	-6%
286	206	SSW	10.1	8.6	-14%	-26%
295	206	SSW	17.6	15.8	-10%	-20%
302	206	SSW	12.6	11.0	-13%	-24%
20	207	SSW	15.1	12.3	-19%	-34%
99	207	SSW	15.7	12.6	-20%	-35%
178	207	SSW	15.0	13.7	-9%	-16%
257	207	SSW	16.4	13.9	-16%	-29%
59	212	SSW	10.9	9.4	-13%	-24%
138	212	SSW	12.2	10.2	-16%	-30%
217	212	SSW	11.8	11.1	-6%	-11%
296	212	SSW	11.9	11.1	-7%	-13%
19	215	SW	15.7	13.9	-12%	-22%
98	215	SW	16.8	14.1	-16%	-30%
177	215	SW	16.4	14.1	-14%	-26%
256	215	SW	17.0	15.0	-12%	-22%

10	217	SW	10.8	9.8	-9%	-17%
89	217	SW	11.6	10.3	-11%	-21%
168	217	SW	11.8	11.6	-2%	-4%
247	217	SW	11.6	11.4	-2%	-4%
70	218	SW	10.2	8.1	-20%	-36%
149	218	SW	11.0	8.7	-21%	-37%
228	218	SW	9.9	10.2	3%	6%
307	218	SW	11.2	9.5	-16%	-29%
5	220	SW	16.2	13.7	-15%	-28%
84	220	SW	16.9	14.0	-17%	-32%
163	220	SW	16.2	14.4	-11%	-21%
242	220	SW	17.1	15.1	-12%	-22%
46	221	SW	9.4	8.0	-15%	-28%
125	221	SW	10.8	8.5	-21%	-38%
204	221	SW	9.7	9.4	-3%	-5%
283	221	SW	10.5	9.1	-13%	-24%
52	223	SW	10.8	9.4	-13%	-24%
131	223	SW	11.7	9.7	-17%	-32%
210	223	SW	11.3	11.2	-1%	-1%
289	223	SW	12.0	10.7	-11%	-21%
67	227	SW	14.8	11.7	-21%	-37%
146	227	SW	15.3	12.0	-22%	-39%
225	227	SW	13.9	12.7	-9%	-17%
304	227	SW	15.7	13.0	-17%	-32%
1	229	SW	10.7	8.4	-21%	-38%
62	229	SW	13.2	11.3	-14%	-27%
80	229	SW	11.3	8.6	-24%	-42%
141	229	SW	14.1	11.8	-17%	-31%
159	229	SW	10.7	10.3	-4%	-8%
220	229	SW	13.8	13.0	-5%	-10%
238	229	SW	11.6	9.4	-18%	-34%
299	229	SW	14.4	12.9	-10%	-20%
2	232	SW	14.4	10.7	-26%	-45%
81	232	SW	14.7	10.7	-27%	-47%
160	232	SW	13.2	10.9	-17%	-32%
239	232	SW	14.8	11.2	-24%	-43%
31	233	SW	14.4	11.6	-19%	-35%
110	233	SW	16.1	13.3	-17%	-32%
189	233	SW	15.5	13.8	-11%	-21%
268	233	SW	15.7	14.3	-9%	-16%

34	234	SW	13.3	10.6	-20%	-36%
113	234	SW	13.7	10.7	-22%	-40%
192	234	SW	12.5	12.4	-1%	-2%
271	234	SW	14.0	11.6	-17%	-31%
48	238	WSW	16.5	17.5	7%	13%
127	238	WSW	16.5	17.8	8%	16%
206	238	WSW	20.2	19.9	-1%	-3%
285	238	WSW	17.6	18.9	7%	15%
35	244	WSW	18.1	15.8	-13%	-24%
114	244	WSW	18.8	16.6	-12%	-23%
193	244	WSW	18.9	17.2	-9%	-17%
272	244	WSW	19.3	17.6	-9%	-17%
8	246	WSW	17.4	14.4	-17%	-32%
87	246	WSW	17.9	14.8	-17%	-31%
166	246	WSW	16.9	14.8	-13%	-24%
245	246	WSW	17.5	15.2	-13%	-24%
21	248	WSW	21.4	17.5	-18%	-33%
41	248	WSW	13.7	11.8	-14%	-27%
100	248	WSW	22.1	16.9	-24%	-42%
120	248	WSW	14.0	11.7	-16%	-30%
179	248	WSW	17.5	14.5	-17%	-31%
199	248	WSW	14.0	13.5	-3%	-6%
258	248	WSW	21.5	17.8	-17%	-32%
278	248	WSW	14.6	12.8	-12%	-23%
50	261	W	18.4	14.1	-23%	-41%
129	261	W	18.7	13.2	-29%	-50%
208	261	W	14.3	12.3	-14%	-27%
287	261	W	18.0	13.8	-23%	-41%
37	262	W	22.3	18.6	-17%	-31%
116	262	W	23.8	19.8	-17%	-31%
195	262	W	19.5	16.0	-18%	-32%
274	262	W	22.3	19.0	-15%	-27%
78	268	W	18.8	13.3	-29%	-50%
157	268	W	19.2	15.7	-18%	-33%
236	268	W	17.6	14.7	-16%	-30%
315	268	W	19.5	16.7	-14%	-27%
71	270	W	21.0	17.1	-18%	-33%
150	270	W	22.2	17.8	-20%	-35%
229	270	W	18.4	14.7	-20%	-36%
308	270	W	21.5	18.1	-16%	-29%

36	271	W	22.7	18.0	-21%	-37%
40	271	W	17.4	13.9	-20%	-36%
72	271	W	27.3	24.3	-11%	-21%
79	271	W	17.8	14.1	-21%	-37%
115	271	W	23.9	18.2	-24%	-42%
119	271	W	18.0	14.0	-22%	-40%
151	271	W	31.2	27.7	-11%	-21%
158	271	W	18.1	14.1	-22%	-40%
194	271	W	17.8	14.6	-18%	-33%
198	271	W	15.2	12.4	-18%	-33%
230	271	W	24.6	21.2	-14%	-26%
237	271	W	15.6	12.5	-20%	-36%
273	271	W	22.6	18.3	-19%	-34%
277	271	W	17.6	14.5	-17%	-32%
309	271	W	28.1	25.2	-10%	-20%
316	271	W	17.8	14.8	-17%	-31%
33	272	W	19.2	15.3	-20%	-37%
66	272	W	14.3	10.8	-24%	-42%
112	272	W	20.0	15.6	-22%	-39%
145	272	W	14.3	10.8	-25%	-43%
191	272	W	17.0	13.3	-22%	-39%
224	272	W	13.1	11.9	-9%	-18%
270	272	W	19.2	15.8	-18%	-32%
303	272	W	14.6	11.7	-20%	-36%
7	273	W	25.2	22.2	-12%	-22%
14	273	W	20.8	17.5	-16%	-30%
86	273	W	27.8	24.1	-13%	-25%
93	273	W	21.7	17.7	-18%	-33%
165	273	W	23.5	19.3	-18%	-32%
172	273	W	18.7	15.1	-19%	-35%
244	273	W	25.5	22.7	-11%	-21%
251	273	W	20.9	18.1	-14%	-26%
13	276	W	16.1	13.0	-19%	-35%
92	276	W	16.3	12.8	-21%	-38%
171	276	W	15.2	12.9	-15%	-28%
250	276	W	16.8	14.0	-17%	-31%
43	278	W	19.7	16.9	-14%	-27%
75	278	W	16.9	15.6	-8%	-15%
122	278	W	20.7	17.0	-18%	-33%
154	278	W	17.1	15.6	-9%	-17%

201	278	W	17.9	14.7	-18%	-32%
233	278	W	17.8	16.1	-9%	-18%
280	278	W	20.0	17.6	-12%	-23%
312	278	W	17.6	16.6	-5%	-11%
3	279	W	24.2	21.6	-10%	-20%
12	279	W	23.9	21.9	-8%	-16%
64	279	W	20.4	17.2	-15%	-28%
82	279	W	25.1	22.4	-11%	-20%
91	279	W	27.1	23.9	-12%	-22%
143	279	W	21.8	17.2	-21%	-37%
161	279	W	24.4	21.1	-14%	-26%
170	279	W	22.7	18.7	-18%	-33%
222	279	W	17.5	14.2	-19%	-34%
240	279	W	25.4	22.7	-11%	-20%
249	279	W	24.6	22.2	-10%	-18%
301	279	W	20.3	17.0	-16%	-29%
38	280	W	20.9	18.2	-13%	-24%
117	280	W	22.1	18.7	-15%	-28%
196	280	W	19.3	15.5	-20%	-35%
275	280	W	21.6	18.8	-13%	-24%
61	281	W	20.5	19.4	-6%	-11%
68	281	W	20.0	18.3	-9%	-17%
140	281	W	21.3	19.9	-7%	-13%
147	281	W	21.6	19.5	-10%	-19%
219	281	W	21.4	18.7	-12%	-23%
226	281	W	21.2	17.4	-18%	-33%
298	281	W	21.7	20.5	-6%	-11%
305	281	W	21.7	19.3	-11%	-20%
44	282	WNW	23.6	21.1	-11%	-20%
123	282	WNW	25.6	22.5	-12%	-23%
202	282	WNW	21.6	17.2	-20%	-37%
281	282	WNW	24.3	21.0	-14%	-26%
63	284	WNW	23.7	21.8	-8%	-15%
142	284	WNW	27.9	23.8	-15%	-27%
221	284	WNW	22.3	18.0	-19%	-35%
300	284	WNW	24.8	22.8	-8%	-16%
11	286	WNW	20.9	18.9	-9%	-18%
90	286	WNW	22.1	19.8	-10%	-20%
169	286	WNW	21.3	17.7	-17%	-31%
248	286	WNW	21.7	19.9	-8%	-16%

16	288	WNW	18.0	16.6	-8%	-15%
28	288	WNW	20.2	17.9	-11%	-21%
95	288	WNW	18.4	16.5	-10%	-19%
107	288	WNW	21.3	18.3	-14%	-26%
174	288	WNW	18.7	16.3	-13%	-24%
186	288	WNW	19.2	15.3	-20%	-37%
253	288	WNW	18.6	17.4	-7%	-13%
265	288	WNW	20.9	18.3	-12%	-23%
29	289	WNW	21.8	20.7	-5%	-10%
30	289	WNW	21.8	20.6	-6%	-11%
108	289	WNW	23.8	22.1	-7%	-14%
109	289	WNW	24.0	22.4	-7%	-13%
187	289	WNW	22.8	19.0	-16%	-30%
188	289	WNW	23.0	19.4	-16%	-29%
266	289	WNW	23.2	21.2	-9%	-17%
267	289	WNW	23.3	21.3	-9%	-17%
25	291	WNW	24.3	23.6	-3%	-6%
104	291	WNW	27.7	27.1	-2%	-4%
183	291	WNW	27.6	23.8	-14%	-26%
262	291	WNW	26.5	25.3	-5%	-9%
39	292	WNW	20.8	19.5	-6%	-12%
73	292	WNW	21.5	21.2	-2%	-3%
118	292	WNW	22.2	20.6	-7%	-14%
152	292	WNW	23.3	22.9	-2%	-4%
197	292	WNW	22.5	19.3	-14%	-26%
231	292	WNW	23.7	20.8	-12%	-23%
276	292	WNW	22.6	20.8	-8%	-16%
310	292	WNW	23.5	22.0	-7%	-13%
4	293	WNW	20.0	19.4	-3%	-6%
83	293	WNW	21.0	20.3	-4%	-7%
162	293	WNW	23.1	21.3	-8%	-14%
241	293	WNW	22.0	20.9	-5%	-10%
17	294	WNW	20.4	19.3	-6%	-11%
96	294	WNW	20.8	20.1	-3%	-7%
175	294	WNW	20.5	18.5	-10%	-19%
254	294	WNW	21.1	19.6	-7%	-13%
23	295	WNW	22.1	21.8	-1%	-3%
102	295	WNW	24.2	24.3	0%	1%
181	295	WNW	25.3	22.3	-12%	-22%
260	295	WNW	24.1	22.9	-5%	-10%

56	296	WNW	20.3	20.3	0%	0%
57	296	WNW	21.0	20.2	-4%	-7%
74	296	WNW	20.7	21.1	2%	4%
135	296	WNW	21.1	21.6	3%	5%
136	296	WNW	22.1	21.9	-1%	-2%
153	296	WNW	20.8	22.1	6%	12%
214	296	WNW	22.9	21.0	-8%	-15%
215	296	WNW	23.3	20.9	-10%	-20%
232	296	WNW	24.5	22.0	-10%	-20%
293	296	WNW	21.8	20.9	-4%	-8%
294	296	WNW	22.8	21.3	-7%	-13%
311	296	WNW	22.0	21.7	-1%	-3%
53	299	WNW	21.3	20.4	-4%	-8%
132	299	WNW	23.6	23.6	0%	0%
211	299	WNW	24.6	21.8	-12%	-22%
290	299	WNW	24.2	22.5	-7%	-14%
42	302	WNW	21.5	21.0	-3%	-5%
121	302	WNW	22.5	22.8	1%	2%
200	302	WNW	24.3	22.7	-7%	-13%
279	302	WNW	23.3	22.3	-4%	-8%
26	304	NW	21.1	22.2	5%	10%
105	304	NW	22.8	25.1	10%	21%
184	304	NW	26.0	25.0	-4%	-7%
263	304	NW	23.3	24.0	3%	7%
76	306	NW	23.7	23.5	-1%	-2%
155	306	NW	25.9	26.6	2%	5%
234	306	NW	28.2	24.8	-12%	-23%
313	306	NW	25.8	25.3	-2%	-4%
27	310	NW	24.5	24.6	0%	1%
106	310	NW	28.0	28.9	3%	6%
185	310	NW	29.8	27.7	-7%	-14%
264	310	NW	27.5	27.1	-2%	-3%
15	315	NW	19.6	21.3	8%	18%
94	315	NW	19.9	22.8	15%	32%
173	315	NW	23.9	24.1	1%	2%
252	315	NW	21.0	23.1	10%	21%
24	321	NW	23.0	22.9	-1%	-1%
103	321	NW	24.6	25.7	4%	9%
182	321	NW	26.9	25.3	-6%	-12%
261	321	NW	25.2	24.4	-3%	-6%

45	330	NNW	17.3	17.1	-1%	-3%
124	330	NNW	18.9	21.8	15%	32%
203	330	NNW	23.2	23.2	0%	0%
282	330	NNW	20.5	22.6	11%	22%

SOUTH JETTY – BY HEIGHT

Table B-2: Wave heights at the South Jetty, under the Existing Condition and 2023 PA, organized by wave direction (from south to north). Grey: wave heights decrease under the PA; White: wave heights increase under the PA.

Storm Number	Offshore Direction		Nearshore Wave Height (ft)		Change in ... (%)	
	°N	Cardinal Direction	Existing	2023 PA	Wave Height	Wave Energy
60	195	SSW	8.3	9.8	18%	40%
139	195	SSW	9.1	9.7	7%	14%
218	195	SSW	9.5	10.2	7%	15%
297	195	SSW	8.3	9.6	16%	35%
18	197	SSW	8.6	9.0	5%	11%
97	197	SSW	10.2	9.7	-5%	-10%
176	197	SSW	10.0	9.2	-8%	-15%
255	197	SSW	9.2	9.1	-1%	-1%
54	198	SSW	8.9	10.6	18%	39%
55	198	SSW	12.7	12.5	-1%	-3%
69	198	SSW	8.8	10.3	17%	36%
133	198	SSW	9.9	10.3	4%	8%
134	198	SSW	13.9	13.9	-1%	-1%
148	198	SSW	9.6	9.8	2%	4%
212	198	SSW	10.4	11.0	6%	12%
213	198	SSW	14.4	14.0	-3%	-6%
227	198	SSW	10.2	10.9	7%	14%
291	198	SSW	9.1	10.2	13%	27%
292	198	SSW	13.7	13.3	-3%	-6%
306	198	SSW	9.0	10.0	11%	23%
9	200	SSW	11.1	11.8	6%	13%
88	200	SSW	12.7	12.6	-1%	-2%
167	200	SSW	12.9	13.1	1%	3%
246	200	SSW	12.0	11.9	-1%	-2%
51	201	SSW	8.1	9.0	10%	21%
130	201	SSW	8.8	9.5	7%	15%
209	201	SSW	9.0	8.9	-1%	-1%
288	201	SSW	8.2	9.0	11%	23%
47	202	SSW	8.3	9.7	17%	36%
77	202	SSW	12.4	12.6	1%	3%
126	202	SSW	9.0	9.3	4%	7%
156	202	SSW	13.6	13.7	1%	2%
205	202	SSW	9.3	9.5	3%	6%

235	202	SSW	14.3	14.4	1%	1%
284	202	SSW	8.2	9.5	16%	33%
314	202	SSW	13.4	13.2	-1%	-3%
22	203	SSW	8.8	10.0	14%	29%
101	203	SSW	9.8	10.1	2%	5%
180	203	SSW	10.0	10.3	3%	5%
259	203	SSW	9.0	9.9	10%	21%
6	204	SSW	10.7	11.5	7%	15%
32	204	SSW	8.5	9.7	14%	31%
85	204	SSW	11.8	12.0	2%	4%
111	204	SSW	9.2	10.0	8%	18%
164	204	SSW	12.4	13.0	5%	11%
190	204	SSW	9.4	9.9	6%	12%
243	204	SSW	11.3	11.4	1%	2%
269	204	SSW	8.5	9.8	16%	33%
49	206	SSW	9.0	10.8	19%	43%
58	206	SSW	14.1	13.8	-2%	-5%
65	206	SSW	11.0	12.0	9%	19%
128	206	SSW	10.0	10.4	4%	8%
137	206	SSW	15.2	15.1	-1%	-2%
144	206	SSW	12.2	12.1	0%	-1%
207	206	SSW	10.7	11.6	8%	16%
216	206	SSW	15.9	16.0	1%	2%
223	206	SSW	13.0	13.3	2%	5%
286	206	SSW	9.5	10.5	11%	23%
295	206	SSW	15.5	14.9	-4%	-8%
302	206	SSW	11.8	12.0	1%	2%
20	207	SSW	15.6	16.2	4%	8%
99	207	SSW	15.7	16.7	6%	13%
178	207	SSW	17.5	18.9	8%	16%
257	207	SSW	16.3	17.3	6%	12%
59	212	SSW	9.6	10.7	11%	23%
138	212	SSW	10.9	11.4	5%	10%
217	212	SSW	10.9	11.4	5%	11%
296	212	SSW	9.8	10.7	9%	19%
19	215	SW	12.6	12.0	-4%	-9%
98	215	SW	14.5	13.8	-5%	-9%
177	215	SW	14.2	12.9	-9%	-17%
256	215	SW	14.2	13.2	-7%	-14%
10	217	SW	8.3	9.4	12%	26%

89	217	SW	9.5	10.0	5%	11%
168	217	SW	9.4	9.6	2%	5%
247	217	SW	8.5	9.5	12%	25%
70	218	SW	10.1	11.4	13%	28%
149	218	SW	11.3	11.3	0%	0%
228	218	SW	12.0	12.4	4%	8%
307	218	SW	10.7	11.2	5%	11%
5	220	SW	14.0	13.4	-4%	-8%
84	220	SW	14.9	14.8	0%	-1%
163	220	SW	15.1	14.9	-1%	-3%
242	220	SW	15.0	14.2	-6%	-11%
46	221	SW	8.7	9.5	9%	19%
125	221	SW	9.9	10.6	7%	16%
204	221	SW	9.8	10.1	3%	7%
283	221	SW	9.0	9.9	9%	20%
52	223	SW	9.2	10.1	9%	19%
131	223	SW	10.9	10.6	-3%	-5%
210	223	SW	10.5	10.4	-1%	-3%
289	223	SW	9.9	10.1	2%	4%
67	227	SW	14.9	15.4	3%	6%
146	227	SW	15.1	15.8	4%	9%
225	227	SW	17.1	18.4	8%	17%
304	227	SW	15.4	15.7	2%	4%
1	229	SW	10.3	11.1	8%	17%
62	229	SW	11.7	12.0	3%	6%
80	229	SW	11.5	11.4	-1%	-2%
141	229	SW	13.0	12.8	-1%	-3%
159	229	SW	11.6	11.5	-1%	-2%
220	229	SW	13.5	13.2	-2%	-4%
238	229	SW	11.1	11.1	1%	1%
299	229	SW	12.7	12.5	-2%	-3%
2	232	SW	16.3	17.1	5%	10%
81	232	SW	16.8	18.6	10%	22%
160	232	SW	17.3	19.1	10%	22%
239	232	SW	16.4	17.9	9%	19%
31	233	SW	12.2	11.1	-8%	-16%
110	233	SW	14.0	13.8	-1%	-3%
189	233	SW	13.5	13.4	0%	-1%
268	233	SW	13.4	12.7	-6%	-11%
34	234	SW	12.4	12.4	0%	0%

113	234	SW	13.6	13.5	-1%	-2%
192	234	SW	14.0	13.4	-4%	-8%
271	234	SW	13.4	12.9	-3%	-7%
48	238	WSW	9.0	9.2	3%	6%
127	238	WSW	10.8	9.7	-10%	-19%
206	238	WSW	10.7	9.3	-13%	-24%
285	238	WSW	9.4	9.2	-2%	-3%
35	244	WSW	14.9	14.9	0%	0%
114	244	WSW	15.5	15.9	3%	5%
193	244	WSW	17.4	18.3	5%	10%
272	244	WSW	15.9	15.6	-2%	-3%
8	246	WSW	17.0	17.5	2%	5%
87	246	WSW	18.1	19.7	9%	18%
166	246	WSW	18.5	19.8	7%	14%
245	246	WSW	17.9	18.6	4%	8%
21	248	WSW	21.1	21.2	0%	1%
41	248	WSW	11.3	11.2	-1%	-2%
100	248	WSW	23.1	25.0	8%	16%
120	248	WSW	13.0	12.2	-6%	-12%
179	248	WSW	21.7	23.1	6%	13%
199	248	WSW	12.6	11.6	-8%	-15%
258	248	WSW	22.7	23.5	4%	7%
278	248	WSW	12.4	11.7	-6%	-11%
50	261	W	17.1	17.1	0%	0%
129	261	W	19.0	20.0	5%	10%
208	261	W	19.1	19.5	2%	4%
287	261	W	18.8	18.8	0%	1%
37	262	W	20.5	20.0	-3%	-5%
116	262	W	23.6	24.6	4%	9%
195	262	W	21.7	21.7	0%	0%
274	262	W	22.6	23.0	2%	4%
78	268	W	16.2	13.3	-18%	-32%
157	268	W	17.6	18.0	2%	4%
236	268	W	17.6	17.0	-3%	-6%
315	268	W	17.6	16.7	-5%	-10%
71	270	W	19.8	19.1	-3%	-6%
150	270	W	22.4	23.3	4%	9%
229	270	W	20.8	20.9	0%	1%
308	270	W	21.8	22.2	2%	4%
36	271	W	21.2	20.8	-2%	-3%

40	271	W	15.6	14.9	-4%	-9%
72	271	W	22.6	22.2	-2%	-3%
79	271	W	15.8	15.3	-3%	-6%
115	271	W	24.4	25.5	4%	9%
119	271	W	17.4	17.7	1%	3%
151	271	W	27.0	27.3	1%	2%
158	271	W	17.6	18.0	2%	5%
194	271	W	22.4	22.7	2%	3%
198	271	W	17.2	16.3	-5%	-10%
230	271	W	24.7	25.4	3%	6%
237	271	W	17.4	16.6	-5%	-9%
273	271	W	23.3	24.1	4%	8%
277	271	W	16.8	16.1	-4%	-8%
309	271	W	24.9	24.9	0%	-1%
316	271	W	17.1	16.8	-2%	-5%
33	272	W	18.0	17.5	-3%	-6%
66	272	W	13.7	13.5	-1%	-2%
112	272	W	20.8	21.2	2%	5%
145	272	W	14.9	15.4	3%	7%
191	272	W	19.2	18.7	-2%	-5%
224	272	W	15.4	15.2	-1%	-2%
270	272	W	19.6	19.5	0%	0%
303	272	W	14.5	14.4	-1%	-2%
7	273	W	21.0	20.3	-4%	-7%
14	273	W	17.9	17.4	-3%	-6%
86	273	W	24.5	24.7	1%	1%
93	273	W	20.6	20.6	0%	1%
165	273	W	22.7	21.8	-4%	-8%
172	273	W	19.4	18.5	-5%	-9%
244	273	W	23.5	23.9	2%	3%
251	273	W	19.8	19.2	-3%	-5%
13	276	W	13.9	13.4	-3%	-6%
92	276	W	15.4	15.2	-1%	-2%
171	276	W	15.6	14.5	-7%	-14%
250	276	W	15.3	14.6	-4%	-9%
43	278	W	16.5	15.8	-4%	-8%
75	278	W	11.7	10.3	-12%	-22%
122	278	W	18.6	18.6	0%	0%
154	278	W	13.6	12.4	-9%	-17%
201	278	W	18.2	16.7	-9%	-16%

233	278	W	12.5	10.7	-14%	-26%
280	278	W	18.0	17.4	-4%	-7%
312	278	W	12.7	10.9	-14%	-26%
3	279	W	19.1	17.7	-8%	-15%
12	279	W	19.8	18.9	-5%	-9%
64	279	W	17.1	16.1	-6%	-12%
82	279	W	21.3	20.9	-2%	-4%
91	279	W	23.4	23.0	-2%	-3%
143	279	W	19.7	19.2	-2%	-5%
161	279	W	19.9	18.9	-5%	-10%
170	279	W	21.2	19.9	-6%	-12%
222	279	W	18.1	16.0	-12%	-22%
240	279	W	21.2	20.2	-5%	-9%
249	279	W	22.2	21.8	-2%	-4%
301	279	W	18.9	17.5	-7%	-14%
38	280	W	17.5	15.9	-9%	-17%
117	280	W	19.7	19.3	-2%	-5%
196	280	W	18.5	16.9	-8%	-16%
275	280	W	18.9	17.5	-8%	-14%
61	281	W	15.6	14.1	-10%	-19%
68	281	W	15.8	14.2	-10%	-19%
140	281	W	17.5	16.9	-3%	-6%
147	281	W	18.5	17.8	-4%	-8%
219	281	W	16.7	14.2	-15%	-27%
226	281	W	16.7	14.7	-12%	-22%
298	281	W	17.4	15.9	-9%	-17%
305	281	W	17.0	15.1	-11%	-22%
44	282	WNW	18.8	16.7	-11%	-21%
123	282	WNW	21.6	20.1	-7%	-13%
202	282	WNW	18.8	16.8	-11%	-21%
281	282	WNW	20.8	18.5	-11%	-21%
63	284	WNW	20.0	19.2	-4%	-8%
142	284	WNW	23.6	23.5	0%	-1%
221	284	WNW	21.5	21.2	-2%	-3%
300	284	WNW	22.4	22.2	-1%	-2%
11	286	WNW	16.9	16.5	-3%	-6%
90	286	WNW	18.9	19.1	1%	1%
169	286	WNW	18.3	17.4	-5%	-10%
248	286	WNW	18.6	18.0	-3%	-6%
16	288	WNW	13.2	11.8	-10%	-20%

28	288	WNW	15.1	13.1	-13%	-24%
95	288	WNW	15.5	14.3	-8%	-15%
107	288	WNW	17.4	16.1	-8%	-15%
174	288	WNW	14.2	11.8	-17%	-31%
186	288	WNW	15.8	12.9	-19%	-34%
253	288	WNW	14.6	12.8	-12%	-23%
265	288	WNW	16.5	14.1	-15%	-27%
29	289	WNW	15.8	13.4	-15%	-28%
30	289	WNW	16.2	14.3	-12%	-23%
108	289	WNW	18.1	16.6	-8%	-16%
109	289	WNW	19.0	17.8	-6%	-12%
187	289	WNW	16.4	13.6	-17%	-31%
188	289	WNW	16.8	14.2	-15%	-28%
266	289	WNW	17.2	14.4	-16%	-30%
267	289	WNW	17.5	14.9	-15%	-27%
25	291	WNW	18.0	16.3	-9%	-18%
104	291	WNW	21.1	19.6	-7%	-13%
183	291	WNW	19.0	16.3	-14%	-27%
262	291	WNW	20.1	18.0	-11%	-20%
39	292	WNW	15.0	13.5	-10%	-19%
73	292	WNW	14.8	13.5	-8%	-16%
118	292	WNW	17.3	16.6	-4%	-8%
152	292	WNW	17.3	16.0	-7%	-14%
197	292	WNW	16.4	14.5	-11%	-22%
231	292	WNW	15.7	12.9	-18%	-32%
276	292	WNW	16.4	14.7	-10%	-19%
310	292	WNW	16.3	14.4	-12%	-22%
4	293	WNW	14.0	12.5	-11%	-20%
83	293	WNW	16.0	15.4	-4%	-7%
162	293	WNW	15.6	14.2	-9%	-17%
241	293	WNW	15.0	13.5	-10%	-19%
17	294	WNW	13.9	12.2	-12%	-22%
96	294	WNW	16.6	15.2	-8%	-16%
175	294	WNW	14.4	11.9	-18%	-32%
254	294	WNW	15.6	13.6	-12%	-23%
23	295	WNW	14.9	13.4	-10%	-18%
102	295	WNW	17.2	16.5	-4%	-8%
181	295	WNW	15.8	13.6	-14%	-26%
260	295	WNW	15.8	14.1	-11%	-20%
56	296	WNW	12.0	10.6	-11%	-21%

57	296	WNW	13.8	11.9	-14%	-25%
74	296	WNW	11.8	10.4	-12%	-23%
135	296	WNW	14.7	13.2	-10%	-19%
136	296	WNW	16.3	15.0	-8%	-16%
153	296	WNW	13.9	12.1	-13%	-25%
214	296	WNW	13.2	10.4	-21%	-38%
215	296	WNW	15.0	11.7	-22%	-40%
232	296	WNW	12.0	9.6	-20%	-36%
293	296	WNW	12.9	11.2	-13%	-24%
294	296	WNW	15.0	13.2	-12%	-22%
311	296	WNW	12.4	11.2	-10%	-19%
53	299	WNW	13.0	11.3	-13%	-24%
132	299	WNW	15.3	13.9	-9%	-17%
211	299	WNW	14.2	10.7	-25%	-43%
290	299	WNW	14.0	12.3	-12%	-22%
42	302	WNW	14.0	12.3	-12%	-23%
121	302	WNW	16.4	15.4	-6%	-12%
200	302	WNW	15.3	12.9	-16%	-29%
279	302	WNW	15.0	13.3	-11%	-22%
26	304	NW	12.7	11.5	-9%	-18%
105	304	NW	15.7	13.7	-13%	-24%
184	304	NW	14.1	10.8	-23%	-41%
263	304	NW	13.1	12.2	-7%	-14%
76	306	NW	15.7	14.0	-11%	-21%
155	306	NW	18.1	16.5	-9%	-17%
234	306	NW	16.3	13.5	-17%	-31%
313	306	NW	16.5	14.6	-12%	-22%
27	310	NW	17.1	14.6	-14%	-27%
106	310	NW	19.4	17.7	-9%	-16%
185	310	NW	17.7	15.0	-15%	-28%
264	310	NW	17.8	15.7	-12%	-22%
15	315	NW	10.0	9.5	-6%	-11%
94	315	NW	12.1	9.8	-19%	-35%
173	315	NW	11.8	9.5	-20%	-35%
252	315	NW	10.0	10.1	1%	1%
24	321	NW	13.5	11.1	-18%	-32%
103	321	NW	16.3	14.4	-11%	-21%
182	321	NW	15.0	12.0	-20%	-36%
261	321	NW	13.4	11.6	-14%	-26%
45	330	NNW	8.4	7.9	-6%	-12%

124	330	NNW	10.8	9.1	-15%	-28%
203	330	NNW	10.7	9.0	-15%	-28%
282	330	NNW	9.6	9.3	-4%	-8%